UNIVERSITY OF SOUTHAMPTON

FACULTY OF NATURAL AND ENVIRONMENTAL SCIENCES

Ocean and Earth Science

2016/2017

RECONSTRUCTING ONTOGENETIC MOVEMENTS IN PELAGIC SHARKS COUPLING OCEAN MODELS AND STABLE ISOTOPE DATA IN INCREMENTALLY GROWN TISSUES

by

Sarah Magozzi

Thesis for the degree of Doctor of Philosophy

April 2017

Abstract

Ecological interactions in the marine pelagic environment are difficult to study, mostly because the open-ocean is vast and largely inaccessible. Migration is a common ecological trait in pelagic settings, with large impacts on community structure and dynamics, and ecosystem functioning. However, migratory predators are rapidly declining worldwide, with unclear ecological consequences.

Pelagic sharks have declined regionally by > 90% in the past 15 years, largely as a result of overfishing and by-catch. Shark vulnerability to fishery capture depends on individual movements, and on the presence of movement traits across individuals, populations or species, which may imply shared vulnerability. Yet, the movements of pelagic sharks and other migratory oceanic animals are difficult to monitor or reconstruct.

Natural-abundance stable isotopes allow retrospective movement reconstruction, by relating the isotopic composition of animal tissues to geographically indexed measurements or predictions of isotopic ratios at the base of the food web (isoscapes). Where incrementally grown, metabolically inert tissues are available, movements can be reconstructed throughout life. However, the application of stable isotopes in bulk tissues to study migration is complicated by mixed baseline and trophic effects and, in pelagic settings, by large uncertainties in the spatio-temporal distributions of isotopic baselines.

In this study, I explored how the ontogenetic movements of two pelagic shark model species, the blue (*Prionace glauca*) and porbeagle (*Lamna nasus*) sharks, could be reconstructed using modelled global ocean carbon isoscapes, and carbon and nitrogen isotopes in bulk cartilage collagen and single amino acids from vertebrae.

To provide a possible solution for poor sampling of isotopic baselines, I developed a process-based, mechanistic carbon isotope model, predicting the likely spatio-temporal distributions of the carbon isotopic composition of phytoplankton across the global ocean.

To provide information on pelagic shark life-history traits, I recovered individual-level life-history carbon and nitrogen isotope records for bulk cartilage collagen from vertebrae of sharks caught across the North Atlantic. I also recovered comparable carbon isotope records for single amino acids, producing the first compound-specific isotopic dataset of within-individual ontogenetic variance in sharks. Consistent ontogenetic isotope patterns across individuals of each species revealed species-level life-history traits. Whilst the interpretation of traits for bulk collagen using modelled isoscapes was ultimately limited from confounding influences from trophic level change, that of traits for essential amino acids conclusively demonstrated ontogenetic and transgenerational movement traits.

During juvenile growth, blue sharks increasingly utilised foraging grounds with more positive carbon isotopic baselines, whereas porbeagles made increasing use of isotopically more negative grounds. Blue shark pupping and maternal foraging occurred in isotopically distinct grounds, with the possibility of natal homing by adult individuals. Pregnant female porbeagles, by contrast, migrated to isotopically distinct foraging grounds prior to giving birth.

Isotope-derived information on ontogenetic movements complements tag-derived information over a snap-shot of the entire life of individuals, but explicit isoscape-based geo-location is limited by large uncertainties in isoscape models, and trophic influences on bulk tissue isotopic compositions.

Table of Contents

List of Tables

APPENDIX 4.D

List of Figures

CHAPTER 1

CHAPTER 2

CHAPTER 3

APPENDICES

Declaration of authorship

I, SARAH MAGOZZI

declare that this thesis and the work presented in it are my own and has been generated by me as the result of my own original research.

RECONSTRUCTING ONTOGENETIC MOVEMENTS IN PELAGIC SHARKS COUPLING OCEAN MODELS AND STABLE ISOTOPE DATA IN INCREMENTALLY GROWN TISSUES

I confirm that:

1) This work was done wholly or mainly while in candidature for a research degree at this University;
2) Where any part of this thesis has previously been submitted for a degree or any other qualification at this University or any other institution, this has been clearly stated;
3) Where I have consulted the published work of others, this is always clearly attributed;
4) Where I have quoted from the work of others, the source is always given. With the exception of such quotations, this thesis is entirely my own work;
5) I have acknowledged all main sources of help;
6) Where the thesis is based on work done by myself jointly with others, I have made clear exactly what was done by others and what I have contributed myself (see individual chapters);
7) Part of this work has been published as a research article in the peer-review journal Ecosphere as: Magozzi, S., A. Yool, H. B. Vander Zanden, M. B. Wunder, and C. N. Trueman. 2017. Using ocean models to predict spatial and temporal variation in marine carbon isotopes. Ecosphere. *In press*.

Signed:

Date:

Acknowledgements

I would first like to thank my supervisor Clive Trueman for his expertise, guidance and endless patience throughout this PhD. You have been such an exceptional mentor, I could not be more greatful.

I would also like to thank Simon Thorrold and Leah Houghton for their hospitality and valuable advice during my exchange at WHOI. In parallel, I am also greatful to Micheael Wunder and Hannah Vander Zanden for their knowledge and precious help over my time at University of Colorado Denver.

At NOCS, I would like to thank all the scientists in the SUMIE group for sharing their expertise and being always open to discussion: Kirsteen MacKenzie, Ming-Tsung Chung, Rhiannon Meier, Diana Shores, Katie Quaeck, Rui Pedro Vieira, Christopher Bird, Clare Prebble, Katie St. John Glew and Matthew Cobain. I am also thankful to Bob and John for their help and humour when preparing samples. I would like to thank Gregory Skomal, Lisa Natanson, Miguel Neves dos Santos, Rui Coelho, David Sims, Nuno Queiroz, Victoria Bendall, Stuart Hetherington and Jim Ellis for providing shark vertebral samples. I am also greatful to Kelton McMahon and Christopher Somes for providing model validation datasets, and to Katie Quaeck and Christopher Bird for providing eye lens isotope data.

Additionally, I would like to express my gratitude to the University of Southampton for providing financial support for both this PhD and the NOCS-WHOI Exchange Programme. I also thank the National Science Foundation for funding the Research-In-Residence program.

The greatest thank you goes to my parents. Thank you for your never-ending love and support in all the decisions I have taken, even the wrong ones. I am stubborn, so I would have taken them anyway, but without your support the consequences would have felt much harder.

These four years have been tough, surely I have not been the easiest person to get along with. But I am greatful to all the people who have loved me, and to those who love me still.

And thank you, little lovely Rimmelina, you always manage to make me smile!

Abbreviations

$^{13}C/^{12}C$	Ratio of the heavy to the light carbon isotopes
$^{15}N/^{14}N$	Ratio of the heavy to the light nitrogen isotopes
^{14}C	Radiocarbon isotope
$\delta^{13}C$	Carbon isotopic composition
$\delta^{15}N$	Nitrogen isotopic composition
$\delta^{2}H$ (or δD)	Hydrogen isotopic composition
$\delta^{18}O$	Oxygen isotopic composition
$\delta^{87}S$	Strontium isotopic composition
$\delta^{13}C_{PLK}$	Carbon isotopic composition of phytoplankton
$\delta^{15}N_{PLK}$	Nitrogen isotopic composition of phytoplankton
$\delta^{13}C_{ZPLK}$	Carbon isotopic composition of zooplankton
$\delta^{13}C_{PLK\text{-}SS}$	Carbon isotopic composition of phytoplankton as predicted by the UVic model (Schmittner & Somes, 2016)
$\delta^{13}C_{DIC}$	Carbon isotope composition of dissolved inorganic carbon
$\delta^{13}C_{CO2(aq)}$	Carbon isotopic composition of dissolved CO_2
$n\delta^{13}C$	Life history-normalised carbon isotope values (of bulk cartilage collagen)
$n\delta^{15}N$	Life history-normalised nitrogen isotope values (of bulk cartilage collagen)
$\delta^{13}C_{bulk}$	Carbon isotopic composition of bulk cartilage collagen
$\delta^{15}N_{bulk}$	Nitrogen isotopic composition of bulk cartilage collagen
$\delta^{13}C_{EAA}$	Carbon isotopic compositions of essential amino acids
$\delta^{13}C_{nonEAA}$	Carbon isotopic compositions of non-essential amino acids
$\delta^{13}C_{norm\text{-}EAA}$	Sample-normalised carbon isotope values of essential amino acids
$\delta^{13}C_{norm\text{-}nonEAA}$	Sample-normalised carbon isotope values of non-essential amino acids
ε_p	Overall carbon isotopic fractionation during photosynthesis
ε_{pi}	Carbon isotopic fractionation for the phytoplankton group i
μ_i	Specific growth rate for the phytoplankton group i
r_i	Cell radius for the phytoplankton group i
S_i	Cell surface area for the phytoplankton group i
V_i	Cell volume for the phytoplankton group i
γ_i	Cell carbon content for the phytoplankton group i
ε_f	Enzymatic carbon isotope fractionation during carbon fixation
ε_d	Diffusive carbon isotope fractionation of $CO_{2(aq)}$ in seawater
D_t	Temperature-sensitive diffusivity of $CO_{2(aq)}$
r_k	Reacto-diffusive length
P	Cell wall permeability
GCM	General circulation model
NEMO	Nucleus for the European modelling of the ocean
MEDUSA	Model of ecosystem dynamics, nutrient utilization, sequestration and acidification
SST	Sea surface temperature
DIC	Dissolved inorganic carbon
POC	Particulate organic carbon
DOC	Dissolved organic carbon
$CO_{2(aq)}$ ($[CO_{2(aq)}]$)	Dissolved CO2 (concentration of)
H_2CO_3 ($[H_2CO_3]$)	Carbonic acid (concentration of)
HCO_3^- ($[HCO_3^-]$)	Bicarbonate ion (concentration of)
CO_3^{2-} ($[CO_3^{2-}]$)	Carbonate ion (concentration of)
HCl	Hydrochloric acid
EDTA	Ethylenediaminetetraacetic acid
USGS-41	Glutamic acid standard for bulk isotope analysis
NIST 1577	Bovine liver standard for bulk isotope analysis
MCF	Methyl chloroformate
TFAA	Trifluoroacetic acid
NACME	N-acetyl methyl ester
AA1, AA2	Amino acid standards for compound-specific isotope analysis

GM	Atlantic cod (*Gadus morhua*) standard
GC-C-irm-MS	Gas chromatography-combustion-isotope ratio monitoring mass spectrometry
Val	Valine
Ileu	Isoleucine
Leu	Leucine
Thr	Threonine
Phe	Phenylalanine
Ala	Alanine
Gly	Glycine
Pro	Proline
Asp	Aspartic acid
Glu	Glutamic acid
VR	Vertebral radius
FL	Fork Length
N	Number of samples along VR
ID	ID of single or combined samples
Av Int	Average interval between adjacent samples
d	Median distance between adjacent samples
BSH (or bsh)	Blue shark (*Prionace glauca*)
POR (or por)	Porbeagle shark (*Lamna nasus*)
MAR	Mid-Atlantic Ridge
CI	Canary Islands
NWA	Northwest Atlantic
WEC	Western English Channel
FI	Faroe Islands
PB	Pre-birth life stage
JUV	Juvenile life stage
AD	Adult life stage
GAMMs	Generalised additive mixed models
GLMMs	Generalised linear mixed models
AIC	Akaike information criteria
SEAc	Standard ellipse area corrected for small sample size
SEA.B	Posterior draws of Bayesian-estimated standard ellipse areas
PCA	Principal component analysis
PC1, PC2	First and second principal components (scores)
PC1.EAA	PC1 scores from PCA with raw carbon isotopic compositions of essential amino acids
PC1.norm-EAA	PC1 scores from PCA with sample-normalised carbon isotopic compositions of essential amino acids
PC1.nonEAA	PC1 scores from PCA with raw carbon isotopic compositions of non-essential amino acids
PC1.norm-nonEAA	PC1 scores from PCA with sample-normalised carbon isotopic compositions of non-essential amino acids
nPC1	Life-history normalised PC1 scores for any of the above
LDA	Linear discriminant function analysis
LD1, LD2	First and second linear discriminants

Chapter 1: Thesis introduction

The populations of marine pelagic sharks have significantly declined worldwide over the past century. The primary cause of such population declines is overfishing, both targeted and incidental (by-catch), followed by habitat destruction, persecution and climate change. The global fin trade is also a major driver of shark mortaility, other than the demand for their meat (Baum *et al.*, 2003; Clarke *et al.*, 2006; Camhi *et al.*, 2008; Worm *et al.*, 2013). As highly migratory predators, pelagic sharks play important ecological roles within marine ecosystems, however, the ecological consequences of their decline are yet mostly unclear (Heupel *et al.*, 2014; Grubbs *et al.*, 2016; Roff *et al.*, 2016; Ruppert *et al*., 2016).

Recently, a systematic global analysis of the threat status of all 1041 chondrichthyan species, including sharks, rays and chimaera, estimated that one fourth are threatened according to the International Union for Conservation of Nature (IUCN) Red List Criteria, due to overfishing (Dulvy *et al.*, 2014). Large-bodied sharks are at greatest risk of extinction, mainly because of typical life-history traits such as slow growth rate, late age at maturity, and small number of offsprings (Cortes, 2000; Jennings *et al.*, 1998; Garcia *et al.*, 2008; Hutchings *et al.*, 2012). Improved management and conservation are urgently needed to avoid extinction and promote population recovery (Baum *et al.*, 2003; Dulvy *et al.*, 2014).

Many pelagic shark species are highly migratory, and move large distances across the open-ocean, spanning multiple management zones. The pelagic environment, particularly high-seas outside national jurisdictions, is heavily targeted by fisheries. Therefore, management of migratory oceanic animals that may be transient components within disparate fished ecosystems is extremely challenging, and requires knowledge of the migratory life-histories of pelagic animals.

The movements of migratory pelagic animals are, however, difficult to monitor or reconstruct. Electronic archival tags provide the best currently available tool to track the movements of individual fish at fine spatio-temporal scales, however, they can only be applied to a small number of individuals, large species and adult life stages. The analysis of stable isotopes in animal tissues allow retrospective movement reconstruction, by relating variance in tissue isotopic compositions to geographic variations in compositions at the base of the food web (for reviews, see Hobson, 1999; Graham *et al.*, 2010; Trueman *et al.*, 2012; McMahon *et al.*, 2013a). It can be applied to every captured fish, including small, rare and/or elusive species, and juvenile stages. Additionally, where incrementally grown tissues are available, movements can be reconstructed throughout the entire life of individual fish.

Forensic applications of stable isotope analysis, therefore, can potentially provide a valuable complementary tool to satellite tags to gather information on the ontogenetic movement and habitat use patterns of threatened species. These applications can, for instance, help in the identification of

essential habitat areas across life-history, as well as areas of high use by multple individuals, populations or species, where interactions with fisheries are of greater concern for survival, recruitment, reproduction and maintenance of ecosystem functions.

1.1 Migration

Migration is a common ecological trait in most habitats on Earth, and as such has stimulated a large literature. Although this literature has primarily focussed on migration itself (Bowlin *et al.*, 2010), the potential impacts of migration on community structure and dynamics, and ecosystem functioning are now being recognised (Lundberg & Moberg, 2003; Holdo *et al.*, 2011; Bauer & Hoye, 2014). The effects of migration on ecological networks have been reviewed by Bauer & Hoye (2014) for a range of terrestrial and marine systems (Fig. 1.1).

By moving, migratory animals transport nutrients and energy (Varpe *et al.*, 2005; Michelutti *et al.*, 2009; Holtgrieve & Schindler, 2011), as well as other organisms, including propagules (Viana *et al.*, 2013) and parasites (Altizer *et al.*, 2011), and toxicants (Brimble *et al.*, 2009) across disparate locations and food webs. Furthermore, migrants also forage (Brönmark *et al.*, 2014) and are preyed upon (Holdo *et al.*, 2011) along their routes, establishing transport and trophic interactions within local communities (Holdo *et al.*, 2011; Bauer & Hoye, 2014).

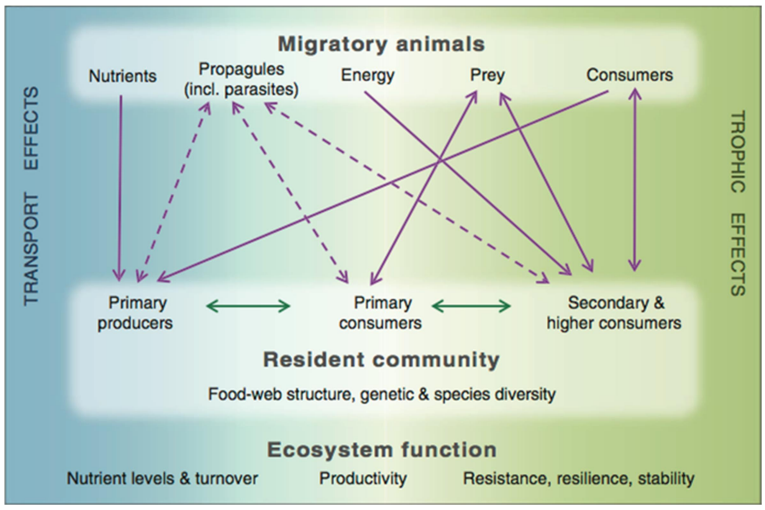

Figure 1.1 Schematics of the transport and trophic effects of migratory animals on community structure and dynamics, and ecosystem functioning. Taken from Bauer & Hoye (2014).

The inputs of allochthonous nutrients and energy by migratory animals result in increased resource availability, with consequences for productivity at various trophic levels (Moore & Schindler, 2004; Varpe *et al.*, 2005; Michelutti *et al.*, 2009; Holtgrieve & Schindler, 2011), and can potentially result in transitions between alternate stable states (Holtgrieve & Schindler, 2011). Furthermore, the long-distance dispersal of propagules or other organisms mediated by migrants may result in the establishment of new or lost species, and lead to maintenance of gene flow and mixing among resident populations (Clausen *et al.*, 2002; Leibold *et al.*, 2004; Viana *et al.*, 2013). Similarly, migratory

animals may alter parasite transmission, diversity and evolution, by either facilitating or challenging parasite dispersal (Buehler *et al.*, 2008; Krauss *et al.*, 2010; Altizer *et al.*, 2011).

Foraging by migrants throughout their journeys may also establish consumer-resource interactions across several locations. By grazing on local primary producers, migratory herbivores may alter nutrient cycling, primary productivity and biomass, competitive interactions between primary production functional groups, and ultimately the composition of the primary producing community (Zacheis *et al.*, 2001; Holdo *et al.*, 2007; Dobson, 2009; Rooney & McCann, 2012). Migratory predators have the potential to exert top-down controls on resident communities through trophic cascades (Brönmark *et al.*, 2014). Migratory predators may also mediate interactions between prey species at spatially distant locations, generating spatial patterns in trophic cascades. Prey availability at one location influences predator abundance, and therefore may indirectly influence the intensity of predator top-down regulations at other locations (Holdo *et al.*, 2011). Spatial coupling of food webs by highly mobile opportunistic predators can potentially lead to increased food web stability (Polis *et al.*, 1997; Lundberg & Moberg, 2003; McCann *et al.*, 2005; Rooney *et al.*, 2006; McCauley *et al.*, 2012; Rooney & McCann, 2012). Additionally, migratory predators compete against resident predators, whereas migratory lower-trophic-level consumers are prey for resident predators (Holdo *et al.*, 2011). The pulsed nature of resource utilisation by migrants, and the timing of their interactions with local communities define the relationship between migrant abundance and primary production for herbivores, or food web stability for predators (Fryxell *et al.*, 1988; McCann *et al.*, 1998; Holdo *et al.*, 2007; 2011; Rooney & McCann, 2012).

In an evolutionary context, migration may determine the genetic structure of geographically separated populations. For example, natal homing may result in genetic isolation and adaptation to local environments, if dispersal is sufficiently low to allow genetic variation to occur (McMahon *et al.*, 2013a).

Given the potential of migrants to uniquely alter community structure and dynamics, ecosystem functioning, population stability, and even speciation and extinction, "migrations are not simply the movements of animals; they are ecological processes intimately embedded in, and interacting with, resident communities" (Bauer & Hoye, 2014). Migration routes and timing may be shaped by resident communities, and resident communities are, in turn, influenced by migrants, by the carryover effects of previous locations on migrants, and the effects of consumer-resource interactions after migrants' departure (Bauer & Hoye, 2014). Migrations are increasingly threatened worldwide through habitat loss, construction of artificial barriers, overexploitation and climate change (Wilcove & Wikelski, 2008; Bauer & Hoye, 2014). The loss of migrants and migratory behaviour implies the loss of the ecosystem functions that they provide. Nevertheless, protection of migratory animals is extremely difficult and inherently transnational, given that it should encompass entire migratory ranges, and all stages of migratory cycles (Wilcove & Wikelski, 2008; Harrison *et al.*, 2011; Bauer &

Hoye, 2014). Targeted management and conservation actions should, therefore, identify ideal collaborations across jurisdictions (Bauer & Hoye, 2014).

Marine pelagic ecosystems are particulalry conducive to migratory traits, as long-distance movement is relatively energetically efficient. Every year, large numbers of pelagic animals migrate across large distances in the open-ocean in pursuit of increased foraging opportunities, improved safety, and higher reproductive output (Dingle, 1996; Alerstam *et al.*, 2003; Bauer & Hoye, 2014). Ontogenetic shifts in movement behaviour and habitat use associated with life-time changes in energy allocation are also common (Werner & Gilliam, 1984; Morris, 2003; Grubbs, 2010; Carlisle *et al.*, 2015).

1.2 Pelagic environment

The pelagic environment is defined as the ecological realm that includes the entire ocean water column. Of all the inhabited Earth's systems, the pelagic zone has the largest volume ($1368 \cdot 10^6$ km^3) and the largest vertical range (0-11000 m; Angel, 1993). Within the pelagic zone, the neritic province includes waters above the continental shelf, the oceanic province open-ocean waters beyond the shelf. The neritic province is mainly distinguished from the oceanic because of higher nutrient concentrations from riverine runoff and upwelling. The upper portion of both the neritic and pelagic provinces, the epipelagic zone (0-200 m), is where photosynthesis occurs; below this zone lie the mesopelagic (200-1000 m), bathypelagic (1000-4000 m), abyssalpelagic (4000-6000 m), and hadopleagic (under 6000 m) zones (Fig. 1.2).

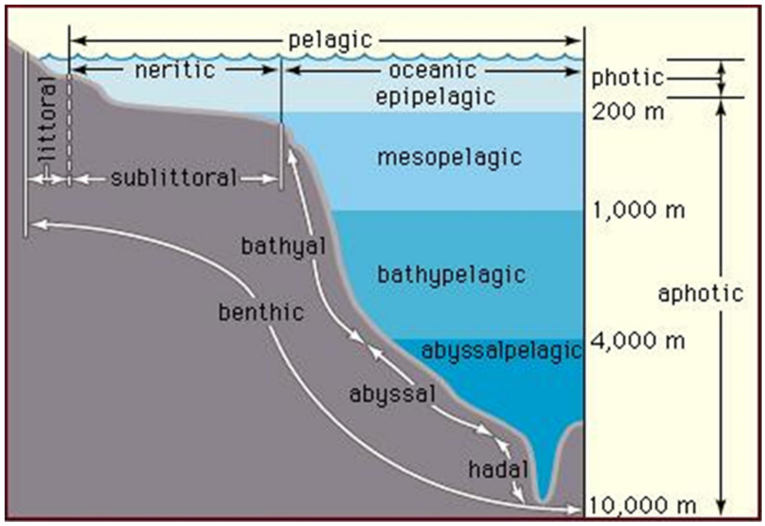

Figure 1.2 Horizontal and vertical zonation in the pelagic environment. Taken from Encyclopedia Britannica.

The pelagic community, therefore, comprises all marine organisms, from primary producers and heterotrophic bacteria to top predators, living in the water column. Pelagic life is found throughout the water column, with variations in abundance, biomass, body size and biodiversity with depth and distance from the shore (Angel, 1986; Backus, 1986; McGowan, 1986). Given that pelagic life, both at

surface and in the deep-sea, is ultimately supported by phytoplankton primary production in the euphotic zone (Gage, 2003; Lampitt *et al.*, 1993), these variations mostly reflect changes in surface primary productivity (Valiela, 1984; Kaiser *et al.*, 2005). Phytoplankton primary production in the euphotic zones varies at a range of spatio-temporal scales, and is generally highest near the coast due to favourable nutrients and temperature, becoming increasingly patchy offshore, with lowest levels in oligotrophic central open-ocean areas (Valiela, 1984; Kaiser *et al.*, 2005). Clearly, coastal and oceanic areas where production is high (e.g. at fronts) can sustain high community standing stocks (i.e. abundance and biomass; Sommer *et al.*, 2002; Kaiser *et al.*, 2005). Patchiness and heterogeneity in physico-chemical variables and biological production are key attributes of the pelagic environment. These attributes, alongside the vast and largely inaccessible nature of the open-ocean, make the pelagic zone extremely difficult to study.

Photosynthetically-derived organic matter in the euphotic zone, together with particles from faecal pellets and animal carcasses known as 'marine snow', is exported to the deep-sea via vertical sinking in the water column (Valiela, 1984; Kaiser *et al.*, 2005). As it sinks, particulate organic matter is diluted into a larger volume of water, resulting in decreasing food availability, and ultimately decreasing standing stocks with increasing depth (Kaiser *et al.*, 2005); however, this is not the case for bacteria (Rex *et al.*, 2006). Other than by food availability, the regional and vertical distributions of pelagic life are regulated by light (Clarke & Denton, 1962; Angel, 1997) and oxygen (Childress & Siebel, 1998; Siebel, 2011) availability, temperature, pressure (Somero, 1992; Yancey *et al.*, 2014), salinity and topography.

1.2.1 Biological and microbial carbon pumps

Primary production by phytoplankton is limited to the euphotic zone. Phytoplankton capture energy from sunlight, and transform inorganic carbon (CO_2) into organic carbon (biomass) via photosynthesis. Approximately 50% of this photosynthetically-originated organic carbon (POC) enters the classic food web *via* zooplankton grazing, or is transported as sinking particles to the deep-sea for long-term storage *via* the biological pump. The remaining 50% of carbon is directly processed by microbial activity (Buchan *et al.*, 2014; Fig. 1.3). As it sinks through the water column, particulate organic carbon enters the microbial loop, where it is first consumed by bacteria and converted into bacterial biomass (bacterial secondary production); it can then either be re-introduced into the classic food web as bacteria are preyed by zooplankton, or undergo continuous recycling within the microbial food web. Alternatively, a fraction of microbially-transformed organic carbon is released into the dissolved phase, some of which resists degradation and contributes to the large pool of recalcitrant dissolved organic carbon (DOC) that is stored in the ocean for thoudands of years *via* the microbial carbon pump). Viral lysis of phytoplankton and bacterial cells is also an important mechanism for the release of both dissolved and particulate organic carbon into the ocean, redirecting carbon away from higher trophic level towards the microbial realm. Dissolved organic carbon is consumed by bacteria

and used for growth. Microbial respiration converts organic carbon to gaseous CO_2, which is eventually utilised by phytoplankton for photosynthesis. Bacteria also regenerate nutrients supporting phytoplankton growth, particularly nitrogen and phosphorus (Buchan *et al.*, 2014; Fig. 1.3).

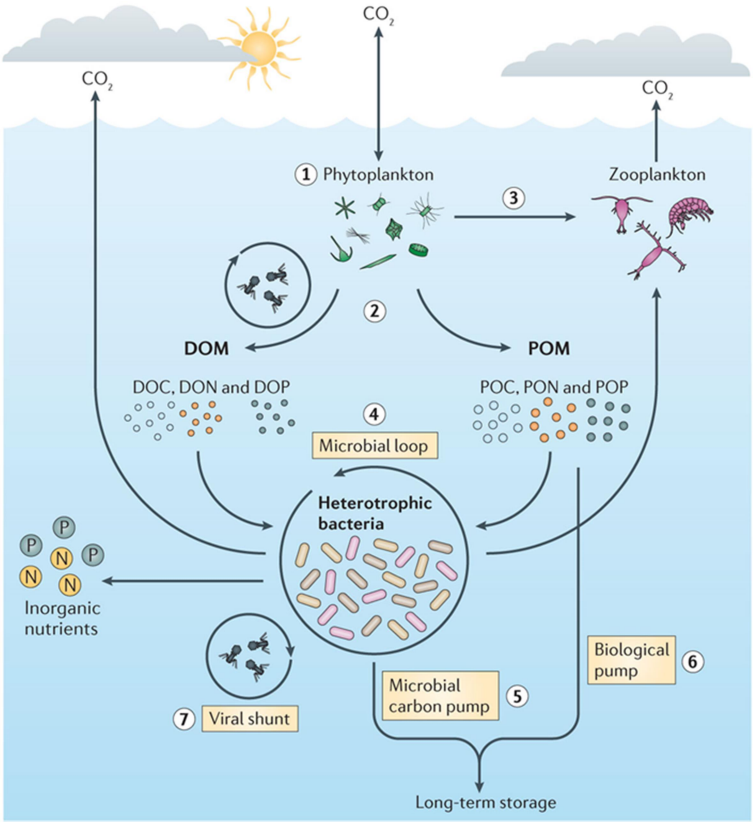

Figure 1.3 Biological and microbial carbon pumps.
1) Conversion of inorganic carbon (CO_2) into organic carbon by phytoplankton *via* photosynthesis; 2) release of particulate (POC) and dissolved (DOC) organic carbon by phytoplankton; 3) consumption of phytoplankton biomass by zooplankton *via* grazing; 4) remineralisation and recycling of POC by heterotrophic bacteria; 5) transformation of POC into recalcitrant DOC *via* the microbial carbon pump; 6) export of POC as sinking particles to the deep-ocean *via* the biological pump; 7) viral lysis of phytoplankton and bacterial cells and release of DOC. Taken from Buchan *et al.* (2014).

1.3 Pelagic sharks

As highly migratory top predators, pelagic sharks play fundamental roles within marine ecosystems. By migrating and foraging across large spatial scales, they alter nutrient and energy flows, ensuring connectivity between otherwise spatially or ecologically separated food webs (McCauley *et al.*, 2012; Heupel *et al.*, 2014; Roff *et al.*, 2016; Ruppert *et al.*, 2016). Such connectivity results in externally-subsidised trophic pyramids (Trebilco *et al.*, 2013; Mourier *et al.*, 2016), and confers resilience to food webs (Polis *et al.*, 1997; Lundberg & Moberg, 2003; McCann *et al.*, 2005; Rooney & McCann, 2012). Additionally, by foraging opportunistically on both resident and migratory species along their routes, pelagic sharks exert top-down controls on lower-trophic-level consumers across several locations or food webs (Holdo *et al.*, 2011; Heupel *et al.*, 2014; Roff *et al.*, 2016; Ruppert *et al.*, 2016).

Pelagic sharks and other marine top predators have declined at a rapid pace in recent decades, largely as a result of unsustainable harvest and by-catch (Pauly *et al.*, 1998; Myers & Worm, 2003). Populations of large sharks have declined regionally by > 90% in the last 15 years (Baum *et al.*, 2003; Clarke *et al.*, 2006; Dulvy *et al.*, 2008; Worm *et al.*, 2013). The ecological consequences of shark population loss are unclear (Heupel *et al.*, 2014; Ruppert *et al.*, 2016; Grubbs *et al.*, 2016), but are thought to include behavioural modifications by prey (Heithaus *et al.*, 2007; 2008), changes in trophic cascades (Ferretti *et al.*, 2010; Heupel *et al.*, 2014), and modifications in ecosystem resilience to change (Polis *et al.*, 1997; Lundberg & Moberg, 2003; McCann *et al.*, 2005).

Managing and conserving the remaining shark populations is problematic, as sharks are capable of travelling for thousands of kilometres over several months in high-seas across jurisdictional borders. This is additionally complicated by a lack of knowledge of their migratory ecology. Shark vulnerability to fishery capture clearly depends on individual movements, as well as on the presence of common, broad movement patterns across individuals, populations or species, which may imply shared vulnerability (Queiroz *et al.*, 2016).

Sharks often share life-history movement and trophic traits, which reflect changes in energy allocation throughout ontogeny, from a juvenile strategy maximising survival and growth, to an adult strategy including reproduction (Werner & Gillam, 1984; Heupel *et al.*, 2007; Grubbs, 2010; Carlisle *et al.*, 2015). A greater understanding of ontogenetic movement patterns would help in characterising areas of essential habitat across life-history (Vandeperre *et al.*, 2014; 2016), where interactions with fisheries are of greater concern, as well as identifying general behaviours influencing shark-human interactions throughout ontogeny.

1.3.1 The blue and porbeagle sharks

This study investigated the movement and habitat use patterns of two pelagic shark model species, the blue (*Prionace glauca*, Linnaeus 1758) and porbeagle (*Lamna nasus*, Bonnaterre 1788) sharks.

The blue shark, of the family Carcharinidae, is an ectothermic shark occurring in temperate and tropical waters worldwide. In the Atlantic, it ranges from Newfoundland to Argentina in the west, over the mid-Atlantic Ridge, and from Norway to South Africa in the east (including the Mediterranean; Compagno, 1984; Nakano & Stevens, 2008). It is mostly oceanic, but can occasionally be associated with shelf, slope and seamount environments (Queiroz *et al.*, 2010; 2012 and references therein).

Compared to most pelagic sharks, blue sharks have a more productive life-history strategy. They are relatively short-lived, fast-growing and fecund (i.e. producing a large number of small offsprings; Hoening & Gruber, 1990; Cortes, 2000; Frisk *et al.*, 2001). In the Atlantic, males are sexually mature at ~ 183 cm fork length (FL; Pratt, 1979), which coincides with an age of ~ 4-5 years (Skomal & Natanson, 2003). Females are subadult at ~ 145 cm FL and ~ 2+ years of age, and can

engage in copulation and store sperm for later fertilisation (Pratt, 1979). Females reach full maturity at ~ 185 cm FL, which corresponds to ~ 5 years of age. Blue sharks are placental viviparous; after 9-12 months of gestation, females give birth to an average of 35 pups (Castro & Mejuto, 1995), though maximum litter size observed is 135 pups. At birth, average size is ~ 45 cm FL (Pratt, 1979).

Blue sharks are known to be highly migratory. Trans-Atlantic movements have often been documented, providing evidence for a single, well-mixed Atlantic population (Casey & Kohler, 1991; Kohler *et al.*, 2002; Kohler & Turner, 2008). However, tagging studies revealed complex spatial structure and dynamics, with segregation by sex and life stage (Stevens 1976; 1990; Queiroz *et al.*, 2005; Mucientes *et al.*, 2009). Different segments of the population (i.e. males and females, juvenile and adults) undergo disparate movements, mainly in relation to seasonal temperature changes, reproductive condition and prey availability (Queiroz *et al.*, 2010; Campana *et al.*, 2011; Vandeperre *et al.*, 2014; see Chapter 3).

Stomach content analysis indicated that blue sharks feed opportunistically primarily on mesopelagic cephalopods, but also on epipelagic and near-bottom fish, crustaceans, birds, other elasmobranchs, mammals and other foaing items (Kohler, 1998; Henderson *et al.*, 2001; McCord & Campana, 2003; Pusinieri *et al.*, 2008).

The blue shark is the most abundant pelagic shark in the Atlantic and globally, despite also being the most frequently caught (Baum *et al.*, 2003; Campana *et al.*, 2011 and references therein). Blue sharks are rarely caught as target species, but are a major by-catch in longline fisheries targeting tuna and swordfish (Buencuerpo *et al.*, 1998; Campana *et al.*, 2006; Mandelman *et al.*, 2008; Mejuto *et al.*, 2009). The combination of high unreported catch, and high discard and mortality rates makes accurate estimates of population abundance and trends difficult to obtain (Burgess *et al.*, 2005; Aires-da-Silva *et al.*, 2008; Campana *et al.*, 2009). Given these challenges, the blue shark is listed in the IUCN Red List as Near Threatened, despite the overall abundance of blue sharks is still considered substantial (Campana *et al.*, 2009).

The porbeagle shark is a lamind endotermic shark coastal and oceanic shark, which is distributed worldwide but apparently restricted to temperate and cold-temperate waters of the North Atlantic (including the Mediterranean and Baltic Seas) and the southern hemisphere (Compagno, 2001; Campana & Joyce, 2004). Porbeagles are most common on continental shelves, but can also occur near the coast or well offshore (Pade *et al.*, 2009; Saunders *et al.*, 2011; Biais *et al.*, 2016).

Similar to most pelagic sharks, porbeagles sharks have relatively slow growth rates, a late age at maturity, and low fecundity (Francis *et al.*, 2008; Natanson *et al.*, 2002). These life history traits making them extremely vulnerable to overexploitation and population depletion. In the Northwest Atlantic, maturity occurs at ~ 174 cm FL in males, and at ~ and 218 cm FL in females (Jensen *et al.*, 2002), which correspond to ~ 8 and 13 years of age, respectively (Natanson *et al.*, 2002). Porbeagle sharks are ovoviviparous, producing an average of four pups, after a gestation period of 8 to 9 months. When pups are born, they are ~ 67 cm FL (Aasen, 1961).

Porbeagle sharks are thought to move short to moderate distances along continental shelves (Stevens, 1976; 1990; Kohler & Turner, 2001), with the possibility of movements far off the shelf by some individuals (Pade *et al.*, 2009; Saunders *et al.*, 2011; Biais *et al.*, 2016). In the Northwest Atlantic, pregnant females are believed to migrate to subtropical pupping grounds as far south as the Sargasso Sea prior to giving birth (Campana *et al.*, 2010; Chapter 3). So far, there has been only one documented case of trans-oceanic migration, implying the existence of two separate populations in the North Atlantic (Francis *et al.*, 2008). Porbeagle sharks are also thought to undergo an ontogentic habitat shift towards slope and offshore settings (Ellis *et al.*, 2015; Biais et al., 2016; see Chapter 3).

Porbeagle sharks are opportunistic predators, mostly feeding on teleost fish, both pelagic and demersal species, and on cephalopods (Joyce *et al.*, 2002).

Porbeagle sharks are commercially valuable, so they have been heavily exploited by target and non-target fisheries in the Northeast Atlantic since the 1930s (Campana et al., 2008). In the late 1950s, the Northeast Atlantic fishery was apparently depleted, and consequently by the 1960s principal finshing grounds moved to the Northwest Atlantic. However, by 1967 the Northwest Atlantic fishery also collapsed. Whilst in the 1990s the Northeast Atlantic population suffered from a further decline due to renewed fishing pressure, the Northwest Atlantic population is considered more depleted (Campana *et al.*, 2003; 2008; 2009). Given to its low reproductive capacity and high commercial value, the porbeagle shark is listed in the IUCN Red List as Vulnerable. The International Council for the Exploration of the Sea (ICES) has estalished a no-take area in the eastern North Atlantic, and the International Commission for the Conservation of Atlantic Tuna (ICCAT) has reccommended that porbeagles should not be taken in international waters. Recently, the porbeagle was also listed in the Appendix II of CITES (Convention on International Trade in Endangered Species) to provide further protection from the high demand in international trade.

Blue and porbeagle sharks have different distribution, habitat and movement patterns, as well as different diets. Whilst these species may sporadically co-occur in some areas of the North Atlantic, fundamental differences in their ontogentic spatial (and trophic) ecology are expcted, which reflect differences in their evolutionary and life histories.

1.4 Artificial physical tags

The movements of highly migratory oceanic animals, including sharks, are difficult to monitor or reconstruct, mostly because the open-ocean is vast and largely inacessible, and because migratory animals conduct extensive movements on seasonal to ontogenetic time-scales (Grubbs, 2010; MacKenzie *et al.*, 2011; Trueman *et al.*, 2012; McMahon *et al.*, 2013a).

To date, direct information on the movements and behaviour of pelagic fish and other marine animals has largely come from fishing and tagging studies (e.g. Stevens, 1976; 1990; Kohler *et al.*, 2002; Queiroz *et al.*, 2005; Block *et al.*, 2011; Queiroz *et al.*, 2016; see also Jennings *et al.*, 2001;

Trueman *et al.*, 2012). Fishing studies are complicated by biased spatio-temporal sampling, whilst tagging studies rely on either the recapture of tagged fishes (e.g. mark-recapture methods), or on the transmission of recorded data (e.g. electronic tagging studies; Trueman *et al.*, 2012).

In conventional mark-recapture methods, fishes are tagged at a known location, and subsequently caught elsewhere by research or commercial fishing vessels. Very large numbers of individuals are required to be tagged in order to produce statistically meaningful results (MacKenzie *et al.*, 2011; Trueman *et al.*, 2012), as a result of high mortality and low recapture rates in the pelagic environment (ICCAT/ICES, 2009). Furthermore, these methods are also inherently biased towards most heavily fished areas, and towards numerically dominant populations and species occurring within capture areas (Kohler & Turner, 2001; Bolle *et al.*, 2005; MacKenzie *et al.*, 2011; Trueman *et al.*, 2012). Consequently, mark-recapture studies provide biased movement information, and are not ideally suited to studying rare species within mixed stocks (Pine *et al.*, 2003; MacKenzie *et al.*, 2011; Trueman *et al.*, 2012).

Recent advances in electronic tagging technology have revolutionised knowledge of the movement ecology of pelagic animals (Block *et al.*, 2011), particularly marine mammals (e.g. Stewart *et al.*, 1989; Mate *et al.*, 1998; McConnel *et al.*, 1999; Andrews *et al.*, 2008), sea turtles (e.g. Godley *et al.*, 2008; Zbinden *et al.*, 2011), tunas (e.g. Block *et al.*, 2001; 2005) and sharks (e.g. Bonfil *et al.*, 2005; Skomal *et al.*, 2009; Campana *et al.*, 2010; Queiroz *et al.*, 2010; Campana *et al.*, 2011; for reviews, see Sims, 2010; Hammerschlag *et al.*, 2011). Electronic archival tags record precise and accurate positional and behavioural data, providing the best currently available tool to track individual movements at fine spatio-temporal scales (Sibert & Nielsen, 2001; Nielsen *et al.*, 2009). However, data storage tags also rely on recapture, and satellite tags on information being transmitted, which may fail due to tag detachment or animals feeding in deep water. Furthermore, whilst satellite tags are becoming cheaper, they are still too expensive and large in size to be applied to large numbers of individuals (but see Block *et al.*, 2011; Queiroz *et al.*, 2016), and juveniles or small species (but see Scott *et al.*, 2014; Vandeperre *et al.*, 2014; 2016). Lastly, electronic tags are typically deployed for no more than 12 months, and thus provide only a small snapshot of individual ontogenetic movements, particularly in long-living species (Hamady, 2014). Electronic tags are not suited for large spatial or population scale studies, or to tracking ontogenetic movements and identifying key habitats across life-histories (Hazen *et al.*, 2012; Shillinger *et al.*, 2012).

Therefore, an urgent need remains for alternative methods to study the movements of pelagic animals at spatio-temporal scales relevant to routine stock management, particularly for widely dispersed stocks, and rare species within mixed stocks (MacKenzie *et al.*, 2011; Trueman *et al.*, 2012).

1.5 Natural chemical tags

Natural chemical tags, where variations in the compositions of animal tissues can be related to geographic variations in the compositions of the local water or food web (see below), can provide valuable complementary information on animal location, movement and diet (Graham *et al.*, 2010; Trueman *et al.*, 2012, McMahon *et al.*, 2013a, b), potentially overcoming some of the limitations associated with artificial tags. These tags can be applied retrospectively to any captured or commercially landed fish, including juveniles, and rare or elusive species. Furthermore, they are considerably cheaper than electronic tags, and can be applied to a larger number of individuals as well as in large-scale studies. Additionally, where incrementally grown tissues, or various tissues with different isotopic incorporation rates are available (see below), movement patterns can be reconstructed throughout time from a single individual (Graham *et al.*, 2010; Trueman *et al.*, 2012). In marine ecology, natural-abundance variations in stable carbon and nitrogen isotopes are commonly used tool to reconstruct the spatial and trophic ecology of animals retrospectively (e.g. Best & Schell, 1996; Cherel *et al.*, 2000; Estrada *et al.*, 2006; Cherel *et al.*, 2009; Newsome *et al.*, 2009; Carlisle *et al.*, 2015; for reviews, see Hobson, 1999; Post, 2002; Graham *et al.*, 2010; Hobson *et al.*, 2010; Boecklen *et al.*, 2011; Ramos & González-Solís, 2012; Trueman *et al.*, 2012; McMahon *et al.*, 2013a). The underlying theory is that the carbon and nitrogen isotopic compositions of animal tissues reflect those of primary producers at the base of the local food web, overlain by relatively predictable trophic modifications (Vander Zanden & Rasmussen, 2001; Post, 2002; McCutchan *et al.*, 2003; Fig. 1.4). The tissues of higher-trophic-level animals are, in fact, enriched in the heavy isotopes (^{13}C, ^{15}N) relative to primary producers, due to preferential excretion of the light isotopes (^{12}C, ^{14}N) during assimilation and metabolism. The isotopic fractionation associated with each trophic step (i.e. trophic fractionation) is highly variable (0-3 ‰ for carbon isotopes, and 2-5 ‰ for nitrogen isotopes, depending on the macromolecule composition of tissue; DeNiro & Epstein, 1977; 1978; 1981; Vander Zanden & Rasmussen, 2001; McCutchan *et al.*, 2003), and dependend on a suite of factors including tissue type, diet quality, and trophic position etc. (Hussey *et al.*, 2014; see also McMahon *et al.*, 2010; 2015b, c; see below). However, trophic fractionation values are conventionally assumed as constant (0.4 ‰ for carbon isotopes and 3.4 ‰ for nitrogen isotopes) when estimating location and/or trophic level. As a result of generally larger trophic fractionation in nitrogen isotopes than in carbon isotopes, carbon isotopes are used to estimate carbon source and location, whereas nitrogen isotopes are used to estimate trophic position (DeNiro & Epstein, 1978; 1981; Peterson & Fry, 1987).

Stable isotope data are generally presented as delta values (e.g. $\delta^{13}C$ and $\delta^{15}N$, ‰), describing the difference in the ratio of the heavy and light isotopes in a sample compared to a standard (Eq. 1.1).

$$\delta^{a}X\ ‰ = [R_{sample}(R_{standard} - 1)^{-1}] \quad (1.1)$$

where a is the atomic mass of the heavy isotope, and R is the ratio of the heavy *versus* light isotopes.

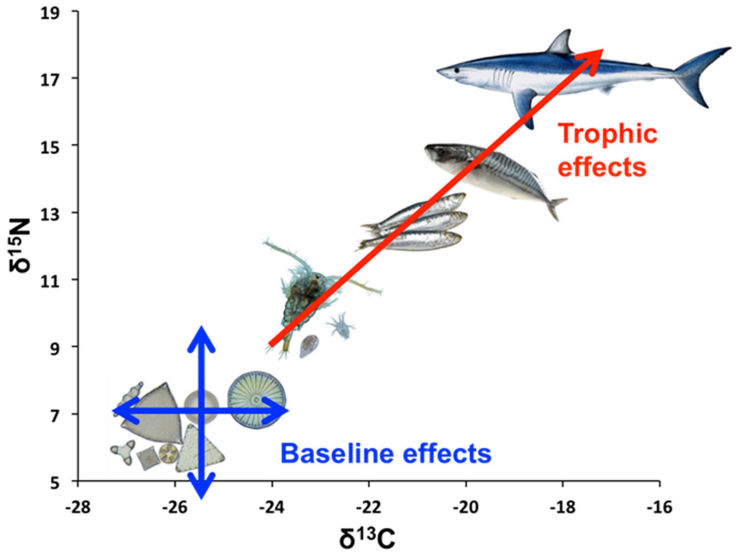

Figure 1.4 Carbon and nitrogen isotope biplot for a typical size-structured marine food web. The carbon and nitrogen isotopic compositions of primary producers at the base are transferred to higher-trophic-level consumers through the food chain, with a relatively predictable isotopic fractionation associated with each trophic step. Variations in isotopic baselines across space (and time) from movement (baseline isotope effects), and variations in prey isotopic compositions from trophic shifts are also transferred to consumers (trophic isotope effects), integrated over the time of tissue synthesis or isotopic incorporation.

The carbon ($\delta^{13}C$) and nitrogen ($\delta^{15}N$) isotopic compositions of phytoplankton at the base of marine food webs vary greatly in space and time in response to changes in physical, chemical and biological variables (Sackett *et al.*, 1965; Rau *et al.*, 1989; Laws *et al.*, 1995; Sigman & Casciotti, 2001; Montoya, 2007). Isotopic variations at the base of the food web are commonly referred to as 'baseline isotope effects' (Fig. 1.4). Spatio-temporal variations in isotopic baselines complicate the use of stable isotopes in food web research, but can provide a geo-location tool (e.g. Jennings & Warr, 2003; Popp *et al.*, 2007; Nielsen *et al.*, 2016; for reviews, see Newsome *et al.*, 2010; Ramos & González-Solís, 2012; Trueman *et al.*, 2012; McMahon *et al.*, 2013b). Animal locations and thus movements can be inferred retrospectively, by relating the isotopic compositions of animal tissues to models of spatial variation in isotopic baselines (Hobson, 1999; Ramos *et al.*, 2009; Graham *et al.*, 2010; Hobson *et al.*, 2010; Trueman *et al.*, 2012; McMahon *et al.*, 2013a). There are, however, several requirements to successfully apply stable isotopes to infer migrations. Firstly, movements must occur between isotopically distinct areas or food webs (Hobson, 1999; Graham *et al.*, 2010; Hobson *et al.*, 2010). Secondly, the sampled tissue must have an isotopic incorporation rate sufficiently long to retain the isotopic signatures of previous feeding locations (Hobson, 1999; Graham *et al.*, 2010; see below). Lastly, any potential influence on tissue isotopic compositions from diet or trophic level change ('trophic isotope effects'; Fig. 1.4) must be accounted for. Equally, trophic shifts may be also inferred from tissue isotopic compositions, if accurate measurements or predictions of variability in isotopic baselines are available (Vander Zanden & Rasmussen, 2001; Post, 2002; McCutchan *et al.*, 2003).

Thus, in general stable isotope analysis povides quantitative information on both habitat and resource use, which are commonly utilised to define the ecological niche space. Whilst the isotopic nice, defined as an area (in δ-space) with isotopic values (δ-values) as coordinates (Newsome *et al.*, 2007; Fig. 1.4), is not directly comparable to other niche formulations, advances in isotope mixing models allow transformation of isotope data into resource contribution values, provding a standardised means for characterising an organism's ecological niche (Newsome *et al.*, 2007). Implicit in this approach, however, is a thorough understanding of the isotopic variation within and among resources (i.e. prey) available to consmers, and the recognition that isotopic analysis does not typically provide information on taxon-specific resource use (Newsome *et al.*, 2007). A commonly used metric for the estimation of isotopic niche width is standard ellipse area (corrected for small sample size, SEAc), as implemented in the SIAR and SIEBER R packages (Parnell & Jackson, 2013). By definition, this metric is related to both location and diet, and can be used for comparing individuals, populations species or higher taxa, or other functional groups (see Jackson *et al.*, 2011).

1.5.1 Tissue types

Any tissue containing the isotope(s) of interest can potentially be sampled to reconstruct location, movements and/or diet. As carbon and nitrogen are structural elements, almost any tissue is suitable for stable isotope analysis. For all tissues, some estimate of length of time represented by the tissue is requred (for reviews of tissue types, see Newsome *et al.*, 2010; Hussey *et al.*, 2012; Kim & Koch, 2012; Trueman *et al.*, 2012). Many tissues sample multiple body pools, and these body pools which be composed of elements derived ditecrly from the diet, or from the replacement (turnover) of biosynthesised tissues. The relative proportion of elements derived from a body turnover pool influences the time period represented by any tissue sample (Carleton & Martinez del Rio, 2010; Newsome *et al.*, 2010; Trueman *et al.*, 2012).

For metabolically active tissues, such as muscle, liver, blood etc., the time period represented by any tissue sample can be difficult to constrain. In rapidly growing juvenile fish, for instance, tissue turnover is relatively small, and body pools of the atoms used to synthesise tissues are tightly linked to the diet. Thus, muscle tissue may reflect weeks to months of life (Trueman *et al.*, 2012 and references therein). In slow growing adult fish, by contrast, the proportion of atoms derived from turnover may be high, and a muscle tissue sample may represent up to several months (or even years in sharks and deep-water fish with slow metabolic rates; Trueman *et al.*, 2012). Liver and blood are even more active metabolically active than muscle, and thus may integrate isotopes over a shorter period of time (Hobson, 1999; Trueman *et al.*, 2012).

Incrementally grown tissues provide an solution to the probem of sample duration. After synthesis, these tissues are metabolically inert, providing a life-time record of the isotopic composition of an animal (Newsome *et al.*, 2010; Hussey *et al.*, 2012; Kim & Koch, 2012; Trueman *et al.*, 2012). Clearly, the tissue isotopic composition at an increment reflects that of the location of isotopic

assimilation at the time of tissue synthesis (or an average if the animal feeds at multple locations; Hobson, 1999; Hobson *et al.*, 2010; Trueman *et al.*, 2012). That is, when interpreting data from incrementally grown tissues, growth rate is a much more important consideration than turnover rate. Examples from marine animals include: fish otoliths (e.g. Elsdon *et al.*, 2008) and scales (MacKenzie *et al.*, 2011), shark vertebrae (Estrada *et al.*, 2006; Kerr *et al.*, 2006; Kim *et al.*, 2012; Carlisle *et al.*, 2015) and eye lenses (Nielsen *et al.*, 2016), sea turtle scute (Vander Zanden *et al.*, 2015a), marine mammal fur, vibrissae, tooth and baleen (Newsome *et al.*, 2010 and references therein).

Elasmobranch vertebral centra are calcified cartilage, composed primarily of the mineral hydroxyapatite deposited within an organic matrix, of which collagen is the primary component (Porter *et al.*, 2006; Hussey *et al.*, 2012; Kim & Koch, 2012). Similar to otoliths in bony fish, vertebrae grow by accretion, and are metabolically inert after synthesis (Pinnegar & Polunin, 1999), providing a life-time record of the isotopic composition of a shark, hence ontogentic movement and feeding information (e.g. Estrada *et al.*, 2006; Kerr *et al.*, 2006; Kim *et al.*, 2012; Carlisle *et al.*, 2015).

In shark vertebrae, the temporal span of the sample can be guided by the apatite increments. To analyse the organic carbon and nitrogen in cartilage collagen, which are references to local food webs, hydroxyapatite must be removed, as it contains inorganic carbon with a different isotopic composition (Hussey *et al.* 2012; Kim & Koch, 2012). Incremental deposition results in vertebral growth bands (Cailliet, 1990). One translucent and one opaque band comprise a band pair, which is often assumed to represent one year of growth (Calliet *et al.*, 1983; Cailliet & Gldmann, 2004; Fig. 1.5A). Age can be estimated by counting vertebral growth band pairs (Campana, 2014); however, not all sharks deposit annual growth band pairs, and many are not easily distinghuishable. Thus, it is necessary to validate the periodicity of growth band pairs with an independent method, including captive rearing, mark-recapture or radiocarbon chronologies (e.g. Natanson et al., 2002; Skomal & Natanson, 2003; Hamady *et al.*, 2014).

Some elasmobranch species, such as the Greenland shark (*Somniosus microcephalus*), lack of calcified tissue, complicating the recovery of time-series isotopes, and age estimations. In vertebraes, the eye lens nucleus is composed of metabolically inactive cristalline proteins, which in the centre (i.e. the embryonic nucleaus), is formed during parental development (Nielsen *et al.*, 2016 and references therein; 1.5B). That is, eye lenses may provide an attractive alternative tissue to vertebrae in studies of isotope ecology (Quaeck *et al.*, *unpubl. data*; Bird *et al.*, *unpubl. data*) and age determination (Nielsen *et al.*, 2016).

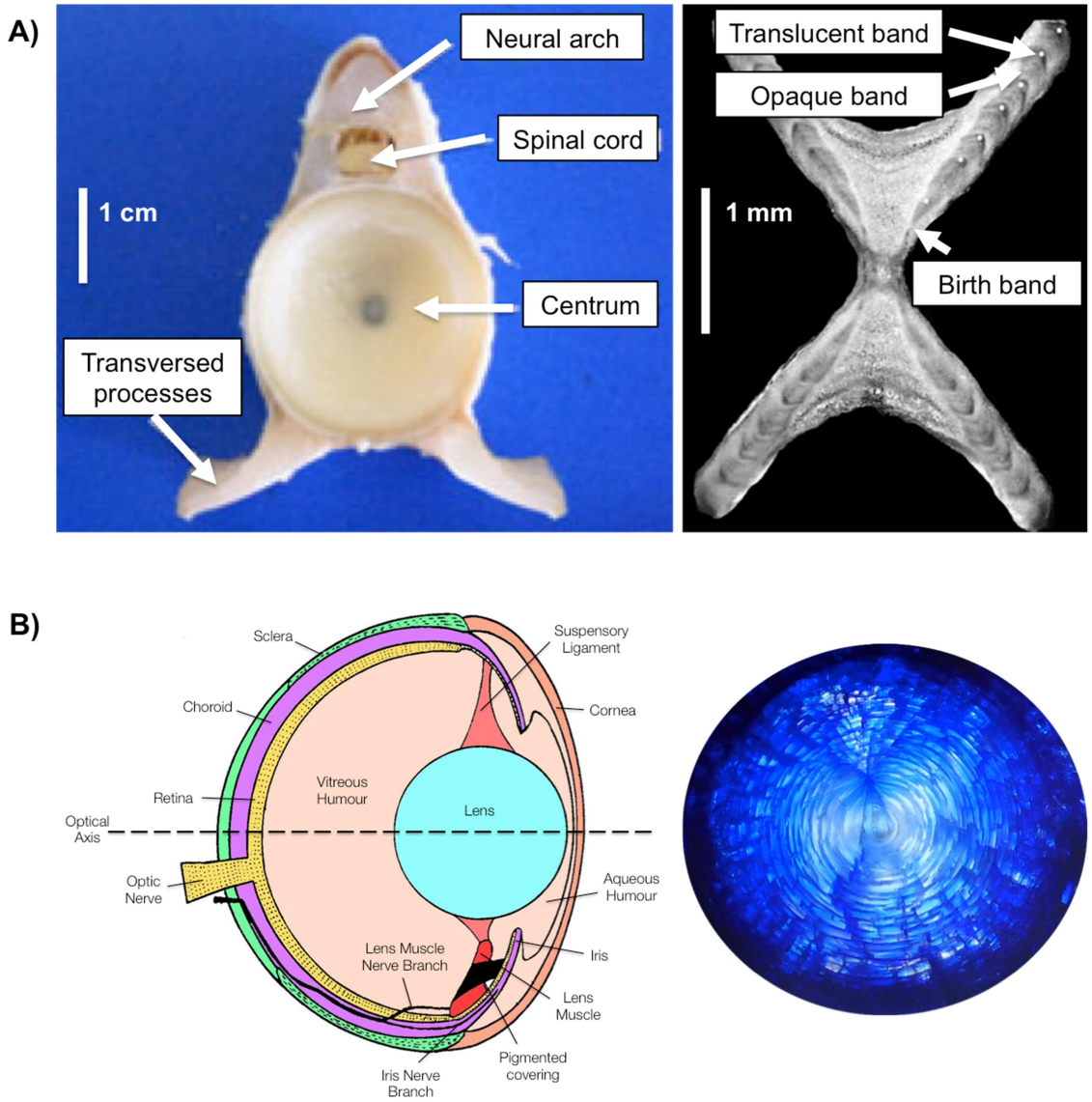

Figure 1.5 Diagrams of A) an elasmobranch vertebra, and B) a teleost eye and eye lens. Panel A) shows a whole vertebrae from a porbeagle shark (*Lamna nasus*), and a vertebral section from a winter skate (*Leucoraja ocellata*). Panel B) shows a typical eye from a teleost, and an eye lens section from a black scabbardfish (*Aphanopus carbo*); this image was obtained from K. Quaeck.

1.5.2 Isoscapes

The use of stable isotopes as an explicit geo-location tool requires the construction of geographically indexed models of the spatio-temporal distributions of baseline isotope values ('isoscapes', *sensu* West *et al.*, 2010; see also Bowen *et al.*, 2005; Bowen & West, 2008; Bowen, 2010a; Graham *et al.*, 2010; McMahon *et al.*, 2013a). Reference isoscapes may be constructed in various ways, from relatively simple interpolation models (Schell *et al.*, 1998; Bowen & Revenaugh, 2003; Bowen *et al.*, 2005; McMahon *et al.*, 2013a) to more complex regression (Jennings & Warr, 2003; Meehan *et al.*, 2004; Radabaugh *et al.*, 2013; MacKenzie *et al.*, 2014) or processed-based, mechanistic models (Hofmann *et al.*, 2000; Tagliabue & Bopp, 2008; Somes *et al.*, 2010; Schmittner & Somes, 2016).

In terrestrial systems, isoscape-based geo-location methods have been applied with great success to reconstruct migrations for a range of taxa, including insects, birds and mammals (e.g. Hobson *et al.*, 2012; Van Wilgenburg *et al.*, 2012; Flockhart *et al.*, 2013; Cryan *et al.*, 2014). Continental- to global-scale isoscapes of stable hydrogen ($\delta^{2}H$) and oxygen ($\delta^{18}O$) isotope ratios in precipitation have been developed, based on the spatial interpolation of large numbers of spatio-temporally distributed isotopic measurements (Bowen & Revenaugh, 2003; Bowen *et al.*, 2005; Fig. 1.6), and on statistical regression relationships between measured isotope values and environmental predictor variables such as latitude, altitude, temperature, and rainout (e.g. Meehan *et al.*, 2004; Bowen, 2010b). These isoscapes have been made web-accessible for custom-tailored application in studies of spatial isotope ecology (www.waterisotopes.org; www.iaea.org/water).

By contrast, in marine environments there has been comparatively little use of isoscape-based methods to study migration, as sampling of isotopic baselines is complicated by both a largely inaccessible environment, and highly dynamic biogeochemical cycles (Trueman *et al.*, 2012, McMahon *et al.*, 2013a). Values of $\delta^{2}H$ and $\delta^{18}O$, and strontium isotope ratios ($\delta^{87}Sr$) are relatively homogenous in seawater (Wassenaar, 2008), whilst $\delta^{13}C$ and $\delta^{15}N$ values show substantial spatio-temporal variations in phytoplankton and low-trophic-level consumers (e.g. Rau *et al.*, 1989; Sigman & Casciotti, 2001; Georicke & Fry, 1994; Montoya, 2007).

Carbon and nitrogen isoscapes have been developed in coastal and shelf systems (e.g. Jennings & Warr, 2003; Radabaugh *et al.*, 2013; MacKenzie *et al.*, 2014; Vander Zanden *et al.*, 2015a). In open-ocean settings, the application of stable isotopes to reconstruct broad-scale animal movements has, to date, been limited to high latitude systems (e.g. Schell *et al.*, 1989a, b; Best & Schell, 1996; Cherel *et al.*, 2000; Jaeger *et al.*, 2010), where strong and predictable temperature-driven gradients dominate the spatial structure in carbon isotopic baselines (e.g. Dunton *et al.*, 1989; Rau *et al.*, 1989; Saupe *et al.*, 1989; Francois *et al.*, 1993; Schell *et al.*, 1998). Indeed, relatively few spatio-temporally explicit $\delta^{13}C$ and $\delta^{15}N$ datasets currently exist for open-ocean settings. Ocean basin-scale isoscapes have been constructed for the Atlantic by interpolating literature-sourced zooplankton $\delta^{13}C$ and $\delta^{15}N$ data (Graham *et al.*, 2010; McMahon *et al.*, 2013a; Fig. 1.6). These isoscapes are based on a relatively few, unevely distributed datapoints, and are strongly influenced by single datapoints or cruises. Additionally, they are influenced by variation associated with season and year of sampling, taxa sampled, and processing methods.

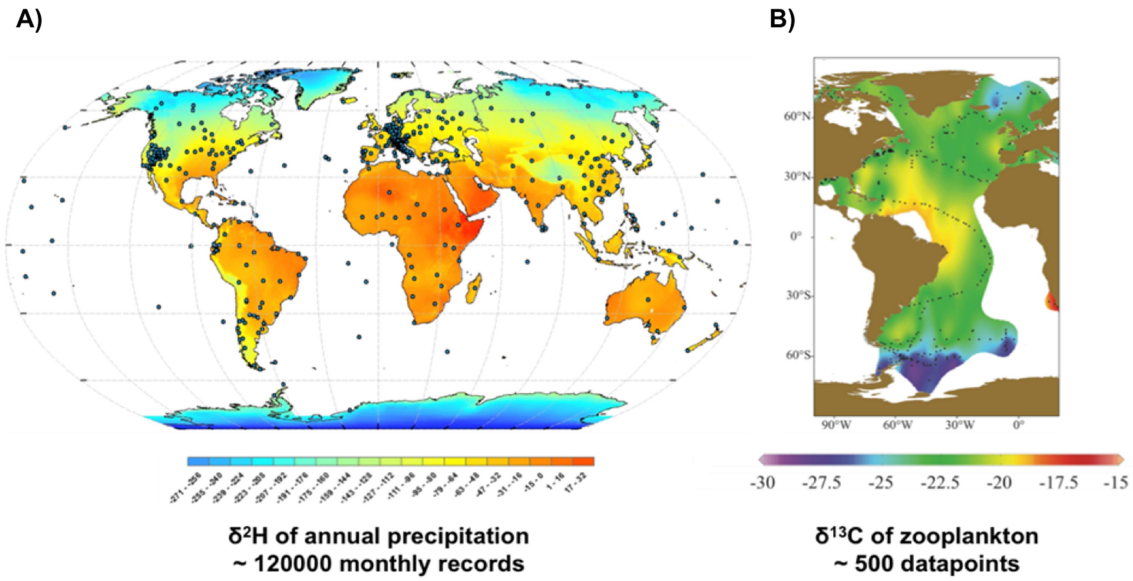

Figure 1.6 Isoscapes of stable A) hydrogen isotope ratios in precipitation and B) carbon isotope ratios in zooplankton across comparable spatial-scales.
The hydrogen isoscape was obtained from the spatial interpolation of ~ 120000 monthly measurements (www.waterisotopes.org), the carbon isoscape from the interpolation of ~ 550 records (McMahon *et al.*, 2013a).

Process-based, mechanistic carbon and nitrogen isotope models have been recently developed within ocean biogeochemical models, predicting the spatio-temporal distributions of isotopic baselines across the global ocean (Hofmann *et al.*, 2000; Tagliabue & Bopp, 2008; Somes *et al.*, 2010; Schmittner & Somes, 2016). Nevertheless, modelled isoscapes are limited by the assumptions implicit in the underlying biogeochemical and fractionation models, and a lack of suitable field validation datasets. Furthermore, they cannot be custom-tailored by isotope ecologists, as isoscape development requires access to the full biogeochemical models.

1.5.2.1 Isoscape-based geographic assignments

Assigning a likely location based on the isotopic composition of an animal's tissue essentially consists of determining the isotopic difference between the measured tissue and each possible location, and assigning a probability of origin to each comparison point (Wunder & Norris, 2008a; Wunder, 2010; e.g. Fig. 1.7). Prior to this comparison, reference isoscapes should be calibrated to tissues, by accounting for trophic and tissue-specific isotopic fractionation (Wunder & Norris, 2008a; Wunder, 2010). Alternatively, reference isoscapes can be constructed directly from consumers of known origin, and used to assign individuals of unknown origin (Vander Zanden *et al.*, 2015a). The accuracy and precision of isoscape-based assignments depends in the first instance on the suitability and quality of the underlying isoscape (Wunder & Norris, 2008a; Graham *et al.*, 2010; Wunder, 2010). Reference isoscapes must predict variation in isotopic values at scales relevant to the movements of the animal or species of interest (Graham *et al.*, 2010; Wunder, 2010). Additionally, where isotopic baselines are highly variable in time (other than in space), temporally explicit isoscapes may be

preferable (MacKenzie *et al.*, 2014; Vander Zanden *et al.*, 2015b). Uncertainties in reference isoscapes must be incorporated into the assignment algorithms, together with other potential sources of variation in tissue isotopic values (i.e. uncertainties in trophic level and trophic and tissue-specific isotopic fractionation, analytical error etc.; Wunder & Norris, 2008a, b; Wunder, 2010).

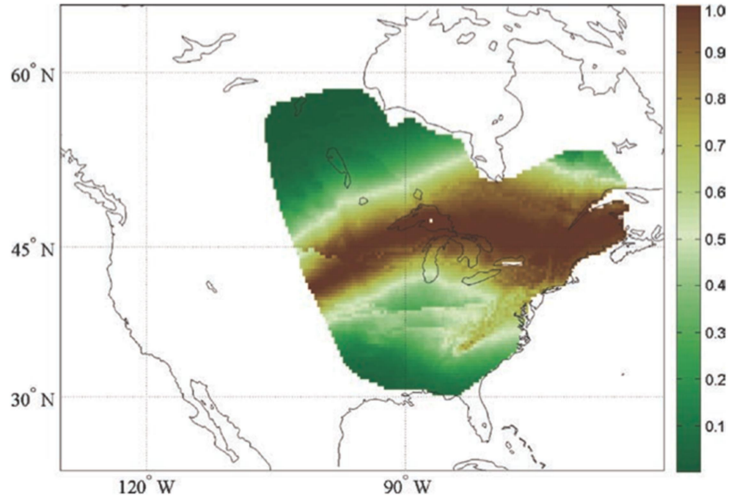

Figure 1.7 Probability density surface for a hypothetical adult bird feather of unknown origin with hydrogen isotopic composition equal to -75‰, based on an isoscape for hydrogen isotope values in precipitation (Bowen *et al.*, 2005) calibrated to feather (Wunder, 2010).
The geography of possible origins for the feather is restricted to the hypothetical breeding range of the bird.

1.5.3 Compound-specific isotope analysis

The use of carbon and nitrogen isotopes (rather than that of hydrogen and oxygen isotopes) to study movement in the marine environment is further complicated by mixed baseline and trophic isotope effects (e.g. Jennings & Warr, 2003; Popp *et al.*, 2007; Nielsen *et al.*, 2016; for reviews, see Newsome *et al.*, 2010; Ramos & González-Solís, 2012; Trueman *et al.*, 2012; McMahon *et al.*, 2013b). Indeed, both carbon and nitrogen isotopes vary greatly across space and time (Graham *et al.*, 2010; Trueman *et al.*, 2012; McMahon *et al.*, 2013a, b), and show variable trophic enrichment factors (Vander Zanden & Rasmussen, 2001; McCutchan *et al.*, 2003; Hussey *et al.*, 2014). Because of these reasons, disentangling mixed baseline and trophic isotope effects is challenging, based on bulk tissue isotope data alone (Trueman *et al.*, 2012; McMahon *et al.*, 2013b).

The analysis of stable carbon and nitrogen isotopes in specific structural compounds within animal tissues, such as individual lipids or amino acids, is increasingly used in movement and trophic studies (e.g. Popp *et al.*, 2007; Lorrain *et al.*, 2009; McMahon *et al.*, 2011a, b; Chikaraishi *et al.*, 2014; for a review, see McMahon *et al.*, 2013b), as it can potentially overcome some of the complications associated with mixed baseline and trophic isotope effects (Trueman *et al.*, 2012; McMahon *et al.*, 2013b). The analysis of amino acid $\delta^{15}N$ values in tropical Pacific tunas, for instance, demonstrated that the observed variance in bulk $\delta^{15}N$ values reflected spatial variations in $\delta^{15}N$ baselines and not trophic level variations (Popp *et al.*, 2007; Graham *et al.*, 2009).

1.5.3.1 Carbon isotopic compositions in amino acids

With regard to carbon metabolism, amino acids are classified as essential, and non-essential, dependent on their synthesis by various organisms (McMahon *et al.*, 2013b; Table 1.1). Essential amino acids can only be synthesised *de novo* by primary producers and bacteria; consumers have lost the enzymatic pathways to synthesise these amino acids, and therefore must acquire them directly through the diet. Conversely, non-essential amino acids can be synthesised by all organisms to maintain normal growth (Hare *et al.*, 1991; Howland *et al.*, 2003; Jim *et al.*, 2006; McMahon *et al.*, 2013b). Essential amino acid $\delta^{13}C$ values show a near zero trophic fractionation, whilst non-essential amino acid $\delta^{13}C$ values display large trophic fractionation, and bulk $\delta^{13}C$ values represent a weighted average (Hare *et al.*, 1991; Hayes, 2001; McMahon *et al.*, 2010; McMahon *et al.*, 2015b). Therefore, values of $\delta^{13}C$ of essential amino acids in a consumer's tissues reflect values in primary producers bacteria (end-members) at the base of the consumer's food web, without confounding influences from trophic discrimination (Lorrain *et al.*, 2009; McMahon *et al.*, 2010; 2015b). Based on this principle, patterns in essential amino acid $\delta^{13}C$ values in consumers are starting to be used to construct isoscapes for phytoplankton (Vokhshoori *et al.*, 2014; Vokhshoori & McCarthy, 2014).

Table 1.1 Classification of amino acids, according to their rate of synthesis by various organisms. Carbon amino acids are divided into essential, non-essential and conditionally essential (indicated by asterisks), nitrogen amino acids into source, trophic and unknown. Modified from Karasov & Martínez del Rio (2007) and McMahon *et al.* (2013b).

		Carbon	
		Essential	**Non-essential**
Nitrogen	**Source**	Lysine	Glycine*
		Phenylalanine	Serine
		Threonine	Tyrosine*
		Methionine	
	Trophic	Isoleucine	Alanine
		Leucine	Aspartic acid
		Valine	Glutamic acid
			Proline*
	Unknown	Hystidine	Arginine*
		Tryptophan	Asparagine
			Taurine*
			Cystine*

The inherent metabolic diversity among various prokaryotic and eukaryotic lineages generates distinct patterns of isotopic fractionation during amino acid biosynthesis among major phylogenetic end-member groups (i.e. bacteria – prokaryotes, fungi, algae and vascular plants – eukaryotes; Abraham & Hesse, 2003; Scott *et al.*, 2006; Larsen *et al.*, 2009; 2013), which are known as 'carbon isotope fingerprints' (*sensu* Larsen *et al.*, 2009; 2013; Fig. 1.8). As these fingerprints are defined downstream of the Calvin cycle by amino acid biosynthetic pathways and associated branching points in the central metabolism (Larsen *et al.*, 2009; 2013), they are largely unaffected by

variation in growth and environmental conditions (Larsen *et al.*, 2013; 2015). Given that patterns in essential amino acid $\delta^{13}C$ values in end-members are transferred to consumers with a near zero trophic fractionation (Hare *et al.*, 1991; Hayes, 2001; Howland *et al.*, 2003; Jim *et al.*, 2006), patterns in consumers can be used to trace the origin of essential amino acids, and thus carbon flow through the food web, even where bulk tissue $\delta^{13}C$ values show considerable variability (Larsen *et al.*, 2009; 2013; 2015). This fingerprinting approach is being increasingly used in marine ecology: to reconstruct residency and movements across habitats or food webs ultimately supported by differing end-members (McMahon *et al.*, 2011a, b; 2012), to determine the proportion of primary *versus* secondary bacterial production within food webs (McMahon *et al.*, 2011a, 2016; see also McCarthy *et al.*, 2007; 2013), to assess the role of hindgut fermentation of consumer metabolism (Arthur *et al.*, 2014), and to reconstruct shifts in the composition of the primary producing community over time (Ruiz-Cooley *et al.*, 2014; Schiff *et al.*, 2014; McMahon *et al.*, 2015a).

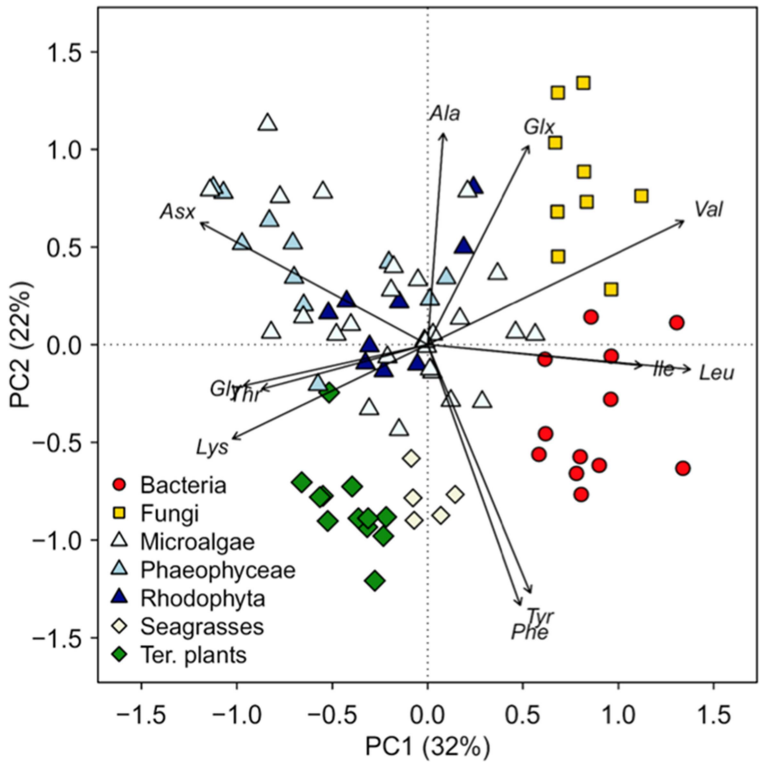

Figure 1.8 Carbon isotope fingerprints for various eukaryotic and prokaryotic lineages, including bacteria, fungi, algae and vascular plants (end-members).
Patterns in carbon isotopic compositions of essential amino acids in end-members are transferred to consumers with a near zero trophic fractionation, therefore patterns in consumers can be used to trace the carbon flow through the food web. Taken from Larsen *et al.* (2013).

Carbon isotopic compositions of non-essential amino acids undergo significant trophic fractionation as amino acids are synthesised (Hare *et al.*, 1991; Hayes, 2001; Howland *et al.*, 2003; Jim *et al.*, 2006; McMahon *et al.*, 2013b). Trophic enrichment factors between consumer and diet (hence $\delta^{13}C$ patterns in non-essential amino acids) vary across taxa and diet types. Previous work has demonstrated that trophic fractionation is related to diet composition and quality, as well as

differential utilisation of dietary constitutents to the bulk carbon pool (McMahon *et al.*, 2010; Newsome *et al.*, 2011; McMahon *et al.*, 2015b). Thus, variations in $\delta^{13}C$ patterns of non-essential amino acids can provide evidence for both *de novo* synthesis from a bulk carbon pool, and routing from dietary protein (O'Brien *et al.*, 2003; Jim *et al.*, 2006; McMahon *et al.*, 2010; Newsome *et al.*, 2011; McMahon *et al.*, 2015b). However, additonal contolled feeding experiemnts are needed to better constrain these effects (McMahon *et al.*, 2013b).

1.5.3.2 Nitrogen isotopic compositions in amino acids

In the case of carbon amino acids, the terms 'essential' and 'non-essential' refer explicitly to the organism's ability to synthesise the side chain (R group). Thus, whilst the carbon isotopic composition of an essential amino acid cannot be altered during diet, the nitrogen isotopic composition, in theory, can. In the context of nitrogen, amino acids have been classified into 'source' and 'trophic', depending on the rate of nitrogen replacement within the amine group (McMahon *et al.*, 2013b; Table 1.1). Values of $\delta^{15}N$ of source amino acids in a consumer are similar to those of its diet, reflecting a near zero trophic fractionation. The reactions associated with the metabolic-processing of source amino acids are assumed to neither form or break bonds containing nitrogen atoms (McClelland & Montoya, 2002; Chikaraishi *et al.*, 2007; Popp *et al.*, 2007). Values of $\delta^{15}N$ of trophic amino acids, by contrast, undergo significant trophic fractionation during nitrogen metabolism, due to the removal and translocation of the amine functional group during deamination and transamination (Macko *et al.*, 1986; McMahon *et al.*, 2015b), which often provide greater sensitivity for defining trophic position than bulk isotope analysis.

When estimating trophic level, a single analysis of $\delta^{15}N$ values of non-essential amino acids in a consumer can provide dual information on isotopic baseline and trophic enrichment (McClelland & Montoya, 2002; Chikaraishi *et al.*, 2009; 2010; 2014). Particulalry, $\delta^{15}N$ values of source amino acids provide a measurement of the isotopic baseline, the difference between $\delta^{15}N$ values of trophic amino acids relative to source provides an estimate of trophic enrichment. Thus, $\delta^{15}N$ values of non-essential amino acids should allow for more accurate estimates of trophic position than those based on bulk $\delta^{15}N$ values alone, particulalry across regions with different isotopic baselines

Chikaraishi *et al.* (2009) recommended the use of the trophic amino acid glutamic acid and the source amino acid phenylalanine to estimate trophic position, due to relatively large and constant isotopic enrichment in glutamic acid relative to phenylalanine with each trophic transfer ($TEF_{glu\text{-}phe}$ = 7.6 ‰), and consistent difference between the trophic and source amino acids in primary production ($\beta_{glu/phe}$ = 3.4 ‰). However, emerging work has demonstrated that early assumptions of a constant $TEF_{glu\text{-}phe}$ value are unfounded, and, similar to bulk $\delta^{15}N$ values (see, for instance, Hussey *et al.*, 2014), $TEF_{glu\text{-}phe}$ values vary systematically with trophic position, feeding ecology, and form of nitrogen excretion (Choy *et al.*, 2012; Hoen *et al.*, 2014; McMahon *et al.*, 2015b, c; Nielsen *et al.*, 2015). The mean measured $\beta_{glu/phe}$ value is also slightly lower than the assumed value and, though no consistent

differences are observed among phytoplankton species, large differences exist between terrestrial and marine plants, and for combinations of other amino acids (Nielsen *et al.*, 2015 and references therein). At present, therefore, further experiments are needed to better constrain variability in the parameters of the trophic position equation. Particulalry, the influence of nutritional quality, form of excretion, differences in isotopic enrichment among amino acids and between tissues should be explored in detail (McMahon *et al.*, 2013b).

1.6 Thesis aim, objectives and hypotheses

The aim of this project is to determine whether the ontogenetic movements of pelagic sharks can be reconstructed retrospectively using stable carbon and nitrogen isotopes. To address this question, this thesis has three main objectives:

1) The development of a process-based, mechanistic carbon isotope model predicting the likely spatio-temporal distributions of the carbon isotopic composition of phytoplankton at the base of pelagic food webs across the global ocean (Chapter 2).
2) The recovery of individual-level life-history records of carbon and nitrogen isotopic compositions of bulk cartilage collagen from vertebrae of two pelagic sharks model species, the blue (*Prionace glauca*) and porbeagle (*Lamna nasus*) sharks (Chapter 3).
3) The recovery of comparable records of carbon isotopic compositions of individual amino acids in vertebrae from the same individual sharks (Chapter 4).

The underlying premise of using stable isotope tracers to infer movement is that the isotopic composition of an animal's tissues reflects that of the local food web, overlain by a relatively predictable trophic enrichment (Fig. 1.4). In principle, therefore, movements across isotopic gradients can be reconstructed by relating variations in tissue isotopic compositions to geographic variations in isotope ratios at the base of the food web. However, interpretations of variance in bulk tissue isotopic compositions to infer movement are limited by mixed baseline and trophic isotope effects, and by large uncertainties in the spatio-temporal distributions of isotopic baselines, particulalry in pelagic settings.

The construction of a reference isoscape is a critical requirement for the application of isotope tracers as a geo-location tool. In pelagic settings, however, the development of reference isoscapes is limited by highly dynamic biogeochemical cycles, and poor spatio-temporal sampling of isotopic baselines. To address these limitations, in Chapter 2 I developed an isotopic extension to an existing ocean biogeochemical model, NEMO-MEDUSA, predicting the likely spatio-temporal distributions of carbon isotopic baselines across the global ocean. Particularly, I hypothesised that: ***H_1 – major spatial (and temporal) patterns in the carbon isotopic composition of phytoplankton can be recovered by a relatively simple function containing the principal controls of carbon isotopic fractionation during photosynthesis***. This carbon isotope model was then used to construct isoscapes

for the global open-ocean, which can be readily custom-tailored by isotope ecologists, and used to investigate the likely influences of spatio-temporal variability in isotopic baselines on tissue isotopic compositions.

The isotopic composition of an animal's tissues reflects the interaction between the animal and its environment (in terms of both location and diet), and can therefore be considered a functional trait. The pattern in the isotopic composition of incrementally grown, metabolically inert tissues reflects the animal-environment interaction throughout time, and thus represents a life-history trait. Variance in ontogenetic isotope patterns among individuals also represents a life-history trait for a population or species. In Chapters 3 and 4, I recover individual-level life-history records of carbon (and nitrogen) isotopic compositions for bulk cartilage collagen and single amino acids from vertebrae of blue and porbeagle sharks caught across the North Atlantic. Pelagic sharks often share life-history traits, such as ontogenetic migrations between pupping and feeding grounds and trophic shifts. Therefore, I hypothesised that: ***H_2 – common, broad ontogenetic patterns in isotopic compositions can be identified across individuals of the same species, indicating species-level life-history isotopic traits*** (e.g. Fig. 1.9).

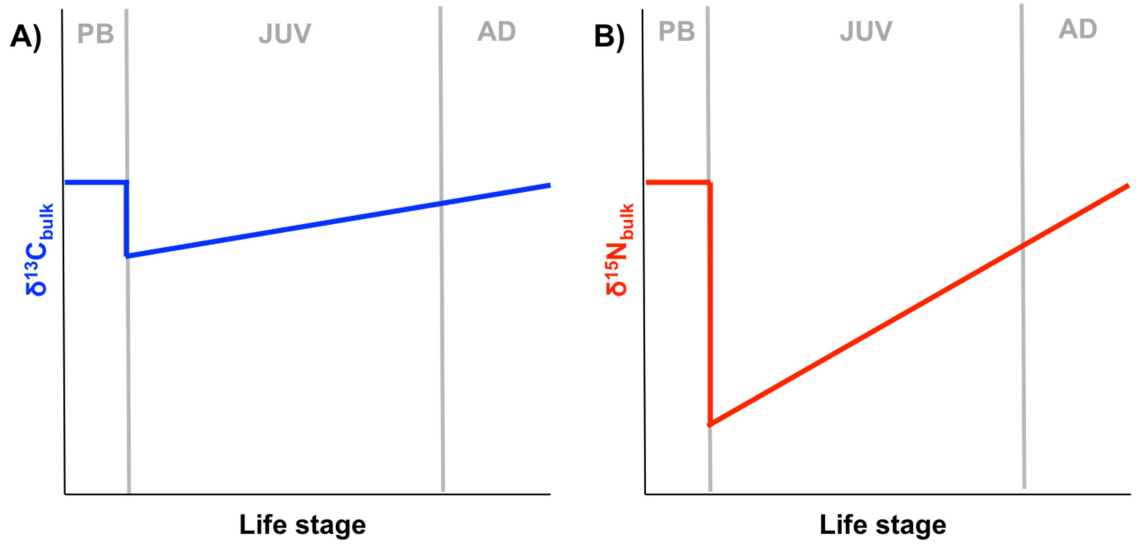

Figure 1.9 Diagram of predicted life-history isotopic traits for A) carbon and B) nitrogen isotopic compositions for an individual shark (or a population, species or functional group) increasing trophic level with size, whilst feeding at the same location throughout ontogeny.
In size-structured ecosystems, trophic level is predicted to increase linearly with size, producing an increase in both carbon and nitrogen isotopic compositions throughout ontogeny, with a larger increase in nitrogen isotope values. In sharks, stepwise increases in trophic level have also been observed, producing step-changes in carbon and nitrogen isotope values (e.g. Estrada *et al.*, 2006). Core regions of the vertebra reflect maternal isotopic compositions (Olin *et al.*, 2011); mothers are predicted to feed at a higher trophic level than newly born and juvenile sharks, and at a comparable level to adults. Clearly, if movement occurs in combination to an increase in trophic level, these patterns may be offset by spatial variations in isotopic baselines.

In traditional bulk tissue isotope analysis, variance in tissue isotopic compositions reflects both variations in isotopic baselines, and fluctuations in diet and trophic level (Fig. 1.4). Thus, whilst interpretations of life-history isotopic traits for bulk collagen using modelled isoscapes may provide

initial movement hypotheses, they are ultimately limited by mixed baseline and trophic isotope effects. Essential amino acids are synthesised *de novo* by primary producers and bacteria (food web end-members), and subsequently assimilated by consumers directly through diet. Consequently, the carbon isotopic compositions of essential amino acids in a consumer's tissues reflect weighted averages of the amino acid isotopic compositions for all the end-members contributing essential amino acids to the consumer's food web, without confounding influences from trophic fractionation. Based on this premise, I hypothesised that: ***H_3 – life-history isotopic traits for essential amino acids can be used to disentangle baseline from trophic effects on traits for bulk collagen, and thus can provide conclusive evidence for movement traits***.

Chapter 2: Using ocean models to predict spatial and temporal variation in marine carbon isotopes

This chapter is modified from a research article published in the peer-review journal Ecosphere: Magozzi, S. M., A. Yool, H. B. Vander Zanden, M. B. Wunder, and C. N. Trueman. 2017. Using ocean models to predict spatial and temporal variation in marine carbon isotopes. Ecosphere. In press. S. Magozzi developed the carbon isotope model, validated it against available zooplankton data, compared it against an alternative published model, and wrote the manuscript. C. Trueman adviced in model development and validation. A. Yool provided outputs from NEMO-MEDUSA, which were used as inputs for the carbon isotope model. M. Wunder and H. Vander Zanden adviced the construction of discrete isoscapes over provinces and clusters. All the co-authors provided feedback on the article.

2.1 Abstract

Natural-abundance stable isotope ratios provide a wealth of ecological information relating to food web structure, trophic level, and location. The correct interpretation of stable isotope data requires an understanding of spatial and temporal variation in the isotopic compositions at the base of the food web. In marine pelagic environments, accurate interpretation of stable isotope data is hampered by a lack of reliable, spatio-temporally distributed measurements of baseline isotopic compositions. In this study, we present a relatively simple, process-based carbon isotope model that predicts the spatio-temporal distributions of the carbon isotope composition of phytoplankton (here expressed as $\delta^{13}C_{PLK}$) across the global ocean at one degree and monthly resolution. The model is driven by output from a coupled physics-biogeochemistry model, NEMO-MEDUSA, and operates off-line; it could also be coupled to alternative underlying ocean model systems.

Model validation is challenged by the same lack of spatio-temporally explicit data that motivates model development, but predictions from our model successfully reproduce major spatial patterns in carbon isotope values observed in zooplankton, and are consistent with simulations from alternative models. Model predictions represent an initial hypothesis of spatial and temporal variation in carbon isotopic baselines in ocean areas where a few data are currently available, and the best currently available tool to estimate spatial and temporal variations in baseline isotopic compositions at ocean basin- to global-scales.

2.2 Introduction

Natural-abundance stable isotope analysis is a routine tool in ecology providing information on food web structuring, trophic interactions, and nutrient flux (e.g. Kelly, 2000; Post, 2002; Boecklen *et al.*, 2011; Layman *et al.*, 2012; Trueman *et al.*, 2014; Choy *et al.*, 2015), and offers a method for retrospective geolocation (e.g. Hobson, 1999; Graham *et al.*, 2010; Hobson *et al.*, 2010; Wunder, 2010; Trueman *et al.*, 2012; Vander Zanden *et al.*, 2015a; Trueman *et al.*, 2016). All ecological applications of stable isotope data require consideration of spatial and temporal variation in the isotopic compositions of nutrients at the base of the food web, or in local precipitation in the case of stable oxygen and hydrogen isotopes. Incomplete knowledge of the likely spatio-temporal variation in baseline isotope values over an animal's foraging range, and/or over seasonal, annual or multi-annual cycles can lead to poor sampling design and inaccurate interpretation of results.

In terrestrial systems, continental- to global-scale isoscapes (*sensu* Bowen & West, 2008; West *et al.*, 2010; for a review, see Bowen, 2010a) of stable hydrogen and oxygen isotope ratios in precipitation have been developed, based on the spatial interpolation of large numbers of spatio-temporally distributed isotopic measurements (e.g. Bowen & Revenaugh, 2003; Bowen *et al.*, 2005), and on statistical regression relationships between measured isotope values and environmental predictor variables such as latitude, altitude, temperature, and rainout (e.g. Meehan *et al.*, 2004; Bowen, 2010b). Over the past decade, geolocation methods using precipitation-based isoscapes have provided the foundation for a formidable body of migration science research in a range of terrestrial taxa, including insects, birds, and mammals (e.g. Wunder, 2010; Hobson *et al.*, 2012; Van Wilgenburg & Hobson, 2011; Van Wilgenburg *et al.*, 2012; Flockhart *et al.*, 2013; Rundel *et al.*, 2013; Cryan *et al.*, 2014; Garcia-Perez & Hobson, 2014).

In marine ecosystems, sampling of baseline isotope compositions is complicated by both highly dynamic biogeochemical cycles and a relatively inaccessible environment (for reviews, see Graham *et al.*, 2010; Trueman *et al.*, 2012; McMahon *et al.*, 2013a). Consequently, the use of stable isotope data in trophic and geolocation studies is particularly challenging in open marine ennvironments. Stable hydrogen, oxygen and strontium isotope ratios show relatively little spatial variation in seawater (Wassenaar, 2008), but by contrast carbon ($\delta^{13}C$) and nitrogen ($\delta^{15}N$) isotope ratios show substantial spatio-temporal variations (e.g. Rau *et al.*, 1989; Francois *et al.*, 1993; Goericke & Fry, 1994; Jennings & Warr, 2003; Barnes *et al.*, 2009; McMahon *et al.*, 2013a and references therein). While carbon and nitrogen isoscapes are beginning to be developed in coastal and shelf areas (e.g. Jennings & Warr, 2003; Barnes *et al.*, 2009; Radabaugh *et al.*, 2013; MacKenzie *et al.*, 2014; Vokhshoori & McCarthy, 2014; Vokhshoori *et al.*, 2014; Vander Zanden *et al.*, 2015a; Trueman *et al.*, 2016), relatively few spatio-temporally explicit $\delta^{13}C$ and $\delta^{15}N$ datasets currently exist for open-ocean settings. Ocean basin-scale isoscapes have been constructed by spatial interpolation of published zooplankton $\delta^{13}C$ and $\delta^{15}N$ data (Graham *et al.*, 2010; McMahon *et al.*, 2013a). However,

such opportunistic compilations of literature data have relatively few, unevenly distributed data points (approximately 550 data points for the Atlantic Ocean; see McMahon *et al.*, 2013a), and consequently are strongly influenced by single data points or specific cruises. Furthermore, isotopic variation associated with season and year of sampling, taxa sampled, and processing methods cannot easily be controlled from opportunistic compilations of literature data.

In open-ocean settings, the application of stable isotopes to reconstruct broad-scale animal movements has been largely limited to high latitude systems (e.g. Schell *et al.*, 1989a, Best & Schell, 1996; Cherel *et al.*, 2000; Cherel & Hobson, 2007; Jaeger *et al.*, 2010), where strong and predictable temperature-driven gradients dominate the spatial structure in baseline carbon isotopes (e.g. Rau *et al.*, 1982; Dunton *et al.*, 1989; Rau *et al.*, 1989; Saupe *et al.*, 1989; Francois *et al.*, 1993; Schell *et al.*, 1998). Realistic predictions of the spatio-temporal distributions of baseline isotope values across the global ocean would help to interpret the isotopic compositions of animal tissues in the context of marine spatial and trophic ecology, and aid the use of stable isotopes as geolocation tools for migratory oceanic animals (Graham *et al.*, 2010; Ramos & González-Solís, 2012; Trueman *et al.*, 2012; McMahon *et al.*, 2013a).

Coupled ocean physics-biogeochemistry models can provide a framework for mechanistic prediction of isotopic compositions of phytoplankton, and stable isotopes have been incorporated into several global system models (Hoffman *et al.*, 2000; Tagliabue & Bopp, 2008; Schmittner & Somes, 2016). Access to full global ocean models is relatively restricted due to processing time, but output from model simulations is widely available. Here we provide an offline extension to ocean ecosystem models predicting isotopic variability of carbon in phytoplankton based on parameters commonly simulated in global ocean biogeochemistry models.

2.2.1 Carbon isotope variation in phytoplankton

Spatial variations in the carbon isotope composition of phytoplankton ($\delta^{13}C_{PLK}$) co-vary with variations in sea surface temperature (Sackett *et al.*, 1965; Fontugne & Duplessy, 1981; Rau *et al.*, 1982; 1989; Goericke & Fry, 1994; Lara *et al.*, 2010), concentration of dissolved CO_2 ($[CO_{2(aq)}]$; Rau *et al.*, 1989; 1992; Goericke & Fry, 1994; Rau *et al.*, 1997; Fischer *et al.*, 1998), and phytoplankton physiology and community dynamics (Wong & Sackett, 1978; Fry & Wainright, 1991; Francois *et al.*, 1993; Goericke *et al.*, 1994; Bidigare *et al.*, 1997; Popp *et al.*, 1999; Maranon, 2009; Lara *et al.*, 2010). At high latitudes, regional- to global-scale patterns in $\delta^{13}C_{PLK}$ values strongly reflect sea surface temperature gradients, as temperature co-varies with direct drivers of isotopic fractionation, such as concentration of dissolved CO_2, phytoplankton growth rates, and community composition (see below). Values of $\delta^{13}C_{PLK}$ are increasingly decoupled from sea surface temperature at lower latitudes, where smaller, often seasonal changes in phytoplankton physiological correlates (e.g. growth rates and cell size) and community dynamics (e.g. community composition) may have greater influences than the

relatively homogenous temperature. Concentration of dissolved CO_2, phytoplankton growth rates, cell size, and community composition act as direct controls on $\delta^{13}C_{PLK}$ values by influencing the degree of carbon isotope fractionation that occurs during photosynthesis (ε_p). In laboratory experiments, ε_p is positively related to the concentration of dissolved CO_2 (Hinga *et al.*, 1994; Laws *et al.*, 1995; 1997; Burkhardt *et al.*, 1999), and negatively related to the specific growth rate of phytoplankton (μ; Laws *et al.*, 1995; Bidigare *et al.*, 1997; Laws *et al.*, 1997; Burkhardt *et al.*, 1999). The extent of isotopic fractionation occurring during photosynthetic carbon assimilation depends on the proportion of intracellular inorganic carbon that diffuses back into the surrounding water (Farquhar *et al.*, 1982; Francois *et al.*, 1993). Assuming that inorganic carbon enters the cell entirely *via* passive diffusion, this proportion is equivalent to the ratio of internal to external concentration of dissolved CO_2, which, in turn, is proportional to the specific growth rate of phytoplankton (Farquhar *et al.*, 1982; Laws *et al.*, 1995; 1997). Concentration of dissolved CO_2 in the environment is also controlled by phytoplankton growth rates, particularly during blooms (Freeman & Hayes, 1992). In addition, because the flux of dissolved CO_2 into and out of the cell is also proportional to the ratio of cell volume to surface area, ε_p is negatively related to phytoplankton cell size, with large phytoplankton cells (e.g. diatoms) showing lower levels of isotopic fractionation (and thus more positive $\delta^{13}C$ values) than small-celled nanoplankton (Popp *et al.*, 1998).

Based on the mechanisms described above, ε_p can be predicted from the concentration of dissolved CO_2, phytoplankton growth rates, size, and community composition. Given ε_p, and the isotopic composition of dissolved CO_2 ($\delta^{13}C_{CO2(aq)}$), $\delta^{13}C_{PLK}$ values can be estimated. Coupled circulation-biogeochemical ocean models can be used to estimate variables influencing carbon isotope fractionation at high spatial and temporal resolutions, and thus to predict $\delta^{13}C_{PLK}$ values at unmonitored sites and under dynamic environmental conditions (e.g. Hofmann *et al.*, 2000; Tagliabue & Bopp, 2008; Somes *et al.*, 2010; Schmittner & Somes, 2016). The choice of the underlying biogeochemical model should reflect a compromise between relatively simple models with a few variables (i.e. degrees of freedom), and more complex models with potentially increased accuracy but also increased computing demand and more opaque relationships between the underlying assumptions and the output.

Here we use an ocean general circulation model (GCM) coupled to a biogeochemistry model of intermediate complexity, NEMO-MEDUSA (Madec, 2008; Yool *et al.*, 2013), combined with general assumptions related to carbon isotope fractionation, to develop a relatively simple, offline, process-based carbon isotope model; this model predicts the spatio-temporal distributions of $\delta^{13}C_{PLK}$ values across the global surface ocean at one degree and monthly resolution. This isotopic extension could be coupled to any existing earth system model that generates predictions of sea surface temperature, concentration of CO_2 and other components within the dissolved inorganic carbon (DIC) pool, and phytoplankton growth rates and proportional abundances.

Based on the underlying mechanisms of isotopic variation included in the model, as well as on observed patterns of variation in nature (e.g. Rau *et al.*, 1989; Francois *et al.*, 1993; Goericke *et al.*, 1994; Goericke & Fry, 1994; McMahon *et al.*, 2013a) we expect: 1) basin- to global-scale variations in simulated $\delta^{13}C_{PLK}$ values to be largely driven by large-scale changes in the concentration and isotopic composition of CO_2, as well as growth rates and proportional abundances of key phytoplankton functional groups, and thus to co-vary with sea surface temperature, 2) regional-scale variations in $\delta^{13}C_{PLK}$ values to be super-imposed on broad latitudinal isotopic gradients, and caused by smaller, often seasonal changes in phytoplankton physiological correlates and community dynamics, and 3) highest temporal variability in $\delta^{13}C_{PLK}$ values to occur in regions characterized by strong, transient phytoplankton blooms (e.g. high/temperate latitudes and upwelling regions) and by periodical oceanographic and/or climatic phenomena.

2.3 Methods

2.3.1 NEMO-MEDUSA

We used the coupled physics-biogeochemistry model, NEMO-MEDUSA, to generate global-scale fields of relevant properties (sea surface temperature, concentration of dissolved CO_2, growth rates and proportional abundances of key phytoplankton functional groups) to estimate the carbon isotope fractionation occurring during photosynthesis (for fractionation occurring within the dissolved inorganic carbon pool and during air-sea CO_2 exchange, see Appendix 2.A). The physical component of this model, NEMO (Nucleus for the European Modelling of the Ocean; Madec, 2008), is a general circulation model, including a sea-ice submodel (LIM2; Timmermann *et al.*, 2005), configured here at approximately 1° horizontal resolution, with vertical space divided into 64 levels with thicknesses increasing from 6 m at the surface to 250 m at 6000 m. The biogeochemical component, MEDUSA-2.0 (Model of Ecosystem Dynamics, nutrient Utilization, Sequestration and Acidification; Yool *et al.*, 2013) is an intermediate complexity ecosystem model founded on the elemental cycles of nitrogen, carbon, silicon, and iron. NEMO-MEDUSA has been extensively described and validated (for a complete description, see Yool *et al.*, 2013), thus here we only report information relevant to the development of the carbon isotope model.

In brief, NEMO-MEDUSA assigns phytoplankton to two functional groups: large-celled 'diatoms' and small-celled 'non-diatoms', which are intended to represent micro- and pico-phytoplankton respectively. Phytoplankton growth is limited by temperature, light, and nutrient (nitrogen and iron) availability, with 'diatoms' being additionally constrained by silicon availability. Within NEMO-MEDUSA, dissolved inorganic carbon is always available in excess to phytoplankton, and is, therefore, entirely assimilated *via* passive diffusion in the form of $CO_{2(aq)}$, although in reality some phytoplankton groups may also actively take up HCO_3^- and CO_3^{2-}, particularly when $CO_{2(aq)}$ is limiting (see Keller & Morel, 1999). NEMO-MEDUSA variables (nutrients, phytoplankton,

zooplankton, and detritus) are simulated for the full 3D water column, but the outputs used in the carbon isotope model (Table 2.1) are taken from the top ~ 6 m of the ocean's surface, with the exception of phytoplankton growth rates and biomass, which are mixed-layer averages.

NEMO-MEDUSA was run for the period 1860-2100 under atmospheric forcing (temperature, humidity, winds, downward heat, and freshwater fluxes) derived from a simulation of the HadGEM2-ES climate model performed as part of Phase 5 of the Coupled Model Intercomparison Project (CMIP5; Collins *et al.*, 2011; Jones *et al.*, 2011). This simulation used the historical atmospheric pCO_2 record to 2005, then Representative Concentration Pathway (RCP) 8.5 out to 2100. The use of such model-derived forcing means that patterns of variability will not exactly match that observed for particular years since the models contain their own internal variability.

For our analysis, we used outputs for the period 2001-2010 at monthly resolution, and re-gridded these onto the standard World Ocean Atlas grid (regular 1° x 1° resolution). To avoid influences from particular years, we averaged outputs for the period 2001-2010 to create a monthly climatology (i.e. of 10 years of Januarys, Februarys, etc.), and then used this climatology to calculate a single annual average and a single intra-annual range (over all averaged months) in $\delta^{13}C_{PLK}$ values. Results of annual average $\delta^{13}C_{PLK}$ values over individual model years for the period 2001-2010 are also presented in Appendix 2.B. In addition, we calculated inter-annual range in $\delta^{13}C_{PLK}$ values as the range of annual average values over individual model years for the period 2001-2010.

Table 2.1 The NEMO-MEDUSA variables and other literature-derived parameters used as inputs in the carbon isotope model. The NEMO-MEDUSA variables are dynamic, and, in general, were simulated for the ocean's surface, with the exception of phytoplankton growth rates and biomass, which were mixed-layer averages. Literature-derived parameters are fixed, and, in general, were assigned base values from Rau *et al.* (1996; 1997), with the exception of 'diatom' and 'non-diatom' cell radii, which were assigned base values from Maranon (2009). The units in which model variables or fixed parameters are expressed in the model are also reported.

Term	**Source**	**Category**	**Layer**	**Value**	**Unit (MEDUSA)**
Sea Surface Temperature (SST)	MEDUSA	Dynamic	Surface	Variable	°C
Concentration of Dissolved Inorganic Carbon ([DIC])	MEDUSA	Dynamic	Surface	Variable	mmol m^{-3}
Concentration of CO_3^{2-} ($[CO_3^{2-}]$)	MEDUSA	Dynamic	Surface	Variable	mmol m^{-3}
Diatom growth rate (μ_d)	MEDUSA	Dynamic	Mixed-layer	Variable	s^{-1}
Non-diatom growth rate (μ_n)	MEDUSA	Dynamic	Mixed-layer	Variable	s^{-1}
Concentration of $CO_{2(aq)}$ ($[CO_{2(aq)}]$)*	MEDUSA	Dynamic	Surface	Variable	mol m^{-3}
Diatom biomass	MEDUSA	Dynamic	Mixed-layer	Variable	mmol N m^2
Non-diatom biomass	MEDUSA	Dynamic	Mixed-layer	Variable	mmol N m^2
Diatom cell radius (r_d)	Maranon, 2009	Fixed	n.a.	$5*10^{-6}$	m
Non-diatom cell radius (r_n)	Maranon, 2009	Fixed	n.a.	$1*10^{-6}$	m
Diatom cell surface (S_d)	Rau *et al.*, 1996; 1997	Fixed	n.a.	$4*\pi*r_d^2$	m^2
Non-diatom cell surface (S_n)	Rau *et al.*, 1996; 1997	Fixed	n.a.	$4*\pi*r_n^2$	m^2
Diatom cell volume (V_d)	Rau *et al.*, 1996; 1997	Fixed	n.a.	$4/3*\pi*r_d^3$	m^3
Non-diatom cell surface (S_n)	Rau *et al.*, 1996; 1997	Fixed	n.a.	$4/3*\pi*r_n^3$	m^3
Diatom cell carbon content (γ_d)	Rau *et al.*, 1996; 1997	Fixed	n.a.	$3.154*10^{-14}*V_d(\mu m^3)^{0.758}$	mol C
Non-diatom cell carbon content (γ_n)	Rau *et al.*, 1996; 1997	Fixed	n.a.	$3.154*10^{-14}*V_n(\mu m^3)^{0.758}$	mol C
Enzymatic fractionation during intracellular C fixation (ε_f)	Rau *et al.*, 1996; 1997	Fixed	n.a.	25	‰
Diffusive fractionation of $CO_{2(aq)}$ in seawater (ε_d)	Rau *et al.*, 1996; 1997	Fixed	n.a.	0.7	‰
Temperature-sensitive diffusivity of $CO_{2(aq)}$ in seawater (D_t)	Rau *et al.*, 1996; 1997	Fixed	n.a.	$1.45*10^{-9}$	$m^2\ s^{-1}$
Reacto-diffusive length (r_k)	Rau *et al.*, 1996; 1997	Fixed	n.a.	$2.06*10^{-4}$	m
Cell wall permeability to $CO_{2(aq)}$ (P)	Rau *et al.*, 1996; 1997	Fixed	n.a.	10^{-4}	m s^{-1}

*Note that, while NEMO-MEDUSA does not distinguish between the concentration of dissolved CO_2 ($[CO_{2(aq)}]$) and the concentration of carbonic acid ($[H_2CO_3]$), $[H_2CO_3]$ in seawater is negligible in comparison to $[CO_{2(aq)}]$ (Zeebe *et al.*, 1999).

2.3.2 $\delta^{13}C_{PLK}$ parameterization

We defined $\delta^{13}C_{PLK}$ as the difference between the isotopic composition of the substrate $CO_{2(aq)}$ ($\delta^{13}C_{CO2(aq)}$; for parameterization, see Appendix 2.A) and the overall carbon isotope fractionation occurring during photosynthesis (ε_p; Freeman & Hayes, 1992). Indeed, ε_p is the major source of variability in $\delta^{13}C_{PLK}$ (Rau *et al.*, 1982; 1989), although carbon isotope fractionation within the DIC pool and during air-sea CO_2 exchange also contribute, to an extent, to variation in $\delta^{13}C_{PLK}$ (i.e. through influencing $\delta^{13}C_{CO2(aq)}$), and thus are also parameterized in the carbon isotope model (see Appendix 2.A). Diazotrophs are not modeled explicitly within NEMO-MEDUSA, but some diazotophs such as *Trichodesmium* are known to display relatively low levels of isotopic fractionation, and thus more positive $\delta^{13}C$ values (Carpenter *et al.*, 1997). We therefore make an assumption that diazotroph contribution to total phytoplankton carbon is relatively minor.

2.3.2.1 Photosynthetic carbon isotope fractionation

We calculated the overall photosynthetic carbon isotope fractionation in each month (ε_p) as the average fractionation of small-celled, and silica-limited large-celled phytoplankton (i.e. 'diatoms' and 'non-diatoms', respectively), weighted by their proportional abundance. In this instance, we parameterized the photosynthetic carbon isotope fractionation of the phytoplankton group i (ε_{pi}) as a linear function of $[CO_{2(aq)}]$, used as a proxy for carbon supply, and the specific growth rate of the phytoplankton group i (μ_i), used as a proxy for carbon demand (Farquhar *et al.*, 1982; Laws *et al.*, 1995); we used the same parameterization of ε_{pi} as Rau *et al.* (1996; 1997) (Eq. 2.1):

$$\varepsilon_{pi} = \varepsilon_f + \frac{b_i}{[CO_{2(aq)}]}; b_i = -(\varepsilon_f - \varepsilon_d)\ \frac{\gamma_i \times \mu_i}{S_i}\left(\frac{r_i}{D_t \times \left(1+\frac{r_i}{r_k}\right)} + \frac{1}{P}\right) \quad (2.1)$$

where the terms $[CO_{2(aq)}]$ and μ_i (i.e. concentration of $CO_{2(aq)}$ and specific growth rate of the phytoplankton group i, respectively) are NEMO-MEDUSA outputs, and all the other terms are fixed values (Table 2.1).

We fixed the cell radius (r_i) at 50µm for 'diatoms', and at 10µm for 'non-diatoms' (Maranon, 2009 and references therein); the cell surface area (S_i) and volume (V_i) depended on r_i, and the cell carbon content (γi), in turn, on V_i. We assigned base values from Rau *et al.* (1996; 1997) to enzymatic isotope fractionation associated with intracellular carbon fixation (ε_f), diffusive isotope fractionation of $CO_{2(aq)}$ in seawater (ε_d), temperature-sensitive diffusivity of $CO_{2(aq)}$ (D_t), reacto-diffusive length (r_k), and cell wall permeability (P). Additionally, to account for the influence of cell size and geometry on ε_{pi} (Popp *et al.*, 1998), and to replicate the observed minimum of ε_{pi} at high values of $\mu_i/[CO_{2(aq)}]$ (Laws *et al.*, 1995; 1997), we constrained ε_{pi} between 5 and 20‰, and between 10 and 26‰ for 'diatoms' and 'non-diatoms', respectively (see Tagliabue & Bopp, 2008).

2.3.2.2 Day-length correction, scaling and latitude-dependent limitation of phytoplankton growth rates

Ocean biogeochemical-ecosystem models frequently struggle to derive growth rate terms consistent with satellite estimates (Schmittner *et al.*, 2013). Phytoplankton growth rates estimated by NEMO-MEDUSA represent the average growth over 24 h, whilst growth rates measured in the laboratory – and used to constrain Eq. 1 – reflect the proportion of growth during the photoperiod (i.e. specific growth rate, μ; Laws *et al.*, 1995; 1997; see also Rau *et al.*, 1996; 1997). To convert NEMO-MEDUSA average growth rates to specific growth rates, therefore, we applied a day-length correction depending on latitude and month (Forsythe *et al.*, 1995). Growth rates in NEMO-MEDUSA integrate growth throughout the mixed-layer, whereas laboratory-derived growth rates in Eq. 2.1 were equivalent to growth at the surface (Laws *et al.*, 1995; 1997; see also Rau *et al.*, 1996; 1997). To provide comparable growth rate units, we scaled NEMO-MEDUSA specific growth rates by a power-law conversion (Eq. 2.2).

$$\mu_{i-scaled} = \beta \times \mu_i{}^{\alpha} \quad (2.2)$$

where β = 1.5 and 2.00, and α = 0.2 and 0.3 for 'diatoms' and 'non-diatoms', respectively. Values of the β coefficient constrain maximum specific growth rate to ~ 1.5 and 2 cell divisions d^{-1} for 'diatoms' and 'non-diatoms', respectively.

The NEMO-MEDUSA model systematically under-estimates phytoplankton growth rates and biomass in oligotrophic regions, attributed in part to the assumption of geographically invariant nutrient kinetics, which does not permit phytoplankton to adapt to oligotrophic conditions (Yool *et al.*, 2013). Therefore, at latitudes between 40 °N and 40 °S, we set growth rate lower limits to 1.25 and 1.75 cell divisions d^{-1} for 'diatoms' and 'non-diatoms', respectively; at latitudes polewards of 60 °N and 60 °S, we set lower limits to 1 cell divisions d^{-1} for both phytoplankton groups. Optimal values of the α and β coefficients for the power-law conversion, cell radii, and latitude-dependent growth rate lower limits were defined to ensure that predicted values remained in the range of $\delta^{13}C$ data for zooplankton provided by McMahon *et al.* (2013a).

2.3.3 Isoscape development

The carbon isotope model estimates the surface water distribution of $\delta^{13}C_{PLK}$ values at one degree and monthly resolution. To reduce the effect of seasonal and decadal variability on $\delta^{13}C_{PLK}$ values, and provide isoscapes more relevant to higher-trophic-level animals assimilating carbon into tissues over longer time-scales (Goering *et al.*, 1990; Bump *et al.*, 2007; see below), we estimated the annually averaged surface water distribution of $\delta^{13}C_{PLK}$ values. To do this, we calculated annual average ε_p as the mean of monthly ε_p values of 'diatoms' and 'non-diatoms', weighted by their proportional contribution to the total annual phytoplankton production. We estimated annual average $\delta^{13}C_{CO2(aq)}$ values simply as the mean of monthly $\delta^{13}C_{CO2(aq)}$ values. In addition, to provide an estimate

of the temporal variability in baseline carbon isotopes, we estimated the intra- and inter-annual range in $\delta^{13}C_{PLK}$ values. Annual average and intra-annual range in $\delta^{13}C_{PLK}$ values, as well as annual average $\delta^{13}C_{CO2(aq)}$ values, are estimated using a monthly climatology for the period 2001-2010, while inter-annual range in $\delta^{13}C_{PLK}$ values is calculated as the range of annual average $\delta^{13}C_{PLK}$ over individual model years for the period 2001-2010.

We displayed annual average and intra- and inter-annual range in $\delta^{13}C_{PLK}$ values as continuous surfaces, within nine (annual average and range, respectively) discrete clusters of 'similar' $\delta^{13}C_{PLK}$ values defined *a posteriori* according to model-based cluster analysis (R function mclust; Fraley *et al.*, 2012), and within 54 biogeographic provinces defined *a priori* by Longhurst (1995; 1998; 2006). Given the simplifications and assumptions inherent in the carbon isotope model, discrete isoscape maps may represent the spatio-temporal variability in $\delta^{13}C_{PLK}$ values at resolutions more realistic than one degree, and at scales more relevant to the movements of migratory oceanic animals.

2.3.4 Validation

Rigorous validation of model isoscapes is challenged by the same lack of spatio-temporally explicit reference isotope data that encourage their development (Graham *et al.*, 2010; Trueman *et al.*, 2012; McMahon *et al.*, 2013a). The most comprehensive compilation of surface ocean $\delta^{13}C$ data is available from McMahon *et al.* (2013a) for zooplankton (i.e. $\delta^{13}C_{ZPLK}$) within the Atlantic Ocean, which we used to tune model parameters as described above. As there are insufficient published $\delta^{13}C$ data to create comparative global continuous surface isoscapes, we divided the global ocean according to Longhurst biogeographic provinces (Longhurst 1995; 1998; 2006), and calculated the mean modeled annual average $\delta^{13}C$ value and its associated standard deviation within each province. We then assembled available literature $\delta^{13}C_{ZPLK}$ data across the global ocean, and estimated mean measured $\delta^{13}C_{ZPLK}$ values within 49 of the 54 discrete provinces (Table 2.2). For each study, we calculated a mean $\delta^{13}C$ value for zooplankton samples recovered within discrete regions. We averaged across the individual study means to estimate mean and variance for $\delta^{13}C_{ZPLK}$ values in each sampled province. We compared modeled and measured values using Monte Carlo resampling and simple linear regression. For each of 500 iterations, we randomly selected 33 of the 49 provinces (67% of cases), and, for each province, drew from the modeled and measured distribution of available $\delta^{13}C$ values. We estimated the intercept, slope and R^2 values, and residual standard error associated with the regression model for each iteration, and reported the resulting mean or median of these regression coefficients across the 500 iterations.

We also conducted a cross-model validation exercise. Alternative models predicting $\delta^{13}C_{PLK}$ values have been described, based on different underlying ocean-biogeochemical model constructs. Schmittner *et al.* (2013), Schmittner & Somes (2016) incorporated carbon and nitrogen isotopes into the UVic earth system model. In this framework, carbon isotopes are explicitly modeled throughout

the ocean carbon cycle, but phytoplankton growth rates are not included in the calculation of isotopic fractionation during photosynthesis.

We also conducted a cross-model validation exercise. Alternative models predicting $\delta^{13}C_{PLK}$ values have been described, based on different underlying ocean-biogeochemical model constructs. Schmittner *et al.*, (2013), Schmittner & Somes (2016) incorporated carbon and nitrogen isotopes into the UVic earth system model. In this framework, carbon isotopes are explicitly modeled throughout the ocean carbon cycle, but phytoplankton growth rates are not included in the calculation of isotopic fractionation during photosynthesis.

Table 2.2 Literature compilation of $\delta^{13}C$ data for zooplankton ($\delta^{13}C_{ZPLK}$) and modeled $\delta^{13}C_{PLK}$ data across Longhurst biogeographic provinces (Longhurst, 1995; 1998; 2006). Reference numbers relate to the reference list in Appendix 2.D.

Longhurst biogeographic province	**Measured mean $\delta^{13}C_{ZPLK}$**	**Measured SD $\delta^{13}C_{ZPLK}$**	**Reference(s)**	**Modeled mean $\delta^{13}C_{PLK}$**	**Modeled SD $\delta^{13}C_{PLK}$**	**Modeled total range $\delta^{13}C_{PLK}$**
Polar - Boreal Polar Province (POLR)	-23.0	1.4	1,2,3,23,24	-27.4	1.1	6.6
Polar - Atlantic Arctic Province	-23.4	1.5	2,5	-26.0	1.0	4.4
Polar - Atlantic Subarctic Province	-23.7	0.9	2,6	-25.0	1.1	4.8
Westerlies - N. Atlantic Drift Province (WWDR)	-21.3	0.0	2	-23.5	1.2	4.2
Westerlies - Gulf Stream Province	-21.1	0.0	2	-20.3	1.1	5.1
Westerlies - N. Atlantic Subtropical Gyral Province (West) (STGW)	-21.2	0.7	2	-20.4	0.9	3.6
Trades - N. Atlantic Tropical Gyral Province (TRPG)	-20.4	0.3	2,4	-20.9	1.1	4.8
Trades - Western Tropical Atlantic Province	-19.6	0.4	2,4	-19.2	0.4	1.7
Trades - Eastern Tropical Atlantic Province	-21.5	0.0	2,7	-19.0	0.5	2.7
Trades - South Atlantic Gyral Province (SATG)	-20.9	0.0	2	-21.6	1.3	5.2
Coastal - NE Atlantic Shelves Province	-21.5	0.5	2,8,9,10	-23.9	1.4	6.7
Coastal - Canary Coastal Province (EACB)	-20.4	0.9	2,7	-20.1	1.5	4.6
Coastal - Guianas Coastal Province	-18.3	0.0	2	-19.4	0.6	3.2
Coastal - NW Atlantic Shelves Province	-21.6	0.5	2	-23.3	2.0	6.2
Westerlies - Mediterranean Sea. Black Sea Province	-21.6	2.3	2,11,12,13	-23.5	0.3	2.7
Trades - Caribbean Province	-21.0	0.7	2	-20.0	0.7	2.9
Westerlies - N. Atlantic Subtropical Gyral Province (East) (STGE)	-21.8	0.5	2,14	-22.3	1.2	4.6
Coastal - Brazil Current Coastal Province	-19.6	1.3	2	-21.4	1.5	5.8
Coastal - SW Atlantic Shelves Province	-22.9	0.0	2	-23.6	1.8	7.6
Coastal - Benguela Current Coastal Province	-19.4	0.0	7	-19.1	0.5	1.9
Trades - Indian Monsoon Gyres Province	-20.1	0.0	51	-18.4	0.4	2.3
Trades - Indian S. Subtropical Gyre Province	-20.5	1.3	15,16,18,51	-21.0	1.4	5.2
Coastal - E. Africa Coastal Province	-19.3	0.8	17,19	-19.4	0.7	4.4
Coastal - Red Sea. Persian Gulf Province	-19.8	1.1	18,20,21	-20.8	1.0	3.3
Coastal - NW Arabian Upwelling Province	-19.8	0.9	18,22	-18.4	0.5	2.7
Coastal - E. India Coastal Province	-19.6	0.0	18	-17.8	0.2	0.9

Coastal - W. India Coastal Province	-19.7	0.6	51	-18.4	0.3	1.4
Polar - N. Pacific Epicontinental Province	-21.7	0.5	23,24	-25.6	1.7	9.2
Westerlies - Pacific Subarctic Gyres Province (East)	-22.0	0.0	3	-24.7	0.8	4.3
Westerlies - Pacific Subarctic Gyres Province (West)	-22.5	1.0	24	-25.6	0.9	4.1
Westerlies - Kuroshio Current Province	-20.7	1.9	26,27,28,29,30	-19.9	1.0	5.0
Westerlies - N. Pacific Polar Front Province	-21.8	2.3	3,23,31	-22.6	1.1	5.1
Westerlies - S. Pacific Subtropical Gyre Province	-23.3	1.7	25	-21.2	1.3	5.1
Trades - N. Pacific Tropical Gyre Province	-18.6	1.2	32,49	-21.6	1.8	6.3
Trades - N. Pacific Equatorial Countercurrent Province	-20.2	1.7	25,33,34,35,36	-18.8	0.4	2.3
Trades - Pacific Equatorial Divergence Province	-20.1	0.0	50	-19.2	0.7	3.2
Trades - W. Pacific Warm Pool Province	-16.2	0.0	27	-19.0	0.3	1.4
Trades - Archipelagic Deep Basins Province	-21.3	0.0	37	-19.3	0.9	3.7
Coastal - Alaska Downwelling Coastal Province	-20.8	1.5	31,38	-23.5	1.0	4.6
Coastal - California Upwelling Coastal Province	-19.0	2.1	31,39,40	-21.4	1.3	5.5
Coastal - Central American Coastal Province	-18.5	0.0	7	-18.4	0.6	2.5
Coastal - Chile-Peru Current Coastal Province	-19.6	1.6	41,50	-21.9	2.3	7.5
Coastal - China Sea Coastal Province	-19.3	0.3	42	-19.6	1.4	5.9
Coastal - East Australian Coastal Province	-21.3	0.3	43,44	-19.5	0.7	2.9
Coastal - New Zealand Coastal Province	-21.3	0.0	52	-22.2	1.3	4.7
Westerlies - S. Subtropical Convergence Province	-19.1	1.1	18,45,51	-21.8	1.0	6.5
Westerlies - Subantarctic Province	-24.2	0.2	2,46	-24.7	1.6	7.8
Polar - Antarctic Province	-27.5	1.0	2	-28.5	0.8	4.0
Polar - Austral Polar Province	-28.7	0.2	2,47,48	-29.2	0.5	2.8

2.4 Results

2.4.1 Spatial patterns in $\delta^{13}C_{PLK}$ values

Predicted annual average $\delta^{13}C_{PLK}$ values range between -31 and -16.5‰ across the global ocean (Fig. 2.1); the mean ± SD predicted annual average $\delta^{13}C_{PLK}$ value is -23.4 ± 3.7‰ for the global ocean. On basin- to global-scales, annual average $\delta^{13}C_{PLK}$ values vary across broad latitudinal gradients, showing steeper variation at high and temperate latitudes than in the tropics. Between 30° N and 30° S, annual average $\delta^{13}C_{PLK}$ values are relatively uniform and positive, varying between -24.5 to -16.5‰ (mean ± SD: -19.9 ± 1.4‰), with peaks of -18 to -16‰ in equatorial upwelling regions. Annual average $\delta^{13}C_{PLK}$ values decrease rapidly from latitudes polewards of 30° N and 30° S, varying between -29 and -17‰ in the subtropics and temperate latitudes, with most positive values of -22 to -20‰ at the subtropical convergence, in upwelling regions and the Gulf Stream current. At latitudes > 60° in the northern hemisphere, annual average $\delta^{13}C_{PLK}$ values range between -30 and -27‰ (mean ± SD: -29.0 ± 0.6‰), with most positive values of -27‰ in the Norwegian Sea and most negative values of -29 to -30‰ in the Chukchi and Beaufort Seas. At comparable latitudes in the southern hemisphere, annual average $\delta^{13}C_{PLK}$ values vary between -31 and -23‰ (mean ± SD: -27.2 ± 1.2‰), and reach most positive values of -28 to -26‰ at the edge of the subantarctic front and near the Antarctic shelf, and most negative values of -30‰ at the polar front (Fig. 2.1). In polar regions, annual average $\delta^{13}C_{PLK}$ values show an inter-hemispheric asymmetry, with overall more positive values in the Arctic Ocean than in the Antarctic Southern Ocean, with the exception of the margins of the Chukchi and Beaufort Seas (Fig. 2.1). These predicted broad-scale spatial patterns are mostly explained by large-scale variations in the concentration and isotopic composition of dissolved CO_2, as well as growth rates and proportional abundances of key phytoplankton functional groups (‘diatoms’- vs. ‘non-diatoms’-dominated phytoplankton communities), and co-vary with sea surface temperature.

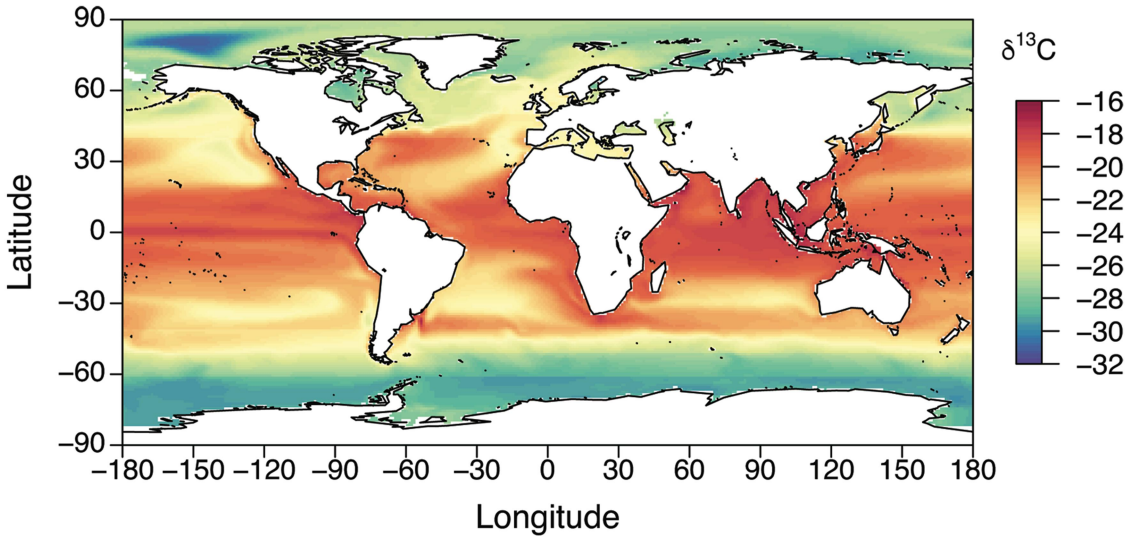

Figure 2.1 Modeled annually averaged surface water distribution of the carbon isotope composition of phytoplankton ($\delta^{13}C_{PLK}$, ‰).
Annual average $\delta^{13}C_{PLK}$ values are calculated using a monthly climatology for the period 2001-2010.

Regional variations in annual average $\delta^{13}C_{PLK}$ values are super-imposed on the broad-scale latitudinal isotopic gradients described above (Fig. 2.1). In general, annual average $\delta^{13}C_{PLK}$ values are relatively positive in the Gulf Stream current, at the subtropical convergence, and in upwelling areas. By contrast, annual average $\delta^{13}C_{PLK}$ values are relatively negative in oligotrophic areas, where nutrients restrict phytoplankton growth, such as subtropical gyres (Fig. 2.1 and 2.2). Modeled annual average $\delta^{13}C_{PLK}$ values are also relatively negative in the Mediterranean Sea, presumably reflecting low phytoplankton growth rates within NEMO-MEDUSA (Fig. 2.1 and 2.2). These predicted regional-scale patterns are mostly explained by smaller-scale, often seasonal changes in the physiological correlates of phytoplankton communities, such as growth rates and proportional abundances of large- and small-celled phytoplankton (Fig. 2.2). As stated above, predictions of phytoplankton growth rates within ocean-biogeochemical models are challenging, and consequently predictions of regional growth rate-dependent variations in $\delta^{13}C_{PLK}$ values are relatively uncertain.

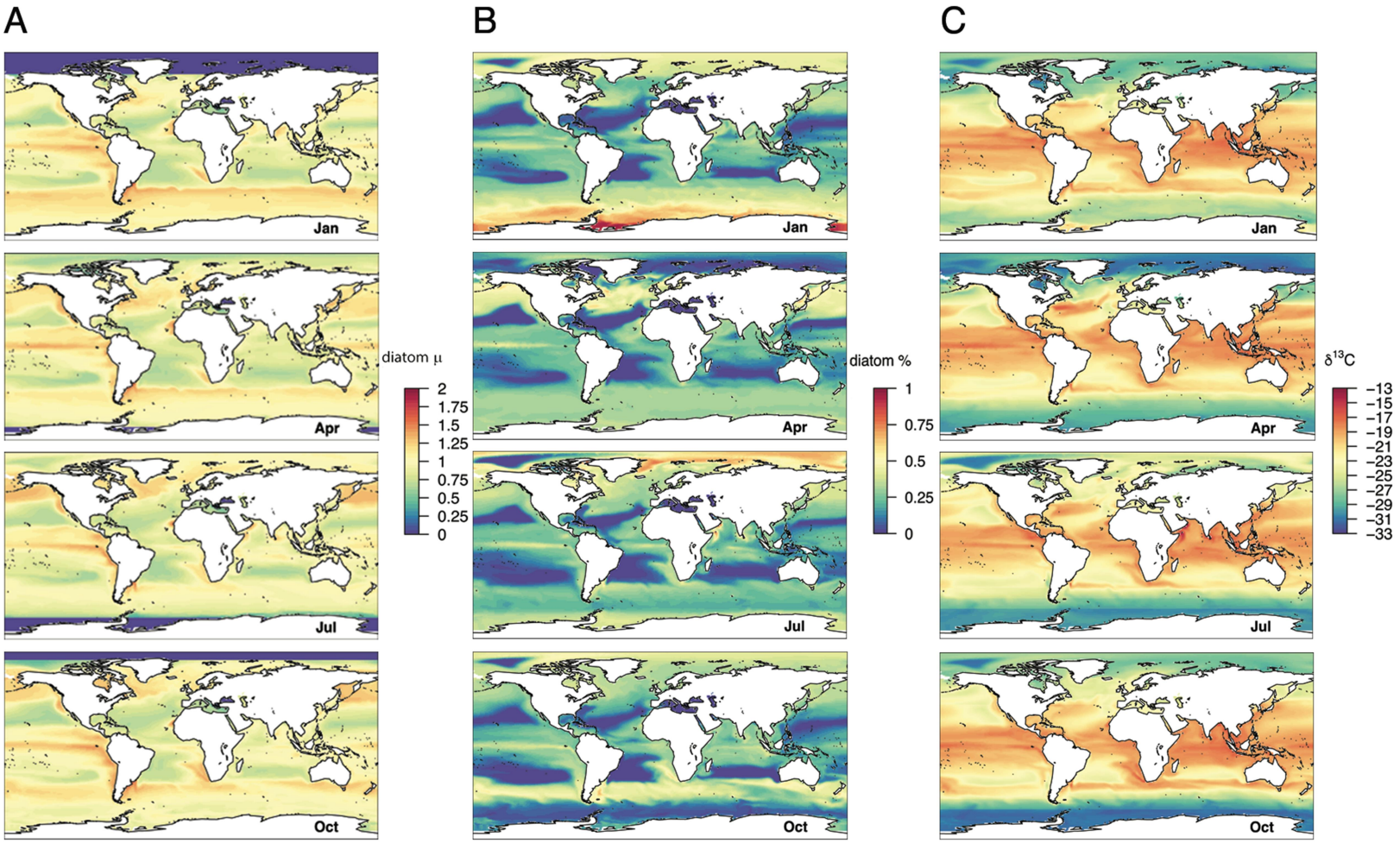

Figure 2.2 Modeled monthly-climatology distributions of: A) day-length corrected, scaled diatom growth rate (μ, number of divisions d^{-1}); B) relative proportion of 'diatoms' (*versus* 'non-diatoms'); C) $\delta^{13}C_{PLK}$ values (‰).
Diatom μ and proportion are simulated for the ocean's mixed layer by NEMO-MEDUSA. To highlight seasonality, outputs for January, April, July, and October for the period 2001-2010 are shown.

2.4.2 Validation

Comparing measured and modeled $\delta^{13}C_{PLK}$ values across Longhurst provinces shows close agreement, with a linear slope approximating 1. Mean (standard deviation) linear regression parameters from 500 iterations accounting for variances in the measured and modeled data are: $\delta^{13}C_{PLK} = 0.85\ (0.15) * \delta^{13}C_{ZPLK} - 3.6\ (3.1)$ ($R^2 = 0.44$; p-value < 0.001; Fig. 2.3A). Thus, the mean slope lies within one standard deviation of a unit line. The median residual standard error associated with any single predicted value was 2.2‰. Predicted $\delta^{13}C_{PLK}$ values are on average ~ 3.5‰ more negative than measured $\delta^{13}C_{ZPLK}$ values, which is within the range expected considering fractionation associated with increases in trophic level (Vander Zanden & Rasmussen, 2001; McCutchan *et al.*, 2003), and potential carnivory and omnivory in larger zooplankton. Modeled annual average $\delta^{13}C_{PLK}$ values reach more positive extreme values compared to measured $\delta^{13}C_{PLK}$ values, particularly in equatorial upwelling regions (Fig 2.3B), although zooplankton in these regions is very sparsely sampled. Estimated annual average $\delta^{13}C_{PLK}$ values are more negative than measured $\delta^{13}C_{PLK}$ averages in the Boreal Polar province due to very negative modeled $\delta^{13}C_{PLK}$ values in the Arctic Ocean north of the Chukchi Sea (Fig. 2.1). However, zooplankton sampling in this area is also limited. As indicated above, modeled annual average $\delta^{13}C_{PLK}$ values are also systematically negative compared to measured $\delta^{13}C_{ZPLK}$ values in the Mediterranean Sea, most likely because of under-prediction of phytoplankton growth rates and possibly under-estimation of 'diatom' relative abundance during winter months by NEMO-MEDUSA (Yool *et al.*, 2013).

NEMO-MEDUSA is an open ocean model that omits coastal processes such as run-off or littoral primary production, and our isotopic extension assumes that all carbon within the food web is derived from atmospheric CO_2. In littoral or coastal ecosystems, isotopically-distinct carbon derived from terrestrial plants, macroalgae and/or benthic remineralized sources can enter the food web, potentially influencing animal tissue isotopic compositions. Accordingly, we did not include zooplankton data recovered from estuarine or littoral systems in the data compilation. However, separating zooplankton data into Longhurst provinces defined as either coastal or open ocean areas did not significantly influence the relationship between modeled and measured values. Whilst this comparison is compromised by the limited abundance and sparse distribution of coastal zooplankton samples, mismatches between modeled and measured values in coastal and littoral areas may indicate incorporation of carbon from sources other than pelagic phytoplankton (e.g. continental-derived carbon).

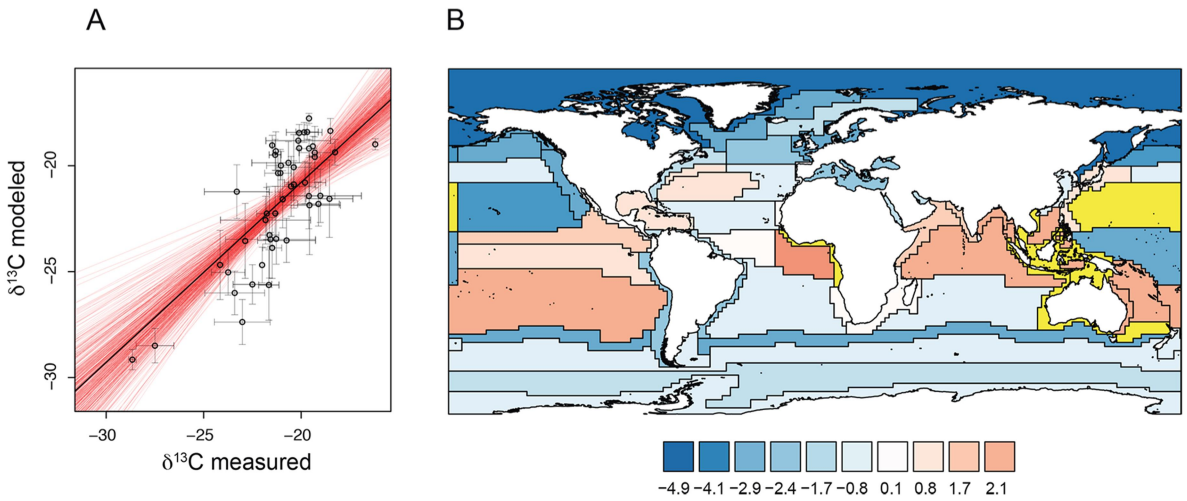

Figure 2.3 Comparison of modeled $\delta^{13}C_{PLK}$ values from our carbon isotope model against measured $\delta^{13}C$ data for zooplankton ($\delta^{13}C_{ZPLK}$, ‰).
A) Estimated linear relationship between modeled annual average $\delta^{13}C_{PLK}$ and $\delta^{13}C_{ZPLK}$ values over the Longhurst biogeographic provinces (Longhurst, 1995; 1998; 2006). Red lines indicate 500 individual linear regression models each reflecting a random selection of 67% of Longhurst provinces with available data and accounting for modeled and measured variance within each province; the black line indicates the mean slope and intercept across the 500 iterations ($\delta^{13}C_{PLK} = 0.85 * \delta^{13}C_{ZPLK} - 3.6$; $R^2 = 0.44$; p-value < 0.001). B) Difference between mean modeled $\delta^{13}C_{PLK}$ and mean measured $\delta^{13}C_{ZPLK}$ values in each province (see Table 2.2); yellow indicates provinces for which no $\delta^{13}C_{ZPLK}$ data were available.

Despite differences in the underlying earth system models, the nature of isotopic incorporation into the models (online *versus* offline isotopic extension), and differences in the variables influencing photosynthetic fractionation, there is strong agreement between our model and the UVic model (Schmittner & Somes, 2016; Fig 2.4). Simple linear regression between annual average $\delta^{13}C_{PLK}$ values predicted by our offline carbon isotope model and $\delta^{13}C$ values estimated by the UVic model ($\delta^{13}C_{PLK\text{-}SS}$) yielded a linear relationship with a slope approximating 1 ($\delta^{13}C_{PLK} = 1.01 * \delta^{13}C_{PLK\text{-}SS} + 1.5$, $R^2 = 0.78$, p-value < 0.001; Fig. 2.4A), and a mean residual standard error of 1.7‰. The close agreement between the two models reflects the first-order control on $\delta^{13}C_{PLK}$ values from surface water concentration and isotopic composition of dissolved CO_2. Annual average $\delta^{13}C_{PLK}$ values modeled within NEMO-MEDUSA were on average 1‰ more positive than those predicted by the UVic model. Values modeled within NEMO-MEDUSA also showed higher regional variability, presumably due to the influence of variable phytoplankton growth rates on fractionation during photosynthesis within the MEDUSA model but not within the UVic model. Accordingly, $\delta^{13}C_{PLK}$ values predicted within MEDUSA were more positive in temperate regions and upwelling areas where phytoplankton growth rates are high, and relatively negative in subtropical gyres where phytoplankton growth is nutrient-limited (Fig 2.4B).

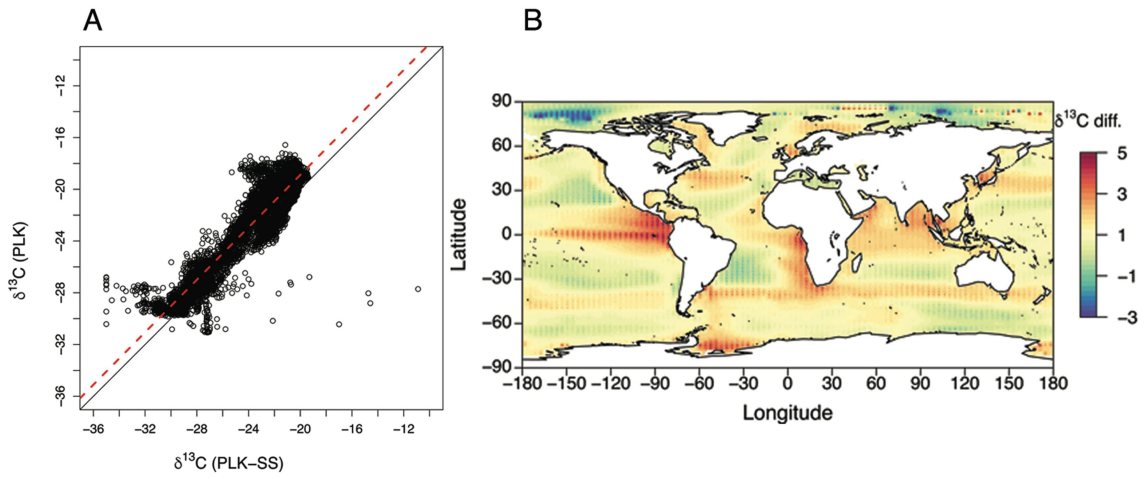

Figure 2.4 Comparison of modeled $\delta^{13}C_{PLK}$ values from our carbon isotope model against modeled $\delta^{13}C_{PLK}$ values from the UVic earth system model ($\delta^{13}C_{PLK\text{-}SS}$, ‰; Schmittner & Somes, 2016). A) Estimated linear relationship between annual average $\delta^{13}C_{PLK}$ values (calculated using a monthly climatology for the period 2001-2010) and annual average $\delta^{13}C_{PLK\text{-}SS}$ values (for the model year 2010; $\delta^{13}C_{PLK} = 1.01 * \delta^{13}C_{PLK\text{-}SS} + 1.5$, $R^2 = 0.78$, p-value < 0.001), indicated by the red dashed line; the black line indicates the unit slope. B) Difference between $\delta^{13}C_{PLK}$ and $\delta^{13}C_{PLK\text{-}SS}$ values interpolated by inverse distance weighting; mean difference across the global ocean was -0.55‰.

2.4.3 Temporal variability in $\delta^{13}C_{PLK}$ values

Our carbon isotope model allows the prediction of temporal patterns in $\delta^{13}C_{PLK}$ values, and thus the construction of temporally-explicit isoscapes, providing isoscapes for a specific point in time, or isoscapes integrated over a defined period. Temporally-explicit isoscape modeling also provides an estimate of the intra- and inter-annual range in baseline carbon isotopes for the global ocean or any given basin. In the Atlantic Ocean, for instance, the predicted intra-annual range in $\delta^{13}C_{PLK}$ reaches ~ 10-12‰ in high and temperate latitudes and upwelling regions characterized by strong, transient phytoplankton blooms, and is limited to 0-2‰ in areas typified by relatively constant temperature and phytoplankton growth rates throughout the year, such as the tropics and subtropical gyres (Fig. 2.5; for inter-annual range in $\delta^{13}C_{PLK}$ values, see Appendix 2.B, Fig. 2.B3). These predicted temporal patterns are influenced by relatively localized seasonal changes in phytoplankton growth rates and proportional abundances of 'diatoms' and 'non-diatoms' (Fig. 2.2). The high intra-annual variability in $\delta^{13}C_{PLK}$ values at high and temperate latitudes in the northern hemisphere reflects, for instance, the strong seasonal variability in phytoplankton growth rates (and concentration of dissolved CO_2) typical of 'diatom' blooms (Fig. 2.2). The reduced variability in $\delta^{13}C_{PLK}$ values at comparable latitudes in the Southern Ocean corresponds to lower overall growth rates throughout the year characteristic of high nutrient low chlorophyll zones, despite 'diatom' blooms in the austral summer (Fig. 2.2).

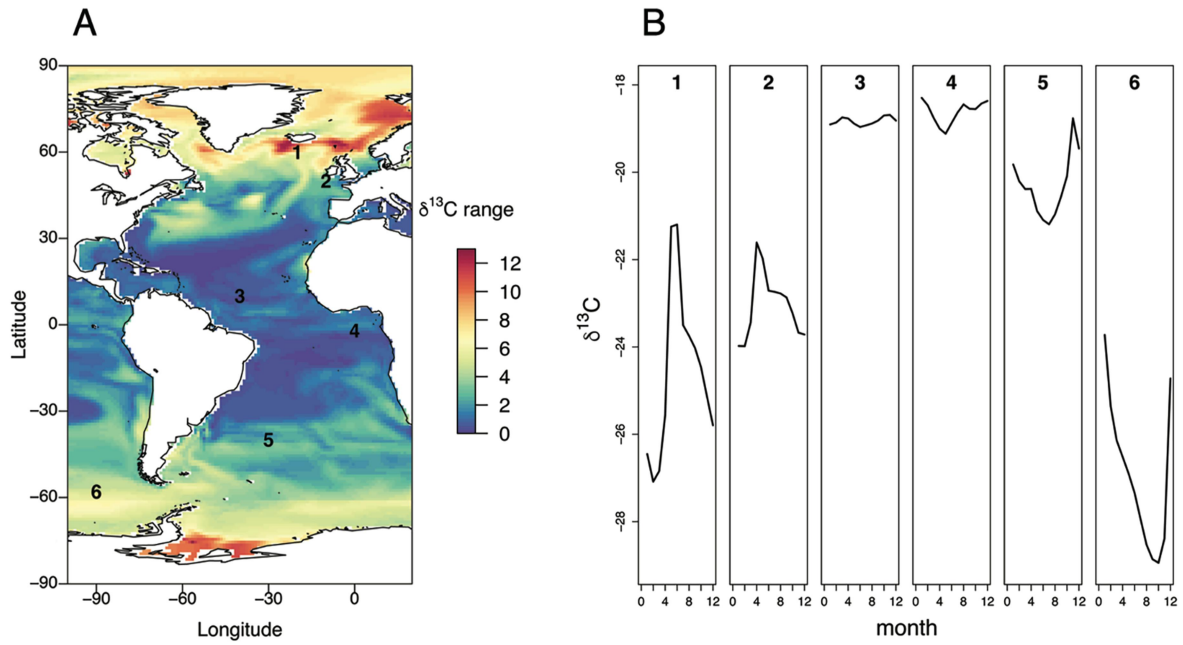

Figure 2.5 Modeled temporal intra-annual variability in $\delta^{13}C_{PLK}$ values (‰).
A) Intra-annual range in $\delta^{13}C_{PLK}$ values across the Atlantic Ocean; intra-annual range of $\delta^{13}C_{PLK}$ values is calculated as the range of monthly-climatology $\delta^{13}C_{PLK}$ values. B) Time-series of monthly-climatology $\delta^{13}C_{PLK}$ values at six locations along a latitudinal gradient, as indicated by numbers in panel A).

2.5 Discussion

The main goal of this study was to develop a relatively simple, offline carbon isotope model to predict the spatio-temporal distributions of the carbon isotope composition of phytoplankton (here expressed as $\delta^{13}C_{PLK}$) at regional- to global-scales. To develop this model, we applied a basic function estimating carbon isotope fractionation during photosynthesis (ε_p; Rau *et al.*, 1996; 1997) to ecological variables (i.e. sea surface temperature, concentration of dissolved CO_2, growth rates and proportional abundances of key phytoplankton functional groups) predicted by the NEMO-MEDUSA coupled physics-biogeochemistry model (Yool *et al.*, 2013). Our simplified model reproduces major spatial patterns in baseline carbon isotopes as observed in nature (Fig. 2.3), and agrees closely with models involving explicit parameterization of ^{12}C and ^{13}C through the underlying biogeochemical model (Schmittner *et al.*, 2013; Schmittner & Somes, 2016; Fig 2.4).

Our carbon isotope model also allows the prediction of temporal variation in baseline carbon isotopes, and thus the construction of temporally-explicit isoscapes (Fig. 2.2C), as well as time-integrated maps of the likely intra- and inter-annual ranges in $\delta^{13}C_{PLK}$ values (Fig. 2.5 and 2.B3A; see also Fig. 2.6B, 2.7B, 2.B6A and 2.B7A). Explicit validation of predicted temporal variability in $\delta^{13}C_{PLK}$ values is, however, even more difficult than validation of geographic variance, particularly over large spatial scales. To our knowledge, a few studies have measured baseline carbon isotope values in open-ocean settings at a relatively high temporal resolution (Fry & Wainright, 1991; Dehairs

et al., 1997), and measurements were all taken at specific point locations usually within an area not larger than a grid cell. However, we argue that if our parameterization of $\delta^{13}C_{PLK}$ reproduces broad-scale spatial patterns in baseline carbon isotopes, it should also be sufficient to recover broad-scale temporal baseline variations. Temporally-explicit isoscapes may, in fact, be less uncertain than annual average isoscapes as annual average $\delta^{13}C_{PLK}$ values must be additionally weighted by the estimates of monthly production. Given the practical limitations concerning temporally-explicit sampling in open-ocean conditions, mechanistic isotope models currently provide the best available tool to explore temporal variability in baseline carbon isotopes.

2.5.1 Model isoscapes' applications in marine ecology

Knowledge or prediction of temporal variations in baseline carbon isotopes may have important implications for the interpretation of animal tissue isotopic compositions for inferences on spatial and trophic ecology (Graham *et al.*, 2010; Trueman *et al.*, 2012; McMahon *et al.*, 2013a). The transfer of temporal baseline variations to animal tissues generally decreases with decreasing tissue isotopic incorporation rate and increasing trophic level (Goering *et al.*, 1990; Bump *et al.*, 2007), potentially leading to the temporal averaging of substantial variability in baseline isotope values in high-trophic-level organisms. Within an organism, tissues with varying turnover rates will also inherit isotopic differences if the animal feeds in a region with high temporal variability in isotopic composition at the base of the food web. Migration across spatio-tempoal isotopic gradients adds additional complexity to the interpretation of stable isotope compsoitions. Simulation modeling provides a tool to explore how spatio-temporal variability in $\delta^{13}C_{PLK}$ values is likely to affect tissue isotopic values.

We stress that modeled isoscapes are limited by the lack of suitable field validation datasets, and by the simplifications and deficiencies implicit in both the biogeochemical and isotopic fractionation models. Here comparison of predicted annual average $\delta^{13}C_{PLK}$ values against measured $\delta^{13}C$ data for zooplankton yields a mean residual standard error around any single point estimate of ~ 2‰, which is more than 10% of the total global range in $\delta^{13}C_{PLK}$ values (Fig. 2.1). Accordingly, we suggest that uncertainty inherent in modeled isoscapes is currently too large to permit explicit geographic assignments based on continuous isoscape surfaces (Wunder & Norris, 2008b; Wunder, 2010). However, the relatively close agreement between modeled and measured estimates of mean $\delta^{13}C$ values in Longhurst biogeographic provinces implies that modeled ocean carbon isoscapes can provide a spatio-temporally explicit reference to which tissue isotopic compositions can be related. Modeled isoscape values can be partitioned to identify isotopically distinct regions within the global ocean (Fig. 2.6), or summarized to describe isotopic variability within biogeographically-defined provinces (Longhurst, 1995; 1998; 2006; Fig. 2.7). In both cases, spatial and temporal isotopic variability can be quantified within each discrete region, and, if required, incorporated into geographic assignment algorithms (Wunder & Norris, 2008b; Wunder, 2010; Vander Zanden *et al.*, 2015a;

Trueman *et al.*, 2016). Given that most marine oceanic animals are highly mobile, and have varying temporal isotopic incorporation rates, discrete isotopic provinces are likely to represent spatio-temporal variability in $\delta^{13}C_{PLK}$ values at scales more realistic and relevant to their spatial and temporal ecology.

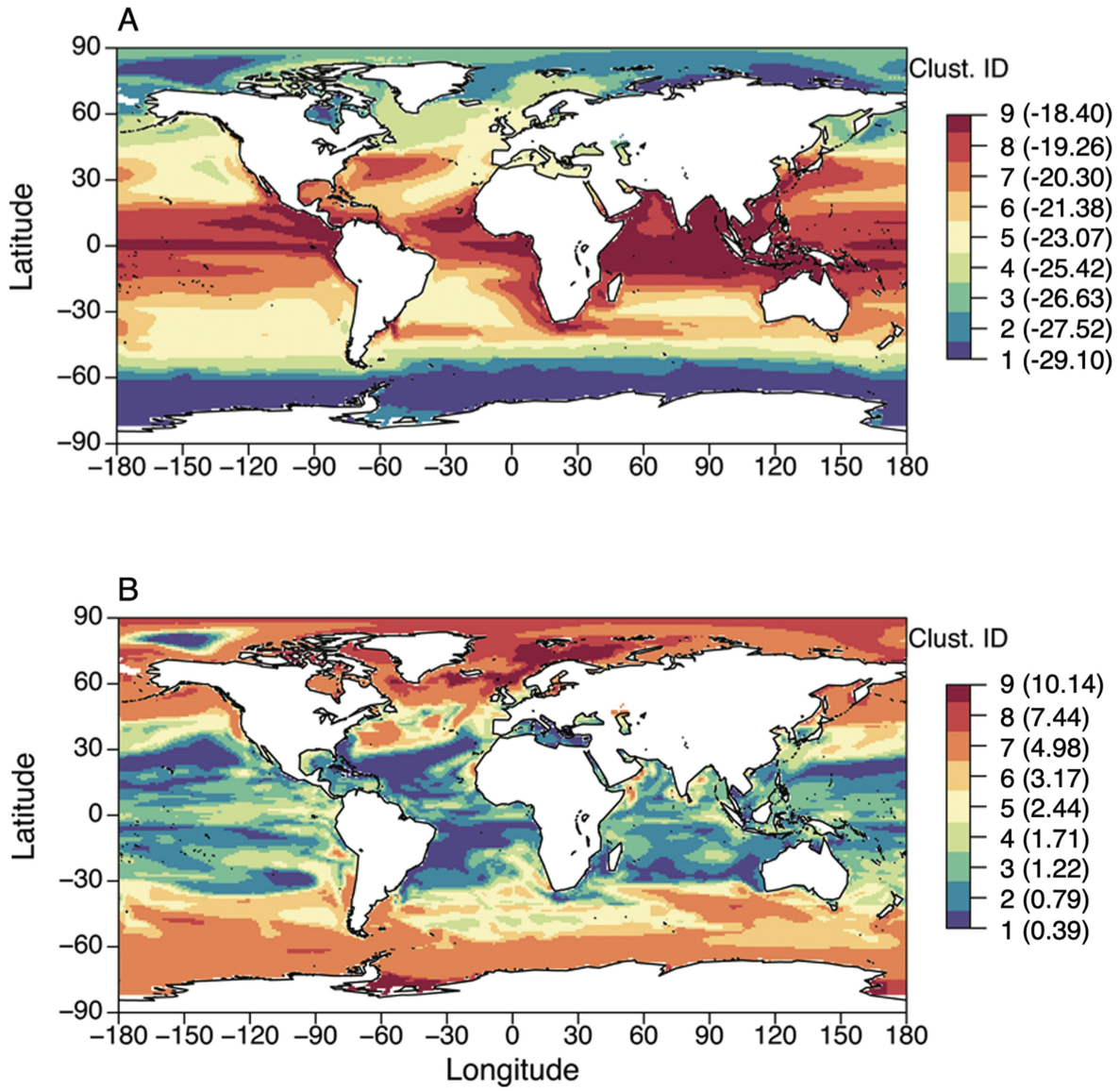

Figure 2.6 Discrete isoscapes showing cluster ID for nine clusters of similar A) annual average $\delta^{13}C_{PLK}$ grid cell values, and B) intra-annual range (i.e. difference between maximum and minimum value) in $\delta^{13}C_{PLK}$ grid cell values. Numbers in brackets are mean annual average and range $\delta^{13}C_{PLK}$ values within each cluster.
Both annual average and intra-annual range in $\delta^{13}C_{PLK}$ values are calculated using a monthly climatology for the period 2001-2010. For standard deviations of $\delta^{13}C_{PLK}$ values within each cluster, see Fig. 2.B4.

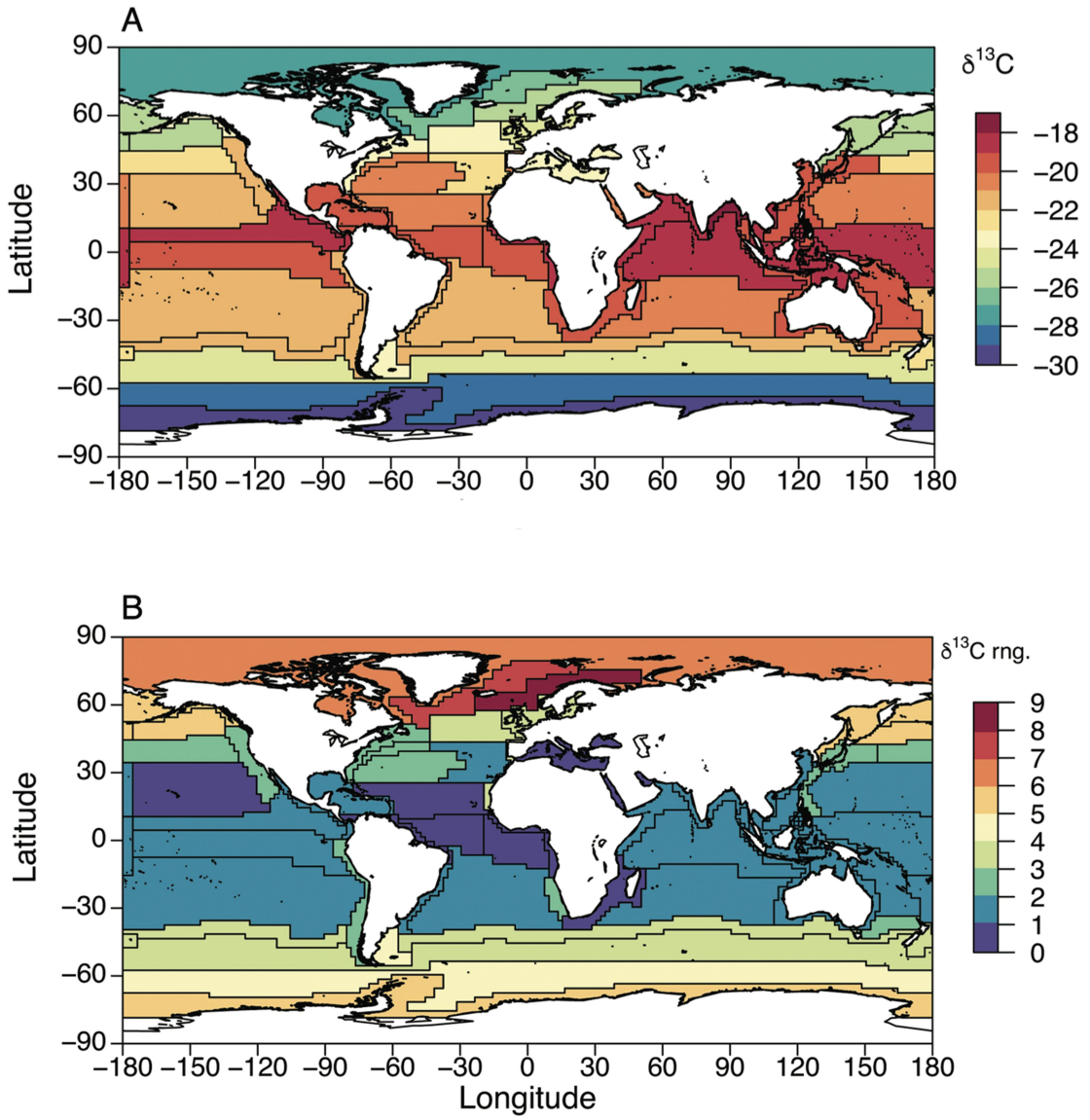

Figure 2.7 Discrete isoscapes across Longhurst biogeographic provinces (Longhurst, 1995; 1998; 2006): A) mean annual average and B) mean intra-annual range in $\delta^{13}C_{PLK}$ grid cell values within each province.
Both annual average and intra-annual range in $\delta^{13}C_{PLK}$ values are calculated using a monthly climatology for the period 2001-2010. For standard deviations of $\delta^{13}C_{PLK}$ values within each province, see Fig. 2.B5.

2.6 Conclusions

1) Process-based carbon isotope models provide spatio-temporally explicit predictions of the carbon isotope composition of phytoplankton ($\delta^{13}C_{PLK}$) at the base of marine pelagic food webs. Modeled isoscapes reproduce major spatial patterns in baseline carbon isotope values as observed in nature and predicted by alternative models.

2) Our offline approach ensures that our model can be coupled to output from a wide range of alternative earth system models to explore mechanisms controlling and influencing

distributions of $\delta^{13}C_{PLK}$ values in space and time. Mismatches between modeled and measured values may indicate the presence of additional carbon sources within food webs (especially in littoral settings), or may be used to compare the performance of competing ocean biogeochemical models.

3) Relatively accurate recovery of major spatial patterns in carbon isotopic baselines implies that modeled isoscapes also capture broad-scale temporal variations in $\delta^{13}C_{PLK}$ values; and carbon isotope models provide the best currently available tool to explore temporal variability in baseline carbon isotope values.

4) Modeled isoscapes provide an estimate of the likely spatial and temporal variation in baseline carbon isotopes over a potential foraging range, and/or over a seasonal, annual or multi-annual cycle; this variation can be explicitly included in statistical models of diet source partitioning or isotopic niche area, as well as taken into account when trying to interpret tissue isotopic compositions to gather information on location and movements.

2.7 Acknowledgements

We would like to thank the University of Southampton (Dean's award) for supporting this study as part of Sarah Magozzi's PhD research. We are also grateful to the National Science Foundation (award #1137336) for supporting Sarah Magozzi's participation to the Inter-university Training in Continental-scale Ecology Research-In-Residence program at University of Colorado Denver, as well as Hannah Vander Zanden's postdoctoral fellowship through the ITCE program (award #1241286). We would also like to acknowledge Kelton W. McMahon and Christopher J. Somes for providing validation datasets. Finally, we would like to thank the reviewers for their valuable feedback on this paper.

Chapter 3: Life-history isotopic traits in pelagic sharks: reconstructing ontogenetic movements and trophic shifts in North Atlantic blue and porbeagle sharks through stable isotope analysis of vertebrae

This chapter is a manuscript in prep. (to be submitted to the peer-review journal Marine Ecology Progress Series in spring 2017): S. Magozzi, S. Thorrold, L. Houghton, G. Skomal, L. Natanson, M. Santos, R. Coelho, N. Queiroz, D. Sims, V. Bendall, S. Hetherington, J. Ellis, K. Quaeck, C. Bird, and C. Trueman. Life-history isotopic traits in pelagic sharks: reconstructing ontogenetic movements and trophic shifts in North Atlantic blue and porbeagle sharks through stable isotope analysis of vertebrae. In prep. S. Magozzi led the research and wrote the manuscript. G. Skomal, L. Natanson, M. Santos, R. Coelho, N. Queiroz, D. Sims, V. Bendall, S. Hetherington and J. Ellis provided the shark vertebral samples, and K. Quaeck and C. Bird eye lens data. L. Houghton advised on sample preparation for bulk stable isotope analysis, and C. Trueman and S. Thorrold on data analysis and interpretation. C. Trueman also provided feedback on the chapter.

3.1 Abstract

Shark populations are rapidly declining worldwide; however, the ecological consequences of such declines remain unclear. Shark vulnerability to fishery capture and roles within marine ecosystems strongly depend on: i) individual ontogenetic movements, and ii) the presence of life-history movement traits across individuals, species, higher taxa and/or functional groups. Electronic archival tags allow tracking individual movements at fine spatio-temporal scales; however, these tags record data over relatively short periods of time, and cannot be applied to juveniles. Stable isotope analysis of incrementally grown tissues, such as shark vertebrae, enables the retrospective reconstruction of the spatial and trophic ecology of individual fishes throughout life. In spite of this, very few individual-level life-history isotopic records currently exist for sharks. Here carbon and nitrogen isotope records were recovered for individual blue (Prionace glauca) and porbeagle (*Lamna nasus*) sharks from across the North Atlantic throughout their life-histories, at a high (i.e. seasonal to multi-annual) temporal resolution. Carbon and nitrogen isotopic compositions varied at multiple levels (i.e. between species, among capture areas, and within and between individuals), indicating spatial and trophic variability. Common, broad ontogenetic patterns in carbon and nitrogen isotope values across

individuals of each species revealed life-history traits in the movement and feeding ecology of blue and porbeagle sharks in the North Atlantic, with super-imposed variability in movement and feeding behaviour among areas and individuals. Furthermore, common patterns in carbon and nitrogen isotope values within many other shark species, and across species, indicated ubiquitous life-history traits in sharks, such as seasonal movements between foraging and breeding sites, ontogenetic movements from juvenile to adult grounds, and trophic shifts. Within individuals, variability in isotopic profiles was generally given by a long-term (ontogenetic) pattern, and super-imposed shorter-term (i.e. seasonal to multi-annual) excursions, which indicated movements and trophic shifts also over relatively short temporal scales. Isotope-derived life-history information on blue and porbeagle shark spatial (and trophic) ecology may complement tag-derived information on short-term movements to implement management and conservation strategies. Nevertheless, interpretations of bulk tissue isotope data are ultimately limited by mixed baseline and trophic isotope effects, as seen in porbeagle sharks in this study.

3.2 Introduction

Marine top predators have declined worldwide at a rapid pace over the past century, largely as a result of overfishing and by-catch (Pauly *et al*., 1998; Myers & Worm, 2003; Worm *et al*., 2005; Estes *et al*., 2011). Populations of large sharks have declined regionally by > 90 % only the past 15 years (Baum *et al*., 2003; Baum & Blanchard, 2010; Worm *et al*., 2013; Dulvy *et al*., 2014). The ecological consequences of such population declines remain unclear (Heupel *et al*., 2014; Ruppert *et al*., 2016; Grubbs *et al*., 2016); however, they may include modifications in anti-predator behaviour by prey (Heithaus & Dill, 2006; Heithaus *et al*., 2007; 2008), cascading effects through food webs such as mesopredator release (Scheffer *et al*., 2005; Myers *et al*., 2007; Ferretti *et al*., 2010; Heupel *et al*., 2014), and changes in ecosystem resilience (Polis *et al*., 1997; Lundberg & Moberg, 2003; McCann *et al*., 2005; Rooney *et al*., 2006).

Large migratory sharks play fundamental roles within marine ecosystems. By migrating and foraging across large spatial scales, they alter nutrient and energy flow, ensuring connectivity between otherwise spatially and/or ecologically separated food webs (McCauley *et al*., 2012; Heupel *et al*., 2014; Roff *et al*., 2016; Ruppert *et al*., 2016). This connectivity confers resilience to food webs (Polis *et al.*, 1997; Lundberg & Moberg, 2003; McCann *et al.*, 2005; Rooney *et al.*, 2006), and can potentially result in externally-subsidised trophic pyramids (Trebilco *et al.*, 2013; Mourier *et al.*, 2016).

Sharks often share life-history traits such as seasonal movements between foraging and breeding sites, ontogenetic movements from juvenile to adult grounds, and trophic shifts (Estrada *et al*., 2006; Campana *et al*., 2010; Vandeperre *et al*., 2014; Carlisle *et al*., 2015). These life-history traits reflect changes in energy allocation throughout ontogeny: i.e. from a juvenile strategy maximising survival and growth (Werner & Gilliam, 1984; Heupel *et al*., 2007; Vandeperre *et al*., 2014) to an

adult strategy, which includes reproduction (Cortes, 2002; Campana *et al*., 2010; Grubbs, 2010; Carlisle *et al*., 2015). Because environmental influences on survival and growth vary by habitat, ontogenetic shifts in habitat use may have profound effects on population growth rates, species interactions, and community dynamics. Ontogenetic shifts in habitat and resource use often define transitions among life stages. Ecological and individual factors can cause variation in the timing and consistency of these transitions, ultimately affecting population and community dynamics through changes in growth and survival.

Shark vulnerability to fishery capture and roles within marine ecosystems strongly depends on: i) individual ontogenetic movements, and ii) the presence of life-history movement traits across individuals, species, higher taxa and/or functional groups. Effective management and conservation strategies to protect sharks and the ecological roles they play should encompass their entire geographic ranges, and include all stages of their migratory cycles (Gillanders *et al*., 2003; Gruess *et al*., 2011; Costa *et al*., 2012; Briscoe *et al*., 2016). The identification of individual ontogenetic movements is needed to define areas of essential habitat across life-history, where interactions with fisheries are of greater concern (e.g. Vandeperre *et al*., 2016). The recognition of common life-history movement traits is required to identify behaviours influencing shark-human interactions, and to define areas of high use where fishing restrictions should be intensified (e.g. Queiroz *et al*., 2016). The movements of highly migratory oceanic animals are difficult to monitor or reconstruct, particularly over ontogenetic time-scales (Graham *et al*., 2010; Trueman *et al*., 2012; McMahon *et al*., 2013a). To date, data-storage and satellite tags provide the best tool to track individual movements at fine spatio-temporal scales (e.g. Block *et al*., 2001; 2005; Campana *et al*., 2010; Queiroz *et al*., 2010; Block *et al*., 2011), by recording precise, accurate and time-resolved positional and behavioural data (Sibert & Nielsen, 2001; Nielsen *et al*., 2009; Sims, 2010; Hammerschlag *et al*., 2011). However, these tags provide movement information over relatively short periods of time (i.e. typically < 12 months), are often too large to be deployed on juveniles (but see Scott *et al*., 2014; Vandeperre *et al*., 2014), and by definition cannot be applied retrospectively. Additionally, they are prohibitively expensive to be applied in large- or population-scale studies (but see Block *et al*., 2001; 2005; 2011; Queiroz *et al*., 2016). Consequently, electronic archival tags are not well suited to studying individual ontogenetic movements, or to identifying life-history movement traits across individuals, populations or species (Hazen *et al*., 2012; Shillinger *et al*., 2012).

Stable isotope analysis allows the retrospective reconstruction of animal spatial and trophic ecology (for reviews, see Post, 2002; Graham *et al*., 2010; Hobson *et al*., 2010; Boecklen *et al*., 2011; Ramos & González-Solís, 2012; Trueman *et al*., 2012; McMahon *et al*., 2013a, b). The underlying premise is that the isotopic composition of an animal's tissues reflects that of primary producers at the base of the food web, overlain by a relatively predictable trophic enrichment (DeNiro & Epstein, 1978; 1981; Vander Zanden & Rasmussen, 2001; McCutchan *et al*., 2003). Therefore, the isotopic

composition of an animal's tissues reflects the interaction between the animal and its environment (in terms of both location and diet), and can be considered functional trait (Fig. 3.1A).

The time of tissue growth or recycling determines the time scale of ecological information (for reviews of tissue types, see Hobson, 1999; Newsome *et al.*, 2010; Trueman *et al.*, 2012; McMahon *et al.*, 2013b). Incrementally grown, metabolically inert tissues, such as shark vertebrae and eye lenses, can provide whole-life, biochemical records containing spatial and trophic information (e.g. Estrada *et al*., 2006; Carlisle *et al*., 2015; Loor-Andrade *et al*., 2015; Quaeck *et al.*, *unpubl. data*). The pattern in isotopic compositions in incrementally grown tissues within an individual reflects the animal-environment interaction throughout life, and can itself be considered a life-history trait for the individual (Fig. 3.1A). Additionally, between-individual variance in both single isotope values and ontogenetic patterns also conveys trait information for the species or population (Fig. 3.1B). Consequently, individual-level life-history isotopic traits provide a means to gather information on the movements throughout the life of single individuals. Additionally, species- or population-level traits may indicate common, broad ontogenetic movement patterns across individuals. Life-history isotopic traits can, therefore, be considered conceptually similar to life-time isotopic niche areas (Newsome *et al.*, 2007): they also allow identifying differences and commonalities across individuals, populations, species, higher taxa and/or functional groups, and provide additional information on ontogenetic patterns.

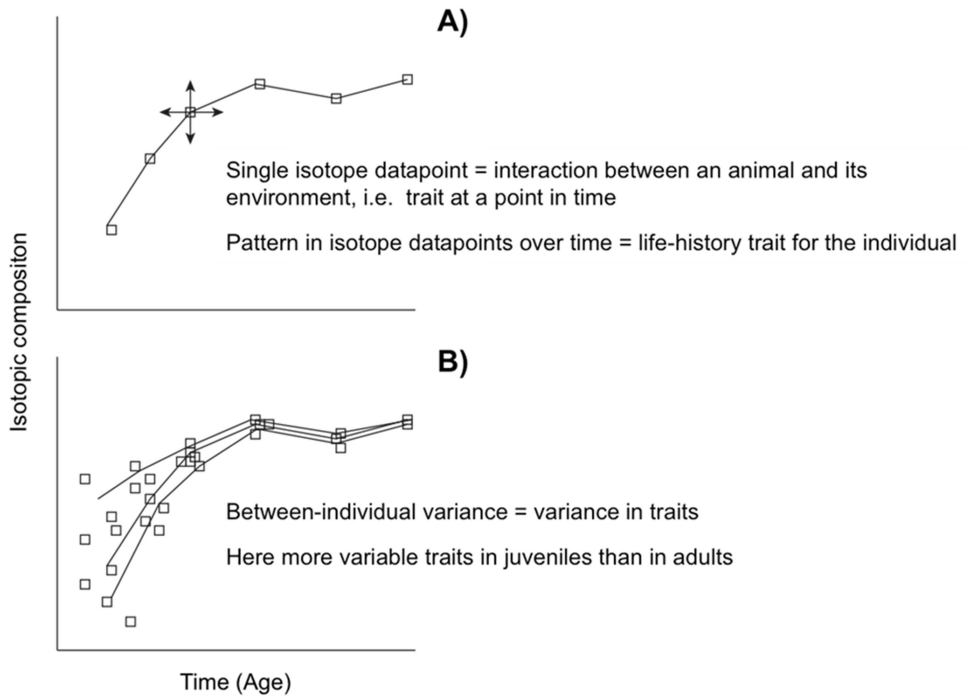

Figure 3.1 Schematics for isotopic traits.
A) Every single isotope value measured in incrementally grown tissues represents the interaction between an animal and its environment at a particular point in time, i.e. an isotopic trait at a point in time; the pattern in isotope values in incrementally grown tissues represents a life-history isotopic trait for the individual. B) Between-individual variances in single isotope values and/or patterns in incrementally grown tissues also represent isotopic traits for the species or population; in this example, a species- or population-level life-history isotopic trait is identified, with more variable traits in juveniles than adults.

3.2.1 Life-history isotopic traits within and among shark species

Only a few individual-level life-history isotopic records currently exist for shark species (Table 3.1). Most of the existing records are for carbon ($\delta^{13}C$) isotopes, which are often measured in association with radiocarbon (^{14}C) data in ageing studies. Fewer records exist for combined carbon and nitrogen ($\delta^{15}N$) isotopes measured in ecological studies (Table 3.1). In the case of vertebrae, central vertebrae are used for isotope analysis where possible, as existing vertebral radius-fork length and fork length-age relationships are most often derived and validated for central vertebrae (e.g. Natanson *et al.*, 2002; Skomal & Natanson, 2003). Shark eye lenses are also grown incrementally, and thus may also provide ecological information throughout ontogeny, though are more focussed on early life-history stages than vertebrae (Quaeck *et al.*, *unpubl. data*; Bird *et al.*, *unpubl. data*). Like vertebrae, eye lenses are also grown allometrically; as yet, however, no validated diameter-age relationships exist for eye lenses.

Where individual-level life-history isotopic records are available, common, broad ontogenetic patterns in isotopic compositions can be identified across individuals and species (Table 3.1; Fig. 3.2), after normalising isotope values at each life stage to the mean values for the individual

shark (see below) to reduce regional variation in isotopic baselines. Carbon isotopic compositions, for instance, consistently decrease throughout life across individual white sharks (Fig. 3.2A), with super-imposed variability in isotopic profiles among areas and individuals (Table 3.1). Similarly, $\delta^{13}C$ values measured in porbeagle eye lenses and salmon shark vertebrae consistently decrease during juvenile growth, and increase until reaching a relatively steady state. In porbeagles, $\delta^{13}C$ values measured in vertebrae increase throughout ontogeny; however, only a few isotope datapoints are available for each individual (Fig. 3.2A). In white and salmon sharks, the observed ontogenetic decrease in $\delta^{13}C$ values may reflect an ontogenetic habitat shift from coastal to oceanic food webs (Hamady, 2014; Carlisle *et al*., 2015).

Common ontogenetic patterns in $\delta^{13}C$ values can also be identified across species. Clear differences in $\delta^{13}C$ values exist, for instance, between early- and mid-juvenile and adult life-history stages across most species. Indeed, whilst ontogenetic patterns in $\delta^{13}C$ values vary among species, a step-change (increase or decrease) in $\delta^{13}C$ values is consistently observed at a point during juvenile life-history stages across most species (Fig. 3.2A). Commonalities in $\delta^{15}N$ patterns across species are more difficult to draw out, as $\delta^{15}N$ records are only available for a few species (Fig. 3.2B).

The identification of life-history isotopic traits across individuals, species, higher taxa and/or functional groups may imply common ontogenetic movement and habitat use patterns, despite potential differences in movement behaviour among areas and individuals, and thus shared vulnerability to fishery capture across their life-histories. In this study, individual-level life-history records of $\delta^{13}C$ and $\delta^{15}N$ values were recovered for two pelagic shark species, the blue (*Prionace glauca*) and porbeagle (*Lamna nasus*) sharks, from across the North Atlantic. Life-history isotopic traits were then tested within each species, and across species. Whilst blue and porbeagle sharks may sporadically co-occur in some ocean areas in the North Atlantic, they are known from tagging studies to have different distribution, habitat and movement patterns across life-history. Blue sharks live primarily in subtropical waters well offshore, and do not show consistent inshore nurseries or juvenile grounds (see below; Queiroz *et al*., 2010; Campana *et al*., 2011; Vandeperre *et al*., 2014; 2016). Porbeagles are restricted to temperate waters, and may present a transition from continental shelves when juveniles towards shelf-edge and slope settings when adults (Pade *et al*., 2009; Campana *et al*., 2010; Saunders *et al*., 2011; Biais *et al.*, 2016). Additionally, blue and porbeagle sharks are known from stomach content analysis to have different prey bases and feeding behaviours (Joyce *et al*., 2002; McCord & Campana, 2003; Pusineri *et al*., 2008). Consequently, differences in ontogenetic movement and feeding ecology between blue and porbeagle sharks are expected to lead to differences in life-history isotopic records.

Table 3.1 Literature-derived individual-level life-history records of carbon ($\delta^{13}C$) and nitrogen ($\delta^{15}N$) isotopic compositions for shark species; studies providing both $\delta^{13}C$ and $\delta^{15}N$ records are in bold.

Species	Capture area	Tissue	N inds.	N samples *per* ind.	Isotopes	Shape	Application	Reference
White shark (*Carcharodon carcharias*)	**Northwest Atlantic**	**Vertebrae**	**n.a.**	**n.a. (27 in total)**	**$\delta^{13}C$, $\delta^{15}N$**	**$\delta^{13}C$ – no pattern; $\delta^{15}N$ –increase**	**Ontogenetic feeding ecology**	**Estrada *et al*., 2006**
White shark (*Carcharodon carcharias*)	**Northwest Atlantic**	**Vertebrae**	**5**	**9-28**	**$\delta^{13}C$, $\delta^{15}N$**	**$\delta^{13}C$ and $\delta^{15}N$ – no pattern**	**Ontogenetic movement and feeding ecology**	**Hamady, 2014**
White shark (*Carcharodon carcharias*)	Northwest Atlantic	Vertebrae	8	2-23	$\Delta^{14}C$, $\delta^{13}C$	$\delta^{13}C$ – decrease	Ageing, changes in carbon source	Hamady *et al*., 2014
White shark (*Carcharodon carcharias*)	**Northeast Pacific**	**Vertebrae**	**11 (6 SI, 9 $\Delta^{14}C$, 4 both)**	**1-5**	**$\Delta^{14}C$, $\delta^{13}C$, $\delta^{15}N$**	**$\delta^{13}C$ – decrease; $\delta^{15}N$ – no pattern**	**Ageing, changes in carbon source, diet and trophic position**	**Kerr *et al*., 2006**
White shark (*Carcharodon carcharias*)	**Northeast Pacific**	**Vertebrae**	**15**	**7-20**	**$\delta^{13}C$, $\delta^{15}N$**	**$\delta^{13}C$ – decrease or no pattern; $\delta^{15}N$ – increase or no pattern**	**Ontogenetic and among- individual variation in foraging strategies**	**Kim *et al*., 2012a**
White shark (*Carcharodon carcharias*)	Southwest Indian	Vertebrae	4	1-3	$\Delta^{14}C$, $\delta^{13}C$	$\delta^{13}C$ – no pattern	Ageing	Christiansen *et al*., 2016
Porbeagle shark (*Lamna nasus*)	Northwest Atlantic	Vertebrae	15	1-4	$\Delta^{14}C$, $\delta^{13}C$	$\delta^{13}C$ – increase	Ageing	Campana *et al*., 2002
Porbeagle shark (*Lamna nasus*)	Southwest Pacific (New Zealand)	Vertebrae	11	3-4	$\Delta^{14}C$, $\delta^{13}C$	$\delta^{13}C$ – decrease	Ageing	Francis *et al*., 2007
Porbeagle shark (*Lamna nasus*)	**Northeast Atlantic**	**Eye lenses**	**47**	**4-26**	**$\delta^{13}C$, $\delta^{15}N$**	**$\delta^{13}C$ and $\delta^{15}N$ – decrease**	**Ontogenetic movement and feeding ecology**	**Quaeck *et al*., *unpubl. data***
Salmon shark (*Lamna ditropis*)	**Northeast Pacific (Alaska)**	**Vertebrae**	**20**	**14 (max)**	**$\delta^{13}C$, $\delta^{15}N$**	**$\delta^{13}C$ and $\delta^{15}N$ – increase**	**Ontogenetic changes in habitat use**	**Carlisle *et al*., 2015**
Smooth hammerhead (*Sphyrna zygaena*)	**East Pacific (Ecuador)**	**Vertebrae**	**20**	**3-8**	**$\delta^{13}C$, $\delta^{15}N$**	**$\delta^{13}C$ – no pattern; $\delta^{15}N$ – increase**	**Population and individual foraging patterns**	**Loor-Andrade *et al*., 2015**
Scalloped hammerhead (*Sphyrna lewini*)	**East Pacific (Ecuador)**	**Vertebrae**	**20**	**3-8**	**$\delta^{13}C$, $\delta^{15}N$**	**$\delta^{13}C$ and $\delta^{15}N$ – no pattern**	**Population and individual foraging patterns**	**Loor-Andrade *et al*., 2015**
Sand tiger shark (*Carcharias taurus*)	Northwest Atlantic, Southwest Indian	Vertebrae	10 (8 NWA, 2 SWI)	2-8	$\Delta^{14}C$, $\delta^{13}C$	$\delta^{13}C$ – increase or no pattern	Ageing	Passerotti *et al*., 2014
Shortfin mako shark (*Isurus oxyrinchus*)	Northwest Atlantic	Vertebrae	8	2-8	$\Delta^{14}C$, $\delta^{13}C$	$\delta^{13}C$ – increase (based on 1 ind.)	Ageing	Campana *et al*., 2002; Ardizzone *et al*., 2006
Great hammerhead shark (*Sphyrna mokarran*)	n.a.	Vertebrae	2	3-7	$\Delta^{14}C$, $\delta^{13}C$	$\delta^{13}C$ – increase	Ageing	Piercy *et al.*, 2010
Spurdog (*Squalus acanthias*)	**Northeast Atlantic**	**Eye lenses**	**25**	**2-11**	**$\delta^{13}C$, $\delta^{15}N$**	**$\delta^{13}C$ – decrease; $\delta^{15}N$ – increase**	**Ontogenetic movement and**	**Quaeck *et al*., *unpubl. data***

Species	Capture area	Tissue	N inds.	N samples *per* ind.	Isotopes	Shape	Application	Reference
							feeding ecology	
Deepwater spiny dogfish (*Centrophorus squamosus*)	Northeast Atlantic (Rockall)	Eye lenses	5	11-16	$\delta^{13}C$, $\delta^{15}N$	$\delta^{13}C$ – increase; $\delta^{15}N$ – no pattern	Ontogenetic movement and feeding ecology	Bird *et al*., *unpubl. data*
Portoguese dogfish (*Centroscymnus coelolepis*)	Northeast Atlantic (Rockall)	Vertebrae, eye lenses	5	10-13	$\delta^{13}C$, $\delta^{15}N$	$\delta^{13}C$ and $\delta^{15}N$ – increase	Ontogenetic movement and feeding ecology	Bird *et al*., *unpubl. data*

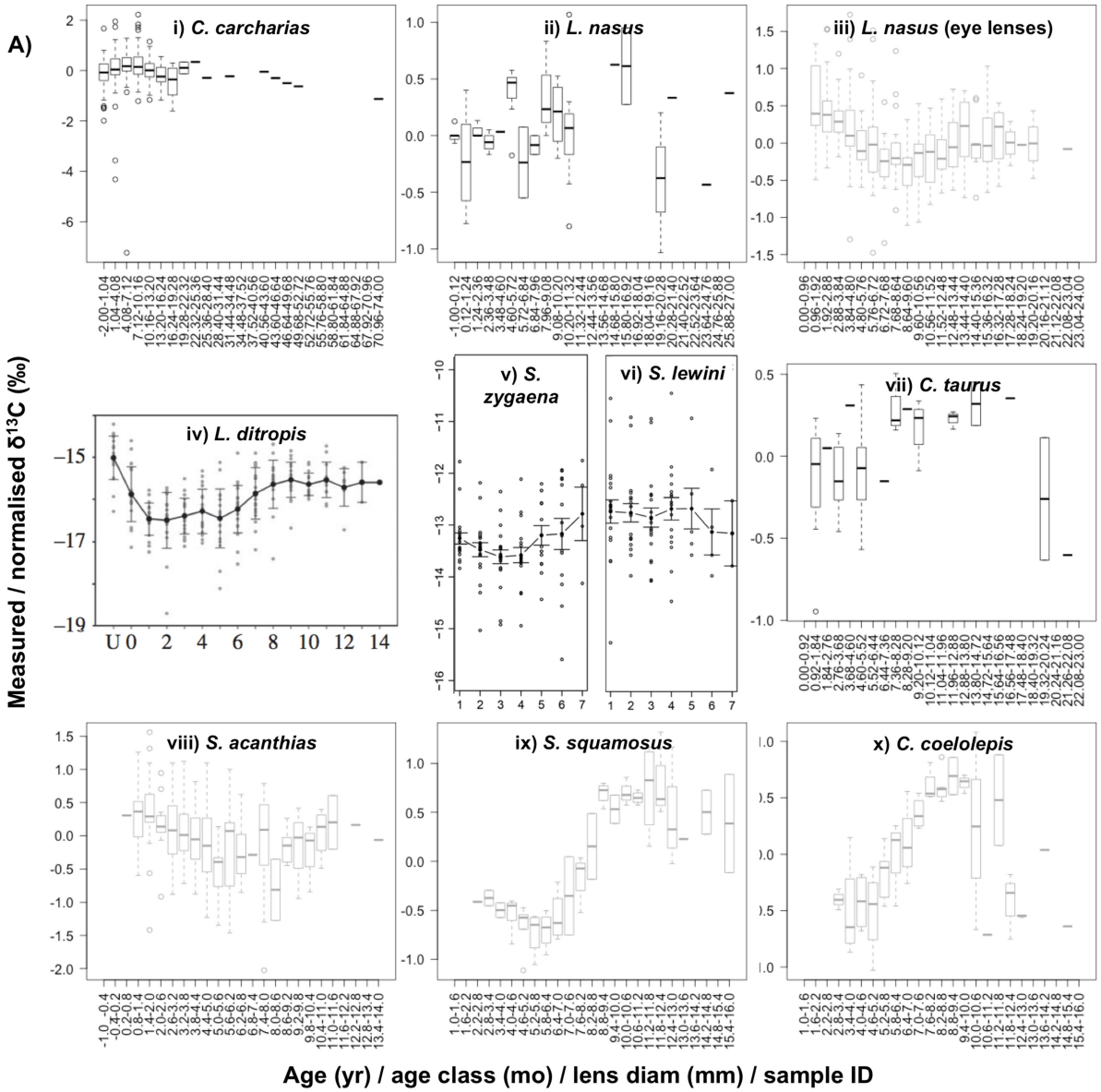

Figure 3.2 Species-level life-history isotopic traits in sharks.
Species-level life-history traits in A) carbon ($\delta^{13}C$) and B) nitrogen ($\delta^{15}N$) isotopic compositions (‰, measured or normalised values: i.e. averaged to the mean values for each individual shark as in Eq. 3.3) for i) white sharks, ii) porbeagles, iii) salmon sharks, iv) smooth and v) scalloped hammerhead sharks, vi) sand tiger sharks, vii) spurdogs, and viii) deep-water sharks. References for raw data are presented in Table 3.1; $\delta^{15}N$ records were not available for porbeagle vertebrae and sand tiger sharks. Isotope records in porbeagles from the Northeast Atlantic, spurdogs and deep-water sharks are for eye lenses (grey plots). For each species and life stage, the boxplot displays the variation in isotope values across individuals. The horizontal line in each boxplot represents the median of the data (i.e. 50% of the data are greater than this value). The lower and upper limits of the boxplot represent the lower and upper quartile (i.e. 25% of the data less or greater than this value), respectively. The lower and upper whiskers represent the minimum and maximum value excluding outliers, respectively. Dots at the bottom or top of whiskers represent outliers (i.e. less and more than 3/2 times of the lower and upper quartile, respectively).

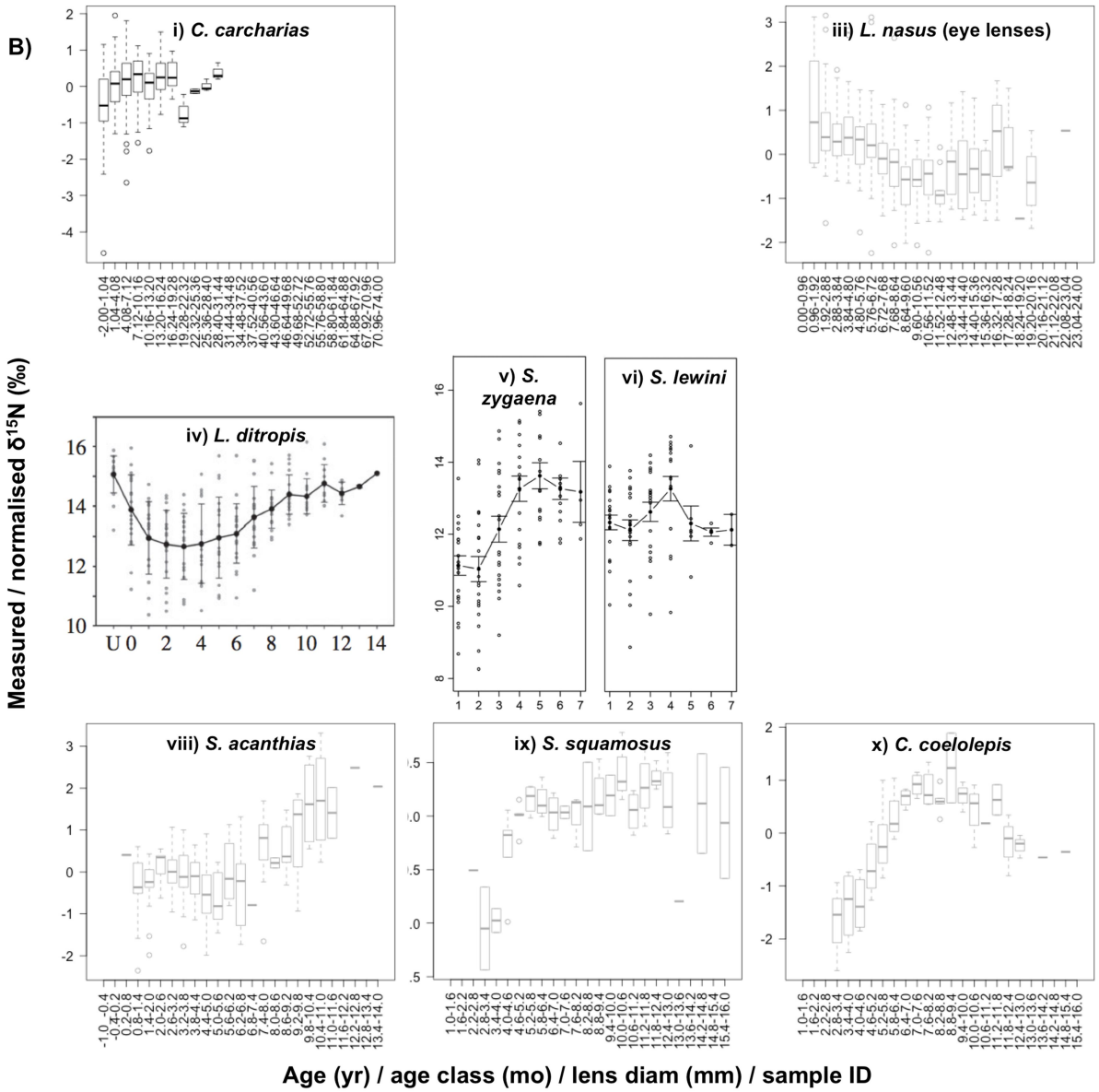

3.2.2 Known ontogenetic movements in blue and porbeagle sharks

Common to most pelagic sharks, current knowledge of blue and porbeagle shark ontogenetic movement ecology is limited and often contradictory. Satellite-tracking studies on blue sharks in the North Atlantic revealed complex spatial dynamics with segregation by sex and life-history stage, influencing population structuring (Queiroz *et al*., 2010; Campana *et al*., 2011; Vandeperre *et al*., 2014; 2016). Juveniles of both sexes of less than two years of age are known to reside in oceanic waters near the Azores in the central North Atlantic (Vandeperre *et al*., 2014; 2016); however, coastal nursery areas are also thought to exist on continental shelves of the Iberian Peninsula and North Africa (Queiroz *et al*., 2010 and references therein). In the eastern North Atlantic, juvenile and subadult females undertake seasonal latitudinal migrations from summerising temperate grounds off Southwest England to wintering subtropical grounds off Portugal and near the Azores (Queiroz *et al*., 2010; 2012;

Vandeperre *et al*., 2014). In the western North Atlantic, juveniles and subadults undergo similar movements from continental shelves off the United States and Canada during summer to offshore warmer waters of the Gulf Stream (as far south as the Sargasso Sea) during winter (Campana *et al*., 2011). Adult females tagged in the Azores are known to undergo directional movements to tropical latitudes during summer utilising pathways on both sides of the Atlantic, which are in sharp contrast with movements by juvenile and subadult females, and possibly associated with parturition and pupping (Vandeperre *et al*., 2014). Adult females tagged in the Northwest Atlantic are also known to move south to deliver their pups, or offshore towards the Northeast Atlantic (Campana *et al*., 2011; Vandeperre *et al*., 2014). Juvenile and adult males tagged in the Azores are known to undergo similar movements, and do not appear to segregate spatially. They move southwest of the Azores during autumn, and aggregate in areas with seamounts, known as 'male clubs', migrate towards the Northwest Atlantic during winter, and finally return to the Azores by the end of spring (Vandeperre *et al*., 2014). Blue sharks show a high degree of individuality in movement behaviour across life-history stages (Queiroz *et al*., 2010; Campana *et al*., 2011; Vandeperre *et al*., 2014; 2016), complicating the identification of clear, common ontogenetic movement and habitat use patterns by different segments of the population.

Satellite-tracking of juvenile and subadult porbeagles in the Northeast Atlantic revealed a general southward movement from warm, seasonally-stratified waters on the continental shelf between 50 and 54 °N during summer to deeper waters over the slope between 47 and 52 °N during winter, with individuals at liberty for long enough showing a return migration (Biais *et al.*, 2016; Fig. 3.3). Porbeagles are not solely restricted to the European shelf edge: some individuals have been observed to move across the mid-Atlantic ridge to the west, as far south as the Azores and the Cape Verde, and as far north as the coast of Norway, indicating large individual variability in movement behavior, at least during juvenile and subadult stages (Pade *et al*., 2009; Saunders *et al*., 2011; Biais *et al.*, 2016; Fig. 3.3). Larger ranges of isotope values in eye lenses during *in situ* periods than during *in utero* periods also suggest an expanded geographic range when juveniles (Quaeck *et al*., *unpubl. data*). In the western North Atlantic, adult females are known to undertake long-distance movements through the winter, at depths down to 1360 m beneath the Gulf Stream, to subtropical pupping grounds in the Sargasso Sea (Campana *et al*., 2010). The movements of adult females in the Northeast Atlantic are still unknown. Additionally, porbeagle sharks are believed to undergo an ontogenetic transition from juvenile grounds on continental shelves towards more offshore, deeper waters, as large individuals are seldom caught in shelf fisheries (Bendall *et al*., 2013; Ellis *et al*., 2015; Biais *et al.*, 2016).

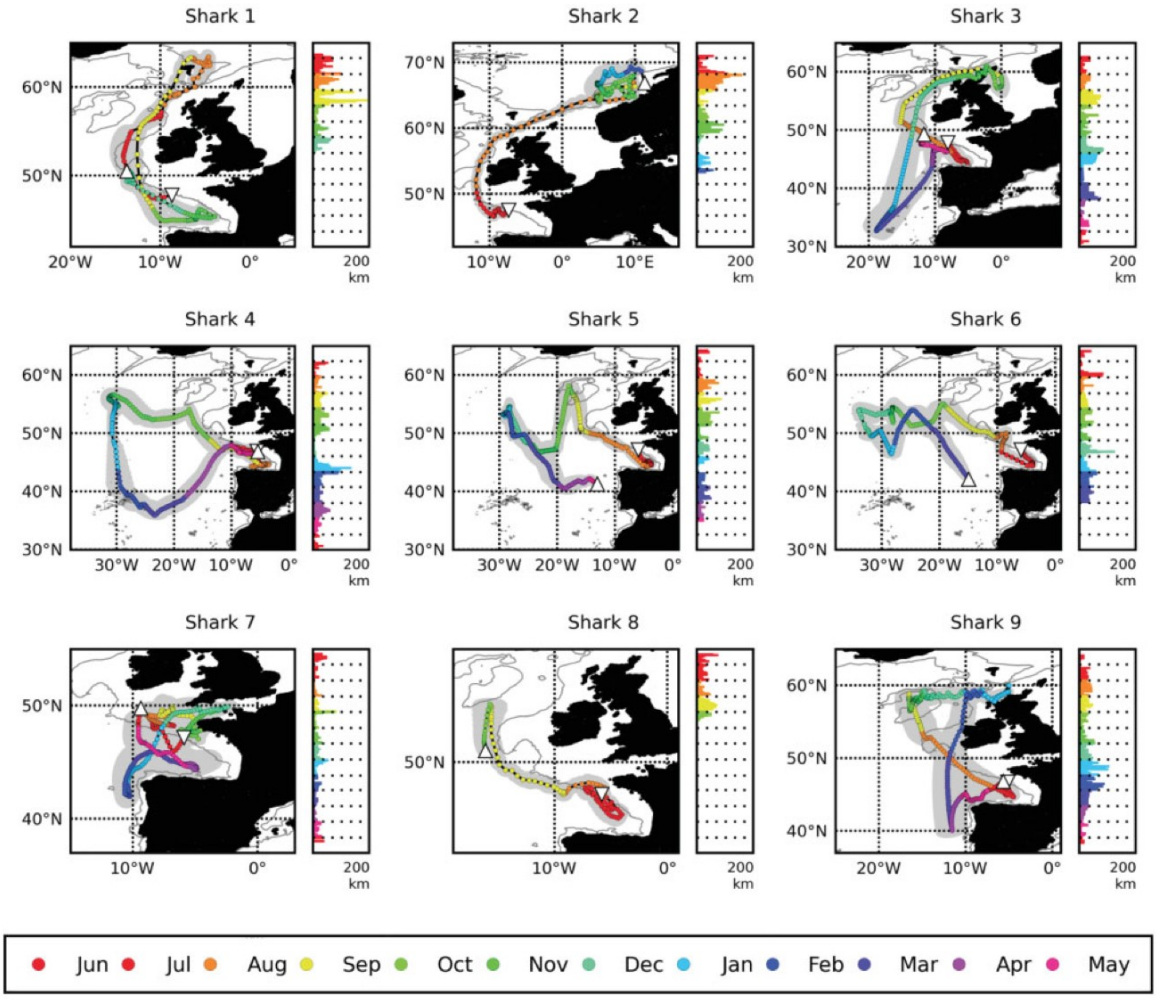

Figure 3.3 Movement patterns of satellite-tracked porbeagle sharks in the Northeast Atlantic. Reconstructed tracks (left) and daily estimated movement distance (right) of the nine porbeagles tagged in the Bay of Biscay in June 2011 (individuals 1-4) and June 2013 (individuals 5-9). 50% Confidence Intervals (CIs) are displayed as grey ellipses and 1000 m contours are shown. Downward and upward triangles denote the tagging and pop-up locations, respectively. Taken from Biais *et al.* (2016).

In this study, individual-level life-history records of $\delta^{13}C$ and $\delta^{15}N$ values were recovered for blue and porbeagle sharks from across the North Atlantic, at a high (i.e. seasonal to multi-annual) temporal resolution. Variation in isotopic profiles was then quantified at multiple levels (i.e. between species, among capture areas, and within and between individuals), and common, broad ontogenetic patterns in isotope records tested for within and across species; commonalities (and differences) in isotopic profiles were also examined across areas and individuals. Shifts in movement and habitat use within individuals may produce individual-level life-history isotopic traits (Fig. 3.1A). Additionally, common, broad movement patterns across individuals may produce life-history isotopic traits for a species or population (Fig. 3.1B). In bulk tissue isotope analysis, variance in tissue isotopic compositions may also reflect shifts in diet and trophic level, due to mixed baseline and trophic isotope effects (e.g. Jennings & Warr, 2003; Popp *et al.*, 2007; Nielsen *et al.*, 2016; for reviews, see

Newsome *et al.*, 2010; Ramos & González-Solís, 2012; Trueman *et al.*, 2012; McMahon *et al.*, 2013b). Isotopic variance in bulk cartilage collagen was interpreted to provide maximum possible inferential information about movements *versus* trophic shifts, given the methodological difficulties in separating baseline from trophic isotope effects. Based on current knowledge of the ontogenetic movement and feeding ecology of blue and porbeagle sharks in the North Atlantic, the following hypotheses were constructed:

1) Values of $\delta^{13}C$ and $\delta^{15}N$ of bulk cartilage collagen from sequential vertebral samples from individual blue and porbeagle sharks vary at multiple levels (i.e. between species, among capture areas, and within and among individuals).
2) Species-level life-history isotopic traits can be identified across individual blue and porbeagle sharks, due to common, broad ontogenetic movements (and/or trophic shifts).
3) Life-history isotopic traits (and life-time isotopic niche areas) differ between species, as a result of different distributions, habitats and movement patterns (and/or trophic ecology) throughout ontogeny.
4) Patterns in isotopic profiles vary among areas and individuals, as a result of movement across different isoscapes in the eastern and western North Atlantic (Schmittner & Somes, 2016; Magozzi *et al.*, 2017; Chapter 2), and a high degree of individuality in movement (and/or trophic) behaviour.
5) Within-individual variability in isotopic profiles has both long- and short-term components, because of ontogenetic and super-imposed seasonal or multi-annual movements (and/or trophic shifts).

3.3 Materials and Methods

3.3.1 Sample description

Vertebrae were removed from nine blue and six porbeagle sharks caught across the North Atlantic. Capture areas included the extremes and centre (at least for blue sharks) of these species' distributional ranges in the North Atlantic, as estimated by electronic tagging studies (e.g. Campana *et al*., 2010; Queiroz *et al*., 2010; Campana *et al*., 2011; Vandeperre *et al*., 2014; Biais *et al*., 2016). For blue sharks, capture areas comprised offshore waters south of Canary Islands (24-26 °N, 20-21 °W) in the Northeast Atlantic, the mid-Atlantic Ridge area north west of the Azores (42 °N, 44-45 °W) in the central North Atlantic, and oceanic waters between Cape Hatteras and the Gulf of Maine in the Northwest Atlantic. For porbeagles, capture areas encompassed shelf waters between the western English Channel and Celtic Sea and around the Faroe Islands in the Northeast Atlantic, and between Massachusetts and Grand Banks (off southern Newfoundland) in the Northwest Atlantic (Fig. 3.4).

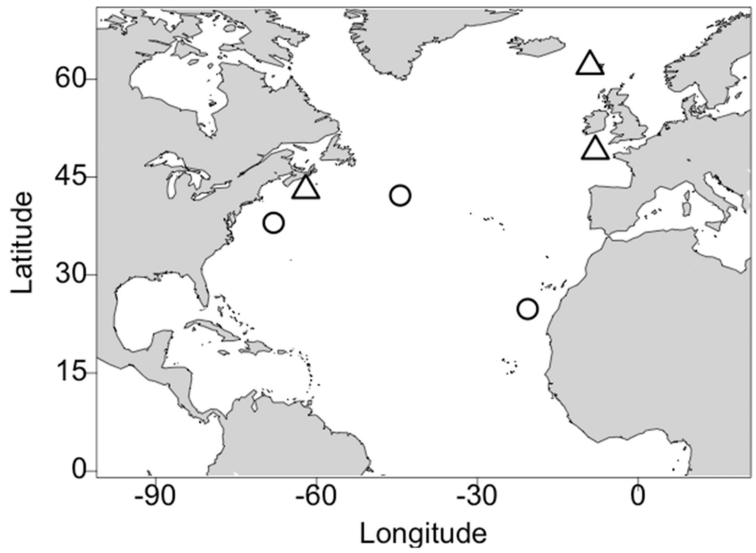

Figure 3.4 Capture areas for blue and porbeagle sharks in the North Atlantic.
Different symbols represent different species: circles identify blue sharks, triangles porbeagles. For blue sharks from the central and eastern North Atlantic, capture position is given by the mean of measured capture latitudes and longitudes for individual sharks. For blue sharks from the Northwest Atlantic and porbeagles, capture position is an estimated value, as capture latitudes and longitudes were not measured.

In the central and eastern North Atlantic, blue sharks were caught by commercial long-lines in 2014. Blue sharks from the Northwest Atlantic were recovered from commercial fishing vessels and during research and recreational fishing cruises, and at sport fishing tournaments in 1996-2001 (Skomal & Natanson, 2003). Porbeagle sharks from the western English Channel were recovered as by-catch from scientific gillnets in 2011 and 2014-2015 (Bendall *et al*., 2013; Ellis *et al*., 2015). Vertebrae from a single individual caught off the Faroe Islands were donated by a local fisherman in 2014. In the Northwest Atlantic, porbeagle sharks were caught by Canadian commercial fishing vessels before 1990 and by commercial and research vessels between 1996 and 1999 (Natanson *et al*., 2002). For each area, vertebrae from the three largest females were selected among all the available samples for isotope analysis. In the case of blue sharks, all individuals were mature; for porbeagles, only western Atlantic individuals were mature, and eastern Atlantic individuals were either immature or maturing (Table 3.2).

Table 3.2 Metadata for individual blue and porbeagle sharks selected for isotope analysis. Data include species, capture area, individual ID, maturity stage (evaluated and estimated from fork length), fork length (FL), vertebral radius (VR), number of samples collected from each vertebra (N) and (achieved) average interval between adjacent samples (Av Int).

Species	Capture area	Individual ID	Maturity (ev.)	Maturity (est.)	FL (cm)	VR (mm)	N	Av Int (mm)
Prionace glauca	mid-Atlantic Ridge	16	Fecunded	Mature	242	11.0	19	0.58
Prionace glauca	mid-Atlantic Ridge	24	Pregnant	Mature	240	11.0	21	0.52
Prionace glauca	mid-Atlantic Ridge	12	Fecunded	Mature	219	10.0	17	0.59
Prionace glauca	Canary Islands	101	NA	Mature	258	12.0	16	0.75
Prionace glauca	Canary Islands	131	NA	Mature	249	12.0	17	0.71
Prionace glauca	Canary Islands	33	NA	Mature	244	11.5	21	0.55
Prionace glauca	Northwest Atlantic	335	NA	Mature	268	17.0	34	0.50
Prionace glauca	Northwest Atlantic	415	NA	Mature	265	15.0	31	0.49
Prionace glauca	Northwest Atlantic	441	NA	Mature	245	14.5	28	0.52
Lamna nasus	western English Channel	11	Maturing	Immature	211	15.0	24	0.63
Lamna nasus	Faroe Islands	1000	NA	Immature	210	15.5	24	0.65
Lamna nasus	western English Channel	40	Immature	Immature	197	12.5	24	0.52
Lamna nasus	Northwest Atlantic	599	NA	Mature	260	17.5	32	0.55
Lamna nasus	Northwest Atlantic	601	NA	Mature	256.5	17.5	34	0.51
Lamna nasus	Northwest Atlantic	578	NA	Mature	256	17	30	0.57

3.3.2 Sample collection and preservation

For porbeagles and Northwest Atlantic blue sharks, multiple central vertebrae were excised from an area just above the brachial chamber (Natanson *et al*., 2002; Skomal & Natanson, 2003). For central and eastern North Atlantic blue sharks, cervical (rather than central) vertebrae were removed from the skull, as these specimens had commercial value, and thus were not available for full dissections. Vertebrae were preserved frozen. For each shark, a single vertebra from the middle (where possible) was selected for isotope analysis. Porbeagle samples were transported to the Unites States for processing and analysis in accordance with the current regulations, and accompanied by a CITES Export Permit (No. 529713/01).

3.3.3 Sample processing

3.3.3.1 Sectioning

After defrosting, vertebral centra were physically cleaned from excess muscle and connective tissue, and air-dried slowly for 3-10 d, depending on dimensions (Campana, 2014; Kim & Koch, 2012). A 6 mm thick section was cut from each centrum using a low-speed diamond-bladed Isomet® saw. Each section was divided in two symmetrical halves. An additional 0.6-1 mm thick section was cut from one half, and spared for future age determinations; the remaining 5-5.4 mm thick

half section was used for isotope analysis of bulk cartilage collagen. The 6 mm thick half section was used for compound-specific analysis of single amino acids (see Chapter 4).

3.3.3.2 Subsampling

Approximately equidistant samples were cut along the vertebral radius from each section. Whilst a target interval between adjacent samples of 0.5 mm was initially set, as a result of the difficulty of manually cutting small chunks of calcified material, the sampled interval varied slightly within and among vertebrae. Thus, the sampled interval was best approximated by the average interval between adjacent samples (Av Int, mm), which was calculated for each vertebra as in Eq. 3.1.

$$\text{Av Int} = \frac{\text{VR}}{\text{N}} \quad (3.1)$$

where VR (mm) is the vertebral radius, and N the number of samples collected along the radius. N ranged between 16 and 34 among vertebrae (i.e. sharks), averaging at 24.80 ± 6.11 (mean ± SD); the average interval between adjacent samples ranged between 0.48 and 0.75 mm, averaging at 0.59 ± 0.08 mm (mean ± SD; Table 3.2). Vertebral samples were dried and weighed prior to exposure to hydrochloric acid (i.e. pre-treatment weight).

3.3.3.3 Decalcification

To remove any potential influence of ^{13}C-enriched bioapatite on carbon isotopic compositions of bulk cartilage collagen, vertebral samples were decalcified by exposure to 2 ml of 1 M hydrochloric acid (HCl) for 48 hrs (Dean & Summers, 2006; Hussey *et al*., 2012; Kim & Koch, 2012; Christiansen *et al*., 2014). As sample weight was not limiting, and samples were relatively large vertebral chunks, the use of hydrochloric acid should preserve the integrity of cartilage collagen (Tuross *et al*., 1988; Kim & Koch 2012; Christiansen *et al*., 2014), whilst avoiding the risk of contamination by alternative organic solvents (e.g. ethylenediaminetetraacetic acid, EDTA; Quaeck *et al*., *unpubl. data*; for other studies using hydrochloric acid, see Jacob *et al*., 2005; Carabel *et al*., 2006; Kerr *et al*., 2006; Brodie *et al*., 2011). To reduce decalcification rates, and prevent cartilage collagen dissolution and damaging, samples were kept at 4 °C during treatment. Samples were washed five times with 2 ml of Milli-Q water, then frozen, freeze-dried and re-weighted (i.e. post-treatment weight). The proportion of organic collagen (i.e. percentage collagen in the original sample) was calculated for each sample. Percentage collagen ranged between 15.84 and 65.91%, averaging at 37.81 ± 5.57% (mean ± SD); these values are consistent with previously reported ranges (e.g. Porter *et al*., 2006; Quaeck *et al*., *unpubl. data*; this study, test samples), providing further confirmation that decalcification had completely occurred without dissolving or damaging collagen.

3.3.3.4 Combination of 'light' samples and analysis resolution

Samples with a post-treatment weight of < 0.5 mg (i.e. the minimum weight required for reproducibly reliable dual carbon and nitrogen isotope analysis on bulk cartilage collagen using available equipment) were combined with their lighter neighbour(s) until the total weight exceeded 0.5 mg. Single or combined samples with a weight of > 1.5 mg (i.e. the maximum weight accepted for analysis) were physically split, and ~ 1.25 mg of material selected for analysis. Blue shark samples were analysed at full resolution; to minimise analytical costs, porbeagle samples were run at half resolution for distances along the vertebral radius < 7 mm, and at full resolution afterwards. For porbeagles, vertebral radius at maturity is estimated to be ~ 12 mm (Natanson *et al.*, 2002); in this study, a vertebral radius of 7 mm was selected as a more conservative cutoff to account for approximations in the sampled interval. For all specimens, the temporal resolution at which isotopic data were recovered was sufficiently high to depict isotopic variation over relatively short time-scales (i.e. typically over one or a few years; for estimated sample age, see Table 3.3).

3.3.4 Stable isotope analysis

Values of $\delta^{13}C$ and $\delta^{15}N$ of selected samples were measured using a PDZ Europa ANCA-GSL elemental analyser interfaced to a PDZ Europa 20-20 isotope ratio mass spectrometer (Sercon Ltd., Cheshire, UK) at the University of California (UC) Davis Stable Isotope Facility. All samples were run in duplicate. Analytical quality control was assessed through repeated sampling of internal laboratory standards (ILSs), which included nylon, glutamic acid and USGS-41. Nylon was used as a drift reference to correct for variation over the course of a run. Glutamic acid was used both to calculate the elemental totals, and to apply a linearity correction to the isotope values. Finally, the isotope values were scaled to two references of known isotope values, nylon and USGS-41. All internal laboratory standards were calibrated to international references. Precision was 0.03‰ for $\delta^{13}C$ values and 0.10‰ for $\delta^{15}N$ values, accuracy 0.01‰ for $\delta^{13}C$ values and 0.06‰ for $\delta^{15}N$ values. Precision was calculated as the standard deviation for isotope values of bovine liver NIST 1577 across runs (i.e. during the time period samples were analysed), accuracy as the difference between the mean isotope value for bovine liver and the accepted isotope value, based on calibration against international references (Jardine & Cunjak, 2005). Final $\delta^{13}C$ and $\delta^{15}N$ values were expressed relative to international standards V-PDB (Vienna PeeDee Belemnite) and Air, respectively. The raw ratio (R) of the heavy (e.g. ^{13}C) to the light (e.g.^{12}C) isotope in a sample was converted to a delta value, in parts per thousands, using the formula: $\delta X = \left[\left(\frac{R_{sample}}{R_{standard}}\right) - 1\right] * 1000$ (see Chapter 1; Eq. 1.1), where X is the heavier isotope. $R_{standard}$ refers to the raw ratio of an internationally accepted standard gas for the isotope being analysed.

3.3.5 Age estimation

To account for differential vertebral growth rates throughout ontogeny, linear distance along the vertebral radius was converted to age using validated and/or estimated vertebral width:body size and body size:age relationships (Natanson *et al*., 2002; Skomal & Natanson, 2003; this study). The median distance along the vertebral radius (d, mm) was calculated for each sample as in Eq. 3.2.

$$d = (ID * Av\ Int) - (\frac{Av\ Int}{2}) \quad (3.2)$$

where ID is the number of each sample along the vertebral radius (or average sample number for all samples in a combination), and Av Int (mm) is the achieved average interval between adjacent samples for each vertebra (Eq. 3.1).

For central vertebrae from porbeagles and Northwest Atlantic blue sharks, sample age (yr or mo) was estimated from distance along the vertebral radius using validated Von Bertalanffy growth curves and validated vertebral radius-fork length relationships (Natanson *et al*., 2002; Skomal & Natanson, 2003). For cervical vertebrae from central and eastern North Atlantic blue sharks, an estimated linear vertebral radius-fork length relationship was used in place of the validated relationship to account for slower growth rates of cervical than central vertebrae (Fig. 3.5); this relationship was estimated based on vertebral radius and fork length data for central and eastern North Atlantic blue sharks examined in this study, and constrained by mean measured vertebral radius and fork length values at birth. For both blue and porbeagle sharks from all areas, age at birth and at maturity were estimated directly from mean measured fork length values using validated Von Bertalanffy relationships (Natanson *et al*., 2002; Skomal & Natanson, 2003), and used as cutoffs to distinguish pre-birth, juvenile and adult life-history stages in time-series and variance analyses. For this thesis, sample age was estimated with statistical models (for a detailed descriptions of these models and associated uncertainity, see Natanson *et al*., 2002; Skomal & Natanson, 2003); in the view of a forthcoming article, it will also be determined more accurately with *annuli*-count by experienced age researchers and co-authors of the manuscript *in prep.* (G.S. and L.N.).

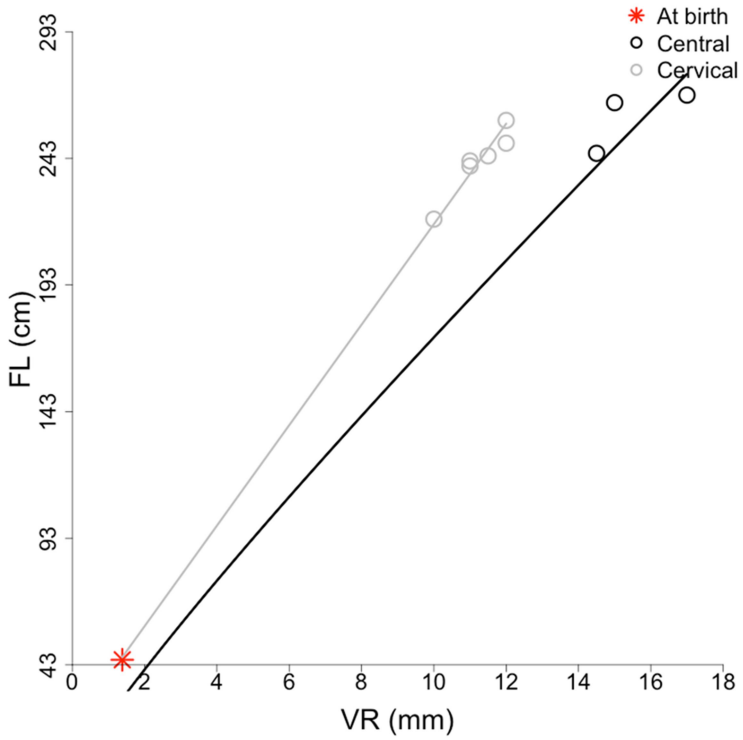

Figure 3.5 Validated vertebral radius-fork length relationship for central vertebrae from generic and Northwest Atlantic blue sharks (Skomal & Natanson, 2003), and estimated linear relationship for cervical vertebrae from central and eastern North Atlantic individuals.
The slope and intercept of the estimated relationship were 19.84 and -18.60, respectively. Lines represent validated and estimated relationships, datapoints measured fork length and vertebral radius data for blue sharks analysed in this study. Black identifies the validated relationship and data for Northwest Atlantic blue sharks, grey the estimated relationship and data for Northeast Atlantic individuals; the red asterisk represents mean measured vertebral radius and fork length values at birth for central vertebrae from generic blue sharks.

3.3.6 Data analysis

Carbon and nitrogen isotopic compositions at each life stage were normalised to the mean isotope values for the individual shark as in Eq. 3.3 (i.e. life-history normalisation). This was done to reduce between-individual variance in isotopic profiles associated with regional variation in isotopic baselines, whilst preserving between-individual variance in the temporal trends of isotopes.

$$n\delta X = \delta X - \text{mean } \delta X_{\text{individual shark}} \quad (3.3)$$

where $n\delta X$ is the delta value of a sample normalised to the mean delta value for all samples from an individual shark, δX is the non-normalised delta value, and mean $\delta X_{\text{individual shark}}$ is the average delta value for all samples from an individual shark. Ontogenetic patterns in isotopic compositions across individual blue and porbeagle sharks were identified using both measured ($\delta^{13}C$, $\delta^{15}N$) and normalised ($n\delta^{13}C$, $n\delta^{15}N$) isotope values, species-level life-history isotopic traits using normalised values. Age classes were determined for each species by subsetting the interval from minimum to maximum age into 25 bins; each age class included 7.80 months in blue sharks, and 11.56 months in porbeagles.

Ontogenetic patterns in measured and normalised isotope values, and the effects of species and capture area on these patterns, were tested with generalised additive mixed models (GAMMs). In this study, the number of sharks sampled varied across life-history, with more individuals sampled during pre-birth and juvenile stages, and fewer sharks sampled with increasing age. Variability in the number of sharks across life-history may influence estimated trends in isotope values (Zuur *et al*., 2014). As the response variables ($\delta^{13}C$, $\delta^{15}N$, $n\delta^{13}C$ and $n\delta^{15}N$ values) were all continuous and potentially varying from $-\infty$ to $+\infty$, a Gaussian linear regression-type distribution, and an identity link function were selected (Zuur *et al*., 2014). As data included multiple isotope measurements from the same shark (i.e. repeated measures), mixed models with random intercept for individual were used (Zuur *et al*., 2014; see also Pinheiro & Bates, 2000). The continuous covariate 'estimated sample age' was added in the models as a smoother. In the full model, the categorical covariates species and area were added as parametric fixed effects (Eq. 3.4).

$$\text{Isotope value}_{is} \sim N(\mu_{is}, \sigma^2)$$

$$E(\text{Isotope value}_{is}) = \mu_{is} \text{ and } \text{var}(\text{Isotope value}_{is}) = \sigma^2$$

$$\mu_{is} = \eta_{is}$$

$$\eta_{is} = \beta_1 + \beta_2 \times \text{fSpecies}_{is} + \beta_3 \times \text{fArea}_{is} + f(\text{Age}_{is}) + a_i \quad (3.4)$$

To test whether patterns in isotopic compositions varied by species and area, and account for potential over-fitting, the full model was compared against the null model using Akaike Information Criteria (AIC). Additionally, separate null and full models were also run and compared for each species (with area as parametric fixed effect). Model parameters were estimated for the full model by fitting the models with maximum likelihood (ML; Zuur *et al*., 2013; 2014). Normalised residuals were plotted against fitted values, and against the covariates included and not included in the model. Residuals were homogenous for models for carbon isotope values (both non-normalised and normalised), and somewhat heterogeneous for nitrogen isotope models; they did not show clear non-linear patterns in any case, and heterogeneity (where present) did not vary between species, or among areas, individuals, and life-history stages.

Normality in measured and normalised isotope values in each combination of species and life stage (i.e. group) was tested with a Shapiro-Wilk test. Homogeneity of variances in measured and normalised isotope values between each pair of groups was tested with a Levene's test where data in both groups were normally distributed, with a Kruskal-Wallis test where data were non-normal. This was done to compare between-individual variance for each species among life stages, and for each life stage between species. Additionally, for each group, variance in measured values was compared against variance in normalised values. Life-history stages (i.e. pre-birth, juvenile and adult) were determined by using estimated ages at birth and at maturity as cutoffs.

Standard ellipse area corrected for small sample size (SEAc) was calculated for each species based on measured isotope values, and used as a proxy for core life-time isotopic niche width (Newsome *et al*., 2007; e.g. Kim *et al*., 2012a; Carlisle *et al*., 2015). Posterior draws of Bayesian-

estimated standard ellipse areas (SEA.B, R = 10000) were also calculated for each species, and the probability that the standard ellipse area for one species is smaller (or larger) than that for the other was determined. The overlap between standard ellipse areas corrected for small sample size for blue and porbeagle sharks was calculated. In order to compare porbeagle samples of comparable age/size between the eastern and western North Atlantic, the same analyses were also repeated after omitting adult samples from Northwest Atlantic porbeagles (i.e. samples with age > age at maturity for porbeagles, i.e. approximately 167 months).

All the analyses were performed using the software package R v.3.2.2 (R Core Team, 2015). Generalised additive mixed models were developed within the mgcv package (Wood, 2006; 2011). Levene's tests for homoscedasticity were performed using the lawstat R package (Gastwirth *et al*., 2015). Standard ellipse areas were estimated using the siar package (Parnell & Jackson, 2013; see also Parnell *et al*., 2010; Jackson *et al*., 2011).

3.4 Results

Raw $\delta^{13}C$ and $\delta^{15}N$ data for each analysed sample are reported in Table 3.3. Carbon isotope values ranged between -16.73 and -13.95 ‰ (mean ± SD: -15.13 ± 0.65 ‰) in blue sharks, and between -15.80 and -13.71 ‰ (-14.55 ± 0. 38 ‰) in porbeagles; $\delta^{15}N$ values varied between 9. 09 and 14.14 ‰ (11. 47 ± 1.11 ‰) in blue sharks, and between 9.42 and 16.29 ‰ (12.84 ± 1.47 ‰) in porbeagles. The range in $\delta^{15}N$ values in porbeagles was strongly influenced by ^{15}N-enriched subadult and adult samples from Northwest Atlantic individuals. When adult samples from Northwest Atlantic porbeagles were omitted, $\delta^{15}N$ values in porbeagles ranged between 10.77-14.00 ‰ (11.90 ± 0.69 ‰). The range, mean and standard deviation for $\delta^{13}C$ and $\delta^{15}N$ values within each individual shark are reported in Table 3.4.

Table 3.3 Raw $\delta^{13}C$ and $\delta^{15}N$ isotope data for each analysed sample; individual ID, sample ID (for combinations of samples, both sample IDs of single samples in the combinations and average sample ID), distance along the vertebral radius (calculated with average sample ID) and age are reported.

Individual ID	Sample ID (combined)	Sample ID (average)	Sample distance (mm)	Sample age (mo)	$\delta^{13}C$ (‰)	$\delta^{15}N$ (‰)
16	1+2	1.5	0.58	-11.82	-15.60	10.23
16	3	3	1.45	-5.95	-15.87	9.93
16	4	4	2.03	-1.82	-16.03	10.45
16	5	5	2.61	2.50	-16.02	10.72
16	6	6	3.18	7.03	-16.29	9.91
16	7	7	3.76	11.80	-15.98	9.09
16	8	8	4.34	16.83	-15.30	9.73
16	9	9	4.92	22.14	-15.38	9.97
16	10	10	5.50	27.78	-15.38	10.40
16	11	11	6.08	33.79	-15.51	10.45
16	12	12	6.66	40.22	-15.53	10.27
16	13	13	7.24	47.13	-15.38	10.51
16	14	14	7.82	54.60	-15.05	10.50
16	15	15	8.39	62.73	-15.08	10.41
16	16	16	8.97	71.64	-15.20	11.24
16	17	17	9.55	81.50	-14.97	11.16
16	18	18	10.13	92.55	-14.70	9.92
16	19	19	10.71	105.10	-14.83	10.08
24	1+2	1.5	0.52	-12.18	-14.92	10.04
24	3	3	1.31	-6.91	-16.01	9.23
24	4	4	1.83	-3.22	-15.61	9.49
24	5	5	2.36	0.62	-15.46	10.12
24	6	6	2.88	4.63	-15.70	10.70
24	7	7	3.40	8.82	-15.97	10.77
24	8	8	3.93	13.21	-16.04	10.12
24	9	9	4.45	17.81	-15.81	10.46
24	10	10	4.98	22.67	-15.82	11.21
24	11	11	5.50	27.78	-15.73	11.19
24	12	12	6.02	33.20	-15.71	10.65
24	13	13	6.55	38.96	-15.78	9.68
24	14	14	7.07	45.10	-15.60	9.40
24	15	15	7.60	51.68	-15.78	9.97
24	16	16	8.12	58.77	-15.32	11.18
24	17	17	8.64	66.44	-14.89	10.79
24	18	18	9.17	74.81	-14.34	10.50
24	19	19	9.69	84.02	-14.39	10.51
24	20	20	10.21	94.24	-14.56	10.81
24	21	21	10.74	105.75	-14.66	10.34
12	1+2	1.5	0.59	-11.76	-15.20	11.37
12	3+4	3.5	1.76	-3.71	-15.76	11.12
12	5	5	2.65	2.82	-15.81	11.40
12	6	6	3.24	7.44	-16.73	10.94
12	7	7	3.82	12.31	-16.49	9.75
12	8	8	4.41	17.45	-15.45	9.47
12	9	9	5.00	22.89	-15.36	11.24
12	10	10	5.59	28.68	-15.38	11.59
12	11	11	6.18	34.85	-15.08	13.03
12	12	12	6.76	41.46	-14.89	11.81
12	13	13	7.35	48.58	-14.53	12.95
12	14	14	7.94	56.30	-13.95	14.13
12	15	15	8.53	64.72	-14.35	13.44
12	16	16	9.12	74.00	-14.22	11.64
12	17	17	9.71	84.30	-14.03	9.43
101	1+2	1.5	0.75	-10.69	-14.43	11.24
101	3	3	1.88	-2.92	-15.49	10.90
101	4	4	2.63	2.65	-15.16	11.55
101	5	5	3.38	8.57	-15.50	11.17
101	6	6	4.13	14.91	-16.03	10.20
101	7	7	4.88	21.71	-15.34	10.18
101	8	8	5.63	29.05	-15.01	10.26
101	9	9	6.38	37.03	-15.22	10.63
101	10	10	7.13	45.76	-14.80	11.03
101	11	11	7.88	55.40	-14.91	11.82
101	12	12	8.63	66.17	-14.40	11.63
101	13	13	9.38	78.36	-14.12	11.01

Individual ID	Sample ID (combined)	Sample ID (average)	Sample distance (mm)	Sample age (mo)	$\delta^{13}C$ (‰)	$\delta^{15}N$ (‰)
101	14	14	10.13	92.42	-14.59	11.79
101	15	15	10.88	109.00	-14.91	11.01
101	16	16	11.63	129.24	-14.35	11.94
131	1	1	0.35	-13.28	-14.36	11.23
131	2	2	1.06	-8.62	-15.07	10.73
131	3	3	1.76	-3.71	-15.81	10.44
131	4	4	2.47	1.47	-16.11	11.05
131	5	5	3.18	6.97	-15.87	11.16
131	6	6	3.88	12.81	-15.05	11.58
131	7	7	4.59	19.05	-14.79	12.03
131	8	8	5.29	25.74	-15.13	11.78
131	9	9	6.00	32.95	-15.08	11.57
131	10	10	6.71	40.78	-14.91	11.67
131	11	11	7.41	49.33	-14.79	11.18
131	12	12	8.12	58.75	-14.59	11.89
131	13	13	8.82	69.24	-14.61	13.25
131	14	14	9.53	81.09	-14.37	11.90
131	15	15	10.24	94.68	-14.73	9.96
131	16	16	10.94	110.62	-14.52	9.39
131	17	17	11.65	129.90	-14.21	9.78
33	1+2	1.5	0.55	-12.02	-14.38	11.32
33	3	3	1.37	-6.50	-15.53	10.17
33	4	4	1.92	-2.62	-15.59	10.91
33	5	5	2.46	1.43	-15.52	11.52
33	6	6	3.01	5.66	-16.26	11.23
33	7	7	3.56	10.09	-15.60	11.19
33	8	8	4.11	14.75	-15.57	11.25
33	9	9	4.65	19.66	-15.27	11.94
33	10	10	5.20	24.84	-14.66	13.49
33	11	11	5.75	30.33	-14.02	13.65
33	12	12	6.30	36.17	-14.76	12.22
33	13	13	6.85	42.40	-15.59	12.30
33	14	14	7.39	49.09	-16.18	12.22
33	15	15	7.94	56.29	-16.00	12.20
33	16	16	8.49	64.11	-14.85	12.53
33	17	17	9.04	72.65	-14.55	10.87
33	18	18	9.58	82.06	-14.83	11.26
33	19	19	10.13	92.54	-14.47	11.49
33	20	20	10.68	104.36	-14.79	11.84
33	21	21	11.23	117.93	-14.54	11.74
335	1	1	0.25	-19.29	-14.54	11.90
335	2+3	2.5	1.00	-14.38	-14.27	12.18
335	4	4	1.75	-9.67	-14.47	11.61
335	5	5	2.25	-6.52	-15.02	10.73
335	6	6	2.75	-3.35	-15.00	11.23
335	7	7	3.25	-0.13	-14.96	11.41
335	8	8	3.75	3.15	-14.96	11.52
335	9	9	4.25	6.50	-15.17	12.01
335	10	10	4.75	9.93	-15.31	12.30
335	11	11	5.25	13.45	-15.19	12.71
335	12	12	5.75	17.07	-15.30	12.93
335	13	13	6.25	20.80	-15.27	13.29
335	14	14	6.75	24.66	-15.19	12.99
335	15	15	7.25	28.64	-15.16	13.53
335	16	16	7.75	32.78	-15.30	14.11
335	17	17	8.25	37.08	-15.27	13.70
335	18	18	8.75	41.56	-15.05	12.90
335	19	19	9.25	46.24	-14.93	12.73
335	20	20	9.75	51.14	-14.80	13.43
335	21	21	10.25	56.28	-14.65	13.39
335	22	22	10.75	61.69	-14.65	14.14
335	23	23	11.25	67.42	-14.72	13.84
335	24	24	11.75	73.49	-14.67	13.86
335	25	25	12.25	79.95	-14.54	11.90
335	26	26	12.75	86.87	-14.37	11.55
335	27	27	13.25	94.32	-14.67	11.33
335	28	28	13.75	102.39	-14.48	11.17
335	29	29	14.25	111.19	-14.60	11.15
335	30	30	14.75	120.89	-14.61	11.20

Individual ID	Sample ID (combined)	Sample ID (average)	Sample distance (mm)	Sample age (mo)	$\delta^{13}C$ (‰)	$\delta^{15}N$ (‰)
335	31	31	15.25	131.68	-14.45	10.83
335	32	32	15.75	143.85	-14.38	10.59
335	33	33	16.25	157.82	-14.24	10.40
335	34	34	16.75	174.23	-14.22	10.39
415	1+2	1.5	0.48	-17.71	-14.54	11.04
415	3	3	1.21	-13.06	-14.96	10.94
415	4	4	1.69	-10.02	-15.40	10.95
415	5	5	2.18	-6.98	-15.40	10.73
415	6	6	2.66	-3.92	-15.73	12.40
415	7	7	3.15	-0.81	-15.66	12.39
415	8	8	3.63	2.35	-15.53	12.08
415	9	9	4.11	5.57	-15.33	12.09
415	10	10	4.60	8.87	-15.24	11.60
415	11	11	5.08	12.24	-15.26	11.83
415	12	12	5.56	15.71	-15.72	12.79
415	13	13	6.05	19.28	-15.79	12.50
415	14	14	6.53	22.96	-15.48	11.44
415	15	15	7.02	26.76	-15.59	11.72
415	16	16	7.50	30.69	-15.86	13.72
415	17	17	7.98	34.77	-15.79	13.22
415	18	18	8.47	39.01	-15.50	12.58
415	19	19	8.95	43.42	-15.37	12.39
415	20	20	9.44	48.03	-15.33	12.11
415	21	21	9.92	52.85	-15.03	11.43
415	22	22	10.40	57.91	-14.99	11.33
415	23	23	10.89	63.23	-14.75	10.97
415	24	24	11.37	68.85	-14.77	10.96
415	25	25	11.85	74.81	-14.66	10.57
415	26	26	12.34	81.14	-14.78	10.78
415	27	27	12.82	87.92	-14.76	10.75
415	28	28	13.31	95.20	-14.72	10.73
415	29	29	13.79	103.07	-14.92	10.93
415	30	30	14.27	111.64	-14.76	10.84
415	31	31	14.76	121.05	-14.35	10.11
441	1	1	0.26	-19.23	-14.55	11.81
441	2	2	0.78	-15.80	-14.88	11.60
441	3	3	1.29	-12.52	-15.24	11.00
441	4	4	1.81	-9.28	-15.51	10.65
441	5	5	2.33	-6.02	-15.76	11.74
441	6	6	2.85	-2.72	-15.97	12.35
441	7	7	3.37	0.63	-15.92	12.48
441	8	8	3.88	4.04	-15.93	12.52
441	9	9	4.40	7.53	-15.83	12.43
441	10	10	4.92	11.11	-15.65	11.37
441	11	11	5.44	14.79	-15.78	11.35
441	12	12	5.96	18.59	-15.90	12.37
441	13	13	6.47	22.51	-15.61	12.33
441	14	14	6.99	26.56	-15.38	12.00
441	15	15	7.51	30.77	-15.38	12.50
441	16	16	8.03	35.14	-15.45	13.92
441	17	17	8.54	39.70	-15.39	13.77
441	18	18	9.06	44.46	-15.07	13.44
441	19	19	9.58	49.45	-14.97	13.06
441	20	20	10.10	54.69	-14.80	12.46
441	21	21	10.62	60.21	-14.90	12.24
441	22	22	11.13	66.06	-14.81	12.32
441	23	23	11.65	72.26	-14.67	11.61
441	24	24	12.17	78.88	-14.50	11.09
441	25	25	12.69	85.98	-14.81	12.34
441	26	26	13.21	93.63	-14.79	11.59
441	27	27	13.72	101.94	-15.14	12.50
441	28	28	14.24	111.03	-14.38	11.57
11	1+2	1.5	0.63	-64.99	-14.05	14.00
11	4	4	2.19	-48.30	-15.00	13.07
11	6	6	3.44	-34.97	-15.22	12.44
11	8	8	4.69	-21.18	-15.38	11.88
11	10	10	5.94	-6.67	-15.80	12.00
11	12	12	7.19	8.75	-14.86	11.19
11	13	13	7.81	16.88	-14.64	11.47

Individual ID	Sample ID (combined)	Sample ID (average)	Sample distance (mm)	Sample age (mo)	$\delta^{13}C$ (‰)	$\delta^{15}N$ (‰)
11	14	14	8.44	25.33	-14.44	11.68
11	15	15	9.06	34.14	-14.57	11.55
11	16	16	9.69	43.35	-14.54	11.58
11	17	17	10.31	53.01	-14.55	11.74
11	18	18	10.94	63.16	-14.39	11.70
11	19	19	11.56	73.88	-14.42	11.57
11	20	20	12.19	85.23	-14.44	11.53
11	21	21	12.81	97.31	-14.25	11.46
11	22	22	13.44	110.24	-14.33	11.53
11	23	23	14.06	124.13	-14.42	11.30
11	24	24	14.69	139.17	-13.94	12.15
40	1+2	1.5	0.52	-66.16	-14.37	11.35
40	4	4	1.82	-52.14	-13.71	11.27
40	6	6	2.86	-41.12	-13.77	11.49
40	8	8	3.91	-29.87	-13.97	11.54
40	10	10	4.95	-18.22	-15.14	10.77
40	11	11	5.47	-12.21	-14.94	11.15
40	12	12	5.99	-6.05	-14.92	11.55
40	13	13	6.51	0.27	-14.43	13.04
40	14	14	7.03	6.76	-14.62	12.72
40	15	15	7.55	13.46	-14.78	12.21
40	16	16	8.07	20.36	-14.81	12.27
40	17	17	8.59	27.50	-14.28	13.28
40	18	18	9.11	34.89	-14.36	13.27
40	19	19	9.64	42.57	-14.47	12.56
40	20	20	10.16	50.55	-14.42	11.96
40	21	21	10.68	58.86	-14.08	12.91
40	22	22	11.20	67.55	-14.10	12.74
40	23	23	11.72	76.65	-14.30	12.46
40	24	24	12.24	86.21	-14.39	12.08
1000	1	1	0.32	-68.44	-15.19	12.98
1000	3	3	1.61	-54.34	-14.79	12.25
1000	5	5	2.91	-40.67	-15.14	12.45
1000	7	7	4.20	-26.65	-15.44	11.87
1000	9	9	5.49	-11.97	-14.71	11.29
1000	11	11	6.78	3.62	-14.58	11.41
1000	12	12	7.43	11.83	-14.49	11.59
1000	13	13	8.07	20.36	-14.18	11.37
1000	14	14	8.72	29.25	-14.15	12.47
1000	15	15	9.36	38.54	-14.19	12.27
1000	16	16	10.01	48.28	-14.33	11.32
1000	17	17	10.66	58.52	-14.30	11.14
1000	18	18	11.30	69.34	-14.57	11.33
1000	19	19	11.95	80.80	-14.47	11.51
1000	20	20	12.59	93.00	-14.83	11.16
1000	21	21	13.24	106.05	-14.74	11.13
1000	22	22	13.89	120.09	-14.77	11.15
1000	23	23	14.53	135.29	-14.88	11.13
1000	24	24	15.18	151.88	-15.13	11.95
599	1	1	0.27	-69.03	-14.96	11.77
599	3	3	1.37	-56.96	-14.60	11.80
599	5	5	2.46	-45.40	-14.16	11.53
599	7	7	3.55	-33.70	-14.32	11.73
599	9	9	4.65	-21.62	-14.24	11.55
599	11	11	5.74	-9.00	-14.23	11.54
599	13	13	6.84	4.31	-15.28	12.73
599	14	14	7.38	11.26	-15.17	12.58
599	15	15	7.93	18.44	-15.13	12.61
599	16	16	8.48	25.87	-14.65	12.83
599	17	17	9.02	33.58	-14.71	12.58
599	18	18	9.57	41.59	-14.30	12.75
599	19	19	10.12	49.94	-14.15	12.50
599	20	20	10.66	58.65	-14.14	12.54
599	21	21	11.21	67.77	-14.02	12.83
599	22	22	11.76	77.35	-14.35	12.72
599	23	23	12.30	87.44	-14.12	13.21
599	24	24	12.85	98.10	-14.11	13.38
599	25	25	13.40	109.40	-13.96	14.42
599	26	26	13.95	121.44	-13.94	15.38

Individual ID	Sample ID (combined)	Sample ID (average)	Sample distance (mm)	Sample age (mo)	$\delta^{13}C$ (‰)	$\delta^{15}N$ (‰)
599	27	27	14.49	134.33	-13.82	15.71
599	28	28	15.04	148.21	-14.26	15.69
599	29	29	15.59	163.23	-14.34	15.77
599	30	30	16.13	179.63	-14.02	14.97
599	31	31	16.68	197.69	-14.29	15.54
599	32	32	17.23	217.79	-14.19	15.45
601	1	1	0.26	-69.22	-15.01	13.94
601	3	3	1.29	-57.82	-14.98	14.09
601	5	5	2.32	-46.94	-14.88	14.00
601	7	7	3.35	-35.96	-14.83	14.06
601	9	9	4.38	-24.68	-14.80	14.14
601	11	11	5.40	-12.96	-14.79	14.04
601	13	13	6.43	-0.67	-15.06	13.06
601	15	15	7.46	12.30	-15.51	12.66
601	16	16	7.98	19.09	-15.07	12.85
601	17	17	8.49	26.10	-14.78	12.63
601	18	18	9.01	33.35	-14.77	12.59
601	19	19	9.52	40.87	-14.88	12.80
601	20	20	10.04	48.69	-14.90	13.24
601	21	21	10.55	56.82	-14.92	12.79
601	22	22	11.07	65.32	-14.68	12.64
601	23	23	11.58	74.20	-14.28	12.77
601	24	24	12.10	83.52	-14.04	12.81
601	25	25	12.61	93.32	-14.53	12.69
601	26	26	13.13	103.66	-14.50	12.94
601	27	27	13.64	114.62	-14.63	13.46
601	28	28	14.15	126.27	-14.56	14.68
601	29	29	14.67	138.71	-14.30	15.06
601	30	30	15.18	152.06	-14.56	15.51
601	31	31	15.70	166.49	-14.64	15.76
601	32	32	16.21	182.17	-14.69	15.53
601	33	33	16.73	199.37	-14.73	15.62
601	34	34	17.24	218.42	-14.59	15.72
578	1	1	0.28	-68.91	-14.53	11.69
578	3	3	1.42	-56.44	-14.33	11.94
578	5	5	2.55	-44.46	-14.33	11.94
578	7	7	3.68	-32.30	-14.36	11.79
578	9	9	4.82	-19.71	-15.09	9.42
578	11	11	5.95	-6.52	-15.31	11.83
578	13	13	7.08	7.43	-14.54	12.17
578	14	14	7.65	14.74	-14.58	12.62
578	15	15	8.22	22.31	-14.48	12.14
578	16	16	8.78	30.16	-14.62	12.00
578	17	17	9.35	38.33	-14.59	12.32
578	18	18	9.92	46.84	-14.56	12.52
578	19	19	10.48	55.73	-14.51	12.67
578	20	20	11.05	65.04	-14.17	13.24
578	21	21	11.62	74.83	-14.27	14.57
578	22	22	12.18	85.15	-14.34	14.01
578	23	23	12.75	96.07	-14.20	15.09
578	24	24	13.32	107.67	-14.31	15.40
578	25	25	13.88	120.04	-14.40	15.66
578	26	26	14.45	133.31	-14.59	15.66
578	27	27	15.02	147.62	-14.29	16.29
578	28	28	15.58	163.16	-14.39	16.15
578	29	29	16.15	180.17	-14.37	15.93
578	30	30	16.72	198.98	-14.39	15.78

Table 3.4 Range, mean and standard deviation (SD) for $\delta^{13}C$ and $\delta^{15}N$ values within each individual shark.

	$\delta^{13}C$ (‰)			$\delta^{15}N$ (‰)			
Individual ID	**Range**	**Mean**	**SD**	**Range**	**Mean**	**SD**	**N**
16	-16.29 -14.70	-15.45	0.45	9.09 - 11.24	10.28	0.50	18
24	-16.04 -14.34	-15.40	0.56	9.23 - 11.21	10.36	0.59	20
12	-16.73 -13.95	-15.15	0.84	9.43 - 14.13	11.55	1.39	15
101	-16.03 -14.12	-14.95	0.52	10.18 - 11.94	11.09	0.59	15
131	-16.11 -14.21	-14.94	0.55	9.39 - 13.25	11.21	0.95	17
33	-16.26 -14.02	-15.15	0.64	10.17 - 13.65	11.77	0.85	20
335	-15.31 -14.22	-14.80	0.35	10.39 - 14.14	12.21	1.16	33
415	-15.86 -14.35	-15.20	0.43	10.11 - 13.72	11.60	0.88	30
441	-15.97 -14.38	-15.25	0.49	10.65 - 13.92	12.16	0.78	28
11	-15.80 -13.94	-14.62	0.47	11.19 - 14.00	11.88	0.69	18
40	-15.14 -13.71	-14.41	0.39	10.77 - 13.28	12.14	0.76	19
1000	-15.44 -14.15	-14.68	0.37	11.13 - 12.98	11.67	0.56	19
599	-15.28 -13.82	-14.36	0.40	11.53 - 15.77	13.31	1.50	26
601	-15.51 -14.04	-14.74	0.29	12.59 - 15.76	13.78	1.12	27
578	-15.31 -14.17	-14.48	0.26	9.42 - 16.29	13.45	1.90	24

3.4.1 Ontogenetic patterns in carbon and nitrogen isotopic compositions within species

3.4.1.1 Patterns in measured (non-normalised) carbon and nitrogen isotope values

Distributions of measured carbon ($\delta^{13}C$) and nitrogen ($\delta^{15}N$) isotopic compositions for each age class across individual blue sharks are presented in Fig. 3.6, and across individual porbeagles in Fig. 3.7. Common, broad ontogenetic patterns in $\delta^{13}C$ and $\delta^{15}N$ values were identified across individuals of both species (Fig. 3.6 and 3.7), despite variability in isotopic profiles among areas and individuals associated with regional variation in isotopic baselines (see below). Patterns in $\delta^{13}C$ and $\delta^{15}N$ values were non-linear (smoother 'estimated sample age': maximum p-value = $3.260 \cdot 10^{-14} < 0.05$, F = 13.980), and differed significantly between species (maximum p-value = 0.0006 < 0.05, F = 11.938); patterns in $\delta^{15}N$ values also differed significantly among areas (p-value = $1.520 \cdot 10^{-9} < 0.05$, F = 12.600), whereas patterns in $\delta^{13}C$ values did not (p-value = 0.079, F = 2.116; Table 3.5 and 3.6A).

In blue sharks, $\delta^{13}C$ values consistently progressively increased by ~ 1‰ during juvenile and subadult life-history stages until reaching a relatively steady state during the adult stage (Fig. 3.6A). Values of $\delta^{15}N$ also increased by ~ 1‰ during the juvenile stage, but decreased by ~ 2‰ during subadult and adult stages (Fig. 3.6B). Both $\delta^{13}C$ and $\delta^{15}N$ values decreased sharply by ~ 1‰ around birth (Fig. 3.6). Patterns in $\delta^{13}C$ and $\delta^{15}N$ values in blue sharks were non-linear (smoother: maximum p-value = $1.720 \cdot 10^{-14} < 0.05$, F = 18.700), and differed significantly among areas (minimum p-value = 0.036, F =3.386; Table 5 and 3.6B).

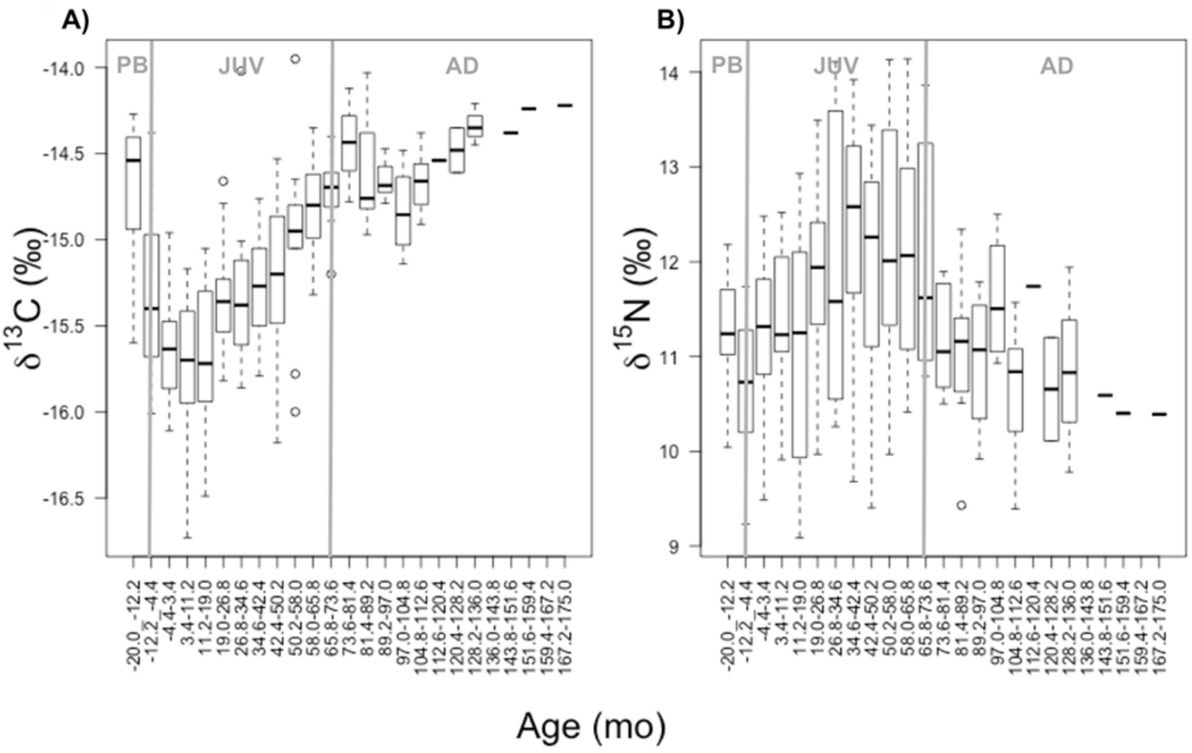

Figure 3.6 Ontogenetic patterns in carbon and nitrogen isotopic compositions in blue sharks. Distributions of measured carbon ($\delta^{13}C$) and nitrogen ($\delta^{15}N$) isotopic compositions for each age class (7.80 months) across individual blue sharks. Grey vertical lines represent estimated age at birth and age at maturity. Accordingly, samples with age < age at birth represent pre-birth (PB) life stages, with age > age at birth and < age at maturity juvenile (JUV) stages, and with age > age at maturity adult (AD) stages. For each life stage, the boxplot displays the variation in isotope values across individuals. The horizontal line in each boxplot represents the median of the data (i.e. 50% of the data are greater than this value). The lower and upper limits of the boxplot represent the lower and upper quartile (i.e. 25% of the data less or greater than this value), respectively. The lower and upper whiskers represent the minimum and maximum value excluding outliers, respectively. Dots at the bottom or top of whiskers represent outliers (i.e. less and more than 3/2 times of the lower and upper quartile, respectively).

Table 3.5 Degrees of freedom (DF) and Akaike Information Criteria (AIC) for generalised additive mixed effect models (GAMMs) predicting profile measured ($\delta^{13}C$, $\delta^{15}N$) and normalised ($n\delta^{13}C$, $n\delta^{15}N$) carbon and nitrogen isotope values. The null model included sample age as smoother and individual as random effect (random intercept), but no parametric fixed effects. Models with AIC > 2 lower than the null model (in bold) were considered as optimal; otherwise, the null model was considered as optimal.

A) All data

		AIC			
Model	**DF**	**$\delta^{13}C$**	**$\delta^{15}N$**	**$n\delta^{13}C$**	**$n\delta^{15}N$**
δ value ~ age + ind	5	349.463	987.588	305.475	**935.135**
δ value ~ age + ind + sp	6	**337.202**	980.9022	**300.519**	934.675
δ value ~ age + ind + sp + loc	10	338.267	**967.050**	306.329	938.796

B) Blue sharks

		AIC			
Model	**DF**	**$\delta^{13}C$**	**$\delta^{15}N$**	**$n\delta^{13}C$**	**$n\delta^{15}N$**
δ value ~ age + ind	5	**181.033**	504.001	**160.356**	**470.997**
δ value ~ age + ind + sp + loc	7	179.798	**497.848**	160.619	473.811

C) Porbeagles

		AIC			
Model	**DF**	**$\delta^{13}C$**	**$\delta^{15}N$**	**$n\delta^{13}C$**	**$n\delta^{15}N$**
δ value ~ age + ind	5	**102.358**	391.487	**87.761**	380.280
δ value ~ age + ind + sp + loc	7	104.925	**380.354**	90.7832	**376.463**

Table 3.6 Results for full GAMMs predicting profile $\delta^{13}C$, $\delta^{15}N$, $n\delta^{13}C$ and $n\delta^{15}N$ values. Estimated sample age was added into models as smoother (f(Age)), individual as random effect (random intercept), and species and/or capture area as parametric fixed effects (fSpecies, fArea; full model), predictors with p-values < 0.05 (in bold) were considered significant. Model parameter estimates for fixed effects are reported in Table 3.7.

A) All data

	$\delta^{13}C$ (‰)			$\delta^{15}N$ (‰)			$n\delta^{13}C$ (‰)			$n\delta^{15}N$ (‰)		
Parameters	**DF**	**F**	**p-value**	**DF**	**F**	**p-value**	**DF**	**F**	**p-value**	**DF**	**F**	**p-value**
fSpecies	1	11.938	**0.0006**	1	23.760	**$1.710 \cdot 10^{-6}$**	1	4.688	**0.031**	1	4.157	**0.042**
fArea	4	2.116	0.079	4	12.600	**$1.520 \cdot 10^{-9}$**	4	0.540	0.707	4	0.959	0.430
f(Age)	7.377	28.430	**$< 2.000 \cdot 10^{-16}$**	5.973	13.980	**$3.260 \cdot 10^{-14}$**	7.433	29.310	**$< 2.000 \cdot 10^{-16}$**	5.988	14.340	**$1.070 \cdot 10^{-14}$**
R^2 (adj.)	0.536			0.537			0.384			0.191		
Scale est.	0.131			0.871			0.126			0.833		
n	339			339			399			339		

B) Blue sharks

	$\delta^{13}C$ (‰)			$\delta^{15}N$ (‰)			$n\delta^{13}C$ (‰)			$n\delta^{15}N$ (‰)		
Parameters	**DF**	**F**	**p-value**	**DF**	**F**	**p-value**	**DF**	**F**	**p-value**	**DF**	**F**	**p-value**
fArea	2	3.386	**0.036**	2	9.451	**0.0001**	2	1.864	0.158	2	0.586	0.558
f(Age)	7.866	38.520	**$< 2.000 \cdot 10^{-16}$**	4.512	18.700	**$1.720 \cdot 10^{-14}$**	7.896	39.360	**$< 2.000 \cdot 10^{-16}$**	4.562	19.500	**$1.070 \cdot 10^{-14}$**
R^2 (adj.)	0.597			0.431			0.601			0.297		
Scale est.	0.107			0.544			0.103			0.524		
n	204			204			204			204		

C) Porbeagles

	$\delta^{13}C$ (‰)			$\delta^{15}N$ (‰)			$n\delta^{13}C$ (‰)			$n\delta^{15}N$ (‰)		
Parameters	**DF**	**F**	**p-value**	**DF**	**F**	**p-value**	**DF**	**F**	**p-value**	**DF**	**F**	**p-value**
fArea	2	0.783	0.459	2	26.240	**$2.780 \cdot 10^{-10}$**	2	0.480	0.620	2	4.173	**0.017**
f(Age)	4.927	8.499	**$6.020 \cdot 10^{-7}$**	3.492	30.990	**$< 2.000 \cdot 10^{-16}$**	5.028	8.840	**$2.430 \cdot 10^{-7}$**	3.553	31.45	**$< 2.000 \cdot 10^{-16}$**
R^2 (adj.)	0.207			0.608			0.245			0.451		
Scale est.	0.097			0.828			0.093			0.803		
n	135			135			135			135		

Table 3.7 Parameter estimates, t- and p-values for fixed effects in full GAMMs predicting profile profile $\delta^{13}C$, $\delta^{15}N$, $n\delta^{13}C$ and $n\delta^{15}N$ values; fixed effects are species and/or capture area, depending on whether models include all data, or blue or porbeagle shark data.

A) All data

	$\delta^{13}C$ (‰)			**$\delta^{15}N$ (‰)**			**$n\delta^{13}C$ (‰)**			**$n\delta^{15}N$ (‰)**		
Parameters	**Estimate ± SD**	**t-value**	**p-value**	**Estimate ± SD**	**t-value**	**p-value**	**Estimate ± SD**	**t-value**	**p-value**	**Estimate ± SD**	**t-value**	**p-value**
Intercept	-14.949 ± 0.087	-171.270	**$< 2 \cdot 10^{-16}$**	11.449 ± 0.190	60.323	**$< 2 \cdot 10^{-16}$**	0.044 ± 0.049	0.899	0.369	0.081 ± 0.127	0.638	0.524
Species: POR	0.406 ± 0.117	3.455	**0.0006**	1.218 ± 0.250	4.874	**$1.71 \cdot 10^{-6}$**	-0.129 ± 0.059	-2.165	**0.031**	-0.311 ± 0.152	-2.039	**0.042**
Area: FI	-0.208 ± 0.208	-1.002	0.317	-0.984 ± 0.447	-2.203	**0.028**	0.012 ± 0.111	0.111	0.912	0.240 ± 0.286	0.842	0.400
Area: MAR	-0.308 ± 0.308	-2.518	**0.012**	-0.658 ± 0.266	-2.481	**0.014**	0.041 ± 0.068	0.596	0.551	0.017 ± 0.175	0.096	0.924
Area: NWA	-0.088 ± 0.088	-0.747	0.456	0.596 ± 0.253	2.354	**0.019**	-0.016 ± 0.061	-0.268	0.789	-0.021 ± 0.158	-0.137	0.891
Area: WEC	0.022 ± 0.022	0.123	0.902	-0.528 ± 0.385	-1.372	0.171	0.066 ± 0.095	0.697	0.486	0.324 ± 0.244	1.328	0.185

B) Blue sharks

	$\delta^{13}C$ (‰)			**$\delta^{15}N$ (‰)**			**$n\delta^{13}C$ (‰)**			**$n\delta^{15}N$ (‰)**		
Parameters	**Estimate ± SD**	**t-value**	**p-value**	**Estimate ± SD**	**t-value**	**p-value**	**Estimate ± SD**	**t-value**	**p-value**	**Estimate ± SD**	**t-value**	**p-value**
Intercept	-14.983 ± 0.081	-185.181	**$< 2 \cdot 10^{-16}$**	11.360 ± 0.235	48.358	**$< 2 \cdot 10^{-16}$**	0.010 ± 0.044	0.237	0.813	-0.0003 ± 0.099	-0.004	0.997
Area: MAR	-0.295 ± 0.114	-2.592	**0.010**	-0.744 ± 0.332	-2.245	**0.026**	0.051 ± 0.062	0.829	0.408	-0.083 ± 0.139	-0.595	0.552
Area: NWA	-0.127 ± 0.111	-0.151	0.251	0.669 ± 0.325	2.055	**0.041**	-0.054 ± 0.056	-0.975	0.331	-0.052 ± 0.125	0.412	0.681

C) Porbeagles

	$\delta^{13}C$ (‰)			**$\delta^{15}N$ (‰)**			**$n\delta^{13}C$ (‰)**			**$n\delta^{15}N$ (‰)**		
Parameters	**Estimate ± SD**	**t-value**	**p-value**	**Estimate ± SD**	**t-value**	**p-value**	**Estimate ± SD**	**t-value**	**p-value**	**Estimate ± SD**	**t-value**	**p-value**
Intercept	-14.679 ± 0.142	-103.225	**$< 2 \cdot 10^{-16}$**	11.799 ± 0.121	55.677	**$< 2 \cdot 10^{-16}$**	-0.0007 ± 0.071	-0.010	0.992	0.127 ± 0.209	0.606	0.545
Area: NWA	0.130 ± 0.163	0.797	0.427	1.524 ± 0.238	6.394	**$2.740 \cdot 10^{-9}$**	-0.020 ± 0.080	-0.249	0.804	-0.323 ± 0.235	-1.376	0.171
Area: WEC	0.217 ± 0.174	1.245	0.215	0.573 ± 0.259	2.214	**0.029**	0.042 ± 0.087	0.481	0.631	0.199 ± 0.255	0.783	0.435

In porbeagles, $\delta^{13}C$ values consistently increased by < 1‰ during the juvenile stage until an age of ~ 57-69 months, and remained relatively constant until capture (Fig. 3.7A). Values of $\delta^{15}N$ showed two stepwise increases throughout ontogeny: a smaller increase (< 1‰) just after birth, and a larger increase (> 2‰) at an age of ~ 92-103 months; during intermediate juvenile and adult periods, they remained relatively constant (Fig. 3.7B). The ontogenetic pattern in $\delta^{15}N$ values in porbeagles was strongly driven by a stepwise increase in $\delta^{15}N$ values during subadult life-history stages in Northwest Atlantic individuals; when adult samples from Northwest Atlantic porbeagles were omitted, $\delta^{15}N$ values showed a similar ontogenetic pattern, except that they did not reach a plateau, as the plateau-phase only regarded adult samples from Northwest Atlantic individuals. Both $\delta^{13}C$ and $\delta^{15}N$ values decreased sharply by < 1‰ and > 1‰ respectively immediately after birth (Fig. 3.7). Patterns in $\delta^{13}C$ and $\delta^{15}N$ values in porbeagles were non-linear (smoother: maximum p-value = $6.020 \cdot 10^{-7}$ < 0.05, F = 8.499; Table 5 and 3.6C); patterns in $\delta^{15}N$ values differed significantly between eastern and western North Atlantic individuals (F = 26.240, p-value = $2.780 \cdot 10^{-10}$ < 0.05), whereas patterns in $\delta^{13}C$ values did not (F = 0.783, p-value = 0.459; Table 5 and 3.6C).

Results for comparisons of variance in $\delta^{13}C$ and $\delta^{15}N$ values between species and among life-history stages are reported in Table 3.8; note that between-individual variance in measured (non-normalised) isotope values is affected by regional variation in isotopic baselines.

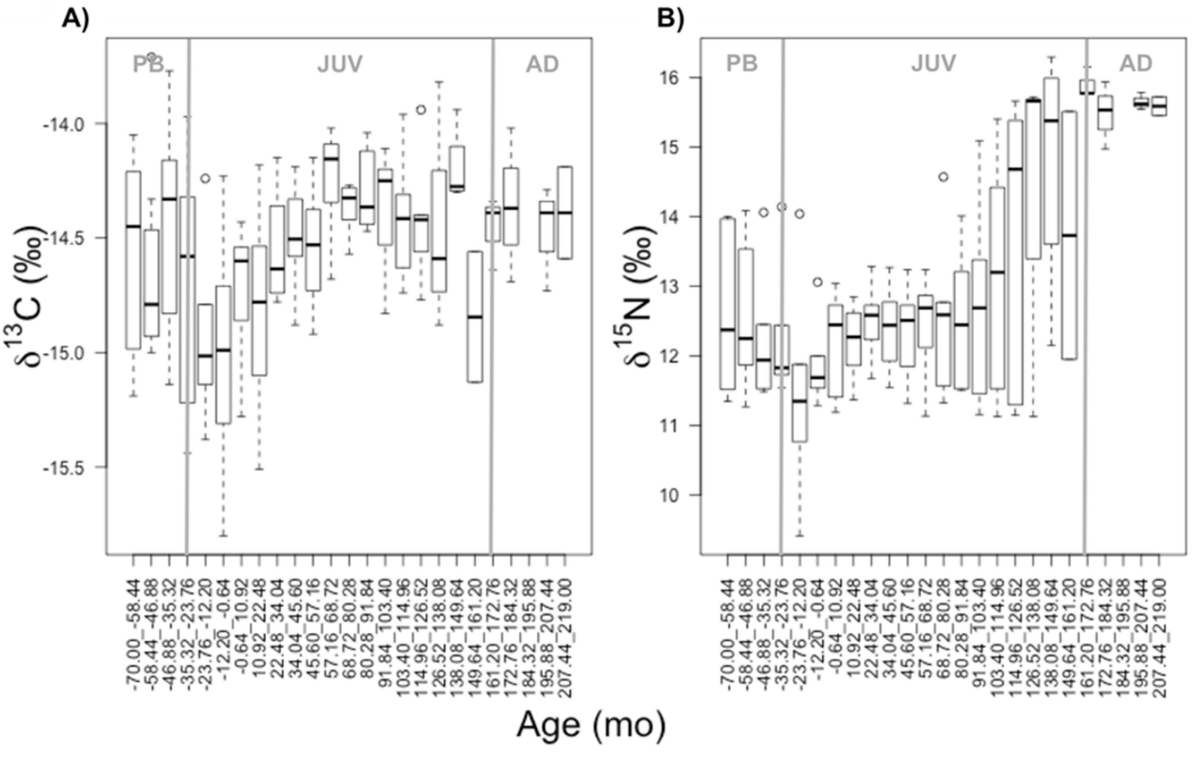

Figure 3.7 Ontogenetic patterns in carbon and nitrogen isotopic compositions in porbeagle sharks. Distributions of $\delta^{13}C$ and $\delta^{15}N$ values for each age class (11.56 months) across individual porbeagles. Grey vertical lines represent estimated age at birth and age at maturity. PB, JUV and AD represent pre-birth, juvenile and adult life stages.

Table 3.8 Results for comparisons of between-individual variance in $\delta^{13}C$, $\delta^{15}N$, $n\delta^{13}C$ and $n\delta^{15}N$ values between pairs of combinations of species (i.e. blue shark – bsh, porbeagle – por) and life-history stage (i.e. pre-birth – PB, juvenile – JUV, and adult – AD): i.e. groups. Difference in standard deviation (SD diff), Levene's test (or Kruskal-Wallis' test, where data were non-normally distributed) result, and p-value are reported; where p-value were < 0.05 (in bold), variances are considered non-equal.

		$\delta^{13}C$ (‰)			**$\delta^{15}N$ (‰)**			**$n\delta^{13}C$ (‰)**			**$n\delta^{15}N$ (‰)**		
Level	**Comparison**	**SD diff**	**L (K-W)**	**p-value**	**SD diff**	**L (K-W)**	**p-value**	**SD diff**	**L (K-W)**	**p-value**	**SD diff**	**L (K-W)**	**p-value**
bsh	PB-JUV	0.031	1.624	0.202	-0.489	10.387	**0.001**	-0.046	1.729	0.188	-0.428	9.457	**0.003**
bsh	PB-AD	0.244	15.816	**$6.980 \cdot 10^{-5}$**	-0.279	2.407	0.121	0.119	9.764	**0.002**	-0.546	15.694	**0.0002**
bsh	AD-JUV	-0.213	16.872	**$6.117 \cdot 10^{-5}$**	-0.210	5.952	**0.015**	0.165	7.081	**0.008**	-0.118	2.070	0.152
por	PB-JUV	0.082	4.646	**0.031**	-0.363	0.0003	0.985	0.024	0.911	0.340	0.074	4.436	**0.036**
por	PB-AD	0.208	5.431	**0.027**	0.751	10.383	**0.001**	0.282	8.369	**0.007**	0.913	15.349	**$8.935 \cdot 10^{-5}$**
por	AD-JUV	-0.126	0.771	0.380	-1.113	8.258	**0.004**	0.258	8.192	**0.004**	0.893	9.479	**0.002**
PB	BSH-POR	0.041	0.317	0.573	-0.344	6.086	**0.013**	-0.008	0.934	0.761	-0.798	24.339	**$8.079 \cdot 10^{-7}$**
JUV	BSH-POR	0.093	5.489	**0.019**	-0.218	0.221	0.638	0.062	2.620	0.106	-0.296	4.759	**0.029**
AD	BSH-POR	0.005	0.032	0.859	0.685	8.734	**0.003**	0.155	5.337	**0.024**	0.661	6.723	**0.012**

3.4.1.2 Patterns in normalised isotope values: species-level life-history isotopic traits

Distributions of normalised carbon ($n\delta^{13}C$) and nitrogen ($n\delta^{15}N$) isotope values for each age class across individual blue sharks are presented in Fig. 3.8, and across individual porbeagles in Fig. 3.9. Common, broad ontogenetic patterns in $n\delta^{13}C$ and $n\delta^{15}N$ values across blue and porbeagle sharks identified species-level life-history isotopic traits, after between-area and individual variance associated with regional variation in isotopic baselines was removed. Patterns in $n\delta^{13}C$ and $n\delta^{15}N$ values were non-linear (smoother: maximum p-value = $1.070 \cdot 10^{-14} < 0.05$, F = 14.340), and differed significantly between species (maximum p-value = 0.042 < 0.05, F = 4.157), but not among areas (minimum p-value = 0.430, F = 0.959; Table 5 and 3.6A). Patterns in normalised isotope values were similar to patterns in non-normalised values (see Fig. 3.6 and 3.7), and generally showed smaller between-individual variance, except for carbon isotopes in adult blue shark samples, and nitrogen isotopes in pre-birth and adult porbeagle samples (Table 3.9; Fig. 3.6-3.9). Differences in variances between normalised and non-normalised isotope values were generally not statistically significant (minimum p-value = 0.057, Levene's test = 3.625), except for carbon isotopes in juvenile blue sharks, and juvenile and adult porbeagles (maximum p-value = 0.035 < 0.05, Levene's test = 5.470; Table 3.9).

Table 3.9 For each combination of species and life-history stage (i.e. group), comparison of variance between $\delta^{13}C$, $\delta^{15}N$ and $n\delta^{13}C$, $n\delta^{15}N$ values.

A) Blue sharks

	bsh.PB			**bsh.JUV**			**bsh.AD**		
Comparison	**SD diff**	**L (K-W)**	**p-value**	**SD diff**	**L (K-W)**	**p-value**	**SD diff**	**L (K-W)**	**p-value**
$\delta^{13}C$-$n\delta^{13}C$ (‰)	0.119	3.625	0.057	0.043	6.188	**0.013**	-0.005	0.007	0.933
$\delta^{15}N$-$n\delta^{15}N$ (‰)	0.285	2.479	0.115	0.345	0.960	0.327	0.018	0.100	0.752

B) Porbeagles

	por.PB			**por.JUV**			**por.AD**		
Comparison	**SD diff**	**L (K-W)**	**p-value**	**SD diff**	**L (K-W)**	**p-value**	**SD diff**	**L (K-W)**	**p-value**
$\delta^{13}C$-$n\delta^{13}C$ (‰)	0.070	1.652	0.205	0.013	7.309	**0.006**	0.145	5.470	**0.035**
$\delta^{15}N$-$n\delta^{15}N$ (‰)	-0.168	0.930	0.340	0.268	1.384	0.239	-0.006	0.422	0.526

In blue sharks, $n\delta^{13}C$ values decreased sharply by ~ 1‰ immediately after birth, and increased progressively during juvenile and subadult stages by 1‰, until reaching a plateau during the adult stage; $n\delta^{13}C$ values during the adult stages were similar to pre-birth levels (Fig. 3.8A). Values of $n\delta^{15}N$ decreased slightly by ~ 0.5‰ around birth, increased by 1‰ during the juvenile stage, and decreased by 2‰ during subadult and adult stages (Fig. 3.8B). Patterns in $n\delta^{13}C$ and $n\delta^{15}N$ values in blue sharks were non-linear (smoother: maximum p-value = $1.070 \cdot 10^{-14} < 0.05$, F = 19.500), and did not differ significantly among areas (minimum p-value = 0.158, F =1.864, Table 5 and 3.6B). Between-individual variances in $n\delta^{13}C$ values during pre-birth and juvenile life-history stages were significantly larger than variance during the adult stage (maximum p-value = 0.002 < 0.05, Levene's test = 9.764), but statistically comparable to one another (Levene's test = 1.729, p-value = 0.188).

Variances in $n\delta^{15}N$ values during juvenile and adult stages were significantly larger than variance during the pre-birth stage (maximum p-value = 0.003 < 0.05, Levene's test = 9.457), and were comparable to one another (Levene's test = 2.070, p = 0.152, Table 3.8).

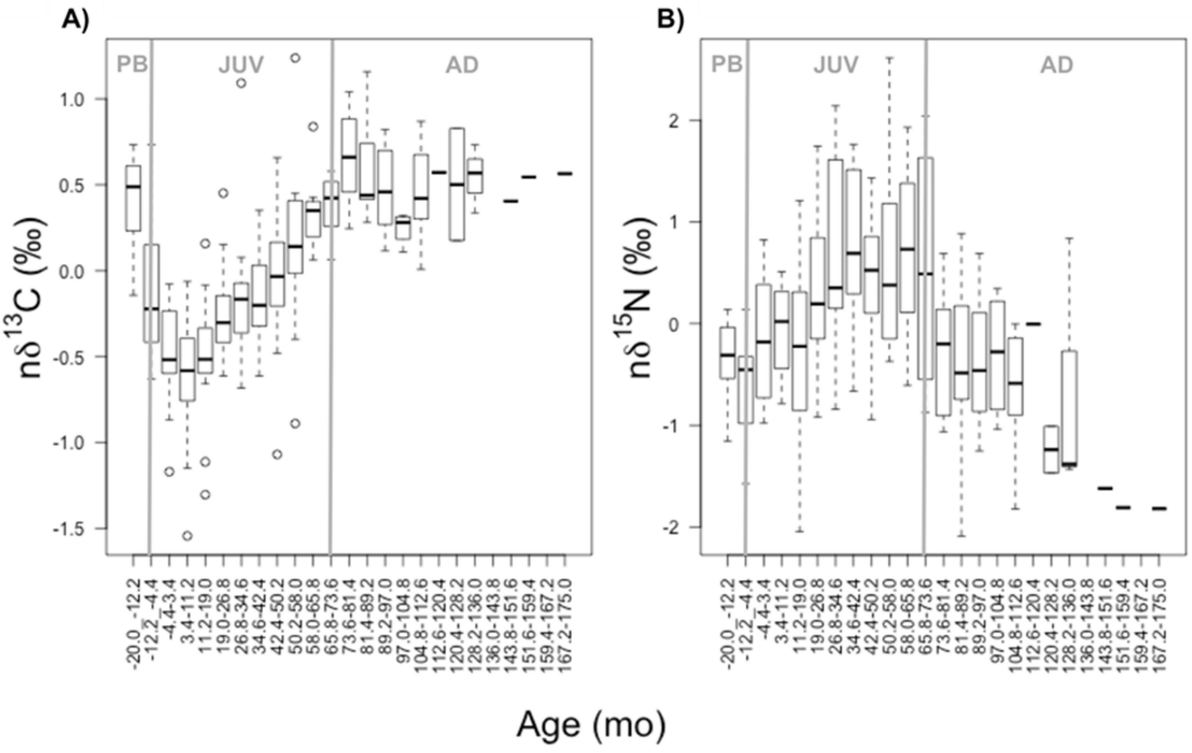

Figure 3.8 Life-history traits in carbon and nitrogen isotopic compositions in blue sharks. Distributions of sample-normalised carbon ($n\delta^{13}C$) and nitrogen ($n\delta^{15}N$) isotopic compositions for each age class (7.80 months) across individual blue sharks. Grey vertical lines represent estimated age at birth and age at maturity. PB, JUV and AD represent pre-birth, juvenile and adult life stages.

In porbeagles, $n\delta^{13}C$ values decreased sharply by < 1‰ just after birth, increased by ~ 1‰ during the juvenile stage until an age of ~ 57-69 months, and remained relatively constant until capture (Fig. 3.9A). Values of $n\delta^{15}N$ increased slightly slightly by ~ 0.5‰ around birth, increased by another 0.5‰ and remained relatively constant during the juvenile stage, and increased stepwise by > 2‰ to a plateau during subadult stages, from an age of ~ 115 months to an age of ~ 138 months (Fig. 3.9B). Neither $n\delta^{13}C$ nor $n\delta^{15}N$ values showed a clear pattern during pre-birth stages (Fig. 3.9). Patterns in $n\delta^{13}C$ and $n\delta^{15}N$ values in porbeagles were non-linear (smoother: maximum p-value = $2.430 \cdot 10^{-7}$ < 0.05, F = 8.840); patterns in $n\delta^{15}N$ values differed significantly between eastern and western North Atlantic individuals (F = 4.173, p-value = 0.017 < 0.05), whereas patterns in $n\delta^{13}C$ values did not (F = 0.480, p-value = 0.620; Table 5 and 3.6C). Between-individual variances in $n\delta^{13}C$ values during pre-birth and juvenile life-history stages were significantly larger than variance at the adult stage (maximum p-value = 0.007 < 0.05, Levene's test = 8.369), but comparable to one another (Levene's test = 0.911, p-value = 0.340). Variances in $n\delta^{15}N$ values differed significantly among all three life-history stages (maximum p-value = 0.036, Levene's test = 4.436, Table 3.8), with highest

and lowest variance in pre-birth and adult samples, respectively (as adult samples only regarded Northwest Atlantic individuals).

Finally, variance in $n\delta^{13}C$ values in blue sharks was significantly higher than variance in porbeagles at the adult stage (Levene's test = 5.337, p-value = 0.024 < 0.05), and comparable to that in porbeagles during pre-birth and juvenile stages (minimum p-value = 0.106, Levene's test = 2.620, Table 3.8). Variances in $n\delta^{15}N$ values differed significantly between blue and porbeagle sharks during all stages (maximum p-value = 0.029 < 0.05, Levene's test = 4.759, Table 3.8), with highest and lowest variance in porbeagle pre-birth and adult samples, respectively.

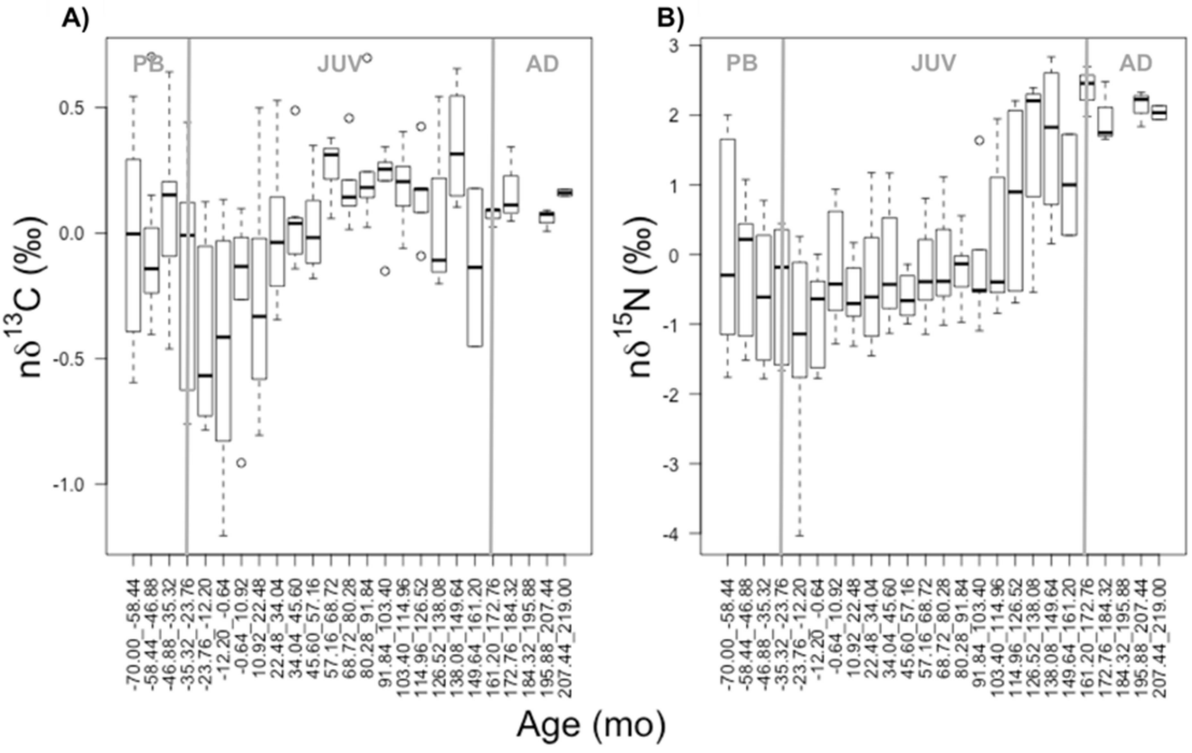

Figure 3.9 Life-history traits in carbon and nitrogen isotopic compositions in porbeagle sharks. Distributions of $n\delta^{13}C$ and $n\delta^{15}N$ values for each age class (11.56 months) across individual porbeagles. Grey vertical lines represent estimated age at birth and age at maturity. PB, JUV and AD represent pre-birth, juvenile and adult life stages.

3.4.2 Between-species differences in life-time isotopic niche areas

Blue and porbeagle shark samples were well separated in the carbon-nitrogen isotope space (Fig. 3.10), indicating between-species differences in life-time isotopic niche areas. In general, blue shark samples showed more negative $\delta^{13}C$ and $\delta^{15}N$ values than porbeagle samples, and had larger isotopic ranges, particularly in $\delta^{13}C$ values (Fig. 3.10). Standard ellipse area (calculated using measured isotope values, and corrected for small sample size, SEAc) was 1.93 for blue sharks, and 1.75 for porbeagles. The posterior probability that Bayesian-estimated standard ellipse area (SEA.B) is larger for blue sharks than for porbeagles was 73%. The overlap between standard ellipse areas for blue and porbeagle sharks was 0.27 (overlap = 0 – no overlap, overlap = 1 – same ellipse). When adult

samples from Northwest Atlantic porbeagles were omitted, the standard ellipse area for porbeagles was smaller: 1.61; consequently, the probability that standard ellipse area for blue sharks is larger than that for porbeagles was larger: 90%. The overlap between standard ellipse areas for blue and porbeagle sharks was also larger: 0.30.

In both species, samples from different areas and individuals were also somewhat separated in the isotope space (Fig. 3.10), indicating between-area and individual variability in isotopic niches. In porbeagles, separation between eastern and western North Atlantic individuals was strongly driven by ^{15}N-enriched subadult and adult samples from Northwest Atlantic individuals; when adult samples were removed, samples from Northeast and Northwest Atlantic individuals were still separated, though to a lesser extent, due to ^{15}N-enrichment in subadult samples from Northwest Atlantic individuals.

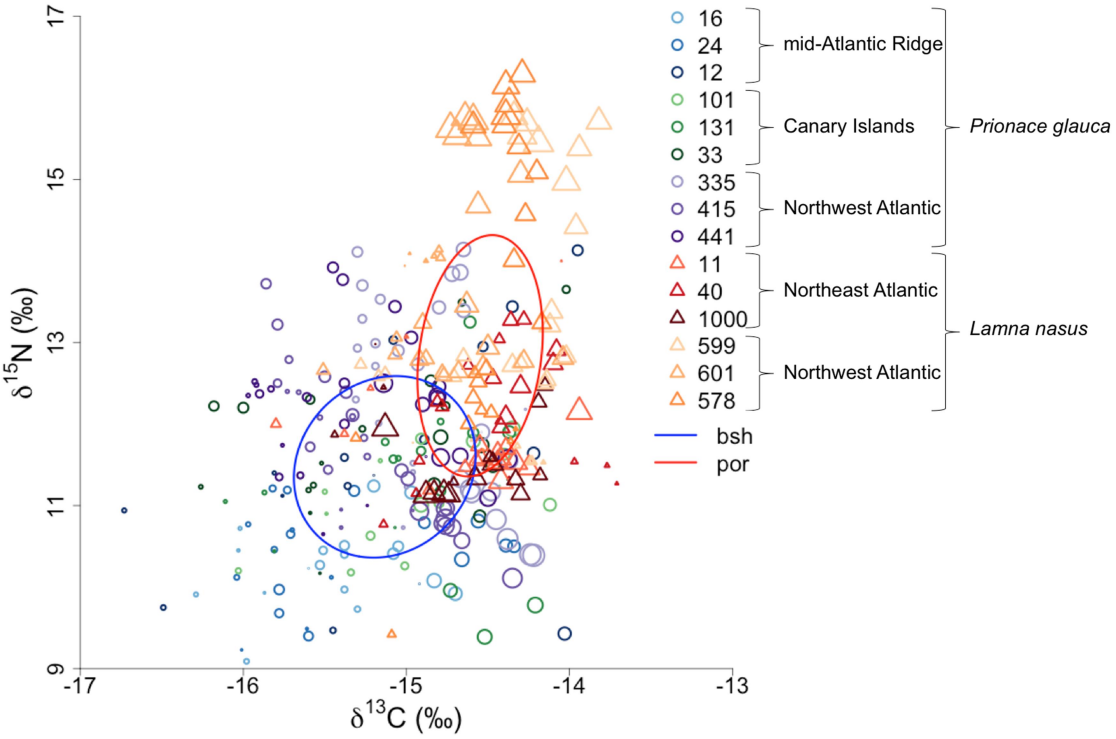

Figure 3.10 Life-time isotopic niches of blue and porbeagle sharks.
Values of δ^{13}C *versus* δ^{15}N values of bulk cartilage collagen from sequential vertebral samples from individual blue and porbeagle sharks. Different symbols represent different species: circles identify blue sharks, triangles porbeagles. Different colour scales represent different species and capture areas: blues identify blue sharks from the mid-Atlantic Ridge, greens blue sharks from the Canary Islands, purples blue sharks from the Northwest Atlantic, reds porbeagles from the Northeast Atlantic (with lightest reds representing porbeagles from the western English Channel and the darkest red the porbeagle from the Faroe Islands), and oranges porbeagles from the Northwest Atlantic. Different colour shades represent different individual sharks as in figure legend. Symbol size is proportional to sample distance along the vertebral radius. Ellipses represent standard ellipse areas corrected for small sample size (SEAc): the blue ellipse is relative to blue sharks (bsh), the red ellipse to porbeagles (por).

3.4.3 Variability in carbon and nitrogen isotopic profiles within and among individuals, and among areas

Individual-level life-history $\delta^{13}C$ and $\delta^{15}N$ records are presented in Fig. 3.11. Within-individual variability in $\delta^{13}C$ and $\delta^{15}N$ profiles was given by a long-term (ontogenetic) pattern, and super-imposed shorter-term excursions in most sharks (with the exception of individual 11; Fig. 3.11). Short-term excursions in $\delta^{13}C$ and $\delta^{15}N$ values typically represented isotopic variance over one or a few years (Table 3.3, Fig. 3.11).

Super-imposed on common, broad ontogenetic patterns in $\delta^{13}C$ and $\delta^{15}N$ values within species (Fig. 3.6 and 3.7; for patterns in $n\delta^{13}C$ and $n\delta^{15}N$ values, see Fig. 3.8 and 3.9), similarities and differences in both long- and short-term patterns in isotopic profiles were identified among capture areas and individuals (Fig. 3.11). In blue sharks, both $\delta^{13}C$ and $\delta^{15}N$ profiles differed significantly among areas (maximum p-value = 0.036 < 0.05, F = 3.386); in porbeagles, $\delta^{15}N$ profiles differed significantly between eastern and western North Atlantic individuals (p-value = $2.780 \cdot 10^{-10}$ < 0.05, F = 26.240), whereas $\delta^{13}C$ profiles did not (p-value = 0.459, F = 0.783).

In blue sharks, for instance, the shape of the increase in $\delta^{13}C$ values throughout life, as well as the frequency, amplitude and time-scales of excursions in $\delta^{13}C$ values, varied among individuals. In more detail, $\delta^{13}C$ values increased linearly throughout life with a few small excursions in individuals 12, 131 and 441, linearly with regular pronounced excursions in sharks 16 and 101, and with a U-shape in individuals 24, 33, 335 and 415 (Fig. 3.11).

In porbeagles, $\delta^{13}C$ and $\delta^{15}N$ profiles in Northeast Atlantic individuals differed from one another, and from profiles in Northwest Atlantic individuals. Specifically, $\delta^{13}C$ values increased linearly throughout life with a few small excursions in individual 11, linearly with regular pronounced excursions in individual 40, and decreased (after increasing slightly at the juvenile stage) in individual 1000, the only individual caught off the Faroe Islands; $\delta^{13}C$ values remained relatively constant throughout ontogeny, showing a pronounced negative excursion just after birth and then moderate excursions, in all three Northwest Atlantic individuals. Values of $\delta^{15}N$ remained relatively constant throughout life in individuals 11 and 1000, and increased slightly with regular pronounced excursions in individual 40; $\delta^{15}N$ values increased stepwise from an age of ~ 62-98 months, and reached a plateau at an age of ~ 138 months in all three western Atlantic porbeagles. Note that, whilst $\delta^{15}N$ values in Northwest Atlantic porbeagles started increasing well before maturity, values in Northeast Atlantic individuals showed no similar increase at comparable ages/sizes, though increased slightly towards the end of life in individuals 11 and 1000 (Fig. 3.11).

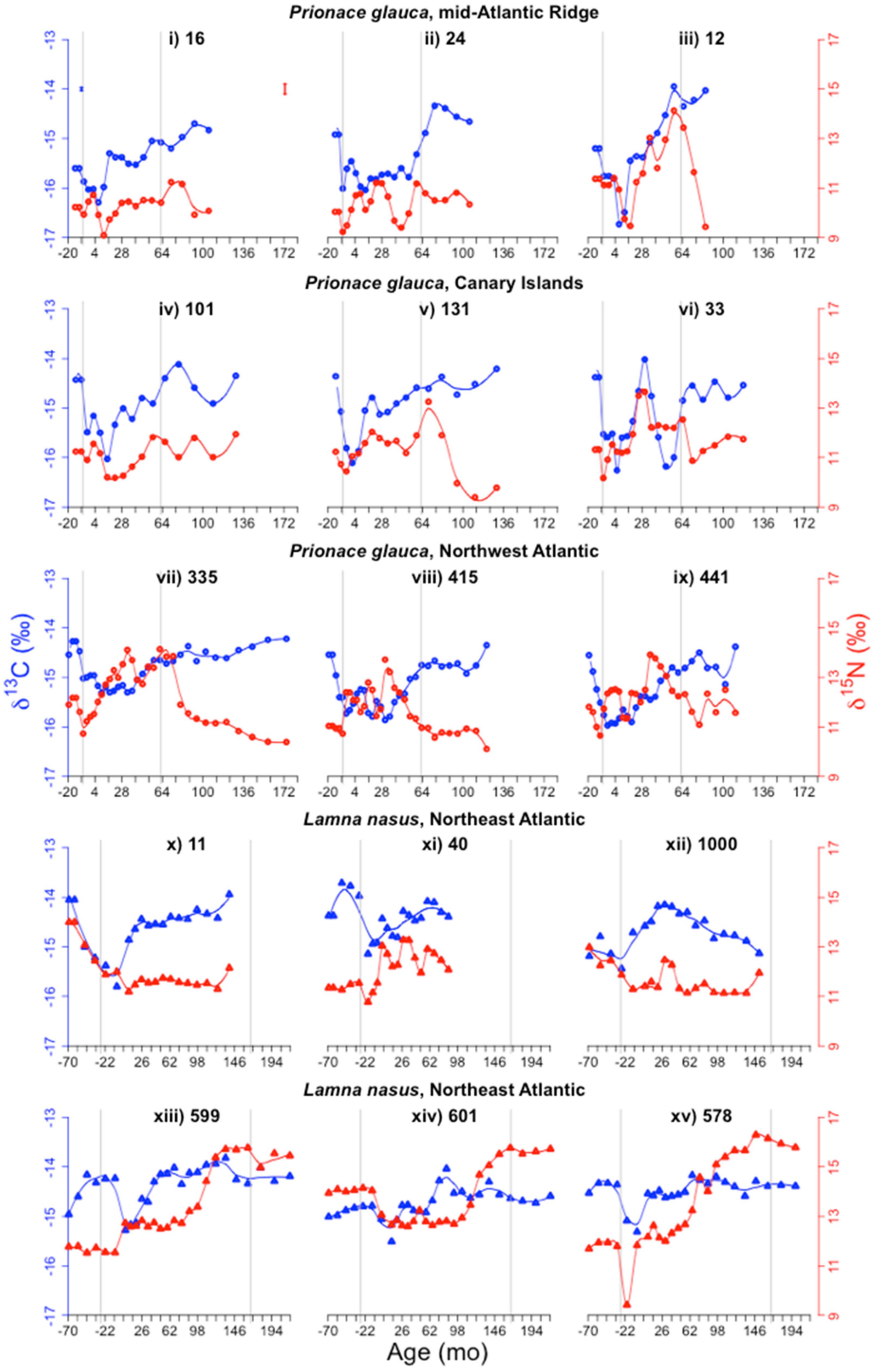

Figure 3.11 Individual-level life-history records of carbon and nitrogen isotopic compositions. From the top-left to the bottom-right, individual-level life-history records of $\delta^{13}C$ and $\delta^{15}N$ values are presented for individuals i) 16, ii) 24, iii) 12 (blue sharks from the mid-Atlantic Ridge), iv) 101, v) 131, vi) 33 (blue sharks from the Canary Islands), vii) 335, viii) 415, ix) 441 (blue sharks from the Northwest Atlantic), x) 11, xi) 40 (porbeagles from the western English Channel), xii) 1000

(porbeagle from the Faroe Islands), xiii) 599, xiv) 601, and xv) 578 (porbeagles from the Northwest Atlantic). Different symbols represent different species as in Fig. 3.10. Different colours represent different isotopes: blue identifies $\delta^{13}C$ values, red $\delta^{15}N$ values. Datapoints are measured isotope values, lines predicted monthly values obtained by fitting the least smooth as possible Loess smoother. The error bars in the top-left panel are the standard deviations for $\delta^{13}C$ and $\delta^{15}N$ values. The grey vertical lines represented estimated age at birth and at maturity.

3.4.3.1 Co-variation between carbon and nitrogen isotope values

Co-variation between $\delta^{13}C$ and $\delta^{15}N$ values was generally insignificant or relatively weak; where present, it did not have a clear ontogenetic component (but see individuals 335 and 415), and resulted from in- or out-of-phase (shifted) excursions in $\delta^{13}C$ and $\delta^{15}N$ values (Fig. 3.11). Similarities and differences in the sign, extent and temporal structure of co-variation between $\delta^{13}C$ and $\delta^{15}N$ values were also identified among areas and individuals. In central and eastern North Atlantic blue sharks, for instance, $\delta^{15}N$ values varied independently from $\delta^{13}C$ values, or were weakly positively related to $\delta^{13}C$ values, due to independent or in-phase, shifted excursions in $\delta^{13}C$ and $\delta^{15}N$ values. In western North Atlantic blue sharks, by contrast, $\delta^{15}N$ values were negatively related to $\delta^{13}C$ values, as a result of both ontogenetic divergence of $\delta^{15}N$ values from $\delta^{13}C$ values, as well as short-term out-of-phase excursions in $\delta^{13}C$ and $\delta^{15}N$ values. In eastern North Atlantic porbeagles, $\delta^{13}C$ and $\delta^{15}N$ time-series varied independently in individuals 11 and 1000, and co-varied positively in individual 40, due to regular and pronounced in-phase excursions in $\delta^{13}C$ and $\delta^{15}N$ values. In Northwest Atlantic porbeagles, $\delta^{15}N$ values were weakly positively related to $\delta^{13}C$ values, mostly due to more positive $\delta^{13}C$ and $\delta^{15}N$ values during subadult and adult life-history stages; whilst $\delta^{15}N$ values increased stepwise at an age of ~ 62-98 months, no corresponding increase in $\delta^{13}C$ values was documented (Fig. 3.11).

3.5 Discussion

In this study, individual-level life-history $\delta^{13}C$ and $\delta^{15}N$ records were recovered for blue and porbeagle sharks caught across the North Atlantic, at a high (i.e. seasonal to multi-annual) temporal resolution. Values of $\delta^{13}C$ and $\delta^{15}N$ varied between species, among capture areas, and within and among individuals, indicating spatial and/or trophic variability at multiple levels (hypothesis 1). A major finding of this study was the identification of common, broad ontogenetic patterns in $\delta^{13}C$ and $\delta^{15}N$ values across individual blue and porbeagle sharks (Fig. 3.6-3.9). Patterns in normalised isotope values (Fig. 3.8 and 3.9) identified species-level life-history isotopic traits, reflecting consistent ontogenetic changes in the interaction between the individuals and their environment, after variability in space use among individuals was removed (hypothesis 2). Life-history isotopic traits can also be identified within many other shark species, and across species (Table 3.1; Fig. 3.2), indicating ubiquitous traits in the movement and feeding ecology of sharks, which may imply shared vulnerability to fishery capture. Nevertheless, differences in life-history isotopic traits were observed (hypothesis 3). Drawing inferences on the underlying biogeochemical and/or ecological mechanisms

of isotopic traits is more challenging. The likely influences from movement across isotopic gradients (baseline isotope effects) and changes in diet and trophic level (trophic isotope effects) on the observed life-history isotopic traits in blue and porbeagle sharks are discussed below.

3.5.1 Species-level life-history isotopic traits

3.5.1.1 Baseline (spatial) arguments for life-history isotopic traits

Generally, the carbon isotopic composition of marine phytoplankton ($\delta^{13}C_{PLK}$) at the base of pelagic food webs co-varies positively with sea surface temperature (SST; Sackett *et al*., 1965; Rau *et al*., 1982; Trueman *et al*., 2012; McMahon *et al*., 2013a; Magozzi *et al*., 2017; Fig. 3.12; Chapter 2). Coastal environments may also be isotopically distinct from offshore settings, depending on latitude and the nature of coastal vegetation (O'Leary, 1981). In theory, then, the consistent shift to more positive $\delta^{13}C$ values during juvenile growth in both blue and porbeagle sharks (Fig. 3.8A and 3.9A) could reflect an ontogenetic movement to warmer southern waters, and/or potentially offshore, if coastal waters contain a high proportion of nutrients derived from ^{13}C-depleted C3 vascular plants (O'Leary, 1981).

Female blue sharks are known from satellite-tracking studies on both sides of the North Atlantic to undergo an ontogenetic shift in movement behaviour, from undertaking seasonal movements between temperate and subtropical latitudes when juvenile and subadult (Queiroz *et al*., 2010; Campana *et al*., 2011; Queiroz *et al*., 2012; Vandeperre *et al*., 2014) to conducting distinctive migrations to tropical waters when adults, possibly associated with parturition and pupping (Vandeperre *et al*., 2014).

Seasonal to annual north-south movements have also been reported for juvenile and subadult female porbeagles in the Northeast Atlantic (Pade *et al*., 2009; Saunders *et al*., 2011; Biais *et al*., 2016; Fig. 3.3), and distinctive migrations to subtropical pupping grounds have been documented for adult females in the Northwest Atlantic (Campana *et al*., 2010). Additionally, porbeagles are thought to undergo an ontogenetic habitat shift, from coastal and shelf systems when juveniles and subadults to shelf-edge and slope environments when adults (Bendall *et al*., 2013; Ellis *et al*., 2015; Biais *et al*., 2016). Thus, the consistent increase in $\delta^{13}C$ values during juvenile life-history stages in both blue and porbeagle sharks (Fig. 3.8A and 3.9A) could potentially be explained by an increase in the frequency and/or duration of movements towards ^{13}C-enriched southern or offshore waters.

For blue sharks, the observed pattern of increasing $\delta^{15}N$ values during juvenile growth, and decreasing $\delta^{15}N$ values during subadult and adult life-history stages (Fig. 3.8B) is consistent with an increase in the utilisation of southern waters. In the North Atlantic, spatial carbon and nitrogen isotopic gradients are predicted to be largely independent (Schmittner & Somes, 2016; Magozzi *et al*., 2017; Fig. 3.11; see also Hofmann *et al*., 2000; Tagliabue & Bopp, 2008; Somes *et al*., 2010; McMahon *et al*., 2013a), due to independent underlying mechanisms of isotopic variation (for reviews,

see Trueman *et al*., 2012; McMahon *et al*., 2013a, b; Chapter 2), and the nitrogen isotopic compositions of phytoplankton ($\delta^{15}N_{PLK}$) is predicted to broadly decrease from north to south (Schmittner & Somes, 2016; Fig. 3.12B).

Assuming that ontogenetic isotopic variation is driven by movements across isotopic gradients, then potential foraging areas can be inferred from available isoscape models (Schmittner & Somes, 2016; Magozzi *et al*., 2017; Chapter 2). In blue sharks, $\delta^{13}C$ values progressively increased by ~ 1‰ from birth to the onset of maturity (Fig. 3.8A), meaning that phytoplankton in juvenile and subadult foraging grounds should have $\delta^{13}C$ values ~ 1 or < 1‰ more negative than in capture areas (Fig. 3.12A). Additionally, because $\delta^{15}N$ values increased by ~ 1‰ during juvenile growth, and decreased by ~ 2 ‰ during subadult and adult stages (Fig. 3.8B), phytoplankton in juvenile and subadult grounds should also have $\delta^{15}N$ values ~ 1 and 2‰ higher than in capture areas, respectively (Fig. 3.12B). Accordingly, blue sharks caught north-west of the Azores, for instance, should have foraged east of the Azores and in the northern Northeast Atlantic when juveniles, then spent an increased proportion of time feeding in the Gulf Stream and further south in the subtropical gyre (Fig. 3.12). Core regions of the vertebra reflect maternal isotopic compositions (Olin *et al*., 2011; Carlisle *et al*., 2015). Interestingly, in blue sharks, maternal $\delta^{13}C$ values were consistently higher than post-birth values, and similar to values during the adult life-history stage, suggesting distinct pupping and maternal foraging grounds, possibly to avoid pup predation by larger sharks. Similar maternal and adult $\delta^{13}C$ values may also suggest a return migration of adult sharks to mothers' foraging grounds. Isotope-inferred foraging areas for all blue sharks are within the known geographic range of this species in the North Atlantic (Queiroz *et al*., 2010; Campana *et al*., 2011; Queiroz *et al*., 2012; Vandeperre *et al*., 2014; 2016), indicating that observed life-history isotopic traits could be explained solely by a southward ontogenetic movement (and no diet and trophic level change).

For porbeagle sharks, by contrast, the stepwise increase in $\delta^{15}N$ values during subadult stages does not seem to be consistent with an increase in the utilisation of southern waters. In porbeagles, $\delta^{13}C$ values increased progressively by < 1‰ during juvenile growth, and $\delta^{15}N$ values increased stepwise by > 2‰ during subadult stages (in large individuals from the Northwest Atlantic; Fig. 3.9). For porbeagles caught in the Northwest Atlantic, the pattern in $\delta^{13}C$ values would require juvenile foraging areas in the northern Northwest Atlantic, whereas that in $\delta^{15}N$ values would require juvenile feeding south of the capture area (Fig. 3.12). Similarly, for individuals caught in the Celtic Sea, patterns in $\delta^{13}C$ and $\delta^{15}N$ values would require juvenile feeding grounds in the northern Northeast Atlantic and in the subtropical gyre, respectively (Fig. 3.12). Due to inconsistencies in isotope-inferred foraging grounds, therefore, life-history isotopic traits in porbeagles cannot be explained only by a southward ontogenetic habitat shift, but must involve trophic shifts.

In addition to latitudinal movement, porbeagles are also believed to undergo an ontogenetic shift towards offshore waters (Bendall *et al*., 2013; Ellis *et al*., 2015; Biais *et al*., 2016); if that is the

case, then drawing inferences on life-time foraging grounds can be more difficult, as isoscape predictions in coastal and shelf systems are likely to be offset (Chapter 2).

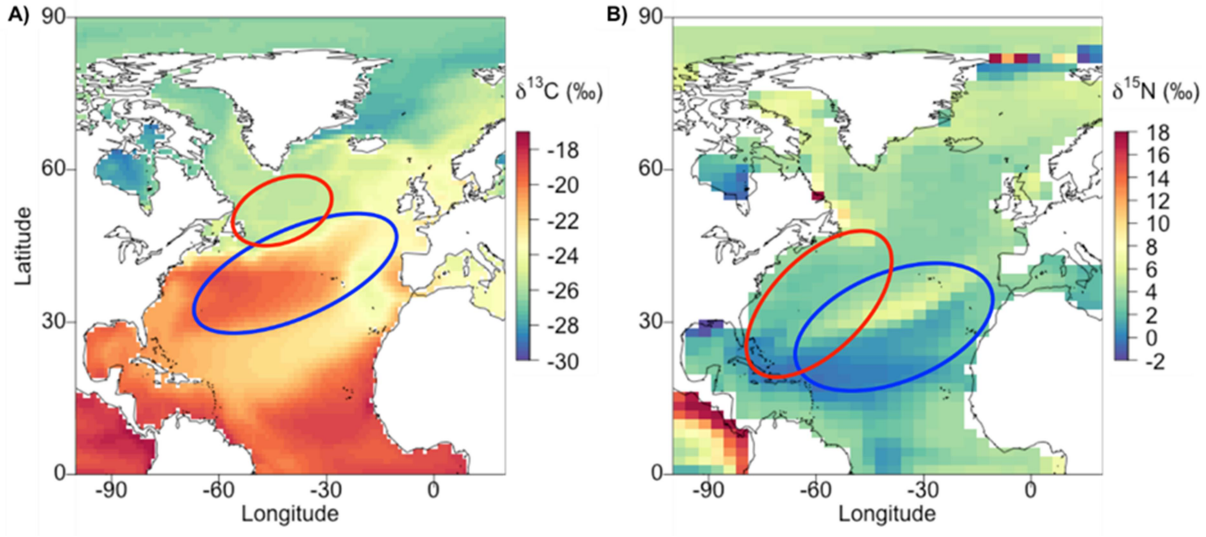

Figure 3.12 Carbon and nitrogen isoscapes for phytoplankton in the North Atlantic. Annually averaged surface water distributions of the A) carbon and B) nitrogen isotopic compositions of phytoplankton ($\delta^{13}C_{PLK}$ and $\delta^{15}N_{PLK}$, respectively) across the North Atlantic Ocean. Both isoscapes are developed using mechanistic, predictive isotope models: the carbon isoscape is constructed using an offline extension to the earth system model NEMO-MEDUSA with a monthly climatology for the period 2001-2010 (Magozzi *et al*., 2017; Chapter 2), the nitrogen isoscape using the isotope-enabled UVic model for the model year 2010 (Schmittner & Somes, 2016). As an example, isotope-inferred life-time foraging areas are represented for blue sharks caught north-west of the Azores, and porbeagles captured off Newfoundland (blue and red ellipses, respectively).

3.5.1.2 Trophic arguments

Whilst life-history isotopic traits in blue sharks (Fig. 3.8) may be explained solely by movements across spatially independent isotopic gradients in the North Atlantic, a potential explanation for progressively increasing $\delta^{13}C$ values throughout ontogeny (Fig. 3.8A) is a size-based increase in trophic level. Size-dependent increases in trophic level have never been reported specifically for blue sharks, but modest correlation between size and trophic level has been documented for other carcharhinid sharks (Cortes, 1999). Assuming a trophic enrichment factor of ~ 1‰ (DeNiro & Epstein, 1978; but see Vander Zanden & Rasmussen, 2001; McCutchan *et al*., 2003), the observed ontogenetic increase in $\delta^{13}C$ values could potentially be explained by an ontogenetic diet shift of one trophic level. However, the lack of a corresponding larger (~ 3.4‰; DeNiro & Epstein, 1981) increase in $\delta^{15}N$ values implies that trophic level change cannot be the only underlying mechanism of isotopic variation, but must be coupled with variations in nitrogen isotopic baselines (Schmittner & Somes, 2016; Magozzi *et al*., 2017; Fig. 3.12).

The most obvious argument for the observed stepwise increase in $\delta^{15}N$ values in porbeagles (Fig. 3.9B) is also a step-change in trophic level. Step-changes in trophic level throughout ontogeny have never been documented specifically for porbeagles, but have been reported for another lamind shark, the white shark, at least for some populations and individuals (Table 3.1; Estrada *et al*., 2006;

Kerr *et al*., 2006; Kim *et al*., 2012a; Hamady, 2014). Similar to blue sharks, the lack of a corresponding (smaller) increase in $\delta^{13}C$ values implies additional movements across carbon isotopic gradients (McMahon *et al*., 2013a; Magozzi *et al*., 2017; Fig. 3.12A), and/or near zero trophic fractionation for carbon isotopes (Vander Zanden & Rasmussen, 2001; McCutchan *et al*., 2003).

The stepwise increase in $\delta^{15}N$ values in porbeagles (Fig. 3.9B) was strongly driven by stepwise increasing $\delta^{15}N$ values during subadult life-history stages in Northwest Atlantic individuals (Fig. 3.11). The lack of a similar pattern in samples of comparable age/size from Northeast Atlantic individuals may indicate a delayed trophic shift in the Northwest Atlantic population (Fig. 3.11), movement across larger nitrogen isotopic gradients in the Northeast Atlantic (McMahon *et al*., 2013a; Schmittner & Somes, 2016; Fig. 3.12B), and/or differences in age estimation models not accounted for in this study.

3.5.2 Area effects on life-history traits

Super-imposed on species-level life-history isotopic traits (Fig. 3.6-3.9), considerable variability existed in carbon and nitrogen isotopic profiles among areas (Fig. 3.11). Between-area variability in isotopic profiles generally regarded both long-term patterns and super-imposed shorter-term excursions in isotope values (see below; Fig. 3.11), suggesting between-area variability in movement and/or feeding behaviour on seasonal to ontogenetic time-scales (hypothesis 4). Commonalities in isotopic profiles were also identified across areas (Fig. 3.11), however, inferences were more difficult to draw due to the small sample size of this study (i.e. three individuals captured in each area). Differences in isotopic profiles among areas most likely indicate movement across different isoscapes in the eastern and western North Atlantic (Schmittner & Somes, 2016; Magozzi *et al*., 2017; Fig. 3.12) and/or spatial differences in prey availability, as no differences in actual movement and feeding patterns are expected between eastern and western North Atlantic individuals from the identification of species-level life-history traits.

3.5.3 Within- and between-individual variability in life-history traits

Both carbon and nitrogen isotopic compositions varied throughout the life of most individual sharks (with the exception of individual 11; Fig. 3.11). Within-individual variability in isotopic profiles was generally given by a long-tem (ontogenetic) pattern, and super-imposed shorter-term excursions (Fig. 3.10), which typically integrated isotopic variance over one or a few years (Table 3.3; Fig. 3.11). Short-term excursions in $\delta^{13}C$ and $\delta^{15}N$ values indicate individual-level movements and/or trophic shifts over seasonal to multi-annual temporal scales (hypothesis 5). Thus, high-resolution sampling and analysis of stable isotopes in incrementally grown tissues may allow investigating individual-scale behaviour over short temporal scales, even in animals with long tissue isotopic incorporation times, such as sharks (Hussey *et al*., 2012; Kim *et al*., 2012b, c). Seasonal movements have been extensively documented in both blue and porbeagle sharks in the North Atlantic (Campana

et al., 2010; Queiroz *et al*., 2010; Campana *et al*., 2011; Biais *et al*., 2016). Seasonal and annual shifts in diet compositions have also been observed for both species, most often in response to oceanographically-driven variation in prey availability, or movements to areas with different prey bases (e.g. Joyce *et al*., 2002; McCord & Campana, 2003; Markaida & Sosa-Nishizaki, 2010; Preti *et al*., 2012; but see MacNeill *et al*., 2005).

Between-individual variability in both the long- and short-term components of variance in isotopic profiles (Fig. 3.11) indicates a high degree of individuality in movement and feeding behaviour over seasonal to ontogenetic time-scales. Whilst general movement patterns have been identified for both species, disparate movements have been documented among individuals (Campana *et al*., 2010; Queiroz *et al*., 2010; Campana *et al*., 2011; Biais *et al*., 2016).

3.6 Conclusions

A major finding of this study was the identification of common, broad ontogenetic patterns in $\delta^{13}C$ and $\delta^{15}N$ values across individual blue and porbeagle sharks (Fig. 3.6-3.9), which indicated life-history traits in the movement and/or feeding ecology of these species in the North Atlantic (Fig. 3.7 and 3.8), with super-imposed variability in movement and/or feeding behaviour among areas and individuals (Fig. 3.11). Consequently, life-history isotopic traits can be considered conceptually similar to life-time isotopic niche areas (Fig. 3.10): they also allow differentiating individuals, populations, species, higher taxa and/or functional groups, as well as identifying commonalities across groups, and provide additional information on ontogenetic patterns.

Species-level life-history isotopic traits were also seen from the literature for many other shark species (Table 3.1; Fig. 3.2), indicating that ontogenetic movements and/or trophic shifts are ubiquitous in sharks. In general, life-history isotopic traits differed between blue and porbeagle sharks (Fig. 3.8 and 3.9), and among other species (Fig. 3.2), indicating between-species differences in ontogenetic movement and/or feeding ecology. The identification of common life-history traits within and across species may have profound implications for determining shark vulnerability to fishery capture, and for designing effective management and conservation strategies to protect sharks and their roles within ecosystems (Gillanders *et al*, 2003; Grubbs, 2010; Gruess *et al*., 2011; Briscoe *et al*., 2016). It may, for instance, help to identify areas of essential habitat across life-history, as well as areas of high use by multiple individuals, populations or species (Vandeperre *et al*., 2016; Queiroz *et al*., 2016), where interactions with fisheries are of greater concern for survival, recruitment, reproduction and maintenance of ecosystem services.

Life-history isotopic traits, however, do not ultimately reflect ontogenetic movements, but may also represent trophic shifts, or more likely a mixture of both. Thus, whilst bulk stable isotope analysis provide an effetive tool to detect the presence of life-history traits in the ecology of sharks, some complementary tools, such as isotope analysis of specific structural compounds within tissues

(i.e. amino acids or lipids) may help disentangling mixed baseline and trophic effects, hence ultimately inferring movement or trophic shifts.

Chapter 4: Reconstructing ontogenetic and transgenerational movements and habitat shifts in pelagic sharks through compound-specific stable isotope analysis of essential amino acids in vertebrae

This chapter is a manuscript in prep. (to be submitted in summer 2017): S. Magozzi, S. Thorrold, L. Houghton, G. Skomal, L. Natanson, M. Santos, R. Coelho, N. Queiroz, D. Sims, V. Bendall, S. Hetherington, J. Ellis, K. Quaeck, C. Bird, and C. Trueman. Reconstructing ontogenetic and transgenerational movements and habitat shifts in pelagic sharks through compound-specific stable isotope analysis of essential amino acids in vertebrae. In prep. S. Magozzi led the research and wrote the manuscript. G. Skomal, L. Natanson, M. Santos, R. Coelho, N. Queiroz, D. Sims, V. Bendall, S. Hetherington and J. Ellis provided the shark vertebral samples. L. Houghton advised on sample preparation and compound-specific isotope analysis. C. Trueman and S. Thorrold aviced on data analysis and interpretations, and provided feedback on the chapter.

4.1 Abstract

Stable isotope analysis of animal tissues has become a mainstream tool in marine ecology to trace nutrient fluxes through food webs, tack trophic shifts within food webs, and reconstruct animal movements. However, interpretations of bulk tissue isotope data are inherently limited by mixed baseline and trophic isotope effects. Isotope analysis of single amino acids in animal tissues is being increasingly used to tease apart baseline from trophic components of variance in bulk tissue isotopic compositions. Essential amino acids can only be synthesised *de novo* by primary producers and bacteria (end-members), and are subsequently assimilated by consumers directly through the diet. Therefore, the carbon isotopic compositions of essential amino acids ($\delta^{13}C_{EAA}$) in consumer tissues reflect those in end-members, without confounding influences from trophic discrmination. The inherent metabolic diversity among major prokaryotic and eukaryotic lineages generates distinct patterns of carbon isotope fractionation during amino acid biosynthesis. These carbon isotope fingerprints can be used to trace the origin of essential amino acids from consumer $\delta^{13}C_{EAA}$ data.

Here individual-level life-history records of $\delta^{13}C_{EAA}$ values were recovered from vertebrae of blue (*Prionace glauca*) and porbeagle (*Lamna nasus*) sharks, and are discussed with reference to bulk collagen isotope data to reconstruct ontogenetic movements across isotopic gradients. Both blue and porbeagle sharks were caught across their known geographic ranges in the North Atlantic. The

recovery of life-history isotopic traits related to movement (i.e. in $\delta^{13}C_{EAA}$ values) across individuals of each species conclusively demonstrated species-level ontogenetic movement traits, implying shared vulnerability to fishery capture across their life-histories. During juvenile growth, blue sharks increasingly utlised foraging grounds with more positive $\delta^{13}C$ baselines, whereas porbeagles made increasing use of more negative $\delta^{13}C$ baselines, whilst also shifting trophic level. Blue shark pupping occurred in isotopically distinct grounds compared to those exploited by mothers and adult sharks, with the possibility of a return migration of adult individuals to maternal foraging grounds. Pregnant female porbeagles, by contrast, migrated to isotopically distinct grounds compared to those exploited by subadult females prior to giving birth. However, immediate post-partum independent feeding resulted in an increasing utilisation of more negative $\delta^{13}C$ baselines. Such isotope-derived inferential information on ontogenetic movement patterns complements tag-derived information on short-term movements to implement effective management strategies.

Ontogenetic and transgenerational changes in the relative contributions of different carbon sources to shark food webs were also investigated, but interpretations were unceratin, given inconsistencies between shark $\delta^{13}C_{EAA}$ patterns and available end-member carbon isotope fingerprints. Finally, patterns in the carbon isotopic compositions of non-essential amino acids ($\delta^{13}C_{nonEAA}$) were also examined, but a coherent physiological framework to interpret variance in carbon isotope data for amino acids that are wholly or partially synthesised *de novo* is currently lacking.

4.2 Introduction

The analysis of stable isotopes in animal tissues has become a routine tool in marine ecology to reconstruct animal movements (e.g. Best & Schell, 1996; Mendes *et al.*, 2007; Cherel *et al.*, 2009; Carlisle *et al.*, 2015) and changes in diet and trophic level (e.g. MacNeill *et al.*, 2005; Estrada *et al.*, 2006; Newsome *et al.*, 2009; Polo-Silva *et al.*, 2013). The basic premise is that the isotopic composition of animal tissues reflects that of primary producers, overlain by a relatively predictable trophic offset (DeNiro & Epstein, 1978; 1981; Vander Zanden & Rasmussen, 2001; McCutchan *et al.*, 2003; for reviews, see Post, 2002; Boecklen *et al.*, 2011; Trueman *et al.*, 2012; McMahon *et al.*, 2013a). In traditional bulk tissue isotope analysis, variance in tissue isotopic compositions reflects both variations in isotope ratios at the base of the food web (baseline isotope effects; e.g. Schmittner & Somes, 2016; Magozzi *et al.*, 2017; Chapter 2), and fluctuations in prey isotopic compositions (trophic isotope effects), significantly complicating the interpretation of bulk tissue isotope data to infer movements and/or diets (e.g. Jennings & Warr, 2003; Popp *et al.*, 2007; Nielsen *et al.*, 2016; for reviews, see Newsome *et al.*, 2010; Ramos & González-Solís, 2012; Trueman *et al.*, 2012; McMahon *et al.*, 2013b).

In Chapter 3, individual-level life-history records of carbon and nitrogen isotopic compositions were recovered for bulk cartilage collagen ($\delta^{13}C_{bulk}$ and $\delta^{15}N_{bulk}$, respectively) from

vertebrae of blue (*Prionace glauca*) and porbeagle (*Lamna nasus*) sharks caught across the North Atlantic. Species-level life-history isotopic traits were identified, and interpreted to infer ontogenetic movements and/or changes in diet and trophic level. Inferences were, however, complicated by mixed baseline and trophic isotope effects. Consistent increases in $\delta^{13}C_{bulk}$ values during juvenile growth in both blue and porbeagle sharks (Chapter 3) were explained by an increase in the utilisation of southern and/or offshore waters (if coastal waters contain a high proportion of nutrients derived from ^{13}C-depleted C3 vascular plants; O'Leary, 1981). For blue sharks, the observed increase in $\delta^{15}N_{bulk}$ values during juvenile life stages, and decrease during subadult and adult stages (Chapter 3) was considered consistent with an increase in the frequency and/or duration of movements towards southern waters, based on modelled carbon and nitrogen isoscapes for phytoplankton in the North Atlantic (Schmittner & Somes, 2016; Magozzi *et al.*, 2017; Chapter 2). By contrast, for porbeagles, the observed stepwise increase in $\delta^{15}N_{bulk}$ values during subadult stages (in mature individuals from the Northwest Atlantic only; Chapter 3) appeared to be incosistent with an ontogenetic movement towards southern waters, based on predicted isoscapes. Thus, life-history traits in $\delta^{13}C_{bulk}$ values in blue sharks could be explained solely by movements across isotopic gradients, whereas equivalent traits in porbeagles must involve a combination of movements and trophic shifts (Chapter 3).

Stable isotope analysis of specific structural compounds within tissues, such as individual lipids or amino acids, is increasingly employed in animal movement (e.g. McMahon, 2011; McMahon *et al.*, 2011a, b; McMahon *et al.*, 2012; Seminoff *et al.*, 2012) and trophic studies (e.g. Popp *et al.* 2007, Chikaraishi *et al.* 2009, Lorrain *et al.* 2009, Chikaraishi *et al.* 2014; for reviews, see McMahon *et al.*, 2013b; Nielsen *et al.*, 2015) to reduce uncertainty in estimates of change in location, trophic position and nutrient source (e.g. McCarthy *et al.*, 2013; Ellis *et al.*, 2014; Schiff *et al.*, 2014; McMahon *et al.*, 2015a; see below). With regard to carbon metabolism, essential amino acids are defined as those that can only be synthesised *de novo* by primary producers and bacteria (end-members), and are subsequently assimilated by consumers directly through the diet (Hare *et al.*, 1991; Reeds, 2000; Jim *et al.*, 2006; for reviews, see Trueman *et al.*, 2012; McMahon *et al.*, 2013b). The carbon isotopic compositions of essential amino acids ($\delta^{13}C_{EAA}$) in a consumer's tissues, therefore, represents weighted averages of the $\delta^{13}C_{EAA}$ values in all the end-members contributing amino acids to the consumer's food web, without confounding influences from trophic fractionation (e.g. Popp *et al.*, 2007; for reviews, see Trueman *et al.*, 2012; McMahon *et al.*, 2013b).

The carbon isotope compositions of essential amino acids ($\delta^{13}C_{EAA}$) in end-members (and thus in consumers) are, in turn, given by the carbon isotopic composition of the inorganic carbon pool ($\delta^{13}C_{CO2(aq)}$), and by the isotopic fractionation during amino acid biosynthesis (F; Eq. 4.1).

$$\delta^{13}C_{EAA} \sim f(\delta^{13}C_{CO2(aq)}, F) \quad (4.1)$$

where $\delta^{13}C_{EAA}$ are the carbon isotopic compositions of essential amino acids, $\delta^{13}C_{CO2(aq)}$ is the isotopic composition of dissolved CO_2, and F the isotopic fractionation associated with amino acid biosynthesis.

The carbon isotopic composition of aqueous CO_2 co-varies with sea surface temperature (SST), concentration of dissolved CO_2 ($[CO_{2(aq)}]$), and other carbon components within the dissolved inorganic carbon (DIC) pool, and thus varies spatially along broad latitudinal gradients (Hofmann *et al.*, 2000; Tagliabue & Bopp, 2008; Schmittner & Somes, 2016; Magozzi *et al.*, 2017). As discussed in Chapter 2, carbon isotope fractionation during photosynthesis (ε_p) is largely determined by the ratio of carbon fixation to carbon flux into the cell (O'Leary, 1981; Farquhar *et al.*, 1982; Larsen *et al.*, 2013), and thus varies with phytoplankton growth rate and external CO_2 concentration (Rau *et al.*, 1989; Freeman & Hayes, 1992; Laws *et al.*, 1995). Isotopic fractionation during amino acid biosynthesis downstream of the Calvin cycle is fundamentally different, as it is largely controlled by amino acid biosynthetic pathways and associated branching points in the central metabolism (Larsen *et al.*, 2009; 2013); therefore, it does not vary substantially with growth and environmental conditions (Larsen *et al.*, 2013; 2015). Recent research has demonstrated that the inherent metabolic diversity among major phylogenetic prokaryotic and eukaryotic lineages (i.e. bacteria – prokaryotes, fungi, algae and vascular plants – eukaryotes) generates unique, distinct patterns in isotopic fractionation during amino acid biosynthesis, named 'carbon isotope fingerprints'(*sensu* Larsen *et al.*, 2009; 2013; see also Scott *et al.*, 2006). Field and laboratory experiments have demonstrated that carbon isotope fingerprints are largely preserved across growth and environmental gradients, despite substantial variation in $\delta^{13}C_{EAA}$ values (due to spatial variations in $\delta^{13}C_{CO2(aq)}$ values; see Eq. 4.1), and $\delta^{13}C$ values of bulk phytoplankton (due to spatial variations in both $\delta^{13}C_{CO2(aq)}$ and ε_p; Larsen *et al.*, 2013; 2015).

Influences from spatial variations in $\delta^{13}C_{CO2(aq)}$ values on $\delta^{13}C_{EAA}$ values in end-members (and thus in consumers) can be removed by sample-normalising the $\delta^{13}C$ values of single amino acids to the mean $\delta^{13}C$ value for all essential amino acids ($\delta^{13}C_{norm\text{-}EAA}$; see Methods). Thus, whilst variance in $\delta^{13}C_{EAA}$ values reflects both spatial variations in $\delta^{13}C_{CO2(aq)}$ values (CO_2 isotope effects), and variations in isotopic fractionation among end-members (F isotope effects), patterns in $\delta^{13}C_{norm\text{-}EAA}$ values only reflect carbon isotopic fingerprints. Based on these premises, differences between $\delta^{13}C_{EAA}$ and $\delta^{13}C_{norm\text{-}EAA}$ values imply movements across spatial $\delta^{13}C_{CO2(aq)}$ gradients, and patterns in $\delta^{13}C_{norm\text{-}EAA}$ values are diagnostic of the origin of essential amino acid (Larsen *et al.*, 2009; 2013; Arthur *et al.*, 2014; McMahon *et al.*, 2015a; 2016).

Here carbon isotopic compositions were recovered for essential amino acids ($\delta^{13}C_{EAA}$) from the same blue and porbeagle shark vertebrae analysed for isotopes in bulk cartilage collagen, to produce comparable individual-level life-history carbon isotope records for bulk collagen and essential amino acids. Variance in raw and sample-normalised essential amino acid carbon isotopic compositions ($\delta^{13}C_{EAA}$ and $\delta^{13}C_{norm\text{-}EAA}$, respectively) was quantified at multiple levels (i.e. between species, among areas, and within and between individuals), and compared against variance in $\delta^{13}C_{bulk}$ values to disentangle baseline from trophic isotope effects. Common, broad ontogenetic patterns in $\delta^{13}C_{EAA}$ and $\delta^{13}C_{norm\text{-}EAA}$ values were analysed across individual blue and porbeagle sharks; where present, these patterns were compared against traits in $\delta^{13}C_{bulk}$ values to test initial hypotheses of

movements *versus* trophic shifts, and provide additional information on movements across spatial $\delta^{13}C_{CO2(aq)}$ gradients and/or shifts in habitat and carbon source. Specifically, for consistent increases in $\delta^{13}C_{bulk}$ values during juvenile growth in both blue and porbeagle sharks, the following scenarios could be expected:

1) Life-history isotopic traits for essential amino acids can be identified, and used to disentangle baseline from trophic isotope effects on traits for bulk collagen, providing conclusive evidence for movement traits.
2) If increases in $\delta^{13}C_{bulk}$ values during juvenile growth in both blue and porbeagle sharks were solely associated with an increase in trophic level, they should not be apparent in $\delta^{13}C_{EAA}$ values (Fig. 4.1A).
3) If increases in $\delta^{13}C_{bulk}$ values reflected movement across spatial isotopic gradients with no accompanying trophic level or carbon source change, they should be retained in $\delta^{13}C_{EAA}$ values but removed by sample-normalisation (Fig. 4.1B).
4) If increases in $\delta^{13}C_{bulk}$ values reflected both movement across spatial isotopic gradients and trophic level change (but no carbon source change), these two effects may be discriminated by contrasting ontogenetic patterns in $\delta^{13}C_{bulk}$ (and $\delta^{15}N_{bulk}$) values, and raw and normalised essential amino acid carbon isotopic compositions ($\delta^{13}C_{EAA}$ and $\delta^{13}C_{norm\text{-}EAA}$, respectively; Fig. 4.1C).
5) If diet changes or spatial movements were associated with changes in the relative contributions of different carbon sources (e.g. algae compared to bacteria or vascular plants) to shark food webs, $\delta^{13}C_{norm\text{-}EAA}$ patterns should co-vary with the estimated contributions of different primary producers, based on available carbon isotope fingerprints (Fig. 4.1D).

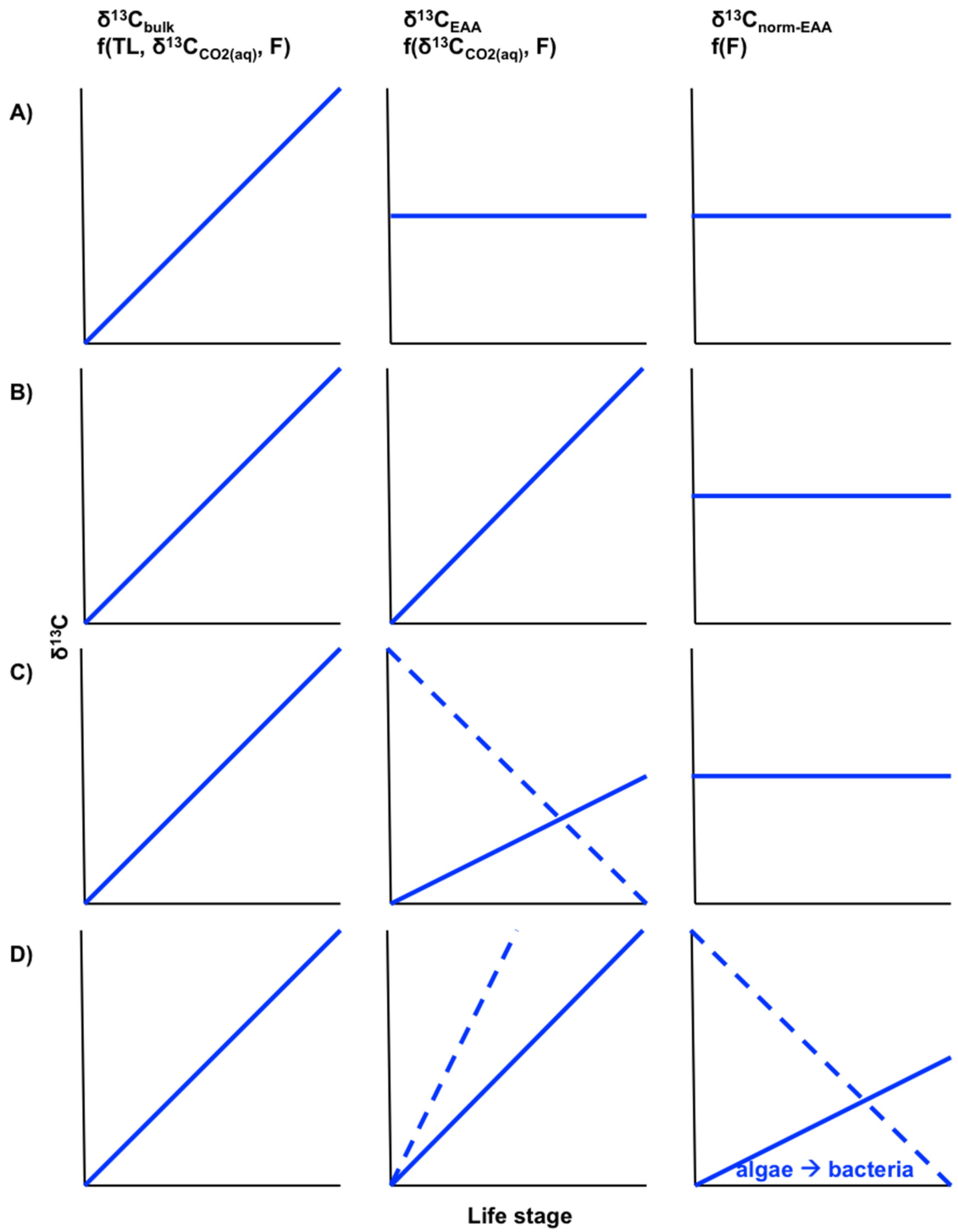

Figure 4.1 Schematics of possible scenarios associated with an increase in the carbon isotopic composition of bulk collagen throughout ontogeny.
A) Increase in trophic level with no movement across spatial isotopic gradients and/or carbon source shift. B) Movement trowards more positive isotopic baselines but no trophic level and/or carbon source shift. C) Increase in trophic level and movement towards more positive isotopic baselines (full line) but no carbon source shift; alternatively, increase in trophic level and movement towards more negative isotopic baselines, with the increase in trophic level producing an isotopic enrichment sufficiently large to offset depletion caused by movement (dashed line). D) Movement towards ^{13}C-enriched waters or carbon source shift toward ^{13}C-enriched sources (full lines) but no increase in trophic level; alternatively, movement towards ^{13}C-enriched waters and carbon source shift toward

^{13}C-depleted sources, with movement producing an isotopic enrichment sufficiently large to offset depletion caused by carbon source shift (dashed line).

As opposed to essential amino acid, non-essential amino acids can be synthesised by all organisms to maintain normal growth, and their isotope values undergo significant trophic fractionation (Hare *et al.*, 2001; Howland *et al.*, 2003; Jim *et al.*, 2006; McMahon *et al.*, 2013b). Patterns in carbon isoopic compositins of non-essential amino acids ($\delta^{13}C_{nonEAA}$) should, in theory, provide evidence for both *de novo* synthesis from bulk dietary carbon pools, and isotopic routing from dietary protein (McMahon *et al.*, 2010; Newsome *et al.*, 2011; McMahon *et al.*, 2015b; see Chapter 1). In this study, pattens in $\delta^{13}C_{nonEAA}$ values were also analysed, but a coherent physiological framework to interpret variance in carbon isotope data for amino acids that are wholly or partially synthesised *de novo* is currently lacking.

4.3 Materials and Methods

4.3.1 Sample description

The same vertebrae analysed for isotopes in bulk collagen (Chapter 3) were analysed for isotopes in single amino acids. In brief, vertebrae were excised from nine blue sharks (*Prionace glauca*, Linnaeus 1758) and six porbeagles (*Lamna nasus*, Bonnaterre 1788) from across the North Atlantic. Capture areas were located at the extremes and centre (at least for blue sharks) of these species' distributional ranges in the North Atlantic, as estimated by electronic tagging studies (e.g. Campana *et al.*, 2010; Queiroz *et al.*, 2010; Campana *et al.*, 2011; Vandeperre *et al.*, 2014; Biais *et al*., 2016). For blue sharks, capture areas included offshore waters south of the Canary Islands (24-26 °N, 20-21 °W) in the Northeast Atlantic, the mid-Atlantic Ridge area north west of the Azores (42 °N, 44-45 °W) in the central North Atlantic, and oceanic waters between Cape Hatteras and the Gulf of Maine in the Northwest Atlantic (Skomal & Natanson, 2003). For porbeagles, capture areas comprised shelf waters between the western English Channel and Celtic Sea (individuals 11 and 40; Bendall *et al.*, 2013; Ellis *et al.*, 2015; Biais *et al*., 2016) and around the Faroe Islands (individual 1000) in the Northeast Atlantic, and between Massachusetts and Grand Banks (off southern Newfoundland) in the Northwest Atlantic (Natanson *et al.*, 2002). Blue sharks were all mature, based on evaluated or fork length-estimated maturity stage. Porbeagles from the Northwest Atlantic were also mature, whereas individuals from the Northeast Atlantic were immature (individual 40) or maturing (individual 11 and 1000; for metadata for individual sharks, see Chapter 3).

4.3.2 Sample collection, preservation, and processing

Procedures for sample collection, preservation and processing for compound-specific isotope analysis were also the same as for bulk analysis, at least until prior to decalcification (Chapter 3). Samples selected for compound-specific analysis were not decalcified, as inorganic biopatite was

removed (and single amino acids liberated from proteins) with hydrolysis (see below). The procedures for bulk and compound-specific analysis, however, presented some differences. Firstly, half vertebral sections for compound-specific isotope analysis were 6 mm (rather than 5 mm) thick, as more sample is required for compound-specific analysis (see below), and equidistant samples from thicker sections are expected to be generally heavier (though sample weight does not depend only on section thickness, but also on intermedialia water and air content; S.M., *pers. obs.*). Furthermore, the minimum weight required for compound-specific isotope analysis was much greater than that for bulk analysis (4 *versus* 0.5 mg, respectively), as determined by analysis of test comparable blue shark samples of varying weight at the Woods Hole Oceanographic Institution Fish Ecology Laboratory. Consequently, whilst the vertebral radius and sample number along the radius (and thus the average interval between adjacent samples, distance along the radius, and age) were the same for bulk and compound-specific isotope analysis, the proportion of samples for compound-specific analysis requiring to be combined was much greater than that of samples for bulk analysis (18 *versus* 4% respectively). Additionally, combinations of samples for compound-specific analysis included up to three (rather than up to two) samples, and were located along the vertebral radius (rather than just at the core of vertebral sections). Finally, compound-specific isotope analysis was run at full resolution along the vertebral radius for blue sharks from the mid-Atlantic Ridge and the Canary Islands, and at half resolution for all other individuals. Thus, the highest possible temporal resolution of ecological information was lower for compound-specific analysis than for bulk analysis, due to a higher number of samples needing to be combined, and generally coarser analysis resolution.

Sample age was estimated from distance along the vertebral radius for single and combined samples for compound-specific isotope analysis in the same way as for samples for bulk analysis, by using validated and estimated body size:age and vertebral radius:body size statistical relationships for blue and porbeagle sharks (Natanson *et al.*, 2002; Skomal & Natanson, 2003; Chapter 3). Additionally, age at birth and at maturity were also estimated directly from measured mean fork length values using validated Von Bertalanffy relationships (Chapter 3), and used as cutoffs to distinguish pre-birth, juvenile and adult life-history stages in time-series and variance analyses (see below).

4.3.3 Sample preparation for compound-specific stable isotope analysis

4.3.3.1 Hydrolysis

After combination, to liberate amino acids from protein, samples were acid-hydrolised in 1 ml 6 N HCl at 110 °C (temperature range: 105-115 °C) for 20 h. To prevent sample and acid evaporation, vials were closed tightly with a lid during hydrolysis. After hydrolysis, samples were dried with a gentle stream of gaseous nitrogen (N_2) at 60 °C (temperature range: 55-65 °C) for 30-60 min, depending on sample weight and excess HCl volume. Samples were re-dissolved in 100 µl 0.1 N HCl, and preserved at 4 °C until derivatisation.

4.3.3.2 Derivatisation

Amino acids are difficult to analyse by gas chromatography-combustion-isotope ratio monitoring mass spectrometry (CG-C-irm-MS), as they contain highly polar functional groups (e.g. carboxylic acid groups). To produce compounds amenable to GC-C-irm-MS analysis, therefore, amino acids must be derivatised through the addition of less polar functional groups (Klee, 1985; McMahon *et al.*, 2011b). Acid-hydrolised samples (i.e. 50 µl of the sample + 100 µl 0.1 N HCl solution) were derivatised by adding 35 µl methanol, 30 µl pyridine, and 15 µl methyl chloroformate (MCF); after additions, the mixture was vortexed for 30 s. The derivatisation method with MCF is one-step, rapid, and substantially decreases the derivative carbon (i.e. exogenous carbon from added functional groups of derivatising agents, such as MCF) contribution, facilitating the determination of carbon isotopic compositions ($\delta^{13}C$) of amino acids (see Husek, 1991; Chen *et al.*, 2010; Walsh *et al.*, 2014). Amino acid-MCF derivates were separated from the reaction mixtures by liquid:liquid extraction using chloroform. Depending on original sample weight, a different volume of chloroform was added to the reaction mixture (i.e. 4-10 mg: 50 µl; 11-22 mg: 75 µl; > 23 mg: 100 µl); after chloroform addition, the mixture was vortexed again for other 30 s. At this stage, the reaction mixture was stratified: the organic layer of amino acid-MCF derivates was separated from the aqueous layer using electrophoresis pipette tips, and used for GC-C-irm-MS analysis.

4.3.3.3 Standards

Derivatisation alters $\delta^{13}C$ values of amino acids through exogenous carbon from added functional groups, and kinetic fractionation associated during derivatisation reactions (Rieley, 1994; Docherty *et al.*, 2001; McMahon *et al.*, 2011b). Two internal laboratory standards (ILSs; i.e. AA1 and AA2 standards) were created from single amino acids with known $\delta^{13}C$ values. Additionally, 20 mg of lyophilised muscle tissue from Atlantic cod (*Gadus morhua*) were acid-hydrolised and re-dissolved in 100 µl 0.1 N HCl, and 50 µl of the solution were also used as standard (i.e. GM standard). All standards were concurrently derivatised with each sample batch, and dissolved in 100 µl chloroform. Derivatisation correction factors were determined for each amino acid, based on known $\delta^{13}C$ values of amino acids in the standards prior to derivatisation, and applied to each sample to adjust for the introduction of exogenous carbon and kinetic fractionation during derivations. As no international standards are currently available for the analysis of carbon isotopes in amino acids, and no large inter-laboratory calibration has yet come up with consensus $\delta^{13}C$ values, mean values across three laboratories (i.e. the Fish Ecology Laboratory, the Marine Biological Laboratory, and UC Davis Stable Isotope Facility; see Table 4.A1A) were used. Precision was determined as the standard deviation for $\delta^{13}C$ values of each amino acid of the in-house cod standard during the time period shark samples were analysed (Table 4.A1B).

The lack of internationally ceritified standards should not be an issue when comparing patterns in carbon isotopic compositions of amino acids in shark samples, as all the samples were run on the same instrument using the same methods, and in the same period of time. By contrast, any potential systemtic bias could be an issue when compating end-member and consumer data within a fingerprinting framework (see below). However, this approach has been previously successfully applied to compare data obtained by different laboratories (e.g. McMahon *et al.*, 2015a).

4.3.4 Compound-specific isotope analysis

Derivatised samples were analysed by gas chromatography-combustion-isotope ratio monitoring mass spectrometry (GC-C-irm-MS) at the Woods Hole Oceanographic Institution Fish Ecology Laboratory. Dervatised samples were dissolved in dichloromethane (DCM), and injected on column in splitless mode at 260 °C and separated on an Agilent VF-23ms column (30 m length, 0.25 mm inner diameter, and 0.25 μm film thickness; Agilent Technologies, Wilmington, Delaware, USA) in an Agilent 6890N Gas Chromatograph (GC). Sample concentrations were adjusted to achieve a minimum 2 V output for all amino acids. Gas chromatography conditions were set to optimise peak separation and shape as follows: initial temperature 80 °C held for 1 min; ramped to 260 °C at 6 °C·min^{-1}; held for 3 min. The separated amino acid peaks were combusted online in a Finnigan GC-C continuous flow interface at 930 °C and then measured as CO_2 on a Thermo Finnigan Mat 253 irm-MS (Agilent Technologies 6890N GC). Standardisation of runs was achieved using intermittent pulses of a CO_2 reference gas of known isotopic composition.

All compound-specific samples were run in duplicate; standards were run interspersed among samples 4-6 times, depending on the number of samples in a particular batch. Carbon isotopic compositions ($\delta^{13}C$, ‰) were recovered for the following amino acids: valine, isoleucine, leucine, threonine, phenylalanine (essential amino acids), alanine, glycine, proline, aspartic acid, and glutamic acid (non-essential amino acids). Carbon isotopic compositions of threonine showed poor chromatography and inconsistencies among replicates, therefore these were omitted from both the sample-normalisation of $\delta^{13}C$ values of amino acids (see below) and data analysis.

A typical chromatogram from the analysis of carbon isotopes in amino acid-MCF derivates showing retention times, peak separation and isotope ratios is displayed in Fig. 4.2. The glutamic acid and aspartic acid peaks contained unknown contributions from glutamine and asparagine, respectively, due to conversion to their dicarboxylic acids during acid hydrolysis. The relative abundance (%) of individual amino acids in vertebrae were calculated from mass 44 peak area based on standards of known concentration.

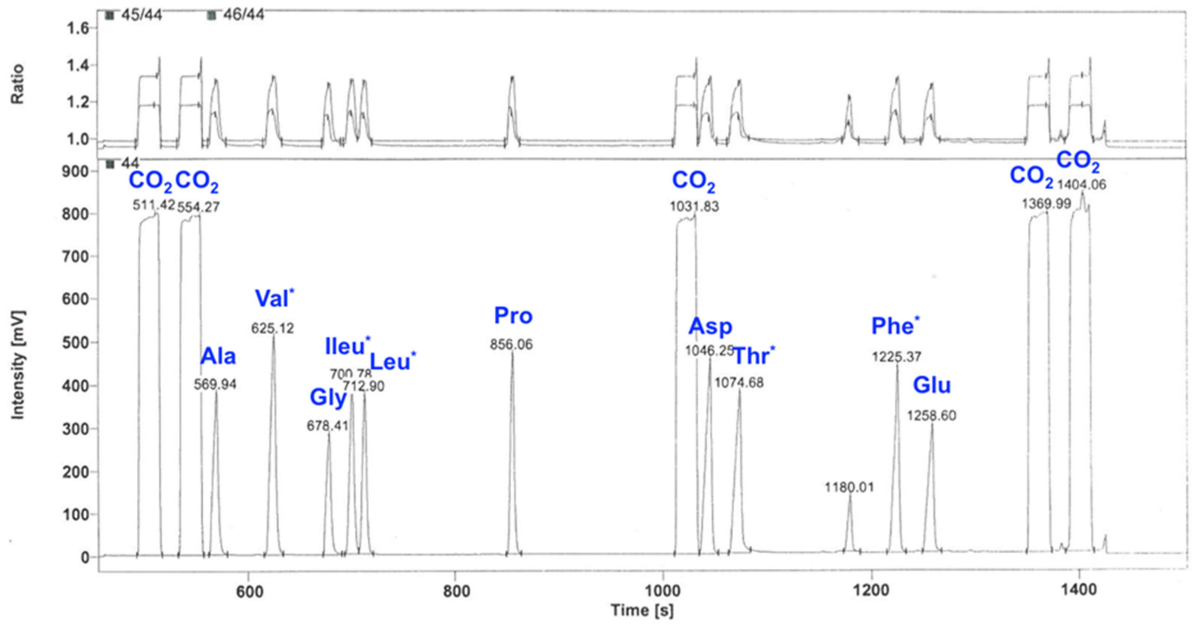

Figure 4.2 Typical chromatogram from the analysis of carbon isotopes in single amino acids from shark vertebral samples.
Peaks are labelled to indicate CO_2 reference and single amino acids. Numbers indicate retention times. The peak with retention time = 1180.01 s is neither a CO_2 reference nor an amino acid peak, hence it is unresolved.

4.3.5 Data analysis

Summary statistics of mean and variance were calculated for the carbon isotopic compositions of all recovered amino acids, including essential and non-essential amino acids, for each species and individual shark. To remove influences from spatial variations in the carbon isotopic composition of aqueous CO_2 ($\delta^{13}C_{CO2(aq)}$), the carbon isotopic compositions of single amino acids in each sample were normalised to the mean $\delta^{13}C$ value for all essential amino acids in that sample (sample-normalisation) as in Eq. 4.2.

$$\delta^{13}C_{norm-AAi} \sim \delta^{13}C_{AAi} - \text{mean } \delta^{13}C_{EAA} \quad (4.2)$$

where $\delta^{13}C_{norm\text{-}AAi}$ is the sample-normalised carbon isotope value for the amino acid i, $\delta^{13}C_{AAi}$ the raw value, and mean $\delta^{13}C_{EAAs}$ the average value for all essential amino acids.

Normality in raw and sample-normalised isotope values for each amino acid was tested with a Shapiro-Wilk test. Homogeneity of variances in isotope values between raw and sample-normalised values was tested with a Levene's test where data in both groups were normally distributed, with a Kruskal-Wallis test where data were non-normal. This was done to test whether variance in sample-normalised values was reduced compared to that in raw values, as sample-normalisation should remove spatial variability in $\delta^{13}C_{CO2(aq)}$ values.

In this thesis, analysis and interpretation of amino acid carbon isotope data were restricted to the essential amino acids. Patterns in carbon isotopic compositions of non-essential amino acids were

also examined, but a coherent physiological framework to interpret variance in carbon isotope values of amino acids that are wholly or partially synthesised *de novo* is currently lacking.

To reduce the number of variables from four essential amino acids (carbon isotopic compositions) to two principal components explaining the largest proportion of variance in amino acids (PC1 and PC2), a principal component analysis (PCA) was applied to both raw and normalised carbon isotopic compositions of essential amino acids ($\delta^{13}C_{EAA}$ and $\delta^{13}C_{norm\text{-}EAA}$, respectively) in shark samples. To examine between-species differences in patterns of $\delta^{13}C_{EAA}$ and $\delta^{13}C_{norm\text{-}EAA}$ values, standard ellipse area corrected for small sample size (SEAc) was calculated for each species, based on PC1 and PC2 scores from PCAs with $\delta^{13}C_{EAA}$ and $\delta^{13}C_{norm\text{-}EAA}$ values.

To allow the comparison of relative changes in $\delta^{13}C_{EAA}$ and $\delta^{13}C_{norm\text{-}EAA}$ values across life-history between individuals, for each PCA, the PC1 score for each sample was normalised to the mean PC1 score across the whole time-series for the individual from where the sample was taken (nPC1; life history-normalisation; Chapter 3). Common, broad ontogenetic patterns in normalised PC1 scores across individuals of both species identified species-level life-history isotopic traits. Ontogenetic patterns in raw and normalised PC1 scores, and the effect of species and capture area on these patterns, were tested with generalised additive mixed models (GAMMs), with generalised linear mixed effect models (GLMMs) where ontogenetic patterns approximated linear relationships (see below), by following the same framework as described in Chapter 3; results and parameter estimates were reported for the full models. Between-individual variances in normalised PC1 scores were compared between each pair of combinations of species and life-history stage with a Levene's test, with a Kruskal-Wallis test where data were non-normal. For each combination, variance in raw PC1 scores was also compared against variance in normalised PC1 scores (see Chapter 3).

4.3.5.1 Definition of carbon source fingerprints

Raw data for carbon isotopic compositions of the essential amino acids recovered for shark samples were literature-sourced for a selection of primary producers and bacteria (end-members), which were considered relevant to blue and porbeagle shark ecology (Scott *et al.*, 2006; Larsen *et al.*, 2009; 2013; 2015; Table 4.B1). The carbon isotopic compositions of essential amino acids in end-member samples were also sample-normalised ($\delta^{13}C_{norm\text{-}EAA}$) as in Eq. 4.2. End-members were classified *a priori* within the following groups: i) autotrophic and ii) heterotrophic bacteri (prokaryotes), iii) microalgae, iv) macroalgae, v) seagrasses and vi) terrestrial plants (eukaryotes).

To assess differences in $\delta^{13}C_{norm\text{-}EAA}$ patterns among these end-member groups, a PCA was first carried out with $\delta^{13}C_{norm\text{-}EAA}$ values (Larsen *et al.*, 2013). To examine combinations of independent variables (i.e. $\delta^{13}C_{norm\text{-}EAA}$ values) that best explained differences between the categorical variables (i.e. the groups defined by the PCA), and to construct a model for predicting group membership of unknown consumer samples, a linear discriminant function analysis (LDA) was performed on the $\delta^{13}C_{norm\text{-}EAA}$ data for end-members. A leave-one-out cross validation approach was

used to calculate the probability of group membership of the classifier sample; accuracy was defined as the proportion (%) of samples that classified within the correct groups (Larsen *et al.*, 2013). The resulting LDA model was then used to predict group membership of shark samples, as well as samples from various consumers (Table 4.B2) and sinking particulate organic matter (Table 4.B3), for which raw $\delta^{13}C_{EAA}$ data were also literature-sourced (Hannides *et al.*, 2013; Larsen *et al.*, 2013; McMahon *et al.*, 2015a, b; Houghton, *unpubl. data*; Sabadel, *unpubl. data*). As stated above, the lack of internationally certified standards may be an issue when comparing end-member and consumer samples analysed on different instruments and with different methods. Nevertheless, such a fingerprinting approch has already been successfully applied to tack phytoplankton regime shifts from amino acid carbon isotope data for corals (McMahon *et al.*, 2015a).

4.4 Results

4.4.1 Variance in $\delta^{13}C$ values of amino acids

128 blue shark vertebral samples were analysed to determine the carbon isotopic compositions in amino acids, and compared to the 196 samples analysed for isotopes in bulk cartilage collagen (Chapter 3). 80 porbeagle vertebral samples were analysed for isotopes in amino acids, and 133 for isotopes in bulk collagen. Raw $\delta^{13}C$ values in all the recovered amino acids, including essential and non-essential amino acids, for each analysed sample are reported in Table 4.1.

In blue sharks, average (mean ± SD, ‰) $\delta^{13}C$ values of single amino acids were -21.25 ± 2.20 for valine, -18.38 ± 2.02 for isoleucine, -26.52 ± 2.22 for leucine, -26.93 ± 1.40 for phenylalanine, -13.69 ± 1.81 for alanine, -3.38 ± 2.15 for glycine, -13.50 ± 1.43 for proline, -12.63 ± 4.58 for aspartic acid, and -8.11 ± 1.87 for glutamic acid. In porbeagles, average (mean ± SD, ‰) $\delta^{13}C$ values of single amino acids were -19.47 ± 1.42 for valine, -17.83 ± 2.01 for isoleucine, -25.34 ± 0.85 for leucine, -25.66 ± 0.73 for phenylalanine, -14.62 ± 1.40 for alanine, -0.95 ± 2.18 for glycine, -11.92 ± 1.27 for proline, -13.24 ± 4.59 for aspartic acid, and -5.03 ± 2.66 for glutamic acid. Values of $\delta^{13}C$ in bulk cartilage collagen averaged at -15.13 ± 0.56 ‰ in blue sharks, and at -14.55 ± 0.38 ‰ in porbeagles. In blue sharks, variances in sample-normalised $\delta^{13}C$ values were significantly smaller than variances in raw values for all essential amino acids and alanine (maximum p-value = 0.013; Levene's test = 6.117); variances in sample-normalised $\delta^{13}C$ values of aspartic and glutamic acids were significantly larger than variances in raw values (maximum p-value = 0.019; Levene's test = 5.540). In porbeagles, variances in sample-normalised $\delta^{13}C$ values were significantly smaller than variances in raw values for isoleucine, leucine, glycine and proline (maximum p-value = 0.026; Levene's test = 5.0278), and significantly larger for phenylalanine (Levene's test = 5.993, p-value = 0.014).

Means and standard deviations (SD) for raw $\delta^{13}C$ values of all the recovered amino acids, including essential and non-essential amino acids, for each individual shark are reported in Table 4.2. Variances in raw and sample-normalised $\delta^{13}C$ values of amino acids, and raw $\delta^{13}C$ values of bulk

cartilage collagen throughout the life of each individual shark are presented in Fig. 4.3. Individual-level life-history records of raw and sample-normalised $\delta^{13}C$ values of amino acids, and raw $\delta^{13}C$ values of bulk cartilage collagen are presented in Fig. 4.4.

Table 4.1 Raw carbon isotopic compositions of all the recovered amino acids, including essential and non-essential amino acids ($\delta^{13}C_{EAA}$ and $\delta^{13}C_{nonEAA}$, respectively), for each analysed sample. Individual ID, sample ID (both IDs of single samples within combinations and average ID), sample distance along the vertebral radius (calculated with average sample ID for combinations), and sample age are reported. Metadata for individual sharks are presented in Chapter 3.

					Essential				Non-essential				
Ind. ID	**ID (comb.)**	**ID (av.)**	**d (mm)**	**age (mo)**	**Val**	**Ileu**	**Leu**	**Phe**	**Ala**	**Gly**	**Pro**	**Asp**	**Glu**
16	1+2+3	2	0.87	-9.90	-23.62	-18.93	-28.46	-28.57	-15.26	-3.17	-15.67	-12.85	-7.32
16	4+5	4.5	2.32	0.31	-24.90	-18.94	-27.80	-28.35	-16.54	-6.89	-14.46	-10.53	-8.48
16	6	6	3.18	7.03	-24.13	-17.61	-28.37	-28.88	-16.27	-5.37	-16.42	-9.59	-7.54
16	7+8	7.5	4.05	14.28	-27.21	-20.97	-28.48	-30.34	-15.02	-7.51	-13.25	-9.11	-12.30
16	9	9	4.92	22.14	-23.74	-18.42	-28.08	-27.38	-13.74	-3.30	-14.48	-7.27	-7.71
16	10	10	5.50	27.78	-24.86	-20.61	-29.06	-29.31	-16.12	-5.42	-16.09	-10.10	-8.25
16	11	11	6.08	33.79	-23.43	-20.41	-30.02	-27.67	-15.55	-5.92	-15.77	-9.45	-7.32
16	12	12	6.66	40.22	-24.19	-20.23	-28.55	-29.87	-16.26	-6.91	-14.79	-11.98	-7.32
16	13	13	7.24	47.13	-24.92	-19.34	-28.49	-27.99	-16.26	-6.86	-16.87	-12.74	-6.45
16	14	14	7.82	54.60	-23.94	-19.41	-28.39	-27.29	-13.55	-3.85	-14.33	-9.90	-9.04
16	15	15	8.39	62.73	-22.61	-19.43	-28.53	-27.80	-14.13	-3.63	-15.69	-9.14	-8.73
16	16	16	8.97	71.64	-22.51	-19.04	-25.49	-28.69	-14.16	-3.40	-12.80	-10.20	-9.95
16	17	17	9.55	81.50	-22.32	-19.70	-27.74	-28.08	-14.55	-2.61	-14.77	-11.66	-7.37
16	18	18	10.13	92.55	-22.52	-18.84	-27.27	-27.90	-13.09	-2.64	-13.30	-9.52	-7.11
16	19	19	10.71	105.10	-21.54	-19.04	-27.29	-28.32	-13.77	-2.54	-13.75	-9.39	-5.94
24	1+2+3	2	0.79	-10.45	-20.13	-17.75	-27.97	-27.33	-13.82	-2.33	-13.05	-4.70	-8.48
24	4+5+6	5	2.36	0.62	-22.31	-18.82	-29.62	-28.07	-14.30	-2.70	-12.83	-9.69	-10.22
24	7+8	7.5	3.67	10.99	-21.39	-18.67	-29.02	-27.64	-13.90	-3.88	-13.65	-9.85	-10.31
24	9+10	9.5	4.71	20.21	-22.87	-19.32	-28.02	-26.14	-15.71	-5.44	-14.49	-8.07	-11.16
24	11	11	5.50	27.78	-22.43	-20.34	-28.65	-26.68	-15.05	-5.52	-14.70	-7.91	-11.16
24	12	12	6.02	33.20	-22.14	-20.25	-27.86	-27.71	-16.19	-7.54	-14.80	-5.17	-11.20
24	13	13	6.55	38.96	-21.34	-20.70	-26.97	-26.41	-16.16	-7.56	-14.96	-5.57	-11.48
24	14	14	7.07	45.10	-22.10	-19.98	-29.22	-27.07	-13.47	-3.08	-14.41	-8.60	-11.06
24	15	15	7.60	51.68	-21.63	-20.71	-29.08	-27.45	-13.66	-3.23	-15.83	-8.67	-11.72
24	16	16	8.12	58.77	-21.78	-19.79	-28.82	-27.72	-13.19	-1.28	-14.01	-6.97	-11.94
24	17	17	8.64	66.44	-20.14	-19.04	-28.21	-27.54	-13.28	-1.96	-14.61	-6.15	-11.67
24	18	18	9.17	74.81	-22.85	-20.27	-27.58	-27.19	-12.93	-4.75	-16.10	-8.53	-9.76
24	19	19	9.69	84.02	-21.66	-19.82	-27.03	-27.13	-13.19	-4.25	-15.16	-8.06	-9.00
24	20	20	10.21	94.24	-19.95	-18.57	-27.72	-27.24	-15.08	-1.93	-11.84	-5.45	-8.85
24	21	21	10.74	105.75	-19.28	-18.04	-26.53	-27.22	-14.94	-0.77	-11.18	-5.86	-8.93
12	1+2+3	2	0.88	-9.81	-21.29	-16.94	-26.62	-28.83	-14.41	-2.39	-13.50	-9.46	-6.38
12	4+5	4.5	2.35	0.59	-23.41	-19.41	-29.13	-29.22	-15.27	-5.21	-14.31	-8.14	-9.97
12	6	6	3.24	7.44	-22.99	-20.73	-29.88	-28.12	-15.48	-5.69	-15.32	-8.34	-9.37
12	7	7	3.82	12.31	-23.07	-19.16	-30.38	-29.43	-14.92	-2.85	-13.22	-8.73	-6.45
12	8+9	8.5	4.71	20.13	-21.75	-18.72	-29.58	-29.01	-14.91	-3.73	-13.37	-9.44	-6.16
12	10+11	10.5	5.88	31.71	-21.97	-18.79	-27.57	-26.23	-12.34	-0.63	-14.06	-9.11	-6.13
12	12	12	6.76	41.46	-21.02	-18.76	-27.76	-27.38	-12.69	-1.56	-14.03	-9.09	-6.67
12	13	13	7.35	48.58	-21.13	-17.79	-26.80	-27.89	-11.09	-1.31	-12.01	-9.72	-6.89
12	14	14	7.94	56.30	-19.57	-16.90	-26.77	-27.71	-11.59	1.10	-11.27	-8.72	-6.19
12	15	15	8.53	64.72	-21.84	-21.47	-28.78	-28.86	-14.84	-6.67	-14.86	-5.41	-7.45
12	16	16	9.12	74.00	-20.60	-20.50	-28.23	-28.18	-14.70	-5.44	-14.03	-5.55	-6.07
12	17	17	9.71	84.30	-21.81	-18.39	-26.87	-28.48	-14.01	-5.92	-10.98	-6.92	-8.05
101	1+2+3	2	1.13	-8.17	-22.88	-21.59	-28.94	-29.26	-16.34	-6.65	-13.59	-16.26	-3.79
101	4	4	2.63	2.65	-24.06	-24.76	-29.69	-28.62	-22.30	-10.44	-17.95	-14.64	-11.82
101	5	5	3.38	8.57	-23.60	-22.06	-30.12	-28.03	-16.59	-8.98	-13.51	-15.94	-7.57

					Essential				Non-essential				
Ind. ID	**ID (comb.)**	**ID (av.)**	**d (mm)**	**age (mo)**	**Val**	**Ileu**	**Leu**	**Phe**	**Ala**	**Gly**	**Pro**	**Asp**	**Glu**
101	6	6	4.13	14.91	-22.36	-20.33	-28.40	-26.20	-16.68	-5.34	-13.82	-10.90	-9.65
101	7	7	4.88	21.71	-23.25	-21.01	-29.11	-28.43	-16.05	-5.42	-13.74	-11.30	-9.29
101	8	8	5.63	29.05	-25.51	-19.34	-29.10	-25.95	-14.59	-6.15	-13.44	-8.90	-8.05
101	9	9	6.38	37.03	-23.16	-19.72	-28.11	-28.39	-15.58	-4.64	-15.68	-8.19	-6.51
101	10	10	7.13	45.76	-23.54	-22.90	-30.82	-27.62	-17.79	-7.70	-13.07	-11.67	-8.64
101	11	11	7.88	55.40	-23.58	-21.75	-29.90	-28.64	-15.78	-5.63	-13.61	-11.29	-5.66
101	12	12	8.63	66.17	-23.25	-20.04	-28.61	-26.05	-14.86	-3.99	-13.39	-9.22	-6.37
101	13	13	9.38	78.36	-21.18	-21.39	-28.17	-26.63	-14.25	-6.37	-12.05	-8.62	-6.11
101	14	14	10.13	92.42	-23.70	-22.57	-27.28	-28.05	-16.20	-3.28	-15.41	-11.10	-6.65
101	15	15	10.88	109.00	-21.72	-21.82	-28.60	-28.34	-14.79	-4.91	-13.82	-8.41	-5.24
101	16	16	11.63	129.24	-24.35	-19.03	-27.51	-26.75	-14.67	-2.79	-12.54	-11.96	-11.73
131	1+2	1.5	0.71	-10.98	-21.14	-19.37	-28.16	-27.48	-13.57	-4.31	-14.62	-11.20	-6.56
131	3	3	1.76	-3.71	-23.24	-18.32	-30.15	-26.53	-13.88	-5.06	-16.92	-9.61	-7.81
131	4+5	4.5	2.82	4.18	-21.96	-20.88	-28.88	-28.35	-15.03	-6.77	-15.76	-10.09	-8.84
131	6+7	6.5	4.24	15.88	-22.30	-16.98	-26.59	-26.59	-15.10	-6.48	-14.06	-11.74	-11.01
131	8	8	5.29	25.74	-21.33	-18.17	-26.92	-26.81	-11.80	-3.28	-14.25	-7.53	-6.78
131	9	9	6.00	32.95	-24.50	-19.08	-28.32	-26.07	-13.16	-2.96	-14.24	-8.55	-8.21
131	10	10	6.71	40.78	-23.52	-20.10	-28.61	-27.67	-14.01	-6.71	-15.32	-8.78	-6.78
131	11	11	7.41	49.33	-23.63	-17.24	-25.52	-26.12	-12.36	-4.12	-12.44	-7.37	-10.18
131	12	12	8.12	58.75	-20.45	-19.98	-28.28	-25.99	-13.13	-4.16	-14.45	-8.78	-6.35
131	13	13	8.82	69.24	-21.35	-19.51	-28.54	-25.80	-14.39	-3.96	-13.88	-9.80	-7.51
131	14	14	9.53	81.09	-22.92	-20.01	-28.41	-26.99	-15.09	-5.89	-15.25	-7.18	-7.34
131	15	15	10.24	94.68	-21.64	-18.03	-27.13	-25.85	-13.66	-4.83	-13.74	-7.39	-8.80
131	16	16	10.94	110.62	-21.88	-18.88	-26.23	-28.18	-12.53	-2.45	-13.97	-5.59	-5.97
131	17	17	11.65	129.90	-21.35	-17.12	-24.76	-26.03	-12.01	-2.44	-11.32	-7.73	-7.75
33	1+2+3	2	0.82	-10.22	-20.51	-15.93	-24.33	-27.38	-11.36	0.64	-12.80	-13.59	-6.11
33	4+5	4.5	2.19	-0.62	-23.39	-18.15	-25.31	-27.29	-15.25	-3.03	-14.84	-14.77	-6.43
33	6+7	6.5	3.29	7.85	-23.90	-17.31	-24.55	-27.21	-15.36	-3.21	-15.28	-16.59	-6.36
33	8+9	8.5	4.38	17.17	-22.87	-16.88	-25.01	-29.10	-10.81	-0.75	-12.95	-13.89	-7.65
33	10	10	5.20	24.84	-21.35	-16.16	-24.26	-28.20	-9.97	-0.50	-13.43	-14.48	-6.71
33	11	11	5.75	30.33	-20.39	-17.91	-26.97	-27.75	-12.67	-1.51	-13.33	-13.11	-8.82
33	12	12	6.30	36.17	-20.69	-16.78	-26.06	-26.58	-11.12	-0.46	-13.85	-14.90	-7.10
33	13	13	6.85	42.40	-22.37	-17.93	-26.15	-27.84	-12.68	-0.82	-12.90	-15.17	-7.78
33	14	14	7.39	49.09	-22.29	-17.92	-26.20	-27.95	-13.28	-1.42	-13.93	-16.32	-7.44
33	15	15	7.94	56.29	-23.10	-18.82	-26.52	-28.11	-12.88	-3.38	-13.93	-13.82	-7.41
33	16	16	8.49	64.11	-22.02	-17.21	-25.73	-28.01	-12.01	-2.48	-14.25	-15.40	-6.03
33	17	17	9.04	72.65	-23.70	-18.97	-26.80	-27.23	-12.14	-2.88	-11.96	-16.13	-8.46
33	18	18	9.58	82.06	-21.80	-18.51	-26.02	-27.98	-12.12	-1.54	-13.82	-16.51	-8.35
33	19	19	10.13	92.54	-22.78	-19.93	-25.93	-27.94	-13.12	-1.82	-13.09	-16.63	-8.05
33	20	20	10.68	104.36	-22.57	-18.80	-25.69	-26.81	-12.63	-1.99	-13.73	-17.74	-7.06
33	21	21	11.23	117.93	-23.84	-20.75	-26.79	-27.99	-12.68	-2.70	-11.88	-5.72	-10.88
335	1+2	1.5	0.50	-17.60	-16.30	-13.88	-22.52	-25.10	-10.86	-2.17	-10.72	-18.65	-4.41
335	5+6	5.5	2.50	-4.94	-18.57	-15.74	-23.60	-24.46	-12.80	-2.19	-12.37	-20.38	-3.97
335	9+10	9.5	4.50	8.20	-19.35	-15.69	-24.58	-26.15	-13.03	-4.98	-12.70	-19.21	-7.04
335	12	12	5.75	17.07	-18.32	-16.48	-25.67	-25.71	-14.32	-3.92	-12.56	-20.66	-7.45
335	14	14	6.75	24.66	-18.64	-14.02	-23.67	-25.32	-13.78	-3.52	-13.07	-17.78	-6.91
335	16	16	7.75	32.78	-17.94	-15.15	-23.17	-25.88	-14.65	-2.26	-13.02	-16.47	-3.00
335	18	18	8.75	41.56	-18.33	-16.91	-25.11	-24.31	-12.01	-3.68	-11.96	-17.09	-5.55
335	20	20	9.75	51.14	-17.55	-14.28	-23.85	-23.95	-14.16	-2.75	-11.62	-16.56	-5.00
335	22	22	10.75	61.69	-18.86	-16.47	-23.67	-25.45	-12.29	-3.32	-11.24	-14.73	-6.05

					Essential				Non-essential				
Ind. ID	**ID (comb.)**	**ID (av.)**	**d (mm)**	**age (mo)**	**Val**	**Ileu**	**Leu**	**Phe**	**Ala**	**Gly**	**Pro**	**Asp**	**Glu**
335	24	24	11.75	73.49	-18.23	-15.93	-23.87	-26.62	-12.34	-1.85	-12.35	-14.64	-7.03
335	26	26	12.75	86.87	-18.35	-16.83	-23.36	-25.09	-10.48	-1.46	-10.88	-18.63	-7.60
335	28	28	13.75	102.39	-17.17	-17.15	-22.70	-24.70	-10.95	-2.50	-10.76	-17.66	-7.78
335	30	30	14.75	120.89	-19.07	-17.56	-24.72	-25.59	-11.55	-1.66	-11.47	-16.46	-9.55
335	32	32	15.75	143.85	-17.11	-16.57	-22.19	-24.24	-11.23	-0.93	-12.57	-15.96	-8.57
335	34	34	16.75	174.23	-17.66	-14.06	-24.17	-24.79	-10.89	-0.68	-10.39	-17.46	-6.03
415	1+2	1.5	0.48	-17.71	-18.08	-17.69	-24.53	-24.20	-11.76	-3.21	-11.54	-14.77	-10.15
415	5+6	5.5	2.42	-5.45	-19.95	-18.52	-26.16	-24.15	-12.81	-3.55	-13.43	-14.41	-9.74
415	8	8	3.63	2.35	-19.01	-17.59	-24.75	-25.40	-14.20	-1.65	-12.17	-17.75	-10.62
415	10	10	4.60	8.87	-20.29	-17.73	-26.24	-24.99	-13.51	-3.07	-13.09	-16.71	-10.25
415	12	12	5.56	15.71	-20.23	-17.34	-24.64	-25.07	-14.15	-2.75	-13.52	-16.13	-10.47
415	14	14	6.53	22.96	-18.01	-18.19	-24.45	-27.15	-13.15	-0.90	-13.43	-15.04	-9.19
415	16	16	7.50	30.69	-19.58	-17.24	-24.49	-27.46	-15.05	-3.75	-14.06	-16.20	-10.15
415	18	18	8.47	39.01	-19.02	-17.43	-24.95	-26.04	-13.30	-3.46	-13.35	-18.66	-9.08
415	20	20	9.44	48.03	-17.87	-18.05	-23.71	-25.14	-13.06	-3.71	-12.04	-19.04	-8.70
415	22	22	10.40	57.91	-17.99	-17.59	-23.38	-25.96	-11.80	-2.13	-12.37	-17.52	-7.82
415	24	24	11.37	68.85	-17.13	-16.55	-23.26	-25.14	-11.55	-0.72	-12.97	-15.73	-7.41
415	26	26	12.34	81.14	-18.13	-17.98	-23.00	-24.98	-11.82	0.69	-13.27	-14.98	-8.36
415	28	28	13.31	95.20	-18.06	-17.64	-23.23	-26.62	-10.31	0.25	-13.58	-15.05	-9.76
415	30	30	14.27	111.64	-18.93	-17.57	-22.95	-25.14	-10.75	0.51	-11.94	-13.29	-9.18
441	1+2	1.5	0.52	-17.48	-19.47	-18.64	-24.72	-26.28	-14.86	-1.87	-12.71	-21.40	-6.88
441	6	6	2.85	-2.72	-20.26	-16.79	-24.28	-25.68	-14.14	-4.02	-13.29	-22.45	-7.80
441	8	8	3.88	4.04	-19.83	-15.30	-24.19	-25.37	-14.05	-3.66	-13.16	-21.52	-8.61
441	10	10	4.92	11.11	-17.82	-15.35	-24.04	-25.20	-12.74	-2.32	-11.86	-19.56	-9.64
441	12	12	5.96	18.59	-19.98	-13.37	-24.90	-25.38	-13.38	-2.60	-13.23	-21.87	-9.19
441	14	14	6.99	26.56	-20.92	-17.20	-25.50	-25.71	-13.72	-3.01	-13.22	-18.15	-10.14
441	16	16	8.03	35.14	-20.36	-17.07	-25.41	-25.94	-12.16	-0.90	-12.80	-17.80	-8.13
441	18	18	9.06	44.46	-20.05	-16.53	-21.79	-26.04	-11.19	-0.79	-12.54	-17.97	-10.34
441	20	20	10.10	54.69	-18.52	-14.72	-23.05	-25.41	-13.00	-2.12	-12.00	-19.06	-8.98
441	22	22	11.13	66.06	-18.29	-13.58	-22.68	-24.90	-11.86	-1.24	-12.59	-21.81	-8.41
441	24	24	12.17	78.88	-20.19	-17.70	-24.58	-26.52	-12.82	-2.58	-12.43	-16.37	-8.27
441	26	26	13.21	93.63	-18.22	-16.29	-23.21	-25.46	-12.74	-1.26	-11.30	-16.25	-6.11
441	28	28	14.24	111.03	-18.85	-16.11	-23.33	-24.84	-11.94	-0.22	-12.08	-18.74	-7.18
11	1+2	1.5	0.63	-64.99	-18.57	-15.57	-24.62	-24.86	-12.39	1.44	-10.08	-3.26	-2.06
11	4+5	4.5	2.50	-44.99	-18.33	-14.18	-24.11	-24.91	-12.09	1.90	-9.38	-3.92	-1.99
11	7	7	4.06	-28.15	-19.48	-14.49	-23.88	-25.79	-13.00	1.47	-9.46	-7.46	-3.94
11	9	9	5.31	-14.03	-18.63	-15.73	-25.74	-25.42	-13.25	0.49	-9.67	-4.90	-3.43
11	11	11	6.56	0.91	-18.60	-16.12	-25.39	-25.78	-12.35	-0.52	-10.05	-7.64	-3.30
11	13	13	7.81	16.88	-19.61	-16.49	-25.75	-25.76	-13.06	-1.54	-10.50	-10.59	-3.99
11	15	15	9.06	34.14	-18.65	-15.02	-24.89	-24.70	-11.94	1.19	-9.81	-7.03	-3.07
11	17	17	10.31	53.01	-18.03	-14.93	-24.76	-24.85	-12.15	1.81	-8.95	-7.56	-3.23
11	19	19	11.56	73.88	-19.88	-16.61	-25.17	-25.39	-12.99	-0.41	-10.26	-8.54	-4.61
11	21	21	12.81	97.31	-18.77	-16.51	-25.02	-25.61	-12.39	0.53	-9.14	-7.26	-3.75
11	23	23	14.06	124.13	-19.20	-17.18	-25.16	-25.89	-12.29	0.78	-9.62	-8.79	-4.09
40	1+2	1.5	0.52	-66.16	-20.91	-18.67	-25.63	-25.60	-16.13	-1.52	-11.47	-10.95	-4.23
40	5	5	2.34	-46.64	-19.08	-19.04	-25.39	-24.83	-15.43	-3.34	-10.91	-11.59	-4.14
40	7	7	3.39	-35.53	-17.78	-20.70	-27.03	-25.92	-15.66	-0.10	-11.60	-11.51	-2.88
40	9	9	4.43	-24.10	-18.59	-20.83	-25.80	-28.08	-17.78	-0.42	-12.61	-11.67	-4.09
40	11	11	5.47	-12.21	-18.80	-20.84	-25.84	-25.30	-16.45	0.42	-13.26	-10.06	-4.38
40	13	13	6.51	0.27	-17.39	-21.42	-24.97	-25.92	-15.77	-1.61	-12.92	-11.06	-4.69

					Essential				Non-essential				
Ind. ID	**ID (comb.)**	**ID (av.)**	**d (mm)**	**age (mo)**	**Val**	**Ileu**	**Leu**	**Phe**	**Ala**	**Gly**	**Pro**	**Asp**	**Glu**
40	15	15	7.55	13.46	-17.62	-21.75	-27.56	-25.81	-14.95	-2.84	-13.36	-10.43	-4.55
40	17	17	8.59	27.50	-20.10	-21.46	-26.65	-25.73	-17.66	-3.91	-12.65	-12.88	-3.52
40	19	19	9.64	42.57	-18.85	-21.28	-26.91	-25.88	-16.21	-2.36	-12.70	-13.73	-3.16
40	21	21	10.68	58.86	-21.48	-22.34	-26.67	-26.13	-15.29	0.37	-12.46	-14.11	-2.63
40	23	23	11.72	76.65	-19.30	-21.28	-26.53	-24.81	-15.56	-3.44	-13.28	-13.76	-4.75
1000	1+2	1.2	0.65	-64.76	-21.31	-16.79	-25.99	-26.20	-16.97	-3.16	-13.23	-7.93	-7.38
1000	4	4	2.26	-47.53	-21.83	-17.60	-26.32	-26.53	-16.66	-2.91	-13.15	-11.23	-7.49
1000	6	6	3.55	-33.73	-20.69	-16.88	-25.78	-26.08	-16.80	-1.50	-13.34	-9.96	-8.13
1000	8	8	4.84	-19.41	-22.29	-18.21	-25.38	-25.31	-15.36	-0.23	-13.29	-8.92	-9.10
1000	10	10	6.14	-4.30	-22.04	-18.58	-25.62	-25.43	-14.06	-3.52	-13.62	-8.82	-8.44
1000	12	12	7.43	11.83	-22.97	-19.05	-25.81	-25.88	-14.02	-3.14	-13.16	-9.94	-8.78
1000	14	14	8.72	29.25	-21.32	-18.15	-25.10	-25.52	-14.96	-3.43	-13.31	-7.66	-7.41
1000	16	16	10.01	48.28	-21.76	-18.98	-25.54	-25.01	-15.09	-4.47	-13.52	-9.29	-5.78
1000	18	18	11.30	69.34	-23.52	-21.00	-26.53	-25.76	-15.88	-5.13	-14.35	-10.87	-9.94
1000	20	20	12.59	93.00	-22.22	-19.92	-25.69	-26.11	-15.01	-3.06	-14.65	-6.81	-10.31
1000	22	22	13.89	120.09	-22.46	-19.48	-25.32	-25.72	-14.42	-1.67	-14.20	-8.32	-12.29
1000	24	24	15.18	151.88	-25.09	-19.39	-25.04	-25.81	-16.06	-2.30	-12.69	-11.37	-12.43
599	1	1	0.27	-69.03	-17.35	-16.55	-23.22	-25.64	-14.89	1.70	-10.78	-21.62	-5.59
599	3	3	1.37	-56.96	-18.72	-15.93	-25.43	-25.73	-15.62	0.93	-10.66	-19.77	-6.09
599	5	5	2.46	-45.40	-19.23	-16.09	-24.63	-25.28	-15.15	3.85	-10.62	-20.19	-8.41
599	7	7	3.55	-33.70	-18.36	-16.84	-24.28	-25.84	-16.01	4.39	-10.78	-17.37	-5.73
599	9	9	4.65	-21.62	-18.74	-15.85	-24.76	-25.55	-16.36	0.11	-11.56	-21.05	-5.68
599	11	11	5.74	-9.00	-19.52	-16.85	-24.26	-25.29	-12.93	0.45	-12.90	-19.74	-9.86
599	13	13	6.84	4.31	-18.11	-17.26	-24.00	-25.05	-13.50	0.71	-11.84	-19.27	-9.38
599	15	15	7.93	18.44	-19.37	-16.55	-23.99	-25.25	-14.44	0.89	-12.17	-17.60	-8.93
599	17	17	9.02	33.58	-17.61	-19.07	-24.73	-29.21	-12.99	-0.09	-11.58	-16.04	-7.50
599	19	19	10.12	49.94	-19.10	-20.43	-25.77	-26.32	-14.09	0.16	-11.26	-21.16	-7.74
599	21	21	11.21	67.77	-19.02	-18.56	-25.12	-27.07	-13.65	0.65	-10.40	-17.60	-4.22
599	23	23	12.30	87.44	-18.12	-19.76	-25.52	-26.20	-13.88	1.14	-11.58	-20.90	-5.74
599	25	25	13.40	109.40	-18.09	-19.74	-25.56	-25.45	-13.48	2.18	-11.13	-20.98	-3.96
599	27	27	14.49	134.33	-18.16	-20.02	-25.91	-26.58	-12.38	1.15	-11.19	-18.07	-8.52
599	29	29	15.59	163.23	-18.29	-19.14	-24.98	-25.19	-14.48	1.08	-11.39	-18.28	-7.43
599	31	31	16.68	197.69	-19.59	-19.02	-25.82	-26.05	-14.43	-0.04	-11.79	-18.53	-7.92
601	1+2	1.5	0.51	-66.23	-19.34	-17.14	-24.68	-26.68	-15.41	-1.11	-11.91	-12.62	-2.15
601	4+5	4.5	2.06	-49.65	-19.76	-16.73	-25.30	-25.84	-15.22	-2.12	-11.80	-12.62	-3.10
601	7+8	7.5	3.60	-33.18	-17.57	-15.97	-25.56	-26.36	-16.85	2.05	-11.68	-11.89	-2.80
601	10	10	4.89	-18.88	-17.89	-15.15	-24.64	-26.30	-16.01	4.00	-10.80	-12.15	-3.30
601	12+13	12.5	6.18	-3.80	-17.80	-16.64	-26.20	-26.64	-16.55	-0.31	-12.45	-12.02	-3.17
601	15	15	7.46	12.30	-19.02	-14.30	-23.60	-25.26	-14.41	-0.60	-11.38	-10.97	-1.72
601	17	17	8.49	26.10	-19.97	-16.75	-26.13	-24.59	-14.72	-2.24	-12.34	-10.37	-2.64
601	19	19	9.52	40.87	-19.04	-15.82	-24.92	-26.06	-14.22	-0.40	-11.13	-10.95	-2.90
601	21	21	10.55	56.82	-19.38	-17.03	-24.92	-25.58	-15.22	-2.86	-12.27	-10.74	-1.89
601	23	23	11.58	74.20	-17.85	-17.83	-26.70	-25.38	-16.57	-3.00	-12.19	-11.62	-2.84
601	25	25	12.61	93.32	-19.35	-14.06	-24.44	-25.26	-13.96	-0.62	-11.95	-11.92	-2.86
601	27	27	13.64	114.62	-17.78	-14.95	-25.30	-24.42	-13.90	0.58	-11.99	-12.13	-2.49
601	29	29	14.67	138.71	-19.67	-16.33	-25.71	-26.18	-14.02	-3.26	-13.42	-10.94	-3.32
601	31	31	15.70	166.49	-18.10	-17.43	-25.86	-25.50	-14.18	-1.23	-13.45	-10.07	-1.50
601	33	33	16.73	199.37	-19.25	-15.80	-26.34	-25.74	-15.82	-2.76	-12.76	-10.98	-3.32
578	1+2	1.5	0.57	-65.64	-19.23	-15.85	-24.03	-24.47	-13.56	1.69	-10.98	-19.60	-2.33
578	4	4	1.98	-50.45	-18.09	-17.51	-24.54	-25.29	-13.80	0.47	-11.35	-18.01	-3.45

					Essential				Non-essential				
Ind. ID	**ID (comb.)**	**ID (av.)**	**d (mm)**	**age (mo)**	**Val**	**Ileu**	**Leu**	**Phe**	**Ala**	**Gly**	**Pro**	**Asp**	**Glu**
578	6	6	3.12	-38.42	-19.27	-16.40	-24.96	-25.62	-14.89	0.28	-11.16	-16.48	-2.24
578	8	8	4.25	-26.07	-20.39	-18.06	-26.79	-26.46	-14.50	-2.01	-12.23	-17.27	-2.27
578	10	10	5.38	-13.20	-20.11	-17.13	-25.07	-25.93	-13.42	-2.93	-13.00	-16.65	-0.67
578	12	12	6.52	0.34	-20.14	-16.61	-24.37	-25.33	-13.42	-4.01	-12.40	-17.65	-4.78
578	14	14	7.65	14.74	-19.86	-19.29	-25.14	-25.04	-13.18	-3.41	-12.33	-16.63	-3.82
578	16	16	8.78	30.16	-21.27	-19.66	-27.14	-25.31	-16.54	-5.35	-13.50	-16.95	-3.40
578	18	18	9.92	46.84	-19.93	-18.64	-25.03	-25.12	-15.09	-3.23	-12.63	-16.81	-3.70
578	20	20	11.05	65.04	-19.83	-19.18	-25.32	-24.85	-14.29	-4.53	-12.47	-19.80	-5.69
578	22	22	12.18	85.15	-18.95	-19.35	-24.62	-25.03	-13.18	-1.89	-12.11	-15.71	-4.89
578	24	24	13.32	107.67	-18.89	-17.82	-24.66	-24.80	-14.96	-1.32	-12.32	-16.48	-8.70
578	26	26	14.45	133.31	-19.16	-18.82	-25.56	-25.29	-14.38	-3.38	-12.63	-17.17	-3.58
578	28	28	15.58	163.16	-19.35	-17.73	-24.66	-24.89	-14.60	-3.99	-12.62	-16.15	-7.53
578	30	30	16.72	198.98	-18.89	-18.26	-25.11	-25.69	-14.35	-1.62	-11.90	-17.72	-4.84

Table 4.2 Mean and standard deviations (SD) for $\delta^{13}C_{EAA}$ and $\delta^{13}C_{nonEAA}$ values, and for carbon isotopic compositions of bulk cartilage collagen ($\delta^{13}C_{bulk}$) for each individual shark. The numbers of samples (N) for bulk and compound-specific isotope analysis are also reported. Raw $\delta^{13}C_{EAA}$ and $\delta^{13}C_{nonEAA}$ data for amino acids for each analysed sample are presented in Table 4.1, raw $\delta^{13}C_{bulk}$ data and metadata for individual sharks in Chapter 3.

	Essential				**Non-essential**							
Ind. ID	**Val**	**Ileu**	**Leu**	**Phe**	**Ala**	**Gly**	**Pro**	**Asp**	**Glu**	**Bulk**	**N-CS**	**N-bulk**
16	-23.76 ± 1.41	-19.39 ± 0.88	-28.13 ± 1.00	-28.43 ± 0.88	-14.95 ± 1.17	-4.67 ± 1.81	-14.83 ± 1.23	-10.23 ± 1.51	-8.06 ± 1.55	-15.45 ± 0.45	15	18
24	-21.47 ± 1.11	-19.47 ± 0.95	-28.15 ± 0.91	-27.24 ± 0.51	-14.32 ± 1.12	-3.75 ± 2.01	-14.11 ± 1.38	-7.28 ± 1.69	-10.46 ± 1.19	-15.40 ± 0.56	15	20
12	-21.70 ± 1.10	-18.96 ± 1.42	-28.20 ± 1.33	-28.28 ± 0.90	-13.85 ± 1.52	-3.36 ± 2.46	-13.41 ± 1.36	-8.22 ± 1.48	-7.15 ± 1.32	-15.15 ± 0.84	12	15
101	-23.3 ± 1.08	-21.31 ± 1.55	-28.88 ± 1.00	-27.64 ± 1.10	-16.18 ± 2.02	-5.88 ± 2.01	-13.97 ± 1.48	-11.31 ± 2.68	-7.65 ± 2.37	-14.95 ± 0.52	14	15
131	-22.23 ± 1.16	-18.83 ± 1.23	-27.61 ± 1.47	-26.75 ± 0.87	-13.55 ± 1.12	-4.53 ± 1.50	-14.30 ± 1.36	-8.67 ± 1.69	-7.85 ± 1.46	-14.94 ± 0.55	14	17
33	-22.35 ± 1.15	-18.00 ± 1.30	-25.77 ± 0.87	-27.71 ± 0.61	-12.50 ± 1.41	-1.74 ± 1.16	-13.50 ± 0.91	-14.67 ± 2.72	-7.54 ± 1.23	-15.15 ± 0.64	16	20
335	-18.10 ± 0.82	-15.78 ± 1.24	-23.79 ± 0.96	-25.16 ± 0.76	-12.36 ± 1.39	-2.25 ± 1.18	-11.85 ± 0.90	-17.49 ± 1.80	-6.40 ± 1.78	-14.80 ± 0.35	15	33
415	-18.73 ± 0.99	-17.65 ± 0.47	-24.27 ± 1.07	-25.53 ± 1.00	-12.66 ± 1.37	-1.96 ± 1.65	-12.91 ± 0.76	-16.09 ± 1.67	-9.35 ± 1.00	-15.20 ± 0.43	14	30
441	-19.44 ± 0.99	-16.05 ± 1.55	-23.98 ± 1.10	-25.59 ± 0.50	-12.97 ± 1.04	-2.05 ± 1.14	-12.55 ± 0.61	-19.46 ± 2.15	-8.44 ± 1.25	-15.25 ± 0.49	13	28
11	-18.89 ± 0.58	-15.71 ± 0.97	-24.95 ± 0.60	-25.36 ± 0.45	-12.54 ± 0.45	0.65 ± 1.09	-9.72 ± 0.48	-7.00 ± 2.18	-3.42 ± 0.81	-14.62 ± 0.47	11	18
40	-19.08 ± 1.31	-20.87 ± 1.1	-26.27 ± 0.79	-25.82 ± 0.87	-16.08 ± 0.92	-1.70 ± 1.59	-12/47 ± 0.81	-11.98 ± 1.42	-3.91 ± 0.74	-14.41 ± 0.39	11	19
1000	-22.29 ± 1.16	-18.67 ± 1.24	-25.68 ± 0.45	-25.78 ± 0.42	-15.44 ± 1.03	-2.88 ± 1.32	-13.54 ± 0.57	-9.26 ± 1.46	-8.96 ± 2.00	-14.68 ± 0.37	12	19
599	-18.59 ± 0.68	-17.98 ± 1.63	-24.87 ± 0.78	-25.98 ± 1.03	-14.27 ± 1.13	1.20 ± 1.30	-11.35 ± 0.65	-19.26 ± 1.67	-7.04 ± 1.80	-14.36 ± 0.40	16	26
601	-18.78 ± 0.85	-16.13 ± 1.12	-25.35 ± 0.84	-25.72 ± 0.68	-15.14 ± 1.03	-0.93 ± 2.01	-21.10 ± 0.74	-11.47 ± 0.80	-2.67 ± 0.6	-14.74 ± 0.29	15	27
578	-19.56 ± 0.77	-18.02 ± 1.16	-25.13 ± 0.84	-25.27 ± 0.50	-14.28 ± 0.90	-2.35 ± 1.99	-12.24 ± 0.68	-17.27 ± 1.16	-4.13 ± 2.07	-14.48 ± 0.26	15	24

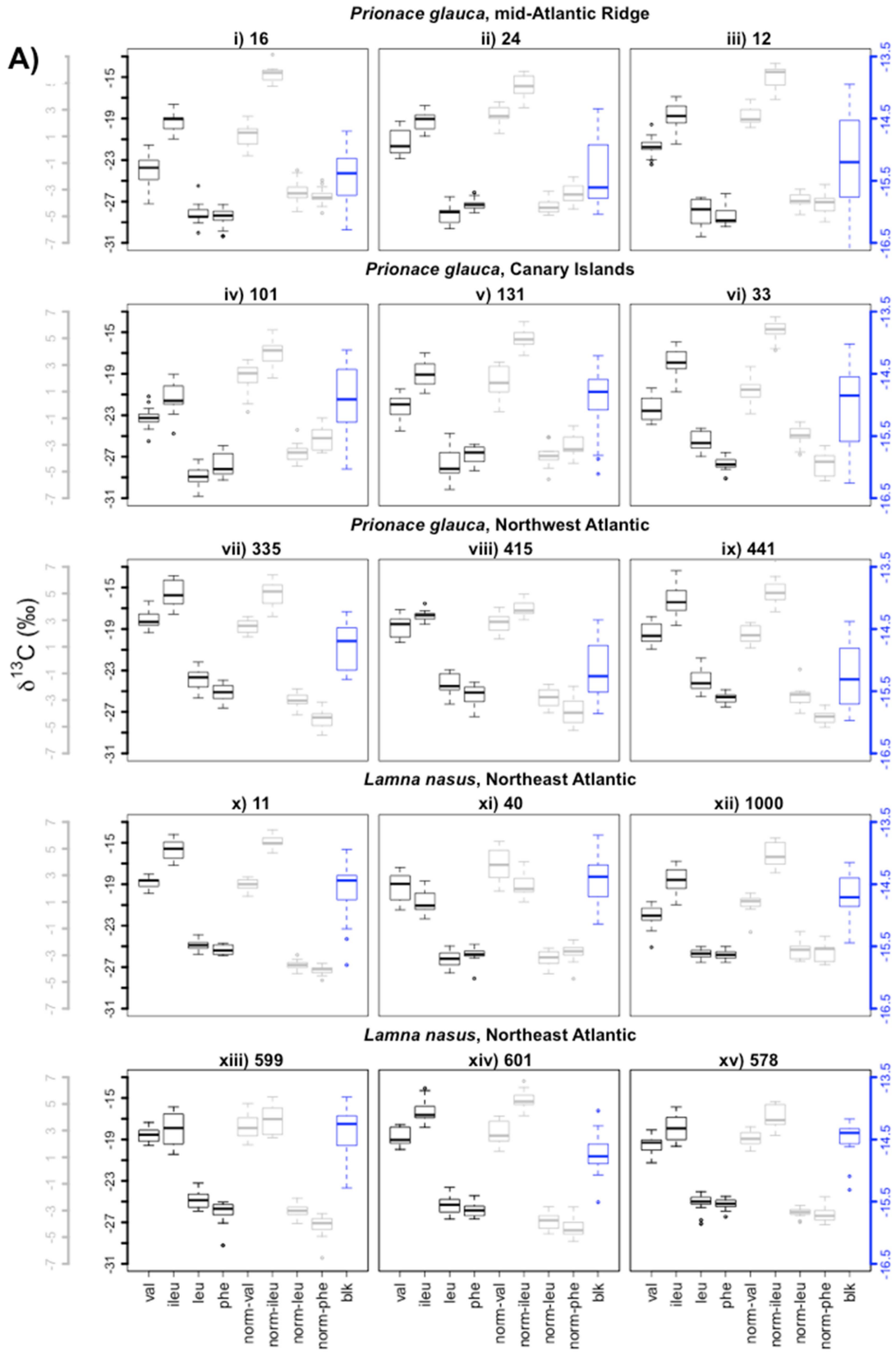

Figure 4.3 Variances in raw and sample-normalised carbon isotopic compositions of all the recovered amino acids, including A) essential ($\delta^{13}C_{EAA}$, $\delta^{13}C_{norm\text{-}EAA}$) and B) non-essential ($\delta^{13}C_{nonEAA}$, $\delta^{13}C_{norm\text{-}nonEAA}$) amino acids, and raw carbon isotope values of bulk cartilage collagen ($\delta^{13}C_{bulk}$) throughout the life of individual sharks.

From the top-left to the bottom-right, variances are presented for individuals i) 16, ii) 24, iii) 12 (blue sharks from the mid-Atlantic Ridge), iv) 101, v) 131, vi) 33 (blue sharks from the Canary Islands), vii) 335, viii) 415, ix) 441 (blue sharks from the Northwest Atlantic), x) 11, xi) 40 (porbeagles from the western English Channel), xii) 1000 (porbeagle from the Faroe Islands), xiii) 599, xiv) 601, and xv) 578 (porbeagles from the Northwest Atlantic). Different colours represent different sets of variables: black indicates raw $\delta^{13}C$ values of amino acids, grey sample-normalised $\delta^{13}C$ values, and blue raw $\delta^{13}C$ values of bulk collagen. For each individual shark and amino acid (or bulk collagen), the boxplot displays the variation in isotope values across samples (i.e. throughout life). The horizontal line in each boxplot represents the median of the data (i.e. 50% of the data are greater than this value). The lower and upper limits of the boxplot represent the lower and upper quartile (i.e. 25% of the data less or greater than this value), respectively. The lower and upper whiskers represent the minimum and maximum value excluding outliers, respectively. Dots at the bottom or top of whiskers represent outliers (i.e. less and more than 3/2 times of the lower and upper quartile, respectively).

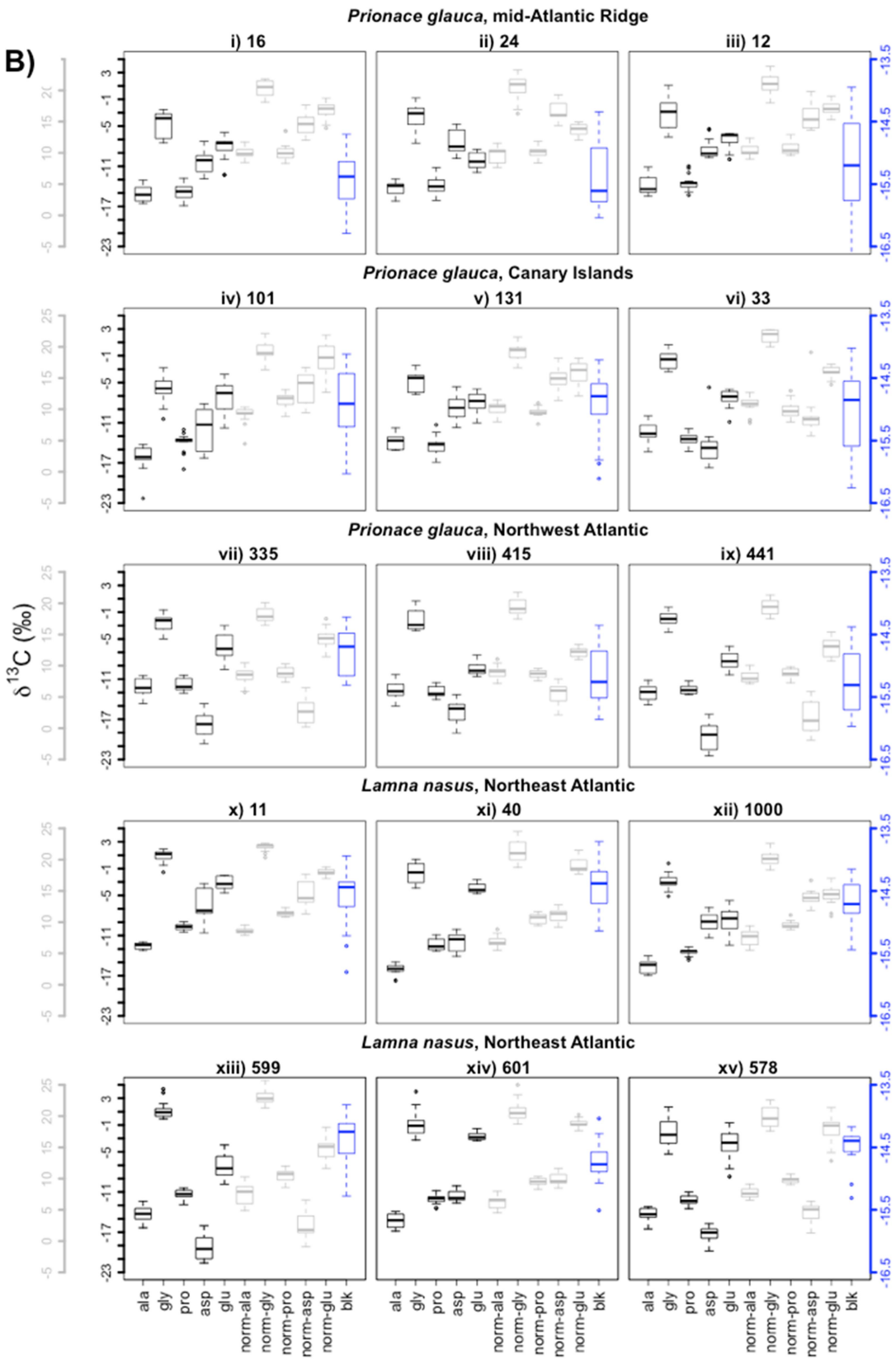
B)
Prionace glauca, mid-Atlantic Ridge
i) 16
ii) 24
iii) 12
Prionace glauca, Canary Islands
iv) 101
v) 131
vi) 33
Prionace glauca, Northwest Atlantic
vii) 335
viii) 415
ix) 441
Lamna nasus, Northeast Atlantic
x) 11
xi) 40
xii) 1000
Lamna nasus, Northeast Atlantic
xiii) 599
xiv) 601
xv) 578
δ13C (‰)
ala
gly
pro
asp
glu
norm-ala
norm-gly
norm-pro
norm-asp
norm-glu
blk

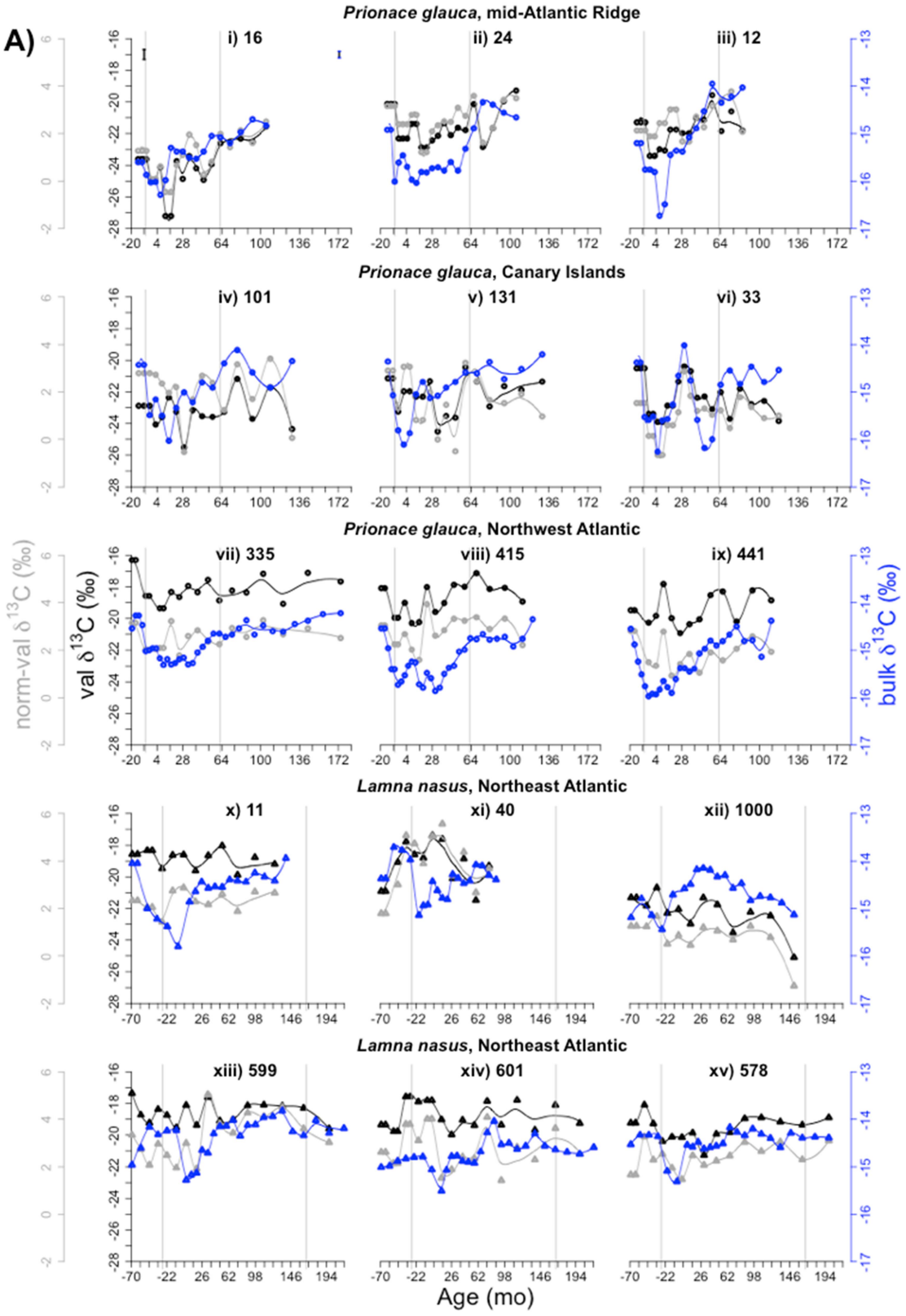

Figure 4.4 Individual-level life-history records of raw and sample-normalised carbon isotopic compositions of A-D) essential ($\delta^{13}C_{EAA}$, $\delta^{13}C_{norm\text{-}EAA}$) and E-I) non-essential ($\delta^{13}C_{nonEAA}$, $\delta^{13}C_{norm\text{-}nonEAA}$) amino acids, and raw carbon isotope values of bulk cartilage collagen ($\delta^{13}C_{bulk}$).
A) valine, B) isoleucine, C) leucine, D) phenylalanine, E) alanine, F) glycine, G) proline, H) aspartic acid, and I) glutamic acid. From the top-left to the bottom-right, records are presented for individuals i)

16, ii) 24, iii) 12 (blue sharks from the mid-Atlantic Ridge), iv) 101, v) 131, vi) 33 (blue sharks from the Canary Islands), vii) 335, viii) 415, ix) 441 (blue sharks from the Northwest Atlantic), x) 11, xi) 40 (porbeagles from the western English Channel), xii) 1000 (porbeagle from the Faroe Islands), xiii) 599, xiv) 601, and xv) 578 (porbeagles from the Northwest Atlantic). Different symbols represent different species: circles identify blue sharks, triangles porbeagles. Different colours represent different sets of variables: black indicates raw $\delta^{13}C$ values of amino acids, grey sample-normalised $\delta^{13}C$ values, and blue raw $\delta^{13}C$ values of bulk collagen. Datapoints represent measured values, lines predicted monthly values by the least smooth as possible Loess smoother. The error bars in plot i) of each panel are the standard deviations for raw $\delta^{13}C$ values of each amino acid and bulk collagen. The grey vertical lines represent estimated age at birth and at maturity.

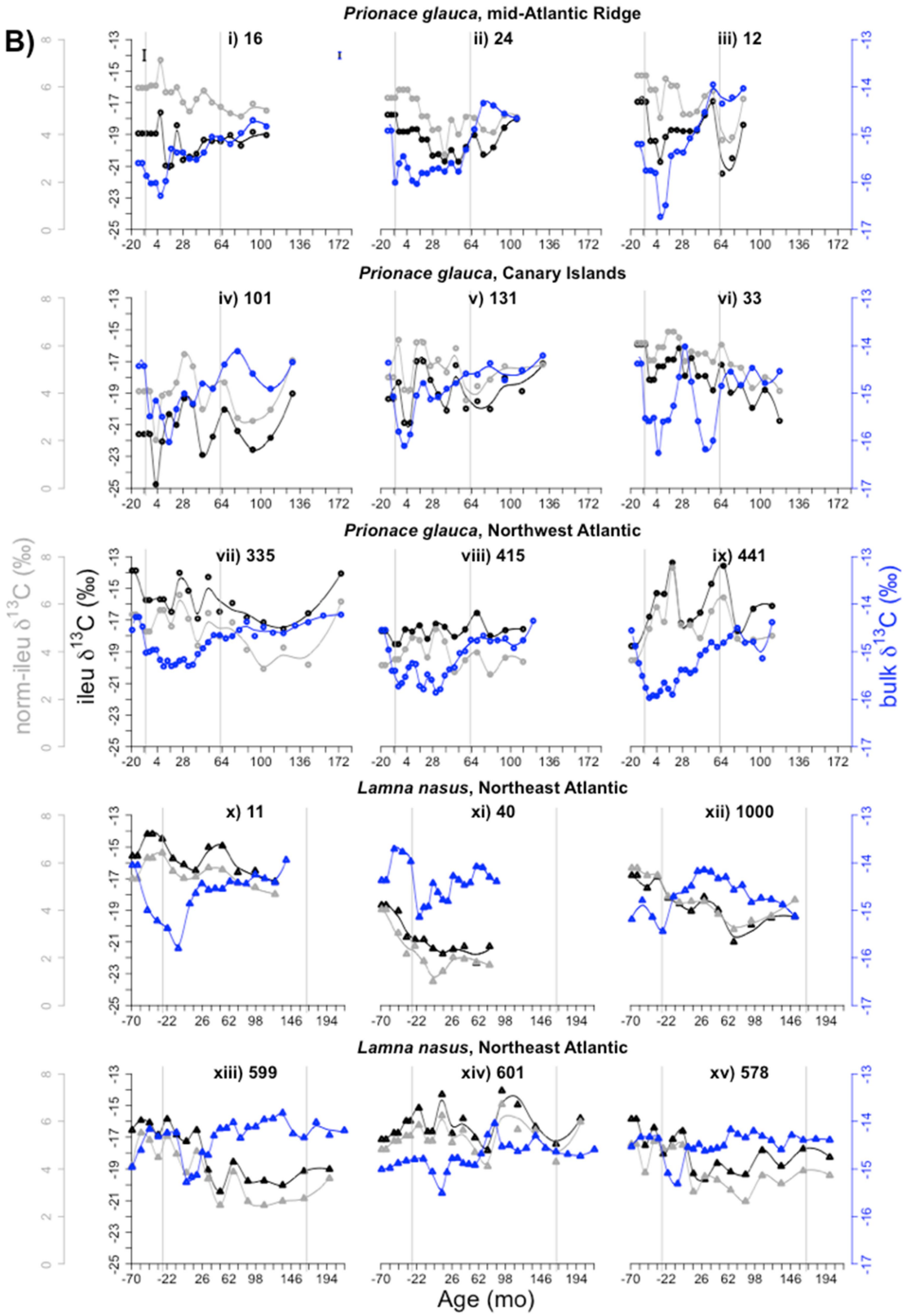
B)
Prionace glauca, mid-Atlantic Ridge
i) 16
ii) 24
iii) 12
Prionace glauca, Canary Islands
iv) 101
v) 131
vi) 33
Prionace glauca, Northwest Atlantic
vii) 335
viii) 415
ix) 441
Lamna nasus, Northeast Atlantic
x) 11
xi) 40
xii) 1000
Lamna nasus, Northeast Atlantic
xiii) 599
xiv) 601
xv) 578
norm-ileu δ13C (‰)
ileu δ13C (‰)
bulk δ13C (‰)
Age (mo)

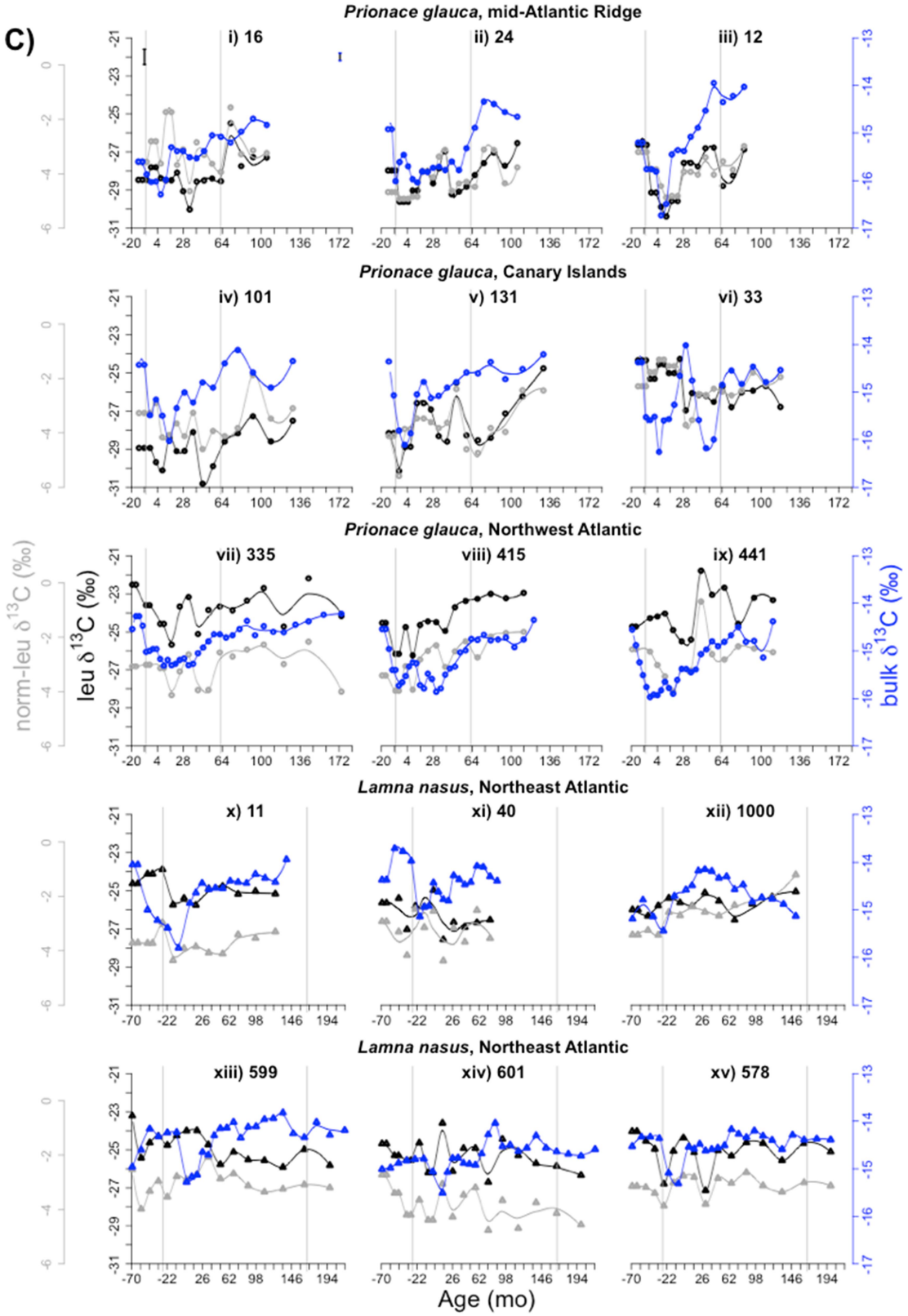
C)
Prionace glauca, mid-Atlantic Ridge
i) 16
ii) 24
iii) 12
Prionace glauca, Canary Islands
iv) 101
v) 131
vi) 33
Prionace glauca, Northwest Atlantic
vii) 335
viii) 415
ix) 441
Lamna nasus, Northeast Atlantic
x) 11
xi) 40
xii) 1000
Lamna nasus, Northeast Atlantic
xiii) 599
xiv) 601
xv) 578
norm-leu δ13C (‰)
leu δ13C (‰)
bulk δ13C (‰)
Age (mo)

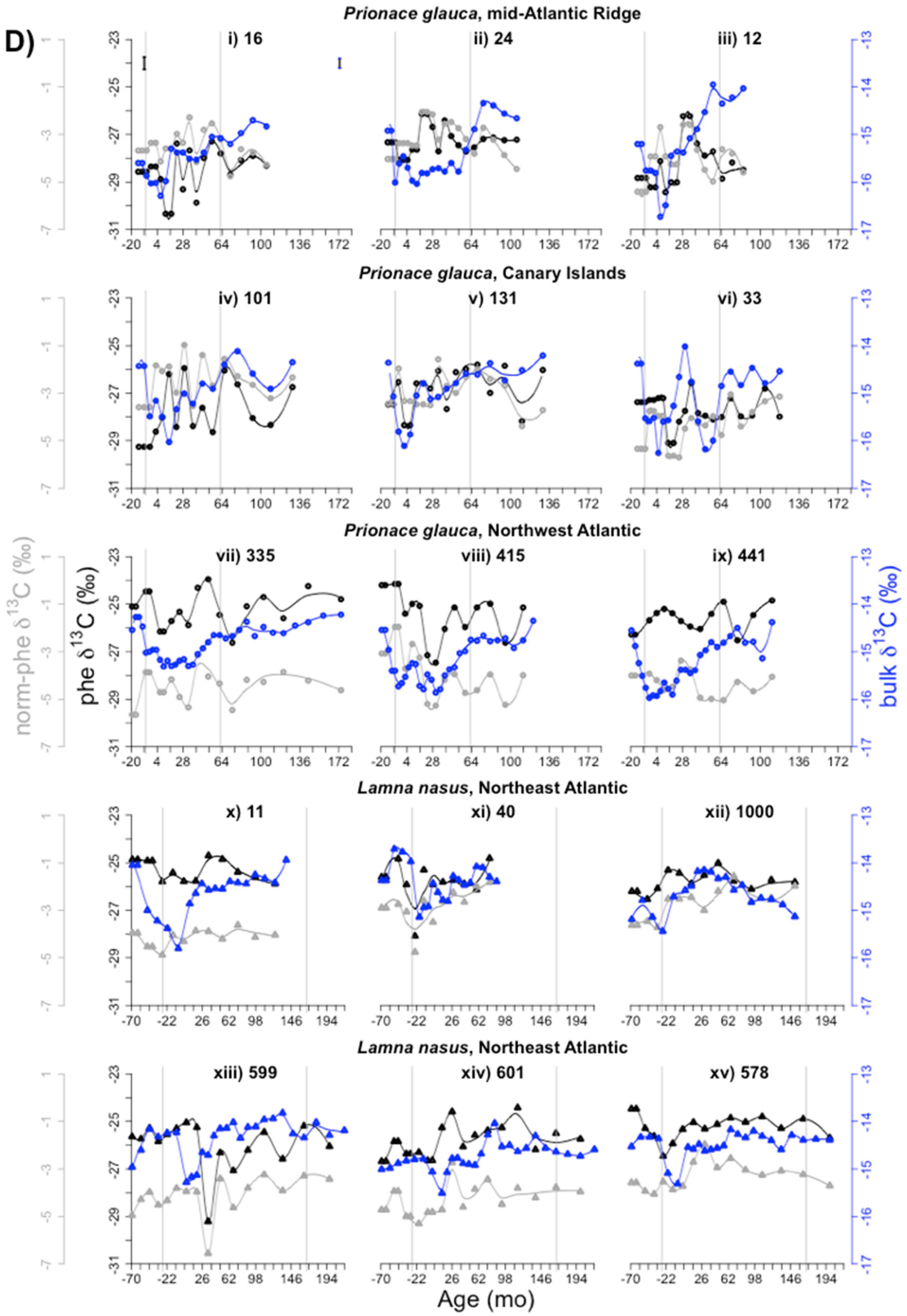
D)
Prionace glauca, mid-Atlantic Ridge
i) 16
ii) 24
iii) 12
Prionace glauca, Canary Islands
iv) 101
v) 131
vi) 33
Prionace glauca, Northwest Atlantic
vii) 335
viii) 415
ix) 441
Lamna nasus, Northeast Atlantic
x) 11
xi) 40
xii) 1000
Lamna nasus, Northeast Atlantic
xiii) 599
xiv) 601
xv) 578
norm-phe δ13C (‰)
phe δ13C (‰)
bulk δ13C (‰)
Age (mo)

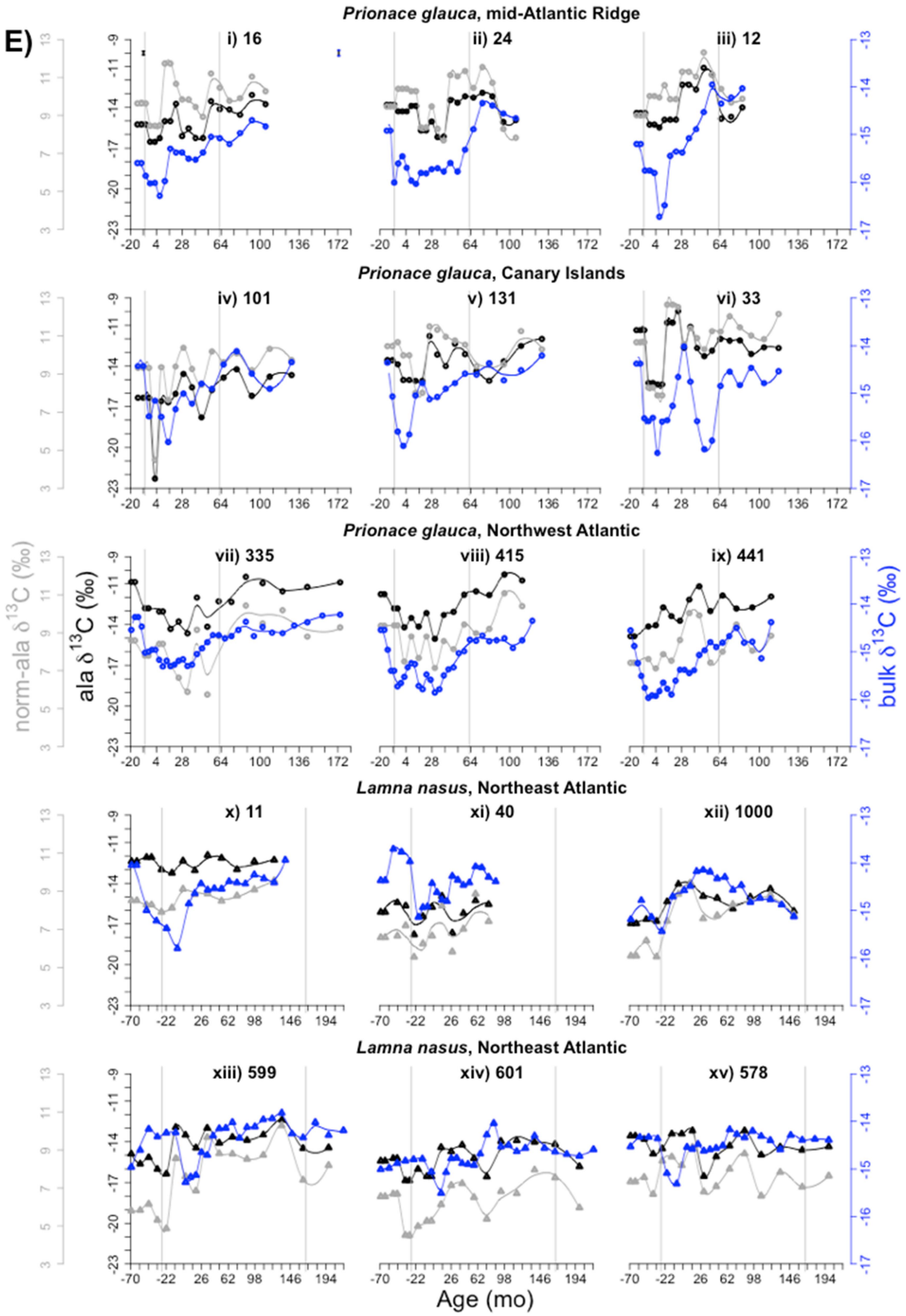
E)
Prionace glauca, mid-Atlantic Ridge
i) 16
ii) 24
iii) 12
Prionace glauca, Canary Islands
iv) 101
v) 131
vi) 33
Prionace glauca, Northwest Atlantic
vii) 335
viii) 415
ix) 441
Lamna nasus, Northeast Atlantic
x) 11
xi) 40
xii) 1000
Lamna nasus, Northeast Atlantic
xiii) 599
xiv) 601
xv) 578
norm-ala δ13C (‰)
ala δ13C (‰)
bulk δ13C (‰)
Age (mo)

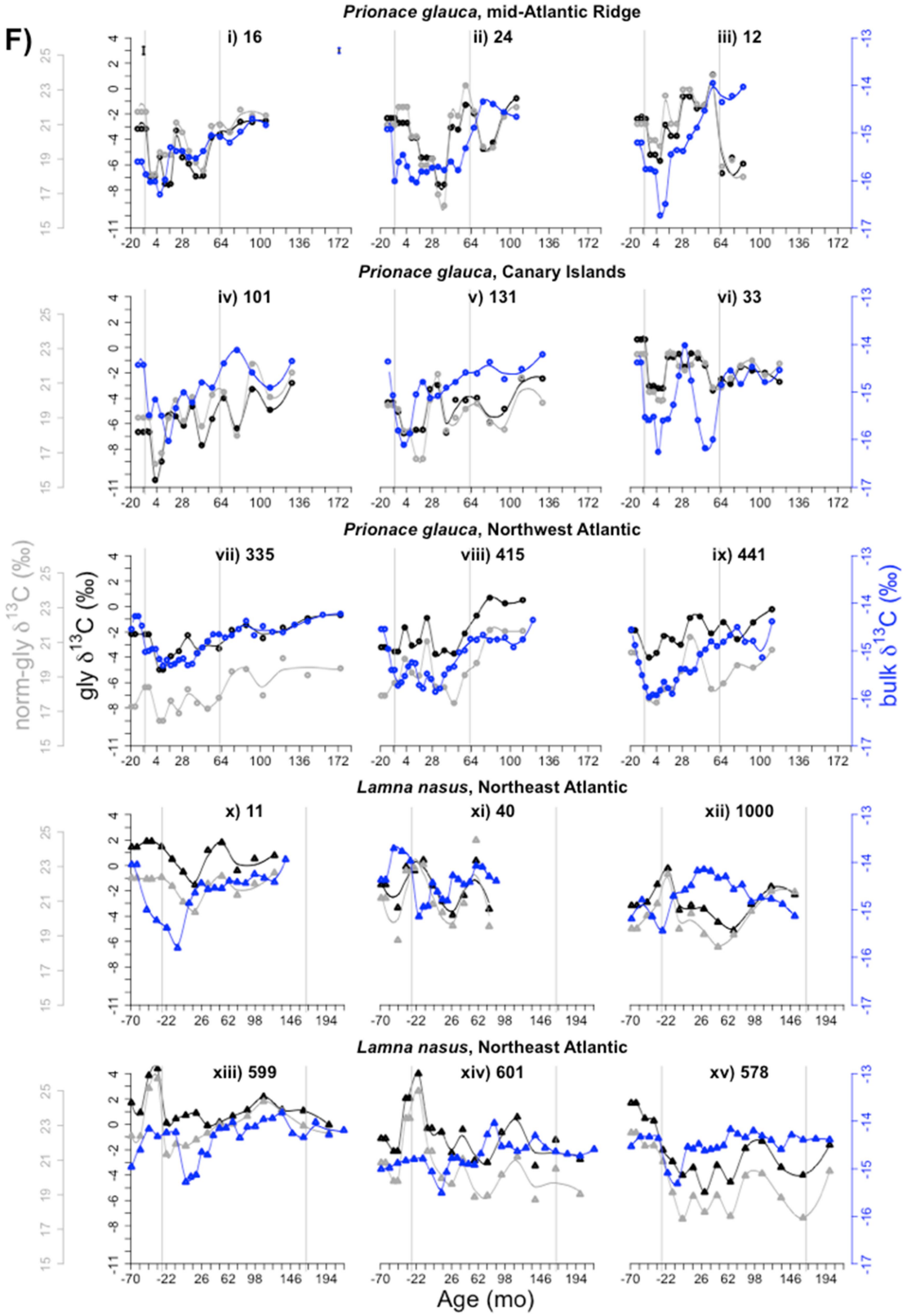
F)
Prionace glauca, mid-Atlantic Ridge
i) 16
ii) 24
iii) 12
Prionace glauca, Canary Islands
iv) 101
v) 131
vi) 33
Prionace glauca, Northwest Atlantic
vii) 335
viii) 415
ix) 441
Lamna nasus, Northeast Atlantic
x) 11
xi) 40
xii) 1000
Lamna nasus, Northeast Atlantic
xiii) 599
xiv) 601
xv) 578
norm-gly δ13C (‰)
gly δ13C (‰)
bulk δ13C (‰)
Age (mo)

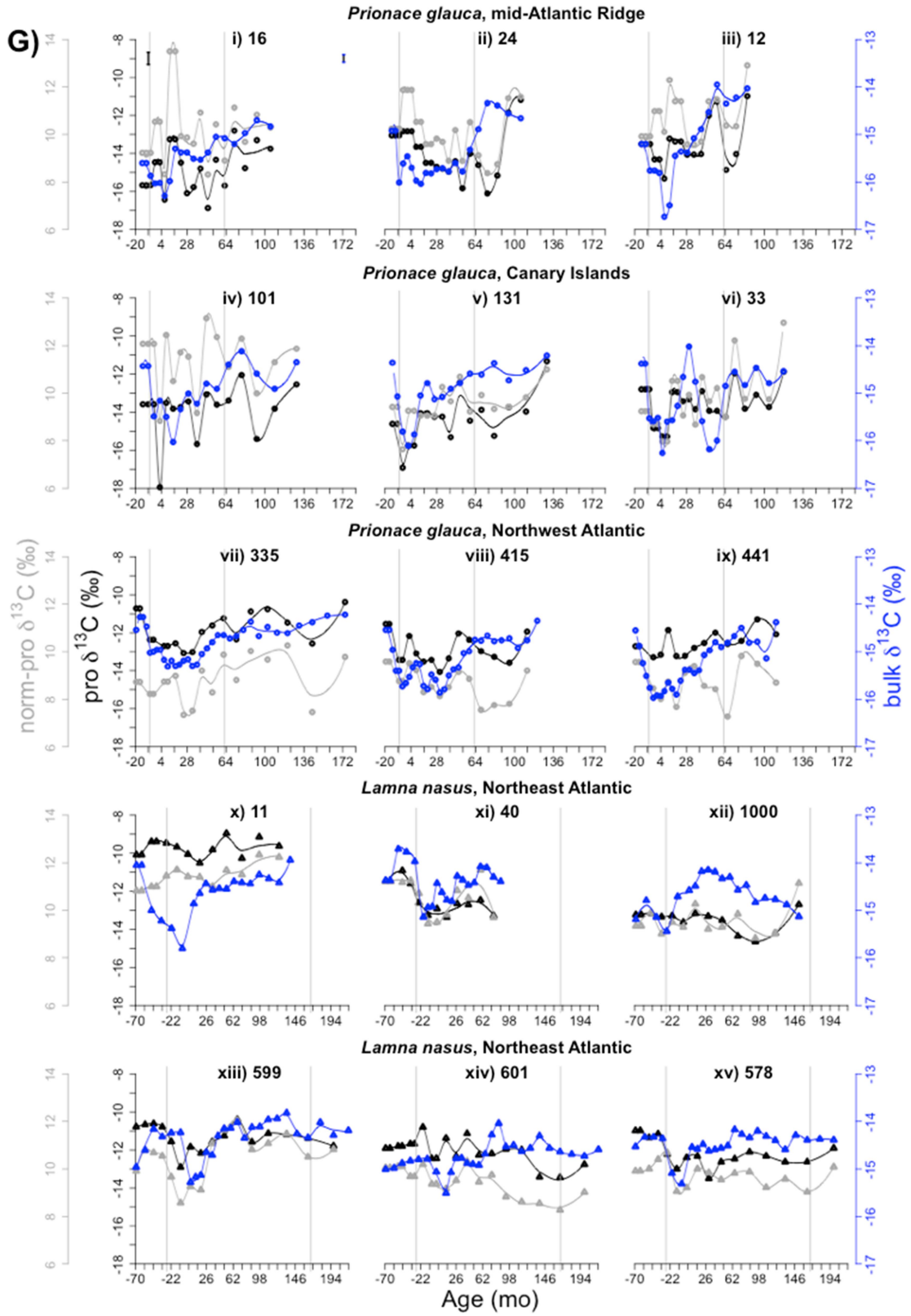
G)
Prionace glauca, mid-Atlantic Ridge
i) 16
ii) 24
iii) 12
Prionace glauca, Canary Islands
iv) 101
v) 131
vi) 33
Prionace glauca, Northwest Atlantic
vii) 335
viii) 415
ix) 441
Lamna nasus, Northeast Atlantic
x) 11
xi) 40
xii) 1000
Lamna nasus, Northeast Atlantic
xiii) 599
xiv) 601
xv) 578
norm-pro δ13C (‰)
pro δ13C (‰)
bulk δ13C (‰)
Age (mo)

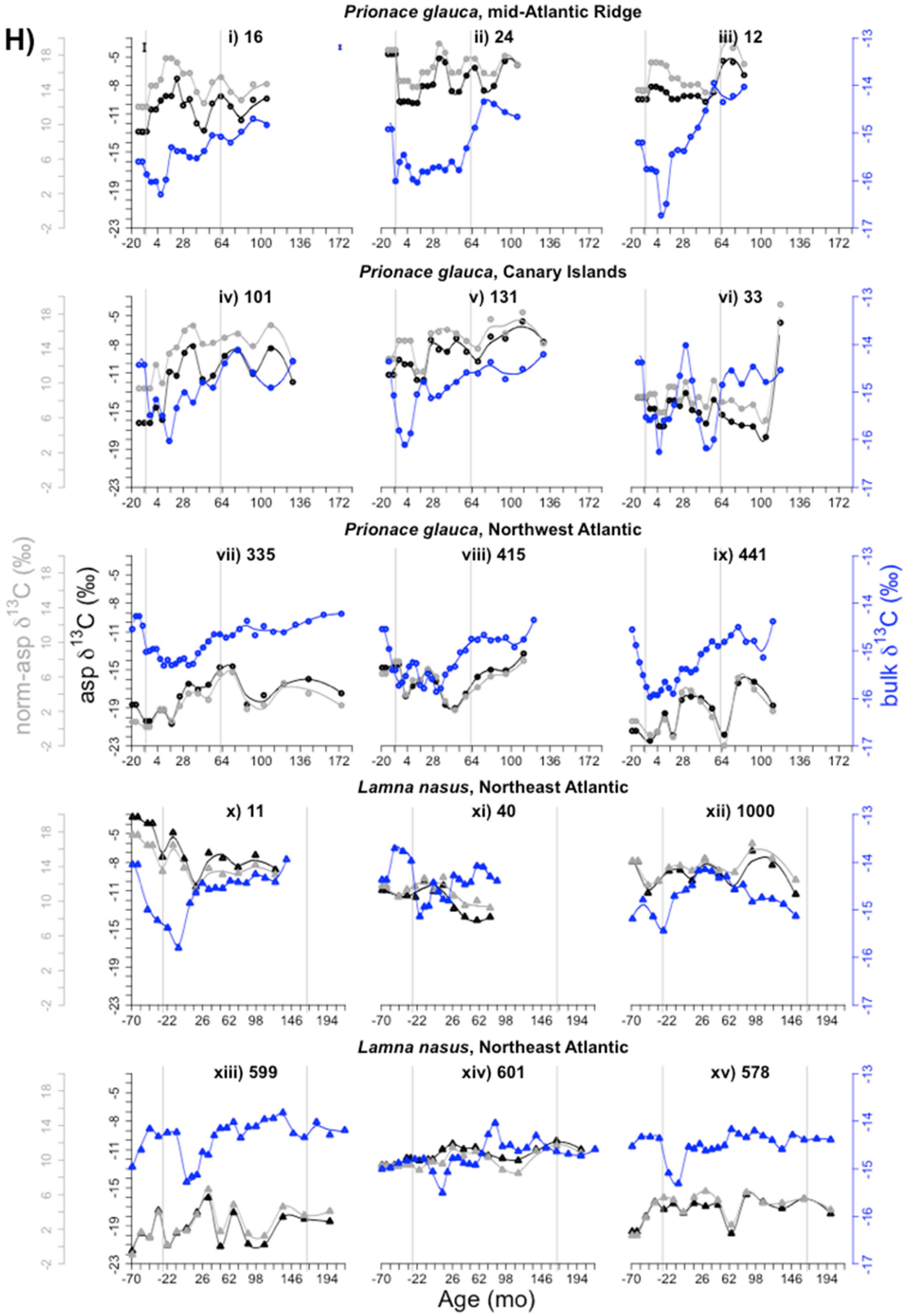
H)
Prionace glauca, mid-Atlantic Ridge
i) 16
ii) 24
iii) 12
Prionace glauca, Canary Islands
iv) 101
v) 131
vi) 33
Prionace glauca, Northwest Atlantic
vii) 335
viii) 415
ix) 441
Lamna nasus, Northeast Atlantic
x) 11
xi) 40
xii) 1000
Lamna nasus, Northeast Atlantic
xiii) 599
xiv) 601
xv) 578
norm-asp δ13C (‰)
asp δ13C (‰)
bulk δ13C (‰)
Age (mo)

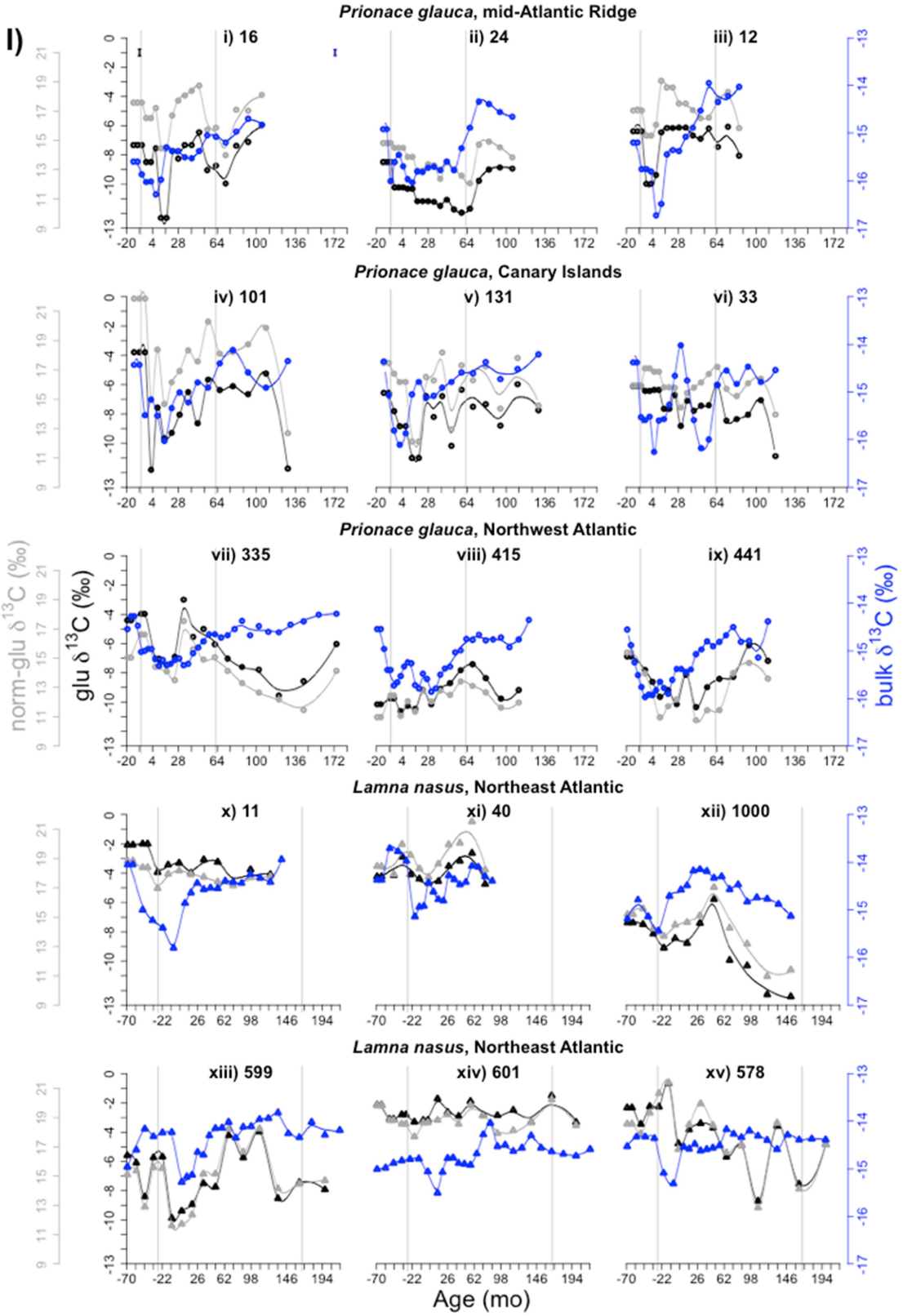
I)
Prionace glauca, mid-Atlantic Ridge
i) 16
ii) 24
iii) 12
Prionace glauca, Canary Islands
iv) 101
v) 131
vi) 33
Prionace glauca, Northwest Atlantic
vii) 335
viii) 415
ix) 441
Lamna nasus, Northeast Atlantic
x) 11
xi) 40
xii) 1000
Lamna nasus, Northeast Atlantic
xiii) 599
xiv) 601
xv) 578
norm-glu δ13C (‰)
glu δ13C (‰)
bulk δ13C (‰)
Age (mo)

4.4.2 Variance in $\delta^{13}C$ values of essential amino acids

4.4.2.1 Variability in $\delta^{13}C$ patterns between species, and among areas and individuals

When principal component analysis (PCA) was carried out with raw carbon isotopic compositions of essential amino acids ($\delta^{13}C_{EAA}$), the first principal component (PC1) explained 72% of the total variance in $\delta^{13}C_{EAA}$ values, the second principal component (PC2) 13% (Table 4.C1A; Fig. 4.5). Most positive PC1 scores corresponded to most positive $\delta^{13}C$ values for all four essential amino acids, as eigenvectors for all amino acids (carbon isotopic compositions) aligned parallel to the PC1 axis, and pointed towards most positive PC1 scores (Fig. 4.5).

Shark samples lie along a gradient on the PC1 axis: blue shark samples from the central and eastern North Atlantic showed the most negative PC1 scores (hence $\delta^{13}C_{EAA}$ values), whereas blue shark samples from the Northwest Atlantic the most positive PC1 values. Porbeagle samples exhibited intermediate PC1 scores, and were also separated, to an extent, by area and individual (at least in the case of samples from the Northeast Atlantic; Fig. 4.5).

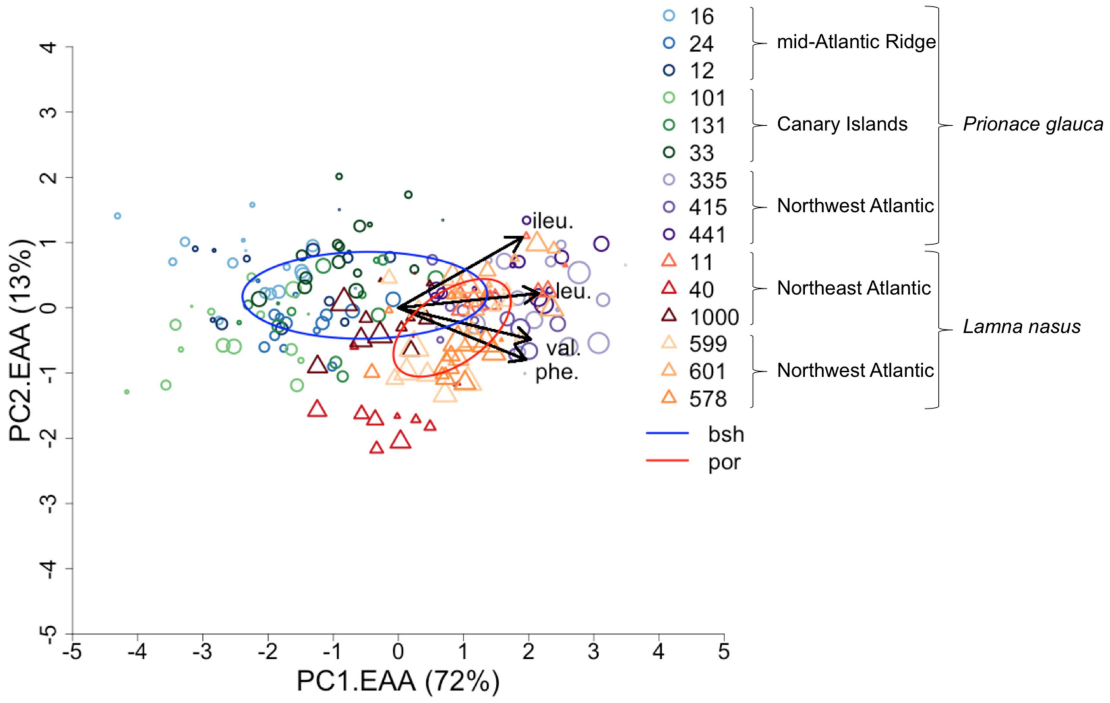

Figure 4.5 Principal component analysis (PCA) with raw carbon isotopic compositions of essential amino acids ($\delta^{13}C_{EAA}$) in sequential vertebral samples from individual blue and porbeagle sharks. Different symbols represent different species: circles identify blue sharks, triangles porbeagles. Different colour scales represent different species and capture areas: blues identify blue sharks from the mid-Atlantic Ridge, greens blue sharks from the Canary Islands, purples blue sharks from the Northwest Atlantic, reds porbeagles from the Northeast Atlantic (with lightest reds representing porbeagles from the western English Channel and the darkest red the porbeagle from the Faroe Islands), and oranges porbeagles from the Northwest Atlantic. Different colour shades represent different individual sharks as in figure legend. Symbol size is proportional to sample distance along the vertebral radius. Ellipses represent standard ellipse areas corrected for small sample size (SEAc): the blue ellipse is relative to blue sharks (bsh), the red ellipse to porbeagles (por).

When PCA was carried out with sample-normalised carbon isotope values of essential amino acids ($\delta^{13}C_{norm\text{-}EAA}$), PC1 and PC2 accounted for 41 and 31% of the total variance in $\delta^{13}C_{norm\text{-}EAA}$ values, respectively (Table 4.C1A; Fig. 4.6). In this case, an increase in PC1 values corresponded to an increase in $\delta^{13}C$ values for valine, and a decrease in $\delta^{13}C$ values of isoleucine; increasing PC2 values were associated with increasing $\delta^{13}C$ values of phenylalanine, and decreasing $\delta^{13}C$ values in leucine. Between-area differences in blue sharks (and porbeagles) were no longer present, and between-species and individual differences considerably reduced compared to PCA with $\delta^{13}C_{EAA}$ values, though the proportion of variance explained by the principal components was also slightly reduced. Indeed, blue shark samples from the eastern-central and western North Atlantic were well-mixed in the PCA space, separating slightly along the PC1 axis. Porbeagle samples also mixed well with blue shark samples, with some individuals (e.g. 40 and 599) showing slightly more positive PC1 scores (Fig. 4.6).

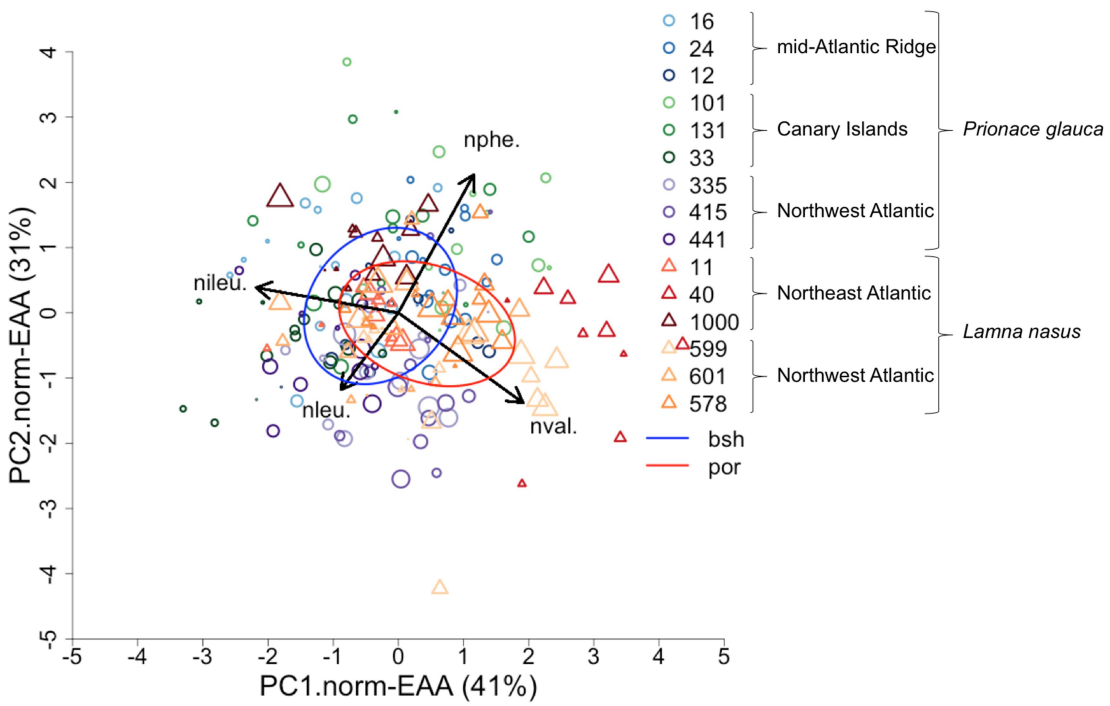

Figure 4.6 PCA with sample-normalised carbon isotopic compositions of essential amino acids ($\delta^{13}C_{norm\text{-}EAA}$) in sequential vertebral samples from individual blue and porbeagle sharks. Different symbols and colours represent different species, capture areas and individuals, symbol size is proportional to sample distance along the vertebral radius, and SEAc are represented for blue and porbeagle sharks as in Fig. 4.5.

4.4.2.2 Species-level life-history isotopic traits

Common, broad ontogenetic patterns in life history-normalised PC1 scores from both PCAs with raw and sample-normalised carbon isotopic compositions of essential amino acids (nPC1.EAA and nPC1.norm-EAA, respectively) were identified across individuals of each species, indicating species-level life-history isotopic traits (Fig. 4.7 and 4.8). When generalised additive mixed models (GAMMs) included data for both species, patterns in both nPC1.EAA and nPC1.norm-EAA values were non-linear (smoother 'estimated sample age': maximum p-value = 0.006 < 0.05, F = 4.357), and did not differ significantly between species (minimum p-value = 0.334, F = 0.937), or areas (minimum p-value = 0.989, F = 0.078; Table 4.3A and 4.4A). Patterns in nPC1.EAA in both blue and porbeagle sharks approximated linear relationships; when modelling these patterns with generalised linear mixed models (GLMMs), species was highly significant (F = 14.807, p-value = 0.0002).

In blue sharks, life history-normalised PC1 scores from PCA with raw amino acid carbon isotopic compositions (nPC1.EAA) showed a sharp decrease of ~ 1% around birth, followed by a progressive increase of ~ 1% during the juvenile stage, and no clear age-related pattern during the adult stage (Fig. 4.7A). Values of nPC1.EAA during pre-birth and adult stages were comparable (Fig. 4.7A). The observed sharp decrease in carbon isotopic compositions of bulk collagen ($\delta^{13}C_{bulk}$) around

birth, and progressive increase during juvenile growth (Chapter 3) were, therefore, retained in carbon isotope values of essential amino acids ($\delta^{13}C_{EAA}$; Fig. 4.7A).

In porbeagle sharks, nPC1.EAA (hence $\delta^{13}C_{EAA}$) values consistently decreased by ~ 1% during juvenile stages up to an age of ~ 60-70 months (Fig. 4.7B), showing an opposite pattern compared to the observed increase in $\delta^{13}C_{bulk}$ values during juvenile growth (Chapter 3); values of nPC1.EAA increased by > 0.5% during late juvenile growth, but showed no clear pattern during subadult and stages (Fig. 4.7B). Values of nPC1.EAA during the pre-birth stage were the highest across life-history, but comparable to immediate post-birth values (Fig. 4.7B).

In both blue and porbeagle sharks, patterns in nPC1.EAA values were non-linear (smoother 'estimated sample age': maximum p-value = 0.019 < 0.05, F = 5.600), and did not differ significantly among areas (minimum p-value = 0.781, F = 0.248; Table 4.3B, C and 4.4B, C).

In both species, between-individual variances in nPC1.EAA scores did not significantly differ among life-history stages (minimum p-value = 0.283; Levene's test = 1.172). Variances during pre-birth and adult stages were statistically comparable between blue and porbeagle sharks (minimum p-value = 0.059, Levene's test = 3.615), whereas variance at the juvenile stage in blue sharks was significantly larger than variance in juvenile porbeagles (Levene's test = 10.142, p-value = 0.003 < 0.05; Table 4.5).

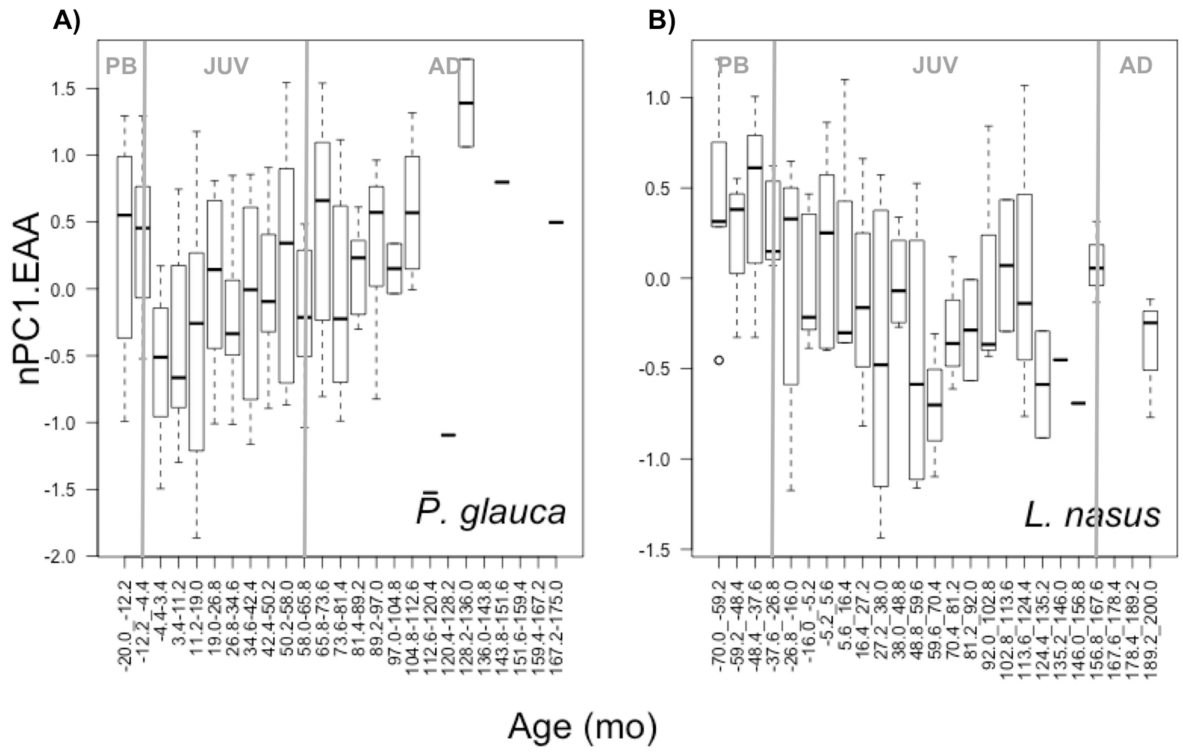

Figure 4.7 Species-level life-history traits in first principal component (PC1) scores from PCA with $\delta^{13}C_{EAA}$ values.
Distributions of life history-normalised PC1 scores from PCA with $\delta^{13}C_{EAA}$ values (nPC1.EAA; Fig. 4.5) for 25 age classes across individual A) blue and B) porbeagle sharks. Each age class represented 7.80 months in blue sharks, and 10.80 months in porbeagles. Grey vertical lines represent estimated age at birth and age at maturity. PB, JUV and AD represent pre-birth, juvenile and adult life stages. For each life stage, the boxplot displays the variation in isotope values across individuals. The horizontal line in each boxplot represents the median of the data (i.e. 50% of the data are greater than this value). The lower and upper limits of the boxplot represent the lower and upper quartile (i.e. 25% of the data less or greater than this value), respectively. The lower and upper whiskers represent the minimum and maximum value excluding outliers, respectively. Dots at the bottom or top of whiskers represent outliers (i.e. less and more than 3/2 times of the lower and upper quartile, respectively).

When PCA was performed with sample-normalised amino acid carbon isotopic compositions, life-history normalised PC1 scores (nPC1.norm-EAA) in blue sharks showed a stepwise increase of ~ 0.5% during the juvenile stage from an age of ~ 11-19 months to ~ 42-50 months, but no clear pattern during subadult and adult stages (Fig. 4.8A). Values nPC1.norm-EAA during the pre-birth stage remained relatively constant (though decreased slightly after birth) and were generally lower than values during adult stages (Fig. 4.8A). Therefore, whilst the observed sharp decrease in $\delta^{13}C_{bulk}$ values around birth, and progressive increase during juvenile growth (Chapter 3) were recovered in $\delta^{13}C_{EAA}$ values (Fig. 4.7A), they were not in nPC.norm-EAA values (Fig. 4.8A).

In porbeagles, nPC1.norm-EAA scores consistently increased by > 0.5% during pre-birth and juvenile stages up to an age of ~ 92-103 months, but showed no clear pattern during subadult and adult stages (Fig. 4.8B). Thus, the observed increase in $\delta^{13}C_{bulk}$ during juvenile growth (Chapter 3) was recovered in nPC1.norm-EAA values (Fig. 4.8B) but not in $\delta^{13}C_{EAA}$ values (Fig. 4.7B); values of

$\delta^{13}C_{EAA}$ and nPC1.norm-EAA showed opposite patterns up to an age of ~ 60-70 months, and both increased and stabilised afterwards (Fig. 4.7B and 4.8B); the increase in $\delta^{13}C_{bulk}$ values around birth was not recovered in either $\delta^{13}C_{EAA}$ or nPC1.norm-EAA values.

In both species, patterns in nPC1.norm-EAA scores were non-linear (smoother 'estimated sample age': maximum p-value = 0.024 < 0.05, F = 2.783), and did not differ significantly among areas (minimum p-value = 0.795, F = 0.230; Table 4.3B, C and 4.4B, C).
Between-individual variance in nPC1.norm-EAA scores did not differ significantly between species or among life-history stages (minimum p-value = 0.134; Levene's test = 2.326; Table 4.5). Finally, variances in nPC1-EAA and nPC1.norm-EAAs scores were statistically comparable across combinations of species and life-history stage (minimum p-value = 0.092, Levene's test = 2.938); variance in nPC1.norm-EAA scores was significantly larger than variance in nPC1.norm-EAA scores in juvenile porbeagles (Levene's test = 4.479, p-value = 0.036 < 0.05; Table 4.5).

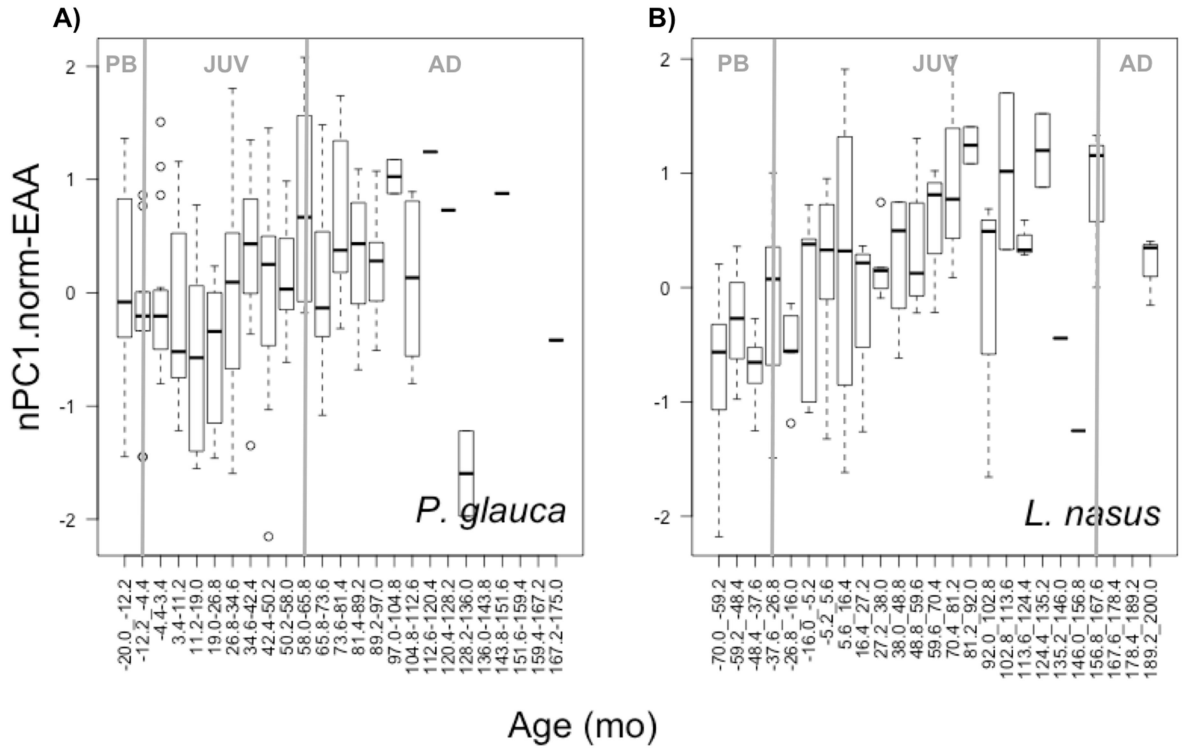

Figure 4.8 Species-level life-history traits in PC1 scores from PCA with $\delta^{13}C_{norm\text{-}EAA}$ values. Distributions of life history-normalised PC1 scores from PCA with $\delta^{13}C_{norm\text{-}EAA}$ values (nPC1.norm-EAA; Fig. 4.6) for 25 age classes across individual A) blue and B) porbeagle sharks. Each age class represented 7.80 months in blue sharks, and 10.80 months in porbeagles. Grey vertical lines represent estimated age at birth and age at maturity. PB, JUV and AD represent pre-birth, juvenile and adult life stages.

Table 4.3 Degrees of freedom (DF) and Akaike Information Criteria (AIC) for generalised additive mixed effect models (GAMMs) predicting profile life history-normalised first principal component (PC1) scores from principal component analysis (PCA) with raw and sample-normalised carbon isotopic compositions of essential amino acids ($\delta^{13}C_{EAA}$, $\delta^{13}C_{norm\text{-}EAA}$; nPC1.EAA and nPC1.norm-EAA, respectively). The null model included sample age as smoother and individual as random effect (random intercept), but no parametric fixed effects. Models with AIC > 2 lower than the null model (in bold) were considered as optimal; otherwise, the null model was considered as optimal.

A) All data

		nPC1.EAA	nPC1.norm-EAA
Model	**DF**	**AIC**	**AIC**
nPC1 ~ age + ind	**5**	**540.132**	**613.579**
nPC1 ~ age + ind + sp	6	539.756	613.965
nPC1 ~ age + ind + sp + loc	10	547.694	621.649

B) Blue sharks

		nPC1.EAA	nPC1.norm-EAA
Model	**DF**	**AIC**	**AIC**
nPC1 ~ age + ind	5	**371.361**	**403.290**
nPC1 ~ age + ind + loc	7	375.306	407.280

C) Porbeagles

		nPC1.EAA	nPC1.norm-EAA
Model	**DF**	**AIC**	**AIC**
nPC1 ~ age + ind	5	**157.430**	**217.504**
nPC1 ~ age + ind + loc	7	160.918	221.035

Table 4.4 Results for full GAMMs predicting profile nPC1.EAA and nPC1.norm-EAA values. Estimated sample age was added into models as smoother (f(Age)), individual as random effect (random intercept), and species and/or capture area as parametric fixed effects (fSpecies, fArea; full model), predictors with p-values < 0.05 (in bold) were considered significant. Model parameter estimates for fixed effects are reported in Table 4.C2.

A) All data

	nPC1.EAA			**nPC1.norm-EAA**		
Parameters	**DF**	**F**	**p-value**	**DF**	**F**	**p-value**
fSpecies	1	0.937	0.334	1	0.557	0.456
fArea	4	0.015	1.000	4	0.078	0.989
f(Age)	3.551	4.357	**0.006**	2.225	12.94	**$2.020*10^{-6}$**
R^2 (adj.)	0.038			0.091		
Scale est.	0.475			0.651		
n	248			248		

B) Blue shark data

	nPC1.EAA			**nPC1.norm-EAA**		
Parameters	**DF**	**F**	**p-value**	**DF**	**F**	**p-value**
fArea	2	0.027	0.973	2	0.005	0.995
f(Age)	1	5.600	**0.019**	3.286	2.783	**0.024**
R^2 (adj.)	0.016			0.057		
Scale est.	0.568			0.661		
n	159			159		

C) Porbeagle data

	nPC1.EAA			**nPC1.norm-EAA**		
Parameters	**DF**	**F**	**p-value**	**DF**	**F**	**p-value**
fArea	2	0.248	0.781	2	0.230	0.795
f(Age)	1	14.03	**0.0003**	1.961	12.630	**$1.010*10^{-5}$**
R^2 (adj.)	0.110			0.226		
Scale est.	0.305			0.578		
n	89			89		

Table 4.5 Results for comparisons of between-individual variances in nPC1.EAA and nPC1.norm-EAA values between pairs of combinations of species (i.e. blue shark – bsh, porbeagle – por) and life-history stage (i.e. pre-birth – PB, juvenile – JUV, and adult – AD): i.e. groups. Differences in standard deviation (SD diff), Levene's test results and p-values are reported; where p-values were < 0.05 (in bold), variances were considered non-equal.

		nPC1.EAA			nPC1.norm-EAA		
Level	**Comparison**	**SD diff**	**L**	**p-value**	**SD diff**	**L**	**p-value**
bsh	PB-JUV	0.022	0.260	0.611	-0.055	0.029	0.866
bsh	PB-AD	-0.012	0.111	0.740	-0.016	0.024	0.876
bsh	AD-JUV	0.034	0.027	0.871	-0.039	0.0005	0.982
por	PB-JUV	-0.130	2.616	0.109	-0.118	0.877	0.352
por	PB-AD	0.119	0.301	0.587	0.427	1.155	0.186
por	AD-JUV	-0.248	1.172	0.283	-0.545	1.789	0.186
PB	BSH-POR	0.286	10.142	**0.003**	0.060	0.434	0.513
JUV	BSH-POR	0.135	3.615	0.059	-0.003	$1.985*10^{-8}$	0.999
AD	BSH-POR	0.416	1.8405	0.182	0.503	2.326	0.134

Table 4.6 For each combination of species and life-history stage (i.e. groups), results for the comparison of variance between nPC1.EAA and nPC1.norm-EAA values.
A) Blue sharks

	bsh.PB			bsh.JUV			bsh.AD		
Comparison	**SD diff**	**L**	**p-value**	**SD diff**	**L**	**p-value**	**SD diff**	**L**	**p-value**
nPC1.EAA-nPC1.norm-EAA	-0.044	0.017	0.896	-0.121	0.639	0.425	-0.048	0.168	0.683

B) Porbeagles

	por.PB			por.JUV			por.AD		
Comparison	**SD diff**	**L**	**p-value**	**SD diff**	**L**	**p-value**	**SD diff**	**L**	**p-value**
nPC1.EAA-nPC1.norm-EAA	-0.270	2.938	0.092	-0.259	4.479	**0.036**	0.038	0.067	0.807

4.4.2.3 Variability in isotopic profiles within and among individuals, and among areas

Individual time-series of PC1.EAA and PC1.norm-EAA values (non life history-normalised), and $\delta^{13}C_{bulk}$ are presented in Fig. 4.9. Similar to $\delta^{13}C_{bulk}$ values, within-individual variability in PC1 profiles was generally given by a long-term (ontogenetic) pattern, and super-imposed shorter-term excursions, which typically represented isotopic variance over one or a few years (Fig. 4.9; for estimated sample ages, see Table 4.1).

Super-imposed on species-level life-history traits (Fig. 4.7 and 4.8), commonalities and differences in profile PC1.EAA and PC1.norm-EAA values were also identified among areas and individuals, with regards to both ontogenetic and short-term patterns in PC1 profiles (Fig. 4.9). When GAMMs included all data, neither PC1.EAA nor PC1.norm-EAA profiles differed significantly between species (minimum p-value = 0.104; F = 2.664). Profile PC1.EAA values differed significantly among areas (F = 17.713; p-value = $9.570 \cdot 10^{-13}$), whereas profile PC1.norm-EAA values did not (F = 0.576; p-value = 0.680). Patterns in nPC1.EAA in both blue and porbeagle sharks approximated linear relationships; when modelling these patterns with generalised linear mixed models (GLMMs), species was significant (F = 14.590, p-value = 0.0002). In blue sharks, profile

PC1.EAA values differed significantly among areas ($F = 30.75$; p-value = $5.66 \cdot 10^{-12}$), but did not in porbeagles ($F = 2.022$; p-value = 0.139); profile PC1.norm-EAA values did not differ among areas in either species (minimum p-value = 0.357; $F = 1.043$).

In blue sharks, PC1.EAA values (hence $\delta^{13}C_{EAA}$ values; Fig. 4.5) increased throughout life in nearly all individuals (except in individual 33), recovering observed ontogenetic increases in $\delta^{13}C_{bulk}$ values, though patterns in $\delta^{13}C_{EAA}$ values were generally more dampened. Values of $\delta^{13}C_{EAA}$ also decreased sharply around birth, and returned to pre-birth levels prior to capture in nearly all individual sharks (except in individuals 441 and 33). Short-term excursions in $\delta^{13}C_{EAA}$ values were generally related to excursions in $\delta^{13}C_{bulk}$ values, and more pronounced or frequent in some individuals (see individuals 335 and 441). Values of PC1.norm-EAA values, by contrast, showed no clear ontogenetic pattern, but increased slightly throughout life in individuals 16, 12, 33 and 335. Excursions in PC1.norm-EAA values were also generally related to excursions in $\delta^{13}C_{EAA}$ and $\delta^{13}C_{bulk}$ values (except in individual 441; Fig. 4.9).

In porbeagles, whilst $\delta^{13}C_{bulk}$ values increased slightly throughout life in nearly all individuals (except in individual 1000), $\delta^{13}C_{EAA}$ values decreased slightly throughout life in Northeast Atlantic individuals and individual 599, and remained relatively constant in individuals 601 and 578. Values of $\delta^{13}C_{EAA}$ also decreased around birth in nearly all individuals (except in individual 1000). Excursions in $\delta^{13}C_{EAA}$ values were generally related to excursions in $\delta^{13}C_{bulk}$ values in Northwest Atlantic individuals, particularly the pronounced negative excursions around birth, but mostly independent in Northeast Atlantic individuals. Values of PC1.norm-EAA values increased slightly throughout ontogeny in most porbeagles (except individuals 1000 and 601), recovering observed increases in $\delta^{13}C_{bulk}$ values, though ontogenetic patterns in PC1.norm-EAA values were more dampened. Values of PC1.norm-EAA decreased sharply around birth in individual 11. Short-term excursions in PC1.norm-EAA values were generally related to excursions in $\delta^{13}C_{EAA}$ and $\delta^{13}C_{bulk}$ values in Northwest, and were independent in Northeast Atlantic individuals (Fig. 4.9).

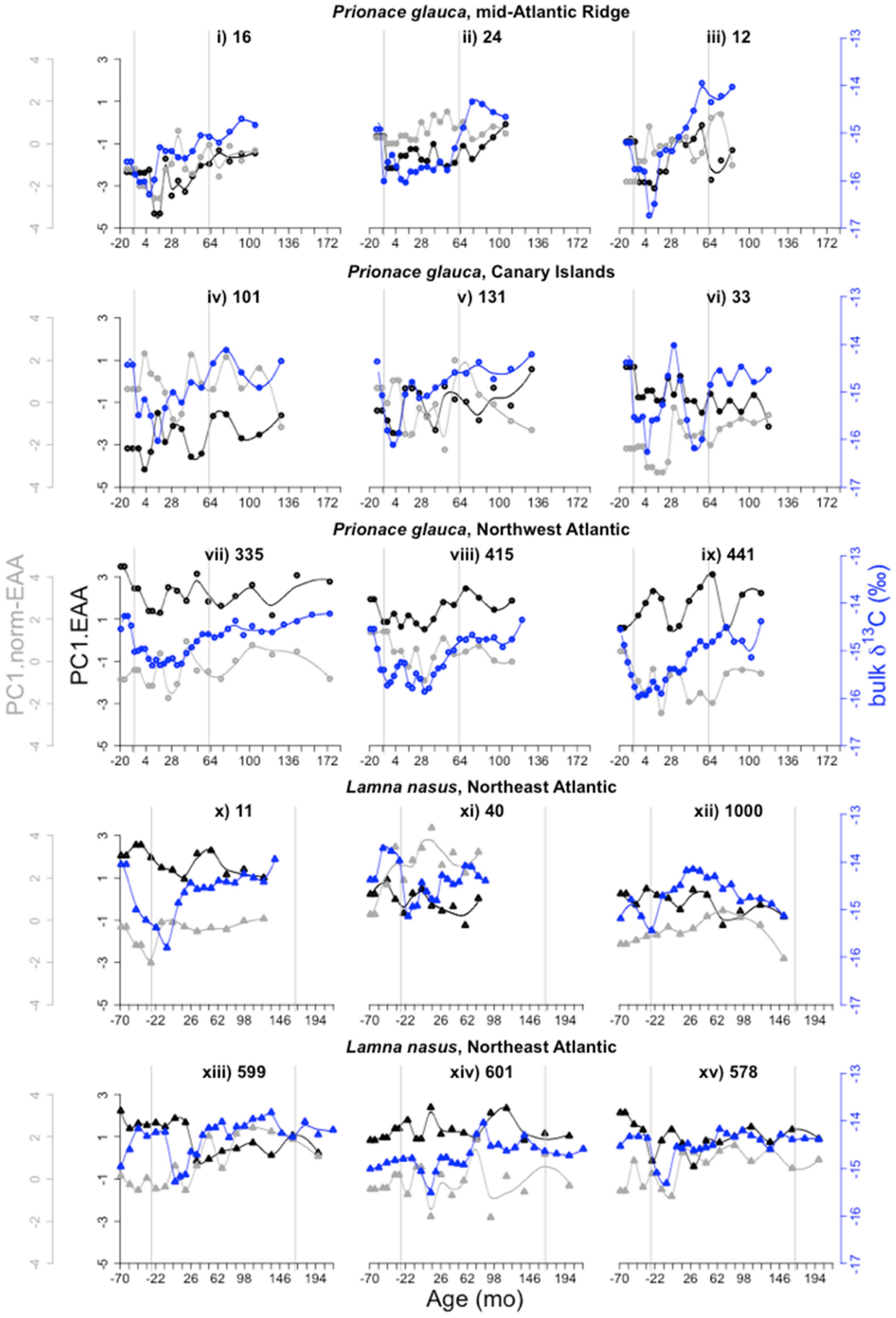

Figure 4.9 Individual-level life-history records of (non life history-normalised) PC1 scores from PCA with $\delta^{13}C_{EAA}$ and $\delta^{13}C_{norm\text{-}EAA}$ values (PC1. EAA and PC1.norm-EAA, respectively). Records are presented in the same order, and different symbols represent different species as in Fig. 4.4. Different colours represent different sets of variables: black indicates PC1.EAA values, grey PC1.norm-EAA values, and blue $\delta^{13}C_{bulk}$ values. Datapoints represent measured values, lines predicted

monthly values by the least smooth as possible Loess smoother. The grey vertical lines represent estimated age at birth and at maturity.

4.4.3 Fingerprinting approach

4.4.3.1 Defining carbon isotope fingerprints

A principal component analysis (PCA) was first carried out with literature-derived sample-normalised carbon isotope compositions of essential amino acids ($\delta^{13}C_{norm\text{-}EAA}$) in primary producers and bacteria (end-members) to test for differences in $\delta^{13}C_{norm\text{-}EAA}$ patterns among the following *a priori*-defined groups: i) autotrophic and ii) heterotrophic bacteria (prokaryotes), iii) macro and iv) microalgae, v) seagrasses, and vi) terrestrial plants (eukaryotes; Fig. 4.10). Raw amino acid carbon isotope data ($\delta^{13}C_{EAA}$) for end-members are reported in Table 4.B1, detailed PCA results in Table 4.D1. Samples clustered in the PCA space according to their major phylogenetic associations: autotrophic bacteria and algae, heterotrophic bacteria, and vascular plants. The four sampled essential amino acids represent three biosynthetic families: pyruvate (leucine and valine), oxaloacetate (isoleucine), and aromatic (phenylalanine); differentiation of samples in the PCA space is assumed to reflect differences in the proportional carbon isotope fractionation associated with these pathways among phylogenetic groups (Table 4.D1; Fig. 4.10). The first principal component (PC1) explained 46% of the total variance in $\delta^{13}C_{norm\text{-}EAA}$ patterns, and separated, to an extent, heterotrophic bacteria, autotrophic bacteria and algae, and vascular plants; the PC1 range for heterotrophic bacteria partially overlapped with the range for autotrophic bacteria and algae. The second principal component (PC2) explained 31% of total variance, and separated heterotrophic bacteria and vascular plants from autotrophic bacteria and algae. Two autotrophic bacteria showed exceptionally negative PC2 scores: *Cyanothece sp*., a genus of photosynthetic Cyanobacteria, and *Aquifex*, a genus of chemolitotroph bacteria (Table 4.D1; Fig. 4.10). In general, therefore, heterotrophic bacteria were relatively negative in both PC1 and PC2 scores, indicating relatively negative $\delta^{13}C$ values (sample-normalised) for phenylalanine and isoleucine and positive $\delta^{13}C$ values for valine and leucine. Vascular plants were positive in PC1 scores but slightly negative in PC2 scores, reflecting relatively isotopically positive phenylalanine and negative valine and leucine, as well as slightly negative isoleucine. Autotrophic bacteria and algae were intermediate in PC1 scores and positive in PC2 scores, indicating relatively isotopically positive valine (Table 4.D1; Fig. 4.10).

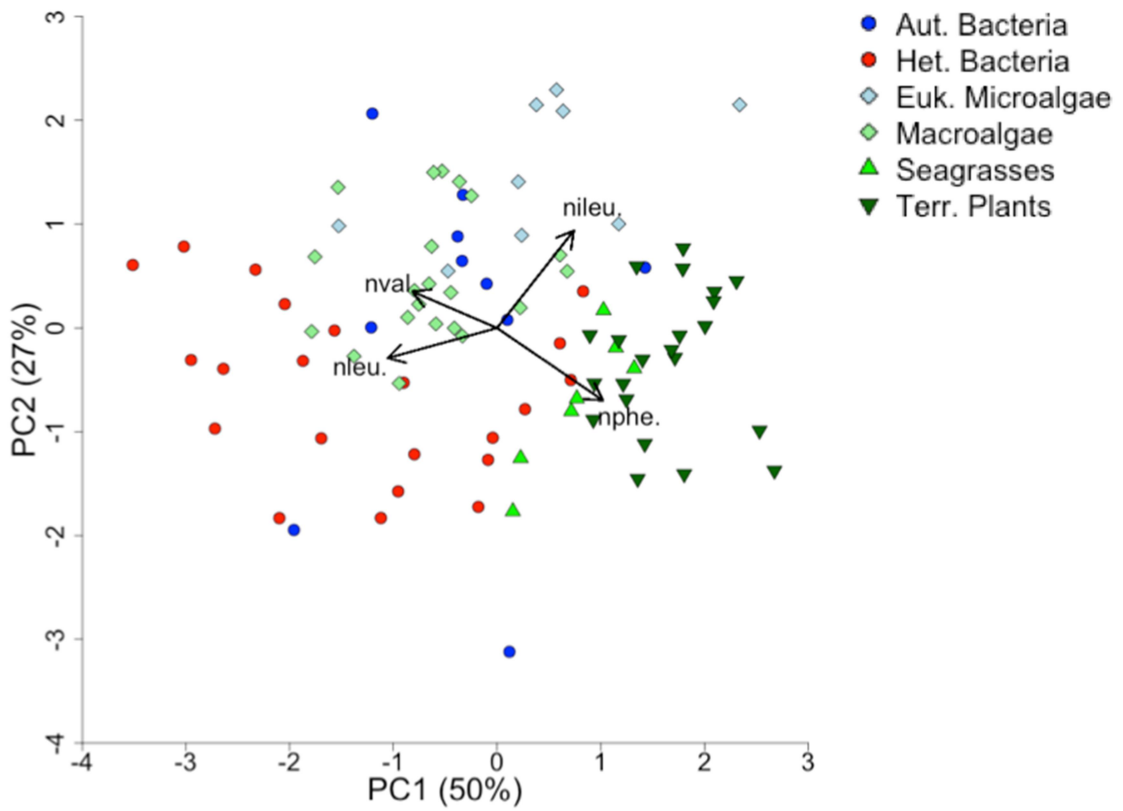

Figure 4.10 PCA with $\delta^{13}C_{norm\text{-}EAA}$ values for end-members.
Different colours and symbols identify different *a priori*-defined end-member groups: i) autotrophic (blue circles) and ii) heterotrophic (red circles) bacteria (prokaryotes), iii) macro (light green diamonds) and iv) microalgae (light blue diamonds), v) seagrasses (green triangles), and vi) terrestrial plants (dark green reverse triangles; eukaryotes).

Linear discriminant function analysis (LDA) was then carried out with $\delta^{13}C_{norm\text{-}EAA}$ data for end-members as independent variables, and end-member groups defined by the PCA as categorical variables: i) autotrophic bacteria and algae, ii) heterotrophic bacteria, and iii) vascular plants (Fig. 4.11). Detailed LDA results are reported in Table 4.D2. The first linear discriminant (LD1) explained 81% of the between-group variance, the second linear discriminant 19% (Table 4.D2A). The most important linear discriminants for separating the three categorical variables were $\delta^{13}C$ values (sample-normalised) of phenylalanine, valine and leucine; $\delta^{13}C$ values of isoleucine were also important for separating algae and autotrophic bacteria from the other groups (Table 4.D2B; Fig. 4.10 and 4.11). The LDA model classified 82% of samples correctly across groups. The proportions of autotrophic bacteria and algae, heterotrophic bacteria and plants classified correctly were 75, 73 and 100%, respectively; within autotrophic bacteria and algae, 60% of autotrophic bacteria, 81% of macroalgae and 89% of microalgae were classified correctly (for posterior probabilities of classification of each samples within the groups, see Table 4.D2C).

4.4.3.2 Classification of shark samples

The LDA model was finally applied to predict group membership of unknown samples from blue and porbeagle sharks, other consumers (Table 4.B2) and particulate organic matter (Table 4.B3) within the end-member groups, and thus to identify the most likely primary carbon sources to shark food webs (Fig. 4.11 and 4.12). Posterior probabilities of classification of unknown samples within the end-member groups are reported in Table 4.D3, 4.D4 and 4.D5 for sharks, other consumers and particulate organic matter, respectively. In the LDA space, shark samples consistently plotted outside end-member ranges, although closer to autotrophic bacteria and microalgae. Shark samples had slightly more negative LD1 values than autotrophic and heterotrophic bacteria and algae, and exceptionally positive LD2 values (i.e. higher than the highest LD2 values for autotrophic bacteria and algae; Fig. 4.11). Negative LD1 values, and positive LD2 values corresponded to more positive $\delta^{13}C$ values (sample-normalised) for valine and leucine, and more negative $\delta^{13}C$ values for phenylalanine (Fig. 4.10 and 4.11). Overall, based on the LDA model, shark samples classified with a posterior probability of 95 ± 5% within autotrophic bacteria and algae (and with probabilities of 5 ± 5 and 0.2 ± 0.7% within heterotrophic bacteria and vascular plants; Table 4.D3), but the classification within a group was imposed by the LDA model. There were no clear between-species, area and individual differences in classification, nor consistent within-individual age-related patterns (Fig. 4.11).

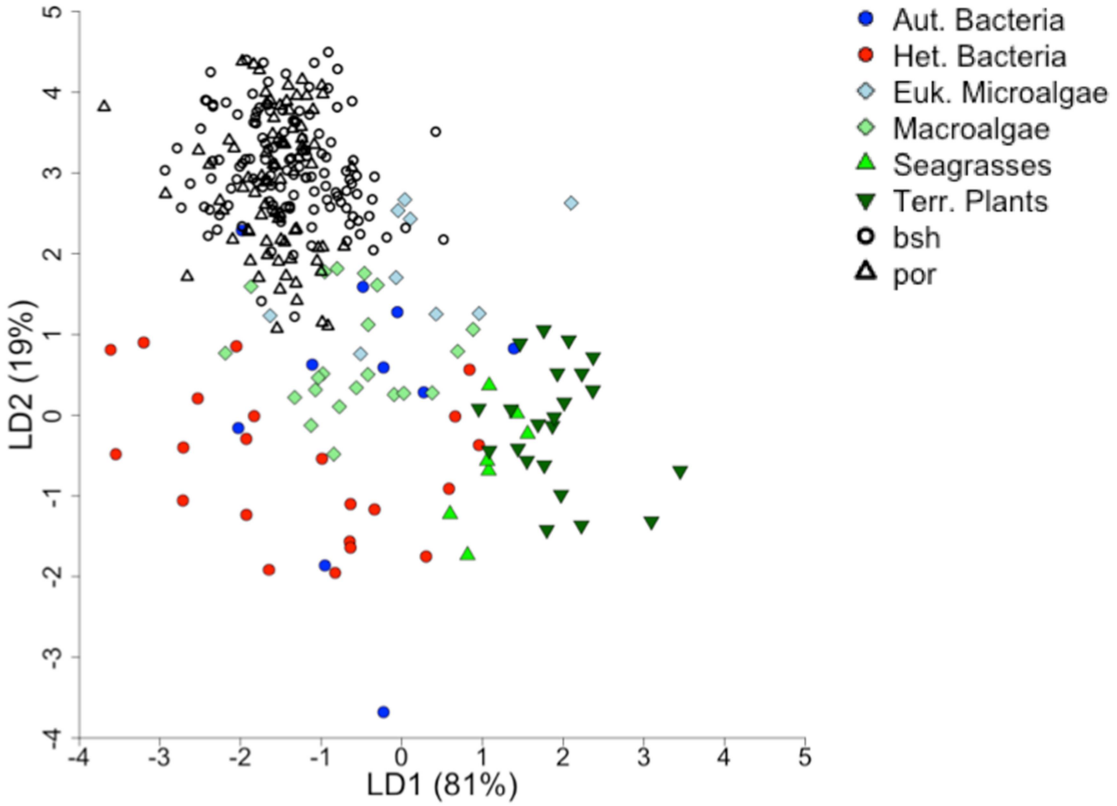

Figure 4.11 Linear discriminant function analysis (LDA) with $\delta^{13}C_{norm\text{-}EAA}$ values for end-members as independent variables, and end-member groups defined by the PCA as categorical variables: i) autotrophic bacteria and algae, ii) heterotrophic bacteria, and iii) vascular plants. The LDA model was then used for predicting group membership of unknown samples from individual blue and porbeagle sharks (Table 4.1).
Filled symbols represent end-member samples, empty symbols unknown samples. For end-members, different colours and symbols identify different *a priori*-defined groups. For sharks, circles identify blue sharks, triangles porbeagles.

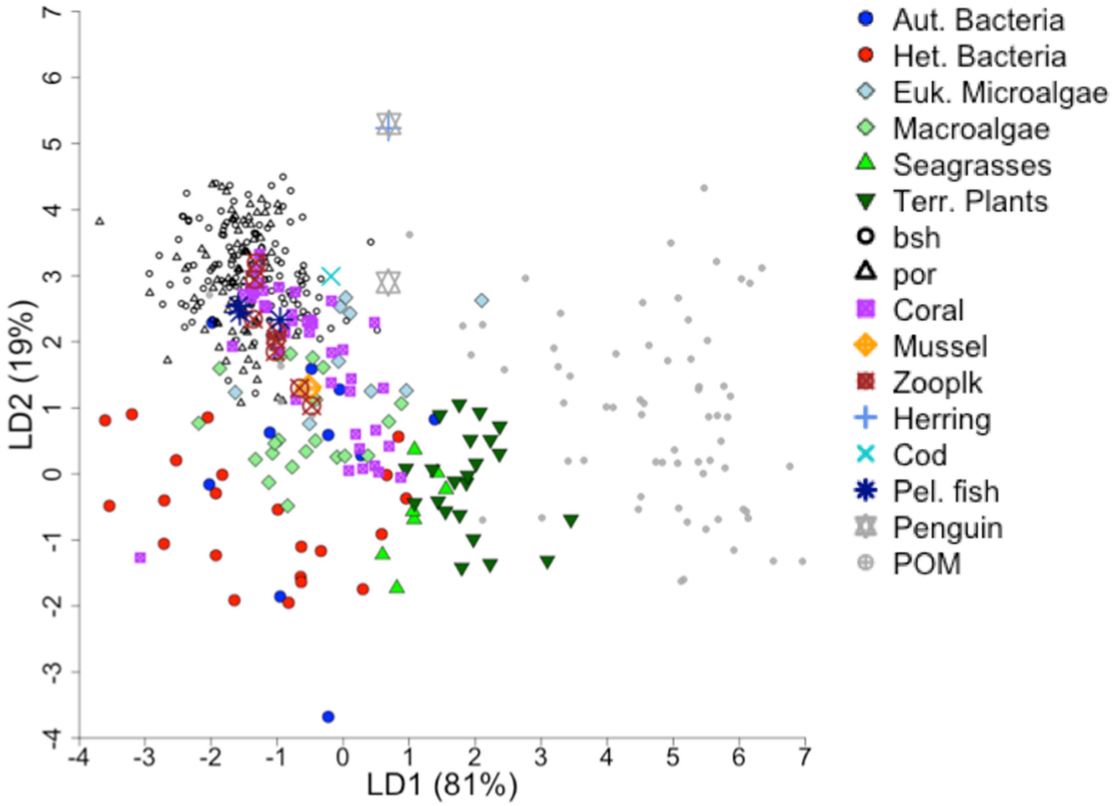

Figure 4.12 LDA with $\delta^{13}C_{norm\text{-}EAA}$ values for end-members as independent variables, and end-member groups defined by the PCA as categorical variables: i) autotrophic bacteria and algae, ii) heterotrophic bacteria, and iii) vascular plants. The LDA model was then used for predicting group membership of unknown samples from individual blue and porbeagle sharks (Table 4.1), various consumers (Table 4.B2) and particulate organic matter (Table 4.B3).
Filled symbols represent end-member samples, empty symbols unknown samples. For end-members, different colours and symbols identify different *a priori*-defined groups. For sharks, circles identify blue sharks, triangles porbeagles. For consumers and organic matter, different colours and symbols identify different organisms as in figure legend.

4.4.4 Variance in $\delta^{13}C$ values of non-essential amino acids

Variances in raw and sample normalised carbon isotopic compositions of non-essential amino acids ($\delta^{13}C_{nonEAA}$ and $\delta^{13}C_{norm\text{-}nonEAA}$, respectively), and $\delta^{13}C_{bulk}$ values throughout the life of each individual sharks are presented in Fig. 4.3B.

The $\delta^{13}C_{bulk}$ value of each sample is the weighted average of the $\delta^{13}C_{EAA}$ and $\delta^{13}C_{nonEAA}$ values (Fig. 4.13). Individual-level life-history records of $\delta^{13}C_{nonEAA}$, $\delta^{13}C_{norm\text{-}nonEAA}$ and $\delta^{13}C_{bulk}$ values are presented in Fig. 4.3E-I. Values of $\delta^{13}C_{nonEAA}$ are more positive than $\delta^{13}C_{EAA}$ values. One third to one fourth of bulk cartilage collagen is constituted by glycine. Whilst patterns in $\delta^{13}C_{bulk}$ values would be expected to recover patterns in $\delta^{13}C$ values of glycine, significant offsets were observed between $\delta^{13}C_{bulk}$ values and $\delta^{13}C$ values of glycine throughout ontogeny in most individual sharks (Fig. 4.4F). In individual 33, for example, $\delta^{13}C_{bulk}$ values were consistently more negative than $\delta^{13}C$ values of glycine during juvenile growth, meaning that $\delta^{13}C$ values in other amino acids (i.e. proline and

aspartic acid, and all the essential amino acids, which are more negative by definition as not influenced by trophic fractionation) must be sufficiently negative to draw down $\delta^{13}C_{bulk}$ values.

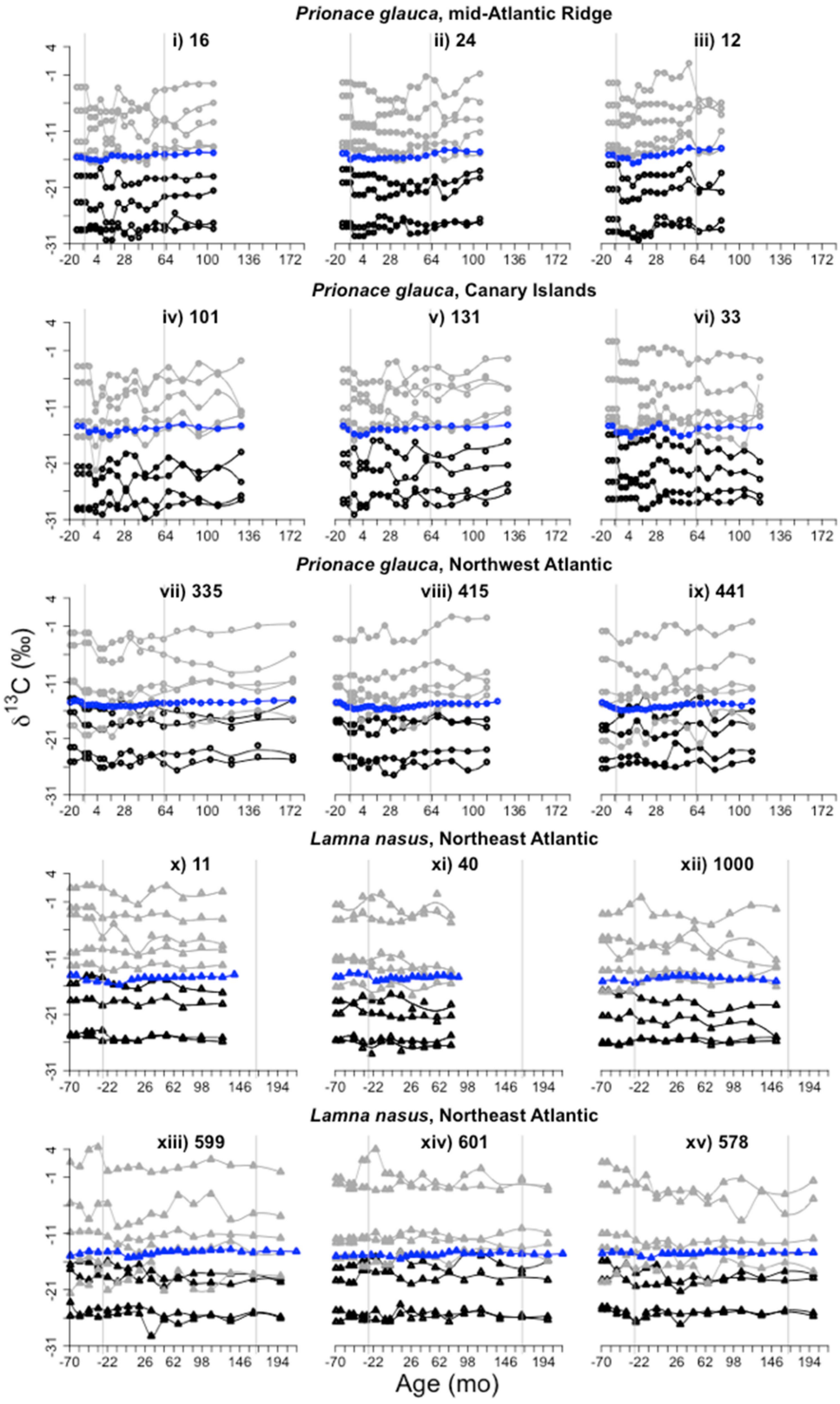

Figure 4.13 Individual-level life-history records of $\delta^{13}C_{EAA}$, $\delta^{13}C_{nonEAA}$, and $\delta^{13}C_{bulk}$ values. Records are presented in the same order, and different symbols represent different species as in Fig. 4.4. Different colours represent different sets of variables: black indicates $\delta^{13}C_{EAA}$ values, grey $\delta^{13}C_{nonEAA}$ values, and blue $\delta^{13}C_{bulk}$ values. Datapoints represent measured values, lines predicted

monthly values by the least smooth as possible Loess smoother. The grey vertical lines represent estimated age at birth and at maturity.

4.4.4.1 Variability in $\delta^{13}C$ patterns between species, and among areas and individuals

When PCA was performed with raw carbon isotopic compositions of non-essential amino acids ($\delta^{13}C_{nonEAA}$), PC1 explained 45% of the total variance in $\delta^{13}C_{nonEAA}$ values, PC2 explained 22% of variance (Fig. 4.14). As for $\delta^{13}C$ values of essential amino acids (Fig. 4.5), most positive PC1 scores corresponded to most positive $\delta^{13}C$ values for all non-essential amino acid except aspartic acid. Most positive PC2 values were associated with most positive $\delta^{13}C$ values for alanine, and most negative $\delta^{13}C$ values for glutamic and aspartic acids (Fig. 4.14).

Patterns of $\delta^{13}C_{nonEAA}$ values in shark samples were similar to patterns of $\delta^{13}C_{EAA}$ values, with additional influences of $\delta^{13}C$ values for aspartic and glutamic acid. Blue shark samples had more negative PC1 values than porbeagles (but see individual 1000), hence more negative $\delta^{13}C$ values for glycine, proline, alanine and glutamic acid, and more positive values for aspartic acid. Additionally, blue shark samples had more positive PC2 values (but see individual 1000), hence more positive $\delta^{13}C$ values for alanine, and more negative values for glutamic and aspartic acids. In both species, individuals from the eastern/central North Atlantic had more negative PC1 and PC2 values compared to insividuals from the western North Atlantic (Fig. 4.14). Patterns of $\delta^{13}C$ values of both essential and non-essential amino acids were similar to patterns of $\delta^{13}C_{nonEAA}$ values (data not shown).

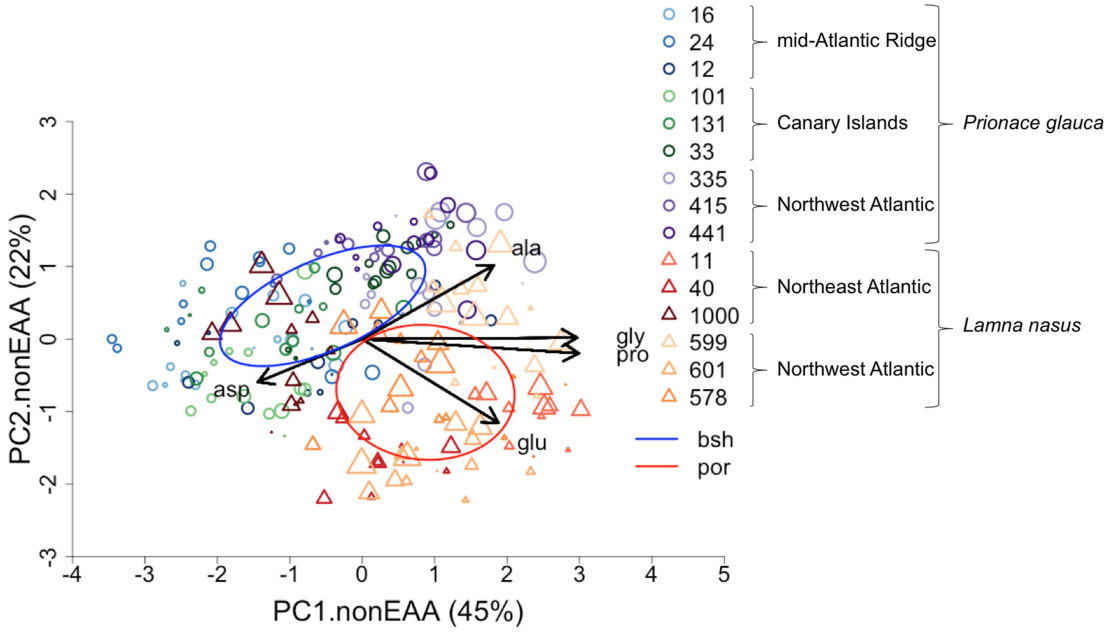

Figure 4.14 PCA with $\delta^{13}C_{nonEAA}$ values in sequential vertebral samples from individual blue and porbeagle sharks.
Different symbols and colours represent different species, capture areas and individuals, symbol size is proportional to sample distance along the vertebral radius, and SEAc are represented for blue and porbeagle sharks as in Fig. 4.5.

When PCA was carried out with normalised carbon isotope values of non-essential amino acids ($\delta^{13}C_{norm\text{-}nonEAA}$), PC1 and PC2 accounted for 38% and 23% of the total variance in $\delta^{13}C_{norm\text{-}nonEAA}$ values, respectively (Fig. 4.15). Most positive PC1 scores corresponded to most negative $\delta^{13}C$ values (sample-normalised) for all non-essential amino acids. Most positive PC2 values were associated with most positive $\delta^{13}C$ values for alanine, and most negative $\delta^{13}C$ values for glutamic acid (Fig. 4.15).

Between-species and area differences in $\delta^{13}C_{norm\text{-}nonEAA}$ patterns were greater than differences in $\delta^{13}C_{norm\text{-}EAA}$ patterns. Blue shark samples had more positive PC2 values than porbeagle samples (but see individual 1000), hence more positive $\delta^{13}C$ values for alanine, and more negative $\delta^{13}C$ values for glutamic acid. Additionally, blue sharks from the western North Atlantic had more positive PC1 values compared to blue sharks from the eastern/central North Atlantic, hence more negative $\delta^{13}C$ values for all non-essential amino acids. Porbeagles had intermediate PC1 values, with individuals from the western North Atlantic having more positive values than individuals from the eastern North Atlantic (Fig. 4.15). When performing PCA with both $\delta^{13}C_{norm\text{-}EAA}$ and $\delta^{13}C_{norm\text{-}nonEAA}$ values, between-species and area differences were reduced (data not shown).

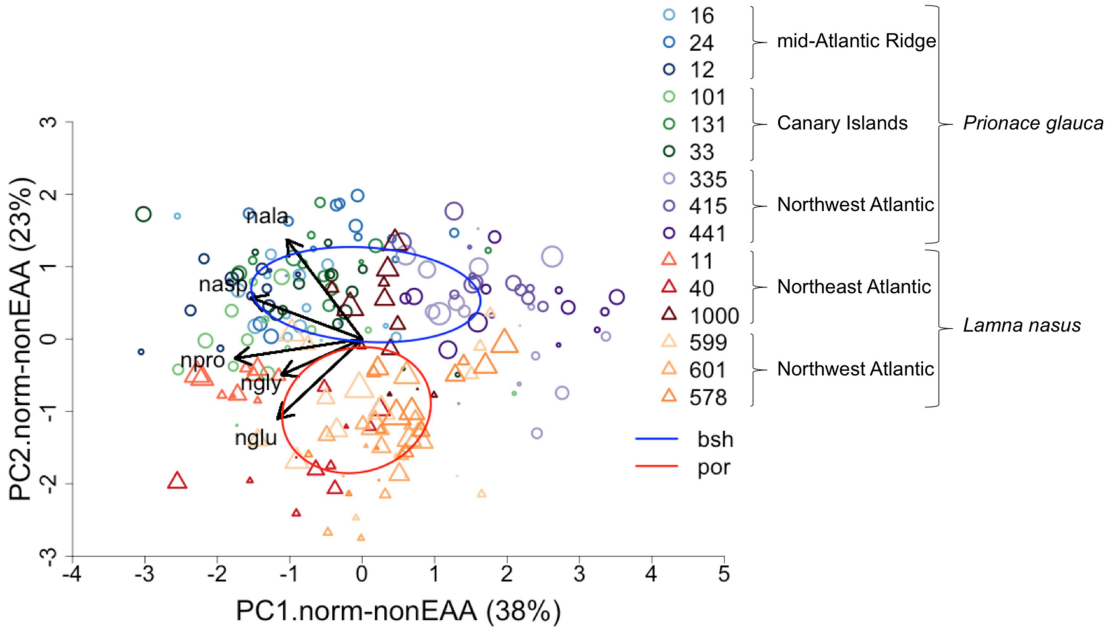

Figure 4.15 PCA with $\delta^{13}C_{norm\text{-}nonEAA}$ values in sequential vertebral samples from individual blue and porbeagle sharks.
Different symbols and colours represent different species, capture areas and individuals, symbol size is proportional to sample distance along the vertebral radius, and SEAc are represented for blue and porbeagle sharks as in Fig. 4.5.

4.4.4.2 Species-level life-history isotopic traits

In blue sharks, life history-normalised PC1 scores from PCA with raw carbon isotope values of non-essential amino acids (nPC1.nonEAA) showed a sharp decrease of ~ 1% around birth, followed by a progressive increase of ~ 1% during juvenile and adult stages (Fig. 4.16A). Values of nPC1.EAA during the pre-birth stage were comparable to values during the adult stage (Fig. 4.16A). The observed

sharp decrease in $\delta^{13}C_{bulk}$ values around birth, and progressive increase during juvenile growth (Chapter 3) were, therefore, retained in $\delta^{13}C_{nonEAA}$ values (with the exception of $\delta^{13}C$ values for aspartic acid; Fig. 4.16A).

In porbeagles, nPC1.nonEAA values showed an increase of ~ 0.5% around birth, and consistently decreased by < 1% during juvenile and subadult stages, whilst also showing excursions (Fig. 4.16B). The observed increase in $\delta^{13}C_{bulk}$ during juvenile growth (Chapter 3) was, therefore, not recovered by $\delta^{13}C_{nonEAA}$ values, with the exception of $\delta^{13}C$ values for aspartic acid.

Life history-normalised PC1 scores from PCA with sample-normalised carbon isotope values of non-essential amino acids (nPC1.norm-nonEAA) showed no clear age-related patterns in either blue or porbeagle sharks (Fig. 4.17).

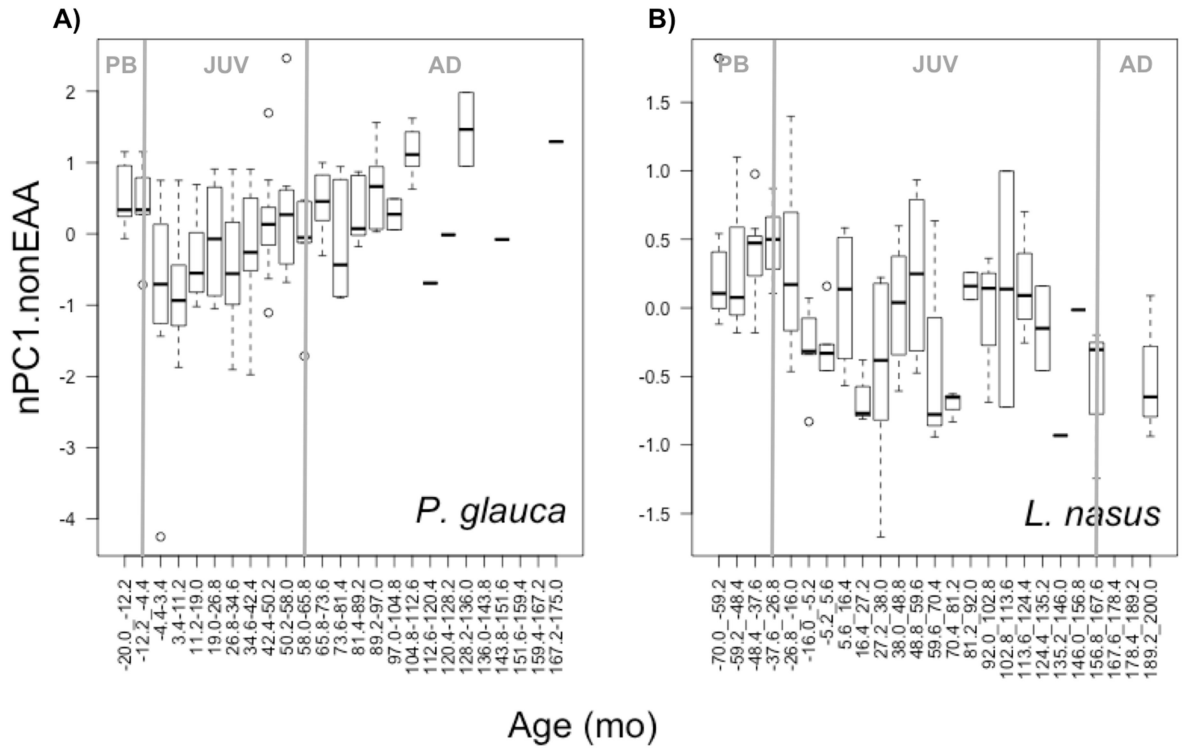

Figure 4.16 Species-level life-history traits in PC1 scores from PCA with $\delta^{13}C_{nonEAA}$ values. Distributions of life history-normalised PC1 scores from PCA with $\delta^{13}C_{nonEAA}$ values (nPC1.nonEAA; Fig. 4.14) for 25 age classes across individual A) blue and B) porbeagle sharks. Each age class represented 7.80 months in blue sharks, and 10.80 months in porbeagles. Grey vertical lines represent estimated age at birth and age at maturity. PB, JUV and AD represent pre-birth, juvenile and adult life stages.

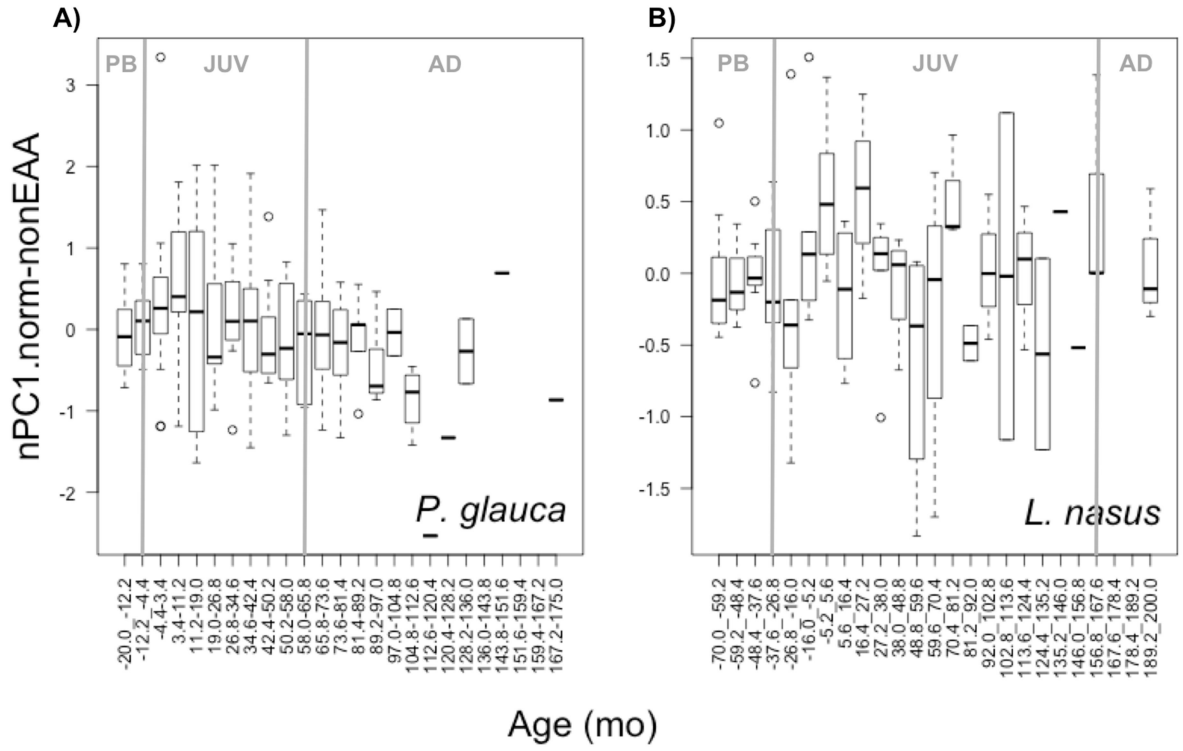

Figure 4.17 Species-level life-history traits in PC1 scores from PCA with $\delta^{13}C_{norm\text{-}nonEAA}$ values. Distributions of life history-normalised PC1 scores from PCA with $\delta^{13}C_{norm\text{-}nonEAA}$ values (nPC1.norm-nnonEAA; Fig. 4.15) for 25 age classes across individual A) blue and B) porbeagle sharks. Each age class represented 7.80 months in blue sharks, and 10.80 months in porbeagles. Grey vertical lines represent estimated age at birth and age at maturity. PB, JUV and AD represent pre-birth, juvenile and adult life stages.

4.4.4.3 Variability in isotopic profiles within and among individuals, and among areas

Individual-level life-history records of PC1.nonEAA and PC1.norm-nonEAA values, and $\delta^{13}C_{bulk}$ values are represented in Fig. 4.18. As for PC1 values from PCAs with $\delta^{13}C_{EAA}$ values, differences (and commonalities) among areas and individuals can be identified (Fig. 4.18).

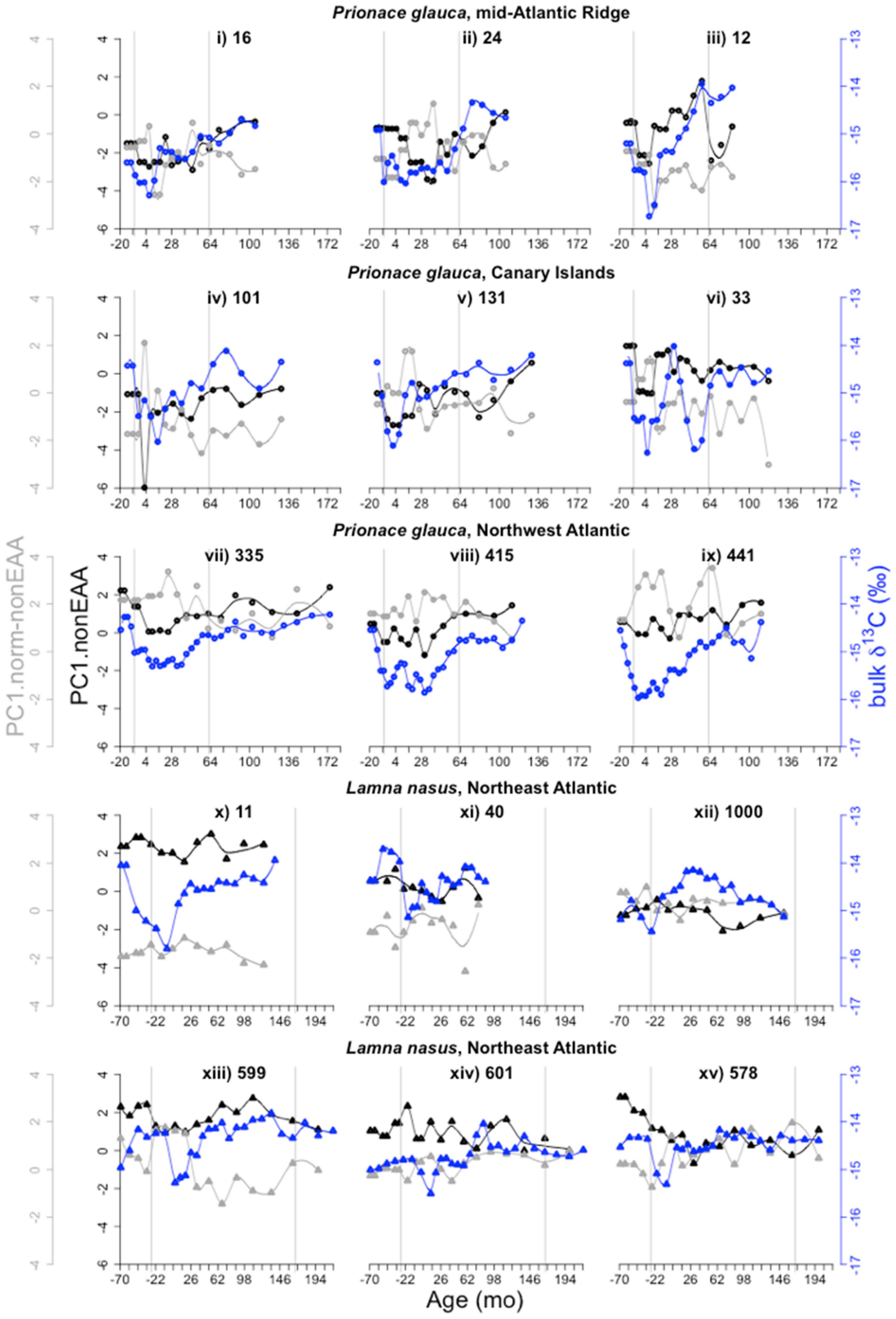

Figure 4.18 Individual-level life-history records of (non life history-normalised) PC1 scores from PCA with $\delta^{13}C_{nonEAA}$ and $\delta^{13}C_{norm\text{-}nonEAA}$ values (PC1.nonEAA and PC1.norm-nonEAA, respectively). Records are presented in the same order, and different symbols represent different species as in Fig. 4.4. Different colours represent different sets of variables: black indicates PC1.nonEAA values, grey PC1.norm-nonEAA values, and blue $\delta^{13}C_{bulk}$ values. Datapoints represent measured values, lines

predicted monthly values by the least smooth as possible Loess smoother. The grey vertical lines represent estimated age at birth and at maturity.

4.4.4.4 Relative spacing between $\delta^{13}C$ values of essential and non-essential amino acids

Individual-level life-history records of the relative spacing between the $\delta^{13}C$ values of each non-essential amino acid and the $\delta^{13}C$ values of an essential amino acid (i.e. phenylalanine or leucine in this case) are presented in Fig. 4.19A-E.

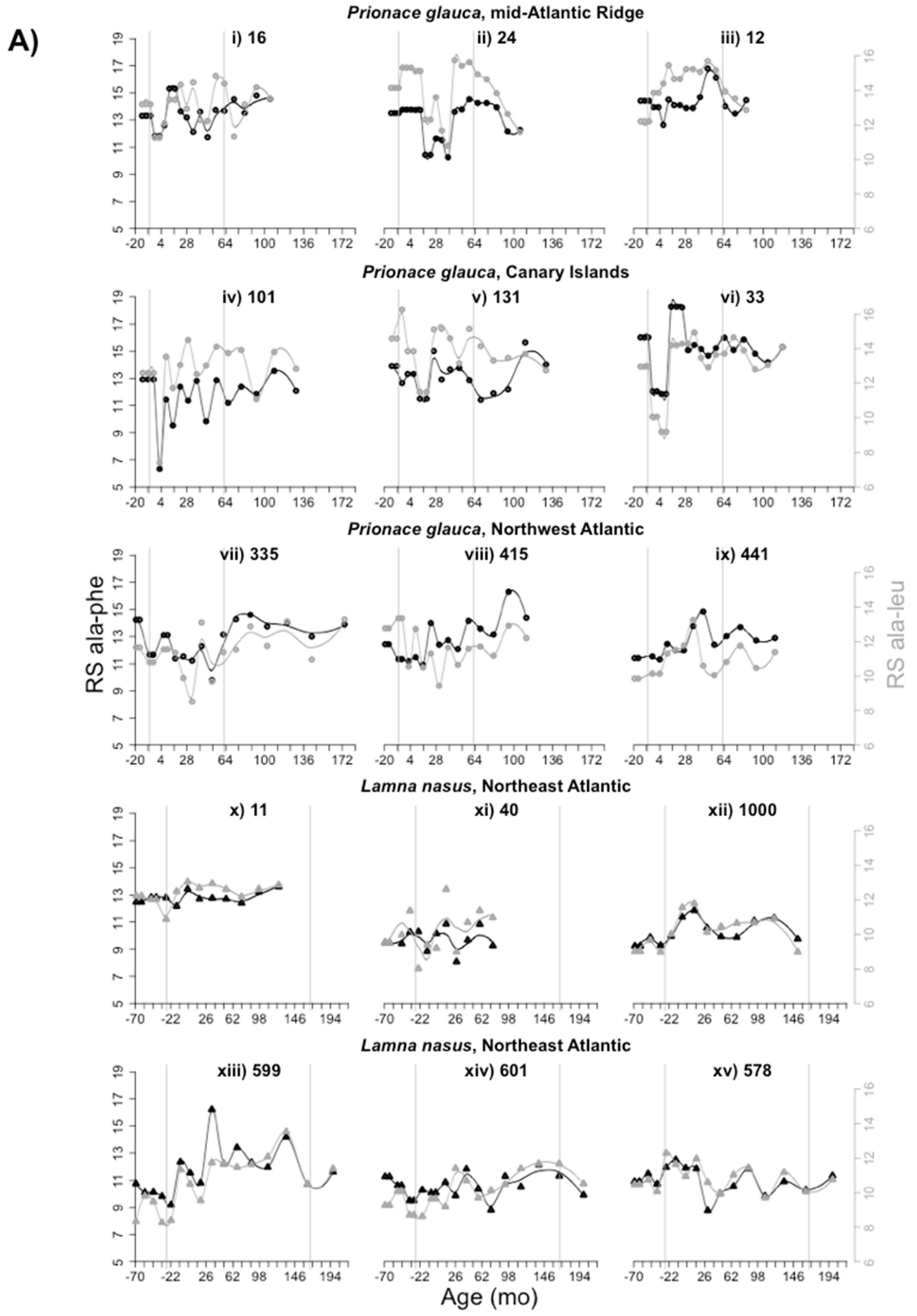

Figure 4.19 Individual-level life-history records of spacing of each non-essential amino acid to two essential amino acids: phenylalanine and leucine.
A) alanine, B) glycine, C) proline, D) aspartic acid, and E) glutamic acid. Records are presented in the same order, and different symbols represent different species as in Fig. 4.4. Different colours represent different sets of variables: black indicates spacing relative to phenylalanine, grey spacing relative to

leucine. Datapoints represent measured values, lines predicted monthly values by the least smooth as possible Loess smoother. The grey vertical lines represent estimated age at birth and at maturity.

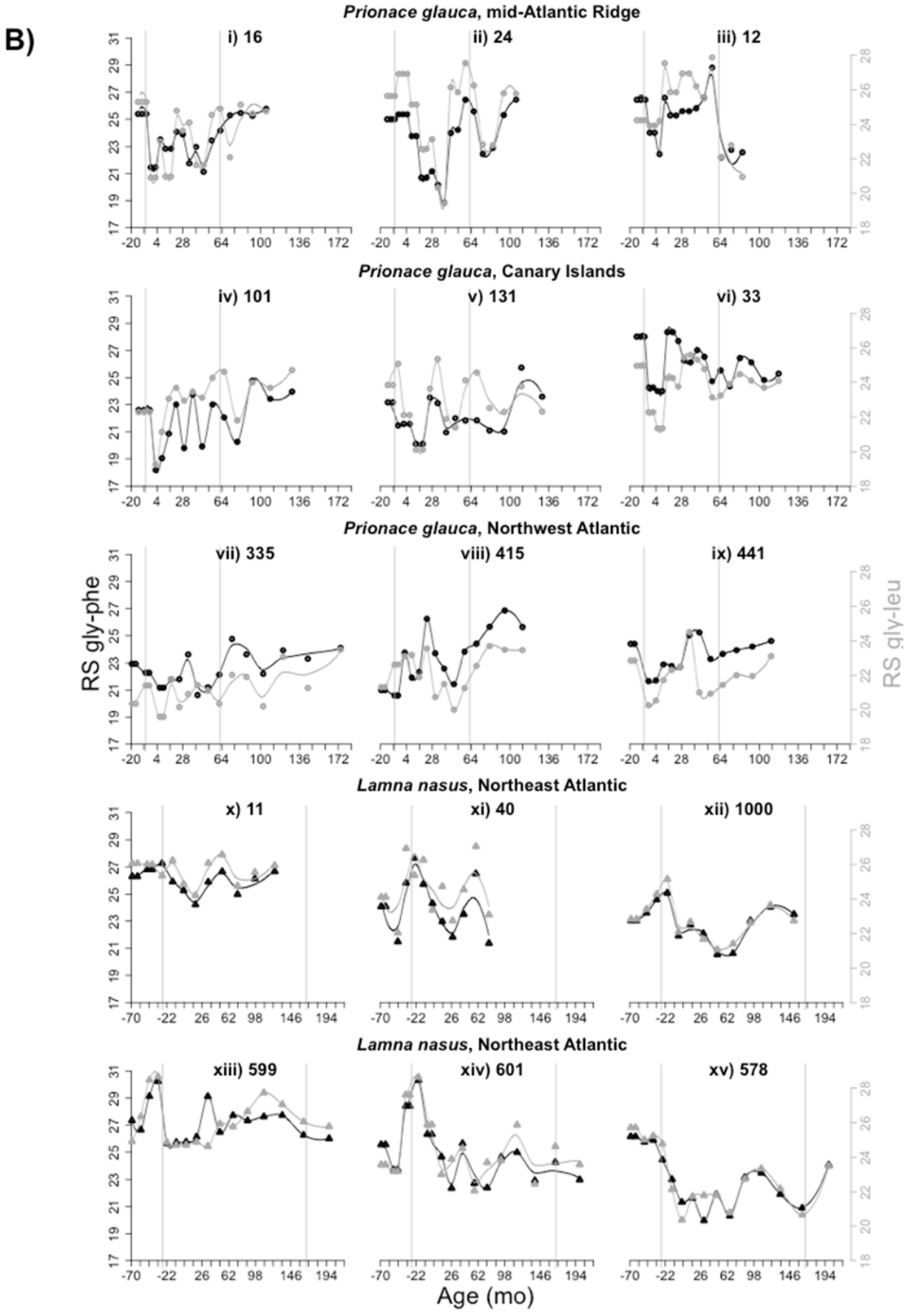

C)

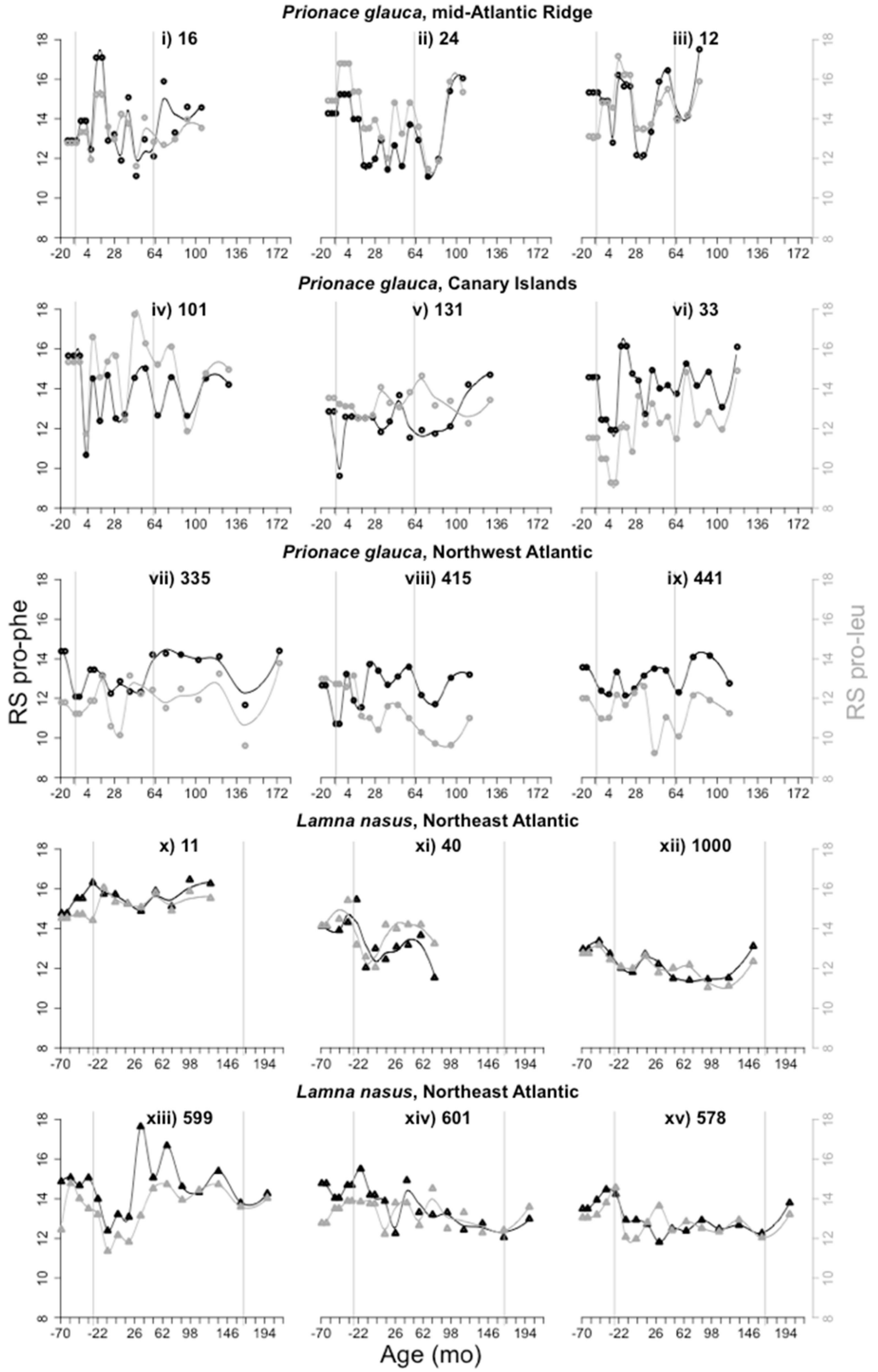
Prionace glauca, mid-Atlantic Ridge
i) 16
ii) 24
iii) 12
Prionace glauca, Canary Islands
iv) 101
v) 131
vi) 33
Prionace glauca, Northwest Atlantic
vii) 335
viii) 415
ix) 441
Lamna nasus, Northeast Atlantic
x) 11
xi) 40
xii) 1000
Lamna nasus, Northeast Atlantic
xiii) 599
xiv) 601
xv) 578
RS pro-phe
RS pro-leu
Age (mo)

D)

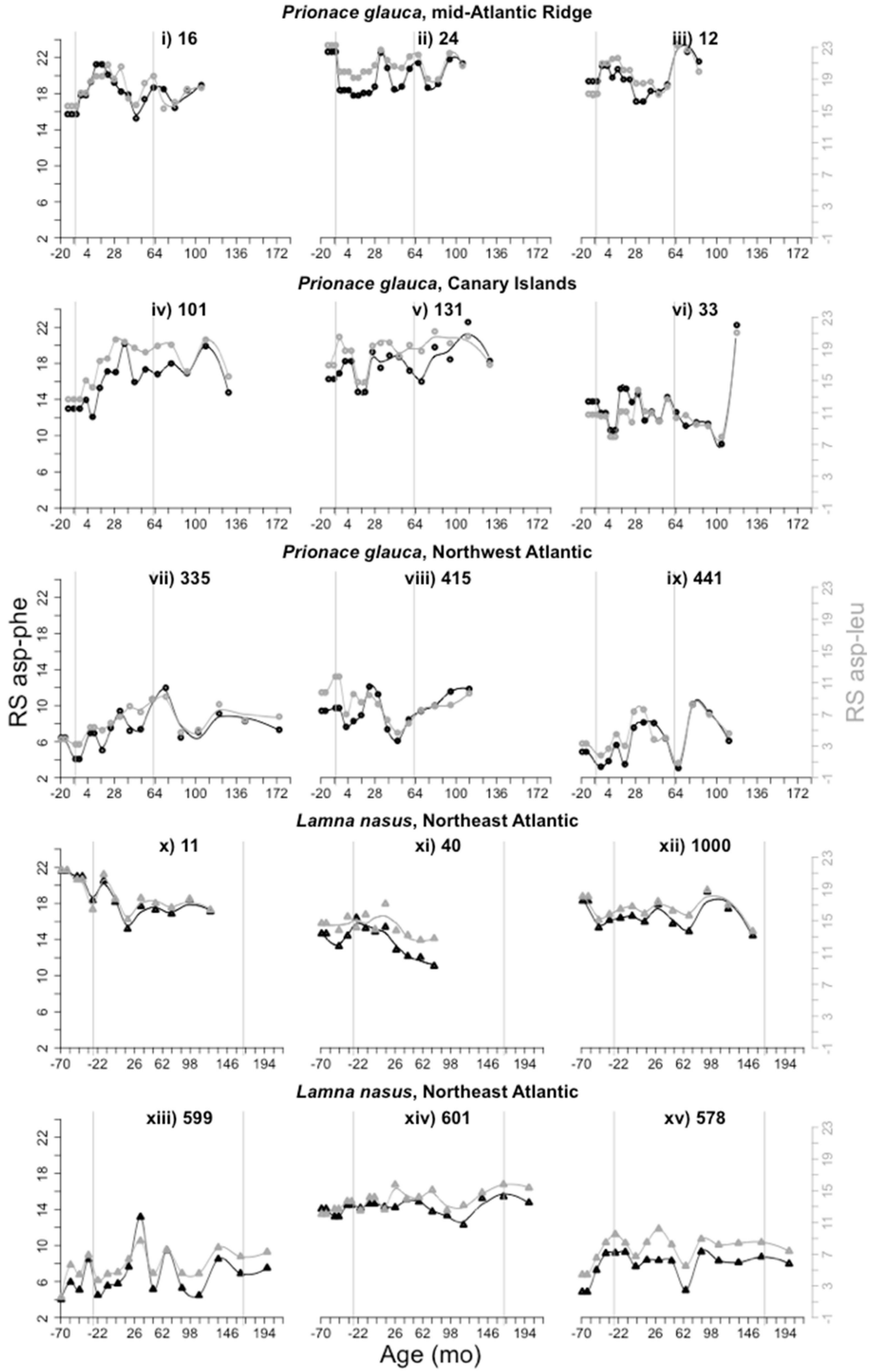
Prionace glauca, mid-Atlantic Ridge
i) 16
ii) 24
iii) 12
Prionace glauca, Canary Islands
iv) 101
v) 131
vi) 33
Prionace glauca, Northwest Atlantic
vii) 335
viii) 415
ix) 441
Lamna nasus, Northeast Atlantic
x) 11
xi) 40
xii) 1000
Lamna nasus, Northeast Atlantic
xiii) 599
xiv) 601
xv) 578
RS asp-phe
RS asp-leu
Age (mo)

E)

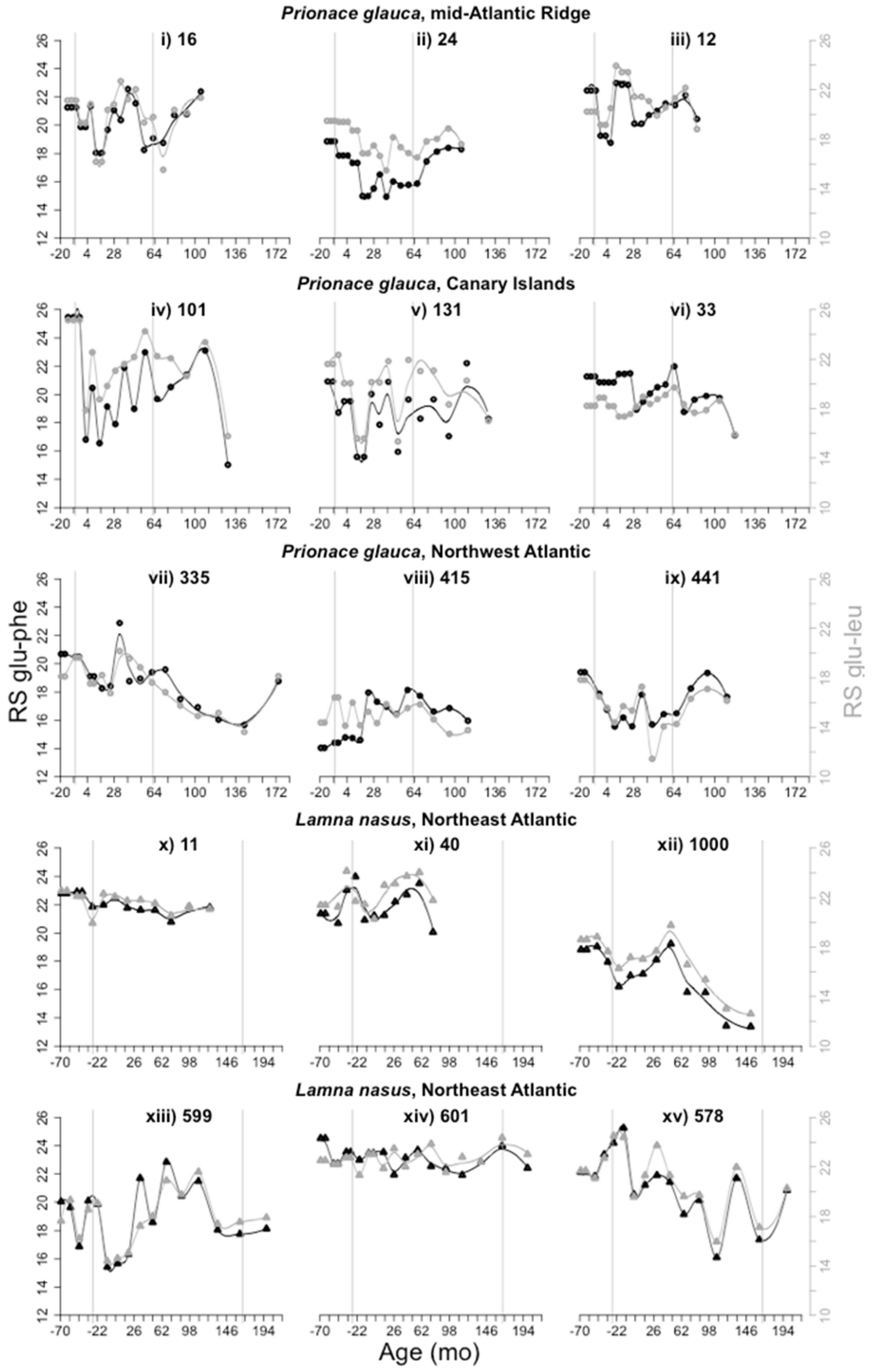
Prionace glauca, mid-Atlantic Ridge
i) 16
ii) 24
iii) 12
Prionace glauca, Canary Islands
iv) 101
v) 131
vi) 33
Prionace glauca, Northwest Atlantic
vii) 335
viii) 415
ix) 441
Lamna nasus, Northeast Atlantic
x) 11
xi) 40
xii) 1000
Lamna nasus, Northeast Atlantic
xiii) 599
xiv) 601
xv) 578
RS glu-phe
RS glu-leu
Age (mo)

4.5 Discussion

In this study, individual-level life-history records of carbon isotopic compositions of essential amino acids ($\delta^{13}C_{EAA}$) comparable to records of carbon isotope values of bulk collagen ($\delta^{13}C_{bulk}$; Chapter 3) were recovered for the same blue and porbeagle sharks. To remove influences from spatial variations in $\delta^{13}C_{CO2(aq)}$ values on $\delta^{13}C_{EAA}$ values, the carbon isotopic compositions of single amino acids were sample-normalised to the mean $\delta^{13}C$ value for all essential amino acids ($\delta^{13}C_{norm\text{-}EAA}$; see Methods). Variance in these sets of variables ($\delta^{13}C_{EAA}$ and $\delta^{13}C_{norm\text{-}EAA}$) was quantified at multiple levels (i.e. between species, among areas and within and between individuals), and compared against variance in $\delta^{13}C_{bulk}$ values to disentangle baseline from trophic isotope effects. Specifically, common, broad ontogenetic patterns in $\delta^{13}C_{EAA}$ and $\delta^{13}C_{norm\text{-}EAA}$ values were analysed across individual blue and porbeagle sharks, and compared against species-level life-history traits in $\delta^{13}C_{bulk}$ values to test i) whether traits in $\delta^{13}C_{bulk}$ values reflect movements across isotopic gradients (baseline isotope effects), changes in diet and trophic level (trophic isotope effects), or both, thus testing initial hypotheses from the interpretation of bulk tissue isotope data using modelled isoscapes (Chapter 3); ii) whether any potential influences from variations in isotopic baselines represent movements across spatial $\delta^{13}C_{CO2(aq)}$ gradients (CO_2 isotope effects) and/or changes in the relative contributions of different carbon sources to shark food webs (F isotope effects).

4.5.1 Blue sharks

4.5.1.1 Movements across isotopic gradients versus trophic shifts

In blue sharks, the interpretation of species-level life-history isotopic traits for bulk collagen ($\delta^{13}C_{bulk}$, $\delta^{15}N_{bulk}$) using modelled isoscapes suggested that the observed increase in $\delta^{13}C_{bulk}$ values during juvenile growth reflects an increase in the utilisation of foraging grounds with more positive $\delta^{13}C$ baselines. To test this hypothesis, this study first asked whether such an increase in $\delta^{13}C_{bulk}$ values is retained in $\delta^{13}C_{EAA}$ values, as variance in $\delta^{13}C_{EAA}$ values in consumers reflects variance in end-members at the base of the food web, without confounding influences from trophic shifts (Trueman *et al.,* 2012; McMahon *et al.,* 2013b).

Principal component analysis (PCA) of $\delta^{13}C$ values of single essential amino acids was used to reduce the number of variables. When analysing raw $\delta^{13}C_{EAA}$ data, the first principal component (PC1) explained 72% of the total variance in $\delta^{13}C_{EAA}$ patterns, and the loadings on the PC1 axis were similar for all sampled amino acids, meaning that relatively more positive PC1 scores reflected relatively more positive $\delta^{13}C$ values for all amino acids (Fig. 4.4).

When combining the PC1 scores for all the individuals to test for species-level life-history isotopic traits, a common, broad pattern of increasing PC1 values during juvenile growth was recovered for blue sharks (Fig. 4.6A). Clearly, therefore, at least a component of the observed increase

in $\delta^{13}C_{bulk}$ values (Chapter 3) must be associated with an increase in the frequency and/or duration of movements towards more positive $\delta^{13}C$ baselines during juvenile growth.

Core regions of the vertebra reflect maternal isotopic compositions (Olin *et al.,* 2011; Carlisle *et al.,* 2015). Maternal $\delta^{13}C_{EAA}$ values were consistently more positive than immediate *post-partum* values (Fig. 4.6A), but comparable to adult values, indicating that pupping consistently occurs in isotopically distinct (i.e. more negative in $\delta^{13}C$) grounds from the principal foraging grounds exploited by mothers and adult sharks, possibly to avoid pup predation by large sharks. After birth, $\delta^{13}C_{EAA}$ values consistently increased until approaching maternal values at ~ 4-5 years of age (FL = 150-165 cm; Skomal & Natanson, 2003; Fig. 4.6A), which approximately corresponds to the onset of maturity (Skomal & Natanson, 2003), possibly suggesting a return migration of adult individuals to maternal foraging grounds (natal homing).

In this study, blue sharks were caught across their entire geographic range in the North Atlantic (Queiroz *et al.,* 2010; Campana *et al.,* 2011; Queiroz *et al.,* 2012; Vandeperre *et al.,* 2014). The recovery of consistent life-history isotopic traits related to movement (i.e. in $\delta^{13}C_{EAA}$ values) across individuals (Fig. 4.6), therefore, implies species-level ontogenetic movement traits. The observation of large between-area and individual variability in $\delta^{13}C_{EAA}$ profiles (Fig. 4.8), however, also indicated movement across differential isotopic gradients in the eastern and western North Atlantic, as well as a high degree of individuality in space and resource use, super-imposed on species-level traits.

4.5.1.2 Spatial movements versus habitat shifts

While life-history traits in $\delta^{13}C_{EAA}$ values in blue sharks conclusively demonstrated ontogenetic movements across isotopic gradients, it is more difficult to define what these movements represent. The isotopic compositions of essential amino acids in end-members are given by the isotopic composition of aqueous CO_2 ($\delta^{13}C_{CO2(aq)}$) which varies spatially along broad latitudinal gradients (Chapter 2), and by the isotopic fractionation during amino acid biosynthesis, which differs among major phylogenetic end-member groups, producing distinct carbon isotope fingerprints (Scott *et al.,* 2006; Larsen *et al.,* 2009; 2013). Thus, inferred movement across isotopic gradients may represent spatial variations in $\delta^{13}C_{CO2(aq)}$ values, or changes in the composition of the primary producing community, or both. To discriminate between these effects, $\delta^{13}C_{EAA}$ values were sample-normalised (effectively removing influences from spatially varying $\delta^{13}C_{CO2(aq)}$ values; $\delta^{13}C_{nEAA}$), and ontogenetic patterns in $\delta^{13}C_{bulk}$, and raw and normalised essential amino acid carbon isotopic compositions ($\delta^{13}C_{EAA}$ and $\delta^{13}C_{norm\text{-}EAA}$, respectively) were contrasted.

When analysing $\delta^{13}C_{norm\text{-}EAA}$ data, PC1 explained 41% of the total variance, and variation in PC1 scores was mostly associated with variation in normalised $\delta^{13}C$ values for valine and isoleucine (Fig. 4.5). Scores of PC1 showed a relatively noisy and unclear ontogenetic pattern (Fig. 4.7A), suggesting that a component of the observed increase in $\delta^{13}C_{EAA}$ values must reflect an ontogenetic

movement towards southern waters, at least during juvenile and subadult growth. This isotope-inferred movement pattern is consistent with tagged-derived movement information, which also indicates an increased utilisation of tropical waters by adult females, possibly associated with pupping and reproduction (Vandeperre *et al.,* 2014). There was, however, a suggestion of a stepwise increase in PC1 scores at ~ 2-3 years of age (FL = 125-155 cm), potentially indicating a shift in habitat and carbon source. Such an increase in PC1 scores reflected relatively more positive normalised $\delta^{13}C$ values for valine, and relatively more negative values for isoleucine (Fig. 4.5). Based on available carbon isotope fingerprints (Scott *et al.,* 2006; Larsen *et al.,* 2009; 2013; 2015; Fig. 4.9), these patterns could indicate an increase in the relative contributions of algally- or bacterially-derived carbon, but these conclusions are highly speculative, given observed inconsistencies between shark and end-member amino acid carbon isotopic compositions (Fig. 4.11).

Maternal PC1 scores were consistently more positive than immediate *post-partum* values (Fig. 4.7A), suggesting that maternal foraging and pupping grounds are primarily fuelled by different carbon sources. A reduction in PC1 scores after birth could indicate a greater contribution from seagrass or vascular plant-derived carbon to juvenile food webs (Fig. 4.9), but these conclusions are uncertain. Blue sharks are believed to feed pelagically across life-history, and an oceanic nursery area has recently been identified in the central North Atlantic near the Azores (Vandeperre *et al.,* 2014; 2016); however, nurseries on continental shelves are also believed to exist in the Northeast Atlantic (Queiroz *et al.,* 2010 and references. therein).

4.5.2 Porbeagle sharks

4.5.2.1 Movements across isotopic gradients versus trophic shifts

In contrast to blue sharks, ontogenetic isotope patterns in bulk collagen ($\delta^{13}C_{bulk}$, $\delta^{15}N_{bulk}$) in porbeagles could not be explained solely by movement across predicted spatial isotopic gradients, so a trophic shift was inferred (Chapter 3). Values of $\delta^{13}C_{EAA}$ consistently decreased during juvenile growth until ~ 5-6 years of age (FL = 155-165 cm; Natanson *et al.,* 2002; Fig. 4.6B), showing an opposite overall trend to that in $\delta^{13}C_{bulk}$ values. These patterns require a combination of movement towards more negative $\delta^{13}C$ baselines, and a trophic shift, producing an increase in $\delta^{13}C$ values of non-essential amino acids sufficiently large to counteract the decrease in $\delta^{13}C_{EAA}$ values, thereby resulting in an increase in $\delta^{13}C_{bulk}$ values. At ~ 5-6 years of age, $\delta^{13}C_{EAA}$ values showed a consistent increase until ~ 8-9 years (FL = 185-190 cm), followed by a subsequent decrease in $\delta^{13}C$ values during subadult life stages, with the possibility of another increase during adult stages, which, however, only regarded adult Northwest Atlantic individuals (Fig. 4.6B). This pattern was clearly distinct from the progressive decrease in $\delta^{13}C_{EAA}$ values during earlier juvenile growth, indicating a shift in movement behaviour between early and late, subadult and possibly adult life stages.

Maternal $\delta^{13}C_{EAA}$ values were the highest across life-history, but not consistently different from immediate *post-partum* values; juvenile $\delta^{13}C_{EAA}$ values, however, started decreasing progressively from just after birth (Fig. 4.6B). These patterns suggest that mothers migrate towards isotopically distinct foraging grounds from those exploited by subadult females to give birth, possibly reflecting an alternative strategy to avoid pup predation compared to that used by blue sharks. Immediate *post-partum* independent feeding, however, results in an increasing utilisation of isotopically distinct (i.e. more negative in $\delta^{13}C$ values) grounds from those provisioning the mother during egg development.

Porbeagles were also captured at the two extremes of their known distributional range in the North Atlantic (Pade *et al.,* 2009; Campana *et al.,* 2010; Saunders *et al.,* 2011; Biais *et al.*, 2016). The recognition of consistent life-history isotopic traits in $\delta^{13}C_{EAA}$ values, therefore, implies common ontogenetic movements for the eastern and western Atlantic populations.

4.5.2.2 Spatial movements versus habitat shifts

Scores of PC1 from the analysis of $\delta^{13}C_{norm\text{-}EAA}$ values, which contain information relative to carbon source rather than water chemistry, showed an overall positive trend throughout ontogeny across individual porbeagles (i.e. the opposite trend to that in $\delta^{13}C_{EAA}$ values, at least until ~ 5-6 years of age; Fig. 4.7B). Such an increase in PC1 scores throughout ontogeny reflected an increase in normalised $\delta^{13}C$ values for valine, and a decrease in values for isoleucine (Fig. 4.5). Based on available carbon isotope fingerprints (Fig. 4.11), these patterns in $\delta^{13}C_{norm\text{-}EAA}$ values could indicate a progressive increase in the relative contributions of algally- and bacterially-derived carbon to juvenile food webs, in association with with spatial movements towards more negative $\delta^{13}C_{CO2(aq)}$ values. This interpretation is broadly consistent with the known occurrence of juvenile porbeagles in shelf settings, and presumed increasing use of shelf-edge and oceanic environments as they grow (Bendall *et al.,* 2013; Ellis *et al.,* 2015; Biais *et al.*, 2016). However, the recovery of life-time minimum PC1 scores in the maternal component of vertebrae is puzzling.

Alternatively, scores of PC1 can tentatively be split into three stages (Fig. 4.7B). Maternal PC1 scores were the most negative across life-history; *post-partum* independent feeding resulted in a sharp increase in PC1 scores, followed by a subsequent gradual (small) decrease until ~ 5-6 years of age. At this stage, PC1 scores newly increased to life-time maximum values, but also showed largest ontogenetic and between-individual variability. The age of ~ 5-6 years is approximately the age at which $\delta^{13}C_{EAA}$ values switched from a decreasing to increasing trend (Fig. 4.6B), and $\delta^{13}C_{bulk}$ values reached a relatively steady state (Chapter 3); after this stage, PC1 scores and $\delta^{13}C_{EAA}$ values broadly co-varied (Fig. 5.6B and 4.7B). These patterns suggested a combination of spatial movement towards more negative $\delta^{13}C_{CO2(aq)}$ values and diet and trophic level change during early juvenile growth, and periodic switches in carbon source during late juvenile, subadult and possibly adult life stages, in association with spatial movements and/or diet changes. These stages, however, seem to be

characterised by higher between-variability in space and resource use. In the Northeast Atlantic, juvenile and subadult porbeagles are known to conduct extensive latitudinal movements, with a high degree of individuality in movement behaviour (Pade *et al.,* 2009; Saunders *et al.,* 2011; Biais *et al.*, 2016).

Whilst life-time lowest maternal PC1 scores are puzzling, life-time highest maternal $\delta^{13}C_{EAA}$ values may indicate a migration of pregnant females towards more positive $\delta^{13}C_{CO2(aq)}$ values possibly associated with parturition, consistent with the observed movement to subtropical grounds by large mature females in the Northwest Atlantic (Campana *et al.* 2010).

4.5.3 Fingerprinting approach

Age-related variance in $\delta^{13}C_{norm\text{-}EAA}$ patterns (Fig. 4.7 and 4.6) suggested ontogenetic changes in the relative contributions of different carbon sources to shark food webs. The application of a fingerprinting approach to shark samples to estimate their most likely carbon source(s), however, revealed inconsistencies between shark amino acid carbon isotopic compositions and available end-member carbon isotope fingerprints (Fig. 4.10). Similar mismatches were also observed for other consumers, including zooplankton, corals, pelagic fishes and penguins (Fig. 4.11). Such systematic offsets in amino acid carbon isotopic compositions between consumers and presumed end-members could not, however, be explained with confidence.

Limited chromatographic separation between peaks for isoleucine and leucine in the example chromatograph (e.g. Fig. 4.1) could potentially result in falsely relatively positive $\delta^{13}C$ values for isoleucine, and relatively negative $\delta^{13}C$ values for leucine, leaving open the possibility of a systematic measurement error. Alternatively, sharks might be feeding in food webs dominated by unsampled end-members, or under-represented in the current selection. Samples of particulate organic matter recovered at various depths in the North Atlantic also showed systematic differences in $\delta^{13}C_{nEAA}$ patterns compared to end-members, but had exceptionally positive LD1 values (Fig. 4.11). Sinking particulate organic matter is degraded and remineralised by heterotrophic bacteria, with the possibility of bacterial overprinting of algal type fingerprints (McCarthy *et al.,* 2007; Hannides *et al.,* 2013; Sabadel, *unpubl. data*). Accordingly, the explanation for inconsistencies between shark and end-member amino acid compositions remains unresolved, and is beyond the scope of the current project. Any potential bias due to the lack of internationally certified standards for the analysis of carbon isotopes in single amino acids could be an issue when comparing data for end-members and consumers within a fingerprinting approach, as data were obtained from different laboratories. Such a fingerprinting approach, however, has already been successfully applied to track phytoplankton regime shifts from corals, and differences in instruments or methods did not seem to create any issue (McMahon et al., 2015b).

4.5.4 Patterns in carbon isotope compositions of non-essential amino acids

Variance in $\delta^{13}C_{nonEAA}$ values reflects shifts in diet and trophic level, in addition to baseline effects (due to variation in $\delta^{13}C_{CO2(aq)}$ values across space and/or variation in isotope fractionation during amino acid biosynthesis among major carbon sources). When analysing variance in $\delta^{13}C_{nonEAA}$ values, patterns in $\delta^{13}C$ values of alanine, glycine and proline were similar to patterns in $\delta^{13}C_{EAA}$ values, whereas $\delta^{13}C$ values of aspartic acid followed the opposite patterns, and $\delta^{13}C$ values of glutamic acid increased separation between blue and porbeagle sharks (Fig. 4.5 and 4.14). Thus, differences in $\delta^{13}C$ values of glutamic acid between blue and porbeagle sharks may suggest differences in trophic position.

Sample-normalisation of $\delta^{13}C_{nonEAA}$ values (i.e. $\delta^{13}C_{norm\text{-}nonEAA}$) removes influences from spatial variation in $\delta^{13}C_{CO2(aq)}$ values. When analysing $\delta^{13}C_{norm\text{-}nonEAA}$ patterns, between-species differences were maintained, and between-area differences became greater (Fig. 4.14 and 4.15). Between-area differences in $\delta^{13}C_{norm\text{-}nonEAA}$ values were also greater than differences in $\delta^{13}C_{norm\text{-}EAA}$ values (Fig. 4.6 and 4.15). Values of $\delta^{13}C$ of all non-essential amino acid were more negative in eastern/central North Atlantic sharks than in western North Atantic sharks. Possible explanations for this pattern may include: feeding at a lower trophic level by eastern/central North Atlantic sharks, a diet richer in lipid, or differences in the primary carbon source, which are less evident when considering only the four essential amino acids. In theory, in fact, carbon isotope fingerprints reflect differences in $\delta^{13}C$ patterns for all amino acids among lineages (Larsen *et al.*, 2013). When trying to identify consumer primary carbon source(s), however, non-essential amino acids are often excluded, to remove confounding influences from trophic effects (e.g. McMahon *et al.*, 2015a).

When examining nitrogen isotopes, the relative spacing between $\delta^{15}N$ values of glutamic acid and phenylalanine is commonly used as proxy for trophic position (Chikaraishi *et al.*, 2009; 2010). If individual sharks increased trophic level throughout ontogeny, an increase in the relative spacing between $\delta^{13}C$ values of these two amino acids with age would also be expected. However, this type of pattern was only seen in individual 101, and within-individual variance in relative spacing was noisy in most sharks. Similalry, if porbeagles fed at a higher trophic level than blue sharks, a higher relative spacing in porbeagles would be expected, but that does not seem to always be the case. Finally, large differences in mean and life stage-specific relative spacing were observed among areas and individuals within each species (Fig. 4.19E). These findings may suggest that $\delta^{13}C_{nonEAA}$ patterns are not so strongly influenced by trophic level as are $\delta^{15}N$ patterns. If that was true, non-essential amino acids could potentially be included when applying a fingerprinting approach to identify consumer carbon source(s), increasing the power of the LDA analysis. However, additional controlled feeding experiments are required to better constrain trophic effects on $\delta^{13}C_{nonEAA}$ values (McMahon et al., 2013b).

4.6 Conclusions

A major result of this study was the identification of species-level life-history traits in the carbon isotopic compositions of essential amino acids ($\delta^{13}C_{EAA}$) in both blue and porbeagle sharks from across the North Atlantic (Fig. 4.6). Traits in $\delta^{13}C_{EAA}$ values are related to movement across isotopic gradients; thus, the recognition of species-level life-history traits in $\delta^{13}C_{EAA}$ values conclusively demonstrated species-level ontogenetic movement traits, implying shared vulnerability to fishery capture across life-history. In blue sharks, a consistent increase in $\delta^{13}C_{EAA}$ values until ~ 5-6 years of age (Fig 4.6A) indicated an ontogenetic movement towards more positive $\delta^{13}C$ baselines during juvenile growth, as hypothesised from the interpretation of life-history isotopic traits in bulk collagen using modelled isoscapes (Chapter 3). In porbeagles, a consistent decrease in $\delta^{13}C_{EAA}$ values until an age of ~ 5-6 years (Fig 4.6B), opposite to the observed increase in $\delta^{13}C_{bulk}$ values (Chapter 3), indicated an ontogenetic movement towards more negative $\delta^{13}C$ baselines, accompanied by a diet change, as also hypothesised from the interpretation of bulk collagen isotope data. At ~ 5-6 years of age, the progressive decrease in $\delta^{13}C_{EAA}$ values switched to periodic oscillations (Fig 4.6B), indicating a change in movement behaviour.

In blue sharks, maternal $\delta^{13}C_{EAA}$ values were consistently more positive than post-birth values, but comparable to values during adult life stages (Fig. 4.6A), indicating isotopically distinct maternal foraging and pupping grounds, and potentially a return migration of adult sharks to maternal foraging grounds. In porbeagles, maternal $\delta^{13}C_{EAA}$ values were the highest across life-history, but comparable to immediate *post-partum* values (Fig. 4.6B), implying that maternal provisioning occurs in isotopically distinct grounds from those exploited by subadult sharks. Immediate post-birth independent feeding, however, results in an increasing utilisation of ^{13}C-depleted foraging grounds.

Movement across isotopic gradients may represent movement across latitudinal gradients in $\delta^{13}C_{CO2(aq)}$, and/or transitions across habitats dominated by different carbon sources. Variance in sample-normalised amino acid carbon isotopic compositions ($\delta^{13}C_{norm\text{-}EAA}$) reflects variance in the relative contributions of different end-member to shark food webs, after influences from spatially varying $\delta^{13}C_{CO2(aq)}$ values are removed. In blue sharks, the comparison of patterns in $\delta^{13}C_{bulk}$, $\delta^{13}C_{EAA}$ and $\delta^{13}C_{norm\text{-}EAA}$ values (Fig. 4.6 and 4.7; Chapter 3) indicated an ontogenetic southerly migration during juvenile growth with no clear accompanying shift in carbon source. It also suggested that pupping and adult foraging grounds are ultimately supported by different carbon sources. Porbeagles, by contrast, were suggested to undertake a spatial movement towards more negative $\delta^{13}C_{CO2(aq)}$ values with no clear change in carbon source during the first 5-6 years of life; then, they appeared to undergo periodic shifts in carbon source associated with spatial movements and/or changes in diet, with late juvenile and subadult life stages showing an expanded geographic range and resource use. However, the application of a fingerprinting approach to estimate the relative contributions of different carbon

sources to shark food webs revealed inconsistences between shark and end-member carbon isotopic compositions, and the underlying mechanisms of these inconsistencies remain unresolved.

Chapter 5: Conclusions

The aim of this project was to determine whether the ontogenetic movements of two model species of pelagic sharks, the blue and the porbeagle sharks, could be reconstructed retrospectively using stable carbon (and nitrogen) isotopes. To answer this question, this thesis had three main objectives:

1) The development of a process-based, mechanistic carbon isotope model predicting the likely spatio-temporal variability of carbon isotopic compositions of phytoplankton across the global ocean (Chapter 2). Particularly, I hypothesised that: ***H_1 – major spatial (and temporal) patterns in the carbon isotopic composition of phytoplankton can be recovered by a relatively simple function containing the principal controls of carbon isotopic fractionation during photosynthesis***.
2) The recovery of individual-level life-history records of carbon and nitrogen isotopic compositions of bulk cartilage collagen from vertebrae of blue and porbeagle sharks (Chapter 3). I hypothesised that: ***H_2 – common, broad ontogenetic patterns in isotopic compositions can be identified across individuals of the same species, indicating species-level life-history isotopic traits***.
3) The recovery of comparable records of carbon isotopic compositions of individual amino acids in vertebrae from the same individual sharks (Chapter 4). I hypothesised that: ***H_3 – life-history isotopic traits for essential amino acids can be used to disentangle baseline from trophic effects on traits for bulk collagen, and thus can provide conclusive evidence for movement traits***.

Records of carbon and nitrogen isotopic compositions of bulk cartilage collagen from vertebrae of individual blue and porbeagle sharks provided information on the movements and diet throughout the entire life of individuals, potentially complementing tag-derived movement information at fine spatio-temporal scales over relatively short periods of time. Interpretations of life-history isotopic traits for bulk collagen to infer movements are limited by large uncertainties in the spatio-temporal distributions of isotopic baselines, and by confounding influences from diet and trophic level change. To address these limitations, in this study I developed a process-based, mechanistic carbon isotope model to predict the likely spatio-temporal variability in isotopic baselines across the global ocean, and compared life-history isotopic traits for bulk collagen against traits for essential amino acids to tease apart influences from movements across isotopic gradients and trophic shifts.

5.1 Modelled global ocean carbon isoscapes

In Chapter 2, I developed an isotopic extension to an existing ocean biogeochemical model, NEMO-MEDUSA, to predict the likely spatio-temporal distributions of the carbon isotopic composition of phytoplankton ($\delta^{13}C_{PLK}$) at the base of pelagic food webs across the global ocean. I demonstrated that a relatively simple transfer function containing the principal controls of carbon isotopic fractionation during photosynthesis (i.e. sea surface temperature, concentration and isotopic compositions of aqueous CO_2, and phytoplankton growth rate and cell size) reproduces major spatial patterns in $\delta^{13}C_{PLK}$ values at regional to ocean-basin scales, as recovered by existing measurements and more complex models (**H_1**; see Chapter 1). Whilst the explicit validation of temporal patterns in $\delta^{13}C_{PLK}$ values is currently not possible (due to the lack of spatio-temporally explicit measurements of isotopic baselines in open-ocean settings), I argue that, if the model reproduces spatial variations in $\delta^{13}C_{PLK}$ values, it should also reproduce temporal ranges (**H_1**).

This carbon isotope model was used to construct spatio-temporally explicit isoscapes for the global ocean (Fig. 2.1 and 2.2), providing a potential solution for the development of reference isoscapes in highly dynamic and poorly sampled open-ocean systems. Modelled global ocean carbon isoscapes provide a means for isotope ecologists to investigate the likely influences from spatio-temporal variability in isotopic baselines on tissue isotopic compositions. For instance, temporal variability in $\delta^{13}C_{PLK}$ values is likely to have large influences on tissue isotope values in ocean areas characterised by a strong seasonality of phytoplankton communities (i.e. high and temperate latitudes and upwelling regions), and in lower-trophic-level animals (Fig. 2.5).

A clear advantage of the current model over more complicated models explicitly incorporating isotope concentrations into biogeochemical models (e.g. HAMOCC 3.1, PISCES, UVic earth system model) is that isoscapes can be generated offline, without requiring access to the full biogeochemical model, and elevated computing skills and demand. Modelled isoscapes can, therefore, be readily custom-tailored by isotope ecologists for specific areas or species.

As yet, however, modelled isoscapes are limited by a lack of suitable field validation datasets, and by the simplifications and deficiencies implicit in both the biogeochemical and isotopic fractionation models. Accordingly, I suggest that uncertainty in continuous isoscapes is too large to permit the explicit geographic assignment of animals, at least over continuous surfaces. However, modelled isoscapes can be partitioned into isotopically distinct regions (i.e. clusters; Fig. 2.6), or summarised over biogeogeographic provinces (Fig. 2.7). In both cases, spatio-temporal variability can be quantified within discrete units, and incorporated into assignment algorithms. Also, temporally-explicit isoscape models can be coupled with agent-based movement models and physiology models to predict the evolution of tissue isotopic compositions during movements across temporally variable spatial isotopic gradients (see Future work).

5.2 Life-history isotopic traits

5.2.1 Ontogenetic patterns in carbon isotopic compositions of bulk cartilage collagen

The recovery of individual-level life-history carbon and nitrogen isotope records for bulk cartilage collagen ($\delta^{13}C_{bulk}$, $\delta^{15}N_{bulk}$) provided information on the movements and diet of individual sharks throughout life. Common, broad ontogenetic patterns in $\delta^{13}C_{bulk}$ and $\delta^{15}N_{bulk}$ values were identified across individual blue and porbeagle sharks (Fig. 3.6-3.9). In this study, blue and porbeagle sharks were caught across their known geographic ranges in the North Atlantic. Thus, the identification of consistent ontogenetic patterns in $\delta^{13}C_{bulk}$ and $\delta^{15}N_{bulk}$ values implied species-level life-history traits (**H_2**; see Chapter 1). Isotope-derived information on life-history traits potentially provides a valuable complement to tag-derived information on short-term movements. Whilst interpretations of life-history isotopic traits for bulk collagen using modelled isoscapes may provide initial movement hypotheses, these interpretations are ultimately limited by mixed baseline and trophic isotope effects.

In blue sharks, for instance, observed life-history isotopic traits could be explained solely by an increased utilisation of southern waters during juvenile growth, based on predicted isoscapes in the North Atlantic (Fig. 3.12); however, a combination of movement across spatially variable $\delta^{15}N$ values and increase in trophic level could not be excluded. In porbeagles, by contrast, observed life-history isotopic traits required a combination of movement across isotopic gradients and trophic level change.

The identification of consistent (or variable) life-history isotopic traits across individuals, populations or species, reflecting common (or variable) ontogenetic movements and/or trophic shifts, has important implications for the management and conservation of pelagic sharks. The presence of consistent traits across individual blue and porbeagle sharks, for instance, implied general behaviours influencing shark-human interactions across life-history, and thus shared vulnerability to fishery capture.

Life-history isotopic traits can, therefore, be considered conceptually similar to isotopic niche areas: they also allow identifying commonalities and differences in movement and/or feeding behaviour among individuals, populations, species, higher taxa and/or functional groups, and provide additional information on ontogenetic patterns.

5.2.2 Patterns in carbon isotopic compositions of essential amino acids

This study provided the first individual-level life-history records of carbon isotopic compositions of essential amino acids ($\delta^{13}C_{EAA}$) for top predators. Given that variation in $\delta^{13}C_{EAA}$ values is directly related to movement across isotopic gradients, the recovery of consistent ontogenetic patterns in $\delta^{13}C_{EAA}$ values across individual blue and porbeagle sharks (Fig. 4.7) conclusively

demonstrated species-level movement traits (**H_3**; see Chapter 1). In blue sharks, observed life-history traits in $\delta^{13}C_{EAA}$ values proved the initial hypothesis of an increase in the utilisation of foraging grounds with more positive $\delta^{13}C$ baselines during juvenile growth. Juvenile porbeagles, by contrast, increasingly utilise grounds with more negative $\delta^{13}C$ baselines, whilst also shifting trophic level (see Chapter 3).

Additionally, differences in $\delta^{13}C_{EAA}$ values between maternal components of vertebrae and immediate *post-partum* independent feeding (Fig. 4.7) provided information on transgenerational movements. Blue shark pupping occurs in isotopically distinct grounds from the principal foraging grounds exploited by mothers and adult sharks, with the possibility of a return migration of adult sharks to maternal grounds. Pregnant female porbeagles, by contrast, migrate towards isotopically distinct foraging grounds from the those exploited by subadult females to give birth; immediate *post-partum* independent feeding, however, results in an increasing utilisation of more negative in $\delta^{13}C$ baselines.

These inferred movements across isotopic gradients may reflect spatial variations in the carbon isotopic composition of aqueous CO_2 ($\delta^{13}C_{CO2(aq)}$), or changes in the composition of the primary producing community, or both. The recovery of ontogenetic variance in sample-normalised carbon isotope values of essential amino acids (i.e. effectively reflecting variance in end-member values, after spatial variability in $\delta^{13}C_{CO2(aq)}$ has been removed; $\delta^{13}C_{nEAA}$; Fig. 4.8) suggested ontogenetic habitat shifts, possibly associated with spatial movement or trophic shifts. As yet, however, inferences on changes in the relative contributions of different carbon sources to shark food webs were highly inconclusive, given inconsistencies between shark $\delta^{13}C_{nEAA}$ patterns and available end-member carbon isotope fingerprints (Fig. 4.11 and 4.12).

In conclusion, the broad ontogenetic movements across isotopic gradients of North Atlantic blue and porbeagle sharks could be reconstructed using a combination of modelled carbon isoscapes, bulk and compound-specific isotope analysis of essential amino acids. The identification of consistent ontogenetic patterns in carbon and nitrogen isotopic compositions across individuals captured at disparate locations implied species-level life-history isotopic traits, reflecting ontogenetic movements and/or trophic shifts. The interpretation of life-history isotopic traits for bulk collagen using modelled isoscapes provided initial movement hypotheses, but was ultimately limited by mixed baseline and trophic isotope effects, as well as uncertainties in modelled isoscapes. The recovery of species-level life-history isotopic traits for essential amino acids, which are directly related to movements, conclusively demonstrated movement traits. Movements across isotopic gradients may represent spatial movements and/or habitat shifts, but changes in the relative contributions of different carbon sources could not be conclusively inferred based on available carbon isotope fingerprints.

Stable isotope analysis of specific compounds (i.e. amino acids) within tissues costs approximately 10 times more than traditional bulk tissue analysis (i.e. ~ 100 *versus* 10 $ for a single

sample). Additionally, the procedures for sample preparation are extremely time-consuming, the precision of analysis is lower and the required sample size larger, resulting in decreased temporal resolution of ecological information. In this study, compound-specific isotope analysis conclusively validated interpretations of movements based on bulk tissue isotope data, and, in porbeagles, revealed the direction of movements. Compound-specific analysis also provided insights on whether baseline effects reflect spatial movements and/or habitat shifts, but failed to quantify changes in the relative contributions of different end-members to shark food webs. Additionally, interpretations of $\delta^{13}C_{nonEAA}$ patterns were only prelimnary and uncertain, as a coherent physiological framework to interpret carbon isotope data for amino acids that are wholly or partially synthesised *de novo* is currently lacking (Chapter 4).

5.3 Future work

Temporal variability plays a key role in defining the isotopic compositions of animal tissues. In pelagic settings, the spatial distributions of isotopic baselines may vary greatly over time. Animal migrations also occur throughout time, and the incorporation of baseline isotopic signatures into animal tissues ultimately depends on tissue elemental turnover rates. Future work should explore how isotope dynamics at the base of the food web, animal behaviour and physiology interact to produce measured tissue isotopic compositions. The likely influences of these traits on tissue isotope values could be investigated, for instance, using a theoretical modelling approach coupling temporally explicit isoscape models, agent-based models of animal movement, and physiological biogeochemical models. Isotope models could also be used to construct hind and forecast predictive isoscapes, which could be linked to historical or archeological samples.

Confidence in isoscape-based geographic assignments could be greatly improved by combining predictions from a range of biogeochemical-isotope models, and by modelling multiple isotope systems.

Whilst this study identified consistent life-history isotopic traits across individual blue and porbeagle sharks from disparate areas in the North Atlantic, the sample size was relatively small (i.e. nine blue sharks and six porbeagles). Future studies should, therefore, recover individual-level life-history isotopic traits for additional individuals to conclusively demonstrate species- and/or population-level movement patterns. Given the high cost of compound-specific isotope analysis, however, I suggest that future studies should identify break-points in time-series of isotopes in bulk tissues, and analyse just break-points for isotopes in essential amino acids to discriminate movements from trophic shifts. A cost- and time-effective combination of bulk and compound-specific isotope analysis could be applied restrospectively to identify focal areas and habitats, as well as general migratory behaviour, for IUCN-listed threatened species, hence inform their management and

conservation. In a more forensic context, it could be applied to characterised and determine the origin species that are illegally caught and sold at markets. It could also

The causes of inconsistencies between essential amino acid carbon isotope patterns in sharks and available carbon isotopic fingerprints for end-members should also be further investigated. Additional end-members that may be relevant to the ecology of pelagic sharks should be fingerprinted, along with other consumers with known and distinct movement and feeding behaviours (i.e. benthic, pelagic, mesopelagic fish).

Finally, additional controlled feeding experiments are required to better constrain the trophic influences on $\delta^{13}C_{nonEAA}$ patterns, and thus to provide a more coherent physiological framework to interpret $\delta^{13}C_{nonEAA}$ data to provide information on resource utilisation, diet and trophic level, or carbon source.

Appendices

Appendix 2.A – Methods

2.A.1 $\delta^{13}C_{CO2(aq)}$ parameterization

We estimated the carbon isotope composition of dissolved CO_2 ($\delta^{13}C_{CO2(aq)}$) as the sum of the carbon isotope composition of dissolved inorganic carbon ($\delta^{13}C_{DIC}$) and the carbon isotope fractionation between $CO_{2(aq)}$ and DIC ($\varepsilon[CO_{2(aq)}–DIC]$).

2.A.1.1 Carbon isotope fractionation within the DIC pool

Carbon isotopic equilibrium in seawater is established on time scales of a few minutes (Zhang *et al.*, 1995; Zeebe *et al.*, 1999, Hofmann *et al.*, 2000; Zeebe & Wolf-Gladrow, 2001). The isotopic fractionation between the carbon components (e.g. $CO_{2(aq)}$) within the DIC pool can, therefore, be considered as an equilibrium fractionation (Hofmann *et al.*, 2000; Zeebe & Wolf-Gladrow, 2001). As a consequence, we parameterized $\varepsilon[CO_{2(aq)}–DIC]$ as the sum of the equilibrium fractionation between $CO_{2(gas)}$ and DIC and the equilibrium fractionation between $CO_{2(gas)}$ and $CO_{2(aq)}$ (Eq. A.1; for a detailed description, see Hofmann *et al.*, 2000):

$$\varepsilon\{CO_{2(aq)} - DIC\} = -\left(0.0144\frac{[CO_3{}^{2-}]}{[DIC]} - 0.1119\right)SST\ (°C) - 11.84 \qquad (A.1)$$

2.A.1.2 Carbon isotope fractionation during air-sea CO_2 exchange, and constant $\delta^{13}C_{DIC}$

While $\delta^{13}C_{DIC}$ values are additionally influenced by the kinetic fractionation occurring during air-sea CO_2 exchange and the biological fractionation occurring during photosynthesis (ε_p; i.e. phytoplankton preferentially takes up ^{12}C, leading to ^{13}C-enriched organic matter; Hofmann *et al.*, 2000; Tagliabue & Bopp, 2008), a full consideration of these fractionation effects on $\delta^{13}C_{DIC}$ would require explicit modeling of [^{12}C] and [^{13}C] through the entire biogeochemical model (e.g. Hofmann *et al.*, 2000; Tagliabue & Bopp, 2008; Schmittner *et al.*, 2013; Schmittner & Somes, 2016). In order to limit model complexity and computational demand, here we ignored the potential effects of kinetic fractionation occurring during air-sea CO_2 exchange and phytoplankton drawdown of [^{12}C], assumed $\delta^{13}C_{DIC}$ as constant (2‰), and thus calculated $\delta^{13}C_{CO2(aq)}$ as 2‰ + $\varepsilon[CO_{2(aq)}–DIC]$. Variations in $\delta^{13}C_{DIC}$ values can be considered as a minor source of variability in $\delta^{13}C_{PLK}$ values; in fact, the global distribution of $\delta^{13}C_{DIC}$ is relatively homogeneous, with values varying around 2‰ (Rau *et al.*, 1982; 1989; Hofmann *et al.*, 2000; Tagliabue & Bopp, 2008; McMahon *et al.*, 2013; Schmittner *et al.*, 2013). While this simplification may result in falsely lower predicted $\delta^{13}C_{PLK}$ values in areas characterized by

high productivity, we argue that, for the purpose of estimating regional- to global-scale variations in $\delta^{13}C_{PLK}$ values, using a simple function (see Methods), assuming a constant $\delta^{13}C_{DIC}$ value is reasonable.

Appendix 2.B – Results

2.B.1 Spatial patterns in $\delta^{13}C_{CO2(aq)}$ values

Predicted annual average $\delta^{13}C_{CO2(aq)}$ values range between -7.5 and -10.5‰ across the global ocean. On ocean basin- to global-scales, average $\delta^{13}C_{CO2(aq)}$ values vary across broad latitudinal gradients, decreasing from the equator (~ 7.5‰) towards both poles (-9 to -10.5‰) as a function of latitude and temperature (Fig. 2.B1). To date, most studies (e.g. Hofmann *et al.*, 2000; Tagliabue & Bopp, 2008; McMahon *et al.*, 2013; Schmittner *et al.*, 2013; Schmittner & Somes, 2016) have represented inorganic isoscapes as distributions of $\delta^{13}C_{DIC}$ values (and not as distributions of $\delta^{13}C_{CO2(aq)}$ values). Predictions of $\delta^{13}C_{CO2(aq)}$ from our model cannot, therefore, be directly compared against $\delta^{13}C_{DIC}$ measurements (McMahon *et al.*, 2013) or $\delta^{13}C_{DIC}$ predictions from other models (Hofmann *et al.*, 2000; Tagliabue & Bopp, 2008; Schmittner *et al.*, 2013; Schmittner & Somes, 2016). The variables from which $\delta^{13}C_{CO2(aq)}$ values are derived ($\delta^{13}C_{DIC}$ and $\varepsilon[CO_{2(aq)}–DIC]$) can, however, be examined. In our model, the value of $\delta^{13}C_{DIC}$ is assumed to be constant (2‰; see Appendix 2.A); when predicting $\delta^{13}C_{CO2(aq)}$, $\varepsilon[CO_{2(aq)}–DIC]$ is, therefore, the only source of variability. This fractionation is strongly temperature-dependent (Eq. A.1), as the ratio of $[CO_3^{2-}]$ to [DIC] is relatively invariant in seawater (Zhang *et al.*, 1995; Hofmann *et al.*, 2000; Zeebe & Wolf-Gladrow, 2001). Thus, the predicted latitudinal gradients in annual average $\delta^{13}C_{CO2(aq)}$ values (Fig. 2.B1) can be explained by latitudinal variations in sea surface temperature (Zhang *et al.*, 1995; Hofmann *et al.*, 2000). Predicted seasonal variations in $\delta^{13}C_{CO2(aq)}$ values are relatively small (~ 0-1‰), and can also be explained by seasonal temperature changes.

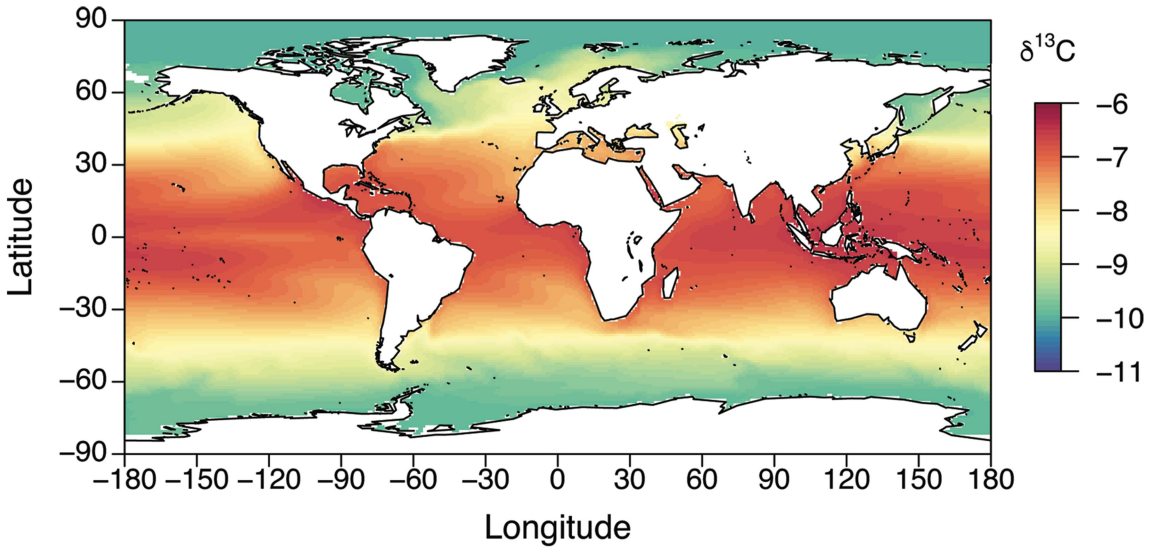

Figure 2.B1 Modeled annually averaged surface water distribution of the carbon isotope composition of dissolved CO_2 ($\delta^{13}C_{CO2(aq)}$, ‰).
Annual average $\delta^{13}C_{CO2(aq)}$ values are calculated using a monthly climatology for the period 2001-2010.

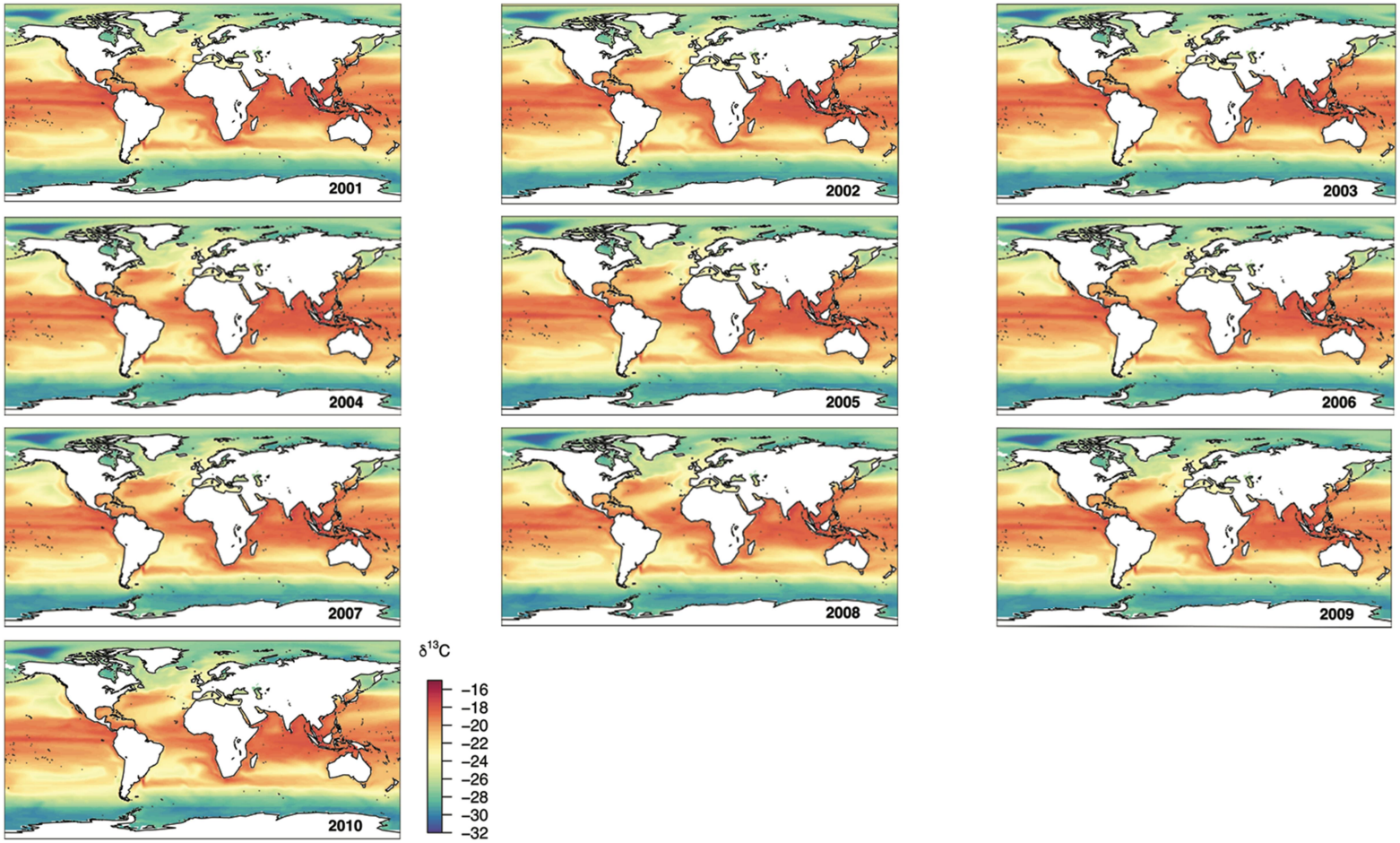

Figure 2.B2 Modeled annually averaged surface water distribution of the carbon isotopic composition of phytoplankton ($\delta^{13}C_{PLK}$, ‰) over individual model years for the period 2001-2010.
Annual average values are calculated as the mean of monthly $\delta^{13}C_{PLK}$ values over each model year.

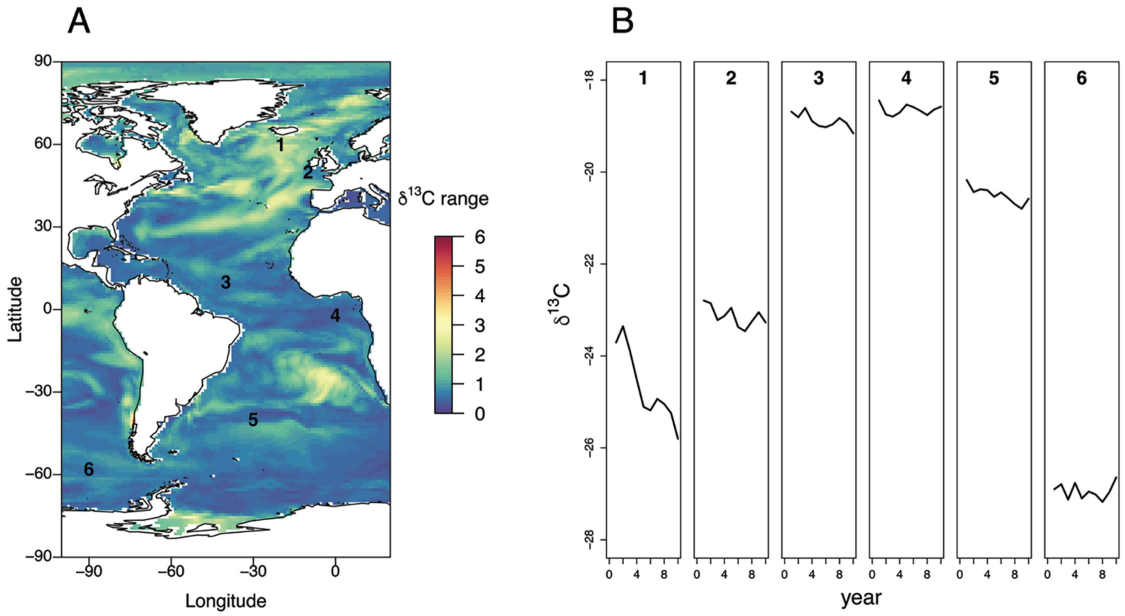

Figure 2.B3 Modeled temporal inter-annual variability in $\delta^{13}C_{PLK}$ values (‰).
A) Inter-annual range in $\delta^{13}C_{PLK}$ values across the Atlantic Ocean; inter-annual range in $\delta^{13}C_{PLK}$ is calculated as the range of annual average $\delta^{13}C_{PLK}$ values over individual model years for the period 2001-2010. B) Time-series of annual average $\delta^{13}C_{PLK}$ values at six locations along a latitudinal gradient, as indicated by numbers in panel A).

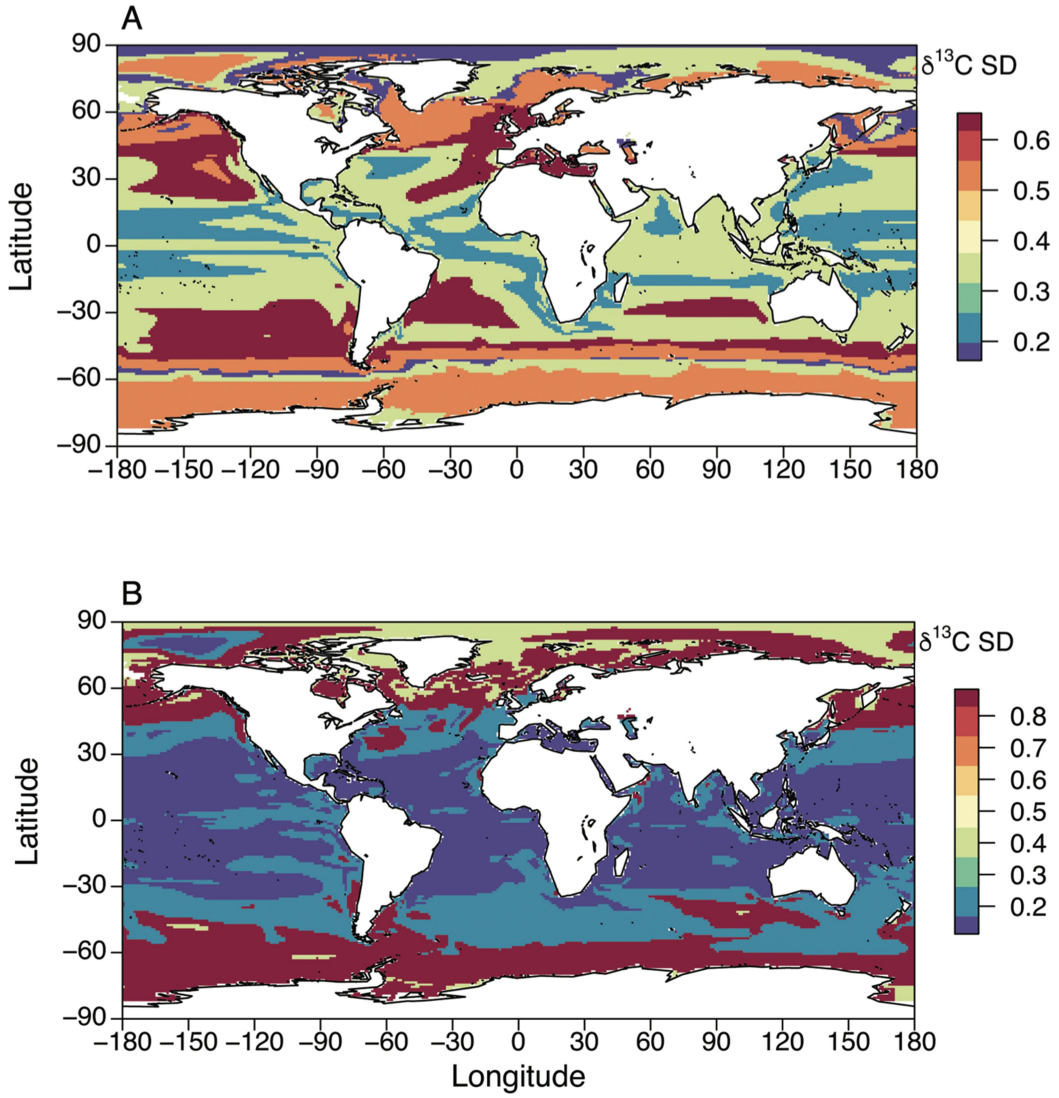

Figure 2.B4 Standard deviations for A) annual average $\delta^{13}C_{PLK}$ grid cell values, and B) intra-annual range in $\delta^{13}C_{PLK}$ grid cell values within each cluster.
Both annual average and intra-annual range in $\delta^{13}C_{PLK}$ values are calculated using a monthly climatology for the period 2001-2010.

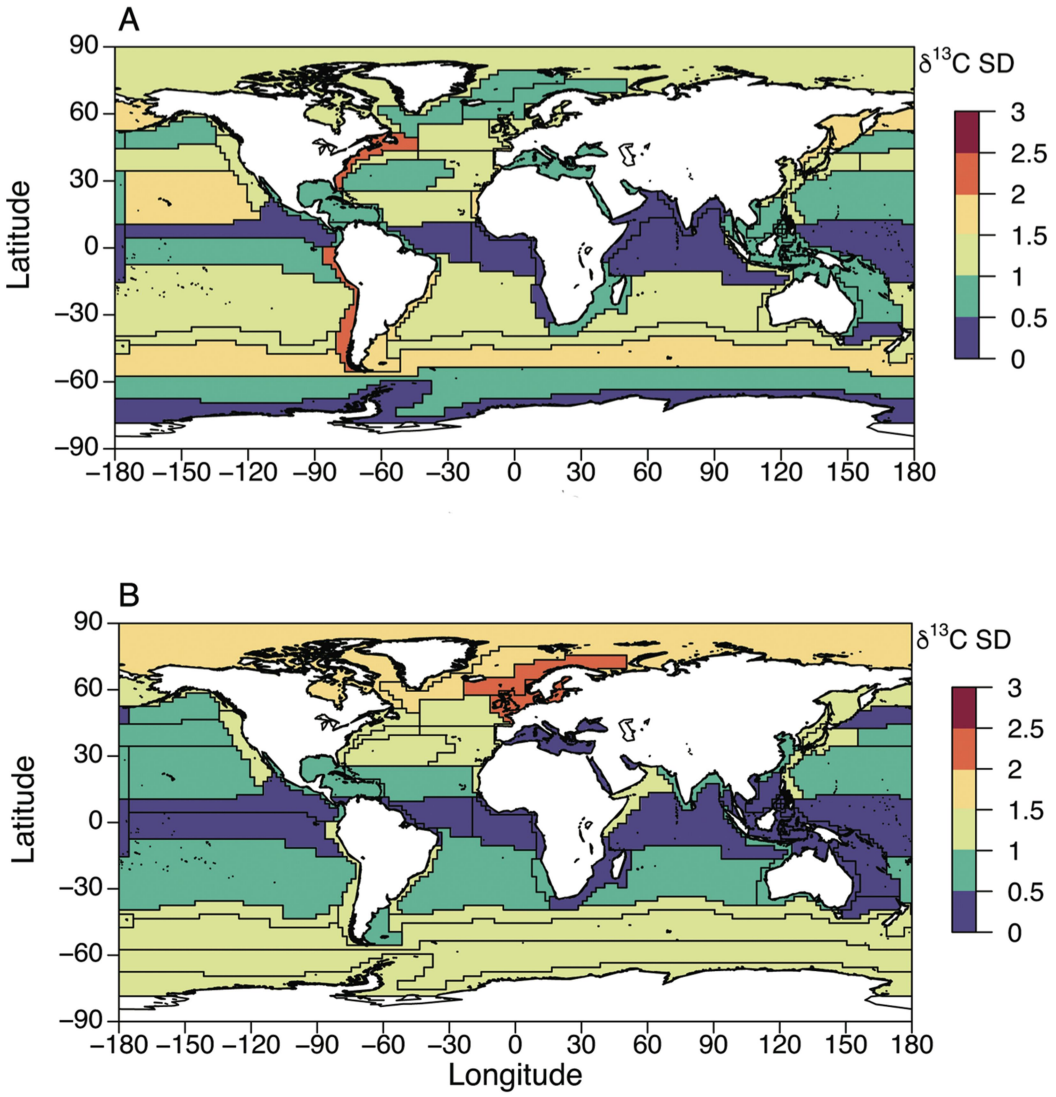

Figure 2.B5 Standard deviations of A) annual average and B) intra-annual range in $\delta^{13}C_{PLK}$ grid cell values within each province.
Both annual average and intra-annual range in $\delta^{13}C_{PLK}$ values are calculated using a monthly climatology for the period 2001-2010.

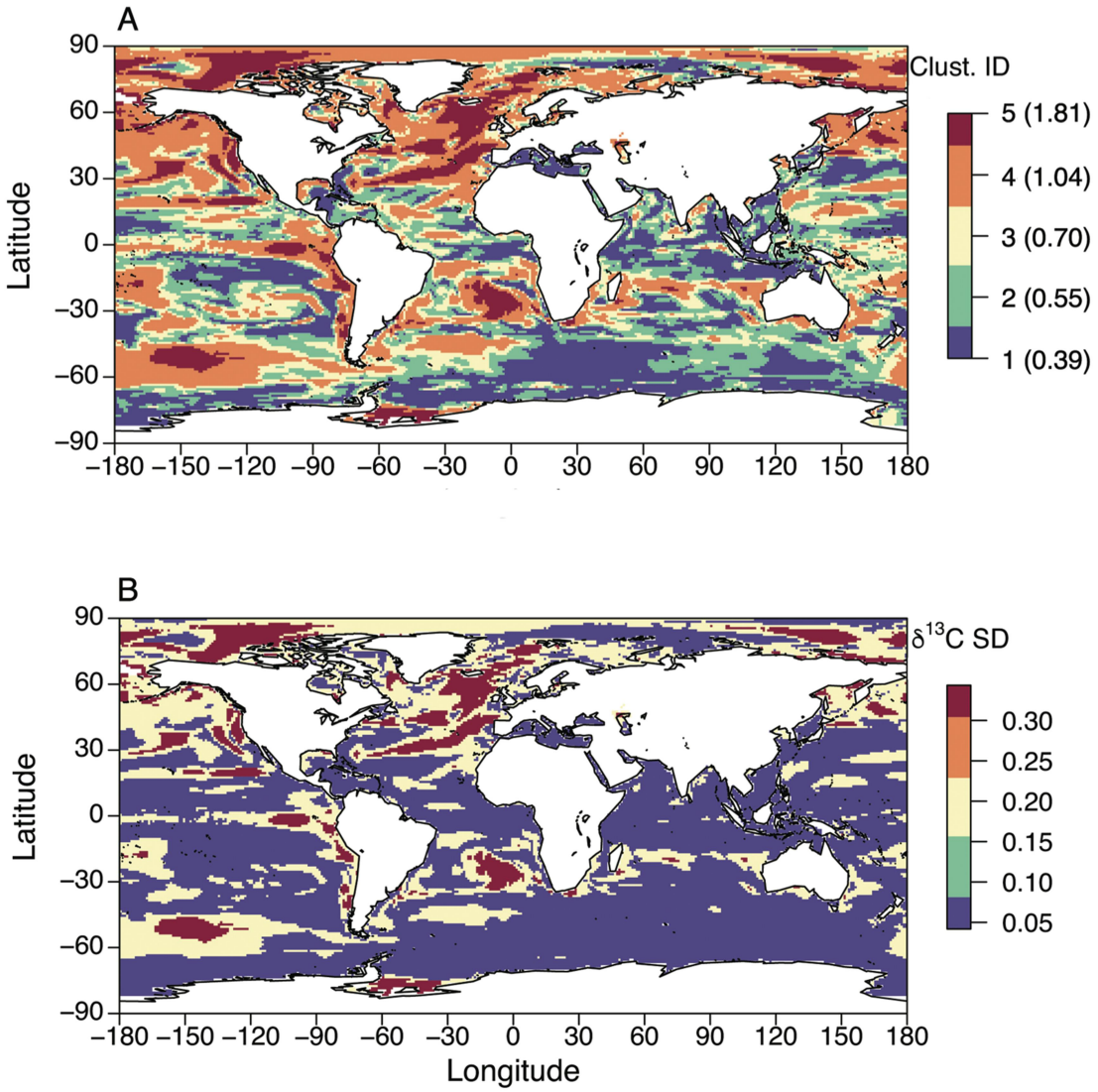

Figure 2.B6 A) Cluster ID for five clusters of similar inter-annual range in $\delta^{13}C_{PLK}$ grid cell values; numbers in brackets are means for inter-annual range in $\delta^{13}C_{PLK}$ values within each cluster. B) Standard deviation for inter-annual range in $\delta^{13}C_{PLK}$ grid cell values within each cluster. Inter-annual range in $\delta^{13}C_{PLK}$ is calculated as the range of annual average $\delta^{13}C_{PLK}$ values over individual model years for the period 2001-2010.

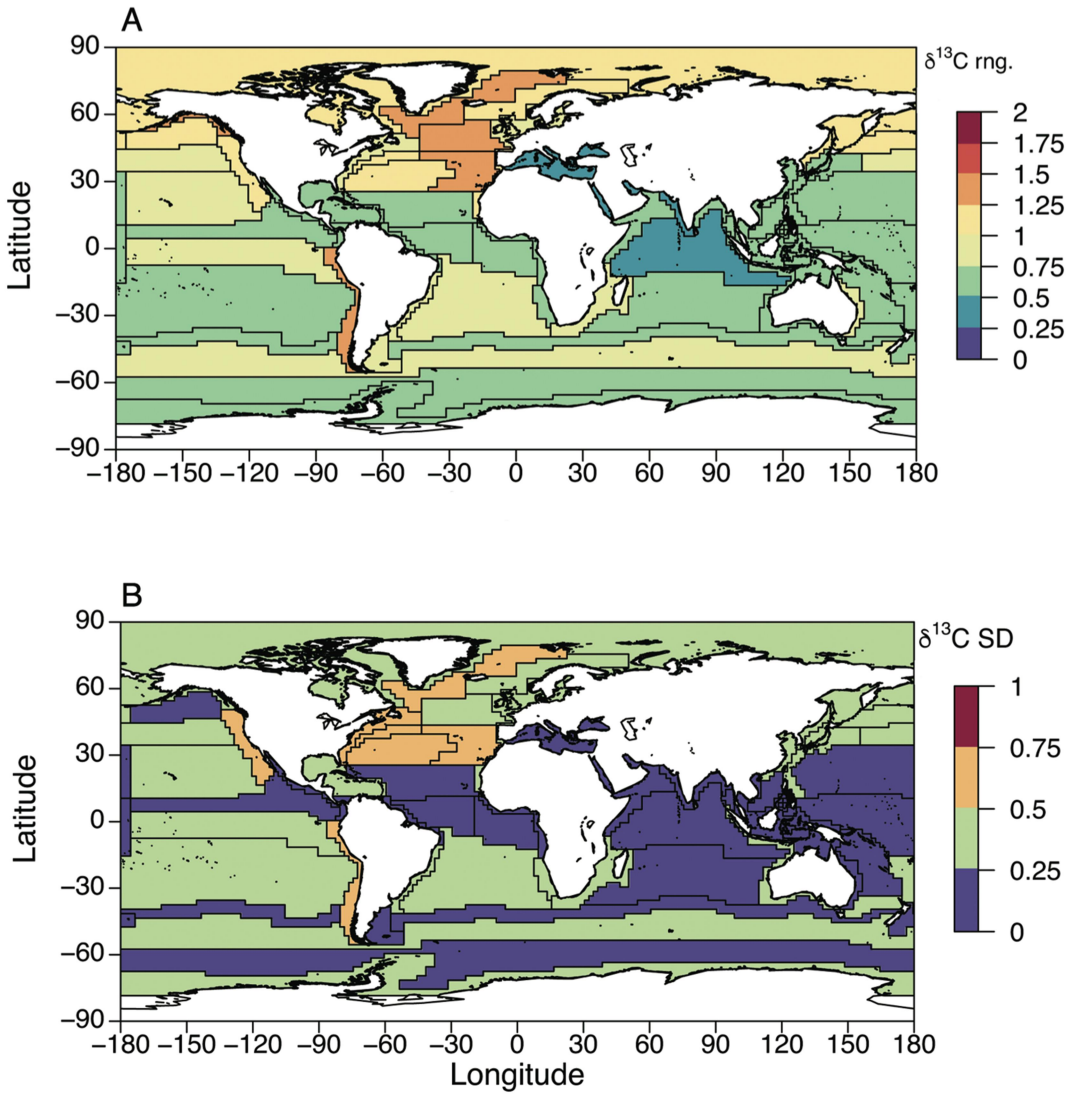

Figure 2.B7 A) Mean and B) standard deviation of inter-annual range in $\delta^{13}C_{PLK}$ grid cell values within each province.
Inter-annual range in $\delta^{13}C_{PLK}$ is calculated as the range of annual average $\delta^{13}C_{PLK}$ values over individual model years for the period 2001-2010.

Appendix 2.C – Polar projection isoscapes

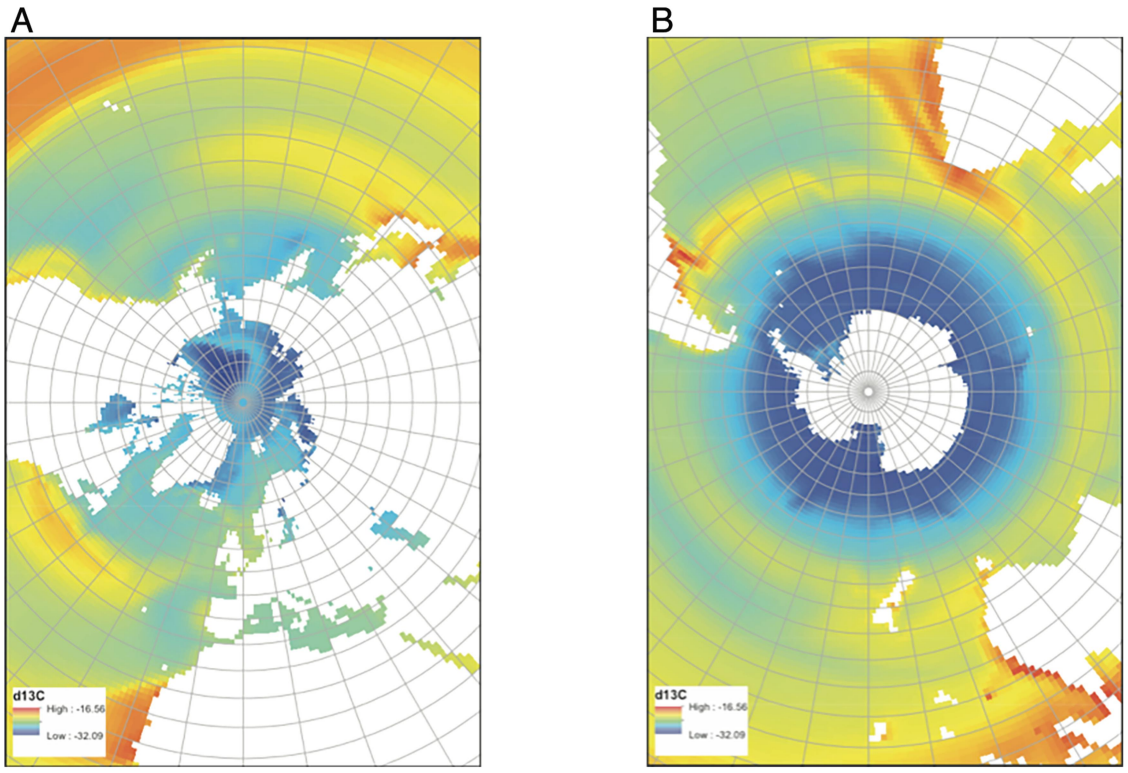

Figure 2.C1 Polar projection of continuous-surface isoscapes of annual average carbon isotopic composition of phytoplankton ($\delta^{13}C_{PLK}$ values, ‰) for A) North, and B) South polar regions. Annual average $\delta^{13}C_{PLK}$ values are calculated using a monthly climatology for the period 2001-2010.

Appendix 2.D Reference list for zooplankton data sources

1 Hobson K.A., W.G. Ambrose Jr., and P.E. Renaud. 1995. Sources of primary production, benthic-pelagic coupling, and trophic relationships within the Northeast Water Polynya: insights from $\delta^{13}C$ and $\delta^{15}N$ analysis. Marine Ecology Progress Series **128**:1-10.

2 McMahon, K.W., L.L. Hamady, and S.R. Thorrold. 2013. A review of ecogeochemistry approaches to estimating movements of marine animals. Limnology and Oceanography **58**:697-714.

3 Pomerleau, C., R.J. Nelson, B.P.V. Hunt, A.R. Sastri, and W.J. Williams. 2014. Spatial patterns in zooplankton communities and stable isotope ratios ($\delta^{13}C$ and $\delta^{15}N$) in relation to oceanographic conditions in the sub-Arctic Pacific and western Arctic regions during the summer of 2008. Journal of Plankton Research **36**:757-775.

4 Sandel, V., R. Kiko, P. Brandt, M. Dengler, L. Stemmann, P. Vandromme, U. Sommer, and H. Hauss. 2016. Nitrogen fuelling of the pelagic food web of the tropical Atlantic. Plos One **10**:e0131258.

5 Hop H., S. Falk-Petersen, H. Svendsen, S. Kwasniewski, V. Pavlov, O. Pavlova, and J.E. Søride. 2006. Physical and biological characteristics of the pelagic system across Fram Strait to Kongsfjorden. Progress in Oceanography **71**:182-321.

6 Søreide, J.E., H. Hop, M.L. Carroll, S. Falk-Petersen, and E.N. Hegseth. 2006. Seasonal food web structures and sympagic-pelagic coupling in the European Arctic revealed by stable isotopes and a two-source mixing model. Progress in Oceanography **71**:59-87.

7 Bode, M., W. Hagen, A. Schukat, L. Teuber, D. Fonseca-Batista, F. Dehairs, and H. Auel. 2015. Feeding strategies of tropical and sub-tropical calanoid copepods throughout the eastern Atlantic Ocean – Latitudinal and bathymetric aspects. Progress in Oceanography **138**:268-282.

8 Chouvelon, T., A. Chappuis, P. Bustamente, S. Lefebvre, F. Mornet, G. Guillou, L. Violamer, and C. Dupuy. 2014. Trophic ecology of European sardine *Sardina pilchardus* and European anchovy *Engraulis encrasicolus* in the Bay of Biscay (north-east Atlantic) inferred from $\delta^{13}C$ and $\delta^{15}N$ values of fish and identified mesozooplanktonic organisms. Journal of Sea Research **85**:277-291.

9 Kopp, D., S. Lefebvre, M. Cachera, M.C. Villanova, and B. Ernande. 2015. Reorganization of a marine trophic network along an inshore-offshore gradient due to stronger pelagic-benthic coupling in coastal areas. Progress in Oceanography **130**:157-171.

10 Kürten B., I. Frutos, U. Struck, S.J. Painting, N.V.C. Polunin, and J.J. Middleburg. 2013. Trophodynamics and functional feeding groups of North Sea fauna: a combined stable isotope and fatty acid approach. Biogeochemistry **113**:189-212.

11 Bode A., P. Carrera, and S. Lens. 2003. The pelagic foodweb in the upwelling ecosystem of Galicia (NW Spain) during spring: natural abundance of stable carbon and nitrogen isotopes. ICES Journal of Marine Science **60**:11-22.

12 Costalgo, D., J. Navarro, I. Álvarez-Calleja, and I. Palomera. 2012. Ontogenetic and seasonal changes in the feeding habits and trophic levels of two small pelagic fish species. Marine Ecology Progress Series **460**:169-181.

13 Valls, M., C.J. Sweeting, M.P. Olivar, M.L. Fernandez de Puelles, C. Pasqual, N.V.C Polunin, and A. Quetglas. 2014. Structure and dynamics of food webs in the water column on shelf and slope grounds of the western Mediterranean. Journal of Marine Systems **138**:171-181.

14 Hirch S., and B. Christiansen 2010. The trophic blockage hypothesis is not supported by the diets of fishes on Seine Seamount. Marine Ecology **31**:107-120.

15 Feunteun, E., M.J. Miller, A. Carpentier, J. Aoyama, C. Dupuy, M. Kuroki, M. Pagano, E. Réveillac, D. Sellos, S. Watanabe, K. Tskamoto, and T. Otake. 2015. Stable isotopic composition of anguilliform leptocephali and other food web components from west of the Mascarene Plateau. Progress in Oceanography **137**:69-83.

16 Waite A.M., B.A. Muhling, C.M. Holl, L.E. Beckley, J.P. Montoya, J. Strzelecki, P.A. Thompson, and S. Pesant. 2007. Food web structure in two counter-rotating eddies based on $\delta^{13}C$ and $\delta^{15}N$ isotopic analyses. Deep-Sea Research II **54**: 1055-1075.

17 Dupuy, C., M. Pagano, P Got, I. Domaizon, A. Chappuis, G. Marchessaux, and M. Bouvy. 2016. Trophic relationships between metazooplankton communities and their plankton food sources in the Iles Eparses (Western Indian Ocean). Marine Environmental Research **116**:18-31.

18 Fontugne M., and J.C. Duplessy. 1981. Organic carbon isotopic fractionation by marine plankton in the temperature range -1 to 31 °C. Oceanologica Acta **4**: 85-90.

19 Prebble, C. Unpublished data, University of Southampton, United Kingdom.

20 Al-Reasi, H.A. F.A. Ababneh, and D.R Lean. 2007. Evaluating mercury biomagnification in fish from a tropical marine environment using stable isotopes ($\delta^{13}C$ and $\delta^{15}N$). Environmental Toxicology and Chemistry **26**:1572-1581.

21 Kürten B., A.M. Al-Aidroos, S. Kürten, M. M. El-Sherbiny, R.P. Devassy, U. Struck, N. Zarokanellos, B.H. Jones, T. Hansen, G. Bruss, and U. Sommer. 2016. Carbon and nitrogen stable isotope ratios of pelagic zooplankton elucidate ecohydrographic features in the oligotrophic Red Sea. Progress in Oceanography **140**:69-90.

22 Al-Habsi S.H., C. J. Sweeting, N.V.C. Polunin, and N.A.J. Greening. 2008. $\delta^{13}C$ and $\delta^{15}N$ elucidation of size-structured food webs in a Western Arabian Sea demersal trawl assemblage. Marine Ecology Progress Series **353**:55-63

23 Saupe, S.M., D.M. Schell, and W.B. Griffths. 1989. Carbon-isotope ratio gradients in western arctic zooplankton. Marine Biology **103**:427-432.

24 Shell, D.M., B.A. Barnett, and K.A. Vinette. 1998. Carbon and nitrogen isotope ratios in zooplankton of the Bering, Chukchi and Beaufort seas. Marine Ecology Progress Series **162**:11-23.

25 Sackett, W.M., W.R. Eckelmann, M.L. Bender, and A.W.H. Be. 1965. Temperature dependence of carbon isotope composition in marine plankton and sediments. Science **148**:235-237.

26. Aita, M.N., K. Tadokoro, N.O. Ogawa, F. Hyodo, R. Ishii, S.L. Smith, T. Saino, M.J. Kishi, S-I Saitoh, and E. Wada. 2011. Linear relationship between carbon and nitrogen isotope ratios along simple food chains in marine environments. Journal of Plankton Research **33**:1629-1642.

27 Chow A., S. Chow, H. Kurogi, S. Katayama, D. Ambe, M. Okazaki, T. Watanabe, T. Ichikawa, M. Kodama, J. Aoyama, A. Shinoda, S. Watanabe, K. Tsukamoto, S. Miyazaki, S. Kimura, Y. Yamada, K. Nomura, H. Tanaka, Y. Kazeto, K. Hata, T. Handa, A. Tawa, and N. Mochioka. 2010. Japanese eel Anguilla japonica do not assimilate nutrition during the oceanic spawning migration: evidence from stable isotope analysis. Marine Ecology Progress Series **402**:233-238.

28 Im D.H., J.H. Wi, and H-L. Suh. 2015. Evidence for ontogenetic feeding strategies in four calanoid copepods in eth East Sea (Japan Sea) in summer, revealed by stable isotope analysis. Ocean Science Journal **50**:481-490.

29 Suzuki, K.W., A. Kasai, T. Isoda, K. Nakamara, and M. Tanaka. 2008. Distinctive stable isotope ratios in important zooplankton species in relation to estuarine salinity gradients: Potential tracer of fish migration. Estuarine, Coastal and Shelf Science **78**:541-550.

30 Weng J.S., M.A. Lee, K.M. Liu, M.S. Hsu, M.K. Hung, and L.J. Wu 2015. Feeding ecology of juvenile yellowfin tuna from waters southwest of Taiwan inferred from stomach contents and stable isotope analysis. Marine and Coastal Fisheries **7**:537-548.

31 Hertz, E., M. Trudel, R.D. Brodeur, E.A. Daley, L. Eisner, E.V. Farley Jr., J.A. Harding, R.B. MacFarlane, S. Mazumder, J.H. Moss, J. M. Murphy, and A. Mazumder. 2015. Continental-scale variability in the feeding ecology of juvenile Chinook salmon along the coastal Northeast Pacific Ocean. Marine Ecology Progress Series **537**:247-263.

32 Eberl, R., and E.J. Carpenter 2007. Association of the copepod *Macrosetella gracillis* with the cyanobacterium *Trichodesmium* spp. in the North Pacific Gyre. Marine Ecology Progress Series **333**:205-212.

33 Max, L.M., S.L. Hamilton, S.D Gaines, and R.R. Warner. 2013. Benthic processes and overlying fish assemblages drive the composition of benthic detritus on a central Pacific coral reef. Marine Ecology Progress Series **482**:281-295.

34 Olson R.J., B.N. Popp, B.S. Graham, G.A. Lopez-Ibarra, F. Galvan-Magana, C.E. Lennert-Cody, N. Bocanegra-Castillo, N.J. Wallsgrove, E. Gier, V. Alatorre-Ramirez, L-T. Balance, and B. Fry. 2010. Food-web inferences of stable isotope spatial patterns in copepods and yellowfin tuna in the pelagic eastern Pacific Ocean. Progress in Oceanography **86**:124-138.

35 Williams, R.L., S. Wakeham, R. McKinney, and K.F. Wishner. 2014. Trophic ecology and vertical patterns of carbon and nitrogen stable isotopes in zooplankton from oxygen minimum zone regions. Deep-Sea Research I **90**:36-47.

36 McCauley D.J., H.S. Young, R.B. Dunbar, J.A. Estes, B.X. Semmens, and F. Micheli. 2012. Assessing the effects of large mobile predators on ecosystem connectivity. Ecological Applications **22**:1711-1717.

37 Loick, N., J. Dippner, H. N. Doan, I. Liskow, and M. Voss. 2007. Pelagic nitrogen dynamics in the Vietnamese upwelling area according to stable nitrogen and carbon isotope data. Deep-Sea Research I **54**:596-607.

38 Whitteveen, B. H., G.A. Worthy, R. Foy, and K. M. Wynne. 2012. Modeling the diet of humpback whales: An approach using stable carbon and nitrogen isotopes in a Bayesian mixing model. Marine Mammal Science **28**:E233-E250.

39 Madigan D.J., Carlisle A.B., H. Dewar, O.E. Snodgrass, S.Y. Litvin, F. Micheli, and B. Block. 2012. Stable isotope analysis challenges wasp-waist food web assumptions in an upwelling pelagic ecosystem. Scientific Reports **2**:654.

40 Miller, T. W., R. D. Brodeur, G. Rau, and K. Omori. 2010. Prey dominance shapes trophic structure of the northern California Current pelagic food web: evidence from stable isotopes and diet analysis. Marine Ecology Progress Series **420**:15-26.

41 Montecinos S., L.R. Castro, and S. Neira. 2016. Stable isotope ($\delta^{13}C$ and $\delta^{15}N$) and trophic position of Patagonian sprat (*Sprattus fuegensis*) from the Northern Chilean Patagonia. Fisheries Research **179**:139-147.

42 Chang, N-N., J-C. Shiao, G-C. Gong, S-J. Kao, and C-H. Hsieh. 2014. Stable isotope ratios reveal food source of benthic fish and crustaceans along a gradient of trophic status in the East China Sea. Continental Shelf Research **84**:23-34.

43 Henschke, N., J.D. Everett, I.M. Suthers, J.A. Smith, B.P.V. Hunt, M.A. Doblin, and M.D. Taylor. 2015. Zooplankton trophic niches respond to different water types of the wastern Tasman Sea: a stable isotope analysis. Deep Sea Research I **104**:1-8.

44 Schlacher, T.A., R.M.Connolly, A.J. Skillington, and T.F. Gaston. 2009. Can export of organic matter from estuaries support zooplankton in nearshore, marine plumes? Aquatic Ecology **43**:383-393.

45 Richoux, N.B., and P.W. Froneman. 2009. Plankton trophodynamics at the subtropical convergance, Southern Ocean. Journal of Plankton Research **31**:1059-1073.

46 Laakmann, S., and H. Auel. 2010. Longitudinal and vertical trends in stable isotope signatures ($\delta^{13}C$ and $\delta^{15}N$) of omnivorous and carnivorous copepods across the South Atlantic Ocean. Marine Biology **157**:463-471.

47 Minks, S.L., C.R. Smith, R.M. Jeffreys, and P.Y.G. Sumida. 2008. Trophic structure on the West Antarctic Peninsula shelf: detritivory and benthic inertia revealed by $\delta^{13}C$ and $\delta^{15}N$ analysis. Deep Sea Research II **55**:2502-2514.

48 Pinkerton M.H., J. Forman, S.J. Bury, J. Brown, P. Horn, and R.L. O'Driscoll. 2013. Diet and trophic niche of Antarctic silverfish *Pleuragramma antarcticum* in the Ross Sea, Antarctica. Journal of Fish Biology **82**:141-164.

49 Choy, C.A., B.N. Popp, C.C.S. Hannides, and J.C Drazen. 2015. Trophic structure and food resources of epipelagic and mesopelagic fishes in the North Pacific. Limnology and Oceanography **60**:1156-1171.

50 Degens, E.T., M. Behrendt, B. Gotthardt, and E. Reppmann. 1968. Metabolic fractionation of carbon isotopes in marine plankton–II. Data on samples collected off the coasts of Peru and Ecuador. Deep-Sea Research 15:11-20.

51 Fontugne M., and J.C. Duplessy. 1978. Carbon isotope ratio of marine plankton related to surface water masses. Earth and Planetary Science Letters 41:365-371.

52 Bury, S. J. Unpublished data, NIWA, New Zealand.

Appendix 2.E – Code for the carbon isotope model

```
# CARBON ISOTOPE MODEL - CLIMATOLOGY 2001-2010

setwd("~/Desktop/carbon_isotope_model/nemo-medusa_outputs_clim/")
month_interval<-c(1,12)

data<-readMat("sosstsst_clim_2001-2010.mat") # medusa output of sst - surface, degrees C
sst<-array(data=data$clim.fld, dim=c(180,360,12))
sst_t<-array(data=NA, dim=c(360,180,12))
for (t in month_interval[1]:month_interval[2]) {
sst_t[,,t]<-t(sst[,,t])
}

data<-readMat("OCN_CO3_clim_2001-2010.mat") # medusa output of [co3] - surface, mmol m^-3
co3<-array(data=data$clim.fld, dim=c(180,360,12))
co3_t<-array(data=NA, dim=c(360,180,12))
for (t in month_interval[1]:month_interval[2]) {
co3_t[,,t]<-t(co3[,,t])
}

data<-readMat("DIC_clim_2001-2010.mat") # medusa output of [dic] - surface, mmol m^-3
dic<-array(data=data$clim.fld, dim=c(180,360,12))
dic_t<-array(data=NA, dim=c(360,180,12))
for (t in month_interval[1]:month_interval[2]) {
dic_t[,,t]<-t(dic[,,t])
}

e_co2aq_dic<-array(data=NA, dim=c(360,180,12)) # e{co2(aq)-dic} (Hofmann et al 2000, eqn.10) - parameterized as sum of equilibrium components of e{co2(gas)-dic} (eqn.8) and e{co2(gas)-co2(aq)} (eqn.9)
        e_co2aq_dic<--(0.0144*(co3_t/dic_t)-0.1119)*sst_t-11.84

d13Cco2aq<-array(data=NA, dim=c(360,180,12)) # d13Cco2(aq) - uses constant (2 per mil) d13Cdic - assumes negligible effects of kinetic component of C isotope fractionation during air-sea gas exchange (eqn.11,12,13,14,15), and of biological C isotope fractionation during photosynthesis (Tagliabue and Bopp 2008) on d13Cdic
        d13Cco2aq<-2+e_co2aq_dic

data<-readMat("ML_PD_G3_clim_2001-2010.mat") # medusa output of large (diatoms) phytoplankton growth rate (u) - mixed-layer, n divisions d^-1 (i.e. during 24 hrs)
dgr<-array(data=data$clim.fld, dim=c(180,360,12))
dgr_t<-array(data=NA, dim=c(360, 180, 12))
for (t in month_interval[1]:month_interval[2]) {
dgr_t[,,t]<-t(dgr[,,t])
}
data<-readMat("ML_PN_G3_clim_2001-2010.mat") # medusa output of small (non-diatoms) phytoplankton u - mixed-layer, n divisions d^-1 (i.e. during 24 hrs)
ngr<-array(data=data$clim.fld, dim=c(180,360,12))
ngr_t<-array(data=NA, dim=c(360, 180, 12))
for (t in month_interval[1]:month_interval[2]) {
ngr_t[,,t]<-t(ngr[,,t])
}

# daylength model (Forsythe et al 1995, eqn.1,2,3)
#J<-
c(15,43,72,113,140,169,205,230,258,288,320,345,380,408,437,478,505,534,570,595,623,653,685,710,745,773,802,843,870,899,935,960,988,1018,1050,1075,1110,1138,1167,
```

```
##1208,1235,1264,1300,1325,1353,1383,1415,1440,1475,1503,1532,1573,1600,1629,1665,1690,1718,1748,178
0,1805,1840,1868,1897,1938,1965,1994,2030,2055,2083,2113,2145,2170,
##2205,2233,2262,2303,2330,2359,2395,2420,2448,2478,2510,2535,2570,2598,2627,2668,2695,2724,2760,278
5,2813,2843,2875,2900,2935,2963,2992,3033,3060,3089,3125,3150,3178,
##3208,3240,3265,3300,3328,3357,3398,3425,3454,3490,3515,3543,3573,3605,3630)
J<-c(15,43,72,113,140,169,205,230,258,288,320,345)
p<-0
theta<-array(data=NA, dim=c(12,180))
sigma<-array(data=NA, dim=c(12,180))
DL<-array(data=NA, dim=c(12,180))
bracket<-array(data=NA, dim=c(12,180))
L=-90:90
for (t in month_interval[1]:month_interval[2]) {
for (i in 1:180) {
theta[t,i]<-0.2163108+(2*atan(0.9671396*tan(0.0086*(J[t]-186))))
sigma[t,i]<-asin(0.39795*(cos(theta[t,i])))
bracket[t,i]<-sin((rad(p)*pi)/180)+sin((L[i]*pi)/180)*sin(sigma[t,i])/(cos((L[i]*pi)/180)*cos(sigma[t,i]))
ifelse (bracket[t,i]<(-1), bracket[t,i]<--1, bracket[t,i])
ifelse (bracket[t,i]>1, bracket[t,i]<-1, bracket[t,i])
DL[t,i]<-24-((24/pi)*acos(bracket[t,i]))
}}

DL_corr_fact<-array(data=NA, dim=c(360,180,12)) # day length correction factor - C isotope fractionation
during photosynthesis reflects the phytoplankton specific u (i.e. phytoplankton u during photoperiod) not the 24
hrs average u (Laws et al 1995,1997)
for (t in month_interval[1]:month_interval[2]) {
for (i in 1:360) {
for (j in 1:180) {
DL_corr_fact[i,j,t]<-24/DL[t,j]
ifelse(is.infinite(DL_corr_fact[i,j,t])==TRUE, DL_corr_fact[i,j,t]<-0, DL_corr_fact[i,j,t])
}}
}

dgr_sp<-array(data=NA, dim=c(360,180,12)) # diatoms specific u - n divisions d^-1
        dgr_sp<-(dgr_t*DL_corr_fact)

ngr_sp<-array(data=NA, dim=c(360,180,12)) # non-diatoms specific u - n divisions d^-1
        ngr_sp<-(ngr_t*DL_corr_fact)

dalpha = 0.2
dbeta = 1.5
nalpha = 0.3
nbeta = 2

#synthetic data to visualise scaling equations
Csyn<-seq(from=0, to=1, by=0.005)
Csyn.sc<-dbeta*(Csyn^dalpha)
CsynN.sc<-nbeta*(Csyn^nalpha)
plot(x<-Csyn, y=Csyn.sc, ylim=c(0,2.5))
par(new=TRUE)
plot(x<-Csyn, y=CsynN.sc, ylim=c(0,2.5), xlab="", ylab="", axes=FALSE, col="red")
par(new=FALSE)

dgr_sc<-array(data=NA, dim=c(360,180,12)) # diatoms specific, scaled u - n divisions d^-1
        dgr_sc<-dbeta*dgr_sp^dalpha

ngr_sc<-array(data=NA, dim=c(360,180,12)) # non-diatoms specific, scaled u - n divisions d^-1
        ngr_sc<-nbeta*ngr_sp^nalpha

d40S40N = 1.25 # -40 to 40 N
```

```
d4050SN = 1.2 # 40 to 50 N, and -40 to -50 N
d5060SN = 1.1 # 50 to 60 N, and -50 to -60 N
d60SN = 1 # > 60 N, < -60 N
n40S40N = 1.75
n4050SN = 1.6
n5060SN = 1.5
n60SN = 1

dgr_lim<-array(data=NA, dim=c(360,180,12)) # diatoms specific, scaled, limited u - n divisions d^-1
for (t in month_interval[1]:month_interval[2]) {
for (i in 1:360) {
for (j in 1:180) {
dgr_lim[i,j,t]<-dgr_sc[i,j,t]
        if(j>=50 & j<=130){
                ifelse (dgr_lim[i,j,t]<d40S40N, dgr_lim[i,j,t]<-d40S40N, dgr_lim[i,j,t])} else
        if(j>130 & j<=140){
                ifelse (dgr_lim[i,j,t]<d4050SN, dgr_lim[i,j,t]<-d4050SN, dgr_lim[i,j,t])} else
        if(j<50 & j>=40){
                ifelse (dgr_lim[i,j,t]<d4050SN, dgr_lim[i,j,t]<-d4050SN, dgr_lim[i,j,t])} else
        if(j>140 & j<=150){
                ifelse (dgr_lim[i,j,t]<d5060SN, dgr_lim[i,j,t]<-d5060SN, dgr_lim[i,j,t])} else
        if(j<40 & j>=30){
                ifelse (dgr_lim[i,j,t]<d5060SN, dgr_lim[i,j,t]<-d5060SN, dgr_lim[i,j,t])} else
        ifelse (dgr_lim[i,j,t]<d60SN, dgr_lim[i,j,t]<-d60SN, dgr_lim[i,j,t])
}}
}
ngr_lim<-array(data=NA, dim=c(360,180,12)) # non-diatoms specific, scaled, limited u - n divisions d^-1
for (t in month_interval[1]:month_interval[2]) {
for (i in 1:360) {
for (j in 1:180) {
ngr_lim[i,j,t]<-ngr_sc[i,j,t]
        if(j>=50 & j<=130){
                ifelse (ngr_lim[i,j,t]<n40S40N, ngr_lim[i,j,t]<-n40S40N, ngr_lim[i,j,t])} else
        if(j>130 & j<=140){
                ifelse (ngr_lim[i,j,t]<n4050SN, ngr_lim[i,j,t]<-n4050SN, ngr_lim[i,j,t])} else
        if(j<50 & j>=40){
                ifelse (ngr_lim[i,j,t]<n4050SN, ngr_lim[i,j,t]<-n4050SN, ngr_lim[i,j,t])} else
        if(j>140 & j<=150){
                ifelse (ngr_lim[i,j,t]<n5060SN, ngr_lim[i,j,t]<-n5060SN, ngr_lim[i,j,t])} else
        if(j<40 & j>=30){
                ifelse (ngr_lim[i,j,t]<n5060SN, ngr_lim[i,j,t]<-n5060SN, ngr_lim[i,j,t])} else
        ifelse (ngr_lim[i,j,t]<n60SN, ngr_lim[i,j,t]<-n60SN, ngr_lim[i,j,t])
}}
}

dgr_lim_s<-array(data=NA, dim=c(360,180,12)) # diatoms specific, scaled, limited u - converted to n divisions
s^-1
        dgr_lim_s<-dgr_lim/86400
ngr_lim_s<-array(data=NA, dim=c(360,180,12)) # non-diatoms specific, scaled, limited u - converted to n
divisions d^-1
        ngr_lim_s<-ngr_lim/86400

rd = 5*(10^(-5)) # diatoms radius - um (Rau et al 1996,1997)
Sd = 4*pi*(rd^2)
Vd = (4/3)*pi*(rd^3)
Vd_um3 = Vd*10^(18)
yd = (3.154*10^(-14))*(Vd_um3)^0.758
rn = 1*(10^(-5)) # non-diatoms radius - um (Rau et al 1996,1997)
Sn = 4*pi*(rn^2)
Vn = (4/3)*pi*(rn^3)
```

```
Vn_um3 = Vn*10^(18)
yn = (3.154*10^(-14))*(Vn_um3)^0.758

data<-readMat("OCN_H2CO3_clim_2001-2010.mat") # medusa output of [h2co3] - surface, mmol m^-3 - same as [co2(aq)], as [h2co3] from dissolution of co2 is negligible in comparison to [co2(aq)] (Zeebe et al 1999)
co2aq_mmol<-array(data=data$clim.fld, dim=c(180, 360, 12))
co2aq_mmol_t<-array(data=NA, dim=c(360, 180, 12))
for (t in month_interval[1]:month_interval[2]) {
co2aq_mmol_t[,,t]<-t(co2aq_mmol[,,t])
}

co2aq_mol_m3<-array(data=NA, dim=c(360,180,12)) # [co2(aq)] - converted to mol m^-3
        co2aq_mol_m3<-co2aq_mmol_t*10^(-3)

ef = 25 # paremeters to calculate C isotope fractionation during photosynthesis (ep) (Rau et al 1996,1997)
ed = 0.7
Dt = 1.45*10^(-9)
rk = 2.06*10^(-4)
P = 1*10^(-4)

db<-array(data=NA, dim=c(360,180,12)) # b (Rau et al. 1996, eqn.15) for diatoms
        db<--(ef-ed)*((yd*dgr_lim_s)/Sd)*((rd/(Dt*(1+rd/rk)))+1/P)
nb<-array(data=NA, dim=c(360,180,12)) # b (Rau et al. 1996, eqn.15) for non-diatoms
        nb<--(ef-ed)*((yn*ngr_lim_s)/Sn)*((rn/(Dt*(1+rn/rk)))+1/P)

dep<-array(data=NA, dim=c(360,180,12)) # ep (Rau et al. 1996, eqn.14) for diatoms - per mil
for (t in month_interval[1]:month_interval[2]) {
for (i in 1:360) {
for (j in 1:180) {
dep[i,j,t]<-ef+(db[i,j,t]/co2aq_mol_m3[i,j,t])
ifelse (dep[i,j,t]<5, dep[i,j,t]<-5, dep[i,j,t]) # ep lower and upper limits (Tagliabue and Bopp 2008)
ifelse (dep[i,j,t]>20, dep[i,j,t]<-20, dep[i,j,t])
}}
}
nep<-array(data=NA, dim=c(360,180,12)) # ep (Rau et al. 1996, eqn.14) for non-diatoms - per mil
for (t in month_interval[1]:month_interval[2]) {
for (i in 1:360) {
for (j in 1:180) {
nep[i,j,t]<-ef+(nb[i,j,t]/co2aq_mol_m3[i,j,t])
ifelse (nep[i,j,t]<10, nep[i,j,t]<-10, nep[i,j,t]) # ep lower and upper limits (Tagliabue and Bopp 2008)
ifelse (nep[i,j,t]>26, nep[i,j,t]<-26, nep[i,j,t])
}}
}

data<-readMat("ML_PD_clim_2001-2010.mat") # medusa output of diatoms biomass - mixed-layer, mmol N m^2
d_biom<-array(data=data$clim.fld, dim=c(180,360,12))
d_biom_t<-array(data=NA, dim=c(360,180,12))
for (t in month_interval[1]:month_interval[2]) {
d_biom_t[,,t]<-t(d_biom[,,t])
}
data<-readMat("ML_PN_clim_2001-2010.mat") # medusa output of non-diatoms biomass - mixed-layer, mmol N m^2
n_biom<-array(data=data$clim.fld, dim=c(180,360,12))
n_biom_t<-array(data=NA, dim=c(360,180,12))
for (t in month_interval[1]:month_interval[2]) {
n_biom_t[,,t]<-t(n_biom[,,t])
}

fd<-array(data=NA, dim=c(360,180,12)) # diatoms relative proportion
```

```
        fd<-(d_biom_t/(d_biom_t+n_biom_t))

meanep<-array(data=NA, dim=c(360, 180, 12)) # average ep - weighted by diatoms and non-diatoms relative proportions - per mil
        meanep<-((dep*fd)+(nep*(1-fd)))

d13Cpoc<-array(data=NA, dim=c(360,180,12)) # d13Cpoc - per mil - assumes co2(aq) as inorganic C source; threfore, d13Cpoc can pe predicted from d13Cco2aq
        d13Cpoc<-(d13Cco2aq-meanep)

## annual average d13Cpoc - weighted by diatoms and non-diatoms proportional contribution to total annual phytoplankton production - per mil
d13Cco2aq_av=array(data=NA, dim=c(360,180))
for (i in 1:360){
for (j in 1:180){
   d13Cco2aq_av[i,j]<-mean(d13Cco2aq[i,j,month_interval[1]:month_interval[2]],na.rm=T)
}}

fd_av=array(data=NA, dim=c(360,180))
for (i in 1:360) {
for (j in 1:180) {
   fd_av[i,j]<-mean(fd[i,j,month_interval[1]:month_interval[2]],na.rm=T)
}}

test <- array(data=NA, dim=c(360,180))
for (i in 1:360) {
for (j in 1:180) {
test[i,j] <- ifelse(sum(d_biom_t[i,j,month_interval[1]:month_interval[2]])==0, 0.0001,
sum(d_biom_t[i,j,month_interval[1]:month_interval[2]]))
}}
sum_d_ep=array(data=NA, dim=c(360,180))
for (i in 1:360){
for (j in 1:180){
   sum_d_ep[i,j]<-
(sum(d_biom_t[i,j,month_interval[1]:month_interval[2]]*dep[i,j,month_interval[1]:month_interval[2]]))/test[i,j]
}}

sum_n_ep=array(data=NA, dim=c(360,180))
for (i in 1:360){
for (j in 1:180){
   sum_n_ep[i,j]<-
(sum(n_biom_t[i,j,month_interval[1]:month_interval[2]]*nep[i,j,month_interval[1]:month_interval[2]]))/(sum(n_biom_t[i,j,month_interval[1]:month_interval[2]]))
}}

ep_av=array(data=NA, dim=c(360,180))
for (i in 1:360) {
for (j in 1:180) {
   ep_av[i,j]<-((sum_d_ep[i,j]*fd_av[i,j])+(sum_n_ep[i,j]*(1-fd_av[i,j])))
}}
d13Cpoc_av=array(data=NA, dim=c(360,180))
for (i in 1:360) {
for (j in 1:180) {
   d13Cpoc_av[i,j]<-d13Cco2aq_av[i,j]-ep_av[i,j]
}}

## intra-annual range in d13Cpoc - per mil
d13Cpoc_rng=array(data=NA, dim=c(360,180))
for (i in 1:360){
for (j in 1:180){
```

```
d13Cpoc_rng[i,j]<-max(d13Cpoc[i,j,month_interval[1]:month_interval[2]])-
min(d13Cpoc[i,j,month_interval[1]:month_interval[2]])
}}
```

CARBON ISOTOPE MODEL - 10 MODEL YEARS

```
setwd("~/Desktop/carbon_isotope_model/nemo-medusa_outputs_2001-2010/")
month_interval<-c(1,120)

data<-readMat("sosstsst_2001-2010.mat") # medusa output of sst - surface, degrees C
sst<-array(data=data$this.fld, dim=c(180,360,120))
sst_t<-array(data=NA, dim=c(360,180,120))
for (t in month_interval[1]:month_interval[2]) {
sst_t[,,t]<-t(sst[,,t])
}

data<-readMat("OCN_CO3_2001-2010.mat") # medusa output of [co3] - surface, mmol m^-3
co3<-array(data=data$this.fld, dim=c(180,360,120))
co3_t<-array(data=NA, dim=c(360,180,120))
for (t in month_interval[1]:month_interval[2]) {
co3_t[,,t]<-t(co3[,,t])
}

data<-readMat("DIC_2001-2010.mat") # medusa output of [dic] - surface, mmol m^-3
dic<-array(data=data$this.fld, dim=c(180,360,120))
dic_t<-array(data=NA, dim=c(360,180,120))
for (t in month_interval[1]:month_interval[2]) {
dic_t[,,t]<-t(dic[,,t])
}

e_co2aq_dic<-array(data=NA, dim=c(360,180,120)) # e{co2(aq)-dic} (Hofmann et al 2000, eqn.10) -
parameterized as sum of equilibrium components of e{co2(gas)-dic} (eqn.8) and e{co2(gas)-co2(aq)} (eqn.9)
        e_co2aq_dic<--(0.0144*(co3_t/dic_t)-0.1119)*sst_t-11.84

d13Cco2aq<-array(data=NA, dim=c(360,180,120)) # d13Cco2(aq) - uses constant (2 per mil) d13Cdic - assumes
negligible effects of kinetic component of C isotope fractionation during air-sea gas exchange
(eqn.11,12,13,14,15), and of biological C isotope fractionation during photosynthesis (Tagliabue and Bopp
2008) on d13Cdic
        d13Cco2aq<-2+e_co2aq_dic

data<-readMat("ML_PD_G3_2001-2010.mat") # medusa output of large (diatoms) phytoplankton growth rate
(u) - mixed-layer, n divisions d^-1 (i.e. during 24 hrs)
dgr<-array(data=data$this.fld, dim=c(180,360,120))
dgr_t<-array(data=NA, dim=c(360, 180, 120))
for (t in month_interval[1]:month_interval[2]) {
dgr_t[,,t]<-t(dgr[,,t])
}
data<-readMat("ML_PN_G3_2001-2010.mat") # medusa output of small (non-diatoms) phytoplankton u -
mixed-layer, n divisions d^-1 (i.e. during 24 hrs)
ngr<-array(data=data$this.fld, dim=c(180,360,120))
ngr_t<-array(data=NA, dim=c(360, 180, 120))
for (t in month_interval[1]:month_interval[2]) {
ngr_t[,,t]<-t(ngr[,,t])
}

# daylength model (Forsythe et al 1995, eqn.1,2,3)
J<-
c(15,43,72,113,140,169,205,230,258,288,320,345,380,408,437,478,505,534,570,595,623,653,685,710,745,773,8
02,843,870,899,935,960,988,1018,1050,1075,1110,1138,1167,
```

```
1208,1235,1264,1300,1325,1353,1383,1415,1440,1475,1503,1532,1573,1600,1629,1665,1690,1718,1748,1780,
1805,1840,1868,1897,1938,1965,1994,2030,2055,2083,2113,2145,2170,
2205,2233,2262,2303,2330,2359,2395,2420,2448,2478,2510,2535,2570,2598,2627,2668,2695,2724,2760,2785,
2813,2843,2875,2900,2935,2963,2992,3033,3060,3089,3125,3150,3178,
3208,3240,3265,3300,3328,3357,3398,3425,3454,3490,3515,3543,3573,3605,3630)
#J<-c(15,43,72,113,140,169,205,230,258,288,320,345)
p<-0
theta<-array(data=NA, dim=c(120,180))
sigma<-array(data=NA, dim=c(120,180))
DL<-array(data=NA, dim=c(120,180))
bracket<-array(data=NA, dim=c(120,180))
L=-90:90
for (t in month_interval[1]:month_interval[2]) {
for (i in 1:180) {
theta[t,i]<-0.2163108+(2*atan(0.9671396*tan(0.0086*(J[t]-186))))
sigma[t,i]<-asin(0.39795*(cos(theta[t,i])))
bracket[t,i]<-sin((rad(p)*pi)/180)+sin((L[i]*pi)/180)*sin(sigma[t,i])/(cos((L[i]*pi)/180)*cos(sigma[t,i]))
ifelse (bracket[t,i]<(-1), bracket[t,i]<--1, bracket[t,i])
ifelse (bracket[t,i]>1, bracket[t,i]<-1, bracket[t,i])
DL[t,i]<-24-((24/pi)*acos(bracket[t,i]))
}}

DL_corr_fact<-array(data=NA, dim=c(360,180,120)) # day length correction factor - C isotope fractionation
during photosynthesis reflects the phytoplankton specific u (i.e. phytoplankton u during photoperiod) not the 24
hrs average u (Laws et al 1995,1997)
for (t in month_interval[1]:month_interval[2]) {
for (i in 1:360) {
for (j in 1:180) {
DL_corr_fact[i,j,t]<-24/DL[t,j]
ifelse(is.infinite(DL_corr_fact[i,j,t])==TRUE, DL_corr_fact[i,j,t]<-0, DL_corr_fact[i,j,t])
}}
}

dgr_sp<-array(data=NA, dim=c(360,180,120)) # diatoms specific u - n divisions d^-1
        dgr_sp<-(dgr_t*DL_corr_fact)

ngr_sp<-array(data=NA, dim=c(360,180,120)) # non-diatoms specific u - n divisions d^-1
        ngr_sp<-(ngr_t*DL_corr_fact)

dalpha = 0.2
dbeta = 1.5
nalpha = 0.3
nbeta = 2

dgr_sc<-array(data=NA, dim=c(360,180,120)) # diatoms specific, scaled u - n divisions d^-1
        dgr_sc<-dbeta*dgr_sp^dalpha

ngr_sc<-array(data=NA, dim=c(360,180,120)) # non-diatoms specific, scaled u - n divisions d^-1
        ngr_sc<-nbeta*ngr_sp^nalpha

d40S40N = 1.25 # -40 to 40 N
d4050SN = 1.2 # 40 to 50 N, and -40 to -50 N
d5060SN = 1.1 # 50 to 60 N, and -50 to -60 N
d60SN = 1 # > 60 N, < -60 N
n40S40N = 1.75
n4050SN = 1.6
n5060SN = 1.5
n60SN = 1

dgr_lim<-array(data=NA, dim=c(360,180,120)) # diatoms specific, scaled, limited u - n divisions d^-1
```

```
for (t in month_interval[1]:month_interval[2]) {
for (i in 1:360) {
for (j in 1:180) {
dgr_lim[i,j,t]<-dgr_sc[i,j,t]
        if(j>=50 & j<=130){
                ifelse (dgr_lim[i,j,t]<d40S40N, dgr_lim[i,j,t]<-d40S40N, dgr_lim[i,j,t])} else
        if(j>130 & j<=140){
                ifelse (dgr_lim[i,j,t]<d4050SN, dgr_lim[i,j,t]<-d4050SN, dgr_lim[i,j,t])} else
        if(j<50 & j>=40){
                ifelse (dgr_lim[i,j,t]<d4050SN, dgr_lim[i,j,t]<-d4050SN, dgr_lim[i,j,t])} else
        if(j>140 & j<=150){
                ifelse (dgr_lim[i,j,t]<d5060SN, dgr_lim[i,j,t]<-d5060SN, dgr_lim[i,j,t])} else
        if(j<40 & j>=30){
                ifelse (dgr_lim[i,j,t]<d5060SN, dgr_lim[i,j,t]<-d5060SN, dgr_lim[i,j,t])} else
        ifelse (dgr_lim[i,j,t]<d60SN, dgr_lim[i,j,t]<-d60SN, dgr_lim[i,j,t])
}}
}
ngr_lim<-array(data=NA, dim=c(360,180,120)) # non-diatoms specific, scaled, limited u - n divisions d^-1
for (t in month_interval[1]:month_interval[2]) {
for (i in 1:360) {
for (j in 1:180) {
ngr_lim[i,j,t]<-ngr_sc[i,j,t]
        if(j>=50 & j<=130){
                ifelse (ngr_lim[i,j,t]<n40S40N, ngr_lim[i,j,t]<-n40S40N, ngr_lim[i,j,t])} else
        if(j>130 & j<=140){
                ifelse (ngr_lim[i,j,t]<n4050SN, ngr_lim[i,j,t]<-n4050SN, ngr_lim[i,j,t])} else
        if(j<50 & j>=40){
                ifelse (ngr_lim[i,j,t]<n4050SN, ngr_lim[i,j,t]<-n4050SN, ngr_lim[i,j,t])} else
        if(j>140 & j<=150){
                ifelse (ngr_lim[i,j,t]<n5060SN, ngr_lim[i,j,t]<-n5060SN, ngr_lim[i,j,t])} else
        if(j<40 & j>=30){
                ifelse (ngr_lim[i,j,t]<n5060SN, ngr_lim[i,j,t]<-n5060SN, ngr_lim[i,j,t])} else
        ifelse (ngr_lim[i,j,t]<n60SN, ngr_lim[i,j,t]<-n60SN, ngr_lim[i,j,t])
}}
}

dgr_lim_s<-array(data=NA, dim=c(360,180,120)) # diatoms specific, scaled, limited u - converted to n divisions
s^-1
        dgr_lim_s<-dgr_lim/86400
ngr_lim_s<-array(data=NA, dim=c(360,180,120)) # non-diatoms specific, scaled, limited u - converted to n
divisions d^-1
        ngr_lim_s<-ngr_lim/86400

rd = 5*(10^(-5)) # diatoms radius - um (Rau et al 1996,1997)
Sd = 4*pi*(rd^2)
Vd = (4/3)*pi*(rd^3)
Vd_um3 = Vd*10^(18)
yd = (3.154*10^(-14))*(Vd_um3)^0.758
rn = 1*(10^(-5)) # non-diatoms radius - um (Rau et al 1996,1997)
Sn = 4*pi*(rn^2)
Vn = (4/3)*pi*(rn^3)
Vn_um3 = Vn*10^(18)
yn = (3.154*10^(-14))*(Vn_um3)^0.758

data<-readMat("OCN_H2CO3_2001-2010.mat") # medusa output of [h2co3] - surface, mmol m^-3 - same as
[co2(aq)], as [h2co3] from dissolution of co2 is negligible in comparison to [co2(aq)] (Zeebe et al 1999)
co2aq_mmol<-array(data=data$this.fld, dim=c(180, 360, 120))
co2aq_mmol_t<-array(data=NA, dim=c(360, 180, 120))
for (t in month_interval[1]:month_interval[2]) {
co2aq_mmol_t[,,t]<-t(co2aq_mmol[,,t])
```

```
}

co2aq_mol_m3<-array(data=NA, dim=c(360,180,120)) # [co2(aq)] - converted to mol m^-3
        co2aq_mol_m3<-co2aq_mmol_t*10^(-3)

ef = 25 # paremeters to calculate C isotope fractionation during photosynthesis (ep) (Rau et al 1996,1997)
ed = 0.7
Dt = 1.45*10^(-9)
rk = 2.06*10^(-4)
P = 1*10^(-4)

db<-array(data=NA, dim=c(360,180,120)) # b (Rau et al. 1996, eqn.15) for diatoms
        db<--(ef-ed)*((yd*dgr_lim_s)/Sd)*((rd/(Dt*(1+rd/rk)))+1/P)
nb<-array(data=NA, dim=c(360,180,120)) # b (Rau et al. 1996, eqn.15) for non-diatoms
        nb<--(ef-ed)*((yn*ngr_lim_s)/Sn)*((rn/(Dt*(1+rn/rk)))+1/P)

dep<-array(data=NA, dim=c(360,180,120)) # ep (Rau et al. 1996, eqn.14) for diatoms - per mil
for (t in month_interval[1]:month_interval[2]) {
for (i in 1:360) {
for (j in 1:180) {
dep[i,j,t]<-ef+(db[i,j,t]/co2aq_mol_m3[i,j,t])
ifelse (dep[i,j,t]<5, dep[i,j,t]<-5, dep[i,j,t]) # ep lower and upper limits (Tagliabue and Bopp 2008)
ifelse (dep[i,j,t]>20, dep[i,j,t]<-20, dep[i,j,t])
}}
}
nep<-array(data=NA, dim=c(360,180,120)) # ep (Rau et al. 1996, eqn.14) for non-diatoms - per mil
for (t in month_interval[1]:month_interval[2]) {
for (i in 1:360) {
for (j in 1:180) {
nep[i,j,t]<-ef+(nb[i,j,t]/co2aq_mol_m3[i,j,t])
ifelse (nep[i,j,t]<10, nep[i,j,t]<-10, nep[i,j,t]) # ep lower and upper limits (Tagliabue and Bopp 2008)
ifelse (nep[i,j,t]>26, nep[i,j,t]<-26, nep[i,j,t])
}}
}

data<-readMat("ML_PD_2001-2010.mat") # medusa output of diatoms biomass - mixed-layer, mmol N m^2
d_biom<-array(data=data$this.fld, dim=c(180,360,120))
d_biom_t<-array(data=NA, dim=c(360,180,120))
for (t in month_interval[1]:month_interval[2]) {
d_biom_t[,,t]<-t(d_biom[,,t])
}
data<-readMat("ML_PN_2001-2010.mat") # medusa output of non-diatoms biomass - mixed-layer, mmol N
m^2
n_biom<-array(data=data$this.fld, dim=c(180,360,120))
n_biom_t<-array(data=NA, dim=c(360,180,120))
for (t in month_interval[1]:month_interval[2]) {
n_biom_t[,,t]<-t(n_biom[,,t])
}

fd<-array(data=NA, dim=c(360,180,120)) # diatoms relative proportion
        fd<-(d_biom_t/(d_biom_t+n_biom_t))

meanep<-array(data=NA, dim=c(360, 180, 120)) # average ep - weighted by diatoms and non-diatoms relative
proportions - per mil
        meanep<-((dep*fd)+(nep*(1-fd)))

d13Cpoc<-array(data=NA, dim=c(360,180,120)) # d13Cpoc - per mil - assumes co2(aq) as inorganic C source;
threfore, d13Cpoc can pe predicted from d13Cco2aq
        d13Cpoc<-(d13Cco2aq-meanep)
```

```
## annual average d13Cpoc - weighted by diatoms and non-diatoms proportional contribution to total annual
phytoplankton production - per mil
month_interval <- c(1,12) # individual model year 2001
#month_interval <- c(13,24) # individual model year 2002
#month_interval <- c(25,36) # individual model year 2003
#month_interval <- c(37,48) # individual model year 2004
#month_interval <- c(49,60) # individual model year 2005
#month_interval <- c(61,72) # individual model year 2006
#month_interval <- c(73,84) # individual model year 2007
#month_interval <- c(85,96) # individual model year 2008
#month_interval <- c(97,108) # individual model year 2009
#month_interval <- c(108,120) # individual model year 2010

d13Cco2aq_av=array(data=NA, dim=c(360,180))
for (i in 1:360){
for (j in 1:180){
   d13Cco2aq_av[i,j]<-mean(d13Cco2aq[i,j,month_interval[1]:month_interval[2]],na.rm=T)
}}

fd_av=array(data=NA, dim=c(360,180))
for (i in 1:360) {
for (j in 1:180) {
   fd_av[i,j]<-mean(fd[i,j,month_interval[1]:month_interval[2]],na.rm=T)
}}

test <- array(data=NA, dim=c(360,180))
for (i in 1:360) {
for (j in 1:180) {
test[i,j] <- ifelse(sum(d_biom_t[i,j,month_interval[1]:month_interval[2]])==0, 0.0001,
sum(d_biom_t[i,j,month_interval[1]:month_interval[2]]))
}}
sum_d_ep=array(data=NA, dim=c(360,180))
for (i in 1:360){
for (j in 1:180){
   sum_d_ep[i,j]<-
(sum(d_biom_t[i,j,month_interval[1]:month_interval[2]]*dep[i,j,month_interval[1]:month_interval[2]]))/test[i,j]
}}

sum_n_ep=array(data=NA, dim=c(360,180))
for (i in 1:360){
for (j in 1:180){
   sum_n_ep[i,j]<-
(sum(n_biom_t[i,j,month_interval[1]:month_interval[2]]*nep[i,j,month_interval[1]:month_interval[2]]))/(sum(n
_biom_t[i,j,month_interval[1]:month_interval[2]]))
}}

ep_av=array(data=NA, dim=c(360,180))
for (i in 1:360) {
for (j in 1:180) {
   ep_av[i,j]<-((sum_d_ep[i,j]*fd_av[i,j])+(sum_n_ep[i,j]*(1-fd_av[i,j])))
}}
d13Cpoc_av=array(data=NA, dim=c(360,180))
for (i in 1:360) {
for (j in 1:180) {
   d13Cpoc_av[i,j]<-d13Cco2aq_av[i,j]-ep_av[i,j]
}}

## inter-annual range in d13Cpoc - per mil (calculated as range of d13Cpoc av for all individual model years)
d13Cpoc_av2001.mf <- readRDS("~/Desktop/plots/d13Cpoc_av2001.rds")
d13Cpoc_av2002.mf <- readRDS("~/Desktop/plots/d13Cpoc_av2002.rds")
```

```
d13Cpoc_av2003.mf <- readRDS("~/Desktop/plots/d13Cpoc_av2003.rds")
d13Cpoc_av2004.mf <- readRDS("~/Desktop/plots/d13Cpoc_av2004.rds")
d13Cpoc_av2005.mf <- readRDS("~/Desktop/plots/d13Cpoc_av2005.rds")
d13Cpoc_av2006.mf <- readRDS("~/Desktop/plots/d13Cpoc_av2006.rds")
d13Cpoc_av2007.mf <- readRDS("~/Desktop/plots/d13Cpoc_av2007.rds")
d13Cpoc_av2008.mf <- readRDS("~/Desktop/plots/d13Cpoc_av2008.rds")
d13Cpoc_av2009.mf <- readRDS("~/Desktop/plots/d13Cpoc_av2009.rds")
d13Cpoc_av2010.mf <- readRDS("~/Desktop/plots/d13Cpoc_av2010.rds")

d13Cpoc_rng20012010<-array(data=NA, dim=c(360,180))
for (i in 1:360){
for (j in 1:180){
d13Cpoc_rng20012010[i,j]<-max(d13Cpoc_av2001.mf[i,j], d13Cpoc_av2002.mf[i,j], d13Cpoc_av2003.mf[i,j],
d13Cpoc_av2004.mf[i,j], d13Cpoc_av2005.mf[i,j], d13Cpoc_av2006.mf[i,j], d13Cpoc_av2007.mf[i,j],
d13Cpoc_av2008.mf[i,j], d13Cpoc_av2009.mf[i,j], d13Cpoc_av2010.mf[i,j])-min(d13Cpoc_av2001.mf[i,j],
d13Cpoc_av2002.mf[i,j], d13Cpoc_av2003.mf[i,j], d13Cpoc_av2004.mf[i,j], d13Cpoc_av2005.mf[i,j],
d13Cpoc_av2006.mf[i,j], d13Cpoc_av2007.mf[i,j], d13Cpoc_av2008.mf[i,j], d13Cpoc_av2009.mf[i,j],
d13Cpoc_av2010.mf[i,j])
}}
```

Appendix 4.A – Standards

Table 4.A1 A) Known $\delta^{13}C$ values of each amino acid in the standards AA1 and AA2 prior to derivatisation. As no international standards are currently available for the analysis of carbon isotopes in amino acids, and no large inter-laboratory calibration has yet come up with consensus values, mean values across three laboratories (i.e. the Fish Ecology Laboratory, the Marine Biological Laboratory and UC Davis Stable Isotope Facility) were used. B) Precision was determined as the standard deviation for $\delta^{13}C$ values of each amino acid of the in-house cod standard during the time period shark samples were analysed.

A) Known $\delta^{13}C$ value

Amino acid	Fish Ecol Lab	MBL	UC Davis	Average	SD
Val	-10.99	-10.55	-10.87	-10.80	0.23
Ile	-10.82	-10.35	-10.69	-10.62	0.24
Leu	-29.83	-30.00	-30.10	-29.97	0.14
Thr	-10.62	-10.05	-10.65	-10.44	0.34
Phe	-11.46	-11.45	-11.54	-11.48	0.05
Ala	-19.45	-19.15	-19.59	-19.40	0.23
Gly	-37.86	-38.25	-38.26	-38.13	0.23
Pro	-10.79	-10.30	-10.67	-10.59	0.26
Asp	-22.17	-22.10	-20.96	-21.74	0.68
Glu	-28.24	-28.55	-28.52	-28.43	0.17

B) Precision

Amino acid	Precision
Val	0.31
Ile	0.34
Leu	0.40
Thr	0.30
Phe	0.26
Ala	0.13
Gly	0.30
Pro	0.32
Asp	0.40
Glu	0.22

Appendix 4.B – Fingerprinting data

Table 4.B1 Literature-derived data for raw carbon isotopic compositions of essential amino acids ($\delta^{13}C_{EAA}$) for a selection of primary producers and heterotrophic bacteria (end-members) presumably relevant to blue and porbeagle shark ecology. Prior to define carbon source fingerprints, $\delta^{13}C_{EAA}$ values were sample-normalised ($\delta^{13}C_{norm\text{-}EAA}$), and end-members classified *a priori* within the following groups: i) autotrophic and ii) heterotrophic bacteria (prokaryotes), iii) eukaryotic miacroalgae, iv) macroalgae, v) seagrasses, and vi) terrestrial plants (eukaryotes; see Materials and Methods).

ID	*A priori*-defined group	Metabolism	Phylogeny	Species	Reference	Val	Ileu	Leu	Phe
AB1	Autotrophic bacteria	N_2 fixing	Cyanobacteria	*A. cylindrica*	Larsen *et al.*, 2013	-20.50	-17.30	-23.30	-19.80
AB2	Autotrophic bacteria	N_2 fixing	Cyanobacteria	*N. muscorum*	Larsen *et al.*, 2013	-24.20	-20.00	-25.80	-24.00
AB3	Autotrophic bacteria	N_2 fixing	Cyanobacteria	*Cyanothece sp.*	Larsen *et al.*, 2013	-24.00	-27.70	-27.80	-24.90
AB4	Autotrophic bacteria	non-N_2 fixing	Cyanobacteria	*M. punctata*	Larsen *et al.*, 2013	-32.80	-28.90	-36.00	-34.60
AB5	Autotrophic bacteria	Chemolithotroph	NA	*Aquifex*	Scott *et al.*, 2006	-38.01	-32.25	-30.83	-30.31
AB6	Autotrophic bacteria	Chemolithotroph	NA	*Nitrosomonas*	Scott *et al.*, 2006	-69.72	-64.44	-70.47	-73.53
AB7	Autotrophic bacteria	Acetogen	NA	*Moorella*	Scott *et al.*, 2006	-29.43	-22.71	-27.32	-28.93
AB8	Autotrophic bacteria	Phototroph	NA	*Chlorobium*	Scott *et al.*, 2006	-17.15	-11.61	-13.40	-17.04
AB9	Autotrophic bacteria	Phototroph	NA	*Synochocystis*	Scott *et al.*, 2006	-25.68	-19.44	-28.25	-23.02
AB10	Autotrophic bacteria	Phototroph	NA	*Spirulina*	Scott *et al.*, 2006	-18.76	-17.06	-24.18	-20.76
HB1	Heterotrophic bacteria	NA	Actinobacteria	*Rhodococcus sp.*	Larsen *et al.*, 2013	-26.40	-23.70	-25.20	-28.90
HB2	Heterotrophic bacteria	NA	Betaprotobacteria	*B. xenovorans*	Larsen *et al.*, 2013	-13.60	-12.00	-12.80	-18.80
HB3	Heterotrophic bacteria	NA	Actinobacteria	*Rhodococcus sp.*	Larsen *et al.*, 2009	-26.80	-27.30	-26.20	-29.20
HB4	Heterotrophic bacteria	NA	Betaprotobacteria	*B. xenovorans*	Larsen *et al.*, 2009	-16.00	-14.20	-12.90	-19.00
HB5	Heterotrophic bacteria	NA	Gammaproteobacteria	*E. coli*	Larsen *et al.*, 2009	-13.60	-12.50	-14.00	-15.50
HB6	Heterotrophic bacteria	NA	Gammaproteobacteria	Gammaproteobacteria *spp.*	Larsen *et al.*, 2009	-30.40	-27.90	-30.10	-31.90
HB7	Heterotrophic bacteria	Organotroph/Acetotroph	Gammaproteobacteria	*E. coli* (aerobic pyruvate)	Scott *et al.*, 2006	-12.41	-11.58	-11.94	-10.65
HB8	Heterotrophic bacteria	Organotroph/Acetotroph	Gammaproteobacteria	*E. coli* (anaerobic pyruvate)	Scott *et al.*, 2006	-11.99	-15.23	-16.59	-19.42
HB9	Heterotrophic bacteria	Organotroph/Acetotroph	Gammaproteobacteria	*E. coli* (acetate)	Scott *et al.*, 2006	-34.61	-32.39	-32.34	-34.45
HB10	Heterotrophic bacteria	Organotroph/Acetotroph/Methylotroph	NA	*S. oneidensis* (aerobe fumarate)	Scott *et al.*, 2006	-30.89	-28.07	-30.69	-30.48
HB11	Heterotrophic bacteria	Organotroph/Acetotroph/Methylotroph	NA	*S. oneidensis* (aerobe nitrate)	Scott *et al.*, 2006	-34.95	-28.68	-30.25	-30.75
HB12	Heterotrophic bacteria	Organotroph/Acetotroph/Methylotroph	NA	*S. oneidensis* (anaerobe fumarate)	Scott *et al.*, 2006	-32.85	-28.96	-34.94	-30.02
HB13	Heterotrophic bacteria	Organotroph/Acetotroph/Methylotroph	NA	*S. oneidensis* (anaerobe nitrate)	Scott *et al.*, 2006	-33.52	-28.43	-35.88	-31.65
HB14	Heterotrophic bacteria	Organotroph	NA	*Desulfobrivio*	Scott *et al.*, 2006	-26.53	-25.52	-29.86	-24.77
HB15	Heterotrophic bacteria	Methylotroph	NA	*Methylophylus*	Scott *et al.*, 2006	-58.63	-60.08	-59.12	-59.02
HB16	Heterotrophic bacteria	Methylotroph	NA	*Methylobacterium* (methylamine)	Scott *et al.*, 2006	-47.96	-48.02	-48.07	-51.15
HB17	Heterotrophic bacteria	Methylotroph	NA	*Methylobacterium* (methanol)	Scott *et al.*, 2006	-51.74	-43.38	-45.86	-47.16
HB18	Heterotrophic bacteria	Organotroph	NA	*Sulfolobus*	Scott *et al.*, 2006	-30.09	-25.54	-31.70	-27.79
HB19	Heterotrophic bacteria	Fermenter	NA	*C. acetobutylicum*	Scott *et al.*, 2006	-30.48	-29.92	-32.37	-29.56
HB20	Heterotrophic bacteria	Organotroph	NA	*Thermotoga*	Scott *et al.*, 2006	-22.54	-23.73	-26.89	-27.57
HB21	Heterotrophic bacteria	Acetotroph	NA	*Desulfomaculum*	Scott *et al.*, 2006	-29.19	-28.22	-29.42	-27.64
HB22	Heterotrophic bacteria	Fermenter	NA	*C. beijerrinckii*	Scott *et al.*, 2006	-29.77	-28.29	-30.78	-26.76
MI1	Microalgae	NA	Chlorophyte	*Dunaliella sp.*	Larsen *et al.*, 2013	-19.10	-15.80	-23.70	-19.70
MI2	Microalgae	NA	Chlorophyte	*P. marinus*	Larsen *et al.*, 2013	-20.60	-15.30	-23.30	-21.40

ID	*A priori*-defined group	Metabolism	Phylogeny	Species	Reference	Val	Ileu	Leu	Phe
MI3	Microalgae	NA	Haptophyte	*E. huxleyi*	Larsen *et al.*, 2013	-24.90	-18.30	-27.20	-23.20
MI4	Microalgae	NA	Haptophyte	*E. huxleyi*	Larsen *et al.*, 2013	-21.00	-19.20	-23.80	-24.60
MI5	Microalgae	NA	Haptophyte	*I. galbana*	Larsen *et al.*, 2013	-26.80	-18.30	-31.40	-25.00
MI6	Microalgae	NA	Diatom	*M. varians*	Larsen *et al.*, 2013	-19.70	-16.50	-22.10	-20.60
MI7	Microalgae	NA	Diatom	*T. weissflogii*	Larsen *et al.*, 2015	-28.80	-21.70	-31.30	-29.60
MI8	Microalgae	NA	Diatom	*T. weissflogii*	Larsen *et al.*, 2015	-28.10	-21.90	-31.40	-29.70
MI9	Microalgae	NA	Diatom	*T. weissflogii*	Larsen *et al.*, 2015	-28.20	-21.20	-31.10	-29.50
MA1	Macroalgae	NA	Rodophyta	*Prionitis sp.*	Larsen *et al.*, 2013	-19.20	-17.30	-20.20	-19.20
MA2	Macroalgae	NA	Rodophyta	*O. spectabilis*	Larsen *et al.*, 2013	-21.30	-15.40	-19.50	-20.70
MA3	Macroalgae	NA	Rodophyta	*C. caniculatus*	Larsen *et al.*, 2013	-25.40	-21.70	-25.80	-25.30
MA4	Macroalgae	NA	Rodophyta	*Calliathron sp.*	Larsen *et al.*, 2013	-19.80	-17.00	-21.90	-23.70
MA5	Macroalgae	NA	Rodophyta	*Corallina sp.*	Larsen *et al.*, 2013	-22.40	-19.50	-22.50	-25.30
MA6	Macroalgae	NA	Rodophyta	*O. floccosa*	Larsen *et al.*, 2013	-20.70	-16.50	-21.00	-21.20
MA7	Macroalgae	NA	Rodophyta	*Mastocarpus sp.*	Larsen *et al.*, 2013	-20.30	-16.70	-21.00	-21.10
MA8	Macroalgae	NA	Rodophyta	*E. muricata*	Larsen *et al.*, 2013	-23.60	-18.00	-23.50	-22.00
MA9	Macroalgae	NA	Rodophyta	*M. flaccida*	Larsen *et al.*, 2013	-20.90	-20.40	-23.40	-22.50
MA10	Macroalgae	NA	Phaeophyceae	*M. pyrifera*	Larsen *et al.*, 2013	-18.80	-17.60	-23.10	-19.40
MA11	Macroalgae	NA	Phaeophyceae	*M. pyrifera*	Larsen *et al.*, 2013	-17.00	-15.20	-21.50	-19.10
MA12	Macroalgae	NA	Phaeophyceae	*M. pyrifera*	Larsen *et al.*, 2013	-20.70	-19.60	-24.80	-22.20
MA13	Macroalgae	NA	Phaeophyceae	*M. pyrifera*	Larsen *et al.*, 2013	-15.70	-16.80	-20.00	-18.90
MA14	Macroalgae	NA	Phaeophyceae	*M. pyrifera*	Larsen *et al.*, 2013	-22.50	-21.40	-26.10	-23.90
MA15	Macroalgae	NA	Phaeophyceae	*Scytosiphon sp.*	Larsen *et al.*, 2013	-10.40	-6.30	-13.30	-12.80
MA16	Macroalgae	NA	Phaeophyceae	*Laminaria sp.*	Larsen *et al.*, 2013	-19.10	-15.60	-23.90	-18.80
MA17	Macroalgae	NA	Phaeophyceae	*Silvetia sp.*	Larsen *et al.*, 2013	-19.60	-19.50	-25.50	-20.40
MA18	Macroalgae	NA	Phaeophyceae	*Petrospongius sp.*	Larsen *et al.*, 2013	-14.50	-10.90	-18.30	-16.70
MA19	Macroalgae	NA	Phaeophyceae	*Peletiopsis sp.*	Larsen *et al.*, 2013	-21.20	-16.90	-23.60	-23.60
MA20	Macroalgae	NA	Phaeophyceae	*Ralfsia sp.*	Larsen *et al.*, 2013	-10.90	-7.30	-14.70	-12.70
MA21	Macroalgae	NA	Phaeophyceae	*C. osmundacea*	Larsen *et al.*, 2013	-22.40	-17.60	-25.20	-21.20
S1	Seagrasses	NA	Posidoniaceae	*P. oceanica*	Larsen *et al.*, 2013	-17.30	-13.90	-19.50	-14.10
S2	Seagrasses	NA	Posidoniaceae	*P. oceanica*	Larsen *et al.*, 2013	-18.30	-14.50	-20.30	-15.10
S3	Seagrasses	NA	Posidoniaceae	*P. oceanica*	Larsen *et al.*, 2013	-19.40	-14.50	-21.70	-15.60
S4	Seagrasses	NA	Posidoniaceae	*P. oceanica*	Larsen *et al.*, 2013	-20.10	-14.90	-22.40	-17.60
S5	Seagrasses	NA	Posidoniaceae	*P. oceanica*	Larsen *et al.*, 2013	-19.50	-15.10	-22.50	-16.50
S6	Seagrasses	NA	Zosteraceae	*P. scouleri*	Larsen *et al.*, 2013	-20.10	-17.50	-21.40	-17.00
S7	Seagrasses	NA	Zosteraceae	*P. torreyi*	Larsen *et al.*, 2013	-21.00	-19.80	-23.10	-17.60
TP1	Terrestrial plants	NA	Fagaceae	*Q. robur*	Larsen *et al.*, 2013	-37.10	-29.20	-38.40	-32.50
TP2	Terrestrial plants	NA	Betulaceae	*A. glutinosa*	Larsen *et al.*, 2013	-36.10	-30.70	-39.70	-33.90
TP3	Terrestrial plants	NA	Salicaceae	*Salix sp.*	Larsen *et al.*, 2013	-31.40	-24.20	-34.40	-27.00
TP4	Terrestrial plants	NA	Polygonaceae	*P. viviparum*	Larsen *et al.*, 2013	-33.30	-27.40	-35.30	-28.80
TP5	Terrestrial plants	NA	Cyperaceae	*C. aquatilis*	Larsen *et al.*, 2013	-31.60	-26.80	-33.50	-27.70
TP6	Terrestrial plants	NA	Poaceae	*C. canadensis*	Larsen *et al.*, 2013	-32.00	-27.10	-34.50	-28.90
TP7	Terrestrial plants	NA	Menyanthaceae	*M. trifoliata*	Larsen *et al.*, 2013	-32.20	-27.50	-33.60	-28.70
TP8	Terrestrial plants	NA	Betulacea	*B. nana*	Larsen *et al.*, 2013	-30.60	-25.20	-35.20	-27.80
TP9	Terrestrial plants	NA	Cyperaceae	*C. utriculata*	Larsen *et al.*, 2013	-32.60	-27.80	-35.40	-28.90
TP10	Terrestrial plants	NA	Malpighiales	*S. reticulata*	Larsen *et al.*, 2013	-30.50	-25.10	-34.50	-26.40

ID	*A priori*-defined group	Metabolism	Phylogeny	Species	Reference	Val	Ileu	Leu	Phe
TP11	Terrestrial plants	NA	Cyperaceae	*E. angustifolium*	Larsen *et al.*, 2013	-30.00	-23.20	-33.00	-27.00
TP12	Terrestrial plants	NA	Polygonaceae	*R. arcticus*	Larsen *et al.*, 2013	-34.10	-27.60	-37.20	-29.90
TP13	Terrestrial plants	NA	Anthophyta	*C. purpuracens*	Larsen *et al.*, 2009	-35.80	-32.10	-38.60	-31.00
TP14	Terrestrial plants	NA	Anthophyta	*C. annum*	Larsen *et al.*, 2009	-36.70	-35.10	-41.80	-33.80
TP15	Terrestrial plants	NA	Anthophyta	*C. bigelowii*	Larsen *et al.*, 2009	-37.70	-33.90	-43.20	-31.70
TP16	Terrestrial plants	NA	Anthophyta	*C. sativus*	Larsen *et al.*, 2009	-35.60	-30.60	-37.40	-32.90
TP17	Terrestrial plants	NA	Anthophyta	*H. annuus*	Larsen *et al.*, 2009	-38.10	-31.80	-39.60	-30.20
TP18	Terrestrial plants	NA	Anthophyta	*O. vulgare*	Larsen *et al.*, 2009	-36.60	-32.10	-38.70	-32.50
TP19	Terrestrial plants	NA	Anthophyta	*S. lycopersicum*	Larsen *et al.*, 2009	-36.80	-31.20	-39.30	-32.60
TP20	Terrestrial plants	NA	Anthophyta	*V. uglinosum*	Larsen *et al.*, 2009	-39.30	-35.20	-40.70	-33.80
TP21	Terrestrial plants	NA	Pteridophyta	*E. pratense*	Larsen *et al.*, 2009	-36.00	-31.10	-37.40	-29.70
TP22	Terrestrial plants	NA	Pteridophyta	*E. scirpoides*	Larsen *et al.*, 2009	-41.30	-35.80	-44.40	-37.30

Table 4.B2 Literature-derived data for $\delta^{13}C_{EAA}$ values for various consumers, including corals and zooplankton from the North Pacific Subtropical Gyre, mussels from a littoral system by the Californian shore, pelagic fish from the central North Pacific, herrings and cod from the North Atlantic, and penguins captive-reared and from the Southern Ocean. Prior to classify unknown consumer samples within end-member groups, $\delta^{13}C_{EAA}$ values were sample-normalised ($\delta^{13}C_{norm\text{-}EAA}$).

ID	Organism	Phylogeny	Species	Reference	Val	Ileu	Leu	Phe
C1	Coral	Parazoanthidae	*K. haumeaae*	McMahon *et al.*, 2015a	-29.50	-24.30	-31.90	-33.30
C2	Coral	Parazoanthidae	*K. haumeaae*	McMahon *et al.*, 2015a	-26.00	-21.10	-28.90	-30.20
C3	Coral	Parazoanthidae	*K. haumeaae*	McMahon *et al.*, 2015a	-24.30	-20.10	-28.10	-28.60
C4	Coral	Parazoanthidae	*K. haumeaae*	McMahon *et al.*, 2015a	-22.50	-28.80	-26.50	-28.00
C5	Coral	Parazoanthidae	*K. haumeaae*	McMahon *et al.*, 2015a	-23.90	-20.40	-28.60	-27.10
C6	Coral	Parazoanthidae	*K. haumeaae*	McMahon *et al.*, 2015a	-23.70	-20.40	-27.30	-22.70
C7	Coral	Parazoanthidae	*K. haumeaae*	McMahon *et al.*, 2015a	-23.60	-20.30	-26.00	-22.50
C8	Coral	Parazoanthidae	*K. haumeaae*	McMahon *et al.*, 2015a	-24.70	-20.50	-26.60	-23.00
C9	Coral	Parazoanthidae	*K. haumeaae*	McMahon *et al.*, 2015a	-24.30	-21.10	-28.50	-25.30
C10	Coral	Parazoanthidae	*K. haumeaae*	McMahon *et al.*, 2015a	-22.30	-21.10	-30.30	-26.80
C11	Coral	Parazoanthidae	*K. haumeaae*	McMahon *et al.*, 2015a	-23.20	-21.10	-30.80	-26.00
C12	Coral	Parazoanthidae	*K. haumeaae*	McMahon *et al.*, 2015a	-23.90	-21.80	-29.60	-28.10
C13	Coral	Parazoanthidae	*K. haumeaae*	McMahon *et al.*, 2015a	-25.70	-22.90	-30.90	-29.70
C14	Coral	Parazoanthidae	*K. haumeaae*	McMahon *et al.*, 2015a	-26.20	-24.10	-31.80	-31.80
C15	Coral	Parazoanthidae	*K. haumeaae*	McMahon *et al.*, 2015a	-24.10	-20.10	-28.40	-24.20
C16	Coral	Parazoanthidae	*K. haumeaae*	McMahon *et al.*, 2015a	-24.10	-20.80	-27.80	-23.70
C17	Coral	Parazoanthidae	*K. haumeaae*	McMahon *et al.*, 2015a	-23.90	-20.30	-26.30	-22.30
C18	Coral	Parazoanthidae	*K. haumeaae*	McMahon *et al.*, 2015a	-24.80	-20.80	-27.20	-22.50
C19	Coral	Parazoanthidae	*K. haumeaae*	McMahon *et al.*, 2015a	-21.80	-20.10	-27.20	-24.10
C20	Coral	Parazoanthidae	*K. haumeaae*	McMahon *et al.*, 2015a	-24.10	-20.90	-29.20	-26.20
C21	Coral	Parazoanthidae	*K. haumeaae*	McMahon *et al.*, 2015a	-22.90	-21.30	-28.60	-27.20
C22	Coral	Parazoanthidae	*K. haumeaae*	McMahon *et al.*, 2015a	-24.30	-22.10	-29.80	-26.10
C23	Coral	Parazoanthidae	*K. haumeaae*	McMahon *et al.*, 2015a	-23.60	-21.70	-29.90	-27.50
C24	Coral	Parazoanthidae	*K. haumeaae*	McMahon *et al.*, 2015a	-26.00	-22.10	-30.10	-28.70
C25	Coral	Parazoanthidae	*K. haumeaae*	McMahon *et al.*, 2015a	-25.90	-23.80	-30.50	-29.60
C26	Coral	Parazoanthidae	*K. haumeaae*	McMahon *et al.*, 2015a	-28.90	-25.20	-33.90	-32.90
C27	Coral	Parazoanthidae	*K. haumeaae*	McMahon *et al.*, 2015a	-29.70	-26.60	-34.20	-34.20
C28	Coral	Parazoanthidae	*K. haumeaae*	McMahon *et al.*, 2015a	-28.60	-22.70	-30.50	-32.10
C29	Coral	Parazoanthidae	*K. haumeaae*	McMahon *et al.*, 2015a	-27.20	-21.40	-28.90	-30.90
C30	Coral	Parazoanthidae	*K. haumeaae*	McMahon *et al.*, 2015a	-24.20	-20.80	-26.60	-28.10
C31	Coral	Parazoanthidae	*K. haumeaae*	McMahon *et al.*, 2015a	-24.00	-19.10	-25.60	-23.00
C32	Coral	Parazoanthidae	*K. haumeaae*	McMahon *et al.*, 2015a	-22.50	-18.00	-24.20	-21.30
C33	Coral	Parazoanthidae	*K. haumeaae*	McMahon *et al.*, 2015a	-24.00	-19.00	-24.40	-22.20
C34	Coral	Parazoanthidae	*K. haumeaae*	McMahon *et al.*, 2015a	-23.50	-20.50	-26.40	-25.30
C35	Coral	Parazoanthidae	*K. haumeaae*	McMahon *et al.*, 2015a	-22.00	-19.70	-28.00	-27.90
C36	Coral	Parazoanthidae	*K. haumeaae*	McMahon *et al.*, 2015a	-23.10	-18.50	-26.90	-25.70
C37	Coral	Parazoanthidae	*K. haumeaae*	McMahon *et al.*, 2015a	-23.70	-19.70	-27.70	-25.50
C38	Coral	Parazoanthidae	*K. haumeaae*	McMahon *et al.*, 2015a	-22.90	-21.10	-29.10	-28.70
C39	Coral	Parazoanthidae	*K. haumeaae*	McMahon *et al.*, 2015a	-24.40	-21.50	-30.30	-30.30

ID	Organism	Phylogeny	Species	Reference	Val	Ileu	Leu	Phe
C40	Coral	Parazoanthidae	*K. haumeaae*	McMahon *et al.*, 2015a	-25.10	-21.80	-29.40	-29.40
C41	Coral	Parazoanthidae	*K. haumeaae*	McMahon *et al.*, 2015a	-24.60	-21.70	-30.10	-29.40
M1	Mussel	Mytilidae	*M. californianus*	Larsen *et al.*, 2013	-23.20	-18.60	-25.10	-24.20
M2	Mussel	Mytilidae	*M. californianus*	Larsen *et al.*, 2013	-21.50	-16.80	-23.40	-22.50
Z1	Zooplankton	NA	NA	Hannides *et al.*, 2013	-22.80	-18.70	-25.40	-25.50
Z2	Zooplankton	NA	NA	Hannides *et al.*, 2013	-23.50	-17.20	-25.40	-27.10
Z3	Zooplankton	NA	NA	Hannides *et al.*, 2013	-24.70	-17.70	-26.40	-28.30
Z4	Zooplankton	NA	NA	Hannides *et al.*, 2013	-23.20	-17.70	-24.80	-26.30
Z5	Zooplankton	NA	NA	Hannides *et al.*, 2013	-22.50	-17.40	-24.70	-25.10
Z6	Zooplankton	NA	NA	Hannides *et al.*, 2013	-24.20	-19.30	-25.50	-24.60
Z7	Zooplankton	NA	NA	Hannides *et al.*, 2013	-24.40	-19.00	-26.10	-26.70
Z8	Zooplankton	NA	NA	Hannides *et al.*, 2013	-24.40	-18.90	-25.30	-25.10
FH1	Herring (mean, n=10)	Clupeidae	*C. harengus*	McMahon *et al.*, 2015b	-20.90	-11.60	-27.00	-24.30
FC1	Cod (mean)	Gadidae	*G. morhua*	Houghton, *unpubl. data*	-23.60	-16.70	-26.80	-25.70
FP1	Pelagic fish	Coryphaenidae	*C. hippurus*	Larsen *et al.*, 2013	-22.10	-18.40	-25.40	-26.70
FP2	Pelagic fish	Lampridae	*L. guttatus*	Larsen *et al.*, 2013	-22.70	-20.30	-27.10	-27.80
FP3	Pelagic fish	Xiphiidae	*X. gladius*	Larsen *et al.*, 2013	-23.20	-20.10	-27.70	-27.10
P1	Penguin (mean, n=5)	Spheniscidae	*P. papua*	McMahon *et al.*, 2015b	-20.60	-11.70	-27.20	-24.30
P2	Penguin (mean, n=5)	Spheniscidae	*P. papua*	McMahon *et al.*, 2015b	-24.10	-14.90	-26.30	-23.90

Table 4.B3 Literature-derived data for $\delta^{13}C_{EAA}$ values for particulate organic matter sampled in the North Pacific Subtropical Gyre and North and South Atlantic at various depths. Prior to classify unknown organic matter within end-member groups, $\delta^{13}C_{EAA}$ values were sample-normalised ($\delta^{13}C_{norm\text{-}EAA}$).

ID	Compound	Area	Depth	Reference	Val	Ileu	Leu	Phe
OM1	Particulate organic matter	North Pacific Subtropical Gyre	25	Hannides *et al.*, 2013	-26.70	-19.20	-25.30	-25.50
OM2	Particulate organic matter	North Pacific Subtropical Gyre	75	Hannides *et al.*, 2013	-19.10	-21.80	-28.10	-27.80
OM3	Particulate organic matter	North Pacific Subtropical Gyre	400	Hannides *et al.*, 2013	-23.10	-17.80	-23.40	-23.90
OM4	Particulate organic matter	North Pacific Subtropical Gyre	750	Hannides *et al.*, 2013	-24.90	-18.00	-24.60	-25.70
OM5	Particulate organic matter	North Atlantic	5	Sabadel, *unpubl. data*	-32.10	-25.30	-39.70	-23.20
OM6	Particulate organic matter	North Atlantic	15	Sabadel, *unpubl. data*	-26.80	-25.10	-43.80	-26.80
OM7	Particulate organic matter	North Atlantic	20	Sabadel, *unpubl. data*	-28.90	-23.70	-37.30	-22.10
OM8	Particulate organic matter	North Atlantic	25	Sabadel, *unpubl. data*	-31.10	-24.50	-37.90	-23.20
OM9	Particulate organic matter	North Atlantic	35	Sabadel, *unpubl. data*	-24.90	-25.10	-44.30	-24.70
OM10	Particulate organic matter	North Atlantic	40	Sabadel, *unpubl. data*	-32.70	-26.10	-39.00	-22.80
OM11	Particulate organic matter	North Atlantic	50	Sabadel, *unpubl. data*	-31.00	-25.10	-39.30	-23.00
OM12	Particulate organic matter	North Atlantic	55	Sabadel, *unpubl. data*	-29.20	-25.10	-37.90	-23.00
OM13	Particulate organic matter	North Atlantic	60	Sabadel, *unpubl. data*	-27.50	-24.20	-37.10	-21.60
OM14	Particulate organic matter	North Atlantic	100	Sabadel, *unpubl. data*	-22.60	-21.40	-36.70	-18.00
OM15	Particulate organic matter	North Atlantic	1000	Sabadel, *unpubl. data*	-23.50	-17.00	-33.40	-17.90
OM16	Particulate organic matter	North Atlantic	2500	Sabadel, *unpubl. data*	-22.90	-11.50	-31.40	-15.80
OM17	Particulate organic matter	North Atlantic	5	Sabadel, *unpubl. data*	-32.20	-26.90	-39.10	-23.90
OM18	Particulate organic matter	North Atlantic	15	Sabadel, *unpubl. data*	-33.60	-28.50	-45.70	-28.90
OM19	Particulate organic matter	North Atlantic	25	Sabadel, *unpubl. data*	-30.30	-24.40	-38.10	-22.10
OM20	Particulate organic matter	North Atlantic	35	Sabadel, *unpubl. data*	-29.20	-23.20	-38.50	-22.20
OM21	Particulate organic matter	North Atlantic	40	Sabadel, *unpubl. data*	-32.50	-26.10	-39.20	-20.80
OM22	Particulate organic matter	North Atlantic	45	Sabadel, *unpubl. data*	-32.10	-26.80	-40.50	-22.60
OM23	Particulate organic matter	North Atlantic	50	Sabadel, *unpubl. data*	-33.10	-27.70	-40.00	-23.80
OM24	Particulate organic matter	North Atlantic	55	Sabadel, *unpubl. data*	-31.50	-26.40	-38.80	-21.40
OM25	Particulate organic matter	North Atlantic	60	Sabadel, *unpubl. data*	-33.70	-27.80	-41.40	-23.70
OM26	Particulate organic matter	North Atlantic	80	Sabadel, *unpubl. data*	-30.50	-26.50	-36.90	-21.10
OM27	Particulate organic matter	North Atlantic	100	Sabadel, *unpubl. data*	-28.90	-23.40	-37.10	-19.40
OM28	Particulate organic matter	North Atlantic	800	Sabadel, *unpubl. data*	-28.90	-24.50	-36.50	-20.60
OM29	Particulate organic matter	North Atlantic	1000	Sabadel, *unpubl. data*	-27.30	-21.10	-35.00	-19.30
OM30	Particulate organic matter	North Atlantic	2500	Sabadel, *unpubl. data*	-28.80	-26.30	-34.90	-24.00
OM31	Particulate organic matter	North Atlantic	4000	Sabadel, *unpubl. data*	-28.50	-23.50	-34.30	-23.30
OM32	Particulate organic matter	South Atlantic	98.8	Sabadel, *unpubl. data*	-34.40	-29.60	-40.80	-27.00
OM33	Particulate organic matter	South Atlantic	44.2	Sabadel, *unpubl. data*	-37.40	-27.40	-44.30	-32.10
OM34	Particulate organic matter	South Atlantic	19	Sabadel, *unpubl. data*	-37.60	-28.50	-40.90	-31.70
OM35	Particulate organic matter	South Atlantic	4.1	Sabadel, *unpubl. data*	-35.60	-27.40	-40.60	-30.70
OM36	Particulate organic matter	South Atlantic	994.3	Sabadel, *unpubl. data*	-36.60	-19.20	-36.20	-24.10
OM37	Particulate organic matter	South Atlantic	297.2	Sabadel, *unpubl. data*	-35.10	-26.90	-37.40	-23.50
OM38	Particulate organic matter	South Atlantic	57.5	Sabadel, *unpubl. data*	-38.10	-32.30	-53.40	-36.70
OM39	Particulate organic matter	South Atlantic	46.4	Sabadel, *unpubl. data*	-35.20	-26.10	-39.40	-28.50
OM40	Particulate organic matter	South Atlantic	53.8	Sabadel, *unpubl. data*	-36.30	-25.20	-41.30	-27.50
OM41	Particulate organic matter	South Atlantic	41.4	Sabadel, *unpubl. data*	-42.40	-29.80	-43.90	-33.10
OM42	Particulate organic matter	South Atlantic	33.7	Sabadel, *unpubl. data*	-41.30	-30.00	-46.00	-34.20

ID	Compound	Area	Depth	Reference	Val	Ileu	Leu	Phe
OM43	Particulate organic matter	South Atlantic	4.1	Sabadel, *unpubl. data*	-43.90	-33.70	-47.20	-36.50
OM44	Particulate organic matter	South Atlantic	136.5	Sabadel, *unpubl. data*	-39.00	-25.90	-40.00	-23.30
OM45	Particulate organic matter	South Atlantic	96.2	Sabadel, *unpubl. data*	-41.90	-32.30	-48.40	-30.50
OM46	Particulate organic matter	South Atlantic	55	Sabadel, *unpubl. data*	-35.70	-24.10	-41.70	-28.40
OM47	Particulate organic matter	South Atlantic	35.7	Sabadel, *unpubl. data*	-34.10	-25.00	-39.90	-28.50
OM48	Particulate organic matter	South Atlantic	0.5	Sabadel, *unpubl. data*	-36.80	-27.20	-41.50	-29.30
OM49	Particulate organic matter	South Atlantic	98.1	Sabadel, *unpubl. data*	-31.20	-22.50	-38.40	-23.60
OM50	Particulate organic matter	South Atlantic	68.3	Sabadel, *unpubl. data*	-32.00	-19.80	-40.50	-24.40
OM51	Particulate organic matter	South Atlantic	41.1	Sabadel, *unpubl. data*	-31.80	-20.80	-38.70	-25.50
OM52	Particulate organic matter	South Atlantic	0.8	Sabadel, *unpubl. data*	-31.30	-23.00	-38.90	-25.10
OM53	Particulate organic matter	South Atlantic	99.5	Sabadel, *unpubl. data*	-31.80	-22.40	-38.30	-22.70
OM54	Particulate organic matter	South Atlantic	65.2	Sabadel, *unpubl. data*	-31.60	-22.00	-41.90	-25.20
OM55	Particulate organic matter	South Atlantic	56.1	Sabadel, *unpubl. data*	-34.60	-25.30	-41.80	-26.00
OM56	Particulate organic matter	South Atlantic	4.9	Sabadel, *unpubl. data*	-33.00	-25.80	-37.50	-24.60
OM57	Particulate organic matter	South Atlantic	79.6	Sabadel, *unpubl. data*	-31.20	-22.30	-37.40	-21.90
OM58	Particulate organic matter	South Atlantic	48	Sabadel, *unpubl. data*	-33.40	-24.90	-39.60	-31.40
OM59	Particulate organic matter	South Atlantic	6.1	Sabadel, *unpubl. data*	-35.10	-25.30	-36.80	-31.50
OM60	Particulate organic matter	South Atlantic	199.6	Sabadel, *unpubl. data*	-36.60	-28.90	-36.30	-30.00
OM61	Particulate organic matter	South Atlantic	149.8	Sabadel, *unpubl. data*	-36.30	-27.60	-39.60	-34.10
OM62	Particulate organic matter	South Atlantic	114.9	Sabadel, *unpubl. data*	-35.70	-26.20	-40.50	-28.40
OM63	Particulate organic matter	South Atlantic	90	Sabadel, *unpubl. data*	-35.70	-26.70	-39.90	-30.80
OM64	Particulate organic matter	South Atlantic	43.8	Sabadel, *unpubl. data*	-36.60	-25.80	-38.40	-33.00
OM65	Particulate organic matter	South Atlantic	5.4	Sabadel, *unpubl. data*	-36.60	-26.80	-38.70	-32.10
OM66	Particulate organic matter	South Atlantic	114.5	Sabadel, *unpubl. data*	-37.20	-25.80	-37.30	-28.40
OM67	Particulate organic matter	South Atlantic	94.7	Sabadel, *unpubl. data*	-35.60	-26.20	-39.80	-31.00
OM68	Particulate organic matter	South Atlantic	82.5	Sabadel, *unpubl. data*	-35.30	-25.10	-39.80	-31.00
OM69	Particulate organic matter	South Atlantic	0	Sabadel, *unpubl. data*	-31.80	-21.30	-34.50	-31.70

Appendix 4.C – Essential amino acids results

Table 4.C1 Results for principal component analysis (PCA) with raw and normalised carbon isotopic compositions of essential amino acids ($\delta^{13}C_{EAA}$ and $\delta^{13}C_{norm\text{-}EAA}$, respectively) for shark samples; for PCA outputs, see Fig. 4.5 and 4.6). Sample ID is given by individual ID and sample ID (IDs of single samples within combinations).

A) Importance of components

	$\delta^{13}C_{EAA}$				$\delta^{13}C_{norm\text{-}EAA}$			
	PC1	**PC2**	**PC3**	**PC4**	**PC1**	**PC2**	**PC3**	**PC4**
Standard deviation	1.70	0.73	0.59	0.48	1.28	1.11	1.06	$2.08*10^{-15}$
Proportion of variance	0.72	0.13	0.09	0.05	0.41	0.31	0.28	0.00
Cumulative proportion	0.72	0.85	0.94	1.00	0.41	0.72	1.00	1.00

B) Vector scores

	$\delta^{13}C_{EAA}$				$\delta^{13}C_{norm\text{-}EAA}$			
	PC1	**PC2**	**PC3**	**PC4**	**PC1**	**PC2**	**PC3**	**PC4**
Valine	0.50	-0.33	0.71	0.35	0.59	-0.49	-0.34	-0.54
Isoleucine	0.47	0.75	-0.19	0.42	-0.67	0.14	-0.46	-0.57
Leucine	0.53	0.15	0.10	-0.82	-0.27	-0.42	0.77	-0.40
Phenylalanine	0.49	-0.55	-0.67	0.13	0.36	0.75	0.29	-0.47

C) Sample scores

	$\delta^{13}C_{EAA}$				$\delta^{13}C_{norm\text{-}EAA}$			
Sample ID	**PC1**	**PC2**	**PC3**	**PC4**	**PC1**	**PC2**	**PC3**	**PC4**
16_1+2+3	-2.341	0.877	-0.013	0.171	-1.195	0.709	-0.532	0.000
16_4+5	-2.380	1.035	-0.512	-0.306	-2.008	1.098	0.606	0.000
16_6	-2.241	1.578	-0.149	0.293	-2.373	0.812	-0.982	0.000
16_7+8	-4.309	1.408	-0.136	-1.009	-2.585	0.577	1.824	0.000
16_9	-1.713	0.625	-0.672	0.209	-1.237	1.579	-0.247	0.000
16_10	-3.461	0.705	0.070	-0.196	-0.966	0.727	0.298	0.000
16_11	-2.754	-0.196	-0.339	0.657	0.604	1.917	-0.943	0.000
16_12	-3.275	1.012	0.562	-0.282	-1.202	-0.204	0.121	0.000
16_13	-2.541	0.687	-0.696	-0.058	-1.429	1.680	0.329	0.000
16_14	-2.045	0.229	-0.706	0.113	-0.638	1.757	0.129	0.000
16_15	-1.961	0.212	-0.015	0.338	-0.059	0.855	-0.644	0.000
16_16	-1.314	0.952	0.583	-0.969	-1.557	-1.350	1.410	0.000
16_17	-1.835	0.246	0.288	-0.040	-0.111	0.082	-0.038	0.000
16_18	-1.484	0.559	0.075	-0.080	-0.801	0.190	0.004	0.000
16_19	-1.458	0.504	0.628	0.007	-0.311	-0.576	-0.408	0.000
24_1+2+3	-0.658	0.299	0.447	0.899	0.288	0.116	-2.097	0.000
24_4+5+6	-2.152	0.414	0.104	0.960	0.007	1.137	-2.021	0.000
24_7+8	-1.576	0.198	0.214	0.925	0.374	0.807	-1.952	0.000
24_9+10	-1.252	-0.348	-0.910	0.260	0.186	2.038	0.096	0.000
24_11	-1.759	-0.622	-0.432	0.339	1.015	1.601	-0.156	0.000
24_12	-1.820	-0.147	0.210	-0.037	0.478	0.284	0.137	0.000
24_13	-1.016	-0.900	-0.080	-0.258	1.354	0.467	0.951	0.000
24_14	-1.899	-0.426	-0.192	0.677	1.027	1.484	-1.015	0.000
24_15	-2.056	-0.602	0.229	0.505	1.512	0.817	-0.786	0.000
24_16	-1.902	-0.106	0.240	0.533	0.716	0.661	-1.040	0.000
24_17	-1.104	-0.110	0.658	0.712	1.027	-0.099	-1.639	0.000
24_18	-1.725	-0.235	-0.269	-0.229	0.211	0.855	0.771	0.000
24_19	-1.164	-0.234	0.084	-0.172	0.429	0.182	0.461	0.000
24_20	-0.703	-0.049	0.553	0.658	0.808	-0.124	-1.527	0.000
24_21	-0.080	0.130	0.779	0.365	0.477	-0.914	-1.141	0.000
12_1+2+3	-0.906	1.504	0.801	0.145	-1.797	-1.138	-1.171	0.000
12_4+5	-2.827	0.880	0.390	0.332	-0.827	0.375	-1.017	0.000
12_6	-2.849	-0.186	0.069	0.558	0.811	1.262	-0.929	0.000
12_7	-3.117	0.904	0.518	0.961	-0.457	0.719	-2.341	0.000
12_8+9	-2.326	0.753	0.750	0.964	-0.113	0.150	-2.442	0.000
12_10+11	-0.823	-0.219	-0.592	0.314	0.180	1.430	-0.233	0.000
12_12	-1.062	0.102	0.283	0.446	0.307	0.216	-1.010	0.000
12_13	-0.776	0.764	0.458	0.165	-0.814	-0.488	-0.784	0.000
12_14	-0.128	0.779	0.805	0.611	-0.437	-0.906	-1.889	0.000
12_15	-2.709	-0.246	0.948	0.044	1.218	-0.458	-0.281	0.000
12_16	-1.790	-0.316	0.960	0.278	1.392	-0.593	-0.786	0.000
12_17	-1.310	0.886	0.578	-0.100	-1.027	-0.710	-0.320	0.000

	$\delta^{13}C_{EAA}$				$\delta^{13}C_{norm\text{-}EAA}$			
Sample ID	**PC1**	**PC2**	**PC3**	**PC4**	**PC1**	**PC2**	**PC3**	**PC4**
101_1+2+3	-3.172	0.023	0.803	-0.122	0.636	-0.267	0.047	0.000
101_4	-4.167	-1.288	0.353	-0.589	2.315	0.691	1.742	0.000
101_5	-3.337	-0.639	-0.065	0.294	1.364	1.535	-0.136	0.000
101_6	-1.496	-0.806	-0.635	0.292	1.143	1.828	0.088	0.000
101_7	-2.871	-0.060	0.204	0.093	0.467	0.708	-0.097	0.000
101_8	-2.113	-0.109	-1.938	0.309	-0.789	3.846	0.433	0.000
101_9	-2.253	0.467	0.144	-0.053	-0.542	0.376	-0.006	0.000
101_10	-3.567	-1.184	-0.206	0.472	2.262	2.069	-0.216	0.000
101_11	-3.419	-0.259	0.227	0.206	0.898	0.977	-0.232	0.000
101_12	-1.642	-0.639	-1.044	0.312	0.624	2.468	0.183	0.000
101_13	-1.556	-1.187	0.084	0.123	2.149	0.730	0.242	0.000
101_14	-2.688	-0.574	0.109	-1.062	0.666	0.082	2.462	0.000
101_15	-2.523	-0.593	0.772	-0.037	1.617	-0.234	0.081	0.000
101_16	-1.610	0.282	-1.100	-0.204	-1.165	1.971	0.907	0.000
131_1+2	-1.381	-0.096	0.329	0.463	0.689	0.306	-0.973	0.000
131_3	-1.846	0.068	-1.047	1.292	-0.035	3.079	-2.049	0.000
131_4+5	-2.443	-0.227	0.593	0.240	1.035	0.125	-0.537	0.000
131_6+7	-0.333	0.729	-0.643	0.178	-1.494	1.040	-0.313	0.000
131_8	-0.555	0.202	-0.115	0.210	-0.263	0.459	-0.415	0.000
131_9	-1.639	-0.058	-1.526	0.179	-0.699	2.968	0.458	0.000
131_10	-2.307	0.047	-0.324	0.096	-0.085	1.296	0.069	0.000
131_11	-0.236	0.733	-1.238	-0.513	-2.232	1.411	1.350	0.000
131_12	-0.855	-1.051	-0.130	0.647	2.000	1.167	-0.808	0.000
131_13	-0.961	-0.836	-0.582	0.728	1.403	1.892	-0.838	0.000
131_14	-1.842	-0.277	-0.460	0.193	0.370	1.490	0.029	0.000
131_15	-0.306	-0.110	-0.720	0.373	-0.085	1.472	-0.364	0.000
131_16	-1.152	0.644	0.486	-0.461	-0.881	-0.826	0.535	0.000
131_17	0.575	0.447	-0.495	-0.434	-1.299	0.150	0.908	0.000
33_1+2+3	0.682	1.345	0.365	-0.366	-2.176	-1.329	0.034	0.000
33_4+5	-0.756	0.857	-0.480	-0.869	-2.081	0.159	1.702	0.000
33_6+7	-0.438	1.276	-0.729	-1.099	-3.057	0.174	2.109	0.000
33_8+9	-0.909	2.014	0.488	-0.826	-3.303	-1.471	0.747	0.000
33_10	0.154	1.734	0.518	-0.663	-2.819	-1.685	0.448	0.000
33_11	-0.627	0.533	0.637	0.348	-0.242	-0.624	-1.161	0.000
33_12	0.245	0.590	-0.103	0.255	-0.919	0.126	-0.701	0.000
33_13	-0.900	0.938	0.068	-0.345	-1.591	-0.262	0.369	0.000
33_14	-0.933	0.970	0.146	-0.319	-1.578	-0.357	0.270	0.000
33_15	-1.481	0.804	0.024	-0.517	-1.446	-0.099	0.819	0.000
33_16	-0.593	1.253	0.223	-0.336	-2.019	-0.659	0.145	0.000
33_17	-1.418	0.458	-0.614	-0.439	-1.263	0.970	1.082	0.000
33_18	-0.915	0.703	0.389	-0.442	-1.046	-0.758	0.506	0.000
33_19	-1.437	0.322	0.182	-0.935	-0.766	-0.543	1.767	0.000
33_20	-0.648	0.261	-0.404	-0.658	-0.966	0.292	1.456	0.000
33_21	-2.138	0.135	-0.114	-0.912	-0.596	0.188	1.967	0.000
335_1+2	3.486	0.655	0.535	0.191	-0.859	-1.948	-1.075	0.000
335_5+6	2.446	-0.028	-0.419	-0.039	-0.408	-0.187	0.144	0.000
335_9+10	1.386	0.727	0.104	0.103	-1.158	-0.696	-0.605	0.000
335_12	1.298	0.006	0.246	0.623	0.368	-0.350	-1.448	0.000
335_14	2.499	0.966	-0.182	0.255	-1.732	-0.572	-0.931	0.000
335_16	2.339	0.710	0.463	-0.138	-1.078	-1.712	-0.332	0.000
335_18	1.860	-0.682	-0.383	0.426	0.945	0.424	-0.536	0.000
335_20	3.141	0.122	-0.485	0.592	-0.434	0.100	-1.195	0.000
335_22	1.829	0.148	0.041	-0.305	-0.486	-0.908	0.439	0.000
335_24	1.624	0.714	0.771	-0.117	-0.828	-1.929	-0.477	0.000
335_26	2.083	-0.187	0.083	-0.396	0.026	-1.043	0.712	0.000
335_28	2.613	-0.596	0.347	-0.516	0.769	-1.608	0.956	0.000
335_30	1.180	-0.249	0.089	-0.126	0.323	-0.552	0.238	0.000
335_32	3.072	-0.539	0.110	-0.562	0.469	-1.447	1.110	0.000
335_34	2.772	0.540	-0.142	0.676	-0.826	-0.328	-1.659	0.000
415_1+2	1.940	-1.007	-0.250	0.064	1.379	0.012	0.251	0.000
415_5+6	0.866	-1.175	-0.904	0.295	1.411	1.548	0.209	0.000
415_8	1.248	-0.350	0.016	-0.090	0.452	-0.417	0.234	0.000
415_10	0.643	-0.491	-0.679	0.356	0.489	1.174	-0.260	0.000
415_12	1.169	-0.194	-0.572	-0.254	-0.258	0.342	0.783	0.000
415_14	0.794	0.016	1.291	-0.353	0.586	-2.454	0.065	0.000
415_16	0.522	0.736	0.830	-0.425	-0.902	-1.884	0.173	0.000
415_18	0.994	-0.042	0.305	-0.035	0.183	-0.797	-0.112	0.000
415_20	1.795	-0.720	0.365	-0.424	1.082	-1.275	0.855	0.000
415_22	1.670	-0.168	0.706	-0.571	0.341	-1.974	0.796	0.000
415_24	2.446	-0.245	0.493	-0.185	0.465	-1.614	0.098	0.000

	$\delta^{13}C_{EAA}$				$\delta^{13}C_{norm\text{-}EAA}$			
Sample ID	**PC1**	**PC2**	**PC3**	**PC4**	**PC1**	**PC2**	**PC3**	**PC4**
415_26	2.008	-0.662	0.229	-0.744	0.729	-1.382	1.531	0.000
415_28	1.445	0.108	1.023	-0.723	0.039	-2.547	0.866	0.000
415_30	1.871	-0.316	0.006	-0.828	-0.010	-1.138	1.681	0.000
441_1+2	0.584	-0.302	0.401	-0.484	0.476	-1.071	0.872	0.000
441_6	1.170	0.294	-0.312	-0.360	-0.934	-0.233	0.696	0.000
441_8	1.756	0.657	-0.460	0.013	-1.478	-0.017	-0.157	0.000
441_10	2.322	0.267	0.138	0.284	-0.362	-0.820	-0.869	0.000
441_12	1.968	1.340	-0.725	0.697	-2.442	0.649	-1.684	0.000
441_14	0.566	0.159	-0.543	-0.028	-0.662	0.576	0.216	0.000
441_16	0.670	0.221	-0.249	0.030	-0.552	0.129	-0.065	0.000
441_18	1.850	0.706	0.043	-1.385	-1.922	-1.810	2.413	0.000
441_20	2.506	0.776	0.002	-0.149	-1.501	-1.096	-0.130	0.000
441_22	3.115	0.981	-0.264	0.016	-1.968	-0.823	-0.452	0.000
441_24	0.586	0.267	0.199	-0.490	-0.585	-0.898	0.767	0.000
441_26	2.148	0.156	0.267	-0.363	-0.402	-1.393	0.430	0.000
441_28	2.232	0.057	-0.275	-0.316	-0.574	-0.551	0.618	0.000
11_1+2	2.054	0.116	-0.291	0.400	-0.320	0.027	-0.833	0.000
11_4+5	2.560	0.654	-0.291	0.503	-1.179	-0.183	-1.271	0.000
11_7	1.963	1.099	-0.195	0.064	-2.015	-0.544	-0.558	0.000
11_9	1.485	0.206	-0.076	0.787	-0.100	0.146	-1.717	0.000
11_11	1.369	0.234	0.168	0.524	-0.107	-0.377	-1.301	0.000
11_13	0.951	0.217	-0.162	0.439	-0.308	0.198	-0.946	0.000
11_15	2.145	0.245	-0.463	0.634	-0.532	0.395	-1.280	0.000
11_17	2.295	0.253	-0.184	0.683	-0.351	-0.040	-1.521	0.000
11_19	1.157	0.110	-0.394	0.154	-0.436	0.301	-0.236	0.000
11_21	1.404	0.076	0.083	0.271	-0.031	-0.407	-0.694	0.000
11_23	1.006	-0.001	0.136	0.094	0.067	-0.464	-0.309	0.000
40_1+2	0.229	-0.442	-0.461	-0.266	0.274	0.528	0.902	0.000
40_5	0.920	-1.161	-0.187	-0.071	1.671	0.188	0.609	0.000
40_7	-0.017	-1.661	0.858	0.400	3.457	-0.632	-0.588	0.000
40_9	-0.674	-0.596	1.739	-0.504	1.897	-2.622	0.475	0.000
40_11	0.269	-1.713	0.287	-0.251	2.832	-0.318	0.996	0.000
40_13	0.486	-1.822	1.165	-0.579	3.405	-1.918	1.280	0.000
40_15	-0.333	-2.162	0.928	0.448	4.362	-0.489	-0.513	0.000
40_17	-0.565	-1.628	0.083	-0.285	2.602	0.216	1.175	0.000
40_19	-0.356	-1.715	0.543	0.055	3.195	-0.282	0.294	0.000
40_21	-1.245	-1.575	-0.095	-0.726	2.230	0.380	2.167	0.000
40_23	0.033	-2.054	-0.118	-0.078	3.226	0.566	0.974	0.000
1000_1+2	0.254	0.533	-0.494	0.158	-1.127	0.654	-0.303	0.000
1000_4	-0.269	0.423	-0.443	0.014	-0.952	0.671	0.034	0.000
1000_6	0.482	0.370	-0.327	0.162	-0.769	0.368	-0.340	0.000
1000_8	0.186	-0.156	-1.095	-0.476	-0.703	1.281	1.517	0.000
1000_10	0.048	-0.302	-0.930	-0.420	-0.322	1.150	1.389	0.000
1000_12	-0.497	-0.161	-0.982	-0.633	-0.652	1.223	1.820	0.000
1000_14	0.431	-0.176	-0.659	-0.447	-0.389	0.571	1.248	0.000
1000_16	0.195	-0.659	-1.003	-0.451	0.188	1.270	1.610	0.000
1000_18	-1.240	-0.903	-1.078	-0.806	0.459	1.650	2.533	0.000
1000_20	-0.573	-0.495	-0.529	-0.766	0.126	0.546	2.008	0.000
1000_22	-0.282	-0.425	-0.825	-0.835	-0.233	0.831	2.244	0.000
1000_24	-0.834	0.078	-1.649	-1.379	-1.815	1.752	3.567	0.000
599_1	2.224	-0.002	0.670	-0.287	0.149	-1.935	0.146	0.000
599_3	1.392	0.299	0.083	0.566	-0.249	-0.242	-1.372	0.000
599_5	1.622	0.199	-0.253	0.146	-0.525	-0.088	-0.344	0.000
599_7	1.548	0.045	0.405	-0.074	0.050	-1.175	-0.142	0.000
599_9	1.660	0.312	0.015	0.306	-0.459	-0.413	-0.836	0.000
599_11	1.477	-0.003	-0.253	-0.221	-0.367	-0.258	0.481	0.000
599_13	1.874	-0.452	0.150	-0.165	0.626	-0.852	0.325	0.000
599_15	1.673	0.090	-0.237	-0.247	-0.533	-0.384	0.481	0.000
599_17	-0.142	0.453	2.516	-0.551	0.637	-4.229	-0.210	0.000
599_19	-0.055	-1.090	0.658	-0.345	2.035	-0.976	0.802	0.000
599_21	0.310	-0.050	0.915	-0.297	0.509	-1.677	0.179	0.000
599_23	0.445	-1.024	0.875	-0.141	2.135	-1.334	0.236	0.000
599_25	0.717	-1.333	0.508	-0.042	2.430	-0.732	0.303	0.000
599_27	0.128	-0.989	1.054	-0.070	2.251	-1.458	0.015	0.000
599_29	1.067	-1.140	0.286	-0.175	1.883	-0.650	0.584	0.000
599_31	0.242	-0.607	0.225	-0.084	1.077	-0.342	0.277	0.000
601_1+2	0.831	0.400	0.503	-0.206	-0.480	-1.262	-0.011	0.000
601_4+5	0.957	0.221	-0.126	0.161	-0.427	-0.057	-0.404	0.000
601_7+8	1.389	0.353	0.776	0.741	0.198	-1.169	-2.067	0.000
601_10	1.785	0.756	0.610	0.467	-0.725	-1.334	-1.607	0.000

	$\delta^{13}C_{EAA}$				$\delta^{13}C_{norm\text{-}EAA}$			
Sample ID	**PC1**	**PC2**	**PC3**	**PC4**	**PC1**	**PC2**	**PC3**	**PC4**
601_12+13	0.897	0.205	0.868	0.813	0.568	-1.064	-2.173	0.000
601_15	2.386	0.903	-0.308	0.109	-1.775	-0.435	-0.549	0.000
601_17	1.123	-0.334	-0.859	0.604	0.207	1.430	-0.765	0.000
601_19	1.366	0.566	0.157	0.283	-0.773	-0.605	-0.932	0.000
601_21	1.178	-0.025	-0.080	0.022	-0.079	-0.242	-0.065	0.000
601_23	0.924	-0.785	0.312	0.897	1.857	0.043	-1.719	0.000
601_25	2.128	0.975	-0.485	0.469	-1.814	0.155	-1.207	0.000
601_27	2.353	-0.013	-0.341	0.996	0.130	0.459	-1.985	0.000
601_29	0.833	0.462	0.014	0.404	-0.601	-0.107	-1.041	0.000
601_31	1.151	-0.481	0.295	0.564	1.173	-0.310	-1.162	0.000
601_33	1.038	0.360	-0.149	0.899	-0.312	0.446	-1.942	0.000
578_1+2	2.140	0.003	-0.646	0.015	-0.560	0.285	0.145	0.000
578_4	1.582	-0.492	0.271	-0.003	0.869	-0.815	-0.027	0.000
578_6	1.325	0.204	-0.085	0.185	-0.385	-0.217	-0.485	0.000
578_8	-0.144	-0.038	0.020	0.365	0.262	0.285	-0.726	0.000
578_10	0.814	0.183	-0.148	-0.088	-0.492	-0.147	0.132	0.000
578_12	1.342	0.190	-0.468	-0.229	-0.815	0.061	0.533	0.000
578_14	0.672	-1.025	-0.305	-0.380	1.239	0.197	1.252	0.000
578_16	-0.406	-0.993	-0.711	0.151	1.255	1.529	0.414	0.000
578_18	0.809	-0.732	-0.345	-0.312	0.761	0.195	1.015	0.000
578_20	0.723	-1.082	-0.410	-0.256	1.321	0.438	1.067	0.000
578_22	1.022	-1.151	0.026	-0.468	1.593	-0.449	1.303	0.000
578_24	1.465	-0.693	-0.216	-0.099	0.841	-0.069	0.474	0.000
578_26	0.738	-0.892	-0.015	-0.010	1.387	-0.027	0.316	0.000
578_28	1.345	-0.551	-0.333	-0.164	0.511	0.067	0.614	0.000
578_30	0.913	-0.526	0.244	-0.083	0.913	-0.607	0.198	0.000

Table 4.C2 Parameter estimates, t- and p-values for fixed effects in full generalised additive mixed models (GAMMs) predicting profile life-history normalised PC1 scores from PCAs with $\delta^{13}C_{EAA}$ and $\delta^{13}C_{norm\text{-}EAA}$ values (nPC1.EAA and nPC1.norm-EAA, respectively); fixed effects are species and/or capture area, depending on whether models include all data, or blue or porbeagle shark data.

A) All data

	nPC1.EAA			**nPC1.norm-EAA**		
Parameters	**Estimate ± SD**	**t-value**	**p-value**	**Estimate ± SD**	**t-value**	**p-value**
Intercept	0.057 ± 0.097	0.590	0.556	-0.071 ± 0.112	-0.634	0.527
Species: POR	-0.144 ± 0.149	-0.968	0.334	0.128 ± 0.172	0.746	0.456
Area: FI	-0.030 ± 0.258	-0.116	0.908	0.045 ± 0.302	0.151	0.880
Area: MAR	0.017 ± 0.133	0.131	0.896	0.030 ±0.155	0.193	0.847
Area: NWA	-0.012 ± 0.139	-0.088	0.930	0.011 ±0.162	0.068	0.964
Area: WEC	-0.029 ± 0.221	-0.131	0.896	0.118 ±0.259	0.455	0.650

B) Blue sharks

	nPC1.EAA			**nPC1.norm-EAA**		
Parameters	**Estimate ± SD**	**t-value**	**p-value**	**Estimate ± SD**	**t-value**	**p-value**
Intercept	-0.010 ± 0.104	-0.095	0.925	-0.006 ± 0.112	-0.052	0.958
Area: MAR	0.029 ± 0.145	0.198	0.844	0.015 ± 0.157	0.093	0.926
Area: NWA	-0.001 ± 0.151	-0.010	0.992	0.002 ± 0.163	0.013	0.990

C) Porbeagles

	nPC1.EAA			**nPC1.norm-EAA**		
Parameters	**Estimate ± SD**	**t-value**	**p-value**	**Estimate ± SD**	**t-value**	**p-value**
Intercept	-0.008 ± 0.156	-0.052	0.959	0.002 ± 0.215	0.008	0.994
Area: NWA	0.042 ± 0.175	0.239	0.812	-0.045 ± 0.241	-0.187	0.852
Area: WEC	-0.056 ± 0.193	-0.292	0.771	0.086 ± 0.266	0.324	0.747

Appendix 4.D – Fingerprinting results

Table 4.D1 Results for PCA with $\delta^{13}C_{norm\text{-}EAA}$ for primary producers and bacteria (end-members); raw amino acid carbon isotope values ($\delta^{13}C_{EAA}$) are reported in Table 4.B1.

A) Importance of components

	PC1	PC2	PC3	PC4
Standard deviation	1.410	1.039	0.966	$1.868*10^{-15}$
Proportion of variance	0.497	0.269	0.233	0.000
Cumulative proportion	0.497	0.767	1.000	1.000

B) Vector scores

	PC1	PC2	PC3	PC4
nValine	-0.444	0.280	0.749	-0.404
nIsoleucine	0.404	0.747	-0.281	-0.447
nLeucine	-0.574	-0.231	-0.554	-0.556
nPhenylalanine	0.557	-0.557	0.230	-0.572

C) Sample scores

ID	PC1	PC2	PC3	PC4
AB1	0.100	0.078	0.392	0.000
AB2	-0.100	0.426	-0.249	0.000
AB3	-1.958	-1.945	2.121	0.000
AB4	-0.328	1.281	0.197	0.000
AB5	0.120	-3.121	-2.914	0.000
AB6	-1.201	2.064	-1.034	0.000
AB7	-0.336	0.645	-1.979	0.000
AB8	-1.212	0.005	-2.276	0.000
AB9	1.427	0.582	-0.216	0.000
AB10	-0.379	0.881	1.383	0.000
HB1	-2.046	0.230	-1.007	0.000
HB2	-3.018	0.783	-0.820	0.000
HB3	-2.719	-0.970	-0.104	0.000
HB4	-2.949	-0.309	-1.456	0.000
HB5	-1.871	-0.317	-0.098	0.000
HB6	-1.567	-0.024	-0.604	0.000
HB7	-1.119	-1.830	-0.070	0.000
HB8	-3.511	0.607	1.833	0.000
HB9	-1.694	-1.063	-1.065	0.000
HB10	-0.899	-0.528	-0.512	0.000
HB11	-0.086	-1.270	-2.464	0.000
HB12	0.712	-0.502	0.157	0.000
HB13	0.831	0.353	-0.085	0.000
HB14	-0.041	-1.058	1.116	0.000
HB15	-2.098	-1.831	0.594	0.000
HB16	-2.637	-0.395	-0.025	0.000
HB17	0.269	-0.783	-3.278	0.000
HB18	0.606	-0.147	-0.179	0.000
HB19	-0.796	-1.217	0.693	0.000
HB20	-2.328	0.562	1.466	0.000
HB21	-0.952	-1.574	0.111	0.000
HB22	-0.180	-1.724	0.350	0.000
MA1	-0.942	-0.534	0.049	0.000
MA2	-0.445	0.341	-1.692	0.000
MA3	-0.589	0.039	-0.533	0.000
MA4	-1.532	1.354	-0.060	0.000
MA5	-1.756	0.685	-0.659	0.000
MA6	-0.655	0.424	-0.716	0.000
MA7	-0.796	0.361	-0.476	0.000
MA8	0.224	0.195	-1.010	0.000
MA9	-1.378	-0.272	0.732	0.000
MA10	-0.412	-0.001	1.227	0.000
MA11	-0.630	0.785	1.057	0.000
MA12	-0.754	0.228	1.123	0.000
MA13	-1.787	-0.034	1.555	0.000
MA14	-0.860	0.102	0.968	0.000
MA15	-0.529	1.510	0.015	0.000

ID	PC1	PC2	PC3	PC4
MA16	0.606	0.702	0.944	0.000
MA17	-0.334	-0.077	1.971	0.000
MA18	-0.362	1.408	0.429	0.000
MA19	-0.610	1.498	-0.190	0.000
MA20	-0.246	1.272	0.456	0.000
MA21	0.677	0.546	0.075	0.000
MI1	0.237	0.892	0.862	0.000
MI2	0.205	1.408	-0.204	0.000
MI3	1.173	1.002	-0.448	0.000
MI4	-1.525	0.982	0.406	0.000
MI5	2.338	2.150	-0.116	0.000
MI6	-0.473	0.549	0.154	0.000
MI7	0.637	2.089	-0.664	0.000
MI8	0.379	2.149	-0.262	0.000
MI9	0.574	2.293	-0.547	0.000
S1	0.716	-0.803	0.325	0.000
S2	0.770	-0.680	0.172	0.000
S3	1.323	-0.390	0.069	0.000
S4	1.027	0.171	-0.086	0.000
S5	1.145	-0.189	0.350	0.000
S6	0.227	-1.254	0.203	0.000
S7	0.153	-1.767	0.790	0.000
TP1	2.094	0.350	-0.859	0.000
TP2	1.346	0.593	0.269	0.000
TP3	2.308	0.452	-0.170	0.000
TP4	1.715	-0.285	-0.200	0.000
TP5	1.216	-0.538	-0.032	0.000
TP6	1.174	-0.115	0.085	0.000
TP7	0.938	-0.534	-0.198	0.000
TP8	1.790	0.573	0.633	0.000
TP9	1.402	-0.304	0.245	0.000
TP10	2.005	0.020	0.528	0.000
TP11	1.793	0.769	-0.177	0.000
TP12	2.087	0.259	0.002	0.000
TP13	1.424	-1.117	0.562	0.000
TP14	0.928	-0.885	1.636	0.000
TP15	2.530	-0.988	1.493	0.000
TP16	0.895	-0.069	-0.190	0.000
TP17	2.673	-1.374	-0.218	0.000
TP18	1.247	-0.689	0.112	0.000
TP19	1.682	-0.210	0.007	0.000
TP20	1.356	-1.454	0.070	0.000
TP21	1.804	-1.407	-0.051	0.000
TP22	1.759	-0.072	0.209	0.000

Table 4.D2 Results for linear discriminant function analysis (LDA) with $\delta^{13}C_{norm\text{-}EAA}$ values for end-members as independent variables, and end-member groups defined by the PCA as categorical variables: i) autotrophic bacteria and algae, ii) heterotrophic bacteria, and iii) vascular plants. C) Posterior probabilities (%) of classification of (known) end-member samples within end-member groups, based on the LDA model with leave-one-out cross-validation.

A) Proportion of trace

	LD1	LD2
Prop. of trace	0.814	0.186

B) Coefficients for linear discriminants

	LD1	LD2
nValine	-0.168	0.195
nIsoleucine	0.142	0.442
nLeucine	-0.360	-0.243
nPhenylalanine	0.402	-0.351

C) Posterior probabilities

ID	Actual group	Aut.bacteria + algae	Het.bacteria	Vasc.plants
AB1	Aut.bacteria + Algae	**0.562**	0.175	0.263
AB2	Aut.bacteria + Algae	**0.706**	0.213	0.081
AB3	Aut.bacteria + Algae	**0.018**	0.970	0.012
AB4	Aut.bacteria + Algae	**0.897**	0.082	0.021
AB5	Aut.bacteria + Algae	**0.000**	0.944	0.056
AB6	Aut.bacteria + Algae	**0.881**	0.119	0.000
AB7	Aut.bacteria + Algae	**0.579**	0.411	0.010
AB8	Aut.bacteria + Algae	**0.138**	0.861	0.001
AB9	Aut.bacteria + Algae	**0.229**	0.013	0.758
AB10	Aut.bacteria + Algae	**0.843**	0.085	0.072
MA1	Aut.bacteria + Algae	**0.280**	0.691	0.029
MA2	Aut.bacteria + Algae	**0.485**	0.502	0.013
MA3	Aut.bacteria + Algae	**0.493**	0.477	0.030
MA4	Aut.bacteria + Algae	**0.759**	0.241	0.001
MA5	Aut.bacteria + Algae	**0.414**	0.585	0.001
MA6	Aut.bacteria + Algae	**0.597**	0.388	0.015
MA7	Aut.bacteria + Algae	**0.572**	0.415	0.013
MA8	Aut.bacteria + Algae	**0.595**	0.269	0.136
MA9	Aut.bacteria + Algae	**0.336**	0.651	0.013
MA10	Aut.bacteria + Algae	**0.587**	0.238	0.175
MA11	Aut.bacteria + Algae	**0.823**	0.141	0.037
MA12	Aut.bacteria + Algae	**0.663**	0.279	0.058
MA13	Aut.bacteria + Algae	**0.387**	0.607	0.007
MA14	Aut.bacteria + Algae	**0.598**	0.356	0.046
MA15	Aut.bacteria + Algae	**0.912**	0.080	0.008
MA16	Aut.bacteria + Algae	**0.533**	0.032	0.435
MA17	Aut.bacteria + Algae	**0.485**	0.157	0.359
MA18	Aut.bacteria + Algae	**0.916**	0.065	0.019
MA19	Aut.bacteria + Algae	**0.898**	0.096	0.006
MA20	Aut.bacteria + Algae	**0.901**	0.068	0.030
MA21	Aut.bacteria + Algae	**0.561**	0.059	0.381
MI1	Aut.bacteria + Algae	**0.764**	0.052	0.184
MI2	Aut.bacteria + Algae	**0.905**	0.049	0.046
MI3	Aut.bacteria + Algae	**0.547**	0.023	0.430
MI4	Aut.bacteria + Algae	**0.700**	0.298	0.002
MI5	Aut.bacteria + Algae	**0.212**	0.000	0.788
MI6	Aut.bacteria + Algae	**0.739**	0.223	0.039
MI7	Aut.bacteria + Algae	**0.951**	0.015	0.034
MI8	Aut.bacteria + Algae	**0.963**	0.015	0.022
MI9	Aut.bacteria + Algae	**0.966**	0.011	0.023
HB1	Het.bactteria	0.239	**0.760**	0.000
HB2	Het.bactteria	0.277	**0.723**	0.000
HB3	Het.bactteria	0.040	**0.960**	0.000
HB4	Het.bactteria	0.049	**0.951**	0.000
HB5	Het.bactteria	0.188	**0.810**	0.001
HB6	Het.bactteria	0.275	**0.723**	0.002
HB7	Het.bactteria	0.054	**0.919**	0.027
HB8	Het.bactteria	0.455	**0.545**	0.000
HB9	Het.bactteria	0.058	**0.940**	0.001
HB10	Het.bactteria	0.259	**0.722**	0.019
HB11	Het.bactteria	0.121	**0.811**	0.068

ID	Actual group	Aut.bacteria + algae	Het.bacteria	Vasc.plants
HB12	Het.bactteria	0.187	**0.055**	0.758
HB13	Het.bactteria	0.443	**0.034**	0.523
HB14	Het.bactteria	0.187	**0.168**	0.645
HB15	Het.bactteria	0.030	**0.968**	0.002
HB16	Het.bactteria	0.098	**0.902**	0.000
HB17	Het.bactteria	0.257	**0.647**	0.097
HB18	Het.bactteria	0.373	**0.091**	0.536
HB19	Het.bactteria	0.195	**0.689**	0.116
HB20	Het.bactteria	0.603	**0.396**	0.001
HB21	Het.bactteria	0.093	**0.858**	0.049
HB22	Het.bactteria	0.101	**0.427**	0.472
S1	Vasc.plants	0.118	0.070	**0.812**
S2	Vasc.plants	0.136	0.069	**0.796**
S3	Vasc.plants	0.074	0.016	**0.910**
S4	Vasc.plants	0.291	0.039	**0.669**
S5	Vasc.plants	0.122	0.020	**0.858**
S6	Vasc.plants	0.144	0.275	**0.581**
S7	Vasc.plants	0.067	0.235	**0.697**
TP1	Vasc.plants	0.082	0.004	**0.914**
TP2	Vasc.plants	0.254	0.012	**0.734**
TP3	Vasc.plants	0.040	0.001	**0.959**
TP4	Vasc.plants	0.045	0.006	**0.948**
TP5	Vasc.plants	0.079	0.023	**0.898**
TP6	Vasc.plants	0.146	0.024	**0.831**
TP7	Vasc.plants	0.146	0.061	**0.793**
TP8	Vasc.plants	0.091	0.002	**0.907**
TP9	Vasc.plants	0.065	0.010	**0.924**
TP10	Vasc.plants	0.026	0.001	**0.973**
TP11	Vasc.plants	0.184	0.005	**0.810**
TP12	Vasc.plants	0.042	0.002	**0.956**
TP13	Vasc.plants	0.015	0.007	**0.978**
TP14	Vasc.plants	0.036	0.011	**0.953**
TP15	Vasc.plants	0.001	0.000	**0.999**
TP16	Vasc.plants	0.279	0.063	**0.658**
TP17	Vasc.plants	0.001	0.000	**0.999**
TP18	Vasc.plants	0.055	0.018	**0.927**
TP19	Vasc.plants	0.048	0.006	**0.946**
TP20	Vasc.plants	0.014	0.013	**0.973**
TP21	Vasc.plants	0.006	0.004	**0.991**
TP22	Vasc.plants	0.045	0.004	**0.951**

Table 4.D3 Posterior probabilities (%) of classification of unknown shark samples within end-member groups, based on the LDA model. ID is given by individual ID and sample ID or IDs of single samples within combinations.

ID	Aut.bacteria + algae	Het.bacteria	Vasc.plants
16_1+2+3	0.990	0.009	0.001
16_4+5	0.981	0.018	0.002
16_6	0.996	0.004	0.001
16_7+8	0.954	0.045	0.001
16_9	0.986	0.010	0.003
16_10	0.977	0.022	0.001
16_11	0.982	0.011	0.007
16_12	0.980	0.019	0.000
16_13	0.980	0.016	0.004
16_14	0.977	0.018	0.005
16_15	0.985	0.013	0.001
16_16	0.938	0.062	0.000
16_17	0.974	0.025	0.001
16_18	0.980	0.019	0.001
16_19	0.981	0.018	0.000
24_1+2+3	0.995	0.005	0.000
24_4+5+6	0.995	0.004	0.001
24_7+8	0.994	0.005	0.001
24_9+10	0.967	0.023	0.010
24_11	0.966	0.028	0.006
24_12	0.964	0.035	0.001
24_13	0.902	0.096	0.002
24_14	0.983	0.013	0.004
24_15	0.976	0.022	0.002
24_16	0.986	0.013	0.001
24_17	0.990	0.010	0.000
24_18	0.947	0.051	0.002
24_19	0.952	0.047	0.001
24_20	0.990	0.010	0.000
24_21	0.986	0.014	0.000
12_1+2+3	0.994	0.006	0.000
12_4+5	0.992	0.007	0.001
12_6	0.983	0.014	0.003
12_7	0.997	0.002	0.001
12_8+9	0.997	0.003	0.000
12_10+11	0.977	0.019	0.004
12_12	0.987	0.012	0.001
12_13	0.989	0.011	0.000
12_14	0.995	0.005	0.000
12_15	0.963	0.037	0.000
12_16	0.974	0.026	0.000
12_17	0.985	0.015	0.000
101_1+2+3	0.962	0.038	0.000
101_4	0.760	0.236	0.004
101_5	0.961	0.032	0.007
101_6	0.956	0.034	0.010
101_7	0.971	0.027	0.002
101_8	0.894	0.015	0.091
101_9	0.979	0.021	0.001
101_10	0.944	0.039	0.017
101_11	0.970	0.027	0.003
101_12	0.952	0.027	0.021
101_13	0.928	0.069	0.003
101_14	0.747	0.251	0.001
101_15	0.942	0.057	0.001
101_16	0.964	0.028	0.008
131_1+2	0.985	0.014	0.001
131_3	0.978	0.003	0.020
131_4+5	0.974	0.025	0.001
131_6+7	0.989	0.010	0.001
131_8	0.983	0.016	0.001
131_9	0.951	0.019	0.030
131_10	0.974	0.023	0.003
131_11	0.967	0.030	0.003
131_12	0.972	0.024	0.004
131_13	0.974	0.017	0.009

ID	Aut.bacteria + algae	Het.bacteria	Vasc.plants
131_14	0.970	0.026	0.005
131_15	0.981	0.015	0.004
131_16	0.965	0.035	0.000
131_17	0.964	0.035	0.001
33_1+2+3	0.985	0.015	0.000
33_4+5	0.947	0.052	0.001
33_6+7	0.949	0.051	0.001
33_8+9	0.982	0.018	0.000
33_10	0.983	0.017	0.000
33_11	0.990	0.010	0.000
33_12	0.990	0.010	0.000
33_13	0.979	0.021	0.000
33_14	0.980	0.020	0.000
33_15	0.967	0.032	0.000
33_16	0.984	0.015	0.000
33_17	0.961	0.037	0.002
33_18	0.968	0.032	0.000
33_19	0.900	0.100	0.000
33_20	0.936	0.063	0.001
33_21	0.887	0.112	0.001
335_1+2	0.990	0.010	0.000
335_5+6	0.972	0.027	0.000
335_9+10	0.989	0.011	0.000
335_12	0.991	0.009	0.000
335_14	0.993	0.007	0.000
335_16	0.983	0.017	0.000
335_18	0.976	0.023	0.001
335_20	0.992	0.008	0.000
335_22	0.962	0.038	0.000
335_24	0.983	0.017	0.000
335_26	0.940	0.060	0.000
335_28	0.895	0.105	0.000
335_30	0.958	0.041	0.000
335_32	0.896	0.104	0.000
335_34	0.995	0.005	0.000
415_1+2	0.941	0.058	0.001
415_5+6	0.948	0.044	0.008
415_8	0.957	0.043	0.000
415_10	0.975	0.022	0.003
415_12	0.953	0.046	0.001
415_14	0.947	0.053	0.000
415_16	0.970	0.030	0.000
415_18	0.970	0.030	0.000
415_20	0.896	0.103	0.000
415_22	0.917	0.083	0.000
415_24	0.954	0.046	0.000
415_26	0.842	0.158	0.000
415_28	0.914	0.086	0.000
415_30	0.867	0.133	0.000
441_1+2	0.918	0.082	0.000
441_6	0.964	0.036	0.000
441_8	0.986	0.013	0.000
441_10	0.987	0.012	0.000
441_12	0.998	0.002	0.000
441_14	0.976	0.023	0.001
441_16	0.979	0.020	0.001
441_18	0.868	0.132	0.000
441_20	0.984	0.016	0.000
441_22	0.990	0.009	0.000
441_24	0.951	0.049	0.000
441_26	0.958	0.042	0.000
441_28	0.959	0.041	0.000
11_1+2	0.988	0.011	0.000
11_4+5	0.994	0.006	0.000
11_7	0.992	0.008	0.000
11_9	0.994	0.006	0.000
11_11	0.991	0.009	0.000
11_13	0.989	0.010	0.001
11_15	0.993	0.007	0.001
11_17	0.994	0.006	0.000
11_19	0.982	0.018	0.001

ID	Aut.bacteria + algae	Het.bacteria	Vasc.plants
11_21	0.984	0.016	0.000
11_23	0.977	0.023	0.000
40_1+2	0.937	0.061	0.002
40_5	0.914	0.085	0.001
40_7	0.931	0.069	0.001
40_9	0.876	0.124	0.000
40_11	0.813	0.186	0.001
40_13	0.675	0.325	0.000
40_15	0.899	0.100	0.001
40_17	0.815	0.183	0.002
40_19	0.877	0.122	0.001
40_21	0.682	0.316	0.003
40_23	0.811	0.186	0.004
1000_1+2	0.987	0.012	0.001
1000_4	0.982	0.017	0.001
1000_6	0.985	0.014	0.001
1000_8	0.933	0.063	0.004
1000_10	0.929	0.067	0.004
1000_12	0.912	0.084	0.004
1000_14	0.935	0.063	0.002
1000_16	0.899	0.095	0.005
1000_18	0.786	0.202	0.012
1000_20	0.856	0.142	0.002
1000_22	0.852	0.145	0.003
1000_24	0.788	0.202	0.009
599_1	0.956	0.044	0.000
559_3	0.992	0.008	0.000
599_5	0.983	0.017	0.000
599_7	0.970	0.029	0.000
599_9	0.988	0.012	0.000
599_11	0.962	0.037	0.000
599_13	0.947	0.053	0.000
599_15	0.964	0.036	0.000
599_17	0.944	0.056	0.000
599_19	0.866	0.134	0.000
599_21	0.950	0.050	0.000
599_23	0.907	0.093	0.000
599_25	0.900	0.100	0.000
599_27	0.918	0.082	0.000
599_29	0.898	0.102	0.000
599_31	0.944	0.056	0.001
601_1+2	0.973	0.027	0.000
601_4+5	0.983	0.016	0.000
601_7+8	0.994	0.006	0.000
601_10	0.994	0.006	0.000
601_12+13	0.994	0.006	0.000
601_15	0.991	0.009	0.000
601_17	0.985	0.012	0.003
601_19	0.990	0.010	0.000
601_21	0.974	0.026	0.000
601_23	0.987	0.012	0.001
601_25	0.995	0.004	0.000
601_27	0.995	0.005	0.001
601_29	0.991	0.009	0.000
601_31	0.983	0.016	0.000
601_33	0.996	0.004	0.001
578_1+2	0.976	0.024	0.001
578_4	0.957	0.042	0.000
578_6	0.984	0.016	0.000
578_8	0.984	0.015	0.001
578_10	0.974	0.026	0.000
578_12	0.968	0.031	0.001
578_14	0.876	0.122	0.001
578_16	0.942	0.050	0.007
578_18	0.914	0.085	0.001
578_20	0.893	0.105	0.002
578_22	0.842	0.157	0.001
578_24	0.942	0.058	0.001
578_26	0.937	0.062	0.001
578_28	0.943	0.056	0.001
578_30	0.949	0.051	0.000

Table 4.D4 Posterior probabilities (%) of classification of unknown consumer samples within end-member groups, based on the LDA model.

ID	Aut.bacteria + algae	Het.bacteria	Vasc.plants
C1	0.959	0.040	0.001
C2	0.966	0.033	0.001
C3	0.969	0.030	0.001
C4	0.020	0.980	0.000
C5	0.959	0.033	0.009
C6	0.465	0.079	0.456
C7	0.503	0.196	0.301
C8	0.464	0.145	0.391
C9	0.834	0.072	0.094
C10	0.971	0.015	0.014
C11	0.912	0.013	0.075
C12	0.956	0.039	0.005
C13	0.961	0.034	0.005
C14	0.966	0.033	0.001
C15	0.729	0.038	0.233
C16	0.612	0.088	0.300
C17	0.416	0.142	0.442
C18	0.273	0.078	0.649
C19	0.873	0.081	0.046
C20	0.922	0.036	0.042
C21	0.941	0.054	0.005
C22	0.861	0.056	0.083
C23	0.958	0.032	0.011
C24	0.950	0.039	0.011
C25	0.910	0.085	0.005
C26	0.976	0.020	0.004
C27	0.958	0.040	0.002
C28	0.964	0.035	0.001
C29	0.957	0.042	0.001
C30	0.867	0.132	0.001
C31	0.678	0.138	0.183
C32	0.605	0.160	0.236
C33	0.533	0.260	0.207
C34	0.812	0.170	0.018
C35	0.978	0.021	0.001
C36	0.961	0.030	0.010
C37	0.925	0.044	0.031
C38	0.972	0.027	0.001
C39	0.985	0.014	0.001
C40	0.957	0.041	0.002
C41	0.975	0.023	0.002
M1	0.852	0.125	0.023
M2	0.860	0.117	0.023
Z1	0.906	0.089	0.005
Z2	0.973	0.026	0.001
Z3	0.981	0.018	0.001
Z4	0.938	0.061	0.001
Z5	0.937	0.059	0.004
Z6	0.809	0.158	0.033
Z7	0.927	0.069	0.004
Z8	0.849	0.133	0.018
FH1	0.994	0.000	0.006
FC1	0.982	0.009	0.009
FP1	0.943	0.056	0.001
FP2	0.936	0.063	0.001
FP3	0.953	0.044	0.003
P1	0.994	0.000	0.005
P2	0.932	0.005	0.063

Table 4.D5 Posterior probabilities (%) of classification of unknown particulate organic matter samples within end-member groups, based on the LDA model.

ID	Aut.bacteria + algae	Het.bacteria	Vasc.plants
OM1	0.778	0.185	0.038
OM2	0.936	0.063	0.000
OM3	0.780	0.209	0.011
OM4	0.883	0.110	0.007
OM5	0.000	0.000	1.000
OM6	0.003	0.000	0.997
OM7	0.000	0.000	1.000
OM8	0.000	0.000	1.000
OM9	0.000	0.000	1.000
OM10	0.000	0.000	1.000
OM11	0.000	0.000	1.000
OM12	0.000	0.000	1.000
OM13	0.000	0.000	1.000
OM14	0.000	0.000	1.000
OM15	0.000	0.000	1.000
OM16	0.000	0.000	1.000
OM17	0.000	0.000	1.000
OM18	0.000	0.000	1.000
OM19	0.000	0.000	1.000
OM20	0.000	0.000	1.000
OM21	0.000	0.000	1.000
OM22	0.000	0.000	1.000
OM23	0.000	0.000	1.000
OM24	0.000	0.000	1.000
OM25	0.000	0.000	1.000
OM26	0.000	0.000	1.000
OM27	0.000	0.000	1.000
OM28	0.000	0.000	1.000
OM29	0.000	0.000	1.000
OM30	0.002	0.000	0.998
OM31	0.002	0.000	0.998
OM32	0.000	0.000	1.000
OM33	0.003	0.000	0.997
OM34	0.007	0.000	0.993
OM35	0.009	0.000	0.991
OM36	0.000	0.000	1.000
OM37	0.000	0.000	1.000
OM38	0.002	0.000	0.998
OM39	0.002	0.000	0.998
OM40	0.000	0.000	1.000
OM41	0.000	0.000	1.000
OM42	0.001	0.000	0.999
OM43	0.001	0.000	0.999
OM44	0.000	0.000	1.000
OM45	0.000	0.000	1.000
OM46	0.000	0.000	1.000
OM47	0.003	0.000	0.997
OM48	0.000	0.000	1.000
OM49	0.000	0.000	1.000
OM50	0.000	0.000	1.000
OM51	0.001	0.000	0.999
OM52	0.000	0.000	1.000
OM53	0.000	0.000	1.000
OM54	0.000	0.000	1.000
OM55	0.000	0.000	1.000
OM56	0.000	0.000	1.000
OM57	0.000	0.000	1.000
OM58	0.152	0.000	0.848
OM59	0.234	0.002	0.764
OM60	0.014	0.004	0.982
OM61	0.391	0.002	0.607
OM62	0.001	0.000	0.999
OM63	0.015	0.000	0.985
OM64	0.255	0.001	0.744
OM65	0.075	0.001	0.924
OM66	0.001	0.000	0.999
OM67	0.022	0.000	0.978

ID	Aut.bacteria + algae	Het.bacteria	Vasc.plants
OM68	0.032	0.000	0.968
OM69	0.940	0.001	0.059

Literature cited

Aasen, O. 1963. Length and growth of the porbeagle (*Lamna nasus*, Bonneterre) in the North West Atlantic. Fisk. Skrift. Ser. Havund. **13**:20-37.

Abraham, W. R., and C. Hesse. 2003. Isotope fractionation in the biosynthesis of cell components by different fungi: a basis for environmental carbon flux studies. Microbial Ecology **46**:121-128.

Aires-da-Silva, A. M., J. J. Hoey, and V. F. Galluci. 2008. A historical index of abundance for the blue shark (*Prionace glauca*) in the western North Atlantic. Fisheries Research **92**:41-52.

Alerstam, T., A. Hedenström, and S. Åkesson. 2003. Long-distance migration: evolution and determinants. Oikos **103**:247-260.

Altizer, S., R. Bartel, and B. A. Han. 2011. Animal migration and infectious disease risk. Science **331**:296-302.

Andrews, R. D., R. L. Pitman, and L. T. Ballance. 2008. Satellite tracking reveals distinct movement patterns for Type B and Type C killer whales in the southern Ross Sea, Antarctica. Polar Biology **31**:1461-1468.

Angel, M. V. 1986. Vertical distribution: study and implications. Pages 3-8 *in* Pelagic Biogeography: Proceedings of an International Conference. UNESCO Technical Papers in Marine Science.

Angel, M. V. 1993. Biodiversity of the pelagic ocean. Conservation Biology **7**:760-772.

Angel, M. V. 1997. What is the deep sea. Pages 1-41 *in* D. J. Randall and A. P. Farrell, editors. Deep-sea Fishes. Academic Press, Amsterdam.

Ardizzone, D., G. M. Cailliet, L. J. Natanson, A. H. Andrews, L. A. Kerr, and T. A. Brown. 2006. Application of bomb radiocarbon chronologies to shortfin mako (*Isurus oxyrinchus*) age validation. Environmental Biology of Fishes **77**:355-366.

Arthur, K. E., S. Kelez, T. Larsen, C. A. Choy, and B. N. Popp. 2014. Tracing the biosynthetic source of essential amino acids in marine turtles using $\delta^{13}C$ fingerprints. Ecology **95**:1285-1293.

Backus, R. H. 1986. Biogeographic boundaries in the open ocean. Pages 9-13 *in* Pelagic Biogeography: Proceedings of an International Conference. UNESCO Technical Papers in Marine Science.

Barnes, C., S. Jennings, and J. T. Barry. 2009. Environmental correlates of large-scale spatial variation in the $\delta^{13}C$ of marine animals. Estuarine Coastal and Shelf Science **81**:368-374.

Bauer, S., and B. J. Hoye. 2014. Migratory animals couple biodiversity and ecosystem functioning worldwide. Science **344**:1242552.

Baum, J. K., and W. Blanchard. 2010. Inferring shark population trends from generalized linear mixed models of pelagic longline catch and effort data. Fisheries Research **102**:229-239.

Baum, J. K., R. A. Myers, D. G. Kehler, B. Worm, S. J. Harley, and P. A. Doherty. 2003. Collapse and conservation of shark populations in the northwest Atlantic. Science **299**:389-392.

Bendall, V. J., J. R. Ellis, S. J. Hetherington, S. R. McCully, D. Righton, and J. F. Silva. 2013. Preliminary observations on the biology and movements of porbeagle *Lamna nasus* around the British Isles. Collective Volume of Scientific Papers ICCAT **69**:1702-1722.

Best, P. B., and D. M. Schell. 1996. Stable isotopes in southern right whale (*Eubalaena australis*) baleen as indicators of seasonal movements, feeding and growth. Marine Biology **124**:483-494.

Biais, G., Y. Coupeau, B. Seret, B. Calmettes, R. Lopez, S. Hetherington, and D. Righton. 2017. Return migration of porbeagle shark (*Lamna nasus*) in the Northeast Atlantic: implications for stock range and structure. Ices Journal of Marine Science. doi:10.1093/icesjms/fsw233.

Bidigare, R. R., A. Fluegge, K. H. Freeman, K. L. Hanson, J. M. Hayes, D. Hollander, J. P. Jasper, L. L. King, E. A. Laws, J. Milder, F. J. Millero, R. Pancost, B. N. Popp, P. A. Steinberg, and S. G. Wakeham. 1997. Consistent fractionation of ^{13}C in nature and in the laboratory: growth-rate effects in some haptophytae algae. Global Biogeochemical Cycles **11**:279-292.

Block, B. A., H. Dewar, S. B. Blackwell, T. D. Williams, E. D. Prince, C. J. Farwell, A. Boustany, S. L. H. Teo, A. Seitz, A. Walli, and D. Fudge. 2001. Migratory movements, depth preferences, and thermal biology of Atlantic bluefin tuna. Science **293**:1310-1314.

Block, B. A., I. D. Jonsen, S. J. Jorgensen, A. J. Winship, S. A. Shaffer, S. J. Bograd, E. L. Hazen, D. G. Foley, G. A. Breed, A. L. Harrison, J. E. Ganong, A. Swithenbank, M. Castleton, H. Dewar, B. R. Mate, G. L. Shillinger, K. M. Schaefer, S. R. Benson, M. J. Weise, R. W. Henry, and D. P. Costa. 2011. Tracking apex marine predator movements in a dynamic ocean. Nature **475**:86-90.

Block, B. A., S. L. H. Teo, A. Walli, A. Boustany, M. J. W. Stokesbury, C. J. Farwell, K. C. Weng, H. Dewar, and T. D. Williams. 2005. Electronic tagging and population structure of Atlantic bluefin tuna. Nature **434**:1121-1127.

Boecklen, W. J., C. T. Yarnes, B. A. Cook, and A. C. James. 2011. On the use of stable isotopes in trophic ecology. Annual Review of Ecology, Evolution, and Systematics **42**:411-440.

Bolle, L. J., E. Hunter, A. D. Rijnsdorp, M. A. Pastoors, J. D. Metcalfe, and J. D. Reynolds. 2005. Do tagging experiments tell the truth? Using electronic tags to evaluate conventional tagging data. ICES Journal of Marine Science **62**:236-246.

Bonfil, R., M. Meyer, M. C. Scholl, R. Johnson, S. O'Brien, H. Oosthuizen, S. Swanson, D. Kotze, and M. Paterson. 2005. Transoceanic migration, spatial dynamics, and population linkages of white sharks. Science **310**:100-103.

Bowen, G. J. 2010a. Isoscapes: spatial pattern in isotopic biogeochemistry. Annual Review of Earth and Planetary Sciences **38**:161-187.

Bowen, G. J. 2010b. Statistical and geostatistical mapping of precipitation water isotope ratios. Pages 139-160 *in* J. B. West, G. J. Bowen, T. E. Dawson, and K. P. Tu, editors. Isoscapes: Understanding Movement, Pattern, and Process on Earth through Isotope Mapping. Springer, Berlin.

Bowen, G. J., and J. B. West. 2008. Isotope landscapes for terrestrial migration research. Pages 79-105 *in* K. A. Hobson and L. I. Wassenaar, editors. Tracking Animal Migration with Stable Isotopes. Elsevier, Amsterdam.

Bowen, G. J., and J. Revenaugh. 2003. Interpolating the isotopic composition of modern meteoric precipitation. Water Resources Research **39**:1299.

Bowen, G. J., L. I. Wassenaar, and K. A. Hobson. 2005. Global application of stable hydrogen and oxygen isotopes to wildlife forensics. Oecologia **143**:337-348.

Bowlin, M. S., I.-A. Bisson, J. Shamoun-Baranes, J. D. Reichard, N. Sapir, P. P. Marra, T. H. Kunz, D. S. Wilcove, A. Hedenstrom, C. G. Guglielmo, S. Akesson, M. Ramenofsky, and M. Wikelski. 2010. Grand challenges in migration biology. Integrative and Comparative Biology **50**:261-279.

Brimble, S. K., K. L. Foster, M. L. Mallory, R. W. MacDonald, J. P. Smol, and J. M. Blais. 2009. High arctic ponds receiving biotransported nutrients from a nearby seabird colony are also subject to potentially toxic loadings of arsenic, cadmium, and zinc. Environmental Toxicology Chemistry **28**:2426-2433.

Briscoe, D. K., S. M. Maxwell, R. Kudela, L. B. Crowder, and D. Croll. 2016. Are we missing important areas in pelagic marine conservation? Redefining conservation hotspots in the ocean. Endangered Species Research **29**:229-237.

Brodie, C. R., M. J. Leng, J. S. L. Casford, C. P. Kendrick, J. M. Lloyd, Y. Zong, and M. I. Bird. 2011. Evidence for bias in C and N concentrations and $\delta^{13}C$ composition of terrestrial and aquatic organic materials due to pre-analysis acid preparation methods. Chemical Geology **282**:67-83.

Brönmark, C., K. Hulthén, P. A. Nilsson, C. Skov, L.-A. Hansson, J. Brodersen, and B. B. Chapmana. 2014. There and back again: migration in freshwater fishes. Canadian Journal of Zoology-Revue Canadienne De Zoologie **92**:467-479.

Buchan, A., G. R. LeCleir, C. A. Gulvik, and J. M. González. 2014. Master recyclers: features and functions of bacteria associated with phytoplankton blooms. Nature Reviews Microbiology **12**:686-698.

Buehler, D. M., T. Piersma, K. Matson, and B. I. Tieleman. 2008. Seasonal redistribution of immune function in a migrant shorebird: annual-cycle effects override adjustments to thermal regime. American Naturalist **172**:783-796.

Buencuerpo, V., S. Rios, and J. Moron. 1998. Pelagic sharks associated with the swordfish, *Xiphias gladius*, fishery in the eastern North Atlantic Ocean and the Strait of Gibraltar. Fishery Bulletin **96**:667-685.

Bump, J. K., K. Fox-Dobbs, J. L. Bada, P. L. Koch, R. O. Peterson, and J. A. Vucetich. 2007. Stable isotopes, ecological integration and environmental change: wolves record atmospheric carbon isotope trend better than tree rings. Proceedings of the Royal Society B-Biological Sciences **274**:2471-2480.

Burgess, G. H., L. R. Beerkircher, G. M. Cailliet, J. K. Carlson, E. Cortes, K. J. Goldman, R. D. Grubbs, J. A. Musick, M. K. Musyl, and C. A. Simpfendorfer. 2005. Is the collapse of shark populations in the Northwest Atlantic Ocean and Gulf of Mexico Real?. Fisheries **30**:19-26.

Burkhardt, S., U. Riebesell, and I. Zondervan. 1999. Stable carbon isotope fractionation by marine phytoplankton in response to daylength, growth rate, and CO_2 availability. Marine Ecology Progress Series **184**:31-41.

Cailliet, G. M. 1990. Elasmobranch age determination and verification; an updated review. Pages 157-165 *in* H. L. Pratt Jr., S. H. Gruber, and T. Taniuchi, editors. Elasmobranchs as living resources: advances in the biology, ecology, systematics and the status of the fisheries. U.S. Department of Commerce, NOAA, Technical Report NMFS 90.

Cailliet, G. M., K. J. Goldman, and M. R. Heithaus. 2004. Age determination and validation in chondrichthyan fishes. Pages 399-447 *in* J. C. Jeffrey, J. A. Musick, and M. R. Heithaus, editors. Biology of Sharks and Their Relatives. CRC Press, Boca Raton, FL.

Cailliet, G. M., L. K. Martin, D. Kusher, P. Wolf, and B. A. Weldon. 1983. Techniques for enhancing vertebral bands in age estimation of California elasmobranchs. Pages 157-165 *in* E.D. Prince, and L.M. Pulos, editors. Proceedings of the international workshop on age determination of oceanic pelagic fishes: tunas, billfishes and sharks. NOAA, Technical Report NMFS 8.

Camhi, M. D., E. Lauck, E. K. Pikitch, and E. A. Babcock. 2008. A global overview of commercial fisheries for open ocean sharks. Pages 166-192 *in* M. D. Camhi, E. K. Pikitch, and E. A. Babcock, editors. Sharks of the Open Ocean: Biology, Fisheries and Conservation. Blackwell Science, Oxford.

Campana, S. E. 2014. Age determination of elasmobranchs, with special reference to Mediterranean species: A technical manual. Studies and Reviews. General Fisheries Commission for the Mediterranean. No. 94. FAO, Rome.

Campana, S. E., A. Dorey, M. Fowler, W. Joyce, Z. Wang, D. Wright, and I. Yashayaev. 2011. Migration pathways, behavioural thermoregulation and overwintering grounds of blue sharks in the Northwest Atlantic. Plos One **6**:e16854.

Campana, S. E., L. Marks, W. Joyce, and N. E. Kohler. 2006. Effects of recreational and commercial fishing on blue sharks (*Prionace glauca*) in Atlantic Canada, with inferences on the North Atlantic population. Canadian Journal of Fisheries and Aquatic Sciences **63**:670-682.

Campana, S. E., L. J. Natanson, and S. Myklevoll. 2002. Bomb dating and age determination of large pelagic sharks. Canadian Journal of Fisheries and Aquatic Sciences **59**:450-455.

Campana, S. E., and W. N. Joyce. 2004. Temperature and depth associations of porbeagle shark (*Lamna nasus*) in the northwest Atlantic. Fisheries Oceanography **13**:52-64.

Campana, S. E., W. Joyce, and L. Marks. 2003. Status of the porbeagle shark (*Lamna nasus*) population in the Northwest Atlantic in the context of species at risk. Canadian Stock Assessment Secretariate Research Document 2003/007.

Campana, S. E., W. Joyce, L. Marks, P. Hurley, L. J. Natanson, N. E. Kohler, C. F. Jensen, J. J. Mello, H. L. J. Pratt, S. Myklevoll, and S. Harley. 2008. The rise and fall (again) of the porbegale shark population in the Northwest Atlantic. Pages 445-461 *in* M. D. Camhi, E. K. Pikitch, and E. A. Babcock, editors. Sharks of the open ocean: biology, fisheries and conservation. Blackwell Publishing, Oxford.

Campana, S. E., W. N. Joyce, and M. J. Manning. 2009. Bycatch and discard mortality in commercially caught blue sharks *Prionace glauca* assessed using archival satellite pop-up tags. Marine Ecology Progress Series **387**:241-253.

Campana, S. E., W. N. Joyce, and M. Fowler. 2010. Subtropical pupping ground for a cold-water shark. Canadian Journal of Fisheries and Aquatic Sciences **67**:769-773.

Carabel, S., E. Godinez-Dominguez, P. Verisimo, L. Fernandez, and J. Freire. 2006. An assessment of sample processing methods for stable isotope analyses of marine food webs. Journal of Experimental Marine Biology and Ecology **336**:254-261.

Carleton, S. A., and Martinez del Rio. 2010. Growth and catabolism in isotopic incorporation: a new foundation and experimental data. Functional Ecology **24**:805-812.

Carlisle, A. B., K. J. Goldman, S. Y. Litvin, D. J. Madigan, J. S. Bigman, A. M. Switherbank, T. C. Kline Jr, and B. A. Block. 2015. Stable isotope analysis of vertebrae reveals ontogentic changes in habitat in an endothermic pelagic shark. Proceedings of the Royal Society B-Biological Sciences **282**:20141446.

Carpenter, E. J., H. R. Harvey, B. Fry, and D. G. Capone. 1997. Biogeochemical tracers of the marine cyanobacterium *Trichodesmium*. Deep-Sea Research Part I-Oceanographic Research Papers **44**: 27-38.

Casey, J. G., and N. E. Kohler. 1991. Long distance movements of Atlantic sharks from the NFS cooperative shark tagging program. Underwater Naturalist **19**:87-91.

Castro, J. A., and J. Mejuto. 1995. Reproductive parameters of blue shark, *Prionace glauca*, and other sharks in the Gulf of Guinea. Marine and Freshwater Research **46**:967-973.

Chen, W.-P., X.-Y. Yang, A. D. Hegeman, W. M. Gray, and J. D. Cohen. 2010. Microscale analysis of amino acids using gas chromatography-mass spectrometry after methyl chloroformate derivatization. Journal of Chromatography B **878**:2199-2208.

Cherel, Y., and K. A. Hobson. 2007. Geographical variation in carbon stable isotope signatures of marine predators: a tool to investigate their foraging areas in the Southern Ocean. Marine Ecology Progress Series **329**:281-287.

Cherel, Y., K. A. Hobson, and H. Weimerskirch. 2000. Using stable-isotope analysis of feathers to distinguish moulting and breeding origins of seabirds. Oecologia **122**:155-162.

Cherel, Y., L. Kernaleguen, P. Richard, and C. Guinet. 2009. Whisker isotopic signature depicts migration patterns and multi-year intra- and inter-individual foraging strategies in fur seals. Biology Letters **5**:830-832.

Chikaraishi, Y., N. O. Ogawa, and N. Ohkouchi. 2010. Further evaluation of the trophic level estimation based on nitrogen isotopic composition of amino acids. Pages 37-51 *in* N. Ohkouchi, I. Tayasu, and K. Koba, editors. Earth, Life, and Isotopes. Kyoto University Press, Japan.

Chikaraishi, Y., N. O. Ogawa, Y. Kashiyama, Y. Takano, H. Suga, A. Tomitani, H. Miyashita, H. Kitazato, and N. Ohkouchi. 2009. Determination of aquatic food-web structure based on compound-specific nitrogen isotopic composition of amino acids. Limnology and Oceanography: Methods **7**:740-750.

Chikaraishi, Y., S. A. Steffan, N. O. Ogawa, N. F. Ishikawa, Y. Sasaki, M. Tsuchiya, and N. Ohkouchi. 2014. High-resolution food webs based on nitrogen isotopic composition of amino acids. Ecology and Evolution **4**:2423-2449.

Chikaraishi, Y., Y. Kashiyama, N. O. Ogawa, H. Kitazato, and N. Ohkouchi. 2007. Metabolic control of nitrogen isotope composition of amino acids in macroalgae and gastropods: implications for aquatic food web studies. Marine Ecology Progress Series **342**:85-90.

Childress, J. J., and B. A. Siebel. 1998. Life at a stable oxygen level: adaptations of animals to oceanic minimum oxygen layers. Journal of Experimental Biology **201**:1223-1232.

Choy, C. A., B. N. Popp, C. C. S. Hannides, and J. C. Drazen. 2015. Trophic structure and food resources of epipelagic and mesopelagic fishes in the North Pacific. Limnology and Oceanography **60**:1156-1171.

Choy, C. A., P. C. Davison, J. C. Drazen, A. Flynn, E. J. Gier, J. C. Hoffman, J. P. McClain-Counts, T. W. Miller, B. N. Popp, S. W. Ross, and T. T. Sutton. 2012. Global trophic position comparison of two dominant mesopelagic fish families (Myctophidae, Stomiidae) using amino acid nitrogen isotopic analyses. Plos One **7**:e50133.

Christiansen, H. M., N. E. Hussey, S. P. Wintner, G. Cliff, S. F. J. Dudley, and A. T. Fisk. 2014. Effect of sample preparation techniques for carbon and nitrogen stable isotope analysis of hydroxyapatite structures in the form of elasmobranch vertebral centra. Rapid Communications in Mass Spectrometry **28**:448-456.

Christiansen, H. M., S. E. Campana, A. T. Fisk, G. Cliff, S. P. Wintner, S. F. J. Dudley, L. A. Kerr, and N. E. Hussey. 2016. Using bomb radiocarbon to estimate age and growth of the white shark, *Carcharodon carcharias*, from the southwestern Indian Ocean. Marine Biology **163**:144.

Clarke, G. L., and E. J. Denton. 1962. Light and animal life. Pages 456-468 *in* M. N. Hill, editor. The Sea Volume I: Physical Oceanography. John Wiley & Sons Lid, New York.

Clarke, S. C., M. K. McAllister, E. J. Milner-Gulland, G. P. Kirkwood, C. G. J. Michielsens, D. J. Agnew, E. K. Pikitch, H. Nakano, and M. S. Shivji. 2006. Global estimates of shark catches using trade records from commercial markets. Ecology Letters **9**:1115-1126.

Clausen, P., B. A. Nolet, A. D. Fox, and M. Klaassen. 2002. Long-distance endozoochorous dispersal of submerged macrophyte seeds by migratory waterbirds in northern Europe – a critical review of possibilities and limitations. Acta Oecologia **23**:191-203.

Collins, W. J., N. Bellouin, M. Doutriaux-Boucher, N. Gedney, P. Halloran, T. Hinton, J. Hughes, C. D. Jones, M. Joshi, S. Liddicoat, G. Martin, F. O'Connor, J. Rae, C. Senior, S. Sitch, I. Totterdell, A. Wiltshire, and S. Woodward. 2011. Development and evaluation of an Earth-system model – HadGEM2. Geoscience Model Development Discussions **4**:997-1062.

Compagno, L. J. V. 1984. Vol. 4. Sharks of the world. An annotated and illustrated catalogue of shark species known to date. Food and Agriculture Organization of the United Nations, Rome.

Compagno, L. J. V. 2001. Vol. 2. Sharks of the world. An annotated and illustrated catalogue of shark species known to date. Food and Agriculture Organization of the United Nations, Rome.

Cortes, E. 1999. Standardized diet compositions and trophic levels of sharks. ICES Journal of Marine Science **56**:707-717.

Cortes, E. 2000. Life history patterns and correlations in sharks. Reviews in Fishery Science **8**:299-344.

Cortes, E. 2002. Incorporating uncertainty into demographic modeling: application to shark populations and their conservation. Conservation Biology **16**:1048-1062.

Costa, D. P., G. A. Breed, and P. W. Robinson. 2012. New insights into pelagic migrations: implications for ecology and conservation. Annual Review of Ecology, Evolution, and Systematics **43**:73-96.

Cryan, P. M., C. A. Stricker, and M. B. Wunder. 2014. Continental-scale, seasonal movements of a heterothermic migratory tree bat. Ecological Applications **24**:602-616.

Dean, M. N., and A. P. Summers. 2006. Mineralized cartilage in the skeleton of chondrichthyan fishes. Zoology **109**:164-168.

Dehairs, F., E. Kopczynska, P. Nielson, C. Lancelot, D. C. E. Bakker, W. Koeve, and L. Goeyens. 1997. $\delta^{13}C$ of Southern Ocean suspended organic matter during spring and early summer: regional and temporal variability. Deep-Sea Research Part II-Topical Studies in Oceanography **44**:129-142.

DeNiro, M. J., and S. Epstein. 1977. Mechanisms of carbon isotope fractionation associated with lipid synthesis. Science **197**:261-263.

DeNiro, M. J., and S. Epstein. 1978. Influence of diet on distribution of carbon isotopes in animals. Geochimica Et Cosmochimica Acta **42**:495-506.

DeNiro, M. J., and S. Epstein. 1981. Influence of diet on the distribution of nitrogen isotopes in animals. Geochimica Et Cosmochimica Acta **45**:341-351.

Dingle, H. 1996. Migration: The Biology of Life on the Move. Oxford University Press, Oxford.

Dobson, A. 2009. Food-web structure and ecosystem services: insights from the Serengeti. Philosophical Transactions of the Royal Society B-Biological Sciences **364**:1665-1682.

Docherty, G., V. Jones, and R. P. Evershed. 2001. Practical and theoretical considerations in the gas chromatography/combustion/isotope ratio mass spectrometry $\delta^{13}C$ analysis of small polyfunctional compounds. Rapid Communications in Mass Spectrometry **15**:730-738.

Dulvy, N. K., J. K. Baum, S. Clarke, L. J. V. Compagno, E. Cortes, A. Domingo, S. Fordham, S. Fowler, M. P. Francis, C. Gibson, J. Martinez, J. A. Musick, A. Soldo, J. D. Stevens, and S. Valenti. 2008. You can swim but you can't hide: the global status and conservation of oceanic pelagic sharks and rays. Aquatic Conservation Marine and Freshwater Ecosystems **18**:459-482.

Dulvy, N. K., S. L. Fowler, J. A. Musik, R. D. Cavanagh, P. M. Kyne, L.R. Harrison, J. K. Carlson, L. N. Davidson, S. V. Fordham, M. P. Francis, C. M. Pollock, C. A. Simpfendorfen, G. H. Burgess, K. E. Carpenter, L. J. Compagno, D. A. Erbert, C. Gibson, M. R. Heupel, S. R. Livingstone, J. C. Sanciargo, J. D. Stevens, S. Valenti, and W. T. White. 2014. Extinction risk and conservation of the world's sharks and rays. eLife **3**:e00590.

Dunton, K. H., S. M. Saupe, A. N. Golikov, D. M. Schell, and S. V. Schonberg. 1989. Trophic relationships and isotopic gradients among arctic and subarctic marine fauna. Marine Ecology Progress Series **56**:89-97.

Ellis, G. S., G. Herbert, and D. Hollander. 2014. Reconstructing carbon sources in a dynamic estuarine ecosystem using oyster amino acid $\delta^{13}C$ values from shell and tissue. Journal of Shellfish Research **33**:217-225.

Ellis, J. R., V. J. Bendall, S. J. Hetherington, J. F. Silva, and S. R. McCully Phillips. 2015. National Evaluation of Populations of Threatened and Uncertain Elasmobranchs (NEPTUNE). Cefas. Lowestoft, UK.

Elsdon, T. S., B. K. Wells, S. E. Campana, B. M. Gillanders, C. M. Jones, K. E. Limburg, D. H. Secor, S. R. Thorrold, and B. D. Walther. 2008. Otolith chemistry to describe movements and life-history parameters of fishes: hypotheses, assumptions, limitations and inferences. Pages 297 *in* R. N. Gibson, R. J. A. Atkinson, and J. D. M. Gordon, editors. Oceanography and Marine Biology: An Annual Review. Vol. 46.

Estes, J. A., J. Tereborgh, J. S. Power, J. Berger, W. J. Bond, S. R. Carpenter, T. E. Essington, R. D. Holt, and J. B. Jackson. 2011. Trophic downgrading of planet Earth. Science **333**:301-306.

Estrada, J. A., A. N. Rice, L. J. Natanson, and G. B. Skomal. 2006. Use of isotopic analysis of vertebrae in reconstructing ontogenetic feeding ecology in white sharks. Ecology **87**:829-834.

Farquhar, G. D., M. H. O'Leary, and J. A. Berry. 1982. On the relationship between carbon isotope discrimination and the inter-cellular carbon dioxide concentration in leaves. Australian Journal of Plant Physiology **9**:121-137.

Ferretti, F., B. Worm, G. L. Britten, M. R. Heithaus, and H. K. Lotze. 2010. Patterns and ecosystem consequences of shark declines in the ocean. Ecology letters **13**:1055-1071.

Fischer, G., P. J. Muller, and G. Wefer. 1998. Latitudinal $\delta^{13}C_{org}$ variations in sinking matter and sediments from the South Atlantic: effects of anthropogenic CO_2 and implications for paleo-pCO_2 reconstructions. Journal of Marine Systems **17**:471-495.

Flockhart, D. T. T., L. I. Wassenaar, T. G. Martin, K. A. Hobson, M. B. Wunder, and D. R. Norris. 2013. Tracking multi-generational colonization of the breeding grounds by monarch butterlies in eastern North America. Proceedings of the Royal Society B-Biological Sciences **280**:20101387.

Fontugne, M. R., and J. C. Duplessy. 1981. Organic carbon isotopic fractionation by marine plankton in the temperature range -1 to 31 °C. Oceanologica Acta **4**:85-90.

Forsythe, W. C., E. J. Rykiel Jr, R. S. Stahl, H. Wu, and R. M. Schoofield. 1995. A model comparison for day-length as a function of latitude and day of the year. Ecological Modelling **80**:87-95.

Fraley, C., A. E. Raftery, T. B. Murphy, and L. Scrucca. 2012. mclust version 4 for R: normal mixture modeling for model-based clustering, classification, and density estimation. Technical report No. 597, Department of Statistics, University of Washington, Washington.

Francis, M. P., L. J. Natanson, and S. E. Campana. 2008. The biology and ecology of the porbeagle shark, *Lamna nasus*. Pages 105-113 *in* M. D. Camhi, E. K. Pikitch, and E. A. Babcock, editors. Sharks of the open ocean: biology, fisheries and conservation. Blackwell Publishing, Oxford.

Francis, M. P., S. E. Campana, and C. M. Jones. 2007. Age under-estimation in New Zealand porbeagle sharks (*Lamna nasus*): is there an upper limit to ages that can be determined from shark vertebrae? Marine and Freshwater Research **58**:10-23.

Francois, R., M. A. Altabet, R. Goericke, D. C. McCorkle, C. Brunet, and A. Poisson. 1993. Changes in the $\delta^{13}C$ of surface water particulate organic matter across the subtropical convergence in the South West Indian Ocean. Global Biogeochemical Cycles **7**:627-644.

Freeman, K. H., and J. M. Hayes. 1992. Fractionation of carbon isotopes by phytoplankton and estimates of ancient carbon dioxide levels. Global Biogeochemical Cycles **6**:185-198.

Frisk, M. G., T. J. Miller, and M. J. Fogarty. 2001. Estimation and analysis of biological parameters in elasmobranch fishes: a comparative life history study. Canadian Journal of Fisheries and Aquatic Sciences **58**:969-981.

Fry, B., and S. C. Wainright. 1991. Diatom sources of ^{13}C rich carbon in marine food webs. Marine Ecology Progress Series **76**:149-157.

Fryxell, J. M., J. Greever, and A. R. E. Sinclair. 1988. Why are migratory ungulates so abundant? American Naturalist **131**:781-798.

Gage, J. D. 2003. Food inputs, utilization, carbon flow and energetics. Pages 313-380 *in* P. A. Tyler, editor. Ecosystems Of The Deep Oceans. Elsevier, Amsterdam.

Garcia, V. B., L. O. Lucifora, and R. A. Myers. 2008. The importance of habitat and life history to extinction risk in sharks, skates, rays and chimaera. Proceedings of the Royal Society B-Biological Sciences **275**:83-89.

Garcia-Perez, B., and K. A. Hobson. 2014. A multi-isotope (δ^2H, $\delta^{13}C$, $\delta^{15}N$) approach to establishing migratory connectivity of Barn Swallow (*Hirundo rustica*). Ecosphere **5**:21.

Gastwirth, J.L., Y. R. Gel, W. L. W. Hui, V. Lyubchich; W. Miao, and K. Noguchi. 2015. lawstat: Tools for Biostatistics, Public Policy, and Law. R package version 3.0.

Gillanders, B. M., K. W. Able, J. A. Brown, D. B. Eggleston, and P. F. Sheridan. 2003. Evidence of connectivity between juvenile and adult habitats for mobile marine fauna: an important component of nurseries. Marine Ecology Progress Series **247**:281-295.

Godley, B. J., J. M. Blumenthal, A. C. Broderick, M. S. Coyne, M. H. Godfrey, L. A. Hawkes, and M. J. Witt. 2008. Satellite tracking of sea turtles: where have we been and where do we go next? Endangered Species Research **4**:3-22.

Goericke, R., and B. Fry. 1994. Variations of marine plankton $\delta^{13}C$ with latitude, temperature, and dissolved CO_2 in the world ocean. Global Biogeochemical Cycles **8**:85-90.

Goericke, R., J. P. Montaya, and B. Fry. 1994. Physiology of isotope fractionation in algae and cyanobacteria. Pages 187-221 *in* K. Lajtha and B. Michener, editors. Stable Isotopes in Ecology. Blackwell Science, Cambridge, MA.

Goering, J., V. Alexander, and N. Haubenstock. 1990. Seasonal variability of stable carbon and nitrogen isotope ratios of organisms in a North Pacific bay. Estuarine Coastal and Shelf Science **30**:239-260.

Graham, B. S., P. L. Koch, S. D. Newsome, K. W. McMahon, and D. Aurioles. 2010. Using isoscapes to trace the movements and foraging behavior of top predators in oceanic ecosystems *in* J. B. West, G. J. Bowen, T. E. Dawson, and K. P. Tu, editors. Isoscapes: Understanding Movement, Pattern, and Process on Earth through Isotope Mapping. Springer, Berlin.

Graham, B.S., B. Fry, B. N. Popp, R. J. Olson, and K. N. Holland. 2009. Tissue turnover rates in captive and wild populations of an endothermic teleost, yellowfin tuna, in captivity and in the wild. Journal of Experimental Marine Biololgy and Ecology.

Grubbs, R. D. 2010. Ontogenetic shifts in movements and habitat use. Pages 319-350 *in* J. C. Carrier, J. A. Musick, and M. R. Heithaus, editors. Sharks and Their Relatives II: Biodiversity, Adaptive Physiology, and Conservation. CRC Press, Boca Raton, FL.

Grubbs, R. D., J. K. Carlson, J. G. Romine, T. H. Curtis, W. D. McElroy, C. T. McCandless, C. F. Cotton, and J. A. Musik. 2016. Critical assessment and ramifications of a purported marine trophic cascade. Scientific Reports **6**:20970.

Gruess, A., D. M. Kaplan, S. Guenette, C. M. Roberts, and L. W. Botsford. 2011. Consequences of adult and juvenile movement for marine protected areas. Biological Conservation **144**:692-702.

Hamady, L. 2014. Age, movements, and feeding ecology of northwest Atlantic white sharks estimated from ecogeochemical profiles in vertebrae. Massachusetts Institute of Technology – Woods Hole Oceanographic Institution.

Hamady, L. L., L. J. Natanson, G. B. Skomal, and S. R. Thorrold. 2014. Vertebral bomb radiocarbon suggests extreme longevity in white sharks. Plos One **9**:e84006.

Hammerschlag, N., A. J. Gallagher, and D. M. Lazarre. 2011. A review of shark satellite tagging studies. Journal of Experimental Marine Biology and Ecology **398**:1-8.

Hannides, C. C. S., B. N. Popp, C. A. Choy, and J. C. Drazen. 2013. Midwater zooplankton and suspended particle dynamics in the North Pacific Subtropical Gyre: a stable isotope perspective. Limnology and Oceanography **56**:1931-1946.

Hare, P. E., M. L. Fogel, T. W. Stafford, A. D. Mitchell, and T. C. Hoering. 1991. The isotopic composition of carbon and nitrogen in individual amino acids isolated from modern and fossil proteins. Journal of Archaeological Science **18**:277-292.

Harrison, X. A., J. D. Blount, R. Inger, D. R. Norris, and S. Bearhop. 2011. Carry-over effects as drivers of fitness differences in animals. Journal of Animal Ecology **80**:4-18.

Hayes, J. M. 2001. Fractionation of carbon and hydrogen isotopes in biosynthetic processes. Reviews in Mineralogy and Geochemistry **43**:225-277.

Hazen, E. L., S. M. Maxwell, H. Bailey, S. J. Bograd, M. Hamann, P. Gaspar, B. J. Godley, and G. L. Shillinger. 2012. Ontogeny in marine tagging and tracking science: technologies and data gaps. Marine Ecology Progress Series **457**:221-240.

Heithaus, M. R., A. Frid, A. J. Wirsing, and B. Worm. 2008. Predicting ecological consequences of marine top predator declines. Trends in Ecology & Evolution **23**:202-210.

Heithaus, M.R., A. Frid, A. J. Wirsing, L. M. Dill, J. W. Fourgurean, D. Burkholder, J. Thomson, and L. Beider. 2007. State-dependent risk taking by green sea turtles mediates top-down effects of tiger shark intimidation in a marine ecosystem. Journal of Animal Ecology **76**:837-844.

Heithaus, M.R., and L. M. Dill. 2006. Does tiger shark predation risk influence foraging habitat use by bottlenose dolphins at multiple spatial scales? Oikos **114**:257-264.

Henderson, A. C., K. Flannery, and J. Dunne. 2001. Observations on the biology and ecology of the blue shark in the North-east Atlantic. Journal of Fish Biology **58**:1347-1358.

Heupel, M. R., D. M. Knip, C. A. Simperdorfen, and N. K. Dulvy. 2014. Sizing up the ecological role of sharks as predators. Marine Ecology Progress Series **495**:291-298.

Heupel, M. R., J. K. Carlson, and C. A. Simpfendorfen. 2007. Shark nursery areas: concepts, definition, characterization and assumptions. Marine Ecology Progress Series **337**:287-297.

Hinga, K. R., M. A. Arthur, M. E. Q. Pilson, and D. Whitaker. 1994. Carbon isotope fractionation by marine phytoplankton in culture – The effects of CO_2 concentration, pH, temperature, and species. Global Biogeochemical Cycles **8**:91-102.

Hobson, K. A. 1999. Tracing origins and migration of wildlife using stable isotopes: a review. Oecologia **120**:314-326.

Hobson, K. A., D. X. Soto, D. R. Paulson, L. I. Wassenaar, and J. H. Matthews. 2012. A dragonfly δ^2H isoscape for North America: a new tool for determining natal origins of migratory aquatic emergent insects. Methods in Ecology and Evolution **3**:766-772.

Hobson, K. A., R. Barnett-Johnson, and T. Cerling. 2010. Using isoscapes to track animal migration. Pages 273-298 *in* B. West, G. J. Bowen, T. E. Dawson, and K. P. Tu, editors. Isoscapes: Understanding Movement, Pattern, and Process on Earth through Isotope Mapping. Springer Science, Berlin.

Hoen, D. K., S. L. Kim, N. E. Hussey, N. J. Wallsgrove, J. C. Drazen, and B. N. Popp. 2014. Amino acid N-15 trophic enrichment factors of four large carnivorous fishes. Journal of Experimental Marine Biology and Ecology **453**:76-83.

Hoening, J. M., and S. H. Gruber. 1990. Life history patterns in the elasmobranchs: implications for fishery management. Pages 1-16 *in* H. L. Pratt Jr., S. H. Gruber, and T. Taniuchi editors. Elasmobranchs as living resources: advances in biology, ecology, systematics and status of the fisheries. U.S. Department of Commerce, NOAA, Technical Report NMFS 90.

Hofmann, M., D. A. Wolf-Gladrow, T. Takahashi, S. C. Sutherland, K. D. Six, and E. Maier-Reimer. 2000. Stable carbon isotope distribution of particulate organic matter in the ocean: a model study. Marine Chemistry **72**:131-150.

Holdo, R. M., R. D. Holt, A. R. E. Sinclair, B. J. Godley, and S. Thirgood. 2011. Migration impacts on communities and ecosystems: empirical evidence and theoretical insights. Pages 131-143 *in* E. J. Milner-Gulland, J. M. Fryxell, and A. R. E. Sinclair, editors. Animal Migration: A Synthesis. Oxford University Press, Oxford.

Holdo, R. M., R. D. Holt, M. B. Coughenour, and M. E. Ritchie. 2007. Plant productivity and soil nitrogen as a function of grazing, migration and fire in an African savanna. Journal of Ecology **95**:115-128.

Holtgrieve, G. W., and D. E. Schindler. 2011. Marine-derived nutrients, bioturbation, and ecosystem metabolism: reconsidering the role of salmon in streams. Ecology **92**:373-385.

Howland, M. R., L. T. Corr, S. M. M. Young, V. Jones, S. Jim, N. J. van der Merwe, A. D. Mitchell, and R. P. Evershed. 2003. Expression of the dietary isotope signal in the compound-specific $\delta^{13}C$ values of pig bone lipids and amino acids. International Journal of Osteoarchaeology **13**:54-65.

Husek, P. 1991. Rapid derivatization and gas chromatographic determination of amino acids. Journal of chromatography **552**:289-299.

Hussey, N. E., M. A. MacNeil, B. C. McMeans, J. A. Olin, S. F. J. Dudley, G. Cliff, S. P Wintner, S. T. Fennessy, and A. T. Fisk. 2014. Rescaling the trophic structure of marine food webs. Ecology Letters **17**:239-350.

Hussey, N. E., M. A. MacNeil, J. A. Olin, B. C. McMeans, M. J. Kinney, D. D. Chapman, and A. T. Fisk. 2012. Stable isotopes and elasmobranchs: tissue types, methods, applications and assumptions. Journal of Fish Biology **80**:1449-1484.

Hutchings, J. A., R. A. Myers, V. B. Garcia, L. O. Lucifora, and A. Kuparinen. 2012. Life-history correlates of extinction risk and recovery potential. Ecological Applications **22**:1061-1067.

ICCAT/ICES. 2009. Report of the 2009 Porbeagle Stock Assessment Meeting. SCRS/2009/014-Sharks Stock Assessment. SCI-032/2009. Copenhagen, Denmark, June 22-27, 2009.

Jackson, A. L., A. C. Parnell, I. R., and S. Bearhop. 2011. Comparing isotopic niche widths among and within communities: SIBER – Stable Isotope Bayesian Ellipses in R. Journal of Animal Ecology **80**:595-602.

Jacob, U., K. Mintenbeck, T. Brey, R. Knust, and K. Beyer. 2005. Stable isotope food web studies: a case for standardized sample treatment. Marine Ecology Progress Series **287**:251-253.

Jaeger, A., V. J. Lecomte, H. Weimerskirch, P. Richard, and Y. Cherel. 2010. Seabird satellite tracking validates the use of latitudinal isoscapes to depict predators' foraging areas in the Southern Ocean. Rapid Communications in Mass Spectrometry **24**:3456-3460.

Jardine, T. D., and R.A. Cunjak. 2005. Analytical error in stable isotope ecology. Oecologia **144**:528-533.

Jennings, S., J. D. Reynolds, and S. C. Millis. 1998. Life history correlates of responses to fish exploitation. Proeedings of the Royal Society B-Biological Sciences **265**:333-339.

Jennings, S., and K. J. Warr. 2003. Environmental correlates of large-scale spatial variation in the $\delta^{15}N$ of marine animals. Marine Biology **142**:1131-1140.

Jennings, S., M. J. Kaiser, and J. D. Reynolds. 2001. Marine Fisheries Ecology. Blackwell Science, Oxford.

Jensen, C. F., L. J. Natanson, H. L. Pratt, N. E. Kohler, and S. E. Campana. 2002. The reproductive biology of the porbeagle shark (*Lamna nasus*) in the western North Atlantic Ocean. Fishery Bulletin **100**:727-738.

Jim, S., V. Jones, S. H. Ambrose, and R. P. Evershed. 2006. Quantifying dietary macronutrient sources of carbon for bone collagen biosynthesis using natural abundance stable carbon isotope analysis. British Journal of Nutrition **95**:1055-1062.

Jones, C. D., J. K. Hughes, N. Bellouin, S. C. Hardiman, G. S. Jones, J. Knight, S. Liddicoat, F. M. O'Connor, R. J. Andres, C. Bell, K. O. Boo, A. Bozzo, N. Butchart, P. Cadule, K. D. Corbin, M. Doutriaux-Boucher, P. Friedlingstein, J. Gornall, L. Gray, P. R. Halloran, G. Hurtt, W. J. Ingram, J. F. Lamarque, R. M. Law, M. Meinshausen, S. Osprey, E. J. Palin, L. Parsons Chini, T. Raddatz, M. G. Sanderson, A. A. Sellar, A. Schurer, P. Valdes, N. Wood, S. Woodward, M. Yoshioka, and M. Zerroukat. 2011. The HadGEM2-ES implementation of CMIP5 centennial simulations. Geoscience Model Development **4**:543-570.

Joyce, W. N., S. E. Campana, L. J. Natanson, N. E. Kohler, H. L. Pratt, and C. F. Jensen. 2002. Analysis of stomach contents of the porbeagle shark (*Lamna nasus* Bonnaterre) in the northwest Atlantic. ICES Journal of Marine Science **59**:1263-1269.

Kaiser, M. J., M. J. Attrill, S. Jennings, D. N. Thomas, D. K. A. Barnes, A. S. Brierley, N. V. C. Polunin, D. G. Raffaelli, and P. J. l. B. Williams. 2005. Marine Ecology: Processes, Systems, and Impacts. Oxford University Press, Oxford and New York.

Karasov, W. H., and C. Martínez del Rio. 2007. Physiological Ecology. Princeton University Press, Princeton, NJ.

Keller, K., and F. M. M. Morel. 1999. A model of carbon isotopic fractionation and active carbon uptake in phytoplankton. Marine Ecology Progress Series **182**:295-298.

Kelly, J. F. 2000. Stable isotopes of carbon and nitrogen in the study of avian and mammalian trophic ecology. Journal of Canadian Zoology **78**:1-27.

Kerr, L. A., A. H. Andrews, G. M. Cailliet, T. A. Brown, and K. H. Coale. 2006. Investigations of $\Delta^{14}C$, $\delta^{13}C$, and $\delta^{15}N$ in vertebrae of white shark (*Carcharodon carcharias*) from the eastern North Pacific Ocean. Environmental Biology of Fishes **77**:337-353.

Kim, S. L., and P. L. Koch. 2012. Methods to collect, preserve, and prepare elasmobranch tissues for stable isotope analysis. Environmental Biology of Fishes **95**:53-63.

Kim, S. L., C. Martinez del Rio, D. Casper, and P. L. Koch. 2012b. Isotopic incorporation rates for shark tissues from a long-term captive feeding study. Journal of Experimental Biology **215**:2495-2500.

Kim, S. L., D. R. Casper, F. Galvan-Magana, R. Ochoa-Diaz, S. Berenice Hernandez-Aguilar, and P. L. Koch. 2012c. Carbon and nitrogen discrimination factors for elasmobranch soft tissues based on a long-term controlled feeding study. Environmental Biology of Fishes **95**:37-52.

Kim, S. L., M. T. Tinker, J. A. Estes, and P. L. Koch. 2012a. Ontogenetic and among-individual variation in foraging strategies of North East Pacific white sharks based on stable isotope analysis. Plos One **7**:e45068.

Klee, M. S. 1985. Modern practice of gas chromatography. Wiley, New York, NY.

Kohler, N. E. 1998. Aspects of the feeding ecology of the blue shark, *Prionace glauca*, in the Western North Atlantic. University of Rhode Island.

Kohler, N. E., and P. A. Turner. 2001. Shark tagging: a review of conventional methods and studies. Environmental Biology of Fishes **60**:191-223.

Kohler, N. E., and P. A. Turner. 2008. Stock structure of the blue shark (*Prionace glauca*) in the North Atlantic Ocean based on tagging data. Pages 339-350 *in* M. D. Camhi, E. K. Pikitch, and E. A. Babcock, editors. Sharks of the open ocean: biology, fisheries and conservation. Blackwell, Oxford.

Kohler, N. E., P. A. Turner, J. J. Hoey, L. J. Natanson, and R. Briggs. 2002. Tag and recapture data for three pelagic shark species: blue shark (*Prionace glauca*), shortfin mako (*Isurus xyrinchus*), and porbeagle (*Lamna nasus*) in the North Atlantic Ocean. Collective Volume of Scientific Papers ICCAT **54**:1231-1260.

Krauss, S., D. E. Stallknecht, N. J. Negovetich, L. J. Niles, R. J. Webby, and R. G. Webster. 2010. Coincident ruddy turnstone migration and horseshoe crab spawning creates an ecological 'hot spot' for influenza viruses. Proceedings of the Royal Society B-Biological Sciences **277**:3373-3379.

Lampitt, R. S., K. F. Wishner, C. M. Turley, and M. V. Angel. 1993. Marine snow studies in the Northeast Atlantic Ocean: distribution, composition and role as a food source for migrating plankton. Marine Biology **116**:689-702.

Lara, R. J., V. Alder, C. A. Franzosi, and G. Kattner. 2010. Characteristics of suspended particulate organic matter in the southwestern Atlantic: influence of temperature, nutrient and phytoplankton features on the stable isotope signature. Journal of Marine Systems **79**:199-209.

Larsen, T., D. L. Taylor, M. B. Leigh, and D. M. O'Brien. 2009. Stable isotope fingerprinting: a novel method for identifying plant, fungal, or bacterial origins of amino acids. Ecology **90**:3526-3535.

Larsen, T., L. T. Bach, R. Salvatteci, Y. V. Wang, N. Andersen, M. Ventura, and M. D. McCarthy. 2015. Assessing the potential of amino acid ^{13}C patterns as a carbon source tracer in marine sediments: effects of algal growth conditions and sedimentary diagenesis. Biogeosciences **12**:4979-4992.

Larsen, T., M. Ventura, N. Andersen, D. M. O'Brien, U. Piatkowski, and M. D. McCarthy. 2013. Tracing carbon sources through aquatic and terrestrial food webs using amino acid stable isotope fingerprinting. Plos One **8**:e73441.

Laws, E. A., B. N. Popp, R. R. Bidigare, M. C. Kennicutt, and S. A. Macko. 1995. Dependence of phytoplankton carbon isotopic composition on growth rate and $CO_{2(aq)}$ – theoretical considerations and experimental results. Geochimica Et Cosmochimica Acta **59**:1131-1138.

Laws, E. A., R. R. Bidigare, and B. N. Popp. 1997. Effect of growth rate and CO_2 concentration on carbon isotopic fractionation by the marine diatom *Phaeodactylum tricornutum*. Limnology and Oceanography **42**:1552-1560.

Layman, C. A., M. S. Araujo, R. Boucek, C. R. Hammerschlag-Peyer, E. Harrison, Z. R. Jud, P. Matich, A. E. Rosenblatt, J. J. Vaudo, L. A. Yeager, D. M. Post, and S. Bearhop. 2012. Applying stable isotopes to examine food-web structure: an overview of analytical tools. Biological Reviews **87**:545-562.

Leibold, M. A., M. Holyoak, N. Mouquet, P. Amarasekare, J. M. Chase, M. F. Hoopes, R. D. Holt, J. B. Shurin, R. Law, D. Tilman, M. Loreau, and A. Gonzalez. 2004. The metacommunity concept: a framework for multi-scale community ecology. Ecology Letters **7**:601-613.

Longhurst, A. R. 1995. Seasonal cycles of pelagic production and consumption. Progress in Oceanography **36**:77-167.

Longhurst, A. R. 1998. Ecological geography of the sea. Academic Press, San Diego, CA.

Longhurst, A. R. 2006. Ecological geography of the sea (2nd Edition). Elsevier, Amsterdam.

Loor-Andrade, P., F. Galván-Magaña, F. R. Elorriaga-Verplancken, C. Polo-Silva, and A. Delgado-Huertas. 2015. Population and individual foraging patterns of two hammerhead sharks using

carbon and nitrogen stable isotopes. Rapid Communications in Mass Spectrometry **29**:821-829.

Lorrain, A., B. Graham, F. Menard, B. Popp, S. Bouillon, P. van Breugel, and Y. Cherel. 2009. Nitrogen and carbon isotope values of individual amino acids: a tool to study foraging ecology of penguins in the Southern Ocean. Marine Ecology Progress Series **391**:293-306.

Lundberg, J., and F. Moberg. 2003. Mobile link organisms and ecosystem functioning: implications for ecosystem resilience and management. Ecosystems **6**:87-98.

Madec, G. 2008. "NEMO ocean engine". Note du Pole de modelisation. No. 27 ISSN No. 1288-1619. Institut Pierre-Simon Laplace, France.

MacKenzie, K. M., C. Longmore, C. Preece, C. H. Lucas, and C. N. Trueman. 2014. Testing the long-term stability of marine isoscapes in shelf seas using jellyfish tissues. Biogeochemistry **121**:441-454.

MacKenzie, K. M., M. R. Palmer, A. Moore, A. T. Ibbotson, W. R. C. Beaumont, D. J. S. Poulter, and C. N. Trueman. 2011. Locations of marine animals revealed by carbon isotopes. Scientific Reports **1**:21.

Macko, S. A., M. L. F. Estep, M. H. Engel, and P. E. Hare. 1986. Kinetic fractionation of stable nitrogen isotopes during amino acid transamination. Geochimica Et Cosmochimica Acta **50**:2143-2146.

MacNeill, M. A., G. B. Skomal, and A. T. Fisk. 2005. Stable isotopes from multiple tissues reveal diet switching in sharks. Marine Ecology Progress Series **302**:199-206.

Magozzi, S. M., A. Yool, H. B. Vander Zanden, M. B. Wunder, and C. N. Trueman. 2017. Using ocean models to predict spatial and temporal variation in marine carbon isotopes. Ecosphere. *In press*.

Mandelman, J. W., P. W. Cooper, T. B. Werner, and K. M. Lageux. 2008. Shark bycatch and depredation in the U.S. Atlantic pelagic longline fishery. Reviews in Fish Biology and Fisheries **18**:427-442.

Maranon, E. 2009. Phytoplankton size structure. Pages 445-452 *in* J. H. Steele, K. Turekian, and S. Thorpe editors. Encyclopedia of Ocean Sciences (2nd Edition). Academic Press, Amsterdam.

Markaida, U., and O. Sosa-Nishizaki. 2010. Food and feeding habits of the blue shark *Prionace glauca* caught off Ensenada, Baja California, Mexico, with a review on its feeding. Journal of the Marine Biological Association of the United Kingdom **90**:977-994.

Mate, B. R., R. Gisiner, and J. Mobley. 1998. Local and migratory movements of Hawaiian humpback whales tracked by satellite telemetry. Canadian Journal of Zoology-Revue Canadienne De Zoologie **76**:863-868.

McCann, K. S., J. B. Rasmussen, and J. Umbanhowar. 2005. The dynamics of spatially coupled food webs. Ecology Letters **8**:513-523.

McCann, K., A. Hastings, and G. R. Huxel. 1998. Weak trophic interactions and the balance of nature. Nature **395**:794-798.

McCarthy, M. D., J. Lehman, and R. Kudela. 2013. Compound-specific amino acid $\delta^{15}N$ patterns in marine algae: tracer potential for cyanobacterial vs. eukaryotic organic nitrogen sources in the ocean. Geochimica Et Cosmochimica Acta **103**:104-120.

McCarthy, M. D., R. Benner, C. Lee, and M. L. Fogel. 2007. Amino acid nitrogen isotopic fractionation patterns as indicators of heterotrophy in plankton, particulate, and dissolved organic matter. Geochimica Et Cosmochimica Acta **71**:4727-4744.

McCauley, D. J., H. S. Young, R. B. Dunbar, J. A. Estes, B. X. Semmens, and F. Micheli. 2012. Assessing the effects of large mobile predators on ecosystem connectivity. Ecological Applications **22**:1711-1717.

McClelland, J. W., and J. P. Montoya. 2002. Trophic relationships and the nitrogen isotopic composition of amino acids in plankton. Ecology **83**:2173-2180.

McConnell, B. J., M. A. Fedak, P. Lovell, and P. S. Hammond. 1999. Movements and foraging areas of grey seals in the North Sea. Journal of Applied Ecology **36**:573-590.

McCord, M. E., and S. E. Campana. 2003. A quantitative assessment of the diet of the blue shark (*Prionace glauca*) off Nova Scotia, Canada. Journal of Northwest Atlantic Fishery Science **32**:57-63.

McCutchan, J. H., W. M. Lewis, C. Kendall, and C. C. McGrath. 2003. Variation in trophic shift for stable isotope ratios of carbon, nitrogen, and sulfur. Oikos **102**:378-390.

McGowan, J. A. 1986. The biogeography of pelagic ecosystems. Pages 191-200 *in* Pelagic Biogeography: Proceedings of an International Conference. UNESCO Technical Papers in Marine Science.

McMahon, K. W. 2011. Functional connectivity of coral reef fishes in a tropical seascape assessed by compound-specific stable isotope analyses. Massachusetts Institute of Technology – Woods Hole Oceanographic Institution.

McMahon, K. W., L. L. Hamady, and S. R. Thorrold. 2013a. A review of ecogeochemistry approaches to estimating movements of marine animals. Limnology and Oceanography **58**:697-714.

McMahon, K. W., L. L. Hamady, S. R. Thorrold, and I. P. Smith. 2013b. Ocean ecogeochemistry: a review. Oceanography and Marine Biology: An Annual Review **51**:327-373.

McMahon, K. W., M. D. McCarthy, O. A. Sherwood, T. Larsen, and T. P. Guilderson. 2015a. Millennial- scale plankton regime shifts in the subtropical North Pacific Ocean. Science **350**:1530-1533.

McMahon, K. W., M. J. Polito, S. Abel, M. D. McCarthy, and S. R. Thorrold. 2015b. Carbon and nitrogen isotope fractionation of amino acids in an avian marine predator, the gentoo penguin (*Pygoscelis papua*). Ecology and Evolution **5**:1278-1290.

McMahon, K. W., M. L. Berumen, and S. R. Thorrold. 2012. Linking habitat mosaics and connectivity in a coral reef seascape. Proceedings of the National Academy of Sciences of the United States of America **109**:15372-15376.

McMahon, K. W., M. L. Berumen, I. Mateo, T. S. Elsdon, and S. R. Thorrold. 2011a. Carbon isotopes in otolith amino acids identify residency of juvenile snapper (Family: Lutjanidae) in coastal nurseries. Coral Reefs **30**:1135-1145.

McMahon, K. W., M. L. Fogel, B. J. Johnson, L. A. Houghton, and S. R. Thorrold. 2011b. A new method to reconstruct fish diet and movement patterns from $\delta^{13}C$ values in otolith amino acids. Canadian Journal of Fisheries and Aquatic Sciences **68**:1330-1340.

McMahon, K. W., M. L. Fogel, T. S. Elsdon, and S. R. Thorrold. 2010. Carbon isotope fractionation of amino acids in fish muscle reflects biosynthesis and isotopic routing from dietary protein. Journal of Animal Ecology **79**:1132-1141.

McMahon, K. W., S. R. Thorrold, L. A. Houghton, and M. L. Berumen. 2016. Tracing carbon flow through coral reef food webs using a compound-specific stable isotope approach. Oecologia **180**:809-821.

McMahon, K. W., S. R. Thorrold, T. S. Elsdon, and M. D. McCarthy. 2015c. Trophic discrimination of nitrogen in amino acids varies with diet quality in a marine fish. Limnology and Oceanography **60**:1076-1087.

Meehan, T. D., J. T. Giermakowski, and P. M. Cryan. 2004. GIS-based model of stable hydrogen isotope ratios in North American growing-season precipitation for use in animal movement studies. Isotopes in Environmental and Health Studies **40**:291-300.

Mendes, S., J. Newton, R. J. Reid, A. F. Zuur, and G. J. Pierce. 2007. Stable carbon and nitrogen isotope ratio profiling of sperm whale teeth reveals ontogenetic movements and trophic ecology. Oecologia **151**:605-615.

Mejuto, J., B. Garcia-Cortes, and A. Ramos-Cartelle. 2005. Tagging-recapture activities of large pelagic sharks carried out by Spain or in collaboration with the tagging programs of other countries. Collective Volume of Scientific Papers ICCAT **58**:974-1000.

Michelutti, N., B. E. Keatley, S. Brimble, J. M. Blais, H. Liu, M. S. V. Douglas, M. L. Mallory, R. W. Macdonald, and J. P. Smol. 2009. Seabird-driven shifts in Arctic pond ecosystems. Proceedings of the Royal Society B-Biological Sciences **276**:591-596.

Montoya, J. P. 2007. Natural abundance of ^{15}N in marine planktonic ecosystems. Pages 176-201 *in* R. Michener and K. Lajtha, editors. Stable Isotopes in Ecology and Environmental Science. Blackwell, Malden, MA.

Moore, J. W., and D. E. Schindler. 2004. Nutrient export from freshwater ecosystems by anadromous sockeye salmon (*Oncorhynchus nerka*). Canadian Journal of Fisheries and Aquatic Sciences **61**:1582-1589.

Morris, D. W. 2003. Toward an ecological synthesis: a case for habitat selection. Oecologia **136**:1-13.

Mourier, J., J. Maynard, V. Parravicini, L. Ballesta, E. Clua, M. L. Domeier, and S. Planes. 2016. Extreme inverted trophic pyramid of reef sharks supported by spawning groupers. Current Biology **26**:2011-2016.

Mucientes, G. R., N. Queiroz, L. L. Sousa, T. P., and D. W. Sims. 2009. Sexual segregation of pelagic sharks and the potential threat from fisheries. Biology Letters **5**:156-159.

Myers, R. A., and B. Worm. 2003. Rapid worldwide depletion of predatory fish communities. Nature **423**:280-283.

Myers, R.A., J. K. Baum, T. D. Shepherd, S. P. Powers, and C. H. Peterson. 2007. Cascading effects of the loss of apex predatory sharks from a coastal ocean. Science **315**:1846–1850.

Nakano, H., and J. D. Stevens. 2008. The biology and ecology of the blue shark *Prionace glauca*. Pages 140-148 *in* M. Camhi, E. Pikitch, and E. A. Babcock, editors. Sharks of the open ocean: biology, fisheries and conservation. Blackwell, Oxford.

Natanson, L. J., J. J. Mello, and S. E. Campana. 2002. Validated age and growth of the probeagle shark, *Lamna nasus*, in the western North Atlantic Ocean. Collective Volume of Scientific Papers ICCAT **54**:1261-1279.

Newsome, S. D., C. M. del Rio, S. Bearhop, and D. L. Phillips. 2007. A niche for isotopic ecology. Frontiers in Ecology and the Environment **5**:429-436.

Newsome, S. D., M. A. Etnier, D. H. Monson, and M. L. Fogel. 2009. Retrospective characterization of ontogenetic shifts in killer whale diets *via* $\delta^{13}C$ and $\delta^{15}N$ analysis of teeth. Marine Ecology Progress Series **374**:229-242.

Newsome, S. D., M. L. Fogel, L. Kelly, and C. Martinez del Rio. 2011. Contribution of direct incorporation from diet and microbial amino acids to protein synthesis in Nile tilapia. Functional Ecology **25**:1051-1062.

Newsome, S. D., M. T. Clementz, and P. L. Koch. 2010. Using stable isotope biogeochemistry to study marine mammal ecology. Marine Mammal Science **26**:509-572.

Nielsen, J. M., B. N. Popp, and M. Winder. 2015. Meta-analysis of amino acid stable nitrogen isotope ratios for estimating trophic position in marine organisms. Oecologia **178**:631-642.

Nielsen, J. L., H. Arrizabalaga, N. Fragoso, A. Hobday, M. Lutcavage, and J. Sibert. 2009. Tagging and tracking of marine animals with electronic devices. Springer Science and Business Media, New York, NY.

Nielsen, J., R. B. Hedeholm, J. Heinemeier, P. G. Bushnell, J. S. Christiansen, J. Olsen, C. Bronk Ramsey, R. W. Brill, M. Simon, K. F. Steffensen, and J. F. Steffensen. 2016. Eye lenses radiocarbon reveals centuries of longevity in the Greenland shark (*Somnius microcephalus*). Science **353**:702-704.

O'Brien, D. M., C. L. Boggs, and M. L. Fogel. 2003. Pollen feeding in the butterfly *Heliconius charitonia*: isotopic evidence for essential amino acid transfer from pollen to eggs. Proceedings of the Royal Society B-Biological Sciences **270**:2631-2636.

O'Leary, M. H. 1981. Carbon isotope fractionation in plants. Phytochemistry **20**:553-567.

Olin, J. A., N. E. Hussey, M. Fritts, M. R. Heupel, C. A. Simpfendorfer, G. R. Poulakis, and A. T. Fisk. 2011. Maternal meddling in neonatal sharks: implications for interpreting stable isotopes in young animals. Rapid Communications in Mass Spectrometry **25**:1008-1016.

Pade, N. G., N. Queiroz, N. E. Humphries, M. J. Witt, C. S. Jones, L. R. Noble, and D. W. Sims. 2009. First results from satellite-linked archival tagging of porbeagle shark, *Lamna nasus*: area fidelity, wider-scale movements and plasticity in diel depth changes. Journal of Experimental Marine Biology and Ecology **370**:64-74.

Parnell, A. C., I. R., S. Bearhop, and A. L. Jackson. 2010. Source partitioning using stable isotopes: coping with too much variation. Plos One **5**:e9672.

Parnell, A., and A. Jackson. 2013. SIAR: Stable Isotope Analysis in R. R package version 4.2.2.

Passerotti, M. S., A. H. Andrews, J. K. Carlson, S. P. Wintner, K. J. Goldman, and L. J. Natanson. 2014. Maximum age and missing time in the vertebrae of sand tiger shark (*Carcharias taurus*): validated lifespan from bomb radiocarbon dating in the western North Atlantic and southwestern Indian Oceans. Marine and Freshwater Research **65**:674-687.

Pauly, D., V. Christensen, J. Dalsgaard, R. Froese, and F. Torres. 1998. Fishing down marine food webs. Science **279**:860-863.

Peterson, B. J., and B. Fry. 1987. Stable isotopes in ecosystem studies. Annual Review of Ecology and Systematics **18**:293-320.

Piercy, A., Carlson, J. K., and Passerotti, M. 2010. Age and growth of the great hammerhead shark, *Sphyrna mokarran*, in the north-western Atlantic Ocean and Gulf of Mexico. Marine and Freshwater Research **61**:992-998.

Pine, W. E., K. H. Pollock, J. E. Hightower, T. J. Kwak, and J. A. Rice. 2003. A review of tagging methods for estimating fish population size and components of mortality. Fisheries **28**:10-23.

Pinheiro, J. C., and D. M. Bates. 2000. Mixed effect models in S and S-Plus. Springer, New York, United States.

Pinnegar, J.K., and N. V. C. Polunin. 1999. Differential fractionation of $\delta^{13}C$ and $\delta^{15}N$ among fish tissues: implications for the study of trophic interactions. Functional Ecology **13**:225-231.

Polis, G. A., W. B. Anderson, and R. D. Holt. 1997. Toward an integration of landscape and food web ecology: the dynamics of spatially subsidized food webs. Annual Review of Ecology and Systematics **28**:289-316.

Polo-Silva, C., S. D. Newsome, F. Galvan-Magana, M. Grijalba-Bendeck, and A. San Juan-Munoz. 2013. Trophic shift in the diet of the pelagic thresher shark based on stomach contents and stable isotope analyses. Marine Biology Research **9**:958-971.

Popp, B. N., B. S. Graham, R. J. Olson, C. C. S. Hannides, M. J. Lott, G. A. Lopez-Ibarra, F. Galvan-Magana, and B. Fry. 2007. Insight into the trophic ecology of yellowfin tuna, *Thunnus albacares*, from compound-specific nitrogen isotope analysis of proteinaceous amino acids. Pages 173-190 *in* T. Dawson and R. Siegwolf, editors. Stable Isotopes as Indicators of Ecological Change. Elsevier, Amsterdam.

Popp, B. N., E. A. Laws, R. R. Bidigare, J. E. Dore, K. L. Hanson, and S. G. Wakeham. 1998. Effect of phytoplankton cell geometry on carbon isotopic fractionation. Geochimica Et Cosmochimica Acta **62**:69-77.

Popp, B. N., T. Trull, F. Kenig, S. G. Wakeham, T. M. Rust, B. Tilbrook, F. B. Griffiths, S. W. Wright, H. J. Marchant, R. R. Bidigare, and E. A. Laws. 1999. Controls on the carbon isotopic composition of Southern Ocean phytoplankton. Global Biogeochemical Cycles **13**:827-843.

Porter, M. E., J. L. Beltran, T. J. Koob, and A. P. Summers. 2006. Material properties and biochemical composition of mineralized vertebral cartilage in seven elasmobranch species (Chondrichthyes). Journal of Experimental Biology **209**:2920-2928.

Post, D. M. 2002. Using stable isotopes to estimate trophic position: models, methods, and assumptions. Ecology **83**:703-718.

Pratt, H. L. 1979. Reproduction in the blue shark, *Prionace glauca*. Fishery Bulletin **77**:445-470.

Preti, A., C. U. Soykan, H. Dewar, R. J. D. Wells, N. Spear, and S. Kohin. 2012. Comparative feeding ecology of shortfin mako, blue and thresher sharks in the California Current. Environmental Biology of Fishes **95**:127-146.

Pusineri, C., O. Chancollon, J. Ringelstein, and V. Ridoux. 2008. Feeding niche segregation among the Northeast Atlantic community of oceanic top predators. Marine Ecology Progress Series **361**:21-34.

Queiroz, N., F. P. Lima, A. Maia, P. A. Ribeiro, J. P. Correia, and A. A. Santos. 2005. Movement of blue shark, *Prionace glauca*, in the north-east Atlantic based on mark-recapture data. Journal of the Marine Biological Association of the United Kingdom **85**:1107-1112.

Queiroz, N., N. E. Humphries, G. Mucientes, N. Hammerschlag, F. P. Lima, K. L. Scales, P. I. Miller, L. L. Sousa, R. Seabra, and D. W. Sims. 2016. Ocean-wide tracking of pelagic sharks reveals extent of overlap with longline fishing hotspots. Proceedings of the National Academy of Sciences of the United States of America **113**:1582-1587.

Queiroz, N., N. E. Humphries, L. R. Noble, A. M. Santos, and D. W. Sims. 2010. Short-term movements and diving behaviour of satellite-tracked blue sharks *Prionace glauca* in the northeastern Atlantic Ocean. Marine Ecology Progress Series **406**:265-279.

Queiroz, N., N. E. Humphries, L. R. Noble, A. M. Santos, and D. W. Sims. 2012. Spatial dynamics and expanded vertical niche of blue sharks in oceanographic fronts reveal habitat targets for conservation. Plos One **7**:e32374.

R Core Team. 2015. R: A language and environment for statistical computing. R Foundation for Statistical Computing, Vienna, Austria.

Radabaugh, K. R., D. J. Hollander, and E. B. Peebles. 2013. Seasonal $\delta^{13}C$ and $\delta^{15}N$ isoscapes of fish populations along a continental shelf trophic gradient. Continental Shelf Research **68**:112-122.

Ramos, R., and J. González-Solís. 2012. Trace me if you can: the use of intrinsic biogeochemical markers in marine top predators. Frontiers in Ecology and the Environment **10**:258-266.

Ramos, R., J. González-Solís, J. P. Croxall, D. Oro, and X. Ruiz. 2009. Understanding oceanic migrations with intrinsic biogeochemical markers. Plos One **4**:e6236.

Rau, G. H., R. E. Sweeney, and I. R. Kaplan. 1982. Plankton ^{13}C-^{12}C ratio changes with latitude – differences between northern and southern oceans. Deep-Sea Research Part I-Oceanographic Research Papers **29**:1035-1039.

Rau, G. H., T. Takahashi, and D. J. D. Marais. 1989. Latitudinal variations in plankton $\delta^{13}C$ – implications for CO_2 and productivity in past oceans. Nature **341**:516-518.

Rau, G. H., U. Riebesell, and D. Wolf-Gladrow. 1996. A model of photosynthetic ^{13}C fractionation by marine phytoplankton based on diffusive molecular CO_2 uptake. Marine Ecology Progress Series **133**:275-285.

Rau, G. H., U. Riebesell, and D. Wolf-Gladrow. 1997. $CO_{2(aq)}$-dependent photosynthetic ^{13}C fractionation in the ocean: a model *versus* measurements. Global Biogeochemical Cycles **11**:267-278.

Reeds, P. 2000. Dispensable and indispensable amino acids for humans. Journal of Nutrition **130**:1835S-1840S.

Rex, M. A., R. J. Etter, J. S. Morris, J. Crouse, C. R. McClain, N. A. Johnson, C. T. Stuart, J. W. Deming, R. Thies, and R. Avery. 2006. Global bathymetric patterns of standing stock and body size in the deep-sea benthos. Marine Ecology Progress Series **317**:1-8.

Rieley, G. 1994. Derivatization of organic compounds prior to gas chromatographic–combustion–isotope ratio mass spectrometry analysis: identification of isotope fraction processes. Analyst **119**:915-919.

Roff, G., C. Doropoulos, A. Rogers, Y.-M. Bozec, N. C. Krueck, E. Aurellando, M. Priest, C. Birrel, and P. J. Mumby. 2016. The ecological role of sharks on coral reefs. Trends in Ecology & Evolution **31**:395-407.

Rooney, N., and K. S. McCann. 2012. Integrating food web diversity, structure and stability. Trends in Ecology & Evolution **27**:40-46.

Rooney, N., K. McCann, G. Gellner, and J. C. Moore. 2006. Structural asymmetry and the stability of diverse food webs. Nature **442**:265-269.

Ruiz-Cooley, R. I., P. L. Koch, P. C. Fiedler, and M. D. McCarthy. 2014. Carbon and nitrogen isotopes from top predator amino acids reveal rapidly shifting ocean biochemistry in the outer California Current. Plos One **9**:e110355.

Rundel, C. W., M. B. Wunder, A. H. Alvarado, K. C. Ruegg, H. R. Harrigan, A. Schuh, J. F. Kelly, R. B. Siegel, D. F. DeSante, T. B. Smith, and J. Novembre. 2013. Novel statistical methods for integrating genetic and stable isotope data to infer individual-level migratory connectivity. Molecular Ecology **22**:4163-4176.

Ruppert, J. L., M.-J. Fortin, and M. G. Meekan. 2016. The ecological role of sharks on coral reefs: response to Roff *et al*. Trends in Ecology & Evolution **31**:586-587.

Sackett, W. M., W. R. Eckelman, M. L. Bender, and A. W. H. Be. 1965. Temperature dependence of carbon isotope composition in marine plankton and sediments. Science **148**:235-237.

Saunders, R. A., F. Royer, and M. W. Clarke. 2011. Winter migration and diving behaviour of porbeagle shark, *Lamna nasus*, in the North East Atlantic. ICES Journal of Marine Science **68**:166-174.

Saupe, S. M., D. M. Schell, and W. B. Griffiths. 1989. Carbon isotope gradients in western Arctic zooplankton. Marine Biology **103**:427-432.

Scheffer, M., S. Carpenter, and B. de Young. 2005. Cascading effects of overfishing marine systems. Trends in Ecology & Evolution **20**:579-581.

Schell, D. M., B. A. Barnett, and K. A. Vinette. 1998. Carbon and nitrogen isotope ratios in zooplankton of the Bering, Chukchi and Beaufort seas. Marine Ecology Progress Series **162**:11-23.

Schell, D. M., S. M. Saupe, and N. Haubenstock. 1989a. Bowhead whale (*Balaena mysticetus*) growth and feeding as estimated by $\delta^{13}C$ techniques. Marine Biology **103**:433-443.

Schell, D. M., S. M. Saupe, and N. Haubenstock. 1989b. Natural isotope abundances in bowhead whale (*Balaena mysticetus*) baleen: markers of ageing and habitat usage. Ecological Studies **68**:260-269.

Schiff, J. T., F. C. Batista, O. A. Sherwood, T. P. Guilderson, T. M. Hill, A. C. Ravelo, K. W. McMahon, and M. D. McCarthy. 2014. Compound specific amino acid $\delta^{13}C$ patterns in a deep-sea proteinaceous coral: implications for reconstructing detailed $\delta^{13}C$ records of exported primary production. Marine Chemistry **166**:82-91.

Schmittner, A., and C. J. Somes. 2016. Complementary constraints from carbon (^{13}C) and nitrogen (^{15}N) isotopes on the Glacial Ocean's soft-tissue biological pump. Paleoceanography **31**:625-913.

Schmittner, A., N. Gruber, A. C. Mix, R. M. Key, A. Tagliabue, and T. K. Westberry. 2013. Biology and air-sea gas exchange controls on the distribution of carbon isotope ratios ($\delta^{13}C$) in the ocean. Biogeosciences **10**:5793-5816.

Scott, J. H., D. M. O'Brien, D. Emerson, H. Sun, G. D. McDonald, A. Salgado, and M. L. Fogel. 2006. An examination of the carbon isotope effects associated with amino acid biosynthesis. Astrobiology **6**:867-880.

Scott, R., A. Biastoch, C. Roder, V. A. Stiebens, and C. Eizaguirre. 2014. Nano-tags for neonates and ocean-mediated swimming behaviours linked to rapid dispersal of hatchling sea turtles. Proceedings of the Royal Society B-Biological Sciences **281**:20141209.

Seminoff, J. A., S. R. Benson, K. E. Arthur, T. Eguchi, P. H. Dutton, R. F. Tapilatu, and B. N. Popp. 2012. Stable isotope tracking of endangered sea turtles: validation with satellite telemetry and $\delta^{15}N$ analysis of amino acids. Plos One **7**:e37403.

Shillinger, G. L., H. Bailey, S. J. Bograd, E. L. Hazen, M. Hamann, P. Gaspar, B. J. Godley, R. P. Wilson, and J. R. Spotila. 2012. Tagging through the stages: technical and ecological challenges in observing life histories through biologging. Marine Ecology Progress Series **457**:165-170.

Sibert, J. R., and J. L. Nielsen. 2001. Electronic tagging and tracking in marine fisheries. Proceedings of the Symposium on Tagging and Tracking Marine Fish with Electronic Devices. February 7–11, 2000, East-West Center, University of Hawaii. Springer, Netherlands.

Siebel, B. A. 2011. Critical oxygen levels and metabolic suppression in oxygen minimum zones. Journal of Experimental Biology **214**:326-336.

Sigman, D. M., and K. L. Casciotti. 2001. Nitrogen isotopes in the ocean. Page 2449 *in* J. H. Steele, K. K. Turekian, and S. A. Thorpe, editors. Encyclopedia of Ocean Sciences. Academic, London, UK.

Sims, D. W. 2010. Tracking and analysis techniques for understanding free-ranging shark movements and behavior. Pages 351-392 *in* J. C. Carrier, J. A. Musick, and M. R. Heithaus, editors. Sharks and Their Relatives II: Biodiversity, Adaptive Physiology, and Conservation. CRC Press, Boca Raton, FL.

Skomal, G. B., and L. J. Natanson. 2003. Age and growth of the blue shark (*Prionace glauca*) in the North Atlantic Ocean. Fishery Bulletin **101**:627-639.

Skomal, G. B., S. I. Zeeman, J. H. Chisholm, E. L. Summers, H. J. Walsh, K. W. McMahon, and S. R. Thorrold. 2009. Transequatorial migrations by basking sharks in the western Atlantic Ocean. Current Biology **19**:1019-1022.

Somero, G. N. 1992. Adaptations to hydrostatic pressure. Annual Review of Physiology **54**:557-577.

Somes, C. J., A. Schmittner, E. D. Galbraith, M. F. Lehmann, M. A. Altabet, J. P. Montoya, R. M. Letelier, A. C. Mix, A. Bourbonnais, and M. Eby. 2010. Simulating the global distribution of nitrogen isotopes in the ocean. Global Biogeochemical Cycles **24**:GB4019.

Sommer, U., H. Stibor, A. Katechakis, F. Sommer, and T. Hansen. 2002. Pelagic food web configurations at different levels of nutrient richness and their implications for the ratio fish production:primary production. Hydrobiologia **484**:11-20.

Stevens, J. D. 1976. First results of shark tagging in Northeast Atlantic, 1972-1975. Journal of the Marine Biological Association of the United Kingdom **56**:929-937.

Stevens, J. D. 1990. Further results from a tagging study of pelagic sharks in the North- East Atlantic. Journal of the Marine Biological Association of the United Kingdom **70**:707-720.

Stewart, B. S., S. Leatherwood, P. K. Yochem, and M.-P. Heide-Jørgensen. 1989. Harbor seal tracking and telemetry by satellite. Marine Mammal Science **5**:361-375.

Tagliabue, A., and L. Bopp. 2008. Towards understanding global variability in ocean carbon-13. Global Biogeochemical Cycles **22**:GB1025.

Timmermann, R., H. Goosse, G. Madec, T. Fichefet , C. Ethe, and V. Duliere. 2005. On the representation of high latitude processes in the ORCA-LIM global coupled sea ice-ocean model. Ocean Modelling **8**:175-201.

Trebilco, R., J. K. Baum, A. K. Salomon, and N. K. Dulvy. 2013. Ecosystem ecology: size-based constraints on the pyramids of life. Trends in Ecology & Evolution **28**: 423-431.

Trueman, C. N., G. Johnston, B. O'Hea, and K. M. MacKenzie. 2014. Trophic interactions of fish communities at midwater depths enhance long-term carbon storage and benthic production on continental slopes. Proceedings of the Royal Society B-Biological Sciences **281**:20140669.

Trueman, C. N., K. M. MacKenzie, and K. St. John Glew. 2016. Stable isotope-based location in a shelf sea setting: accuracy and precision are comparable to light-based location methods. Methods in Ecology and Evolution **8**:232-240.

Trueman, C. N., K. M. MacKenzie, and M. R. Palmer. 2012. Identifying migrations in marine fishes through stable isotope analysis. Journal of Fish Biology **81**:826-847.

Tuross, N., M. L. Fogel, and P. E. Hare. 1988. Variability in the preservation of the isotopic compositions of collagen from fossil bone. Geochimica Et Cosmochimica Acta **52**:929-935.

Valiela, I. 1984. Marine Ecological Processes. Springer, New York and Heidelberg.

Van Wilgenburg, S. L., and K. A. Hobson. 2011. Combining stable-isotope (δD) and band recovery data to improve probabilistic assignments of migratory birds to origin. Ecological Applications **21**:1340-1352.

Van Wilgenburg, S. L., K. A. Hobson, K. R. Brewster, and J. M. Welker. 2012. Assessing dispersal in threatened migratory birds using stable hydrogen isotope (δD) analysis of feathers. Endangered Species Research **16**:17-29.

Vandeperre, F., A. Aires-da-Silva, C. E. Lennert-Cody, R. Serrão Santos, and P. Afonso. 2016. Essential pelagic habitat of juvenile blue shark (*Prionace glauca*) inferred from telemetry data. Limnology and Oceanography **61**:1605-1625.

Vandeperre, F., A. Aires-da-Silva, J. Fontes, M. Santos, R. S. Santos, and P. Afonso. 2014. Movements of blue sharks (*Prionace glauca*) across their life history. Plos One **9**:e103538.

Vander Zanden, H. B., A. D. Tucker, K. M. Hart, M. M. Lamont, I. Fujisaki, D. S. Addison, K. L. Mansfield, K. F. Phillips, M. B. Wunder, G. J. Bowen, M. Pajuelo, A. B. Bolten, and K. A. Bjorndal. 2015a. Determining origin in a migratory marine vertebrate: a novel method to integrate stable isotopes and satellite tracking. Ecological Applications **25**:320-335.

Vander Zanden, H. B., M. B. Wunder, K. A. Hobson, S. Van Wilgenburg, L. I. Wassenaar, J. Welker, and G. J. Bowen. 2015b. Space-time tradeoffs in the development of precipitation-based isoscape models for determining migratory origin. Journal of Avian Biology **46**:1-10.

Vander Zanden, M. J., and J. B. Rasmussen. 2001. Variation in $\delta^{15}N$ and $\delta^{13}C$ trophic fractionation: implications for aquatic food web studies. Limnology and Oceanography **46**:2061-2066.

Varpe, O., O. Fiksen, and A. Slotte. 2005. Meta-ecosystems and biological energy transport from ocean to coast: the ecological importance of herring migration. Oecologia **146**:443-451.

Viana, D. S., L. Santamaría, T. C. Michot, and J. Figuerola. 2013. Migratory strategies of waterbirds shape the continental-scale dispersal of aquatic organisms. Ecography **36**:430-438.

Vokhshoori, N. L., and M. D. McCarthy. 2014. Compound-specific $\delta^{15}N$ amino acid measurements in littoral mussels in the California upwelling ecosystem: a new approach to generating baseline $\delta^{15}N$ isoscapes for coastal ecosystems. Plos One **9**:e98087.

Vokhshoori, N. L., T. Larsen, and M. D. McCarthy. 2014. Reconstructing $\delta^{13}C$ isoscapes of phytoplankton production in a coastal upwelling system with amino acid isotope values of littoral mussels. Marine Ecology Progress Series **504**:59-72.

Walsh, R. G., S. He, and C. T. Yarnes. 2014. Compound-specific $\delta^{13}C$ and $\delta^{15}N$ analysis of amino acids: a rapid, chloroformate-based method for ecological studies. Rapid Communications in Mass Spectrometry **28**:96-108.

Wassenaar, L. I. 2008. An introduction to light stable isotopes for use in terrestrial animal migration studies. Pages 21-44 *in* K. A. Hobson and L. I. Wassenaar, editors. Tracking Animal Migration with Stable Isotopes, Elsevier, Amsterdam.

Werner, E. E., and J. F. Gillam. 1984. The ontogenetic niche and species interactions in size-structured populations. Annual Review of Ecology, Evolution, and Systematics **15**:393-425.

West, J. B., G. J. Bowen, T. E. Dawson, and K. P. Tu, editors. 2010. Isoscapes: Understanding Movement, Pattern, and Process on Earth through Isotope Mapping. Springer Science, Berlin.

Wilcove, D. S., and M. Wikelski. 2008. Going, going, gone: is animal migration disappearing ? Plos Biology **6**:e188.

Wong, W. W., and W. M. Sackett. 1978. Fractionation of stable carbon isotopes by marine phytoplankton. Geochimica Et Cosmochimica Acta **42**:1809-1815.

Wood, S.N. 2006. Generalized Additive Models: An Introduction with R. Chapman and Hall/CRC Press.

Wood, S.N. 2011. Fast stable restricted maximum likelihood and marginal likelihood estimation of semiparametric generalized linear models. Journal of the Royal Statistical Society B:**73**:3-36.

Worm, B., B. Davis, L. Kettemer, C. A. Ward-Paige, D. Chapman, M. R. Heithaus, S. T. Kessel, and S. H. Gruber. 2013. Global catches, exploitation rates, and rebuilding options for sharks. Marine Policy **40**:194-204.

Worm, B., M. Sandow, A. Oschilies, H. K. Lotze, and R. A. Myers. 2005. Global patterns of predator diversity in the open oceans. Science **309**:1365-1369.

Wunder, M. B. 2010. Using isoscapes to model probability surfaces for determining geographic origins. Pages 251-270 *in* J. B. West, G. J. Bowen, T. E. Dawson, and K. P. Tu, editors. Isoscapes: Understanding Movement, Pattern, and Process on Earth through Isotope Mapping. Springer Science, Berlin.

Wunder, M. B., and D. R. Norris. 2008a. Analysis and design for isotope-based studies of migratory animals. Pages 107-128 *in* K. A. Hobson and L. I. Wassenaar, editors. Tracking Animal Migration with Stable Isotopes, Elsevier, Amsterdam.

Wunder, M. B., and D. R. Norris. 2008b. Improved estimates of certainty in stable-isotope-based methods for tracking migratory animals. Ecological Applications **18**:549-559.

Yancey, P. H., M. E. Gerringer, J. C. Drazen, A. A. Rowden, and A. Jamieson. 2014. Marine fish may be biochemically constrained from inhabiting the deepest ocean depths. Proceedings of the National Academy of Sciences of the United States of America **111**:4461-4465.

Yool, A., E. E. Popova, and T. R. Anderson. 2013. MEDUSA-2.0: an intermediate complexity biogeochemical model of the marine carbon cycle for climate change and ocean acidification studies. Geoscientific Model Development **6**:1767-1811.

Zacheis, A., J. W. Hupp, and R. W. Ruess. 2001. Effects of migratory geese on plant communities of an Alaskan salt marsh. Journal of Ecology **89**:57-71.

Zbinden, J. A., S. Bearhop, P. Bradshaw, B. Gill, D. Margaritoulis, J. Newton, and B. J. Godley. 2011. Migratory dichotomy and associated phenotypic variation in marine turtles revealed by satellite tracking and stable isotope analysis. Marine Ecology Progress Series **421**:291-302.

Zeebe, R. E., and D. Wolf-Gladrow, editors. 2001. CO_2 in seawater: equilibirum, kinetics, isotopes. Elsevier, Amsterdam, Netherlands.

Zeebe, R. E., D. A. Wolf-Gladrow, and H. Jansen. 1999. On the time required to establish chemical and isotopic equilibrium in the carbon dioxide system in seawater. Marine Chemistry **65**:135-153.

Zhang, J., P. D. Quay, and D. O. Wilbur. 1995. Carbon isotope fractionation during gas-water exchange and dissolution of CO_2. Geochimica Et Cosmochimica Acta **59**:107-114.

Zuur, A. F., A. A. Saveliev, and E. N. Ieno. 2014. A beginner's guide to generalised additive mixed models with R. Highland Statistics Ltd., Newburgh, United Kingdom.

Zuur, A. F., J. M. Hilbe, and E. N. Ieno. 2013. A beginner's guide to GLM and GLMM with R. Highland Statistics Ltd., Newburgh, United Kingdom.